DEPARTMENT OF CIVIL ENGINEERING
220 CIVIL/ELECTRICAL ENGINEERING BUILDING
UNIVERSITY OF ALBERTA
EDMONTON, ALBERTA, CANADA T6G 2G7
TELEPHONE (403) 432-4235

University of Alberta
Department of Civil Engineering

Structural Engineering Report 162

BEHAVIOR AND DESIGN OF REINFORCED CONCRETE ICE-RESISTING WALLS

by
R. M. ELLIS
and
J. G. MacGREGOR

November 1988

RECENT STRUCTURAL ENGINEERING REPORTS

Department of Civil Engineering

University of Alberta

131. *Inelastic Lateral Buckling of Steel Beam-Columns* by P.E. Cuk, M.A. Bradford and N.S. Trahair, December 1985.

132. *Design Strengths of Steel Beam-Columns* by N.S. Trahair, December 1985.

133. *Behaviour of Fillet Welds as a Function of the Angle of Loading* by G.S. Miazga and D.J.L. Kennedy, March 1986.

134. *Inelastic Seismic Response of Precast Concrete Large Panel Coupled Shear Wall Systems* by M.R. Kianoush and A. Scanlon, March 1986.

135. *Finite Element Prediction of Bin Loads* by A.H. Askari and A.E. Elwi, June 1986.

136. *Shear Behavior of Large Diameter Fabricated Steel Cylinders* by J. Mok and A.E. Elwi, June 1986.

137. *Local Buckling Rules for Structural Steel Members* by S. Bild and G.L. Kulak, May 1986.

138. *Finite Element Prediction of Reinforced Concrete Behavior* by S. Balakrishnan and D.W. Murray, July 1986.

139. *Behavior and Strength of Masonry Wall/Slab Joints* by T.M. Olatunji and J. Warwaruk, July 1986.

140. *Bayesian Analysis of In-Situ Test Data for Estimating the Compressive Strength of Concrete in Existing Structures* by G.J. Kriviak and A. Scanlon, July 1986.

141. *Shear-Moment Transfer in Slab-Column Connections* by S.D.B. Alexander and S.H. Simmonds, July 1986.

142. *Minimum Thickness Requirements for Deflection Control of Two-Way Slab Systems* by D.P. Thompson and A. Scanlon, November 1986.

143. *Shrinkage and Flexural Tests of Two Full-Scale Composite Trusses* by A. Brattland and D.J.L. Kennedy, December 1986.

144. *Combined Flexure and Torsion of I-Shaped Steel Beams* by R.G. Driver and D.J.L. Kennedy, March 1987.

145. *Cyclic and Static Behaviour of Thin Panel Steel Plate Shear Walls* by E.W. Tromposch and G.L. Kulak, April 1987.

146. *Postbuckling Behavior of Thin Steel Cylinders Under Transverse Shear* by V.G. Roman and A.E. Elwi, May 1987.

147. *Incipient Flow in Silos - A Numerical Approach* by R.A. Link and A.E. Elwi, May 1987.

148. *Design of Web-Flange Beam or Girder Splices* by D. Green and G.L. Kulak, May 1987.

149. *Spreadsheet Solution of Elastic Plate Bending Problems* by G.E. Small and S.H. Simmonds, July 1987.

150. *Behaviour of Transversely Loaded Continuous Steel-Concrete Composite Plates* by S.J. Kennedy and J.J. Cheng, July 1987.

151. *Behaviour and Ultimate Strength of Partial Joint Penetration Groove Welds* by D.P. Gagnon and D.J.L. Kennedy, July 1987.

152. *KBES for Design of Reinforced Concrete Columns* by A. Bezzina and S.H. Simmonds, July 1987.

153. *Compressive Behavior of Gusset Plate Connections* by S.Z. Hu and J.J. Cheng, July 1987.

154. *Development of Structural Steel Design Standards* by P.J. Marek and D.J.L. Kennedy, October 1987.

155. *Behaviour of Bolted Joints of Corrugated Steel Plates* by R.W.S. Lee and D.J.L. Kennedy, January 1988.

156. *Masonry Veneer Wall Systems* by W.M. McGinley, J. Warwaruk, J. Longworth and M. Hatzinikolas, January 1988.

157. *Stability of Concrete Plates* by A.O. Aghayere and J.G. MacGregor, February 1988.

158. *The Flexural Creep Behaviour of OSB Stressed Skin Panels* by P.C.K. Wong, L. Bach and J.J. Cheng, April 1988.

159. *Ultimate Strength of Eccentrically Loaded Fillet Welded Connections* by D.F. Lesik and D.J.L. Kennedy, May 1988.

160. *Fatigue Strength of Coped Steel Beams* by M.C.H. Yam and J.J. Cheng, June 1988.

161. *Analysis of Concrete Panels* by B. Massicotte, A.E. Elwi and J.G. MacGregor, July 1988.

162. *Behavior and Design of Reinforced Concrete Ice-Resisting Walls* by R.M. Ellis and J.G. MacGregor, November 1988.

Structural Engineering Report No. 162

BEHAVIOR AND DESIGN OF REINFORCED CONCRETE ICE-RESISTING WALLS

by

Reed M. Ellis

and

James G. MacGregor

Department of Civil Engineering

University of Alberta

Edmonton, Alberta

Canada T6G 2G7

November 1988

"During the next decade it is hoped that the design regulations ... can be ... simplified and given physical significance so that designers can approach unusual design problems in a rational manner".

- ACI-ASCE Shear Committee 1973

"Everything should be made as simple as possible, but not any simpler".

- Albert Einstein

Abstract

The exterior wall used to resist ice loads on offshore structures must be designed to withstand high magnitude concentrated loads. The shape and span-to-depth ratios of these walls are such that their analysis and design fall outside building code design specifications. Possible analysis and design procedures include the strut-and-tie model, and the use of nonlinear finite element analysis.

A research program was carried out to investigate the behavior of two types of reinforced concrete ice resisting walls. Circular arch specimens, modelling an ice-resisting wall of the type proposed for use in the Arctic, and V-shaped arch specimens, modelling the type proposed for use in the Hibernia field off the coast of Newfoundland, were constructed and tested.

Since the strut-and-tie model and the finite element method are viewed as the most suitable design methods and since the two methods complement each other, both methods are examined and applied. Particular attention is paid to the development of strut-and-tie models for different loadings and geometry. The assumptions concerning force-transfer mechanisms in reinforced concrete are critically examined. The possibility of using the graphical capabilities of the micro-computer to aid in the development of strut-and-tie models for reinforced concrete design is considered.

Recommendations concerning the analysis and design of reinforced concrete ice-resisting walls for offshore structures are made. Suggestions for further research are given.

Acknowledgements

I wish to sincerely thank Dr. J. G. MacGregor for his guidance and support throughout this work. The research was funded by Research Grant A1673 from the Natural Sciences and Engineering Research Council of Canada.

I would like to acknowledge the financial support of the Society of Naval Architects and Marine Engineers (Arctic Section) in the form of a Scholarship. The assistance of DYWIDAG Systems International (Canada) Ltd. and Con-Force Structures Ltd. in prestressing matters is gratefully acknowledged.

The construction and testing of the test specimens could not have been completed without the technical assistance of Larry Burden, Richard Helfrich, and Vijay Parmar at the Morrison Structural Laboratory. The assistance of summer employees P. Sundararaj, D. MacGregor, and M. Roberts in the construction of the formwork and reinforcing cages is acknowledged.

I wish to acknowledge the support and encouragement of Professors J. Warwaruk and S. H. Simmonds, and Professor A. Scanlon who, in addition, helped with the pulse-velocity measurements. I am indebted to Professor D. W. Murray and Dr. P. F. Adams who provided encouragement to undertake this task.

I am particularily indebted to two of my colleagues Dr. A. Aghayere, and Y. Budan for their assistance in the

numerous manual strain measurements taken during this project.

I am indebted to Mr. John Hanson, Senior Draftsman at The Engineers Collaborative, Structural Consulting Engineers, Edmonton, who inked the numerous and detailed technical drawings. My appreciation is also extended to Ms. Nola Shaw who typed the text for this document.

Finally, I am most deeply grateful to my wife, Lorna, whose support, understanding, and strength made it possible for me to endure the extreme working hours required over the past four years. To Lorna I extend my gratitude, my respect, and my love.

Table of Contents

List of Tables

List of Figures

Notation

A_s = Area of reinforcing steel

A_v = Area of shear reinforcement

b = Width of specimen

C_i = ith Strut force

d = Distance to center of tension reinforcement

d_b = Reinforcing bar diameter

E_c = Tangent modulus of concrete

E_s = Modulus of steel reinforcement

E_{sh} = Slope of strain hardening portion of reinforcing stress-strain curve

f'_c = Uniaxial compressive strength of concrete

f_{ce} = Effective concrete strength in compression

f_{CD} = Diagonal compressive stress in concrete

f_{cu} = Compressive strength of concrete

f'_t = Uniaxial tensile strength of concrete. Taken to be equal to the split cylinder strength.

f_{te} = Effective concrete strength in tension

f_{tu} = Tensile strength of concrete

f_y = Yield stress of reinforcing steel

G = Shear modulus of uncracked concrete

G_{cr} = Shear modulus of cracked concrete

H = Horizontal force component

h = Depth of D region

h_o = Height of nodal zone

l_d = Development length of reinforcing bar

l_{db} = Basic development length of reinforcing bar

ℓ = Length of fan surface

N_v = Tensile force in reinforcement due to shear

p = Uniformly distributed load. Normal stress acting on fan surface

p' = Normal stress acting on circular surface of fan

P = Applied load.

R = Reaction

r_F = Fan radius to point F

R_o = Force at base of centered fan

s_A = Slope of fan line through point A

T = Tie force

V = Shear force at a section. Vertical force component

w_s = Width of strut

β_L = Equivalent strut angle for left-hand fan

β_R = Equivalent strut angle for right-hand fan

ϵ = Normal strain

E = Non-dimensional coordinate along top surface of fan

ϵ_1 = Strain normal to crack

ϵ_{cr} = Cracking strain of concrete

ϵ_s = Strain in steel

ϵ_{yield} = Yield strain of steel

ϵ_{ut} = Strain at which tensile stress has reduced to zero

ϵ_{gt} = Strain at which G has reduced to the minimum value

ζ = Non-dimensional coordinate for hyperbolic decentered fan

η = Non-dimensional coordinate for hyperbolic decentered fan

θ_0 = Spreading angle

θ_G = Angle of fan line through pt. G

μ_{AVE} = Average bond stress

ν = Concrete effectiveness factor. Poisson's Ratio (Chapter 7)

σ = Stress

σ_0 = Stress at base of radial fan

σ_1 = Major principal stress

σ_2 = Minor principal stress

σ_3 = Principal stress in direction 3

σ_N = Normal stress acting on the actual bearing surface of the fan

σ_T = Tangential (bond) stress acting on the actual bearing surface of the fan

σ_{2c} = Compressive strength in the minor principal stress direction under biaxial compression

τ = Shear or tangential stress acting on fan surface

τ' = Shear or tangential stress acting on circular surface of fan

ω_0 = Non-dimensional distance in hyperbolic decentered fan

1. INTRODUCTION

1.1 General

Reinforced concrete structures have performed entirely successfully in harsh offshore environments such as the North Sea and the Canadian and Alaskan Beaufort Sea. Concrete production structures are being designed for use in the Arctic and it appears that the first production structure off the coast of Newfoundland will be a reinforced concrete gravity structure.

In the design of offshore structures in these environments, it is necessary to consider many types of loads at the various stages of construction, towing, installation, and operations (API, 1982; DnV, 1977; FIP, 1977; MacGregor, Baskin, and Ellis, 1984). In particular, the exterior wall must resist very high magnitude concentrated 'patch' loads, perhaps in the order of 10 MPa on smaller areas. To resist loads of this magnitude, the structural system must include some arrangement of thick exterior walls supported by a system of interior walls. Generally, the interior walls are arranged to provide cells for fluid storage.

A schematic diagram of a typical Arctic reinforced concrete offshore structure is shown in Fig. 1.1. This is based on the Concrete Island Drilling System, developed by Global Marine (Yee et al., 1984). The reinforced concrete ice-resisting module rests on a steel-mud base. The

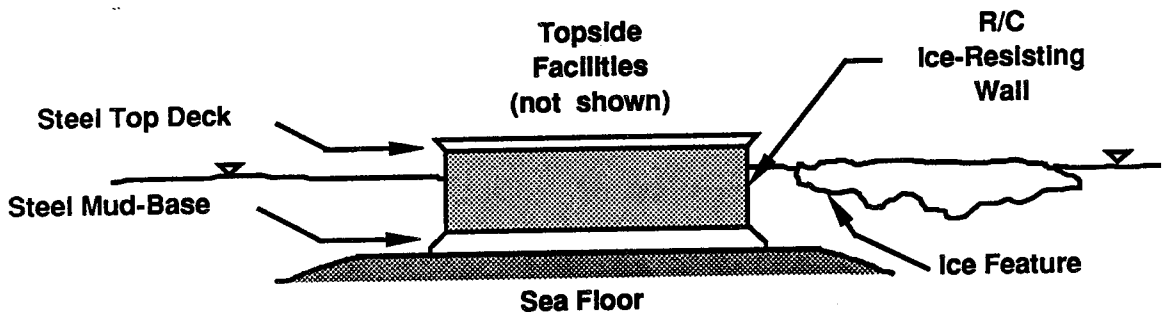

Figure 1.1 Schematic Diagram of Typical Arctic Offshore Structure

reinforced concrete ice resisting wall is located in the splash zone and will be exposed to severe corrosion and temperatures as well as to intense ice loads.

Because of the limited available floating draft for structures being towed into the Arctic, and for cost reasons, it is essential that the weight of the structure be minimized. Furthermore the external ice resisting wall represents a significant portion of the overall construction cost and construction time associated with these structures. It is therefore necessary to optimize the structural performance of the ice-resisting wall system.

This can best be done by choosing a geometrical configuration which will encourage optimum structural and material behavior through 'deep beam' or 'arching' action rather than exclusively beam or plate action. An efficient system will also encourage fracturing of the ice which tends to reduce the ice load. Typical reinforced concrete arrangements that have been proposed include haunched one-way slabs, circular arches, and V-shaped arches (Fig. 1.2). In reinforced concrete, these shapes have the added benefit that they allow a wide spacing of interior walls rather than relying on a close spacing and complex arrangement of ribs and bulkheads as in the case of steel or steel-concrete composite construction.

The proposed ice-resisting walls are not like usual building structures. The reasons for this are as follows:

1. These walls tend to be significantly thicker, relative

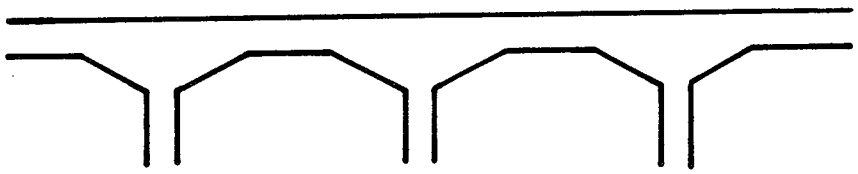

Haunched Slab

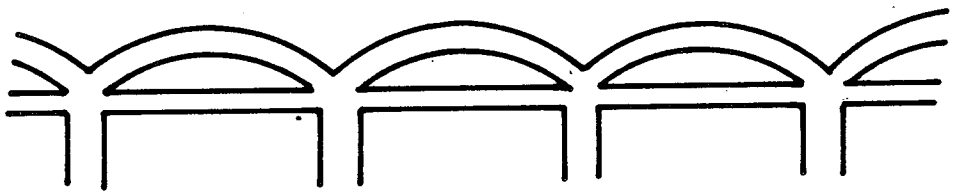

Circular Arch

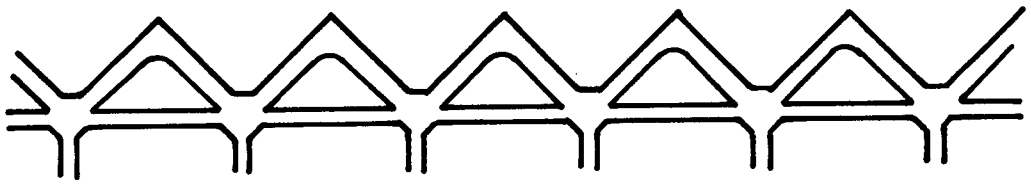

V - Shaped Arch

Figure 1.2 Typical Reinforced Concrete Ice-Resisting Wall Configurations

to the span, than building slabs, walls, or shells.

2. They tend to have significantly more reinforcement than building structures including through-the-wall shear reinforcement. This reinforcement will include prestressing tendons.
3. They may develop high in-plane compressive stresses due to membrane or arching action which will enhance the shear strength of the concrete in the walls. The extent of arching action that can be developed depends on the continuity and the degree of restraint provided by the supporting interior walls.

Design guidelines are lacking for structures with the above characteristics. Conventional shear strength or slab design procedures are overconservative for these types of walls because the beneficial effects of in-plane compression stresses are ignored. The ability of walls of this thickness to carry load through 'deep beam' behavior places the design into a category given only cursory treatment in codes.

Simple analytical tools are needed to predict the ultimate strength of these walls. Because of the importance of the reinforcement detailing a clear understanding of the flow of forces through the structure is necessary. It is also desirable to be able to predict the mode of failure and the overall ductility of the structure. Since a design method capable of doing all of these things reliably and economically is not available, a combination of methods will be required. The research program, described in the next

section, was initiated in order to provide information concerning this problem.

1.2 Objectives and Scope

The Objectives of this research program are:

1. To develop rational models for the analysis/design of arch shaped reinforced concrete ice-resisting walls subjected to high magnitude patch loadings.
2. To calibrate and verify these models experimentally through the construction and testing of large-scale detailed test specimens.
3. To verify the applicability of non-linear finite element analysis in predicting the behavior of these test specimens.
4. To provide recommendations for the analysis and design of reinforced concrete ice-resisting walls and to outline areas of future work.

The effects of the following on the behaviour of arch-shaped reinforced concrete ice-resisting walls are investigated:

1. Shape of the arch (circular or V-shaped)
2. Reinforcing ratio of longitudinal reinforcement
3. Reinforcing ratio of shear reinforcement
4. Lateral and bending stiffness of the support provided the arch.

1.3 Organization of the Thesis

In Chapter 2 of this thesis, a review of the existing research literature on reinforced concrete ice-resisting walls is presented. Details of the experimental research program are presented in Chapter 3 including for each test series, the objectives, the reinforcing and construction details, details of the prestressing operation, measured material properties, and the test set-up and instrumentation particular to that test series. In Chapter 4 are presented the test results including for each specimen failure load, mode of failure, load-deflection response, measured concrete and reinforcing strains, and cracking and damage patterns. In Chapter 5 is presented a detailed discussion of plasticity based strut-and-tie models including basic modelling principles, a discussion of the various compressive stress fields and the different nodal regions, and a discussion of force transfer mechanisms in reinforced concrete with a view towards strut-and-tie modelling. A discussion and application of computer aided strut-and-tie modelling is also included in Chapter 5. In Chapter 6, the development of strut-and-tie models for each type of test specimen are presented. Simple strut-and-tie models and models based on the measured forces and moments and the measured reinforcing strains are presented. In Chapter 7, the application of non-linear finite element analysis to reinforced concrete ice-resisting walls is discussed. A suitable program, FEPARCS, having adequate sophistication

for this type of analysis, is used to predict the crack pattern, load-deflection response, failure load and failure mode for each type of specimen. The conclusions and recommendations are presented in Chapter 8, along with recommendations for further research.

2. LITERATURE REVIEW

2.1 Ice Loading on Offshore Structures

Most specifications for the design of offshore structures (API Bulletin 2N, 1982; ACI 357-R78, 1978;API Rp2A 1982; DnV, 1977; FIP, 1977; MacGregor et al., 1984) make reference to ice loads but there are as yet no quantitative design recommendations. Research in the last decade has improved the understanding of sea ice rheology and ice-structure interaction to the point that consensus is emerging in the literature as to the nature of the ice loads on offshore structures.

The field of ice mechanics and the study of ice-structure interaction are not included within the scope of this thesis. Instead several good references on this subject will be provided. Following this, those aspects of ice loading on offshore structures essential to this thesis will be summarized.

The mechanical behavior of sea ice is given an excellent treatment by Mellor (1983) and by Croasdale (1984a). There are several good references on the nature of ice loading on offshore structures: for eg. Bruen et al. (1982), Watt (1984), Croasdale (1984b and 1985). The nature of ice-structure interaction is discussed by Croasdale (1984b and 1985), and by Bercha et al. (1985), and Allyn (1986). The evaluation of iceberg loads on fixed offshore structures and the topic of iceberg-structure interaction

are discussed by Deleuil et al. (1984) and Brown et al. (1986).

The following points summarize the above research.

1. The maximum pressure which an ice body will exert on a structure depends on many factors such as the rheology of the ice, the loading rate, the area of contact, the geometry of the ice feature, and the geometry of the structure.
2. Ice forces on offshore structures may be categorized into global loads and local loads. The global ice load is of interest in the overall design of the structural system (for eg. the sliding and overturning). Local ice loads are those which act over a small area and govern the design of the exterior wall. Local ice pressures are much larger than global ice pressures. A typical ice pressure vs. loaded area curve is shown in Fig. 2.1. This particular distribution is that proposed by Watt (1984).
3. In iceberg infested water, fixed offshore structures must be designed to resist forces resulting from impact from icebergs, growlers, and smaller pieces called 'bergy bits'. As in the case of other sea ice, consideration must be given to the global force applied to structure and to the pressures generated locally during the ice-structure interaction. Studies indicate that the dynamic interaction between the ice feature and the structure should be considered and that the

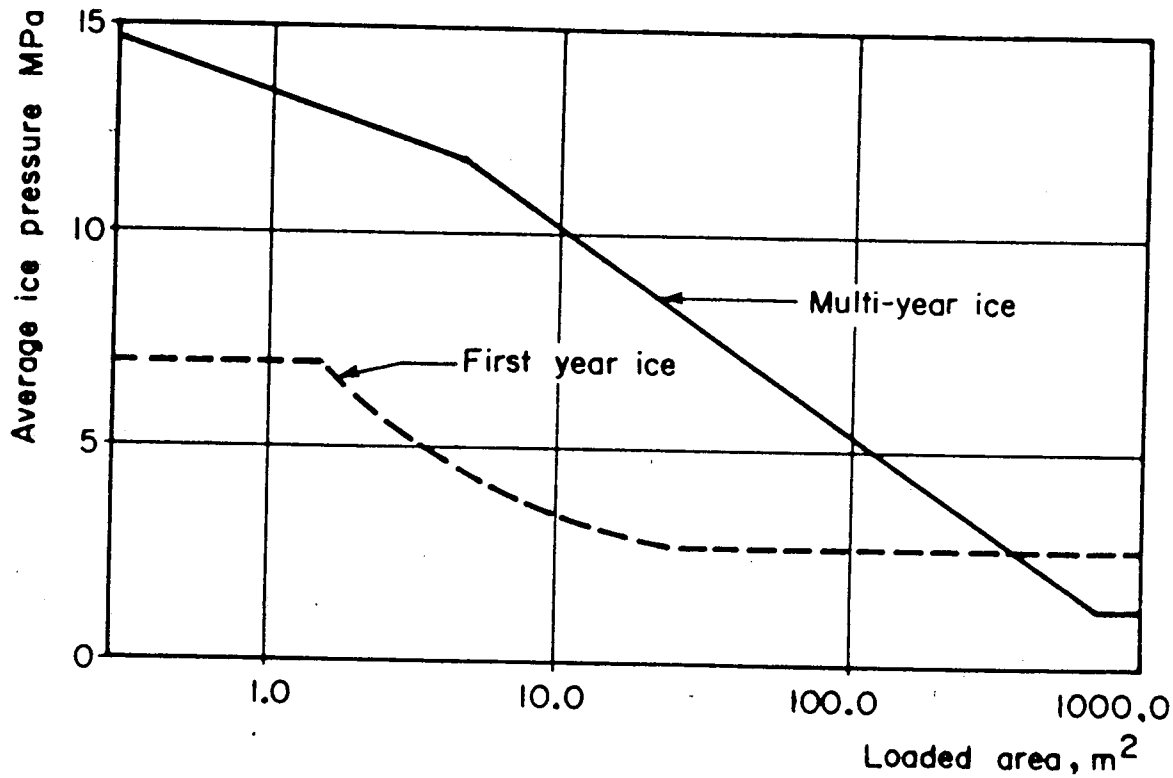

Figure 2.1 Typical Ice Pressure vs. Loaded Area Curve

structural geometry and flexibility in the vicinity of the load is important.

2.2 Research on Reinforced Concrete Offshore Structures

2.2.1 Gerwick, Litton and Reimer (1981)

In this paper, the authors recognized that while the problem of global ice loading had been addressed, a more serious problem is in the 'unprecedently high' shear forces acting on the exterior walls due to the local concentrated loads.

It is suggested that if conventional code procedures are followed, wall thicknesses of up to 4 meters would be required. This would make the structure so heavy that it would not float with reasonable draft, preventing delivery of such a structure into the Arctic.

Research on the impact of floating vessels on concrete offshore structures and on the end slabs of prestressed concrete nuclear reactor vessels is cited to illustrate that arching action will occur in thick slabs. Of particular importance is "the formation within the wall after initial flexural cracking has occurred, of an internal arch". To encourage this behavior, thick reinforced concrete circular arches are proposed as the best alternative for use as ice-resisting walls. Results of a simple finite element analysis are presented. In the analysis, the circular arch is loaded by a 7 MPa patch load applied symmetrically at

midspan.

Of particular interest is the proposal that through-the-wall post-tensioned stirrups be used to strengthen the wall and reduce the thickness. The finite element analysis indicated that the use of the post-tensioned stirrups would inhibit the punching shear and lead to a flexural compressive failure under the applied load, or to a shear-compression failure at the edge of the applied load. It is suggested that this mode of failure would be more ductile if adequate triaxial confinement were provided by using stirrups anchored at their ends by bearing plates.

2.2.2 Bhula, Birdy, and Bruen (1984)

In this paper, the authors present a method for designing reinforced concrete offshore structures to resist ice loads. An ice pressure vs. area curve similar to that shown in Fig. 2.1, is presented based on the probabilistic method described by Vivatrat and Slomski, 1983 , and Slowski and Vivatrat, 1983.

A limit states philosophy similar to that recommended in ACI 357-R78 (1978) is adopted. This considers the serviceability limit state (SLS), the ultimate limit state (ULS), and servivability. It is suggested that the structures be designed for the serviceability and ultimate loads. Then the survivability can be analyzed based on a selected probability of occurrence.

It is recommended that finite element analyses be used to study the global behavior and to provide the necessary boundary conditions for a more detailed local analysis. Presumably, an elastic analysis is implied for the global analysis, and a nonlinear analysis is suggested for the local analysis.

It is suggested that the reinforcement can be proportioned using lower-bound approaches similar to those given by Brondum-Nielsen (1974) and Clark (1976). Equations for proportioning orthogonal reinforcement to resist the in-plane and out-of-plane forces and moments are given. For the out-of-plane shear design, it is recommended that the (nonprestressed) beam-shear provisions of ACI 318-83 be used, including the effects of the in-plane compressive forces resulting from the out-of-plane loads. Thermal effects and the effects of prestressing should also be included. A significant recommendation is that the ice pressure vs area curve relationships require "that shear checks be made for loads smaller than the total design load as this may prove to be critical."

For the SLS, it is recommended that non-linear finite element analysis be used to evaluate the stresses in the reinforcement and in the concrete, and to determine the extent of cracking at the service load level.

2.2.3 Birdy, Bhula, Smith and Wicks (1985)

In this paper, results are presented from a joint industry research program directed towards improving the understanding of the punching shear capacity of typical reinforced concrete panels representing the ice-resisting wall in an Arctic offshore structure. One thick slab, one thick arch, and eight thick shells were tested. The specimens were loaded by circular patch loads. The specimens contained shear reinforcing in the form of open stirrups.

Following a review of pertinent literature, the paper gives a description of the test results for each specimen including a discussion of the effects of the significant test parameters.

Based on these tests, the authors recommend that the flexural design be done in accordance with ACI 318-77 (1977) using the forces, moments, and thrusts determined from a linear-elastic finite element analysis. To determine the punching shear resistance, modified slab-shear expressions are provided. In effect, the slab-shear provisions of ACI 318-77 (1977) are followed concerning the critical section for shear, but the upper limit on the shear strength is increased. The best correlation with the test results is obtained with the test results is obtained if the upper limit from the beam-shear provisions is used.

2.2.4 O'Flynn (1987)

In this study, steel-concrete composite ice-resisting wall specimens were constructed and tested under uniform loading. The specimens were simply supported and contained stud-type shear connectors. Span-to-depth ratios of 3,4 and 5 were tested.

Hyperbolic, de-centered fan stress fields were used to predict the load path and ultimate strength of these specimens. Failure generally occurred in combinations of overall crushing of the concrete core, crushing of the concrete near the support, yielding of the tension steel plates. In the case when failure occurs in the concrete core, the predicted strength depends primarily on the effective concrete strength, f_{ce}. Consequently, a rational expression for the concrete effectiveness factor is proposed.

The general conclusions of the tests were that

1. "Composite ice-resisting walls with span-to-depth ratios varying from 3 to 5 can withstand external pressures in the range of 1.0 MPa to 10.0 MPa.
2. Assuming there are adequate shear connectors, the capacity of an individual wall configuration is a function of the span-to-depth ratio, the concrete strength, the size and mechanical properties of the steel plates, and the loading arrangement".

Specific conclusions concerning construction details were also given.

2.3 Reinforced Concrete Plasticity and Strut-and-Tie Modelling

In Chapter 5, the topic of strut-and-tie modelling is discussed in detail and the literature necessary for this discussion is cited as required. On the topic of reinforced concrete plasticity, the reader is referred to Chen (1982) and Nielsen (1984).

2.4 Finite Element Prediction of Reinforced Concrete Behavior

In Chapter 7, the results of nonlinear finite element analyses are presented. In order to adequately define the full range of behavior, one specimen from each of the major test divisions is considered.

The program selected to do this was FEPARCS, developed at the University of Alberta (Elwi and Murray, 1980; Balakrishnan and Murray, 1986). The development of the program and an excellent treatment of the topic of finite element prediction of reinforced concrete behavior are contained in these references.

3. EXPERIMENTAL RESEARCH PROGRAM

3.1 Introduction

The experimental research program was undertaken to investigate the ultimate strength of arch-shaped reinforced concrete ice-resisting walls for offshore structures. From this information, strut-and-tie models were developed and are presented in Chapter 6. Finite element analyses were performed and are presented and compared to the test results in Chapter 7.

Two large-scale reinforced concrete circular arch specimens were tested (Specimens P1 and P2). These represent a portion of an ice-resisting wall made up of reinforced concrete circular arches (Fig. 3.1). In addition a total of seven V-shaped arches were tested. These represent a portion of an ice-resisting wall made up of reinforced concrete V-shaped arches (Fig.3.2). Specimens A1 to A5 were subjected to a loading which simulates an ice event impacting the arch symmetrically at midspan (Fig. 3.2(a)). Specimens B1 and B2 were subjected to loading which simulates an ice event whose initial impact is perpendicular to one side of the arch (Fig. 3.2 (b)).

The two preliminary circular arch specimens, P1 and P2, were tested first in order to provide information necessary for the analysis and design of the subsequent test series. This made it possible to test the load application set-up, the reaction devices, and the post-tensioning equipment and

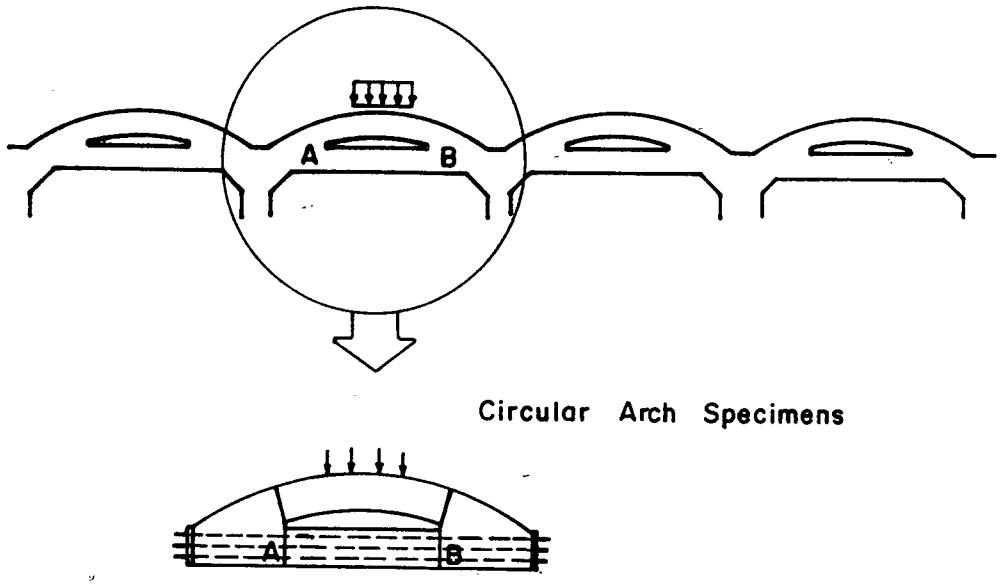

Figure 3.1 Circular Arch Test Specimen from R/C Ice-Resisting Wall

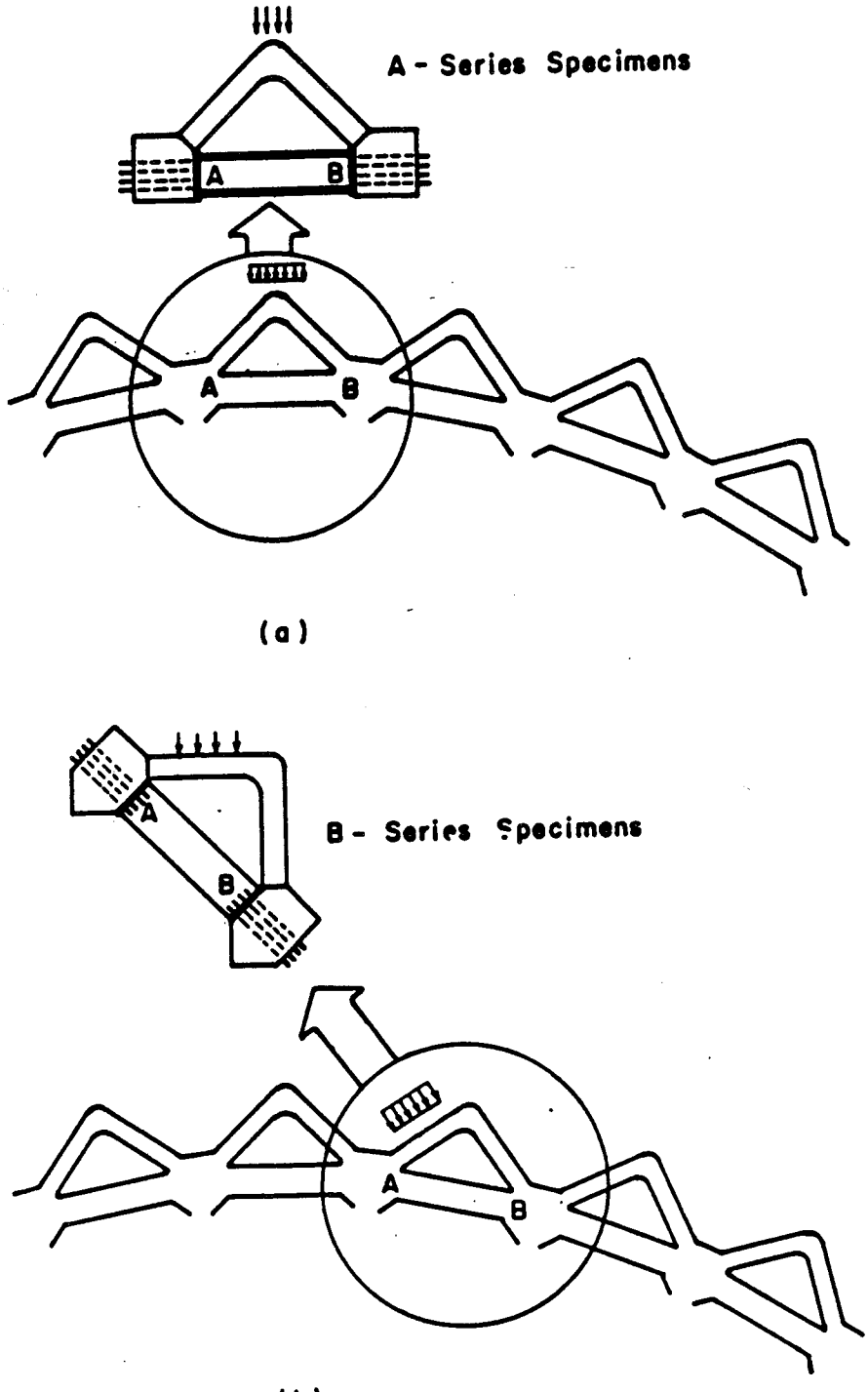

Figure 3.2 V-Shaped Arch Test Specimen from R/C Ice-Resisting Wall

method. In these two specimens, the continuity which exists in the prototype structure was simulated using a prestressed concrete tension member (A-B in Fig. 3.1). The principal test variables were the type and amount of shear reinforcement. The details of these test specimens are given in Sect. 3.2.1.

Following the circular arch specimens, the five A-Series V-shaped arch specimens and the two B-Series V-shaped arch specimens were tested. In the V-shaped arch specimens, a specially made steel beam was used to simulate the continuity existing in the prototype structure (A-B in Fig. 3.2). Although the prestressed concrete restraining beam used in the circular arch specimen was more realistic, it was difficult to instrument. In the V-shaped arch specimens, the use of a steel beam allowed restraining forces to be measured and the effects of beam stiffness to be studied. Properties of the two steel restraining beams are discussed in Sect. 3.3.4. The test variables investigated in the V-shaped arch specimens were the type of loading, the amount of shear reinforcement, the amount of longitudinal reinforcement, and the stiffness of the beam simulating continuity in the prototype structure. The details of the A-Series and B-Series specimens are given in Sects. 3.2.2 and 3.2.3, respectively.

In the following, details of the test specimens are described and the material properties of the concrete and reinforement used in each specimen are given. Following

this, the testing aparatus and test procedures are discussed. Finally, the instrumentation used in the tests to measure applied loads, reactions, strains, and displacements is presented.

3.2 Test Specimens

3.2.1 Preliminary Circular Arch Specimens

3.2.1.1 Objectives

The first objective of the tests on circular arch-shaped specimens was to investigate the behavior of this type of ice-resisting wall when subjected to high magnitude patch loads. The additional objectives of the preliminary tests were to provide guidance for the design and construction of the subsequent test specimens, and to evaluate the performance of the test set-up. This included an evaluation of the load application devices, the reaction devices, and the post-tensioning equipment and method. Since the behavior of post-tensioned stirrups was of interest, the viability of constructing and testing specimens containing these was to be evaluated.

3.2.1.2 Overall Geometry, Loading, and Support

The overall geometry and loading of the circular arch-shaped specimen P1 is shown in Fig. 3.3. The overall geometry and loading of Specimen P2 is shown in Fig. 3.4. In both specimens, the thickness of the arch region is 250mm.

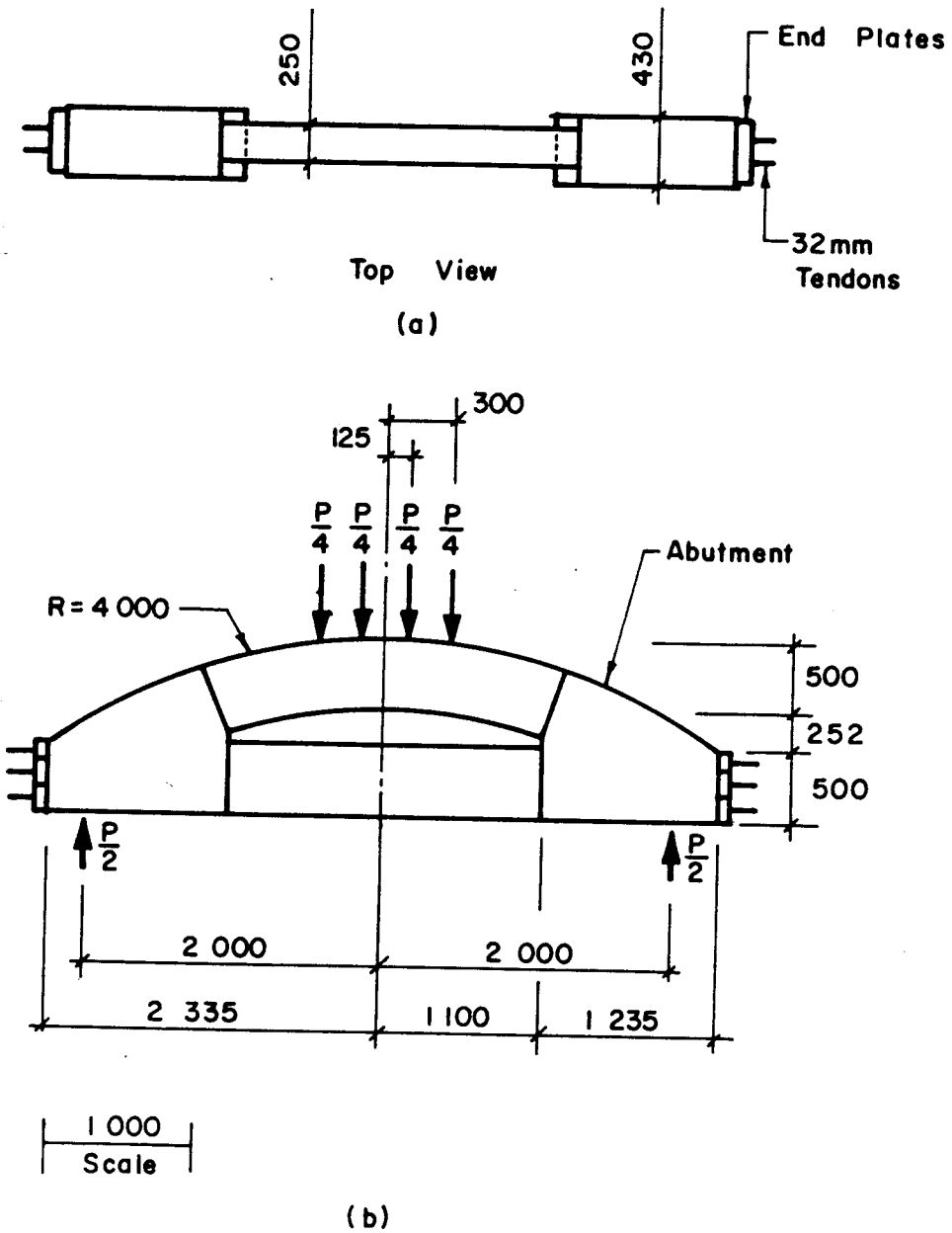

Figure 3.3 Geometry and Loading for Specimen P1

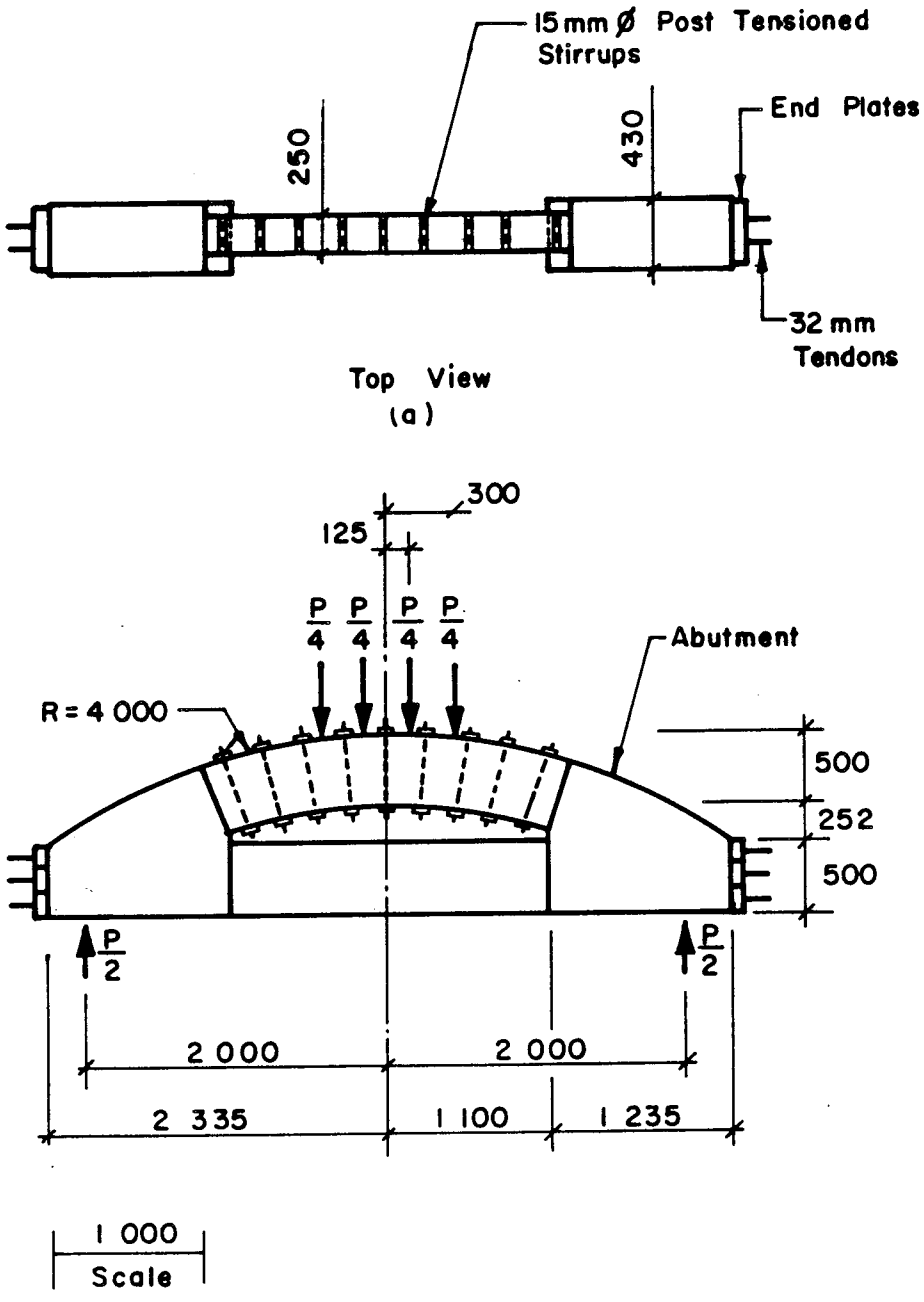

Figure 3.4 Geometry and Loading for Specimen P2

The abutments were thickened in an attempt to ensure that failure would occur within the arch portion. The thickness of the abutments was 430mm, based on the width of a two-by-four on each side.

Both specimens were loaded by four point-loads placed symmetrically about midspan as shown. Knife-edge and roller devices were provided at the suppports to eliminate unwanted reactions. The distance between the supports was 4000mm. The loading and reaction devices are discussed in more detail in Sect. 3.4.1. The test procedure and instrumentation are discussed in Sections 3.4.2 and 3.5, respectively.

A prestressed concrete tension member was used to provide the horizontal and bending reactions for each specimen. The 6 - 32mm diameter tendons, nuts, and end-plates are visible in Fig. 3.3 and 3.4. Specimens P1 and P2 contained identical reinforcement except that Specimen P2 also contained 15mm diameter through-the-wall post-tensioned strirrups. These tendons are also visible in Fig. 3.4.

Specimen P1 had a minimal amount of deformed bar stirrups whose contribution was small enough that the strength of Specimen P1 was expected to be the minimum of this test series. Specimen P2 was expected to delineate the maximum strength of the circular arch specimens planned in the test series.

The design of P1 and P2 was based on an elastic frame analysis using stiff members to simulate the abutments and using cracked section properties in the arch. The effects of

losses on the prestressed concrete tension member were accounted for using the ACI - ASCE Committee recommendations (Zia et al, 1979). The design of the tension tie followed the recommendations of Wheen (1979) and Naaman (1982). The following was satisfied:

1. The tie would remain in the elastic range for a tension force resulting from an applied load which was 30% greater than the estimated failure load.
2. There would be a margin of safety against cracking for an applied load which was 30% greater than the estimated failure load.
3. In the event of cracking, the full tension could be resisted by the tendons acting alone although this would involve a substantial reduction in axial stiffness.

Details of the prestressing and mild reinforcement requirements for specimens P1 and P2 are presented in the next section.

3.2.1.3 Reinforcing Details

The reinforcing layouts for Specimens P1 and P2 are shown in Fig. 3.5 and 3.6, respectively. Details of the reinforcement in these test specimens are summarized in Table 3.1.

All longitudinal reinforcement consisted of Grade 400 deformed reinforcing bars. The stirrups were made from 6mm deformed bars having properties similar to Grade 400 reinforcing steel. In addition, both specimens contained 32 mm diameter prestressing tendons in the restraining beam and

Table 3.1 Reinforcing Details for Specimens P1 and P2

SPECIMEN	TOP STEEL	BOTTOM STEEL	STIRRUPS	
	Type	Type	Type	Spacing
P1	3 - No. 25M	3 - No. 25M	6mm (3 legs)	250 mm
	Fy = 480 MPa	Fy = 480 MPa	Fy = 434 MPa	
P2	3 - No. 25M	3 - No. 25M	6mm (3 legs)	250 mm
	Fy = 480 MPa	Fy = 480 MPa	Fy = 434 MPa	
			and 15mm	
			DYWIDAG Tendons	250 mm
			Fy = 886 MPa	

Specimen P2 contained 15mm post-tensioned stirrups. The 25M longitudinal reinforcing bars were supplied and bent by a local fabricator. The same fabricator also bent the 6mm deformed bar into stirrups. The prestressing tendons, anchorages, and ducts were supplied by DYWIDAG Systems International. The material properties of all reinforcement are discussed in Sect. 3.3.

In Specimens P1 and P2, the top (outside) 25M bars were continued around the periphery of the abutments for development and to provide a frame for tying the abutment cage (Fig. 3.5 and 3.6). The bottom 25M bars were extended into the abutments an amount greater than their tension development length. These 20M bars were provided to contain any cracks that might develop if the cracking strength of the prestressed restraining beam was exceeded.

Miscellaneous 10M and 6mm bars were provided to reinforce the abutments. In particular, closely spaced ties were concentrated at the end of the abutments to resist the tensile ("bursting") stresses which develop due to the post-tensioning. Lifting hooks were not cast into the specimens. Instead, each specimen was lifted out of the form using the 32mm diameter tendons which protruded from the abutments.

Details of the prestressing operations associated with Specimens P1 and P2 are discussed briefly in Sect. 3.2.1.5.

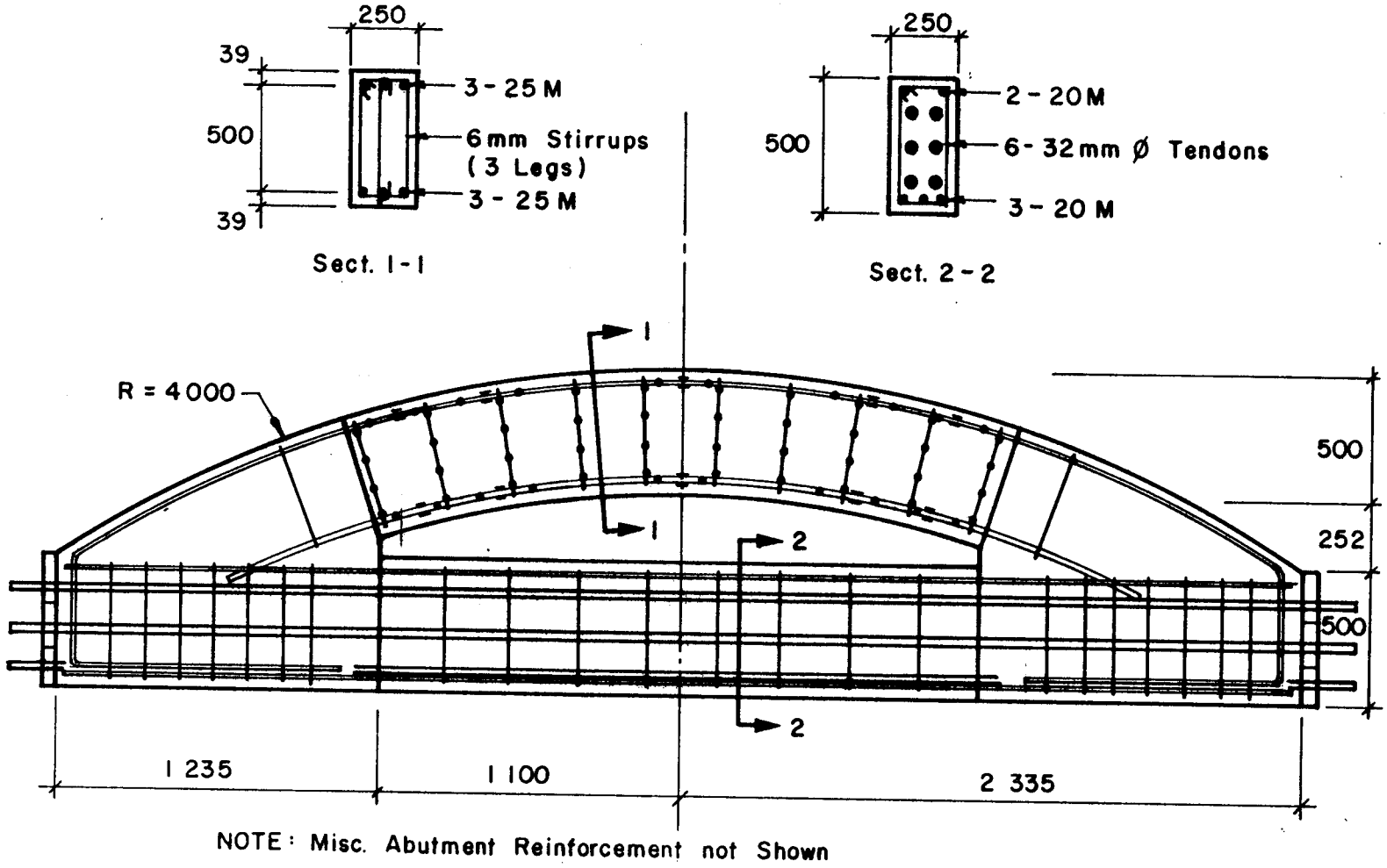

Figure 3.5 Reinforcing Details for Specimen P1

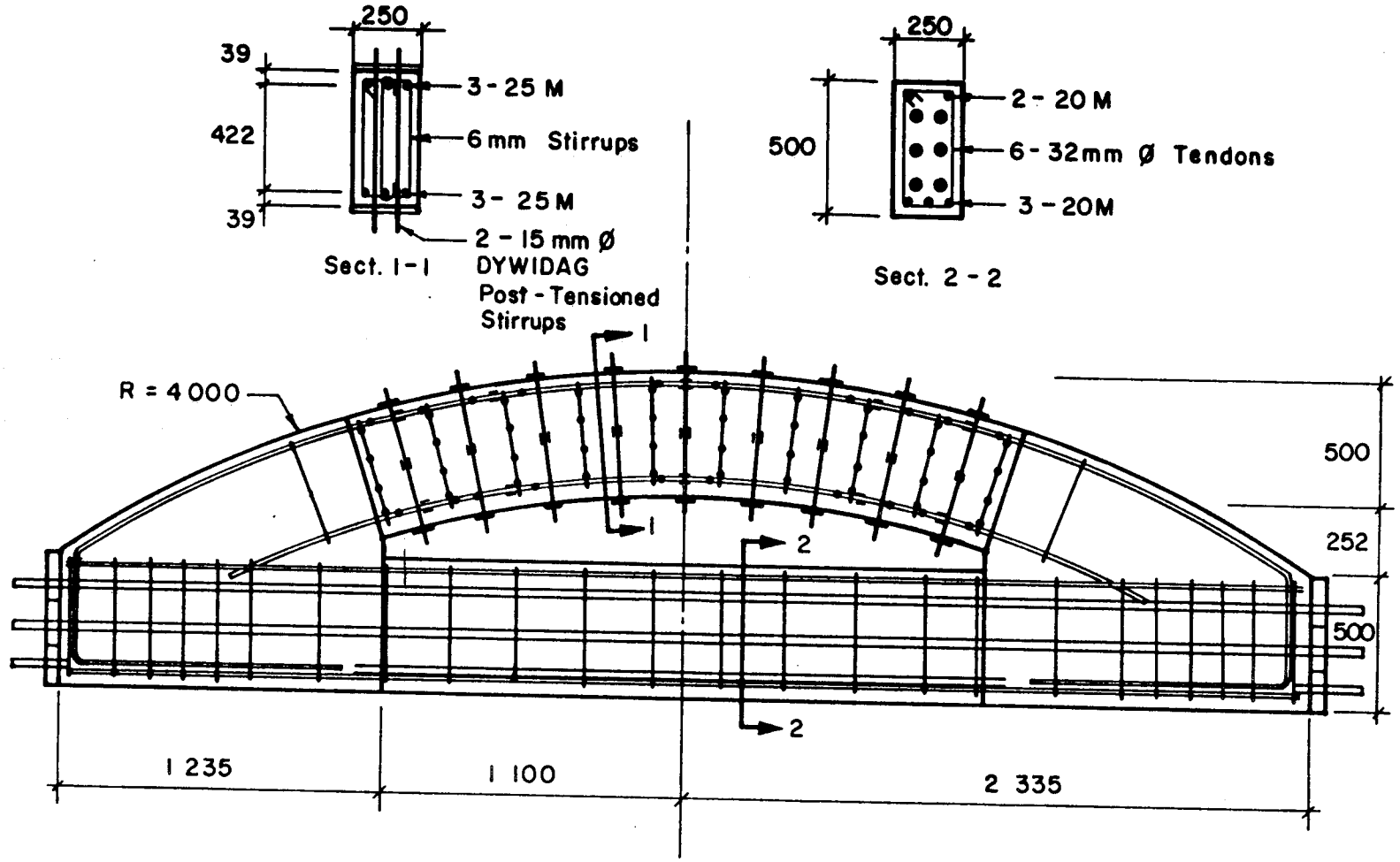

Figure 3.6 Reinforcing Details for Specimen P2

3.2.1.4 Construction Details

The specimens were cast back-to-back in curved wooden formwork (Fig. 3.7). For straight portions, 12mm plywood was used. For the curved regions double layers of 6mm plywood were bent and held in position using preshaped bulkheads. The 250mm thick region of the specimen was formed on a raised platform so that the abutments could be made thicker than the central arch portion.

The formwork for the central void portion had removable wedges which would pull away from the concrete as they are lifted thereby allowing the void formwork to collapse inwards and away from the concrete. The ends and bottom of the arches were removable. The remainder of the formwork was fixed.

In the abutments, the cages were chaired at the appropriate level. In the central arch region, the lugs which were brazed onto the longitudinal bars for DEMEC targets, doubled as chairs for the cage. The 50mm diameter plastic ducts were supported at each end by plywood templates in the form, and along their length using stiff wire ties. The 25mm diameter plastic ducts used for the post-tensioned stirrups in Specimen P2 were held in place using tight-fitting wooden dowels and supported at the proper elevation using removable pins. When the specimen was to be lifted from the forms, the pins were pulled and the dowels were subsequently knocked out.

Figure 3.7 Formwork and Reinforcing Cages for Specimens P1 and P2

The forms were oiled before the cages were installed. Two layers of polyethylene plastic sheet were placed in the forms at the abutments. This was to allow the abutments to slide inward, if necesary, to prevent shrinkage cracks that might develop if the central portion and abutments cured at different rates and the abutments were not free to move. The concrete was placed using the overhead crane and bucket and with the aid of 25mm pencil vibrators.

3.2.1.5 Prestressing Operations

The restraining beams in Specimens P1 and P2 were reinforced as prestressed concrete ties. The 6 - 32mm diameter DYWIDAG tendons were ungrouted so that they could be resused. The ducts provided for these tendons consisted of 50mm diameter ABS plastic pipe.

To satisfy the design requirements discussed in Sect. 3.2.1.2, CSA G279-M Grade 1080 32mm diameter tendons were used. These tendons have an ultimate strength of 1080 MPa. The tendons were given an effective prestress equal to 50% of this value prior to testing.

To monitor the force in each tendon during the prestressing operation and during the test, strain gauges were mounted at one end of each tendon. The strain gauges were protected by using a collar made from A36 extra-strong pipe. The collar was slotted to allow the wires to pass through and machined at each end to ensure good bearing of the steel end plates.

The post-tensioning operation required the fabrication of two high-capacity jack stands and special purpose wrenches. The stands were constructed so that the DYWIDAG bars could be tensioned using 120 kip center-hole jacks and the nuts could be turned in between the legs of the jack stand using these wrenches. It was found that in order to prevent bending stresses from developing in the tendons during post-tensioning, each tendon required separate end plates. The prestressing set-up for the 32mm diameter tendons is shown in Fig. 3.8(a).

CSA G279-M Grade 1080 15mm diameter DYWDAG post-tensioned stirrups were also specified. The bars were given an effective prestress equal to 65% of their ultimate stress in order to provide a vertical stress at mid-depth of the specimen of approximately 4.0 MPa. Standard 25mm diameter corrugated plastic ducts were provided for these tendons.

One bar of each pair of stirrups was instrumented with strain gauges so that the prestress could be verified and losses could be monitored up to the time of testing. A load cell was also used to check the force being applied to each bar. These readings were compared to the pressure gauge attached to the hydraulic jack to verify its accuracy.

The prestressed stirrups were post-tensioned using a 30 kip center-hole jack with a set-up similar to that of the 32mm tendons. The bars were then epoxy grouted using grout nipples installed in the end plates. The entire set-up is

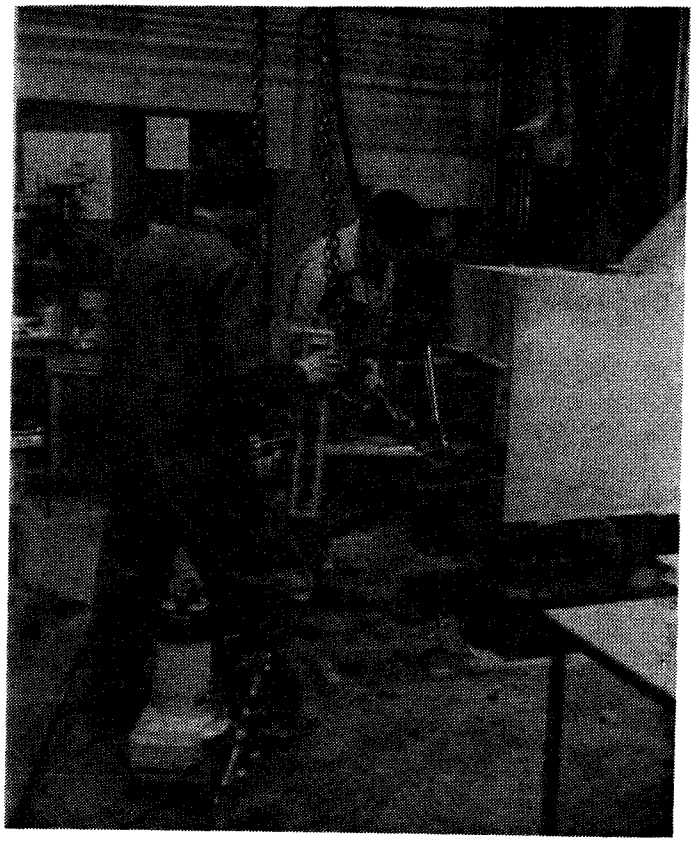

a

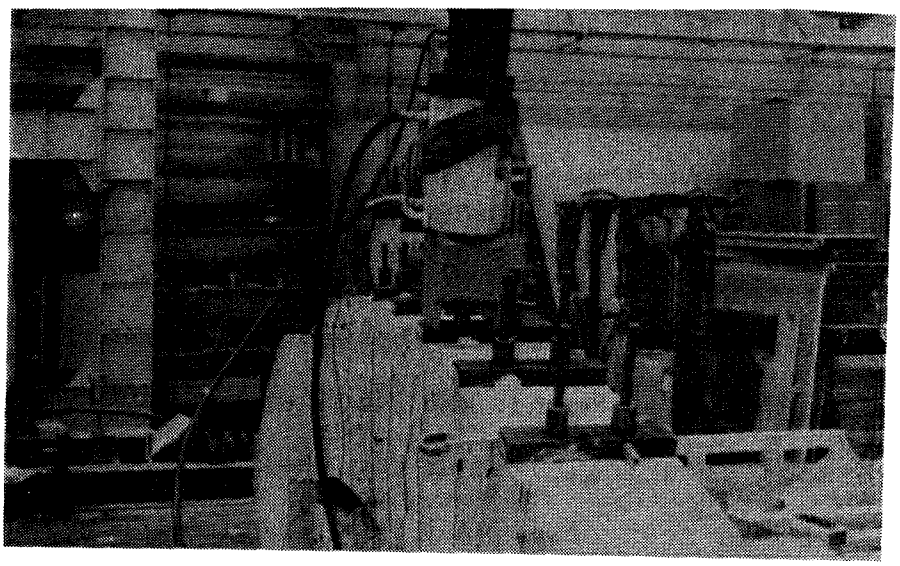

b

Figure 3.8 Prestressing Operations for Specimens P1 and P2

shown in Fig. 3.8(b). In this figure, the jack, the jack-stand, tendons, end-plates, nuts, wrench, and grout nipples may be seen.

3.2.2 A-Series V-Shaped Arch Specimens

3.2.2.1 Objectives

The main objective of the A-Series tests on V-shaped arches was to investigate the behavior of this type of ice-resisting wall when subjected to symmetrically placed high-magnitude patch loading. The parameters studied were the amount of shear reinforcement,the amount of longitudinal reinforcement, and the stiffness of the steel restraining beam.

3.2.2.2 Overall Geometry, Loading, and Support

The overall geometry of the typical A-Series specimen is shown in Fig. 3.9. The thickness of the arch portion is 250mm. The abutments were thickened to 475mm to ensure that the failure of the specimen would occur within the arch portion.

All specimens were loaded by four point loads applied through rollers placed symmetrically about midspan as shown. The center-to-center distance between the supports was always 3300mm. High magnitude loads and a compressive failure mode were anticipated for these specimens. Until experience had been developed regarding the behavior of these specimens, the specimens were not loaded to failure

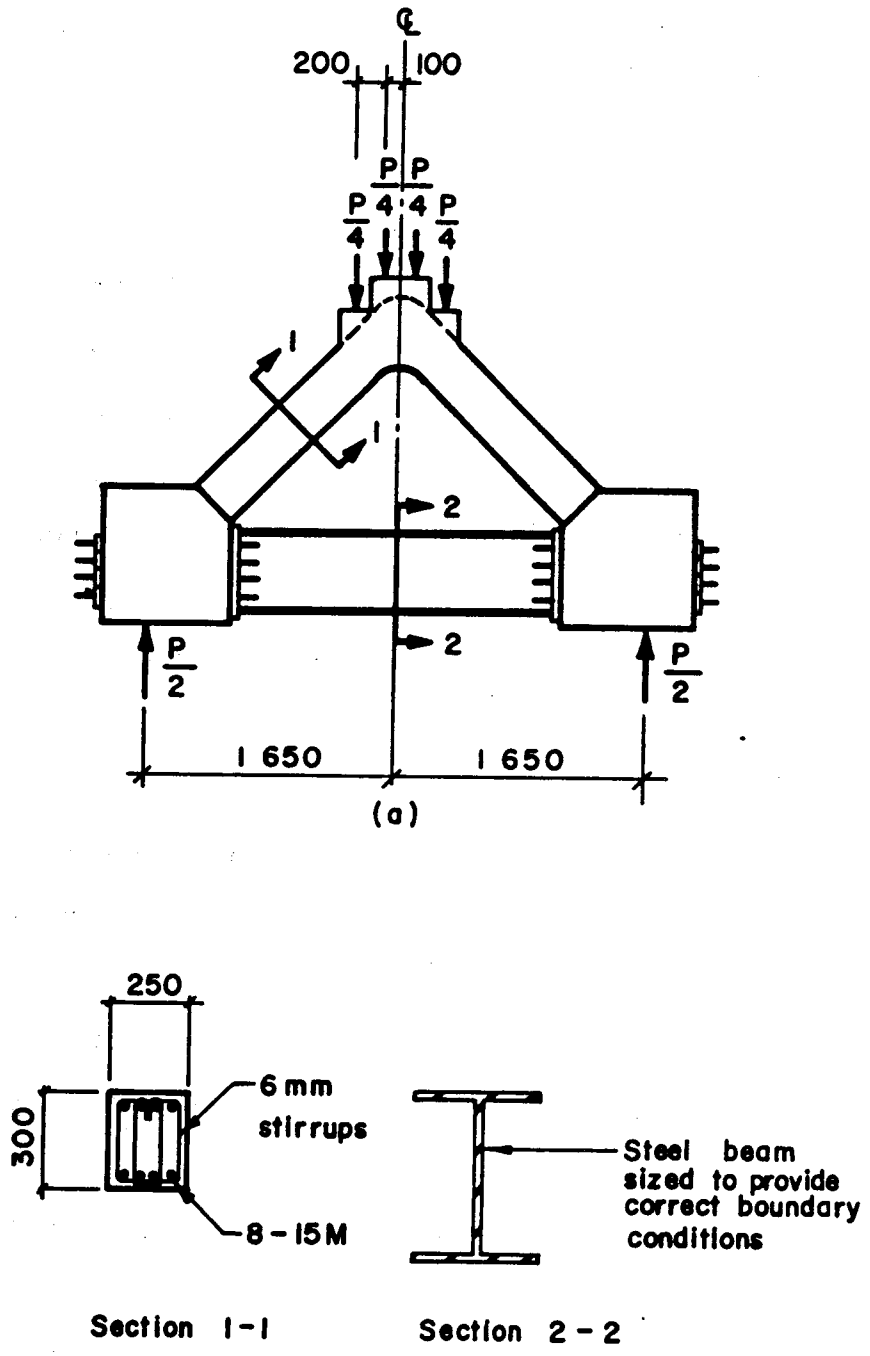

Figure 3.9 Typical Geometry and Load Arrangement for A-Series Specimens

with the load application rollers in place. Instead, the first specimen (A1) was loaded incrementally with the loading of Fig 3.9 only up to the first signs of crushing. Then, the specimen was unloaded, the roller assemblies were removed, and the specimen was loaded to failure using the platten of the testing machine. The load condition is idealized in Fig. 3.10. The same procedure was followed for the next specimen (A2). Specimens A3, A4, and A5 were loaded to failure with the rollers in place under the loading shown in Fig. 3.9. In all cases, detailed measurements were recorded for each load step. The loading and reactions devices are discussed in more detail in Sect. 3.4.2. The test procedure and instrumentation are discussed in Sections 3.4.3 and 3.5, respectively. For both load conditions, the behavior and failure mode was essentially the same, as the analytical models presented in Chapter 6 suggest. The design implications of this insofar as ice loading is concerned is discussed in Chapter 8.

Safety also dictated two other precautions. Specimen A1 had rollers under both supports and horizontal jacks were used to hold the specimen in alignment. For specimens A2-A5, the east roller assemblies were removed to prevent drift of the specimen. This appeared to have influenced the boundary conditions enough to slightly affect the forces and moments acting at the ends of the specimen. This is discussed further in Chapter 4. The support and loading details of the test specimens A1-A5 are summarized in Table 3.2. A second

Table 3.2 Summary of Support and Loading Conditions for V-Shaped Arch Specimens

SPECIMEN	LOAD CONDITION	STEEL BEAM	REACTIONS			
			West		East	
			Rollers	Knife-Edges	Rollers	Knife-Edges
A1	I (0 - 6000 kN)	SB-1	Y	Y	Y	Y
	II (0 - Failure)	SB-1	Y	Y	N	Y
A2	I (0 - 6000 kN)	SB-2	Y	Y	N	Y
	II (0 - Failure)	SB-2	Y	Y	N	Y
A3	I (0 - Failure)	SB-1	Y	Y	N	Y
A4	I (0 - Failure)	SB-1	Y	Y	N	Y
A5	I (0 - Failure)	SB-1	Y	Y	N	Y
B1	I (0 - Failure)	SB-1	Y	Y	N	Y
B2	I (0 - Failure)	SB-1	Y	Y	N	Y

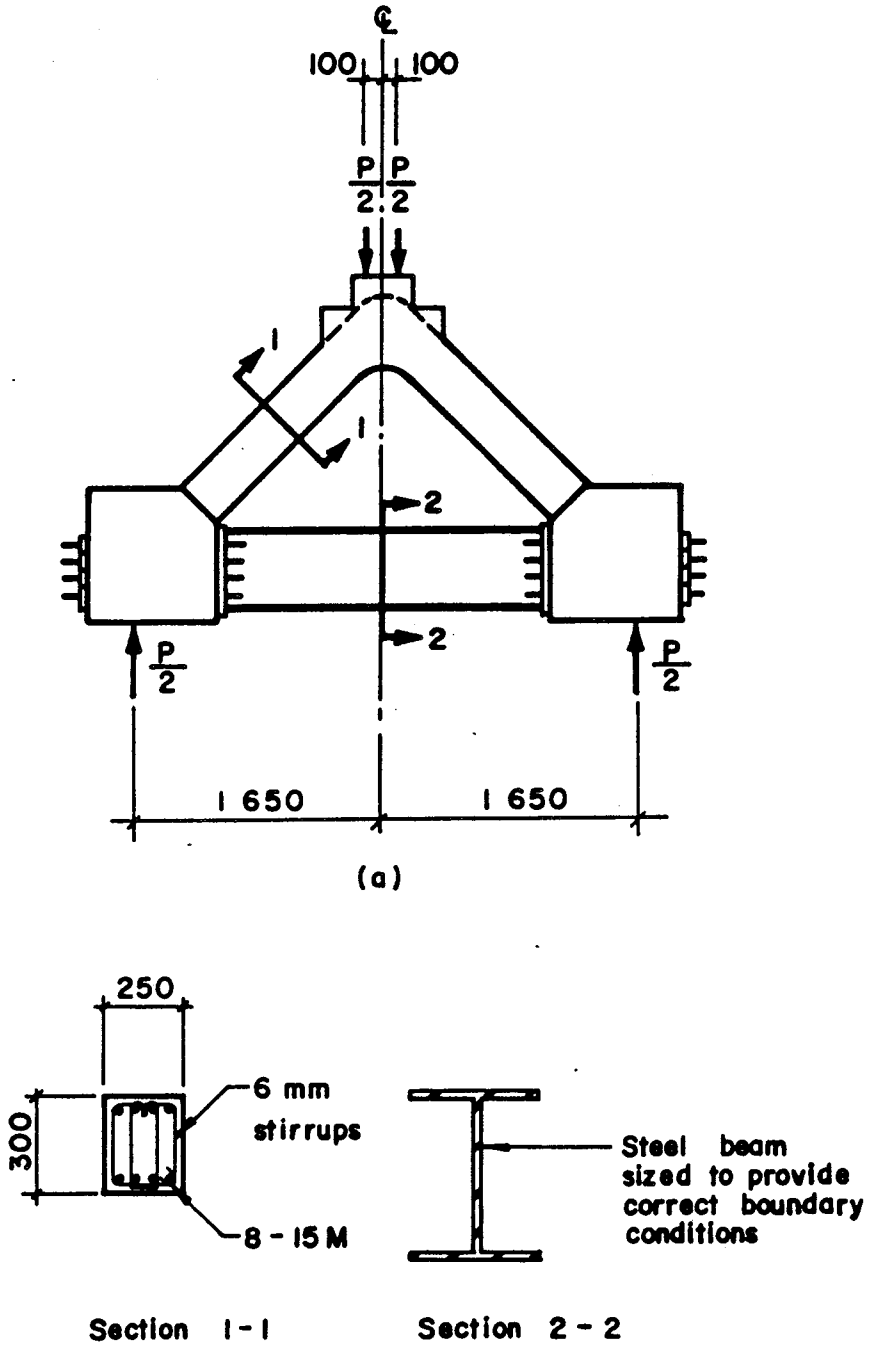

Figure 3.10 Additional Geometry and Load Arrangement for Specimens A1 and A2

precaution was the use of ultra-sonic equipment in an attempt to detect the start of internal microcracking and give warning of imminent failure.

As stated in Sect. 3.1, steel beams were used to provide the restraining forces for the V-shaped arches. Two I-shaped steel beams were designed, SB-1 and SB-2. The out-to-out depth of both beams was 500mm and the flanges were 400mm wide. The beams had stiff end - plates at each end to provide for connection to the specimens using 32mm DYWIDAG threadbars. Both beams were 2180mm long to allow for 10mm of plaster at each end. The different design stiffnesses were achieved by changing the thickness of the web and flange plates. Beam SB-1 was the stiffer of the two beams. The design of these beams was in accordance with CSA S16.1-M84. The geometric and material properties of these beams are discussed in Sect. 3.3.3.

3.2.2.3 Reinforcing Details

The general reinforcing layout for the A-Series specimens is shown in Fig. 3.11. The layouts of the principal reinforcement for each of the five specimens are shown in Fig. 3.12 to 3.15. Details of the reinforcing steel in each specimen are summarized in Table 3.3. From this table, the significant test parameters may be seen for each specimen. Specimens A1, A4, and A5 were tested in order to investigate the importance of stirrup spacing. Specimen A3 was tested to investigate the importance of longitudinal reinforcement. Specimen A2 allowed the effects of the

Table 3.3 Reinforcement Details for V-Shaped Arch Specimens

SPECIMEN	TOP STEEL		BOTTOM STEEL		STIRRUPS		
	Type	Fy (MPa)	Type	Fy (MPa)	Type	Fy (MPa)	Spacing
A1	4 - No. 15M	400	4 - No. 15M	400	6mm (4 legs)	478	50 mm
A2	4 - No. 15M	400	4 - No. 15M	400	6mm (4 legs)	478	50 mm
A3	4 - No. 15M	400	4 - No. 15M	400	6mm (4 legs)	478	100 mm
A4	4 - No. 10M	392	4 - No. 10M	392	6mm (4 legs)	478	50 mm
A5	4 - No. 15M	400	4 - No. 15M	400	6mm (4 legs)	478	300 mm
B1	4 - No. 15M	400	4 - No. 15M	400	6mm (4 legs)	478	50 mm
B2	4 - No. 15M	429	4 - No. 15M	429	6mm (4 legs)	478	100 mm

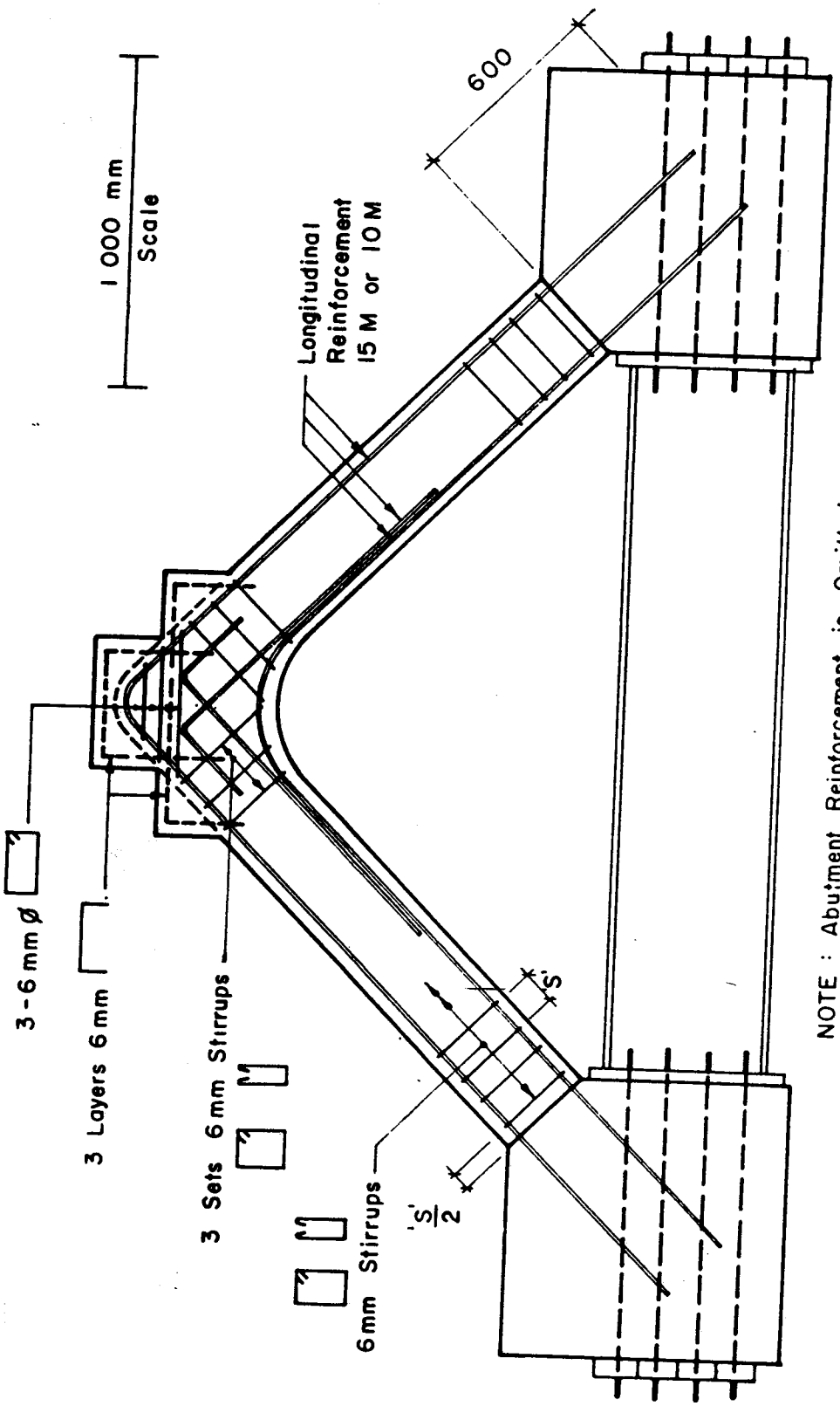

Figure 3.11 General Reinforcing Layout for A-Series Specimens

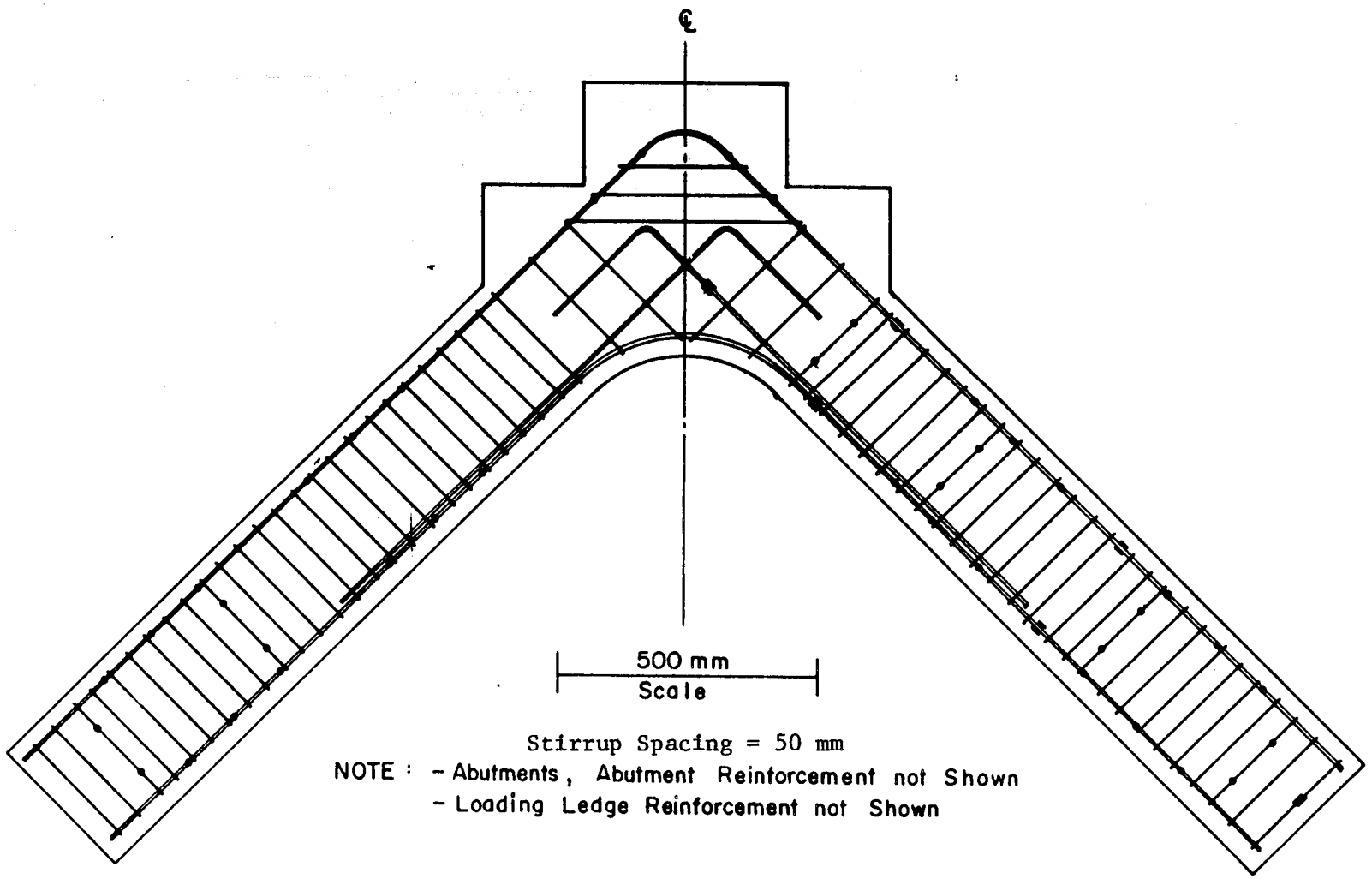

Figure 3.12 Reinforcing Details for Specimens A1 and A2

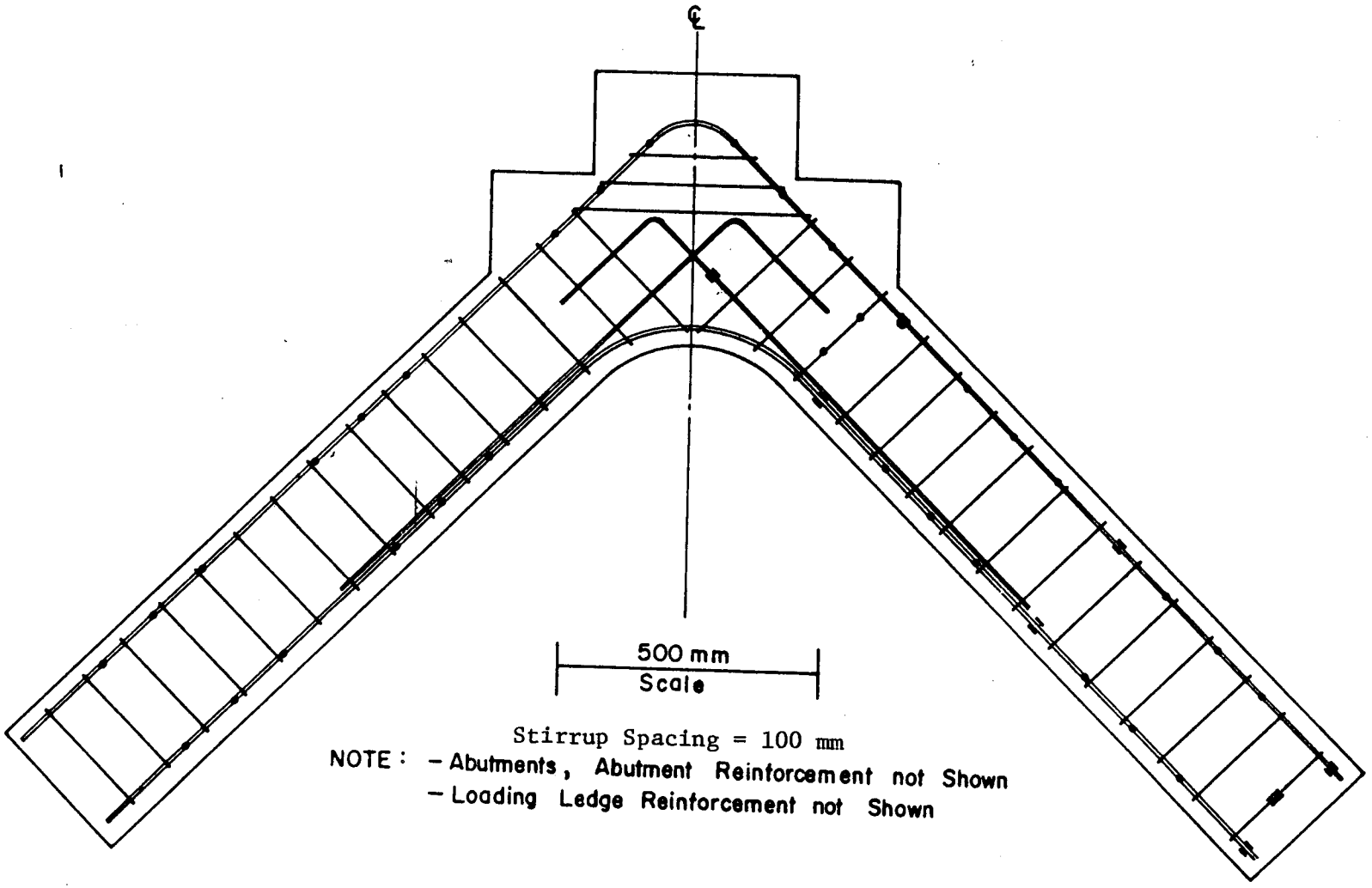

Figure 3.13 Reinforcing Details for Specimen A3

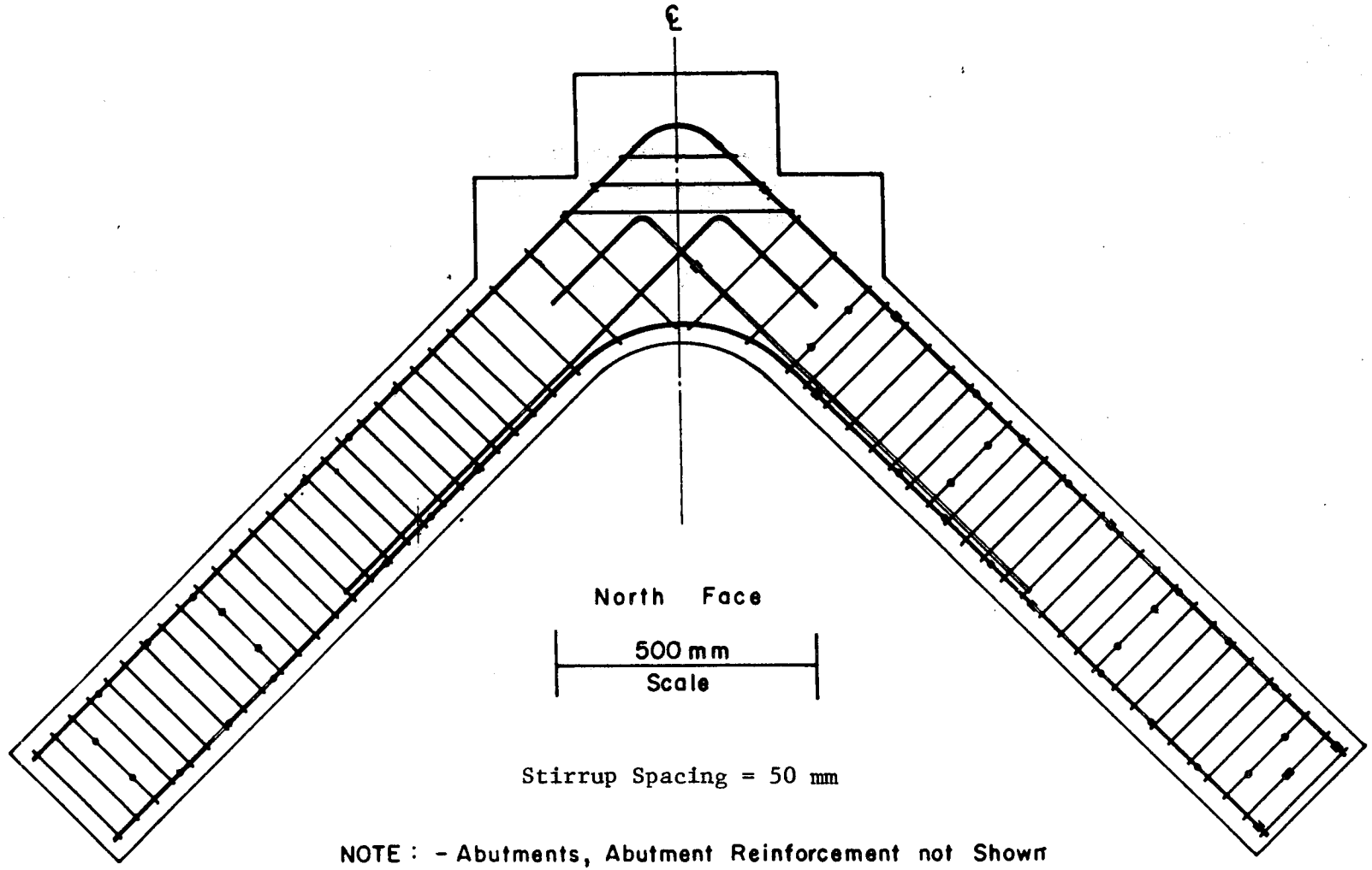

Figure 3.14 Reinforcing Details for Specimen A4

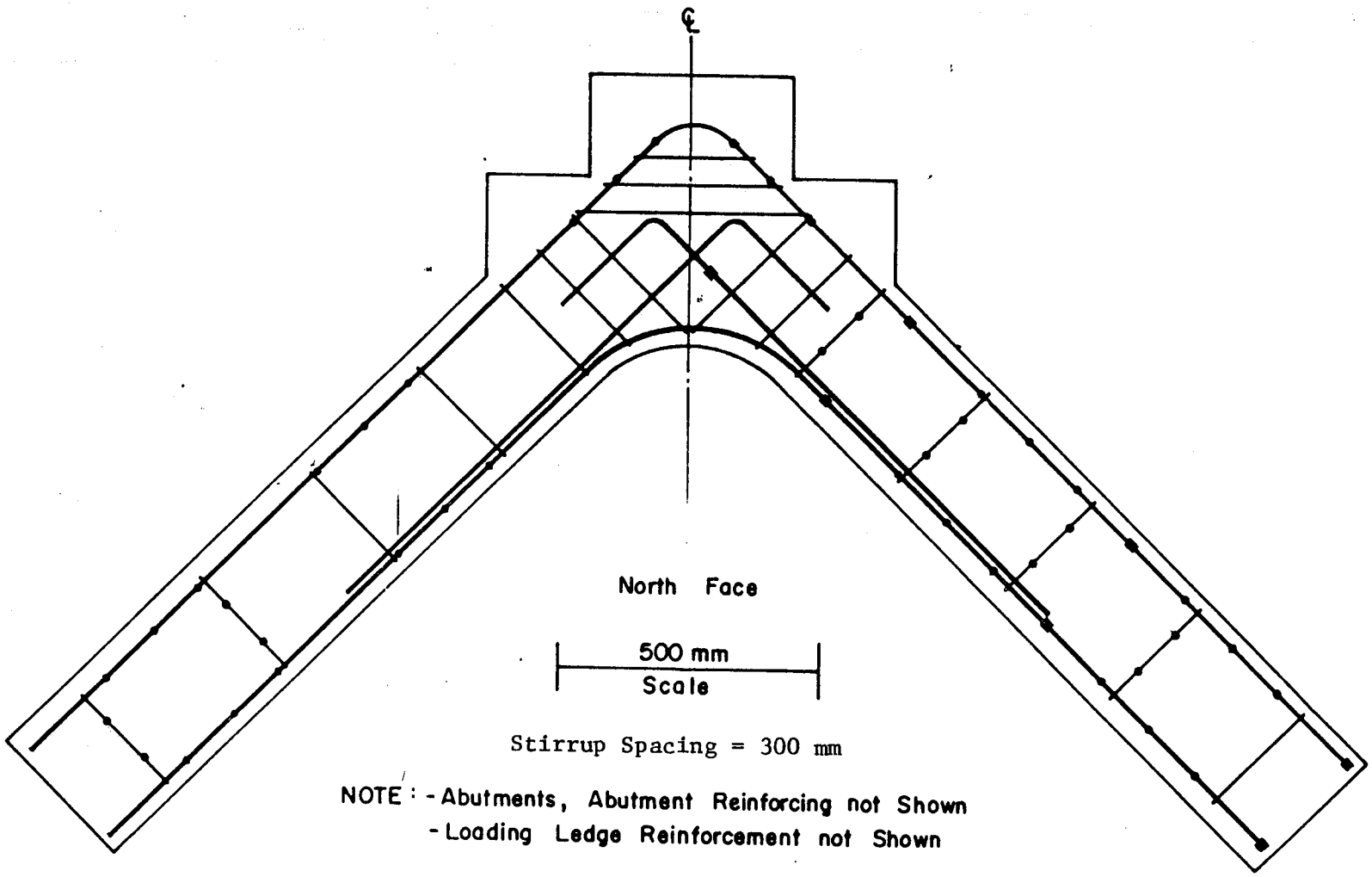

Figure 3.15 Reinforcing Details for Specimen A5

stiffness of the steel restraining beam to be investigated.

All longitudinal reinforcement consisted of Grade 400 deformed reinforcing bars. The stirrups were made from 6mm deformed bar having properties similar to Grade 400 reinforcing steel. The 10M and 15M longitudinal bars and the reinforcement in the abutments were supplied and bent by a local fabricator. All of the 6mm stirrups and all miscellaneous reinforcement were cut and bent in-house. The material properties of all reinforcement are discussed in Sect. 3.3. The top portion of the cage for Specimen A3 is shown in Fig. 3.16.

The longitudinal bars were extended into the allotments to develop their full compressive and tensile strength. The abutments were heavily reinforced by ties in both directions and by cross-ties to ensure adequate performance under the extreme loading and prestressing forces. A nominal amount of 6mm reinforcement was provided to contain the loading ledges used in the A-Series specimens. The number of 6mm stirrups in the corner region was kept constant for the five A-Series specimens. In addition, three extra 6mm ties were added at the outer side of the corner to confine the concrete there. These details are visible in Fig. 3.16. Lifting hooks were not provided. Instead, the specimens were lifted using slings passed under the raised formwork. This was done with the steel beams temporarily attached.

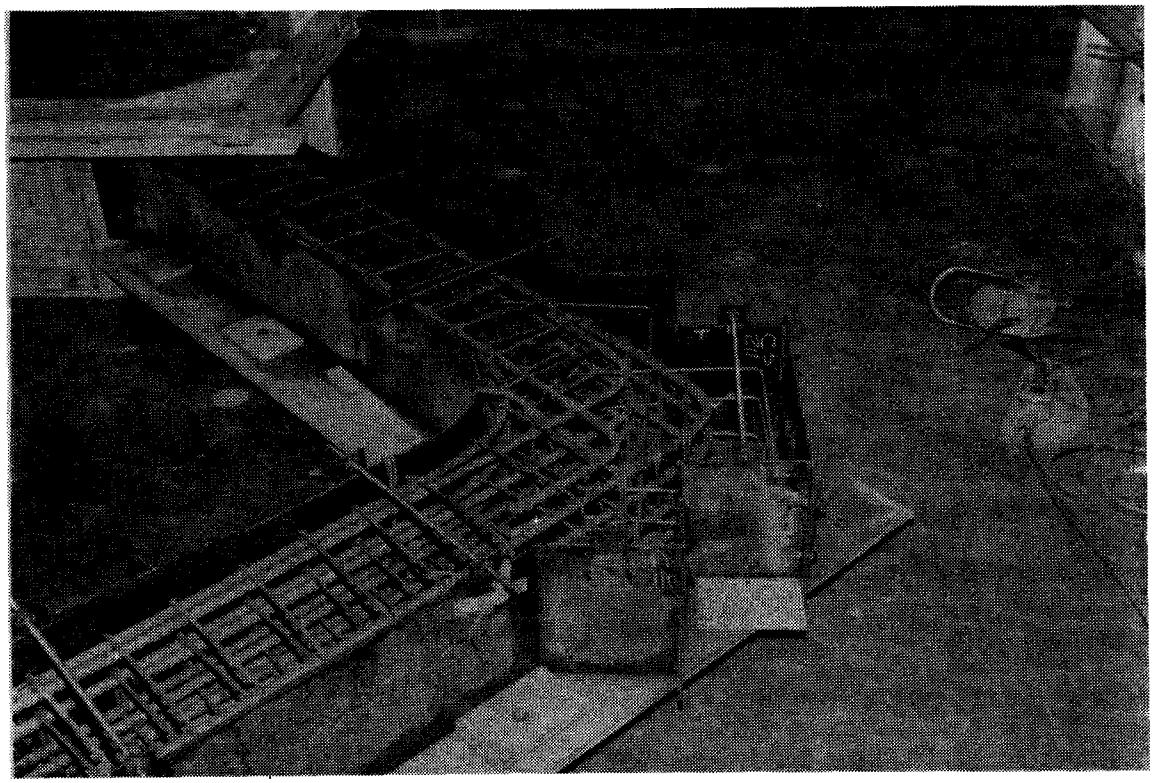

Figure 3.16 Formwork and Details for Specimen A3

3.2.2.4 Construction Details

The V-shaped arch specimens were cast in pairs except for Specimen B2 which was cast alone. Reusable wooden forms were used for the abutments and for the raised platform. The sides of the specimen were formed with steel forms. The steel forms were held in place by threaded rods at the top and by bolted plates at the bottom (Fig. 3.16).

The reinforcement was tied in three separate cages. The two abutment cages were designed to mate with the specimen cage when the cages were placed in the forms. The abutment cages were supported on legs made by tack-welding small diameter rods to the cage. The cage in the arch region was supported on the legs which had been brazed onto the longitudinal bars to be used as DEMEC targets.

The 50mm corrugated post-tensioning ducts were supported at each end by 6mm plywood templates which were inserted into the forms. These templates were drilled to match the holes in the steel beam end-plates to ensure that the duct openings in the concrete would line up with the openings in the steel beam end-plates. The templates were removed after the specimen was lifted out of the forms. The corrugated metal ducts were then ground flush with the surface of the concrete.

The wooden and steel forms were oiled before the cages were installed. The concrete was placed using the overhead crane and bucket and with the aid of 25mm pencil vibrators.

3.2.2.5 Prestressing Operation

For each specimen, the specified steel restraining beam was post-tensioned to the abutments. At each abutment, 8-32mm diameter DYWIDAG threadbars were used. Each tendon required end plates and nuts at each end. There were a total 16 prestressing operations per specimen. Standard 50mm corrugated metal ducts were provided for these tendons. High strength gypsum plaster was placed between the steel beam end plates and the abutment to provide a good bearing surface.

In the V-shaped specimens, the prestressing followed the same procedure as for the circular arch specimens. In this case, the tendons were stressed in pairs and the reading on the pressure gauge was used to determine the jacking force. The pressure gauge had been calibrated against strain gauges and against a load cell and was considered reliable.

3.2.3 B-Series V-Shaped Arch Specimens

3.2.3.1 Objectives

The main objective of the B-Series tests was to investigate the behavior of this type of ice-resisting wall subjected to high magnitude patch loading acting perpendicular to one face of the arch. In particular, the goal was to investigate the effect of varying the spacing of the shear reinforcement on the ultimate strength and failure mode for this load condition.

3.2.3.2 Overall Geometry, Loading, and Support

The overall geometry of the typical B-Series specimen is shown in Fig. 3.17. The shape of these specimens is different from the A-Series specimens in that the loading ledges were not required and in that different shaped abutments were necessary. The thickness of the arch portion is 250mm, while the abutments are 475mm thick.

The specimens were loaded by the same arrangement as the A-Series specimens except that the four point loads are now placed at the midpoint of one side of the arch. The east end of the specimen was supported by a knife-edge and was free to rotate, but since rollers were not used, the specimen was not free to move horizontally. The west end of the specimen was supported on knife-edge and roller supports and was elevated approximately 2.5 m in order to have one side of the arch horizontal. The second steel beam (SB-2) was also designed as a column in order for it to double as the support pedestal for the west end of the B-Series specimens.

Two specimens were tested, Specimens B1 and B2. Both of these used steel beam SB-1 as the restraining beam. The principal difference between the two specimens is the spacing of the stirrups. The details of the reinforcement are discussed in the next section.

3.2.3.3 Reinforcing Details

The reinforcing layouts for Specimens B1 and B2 are shown in Figs. 3.18 and 3.19, respectively. The details of

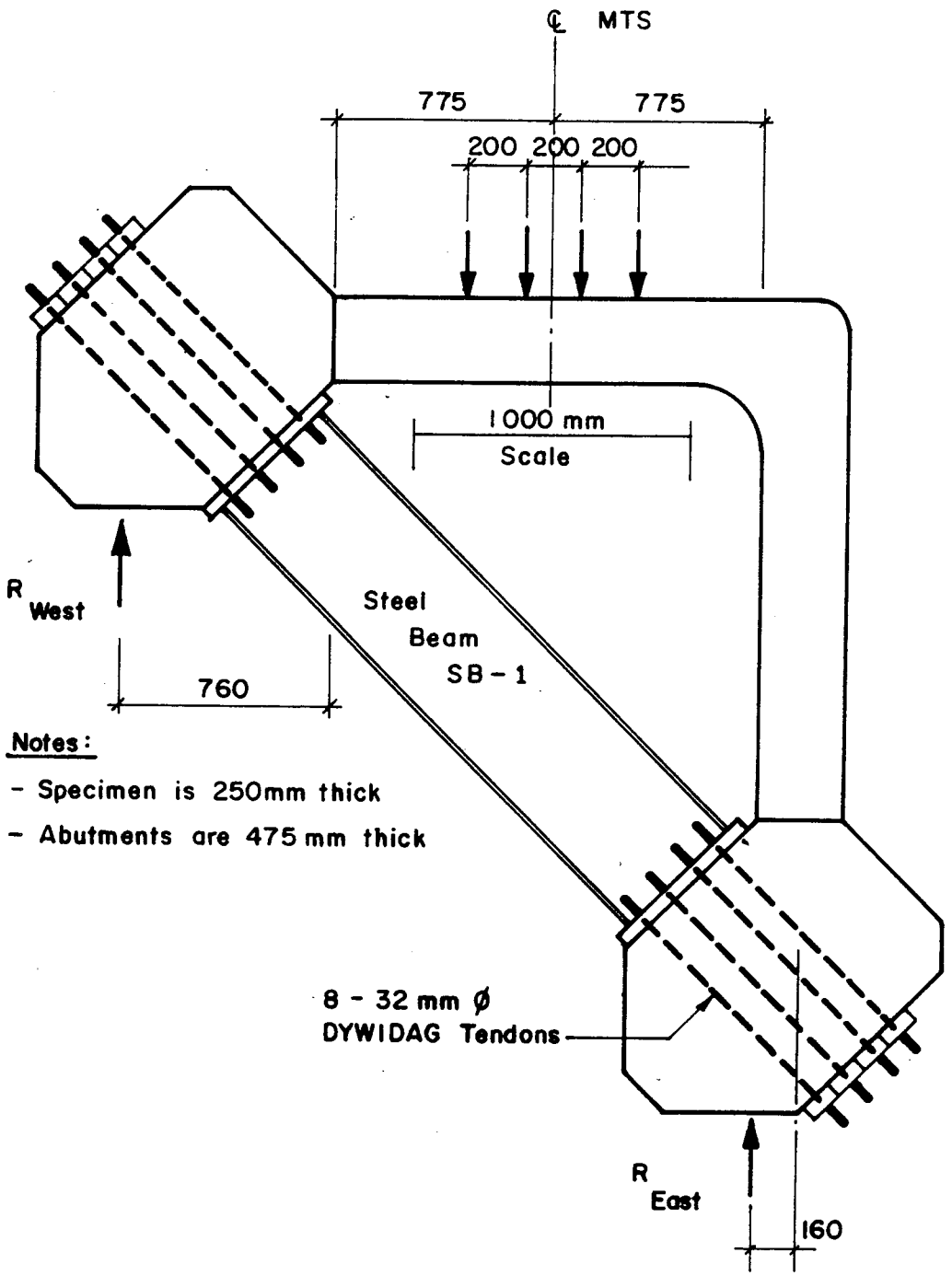

Figure 3.17 Geometry and Loading for Specimens B1 and B2

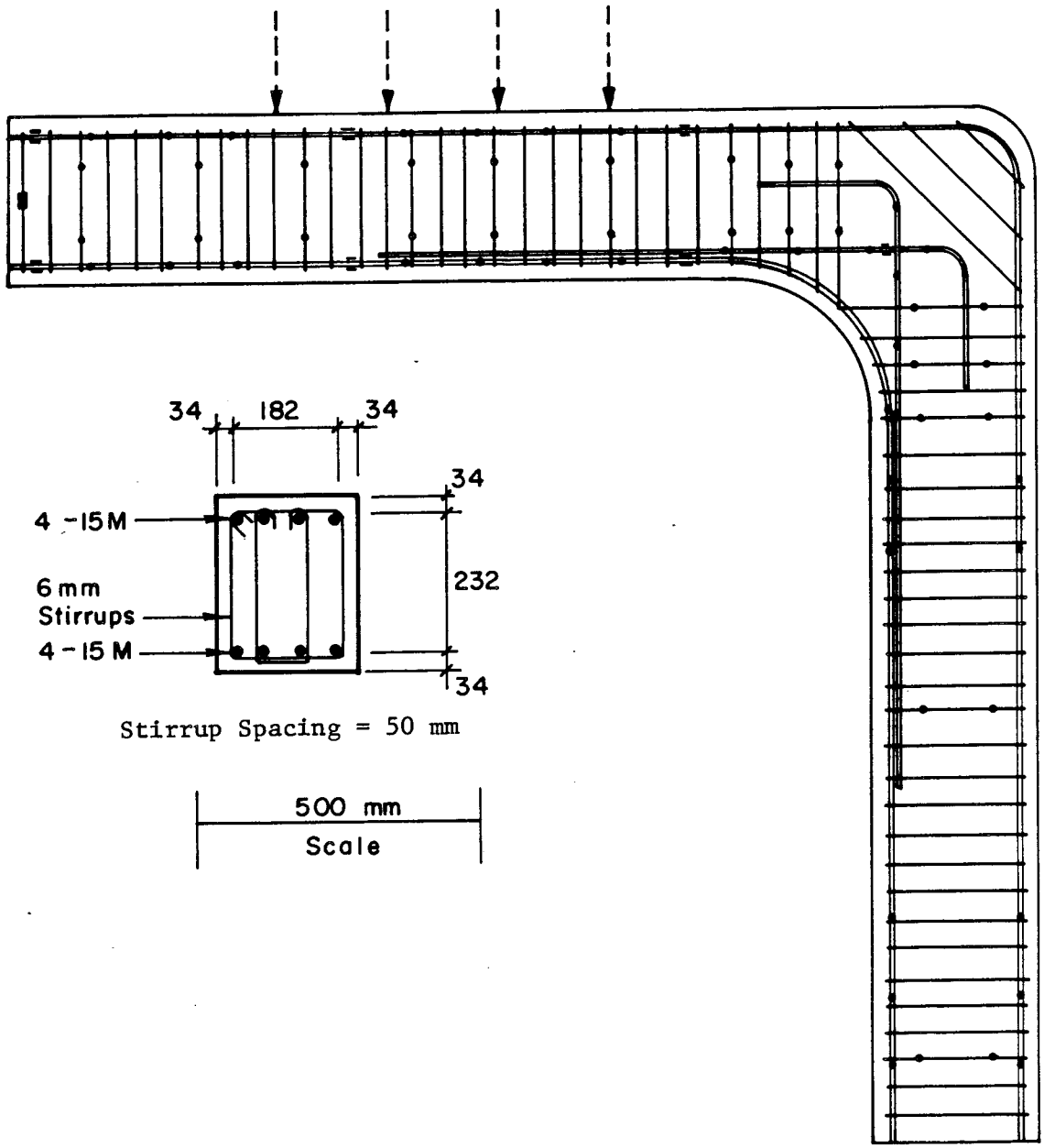

Figure 3.18 Reinforcing Layout for Specimen B1 (Abutments not Shown)

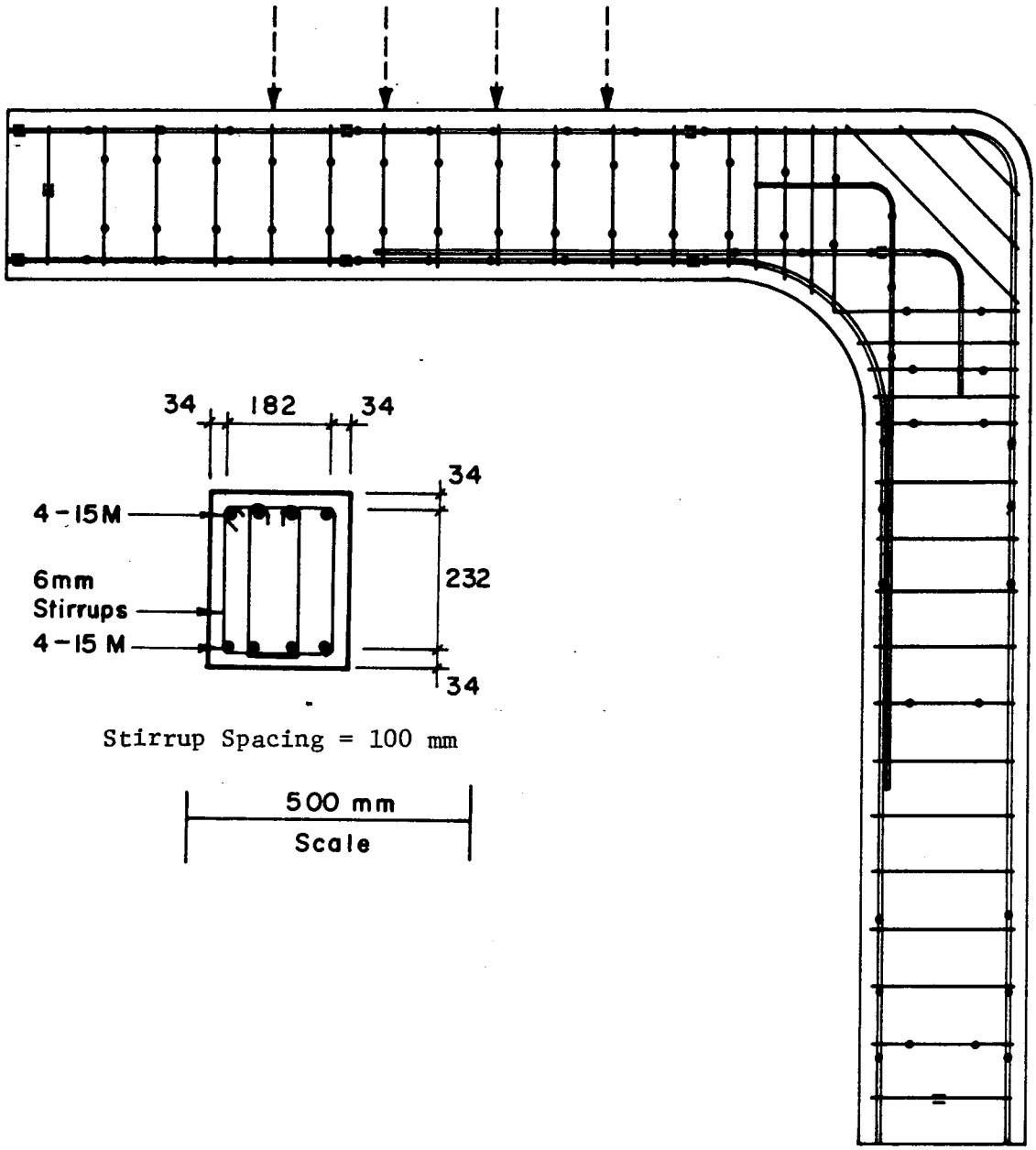

Figure 3.19 Reinforcing Layout for Specimen B2 (Abutments not Shown)

the reinforcement for both specimens are summarized along with that of the A-Series specimens in Table 3.3.

Except for a few minor differences, the details and specifications of the reinforcing in these specimens are the same as that of the A-Series specimens discussed in Sect. 3.2.2.3. The different shape of the abutments required a slightly different reinforcing cage. Also, the minor reinforcement in the loading ledges was no longer necessary.

The hooked bars which were lapped with the bottom reinforcement in all the V-shaped arch specimens were provided in anticipation of the B-Series tests. The inside longitudinal bars were expected to be required to develop their yield strength at midspan under this loading condition. This presents a detailing problem when these bars are bent to follow the inside soffit of the specimen since the bars would tend to want to straighten-out thereby damaging the specimen and leading to premature failure. The detail proposed to remedy this was to provide bars lapped with the main bottom bars and anchored towards the outside of the joint with 90° standard hooks. Also, extra 6mm stirrups were provided in this region to carry the radial component of the force in the bottom steel and to confine the concrete in this critical area (Fig. 3.20).

As will be discussed in Chapter 4, tension forces were measured in the hooked bars during the B-Series tests. The force in the hooked bars is accounted for in the analytical model presented in Chapter 6.

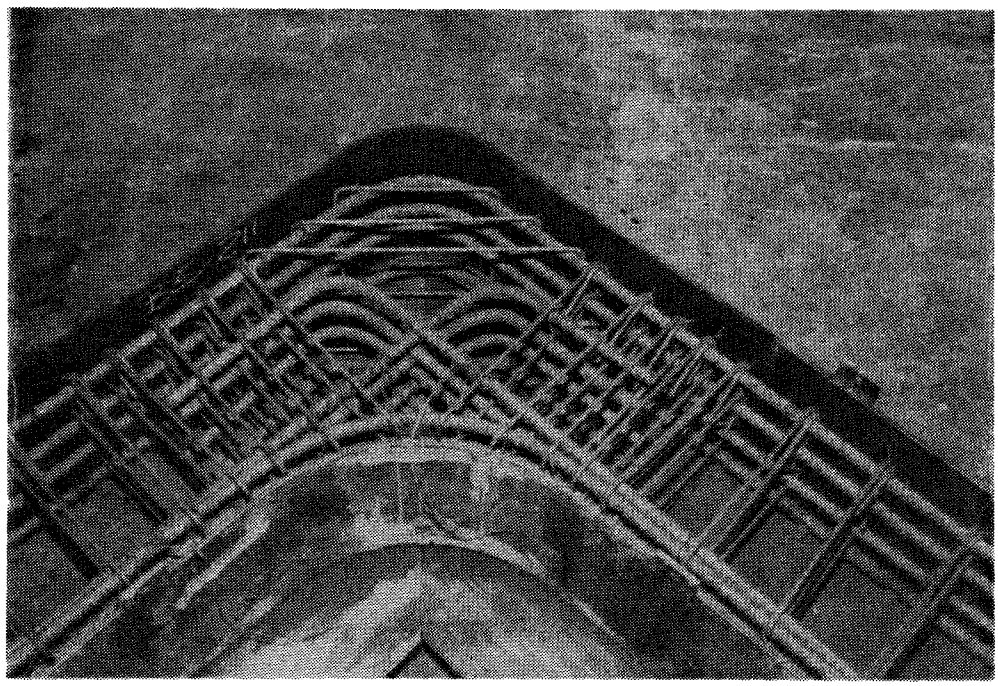

Figure 3.20 Formwork and Details for Specimen B2

3.2.3.4 Construction Details

The construction details of the V-shaped arch specimens were discussed in Sect. 3.2.2.5.

3.2.3.5 Prestressing Operation

The B-Series specimens contained identical prestressing details and were post-tensioned using the same procedure as the A-Series specimens. This was described in Sect. 3.2.2.4.

3.3 Material Properties

3.3.1 Concrete

All of the concrete used in the tests reported in this thesis was batched by a local concrete supplier and delivered by ready-mix trucks. The design specifications for the concrete for the circular arch specimens and the V-shaped arch specimens are shown in Table 3.4.

The specimens were generally cast in pairs with the exception of Specimen B2 which was cast alone. The formwork was removed approximately 24 hours after the concrete had been placed. The specimens were then cured with wet burlap and polyethylene sheets for approximately 4 days. Following this curing period the specimens were stored in the lab with no special curing procedures. Concrete test cylinders and modulus of rupture beams were cast at the same time as the specimens and then cured in a similar manner. A few of these were then tested at 14 days to assess the quality of the concrete. The remaining cylinders and beams were tested

Table 3.4 Concrete Design Specifications

SPECIMENS	SPECIFICATIONS
P1 and P2	40 MPa, Type 10 Cement
	15mm Aggregate
	100 mm Slump
	Non-Air Entrained
	Superplasticized
	4m3
A - Series	35 MPa, Type 10 Cement
B - Series	15mm Aggregate
	100 mm Slump
	Non Fly-Ash
	Non-Air Entrained
	2 oz. Protard Retardant
	Superplasticized

generally on the day following the specimen test. At that time, tests were conducted to determine the compressive strength, modulus of elasticity, split cylinder strength and modulus of rupture. These tests were conducted in accordance with CSA A23.2 M77. The concrete properties determined for each specimen are summarized in Table 3.5.

Several cylinders from the batch of concrete used in Specimens A1 and B1 were instrumented with longitudinal and transverse strain gauges and tested in the MTS testing machine in stroke control mode. This was part of an investigation into the effects of various capping materials on the cylinder strength (Napoleo and Kennedy, 1987). The stress-strain curve for this concrete at approximately 28 days is shown in Fig. 3.21. This cylinder was instrumented with strain gauges, capped with standard sulphur, and tested in accordance with CSA A23.2.

3.3.2 Reinforcing and Prestressing Steel

All principal reinforcement consisted of deformed bars except in Specimen P2 where post-tensioned stirrups were used. Tension coupon tests were performed on samples of all reinforcement to determine their mechanical properties.

In Specimens P1 and P2, the principal reinforcement consisted of Grade 400 25M bars from one heat. The mild shear reinforcement consisted of deformed 6mm bars having properties similar to Grade 400. This reinforcement was already available in the lab and the bars were from one

Table 3.5 Concrete Properties

SPECIMEN	f'c (MPa)	f't (MPa)	f'r (MPa)	Ec (MPa)	Age (Days)
P1	35.1	3.25	4.78	23154	100
P2	35.1	3.25	4.78	23154	100
A1	61.8	3.66	5.05	27498	42
A2	57.8	3.91	4.92	29429	72
A3	51.1	3.88	5.8	26450	97
A4	57.8	3.91	4.92	29429	72
A5	51.2	3.72	5.85	27900	114
B1	59.5	3.9	6.39	31500	120
B2	53.3	3.37	5.5	26101	93

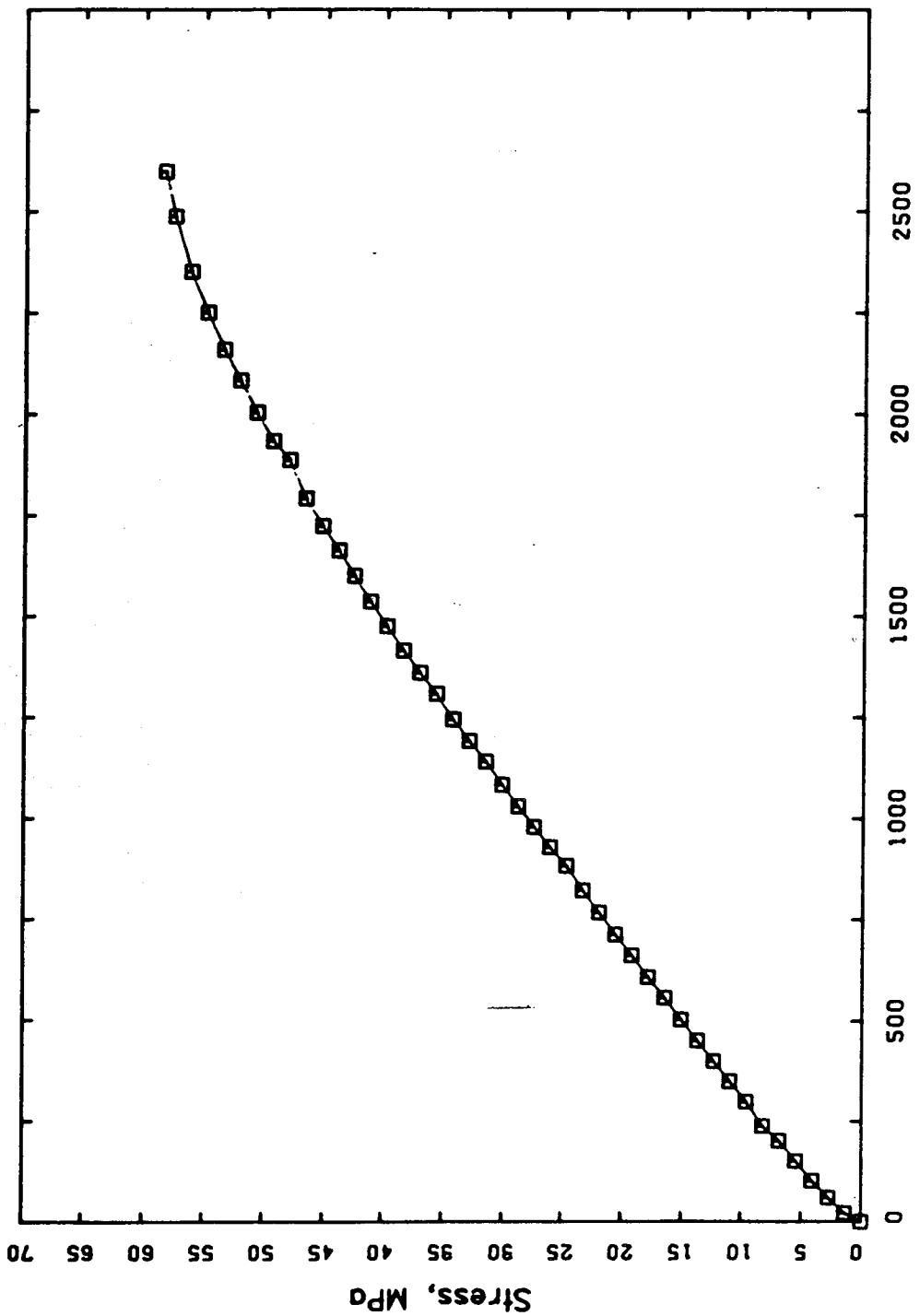

Figure 3.21 Stress-Strain Curve for Concrete in Specimens A1 and B1

heat. The post-tensioned stirrups consisted of 15mm diameter DYWIDAG threadbars. These bars were certified as being from one heat. The 32mm diameter DYWIDAG threadbars used in the prestressed tension member were also obtained from one heat. The yield strength, modulus of elasticity and ultimate strength of the reinforcement used in the circular arch specimen are summarized in Table 3.6. The stress-strain curves of the post-tensioned and mild shear reinforcement are shown in Fig. 3.22. These tension tests were done in a Baldwin testing machine using electrical resistance strain gauges and calipers to determine the strains.

In all the V-shaped arch specimens, the 6mm diameter bars were from one heat obtained from Construction Technology Laboratories, Skokie, Illinois. The 15M Grade 400 bars for specimens A1 - A5 and B1 were from the same heat. The 15M bars for Specimen B2 were from a different heat. The 10M Grade 400 bars for Specimen A4 were from one heat. Tension coupon tests were performed on all reinforcement in the A and B Series specimens. The results of these tests are summarized in Table 3.6. The stress-strain curves are shown in Fig. 3.23. The 32mm diameter threadbars used in Specimens P1 and P2 were also used in the A and B Series specimens to attach the steel beam to the abutments and the properties of these bars are also shown in Table 3.6.

Table 3.6 Reinforcing and Prestressing Steel Properties

SPECIMENS	Bar Size	As (mm2)	fy (Mpa)	Yield Strain mm/mm	fu (Mpa)	Es (Mpa)	Comments
P1	25M	500	479.4	0.00235	745.5	204000	top and bottom
	6mm	31.7	439.4	0.0022O	635.9	199450	stirrups
	32mm	804	-	-	-	211000	all specimens
P2	25M	500	479.4	0.00235	745.5	204000	top and bottom
	6mm	31.7	439.4	0.0022O	635.9	199450	stirrups
	15mm	181	885.7	0.00439	1121	204900	P/T stirrups
A1-A3,A5,B1	15M	200	400.O	0.0023O	646.9	188800	top and bottom
	6mm	31.7	479.5 *	0.00422 *	656.O	185300	stirrups
A4	10M	100	390.8	0.00203	571.5	192770	top and bottom
	6mm	31.7	479.5 *	0.00422 *	656.O	185300	stirrups
B2	15M	200	428.5	0.00251	683.O	187120	top and bottom
	6mm	31.7	479.5 *	0.00422 *	656.O	185300	stirrups
	* Note: For these bars only, fy determined from 0.02% offset						

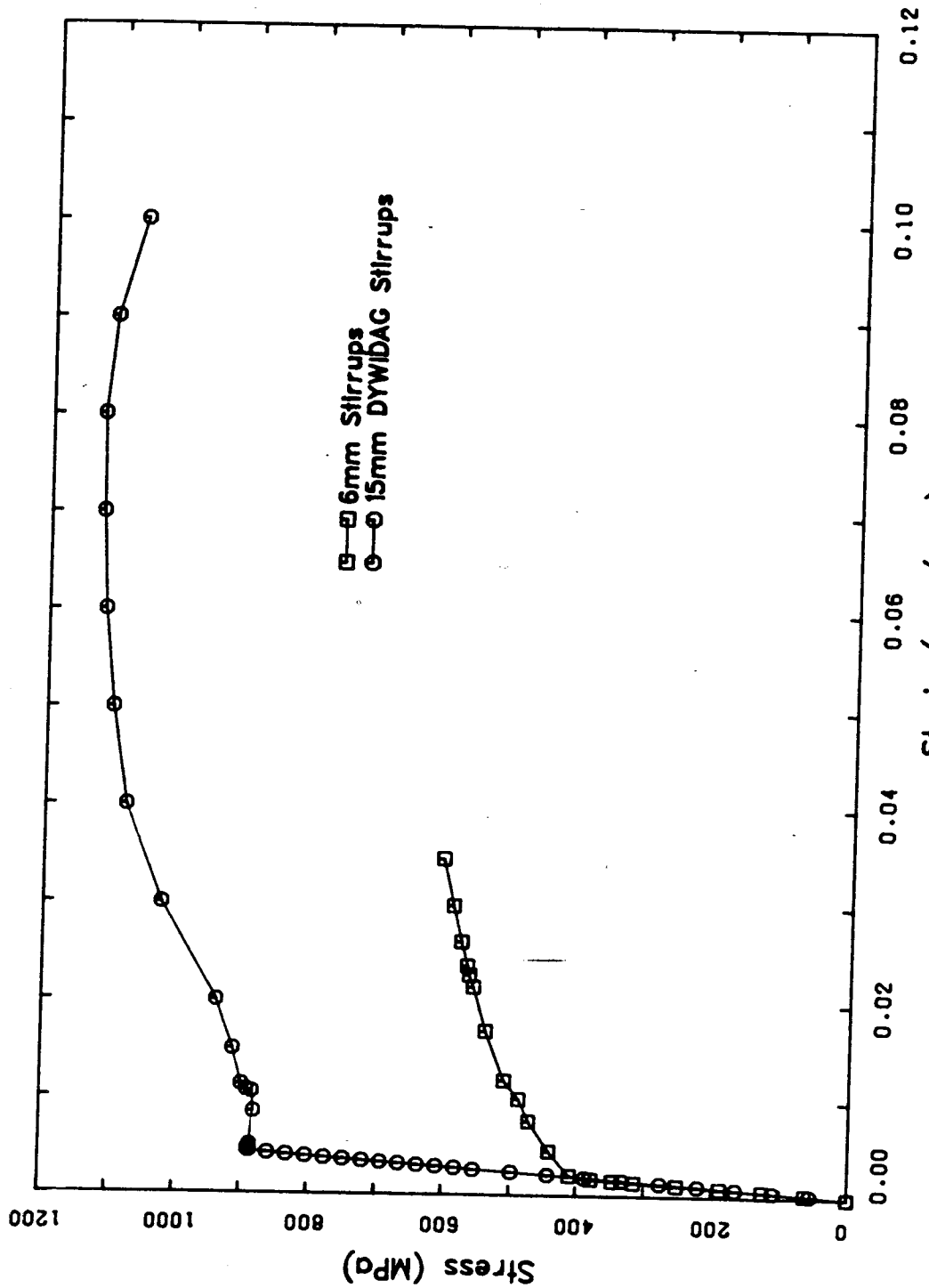

Figure 3.22 Stress-Strain Curves for Shear Reinforcement in Specimens P1 and P2

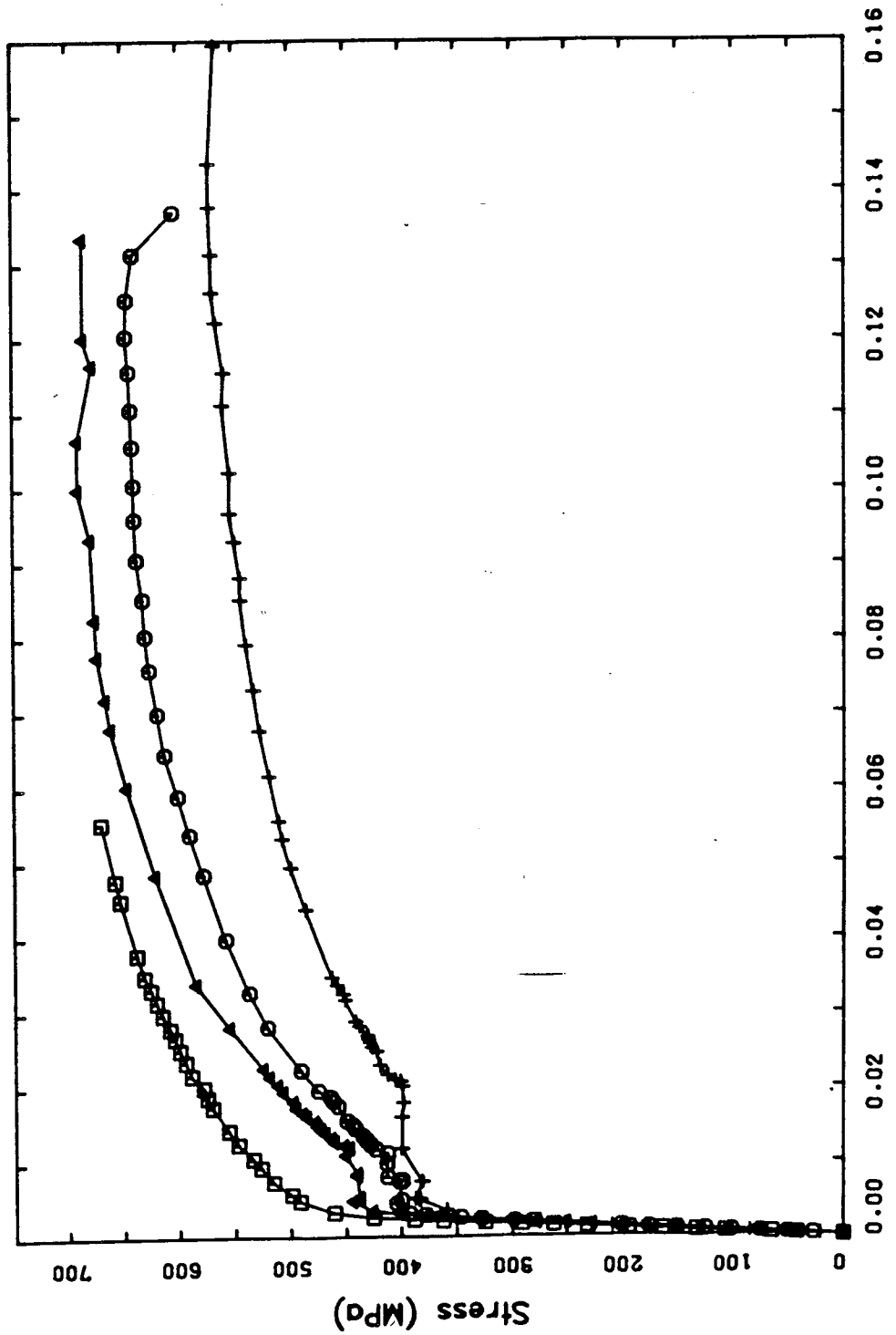

Figure 3.23 Stress-Strain Curves for Reinforcement in V-Shaped Arch Specimens

3.3.3 Steel Restraining Beams

Since the geometry and elastic properties of the steel beams were important, tension coupon tests were performed on the material used in the webs and flanges of each of the two beams. Both beams were I-shaped and fabricated from CSA G40.21-M77 Grade 300W structural steel plate. The important properties of the two steel beams are summarized in Table 3.7.

3.4 Test Set-Up and Procedure

3.4.1 Test Set-Up

The geometry, loading, and support conditions for each specimen were discussed in Sect. 3.2.

The load application system was essentially the same for all the specimens discussed in this thesis. This is illustrated schematically in Fig. 3.24. Load is applied through a stiff steel beam. Two pairs of rollers are free to pivot on knife-edges. This allows displacements and rotation to occur while ensuring that the load is applied evenly to the four load points. As suggested in Sect. 3.2, reactions were also provided by knife-edges and rollers. A typical knife-edge and roller assembly with a flat load cell in between is shown in Fig. 3.25. All knife-edge and roller assemblies were designed to have sufficient capacities and to be serviceable under the extreme loads required in this test program. This was achieved by using a low-alloy steel

Table 3.7 Steel Beam Properties

Steel Beam	Cross-Sectional Properties		Length	Elastic
	Area	Inertia		Modulus
	(mm2)	(mm4 x E6)	(mm)	(MPa)
SB - 1	18069	973	2180	204830
SB - 2	14368	715	2180	205370

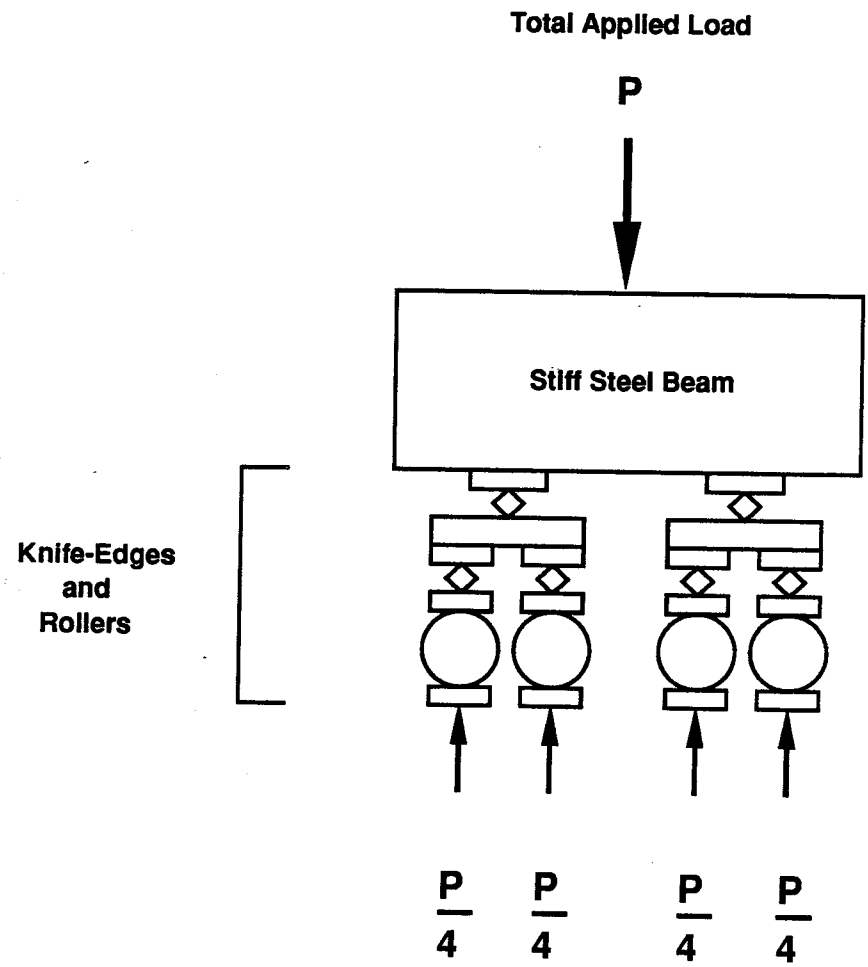

Figure 3.24 Schematic of Typical Load Application Set-up

(AISI-SAE 4140) which was machined in the annealed condition and then heat treated to a hardness of approximately 45 on the Rockwell 'C' scale, and to about 1/3 depth (Ellis, 1985).

The typical test set-up for Specimens P1 and P2 is shown in Fig. 3.26. The test set-up for Specimen A1 subjected to the loading of Fig. 3.9 is shown in Fig. 3.27(a). The test set-up for Specimen B1 subjected to the loading of Fig. 3.17 is shown in Fig. 3.27(b). For the V-shaped arch specimens, platforms were provided in order that the manual measurements could be taken. In the case of the B-Series specimens, these needed to be of considerable elevation.

The specimens were tested vertically in the 6700 kN capacity MTS testing machine. Steel columns were prestressed to the strong-floor of the lab for safety and to attach jacks which could be used to keep the specimen in alignment if necessary. These steel columns could also be used to support instrumentation. Four lateral support beams were provided for the circular arch specimens. Each beam had a roller at the end and was mounted on steel columns on each side of the two abutments. The rollers were backed off approximately 10 mm so as not to interfere with the abutments. These lateral support beams added to the congestion under the testing machine and were not used in the V-shaped arch tests. In the V-shaped arch tests, chains and/or slings were hung around the specimen for safety.

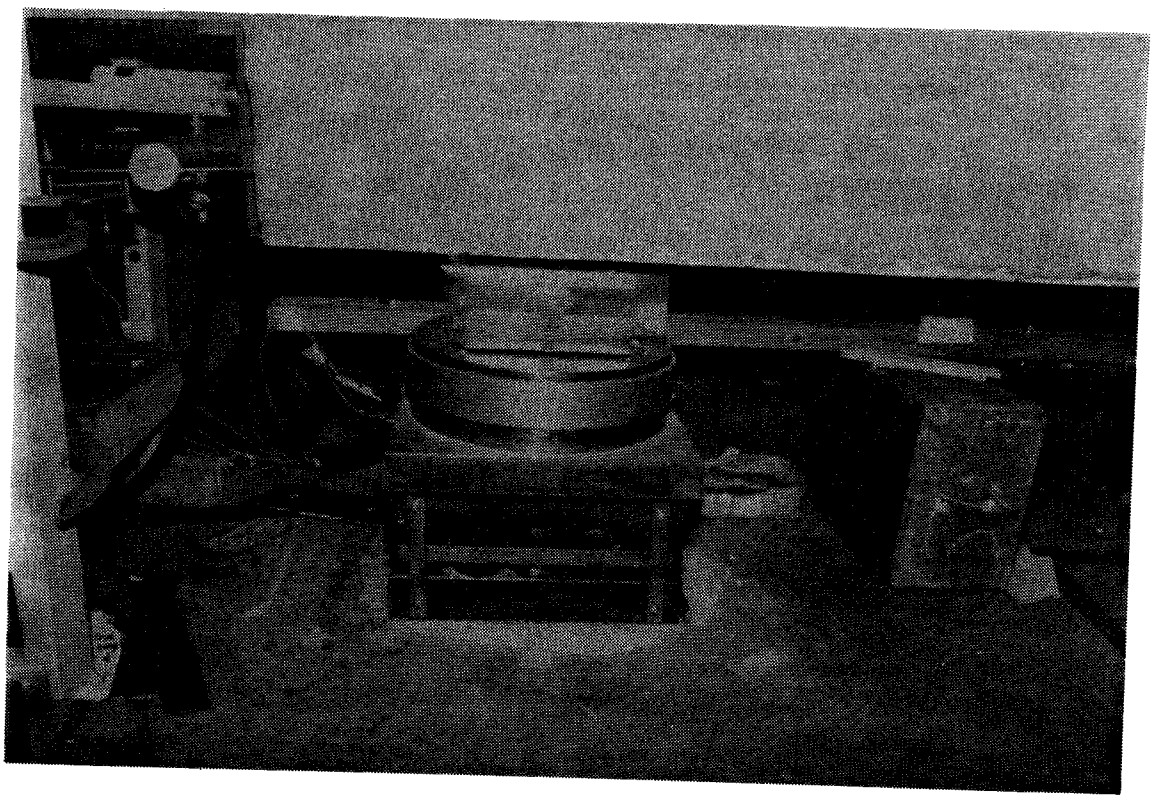

Figure 3.25 Typical Reaction Devices and Load Cell

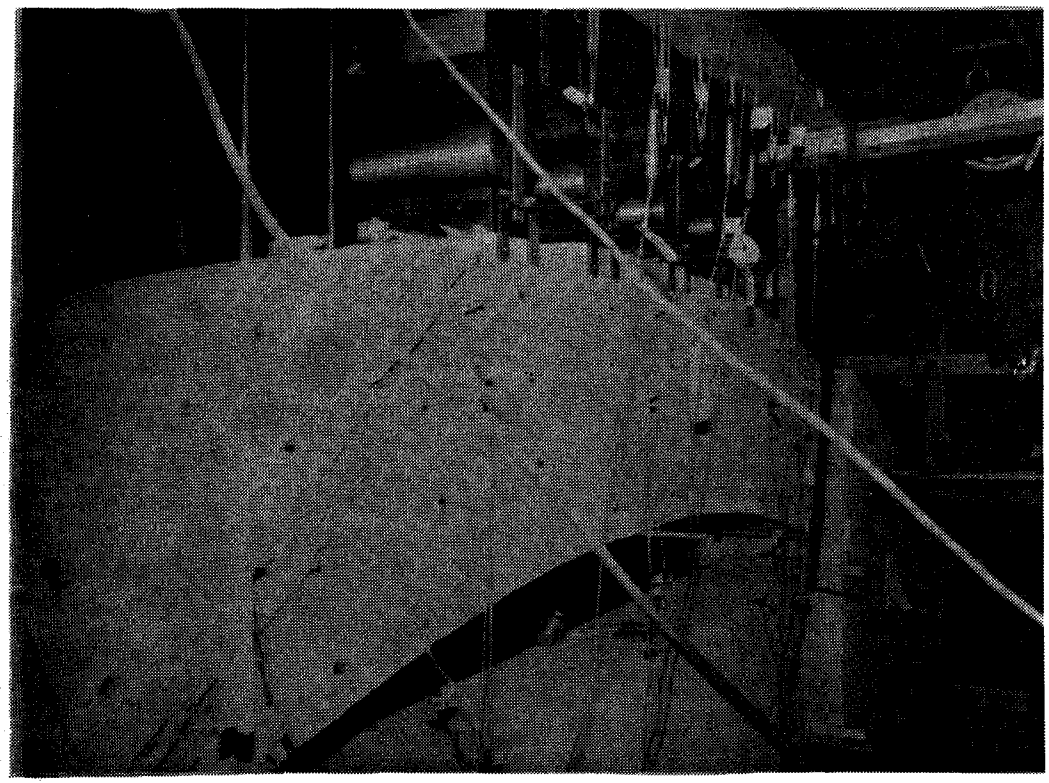

Figure 3.26 Typical Test Set-Up for Specimens P1 and P2

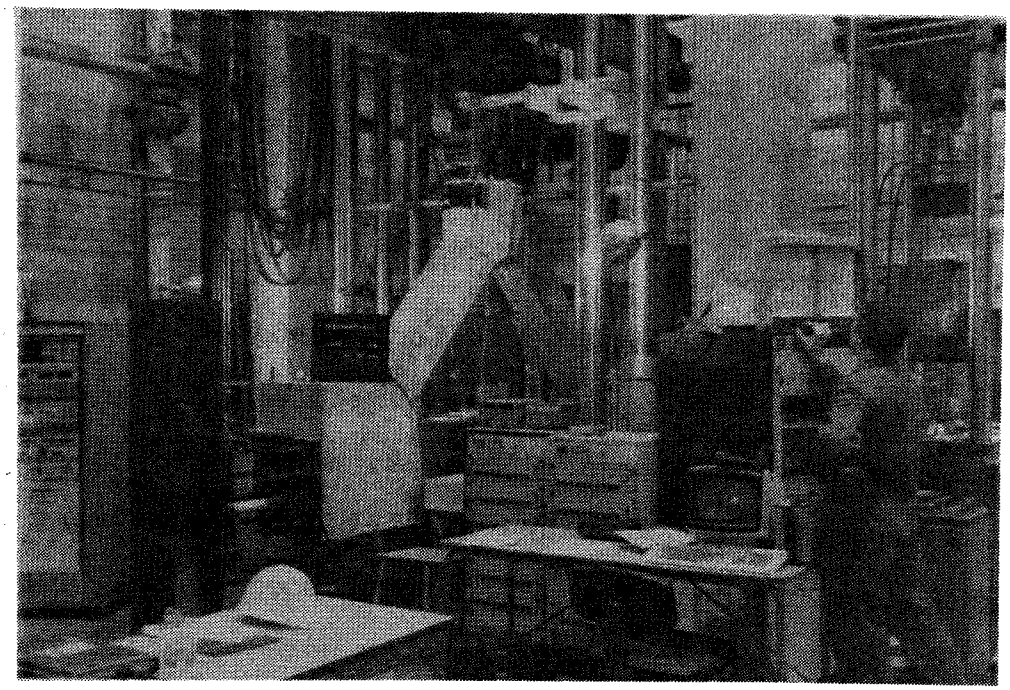

a

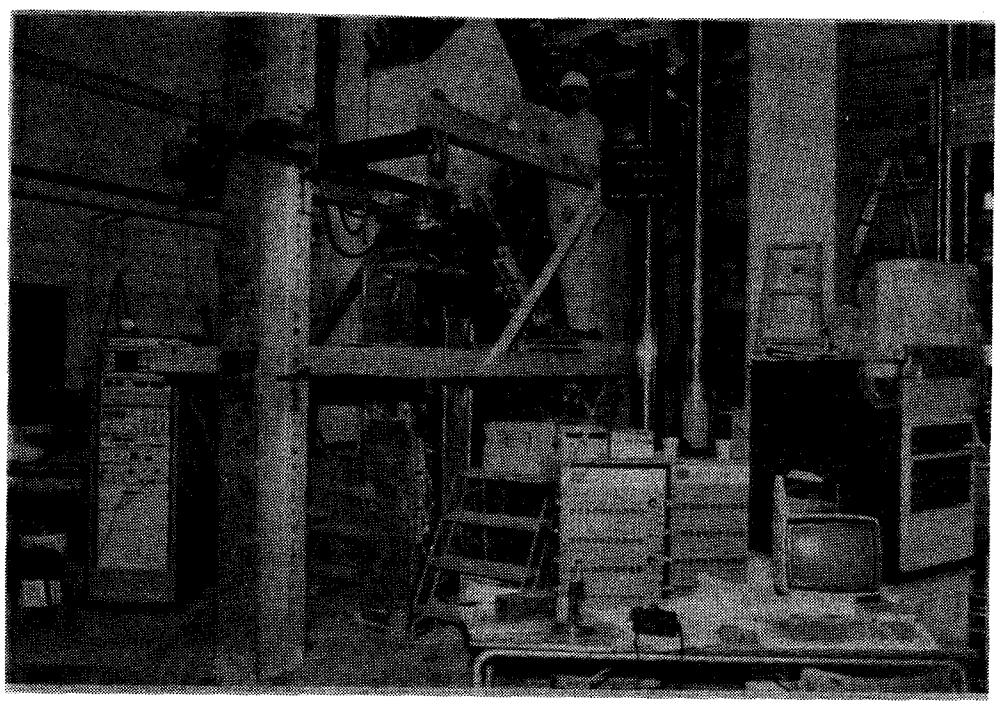

b

Figure 3.27 Typical Test Set-Up for V-Shaped Arch Specimens

For all the test specimens, the displacement transducers and dial gauges were mounted using either magnetic bases attached to the steel columns at each end of the specimen or supported from the overhead beams in the testing machine

3.4.2 Test Procedure

The loads were applied in increments of approximately 100 kN for the circular arch specimens and the A-series specimens. For Specimens B1 and B2, a smaller increment of 50 kN was used. In all cases smaller increments were used nearing the ultimate strength of the specimen.

At each load increment results were recorded using the 256 channel Data General S/120 data acquisition computer system. Each load cell, displacement transducer and strain gauge was assigned a channel. The power supply voltages were also recorded. The total number of channels used was in the order of 90-100. Typically 50-60 of these were for strain gauges. Also at every load increment, cracks were marked using a felttipped pen. At several load increments during the test a full set of manual readings were recorded (crack widths, DEMEC readings, dial gauges). Details of the instrumentation are discussed in Sect. 3.5.

When the specimen was close to failure no manual readings were taken. Also, the more sensitive instrumentation was removed at this time. After the specimen had failed, the specimen was loaded again to determine the

post-ultimate carrying capacity.

3.5 Instrumentation

3.5.1 Loads and Reactions

In all tests, the loads were applied using the 6700kN capacity MTS testing machine. The total applied load was recorded from the MTS pressure transducer. The system of beams, knife-edges and rollers were such that 1/4 of the total load could be assumed to be applied at each of the four load points on each specimen.

In all tests, the reactions were measured using Strainsert FL-500C(C)-2SGKT flat load cells. These load cells have a 500 kip rated capacity in compression and a maximum non-linearity of 0.25% full scale (1.25 kips) and a repeatability of 0.05% full scale (0.25 kips). The calibration of the load cells in the MTS 6700 kN capacity testing machine indicated a very linear response. One of these load cells is visible in Fig. 3.25. The reactions for Specimens P1 and P2 and the B-Series reactions were much less than 500 kips. In the case of the A-Series specimens, however, the reactions exceeded this value. In consultation with the load cell manufacturers this was determined to be acceptable since the load cells have a linear response up to the safe static overload which for these load cells was 200% full scale.

3.5.2 Strain Measurements

3.5.2.1 Concrete Strains

Concrete strains were recorded manually using 50.8mm (2") gauge length DEMEC rosettes. The targets were fastened to the concrete using sealing wax and arranged to form a standard 45 degree strain rosette. Thus there were four gauge lengths per rosette; vertical, horizontal and 45 degrees each way from vertical. In this way, there is redundancy in the strain measurements in that four Mohr's Circles of strain can be constructed from each rosette.

The same DEMEC gauge was used for all concrete strain measurements. Calibration of the gauge using a micrometer indicated that one division on the gauge corresponds to a strain of 25 microstrain. This calibration was verified for each test series.

The 50.8mm gauge length DEMEC rosettes were mounted on one side of each specimen. This was always the south face of the specimen when the specimen was in the MTS testing machine. The layout of the rosettes for Specimens P1 and P2 is given in Fig. 3.28. The rosette layout for the Specimen A1 is shown in Fig. 3.29. The number and location of rosettes was varied in the A-Series specimens to find the optimum in order to reduce the time required to take these manual readings. The remaining A-Series specimens have similar rosette layouts to that of Specimens A1. The differences may be seen in Figs. 4.20, 4.23, and 4.24. The layout of the rosettes for Specimens B1 and B2 is shown in

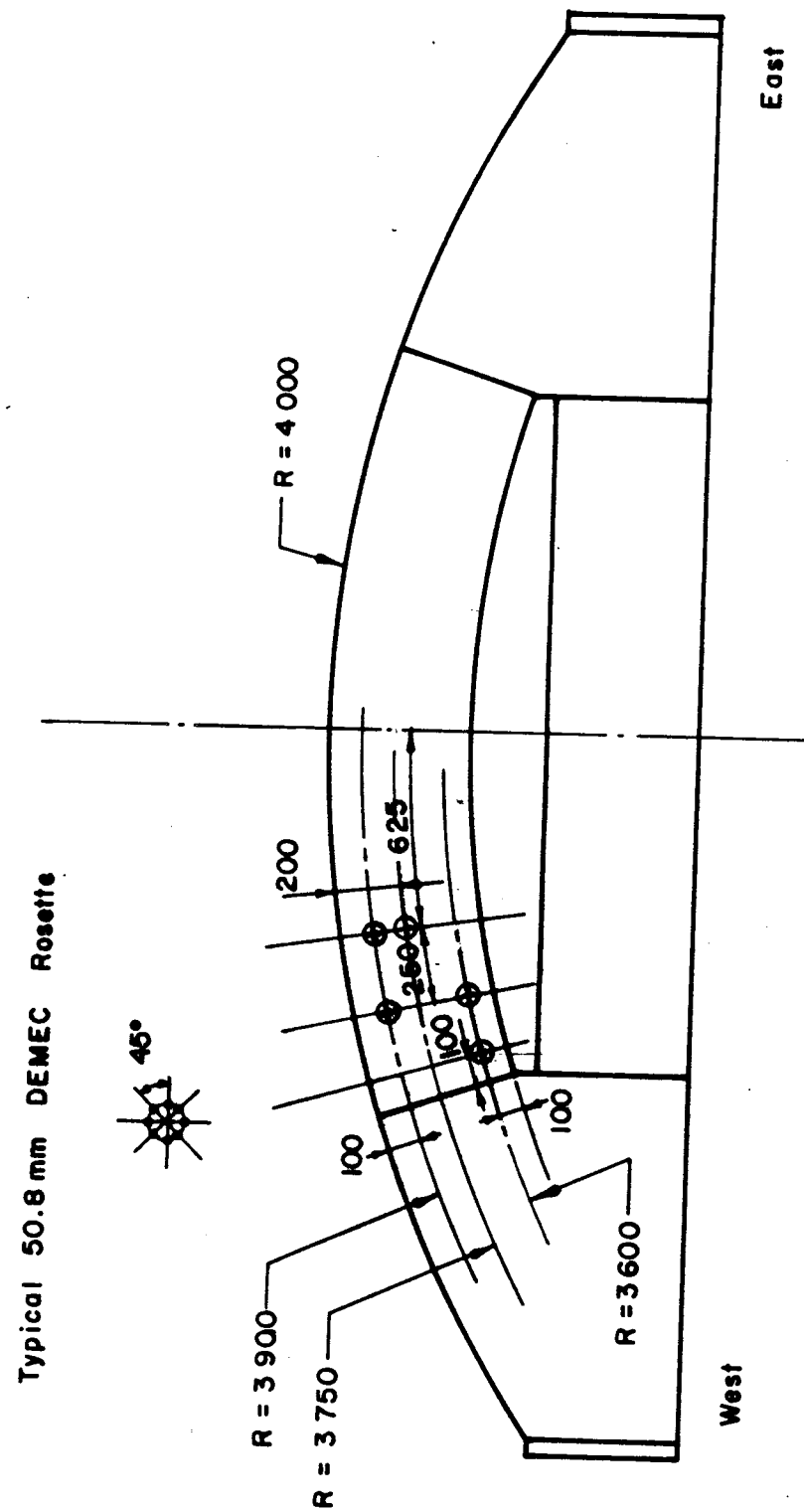

Figure 3.28 Layout of 50.8 mm DEMEC Rosettes for Specimens P1 and P2

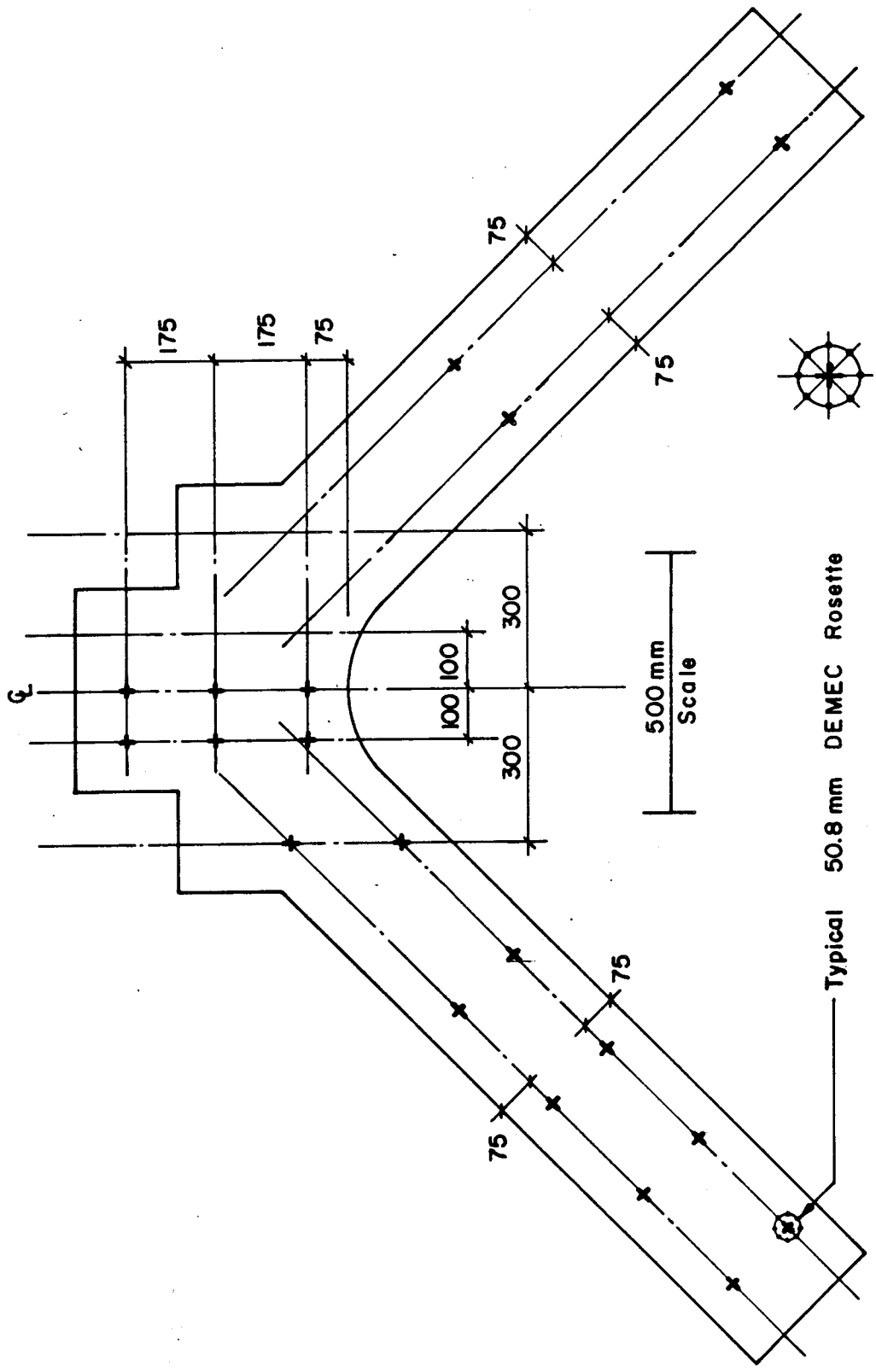

Figure 3.29 Layout of 50.8 mm DEMEC Rosettes for Specimen A1

Fig. 3.30.

3.5.2.2 Reinforcing Steel

The strains in the reinforcing steel were recorded using electrical resistance strain gauges and DEMEC gauges. The strain gauge results were recorded using the computer data acquisition system while the DEMEC readings were recorded manually.

The electrical resistance strain gauges were always mounted in pairs to eliminate any effects due to bending strains in the reinforcement. The gauges used were 5mm gauge length, foil gauges with a nominal resistance of 120 ohms and a gauge factor of 2.11 +/-1%. Each gauge was installed using the three-wire system and calibrated using a shunt resistor. As is the standard in the lab, each gauge uses a 'dummy' gauge for temperature compensation.

In the abrasive environment within a concrete test specimen, the gauges need adequate protection. Several systems were employed for this but the most economical and effective of these used a narrow width of black electrical tape wrapped around and through the leads in such a way as to insulate the leads from each other and from the reinforcing steel. Both gauges were then wrapped again and then sealed using 5-minute epoxy. Less than 2% of the gauges failed to function prior to testing.

The targets for the DEMEC gauges were mounted using sealing wax onto 6mm diameter steel lugs which were brazed onto the reinforcing steel. These lugs were isolated from

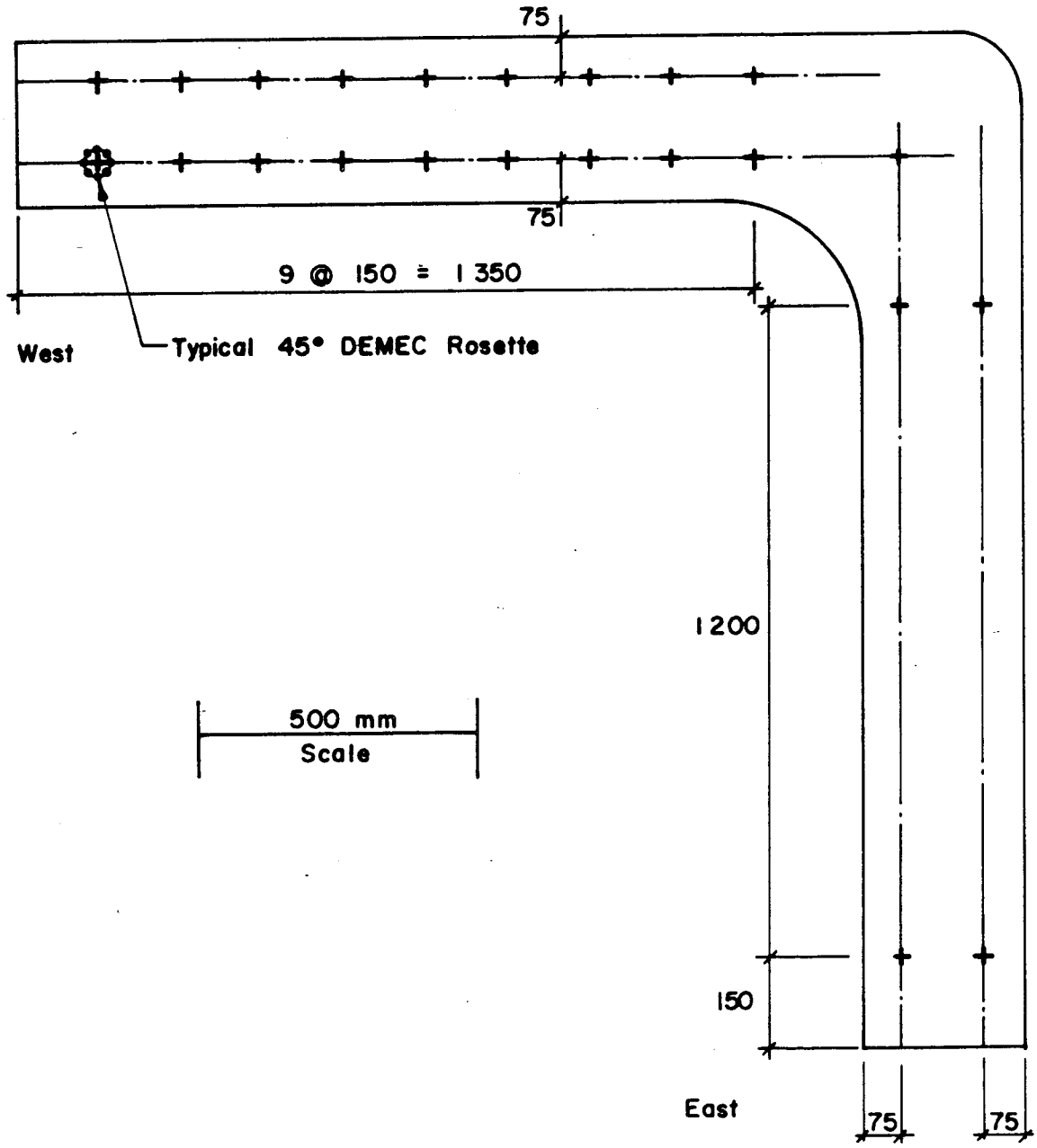

Figure 3.30 Layout of 50.8 mm DEMEC Rosettes for Specimens B1 and B2

the concrete by using a short piece of rubber hose. The hose was lubricated with vaseline and wrapped with polyethylene so that it could be removed after the forms were stripped. The lugs typically doubled as chairs to hold the reinforcing cage at the desired level in the form.

The circular arch specimens P1 and P2 employed a 5" gauge length on the mild shear reinforcement and an 8" gauge length on the 25M longitudinal steel. Electrical resistance strain gauges were used on the 15mm post-tensioned stirrups and on the 25M longitudinal steel. In the V-shaped arch specimens, 5" gauge length DEMECS were used on the stirrups and on the 15M longitudinal steel. In addition, strain gauges were used on the 15M bars and on selected stirrups.

The layout of the DEMEC gauge lengths and the position of the strain gauges on the reinforcing steel are given in Figures 3.5, 3.6, 3.12 to 3.15, 3.18 and 3.19 corresponding to each of the test specimens. In the figures, DEMEC lugs are shown as dots at the appropriate location on the reinforcement. Strain gauge locations are identified by short parallel lines. At many locations both mechanical and electrical measurements were taken in order to have redundancy in the readings.

3.5.3 Strain Measurements in the Steel Restraining Beams

The steel beams used in the A-Series and B-Series tests were heavily instrumented with strain gauges. The layout of these gauges is presented in Sect. 4.3.1 in the discussion

of the steel beam strain measurements.

3.5.4 Displacements

The displacements of the specimens were measured using linear variable displacement transducers (LVDTs). Dial gauges were used for redundancy or to monitor rough overall movements. The LVDT readings were recorded using the computer data acquisition system. Each LVDT was calibrated using a micrometer before using and the accuracy in the linear range is typically 0.1% of full scale.

The typical transducer layout for the circular arch specimens is shown in Fig. 3.31. The full scale range of each LVDT, in mm , is shown at each location. In this schematic only the principal LVDT locations are shown. The typical transducer layouts for the A-Series and B-Series Specimens are shown in Figs. 3.32 and 3.33 respectively.

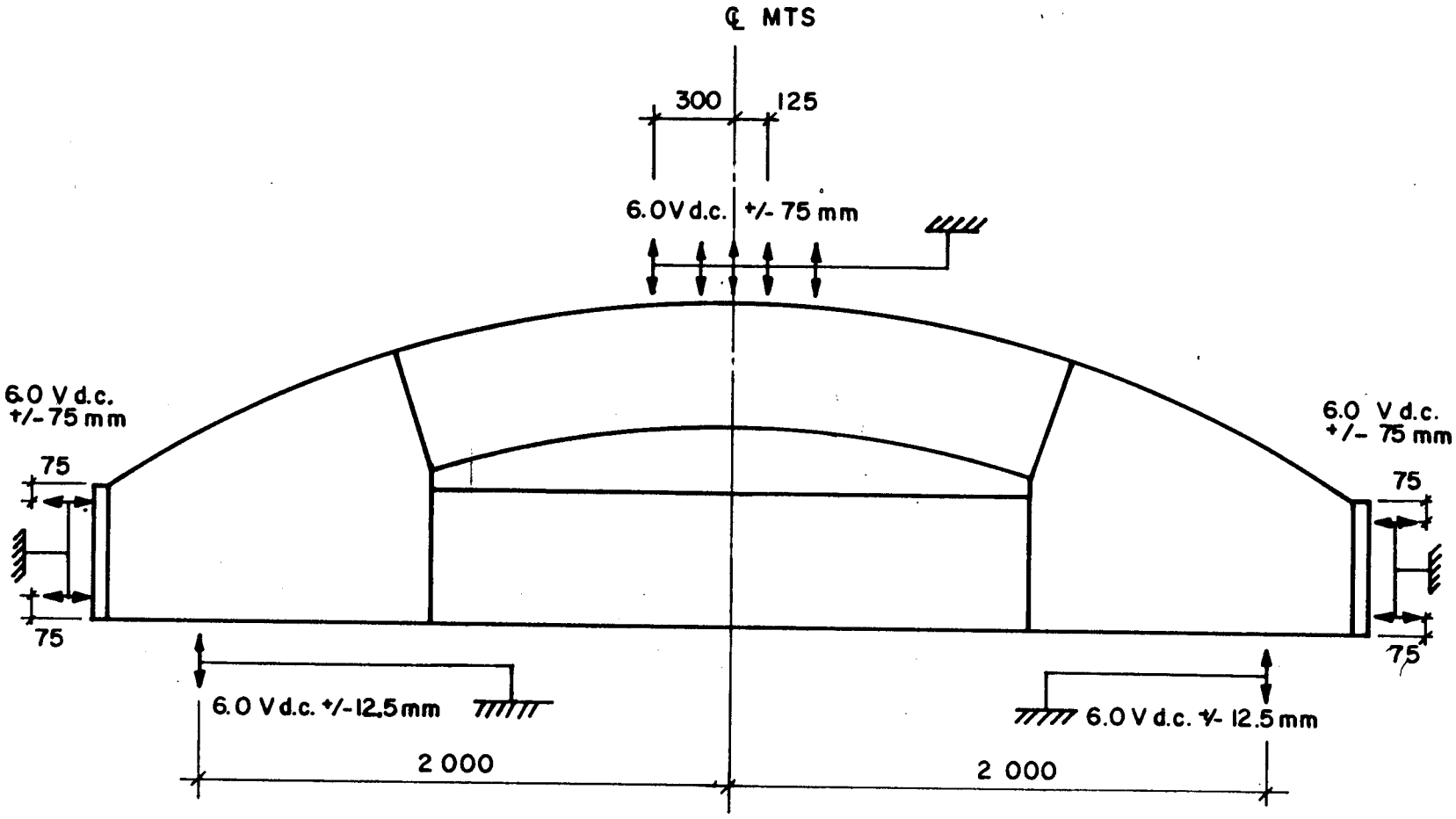

Figure 3.31 Typical Transducer Layout for Specimens P1 and P2

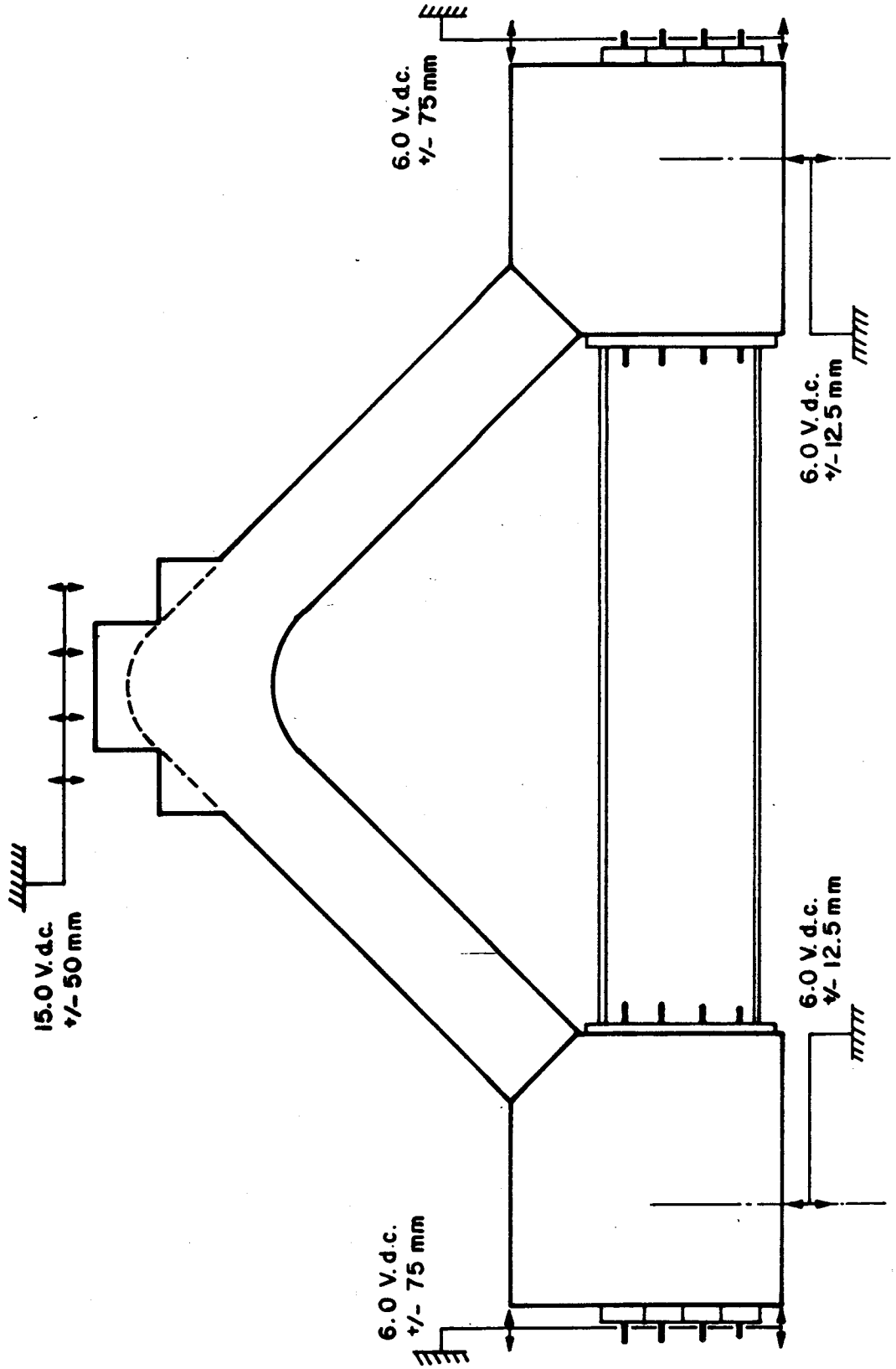

Figure 3.32 Typical Transducer Layout for the A Series Specimens

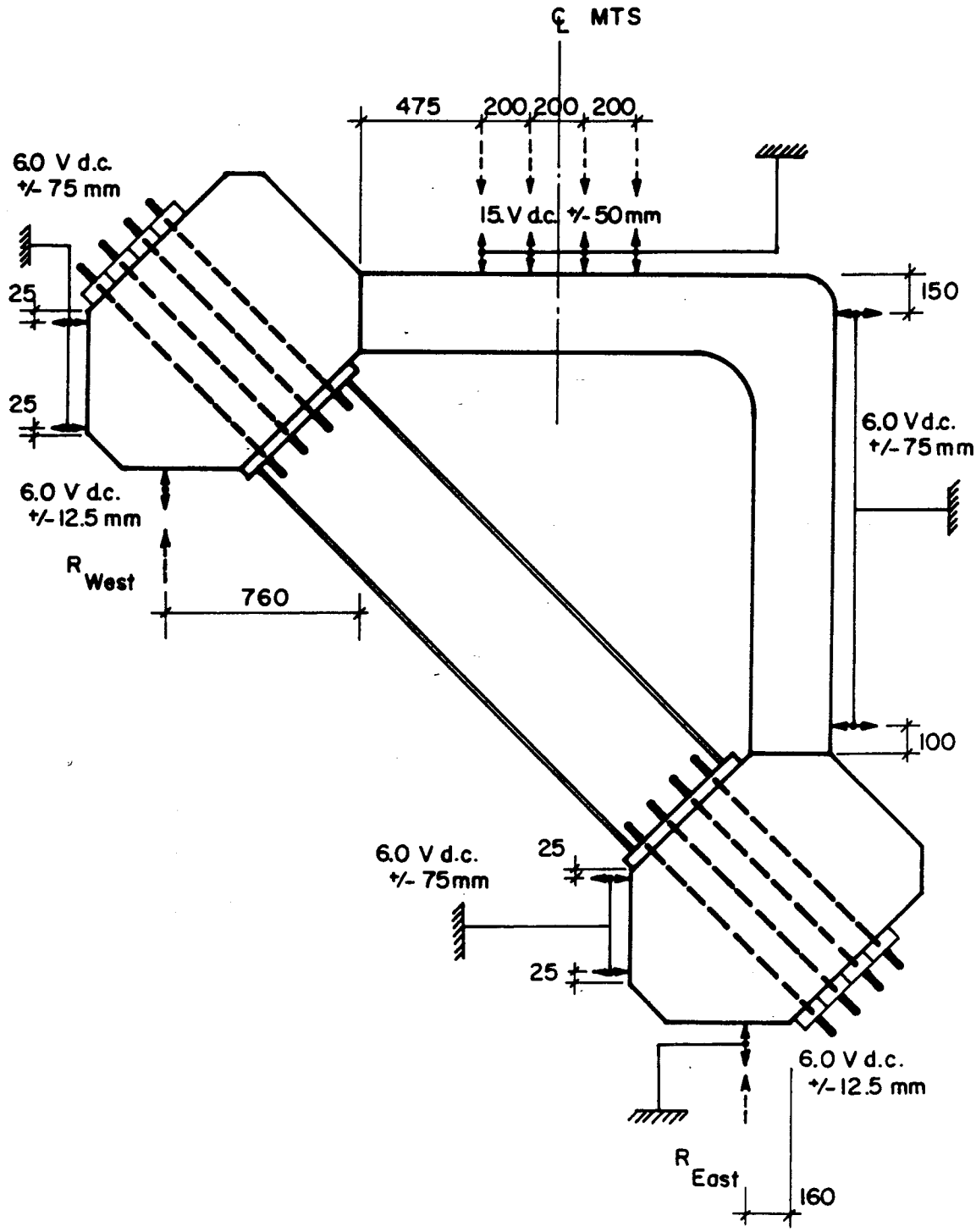

Figure 3.33 Typical Transducer Layout for the B Series Specimens

4. TEST RESULTS

4.1 Presentation of Results

In this chapter, the test results for each of the test specimens are presented. First the results of the tests on circular arch specimens are presented. Next, the results of the A-Series tests on V-shaped arches are presented followed by the results of the B-Series tests.

For each test specimen, the following were recorded at regular intervals for each test:

1. Applied loads
2. Steel strains
3. Concrete strains
4. Concrete crack patterns
5. Vertical and horizontal displacements at various points on the specimen.

The loads, strains and crack patterns were useful for development of the various analytical models presented in Chapter 6. The displacements were used to access the general behavior and ductility of the specimen. In addition, all of the above were compared with the results of the finite element analyses presented in Chapter 7.

Results are presented in graphical form, where possible, to facilitate interpretation. The presentation of concrete strains is always depicted as viewed from the rosette side of the specimen. This was always the south side of the specimen. Strains in the longitudinal reinforcement

are presented as viewed from the north face of the specimen.

4.2 Circular Arch Specimens

4.2.1 Failure Loads

The measured ultimate loads for the two circular arch specimens are given in Table 4.1. In order to compare with an ice pressure, the loads are also given in terms of average effective pressures, expressed in MPa, acting on the loaded surface of the specimen are also given. These values are obtained by dividing the applied load by the area 250 mm x 1000 mm. Throughout this thesis, the reported loads and reactions are as recorded by the data acquisition system. These values do no include the weight of the specimen or the load application and reaction devices since the system was zeroed after the set-up was in place. The weight of these items was very small compared to the magnitude of loads applied in this study.

The type of failure for each specimen is also described in Table 4.1. Details of the tests on Specimens P1 and P2 will be discussed in Sect. 4.2.3 and Sect. 4.2.4, respectively.

4.2.2 Load-Deflection Response

The measured midspan deflections for specimens P1 and P2 are presented in Fig. 4.1. The portion of the deflection due to the support settlement has been subtracted from these

Table 4.1 Failure Loads and Description of Failure for Arch Specimens

Specimen	Failure Load (kN)	Effective Pressure on 0.25m x 1.0m (MPa)	Description of Failure
P1	2900	11.6	First cracking after 2100 kN. Diagonal cracks followed by failure of west strut (Fig. 4.3)
P1 Post-Failure	725	2.9	
P2	3330 (stopped test)	13.3	First cracking in tie and abutments at approximately 3000 kN (Fig. 4.9). Cracking in arch region at 3200 kN due to spreading of tie (sim. Fig. 4.10). Test terminated at 3330 kN due to failure of abutments (Fig. 4.10).

readings.

4.2.3 Test Results for Specimen P1

The specimen carried 2100 kN (or 8.4 MPa) without visible damage. The first cracks were observed at a load of 2200 kN. These cracks were oriented approximately parallel to the principle compressive strains and extended from the lower soffit of the arch at the abutments to the first load point at each end of the arch. These cracks were approximately parallel. The location and extent of cracking at an applied load of 2200 kN is shown in Fig. 4.2. The cracks increased in size and number as the load was increased. As shown in Fig. 4.3, failure occurred in the west shear span at an applied load of 2900 kN (or 11.6 MPa). The amount of shear reinforcement in this specimen was negligible. Consequently the failure occurred suddenly when sufficient cracks had developed in the west shear span to eliminate the load path. A major crack developed through the compressive strut between the support and the first load point. At failure 'popping' sounds were heard as the stirrups crossing this failure plane snapped. After failure, the specimen was reloaded and carried 725 kN (or 2.90 MPa).

Concrete strains were measured at the rosette locations shown in Fig. 3.28 using a 50.8 mm gauge length DEMEC gauge. As discussed in Sect. 3.5.2.1, these readings allow the construction of four Mohr's Circles for each location. The strain gradient across a given rosette will cause these

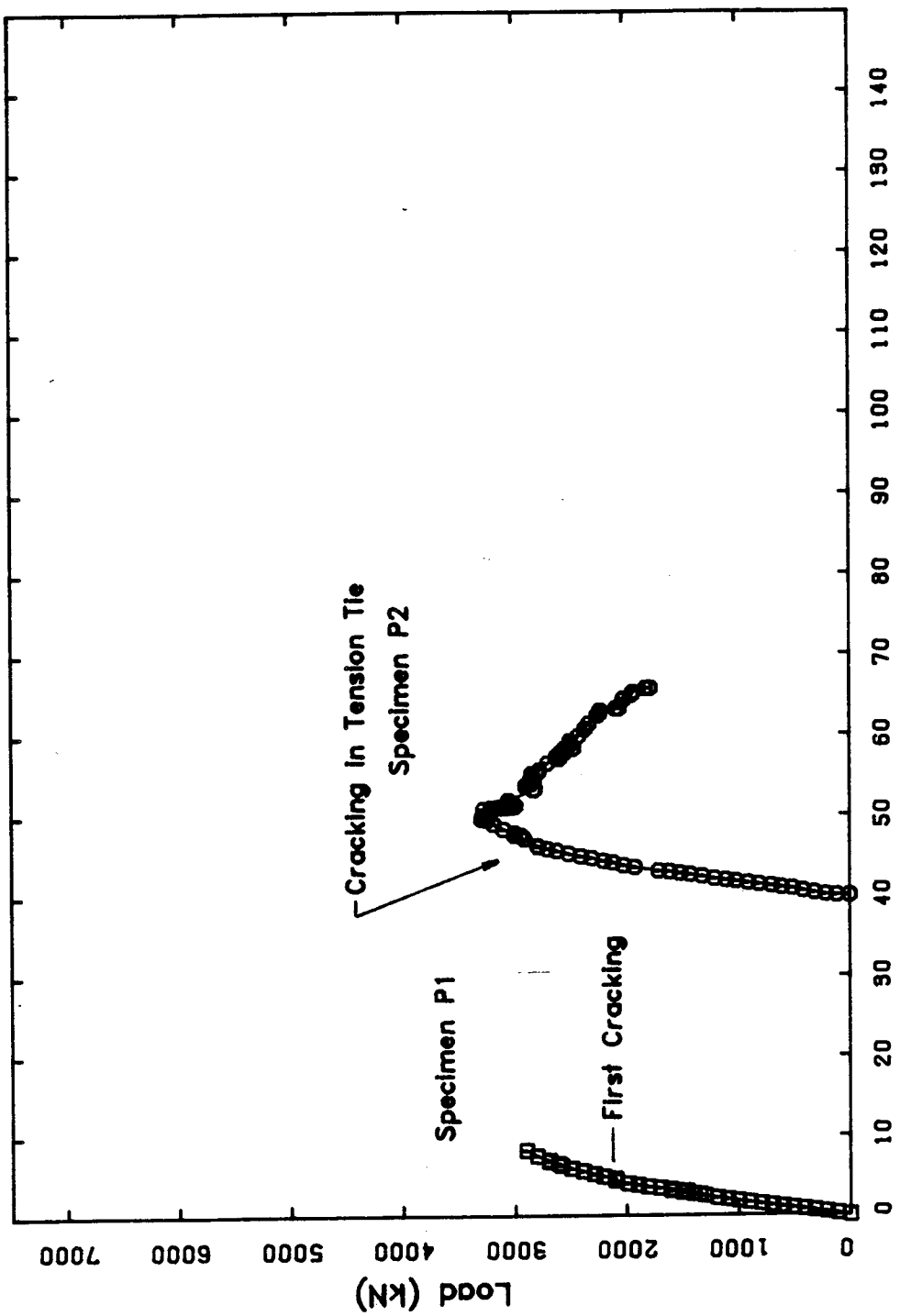

Figure 4.1 Load vs. Midspan Displacement for Specimens P1 and P2

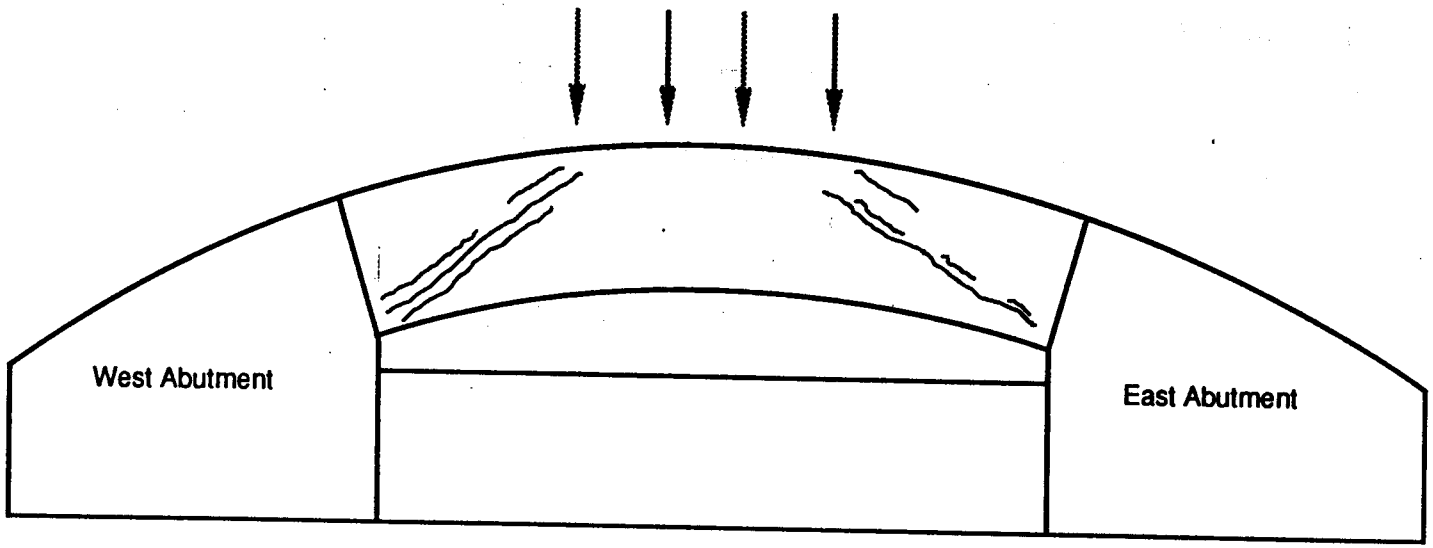

Figure 4.2 Crack Pattern for Specimen P1 at Load = 2200 kN

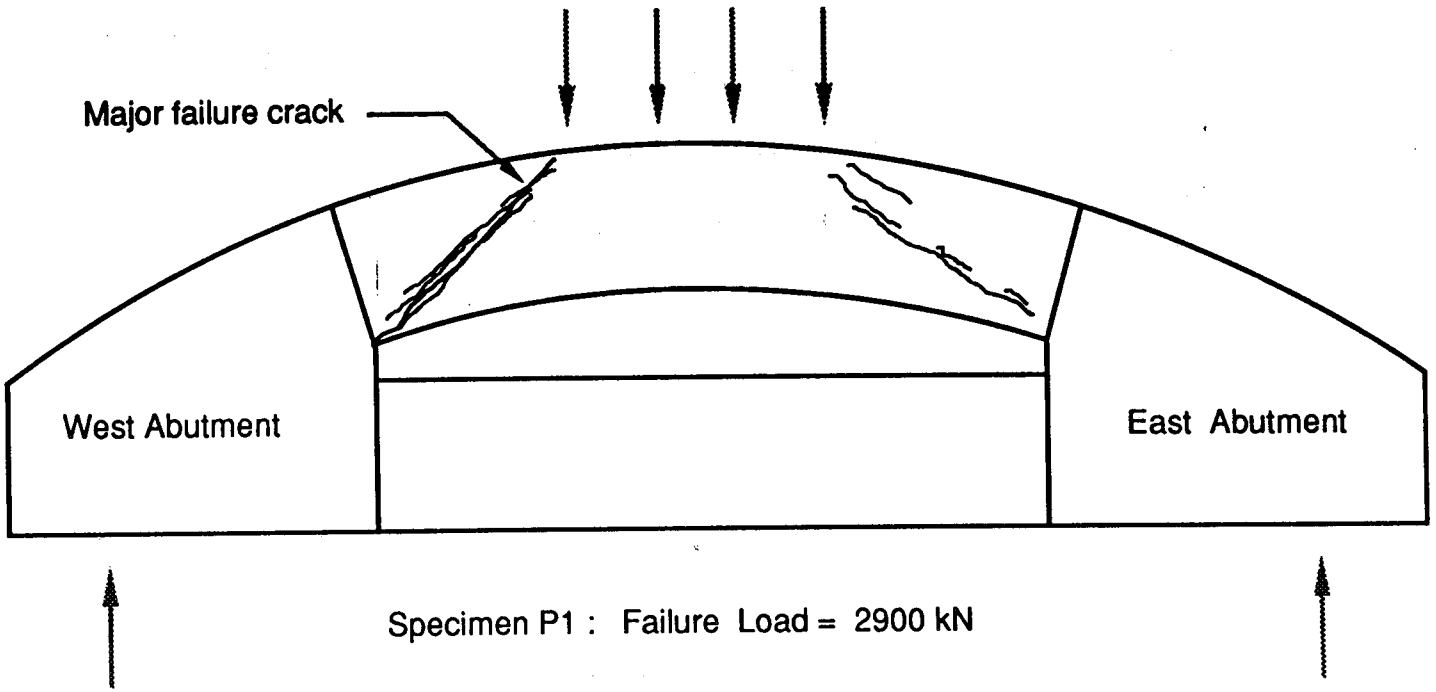

Figure 4.3 Crack Pattern and Major Failure Crack for Specimen P1

circles to differ from each other. Also, the presence of reinforcement in the specimen and the formation of microcracking invalidate the assumption of homogeneity of the strain field, leading to further differences between the circles. The differences will be generally larger where cracks have occurred (for eg. in zones of flexural cracking), and generally smaller in regions with lower strain gradients (for eg. uniaxial strain fields).

To determine the reliability of these rosette readings the four circles were plotted and the principal strains and angles of inclination were determined. The mean and standard deviations of these values were determined, and if for a given rosette, the standard deviations were consistently less than about 10% of the mean values, the rosette was considered reliable. Figure 4.4 shows two acceptable Mohr's Circles, representative of the readings in the circular arch specimens. Figure 4.5 shows the magnitudes and directions of the principal strains at the rosette locations in specimen P1. The results are shown superimposed on one-half of the specimen. Lines with arrowheads indicate tensile strains and the scales are given on the drawing. Figure 4.5(a) shows the principal strains at the load following the development of the first cracks (approx. 2200 kN). Figure 4.5(b) shows the results at an applied load equal to 2500 kN. The trajectories for the two load levels have essentially the same angles of inclination which suggests that the ultimate load path is already established after cracking at the lower

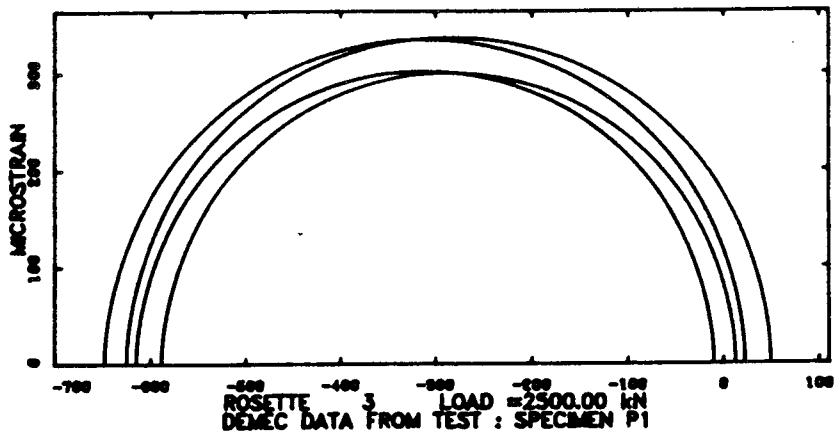

a

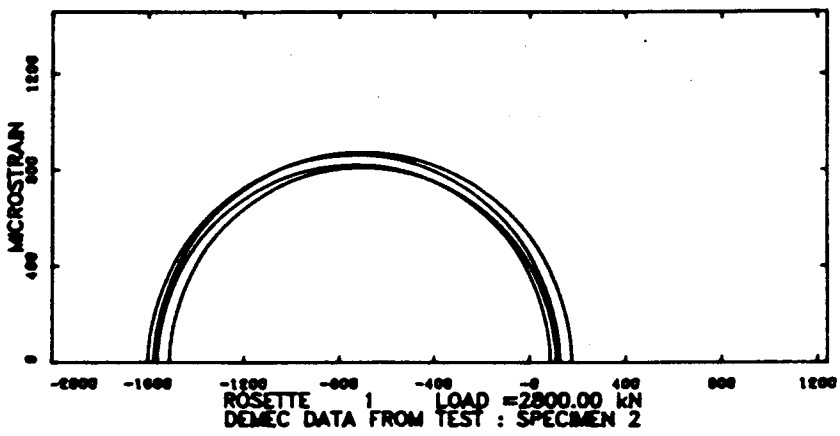

b

Figure 4.4 Typical Mohr's Circles Developed from Measured Strains

load. The cracking observed in the test was approximately at the same angle as the average principal strain trajectory.

The measured strains in the longitudinal reinforcement at an applied load of 2500 kN are shown plotted at the appropriate locations on the top and bottom reinforcement in Figs. 4.6 and 4.7 respectively. Values are plotted at 2500 kN because this is the last load step at which manual readings were taken. In this figure, tensile strains are positive and are plotted above the bar. Scales are as indicated on the drawing. Since the centers of the 203.2 mm DEMEC gauge lengths and the location of the electrical resistance strain gauges coincided, the value shown is the average measured strain using the two values. Also shown are the strains at the ultimate load, 2900 kN, as measured using the electrical resistance strain gauges. These are given in brackets. The yield strain of the bars, as determined from the tension coupon tests, is as indicated on the figure. It is observed that the 25M bars reached yield only at the top midspan and that all locations are in compression except at the bottom midspan.

The stirrups between the abutment and the first load point at each end of the arch began to carry load after cracking occurred around 2200 kN. The stirrups reached yield after 2500 kN and as mentioned above, several of these broke as the specimen failed. The stirrups within the region below the load points did not reach yield during the test.

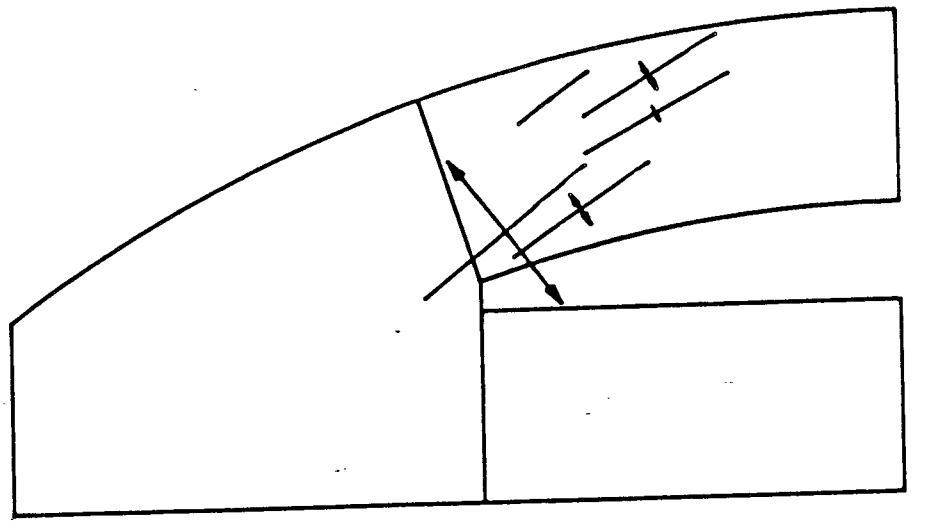

(a) 2 200 kN

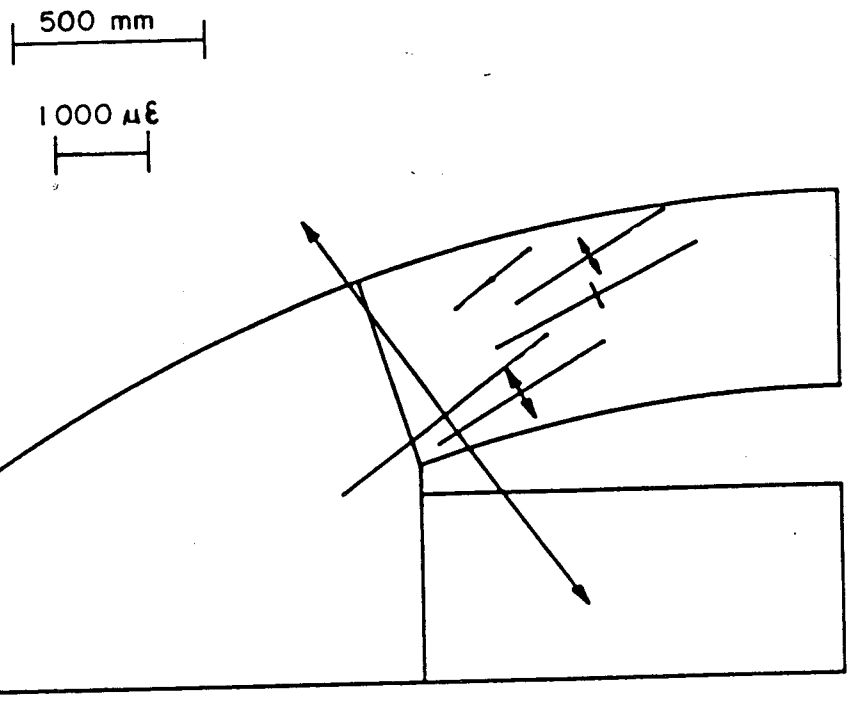

(b) 2 500 kN

Figure 4.5 Principal Strain Plots for Specimen P1

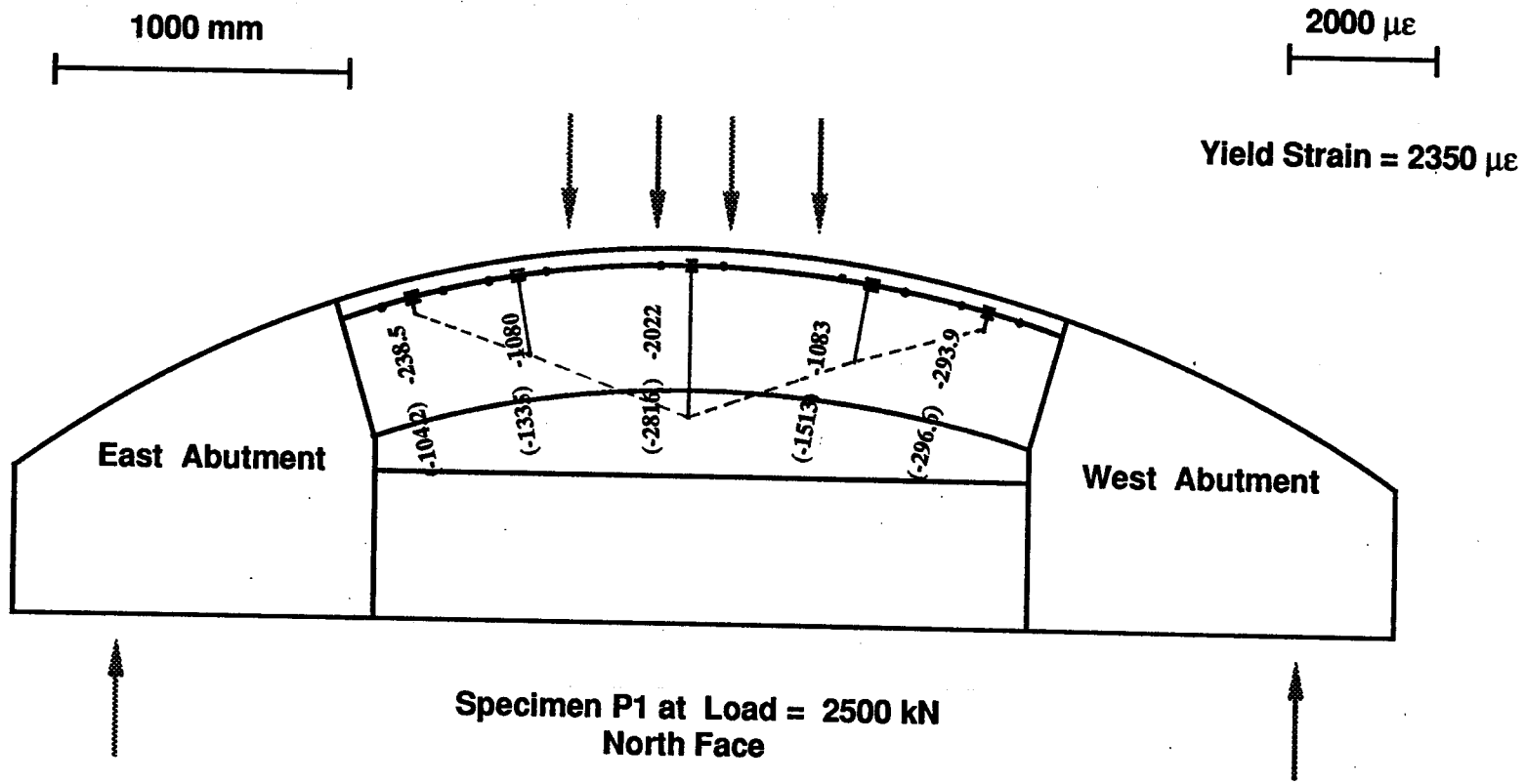

Figure 4.6 Measured Strain Distribution in Top Reinforcing Bars for Specimen P1

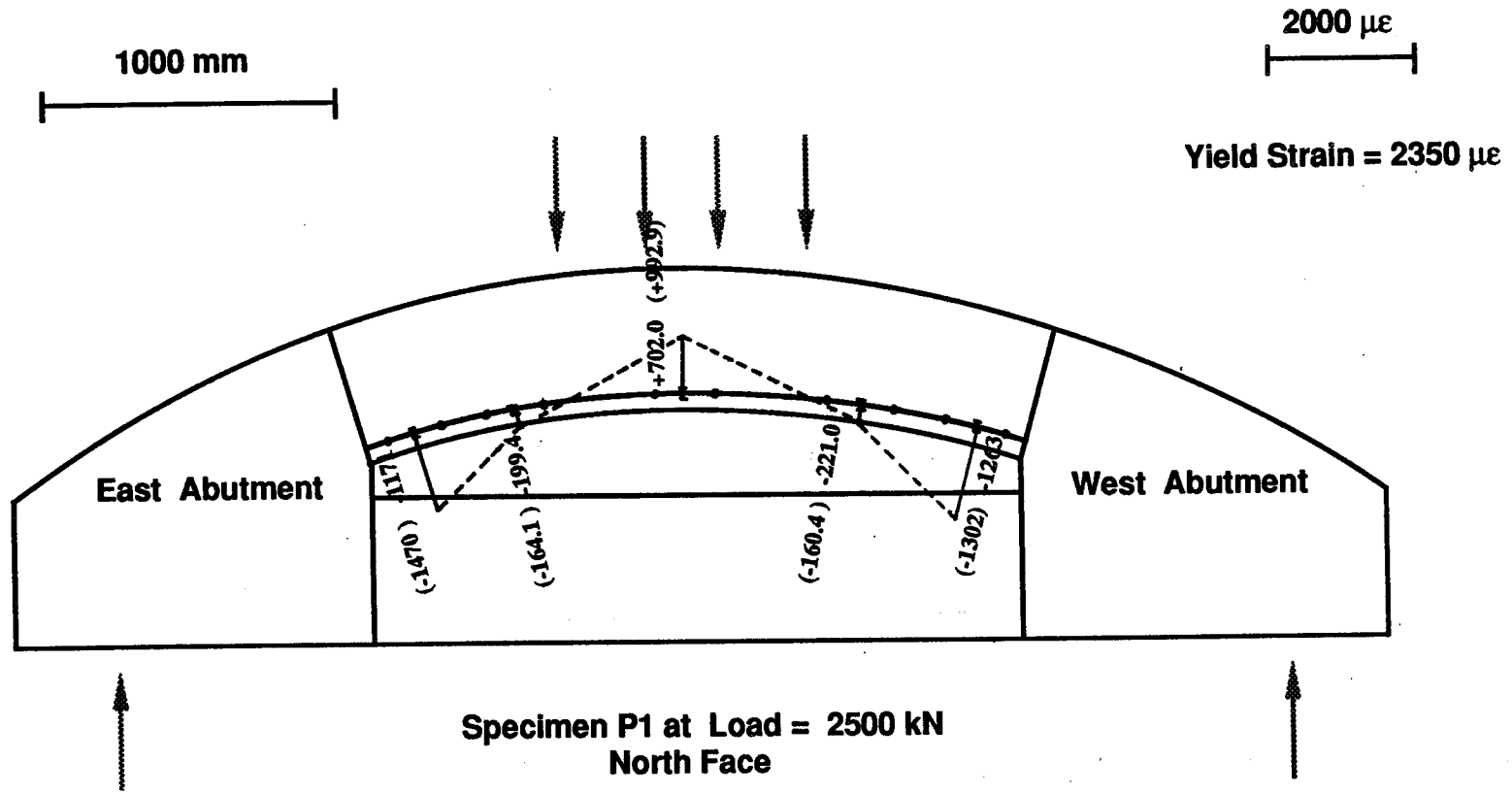

Figure 4.7 Measured Strain Distribution in Bottom Reinforcing Bars for Specimen P1

4.2.4 Test Results for Specimen P2

Specimen P2 was identical to Specimen P1 except that it also contained post-tensioned stirrups. Details of the prestressing and grouting operation have been discussed in Sect. 3.2.1.5. The level of the prestress in these stirrups was monitored using electrical resistance strain gauges for approximately 30 days prior to the test in order to quantify losses. A typical plot of strain vs. time for one of the 15 mm tendons is shown in Fig. 4.8. As expected the gradient was steepest over the first several days and then reduced with time. The magnitude of losses was less than 10% for all sets of tendons.

Specimen P2 carried 2900 kN (or 11.6 MPa) without visible damage. At this point it was apparent that the specimen would carry significantly more load than anticipated and that further increase in load would cause the force in the prestressed concrete tie to approach the design strength. Cracking of an unbonded prestressed concrete tension member is a major event in that all of the load is transferred abruptly to the steel acting alone. The subsequent reduction in axial stiffness means that the arch is not afforded the same lateral support. Nevertheless, it was decided to continue the test and observe the resulting failure since a tie overload is one possible failure mode in a prototype structure.

As the load was increased to 3000 kN, the first cracks in the bottom of the tension tie were observed. With these

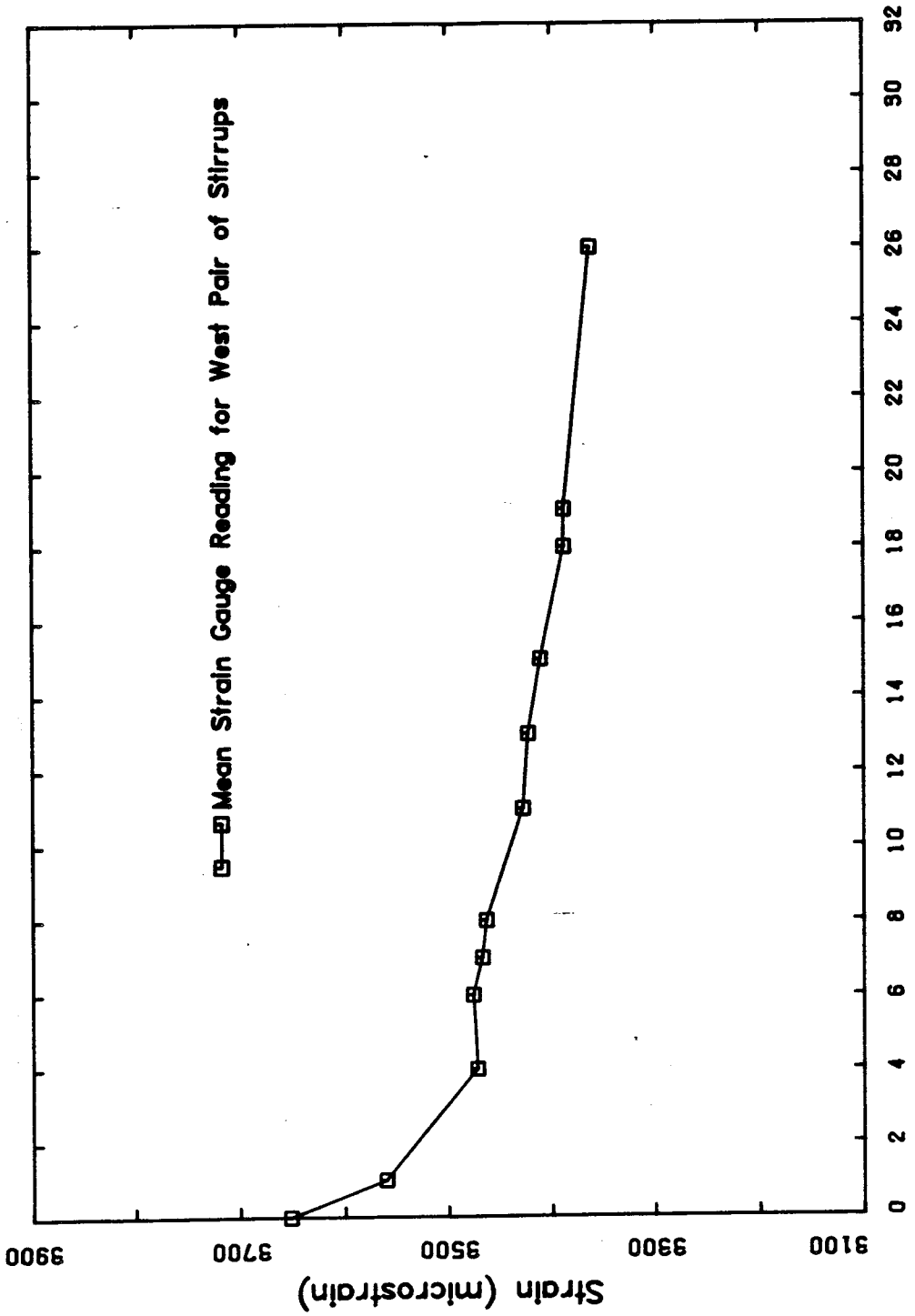

Figure 4.8 Typical Losses in Prestressed Stirrups for Specimen P2

came a few inclined cracks in each abutment (Fig. 4.9). There were no cracks in the arch until the load had reached 3200 kN (or 12.8 MPa). At this point, the spreading of the arch due to the loss of stiffness in the tie led to flexural cracking at the lower soffit of the arch (Fig. 4.10). With increasing load came increasing damage and the failure mode was not representative of the arch region. The test was terminated at a load of 3300 kN (or 13.2 MPa). At this point the tension member had cracked almost all the way across and the abutments were heavily damaged (Fig. 4.10).

Concrete strains were measured as in Specimen P1 (see Fig. 3.28). The principal strain plot at 2500 kN applied load is shown in Figure 4.11(a) . This is seen to be similar to that in Fig. 4.5(a) taken at the same load for Specimen P1. Figure 4.11(b) shows the principal strains at 2800 kN. This was the last load at which manual measurements were taken.

The measured strains in the longitudinal reinforcement at an applied load of 2800 kN are shown plotted at the appropriate locations on the top and bottom reinforcement in Figs. 4.12 and 4.13, respectively. The values are the average of DEMEC and electrical resistance strain gauges. The electrical resistance strain gauge readings at the end of the test, 3300 kN, are also shown in Figs. 4.12 and 4.13.

The strains in the 6 mm stirrups were negligible up to the last measured load (2800 kN). The 15 mm post-tensioned stirrups had negligible change in strain throughout the

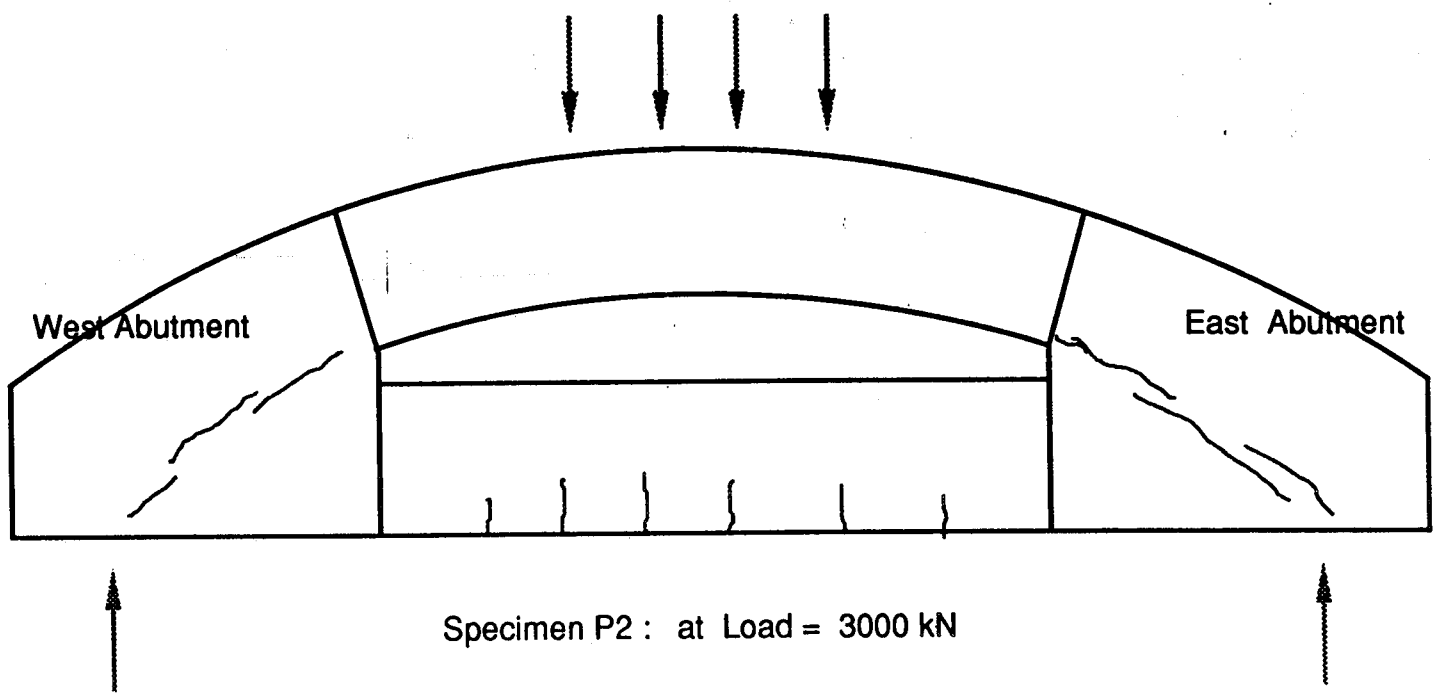

Figure 4.9 Cracking in Prestressed Tie in Specimen P2

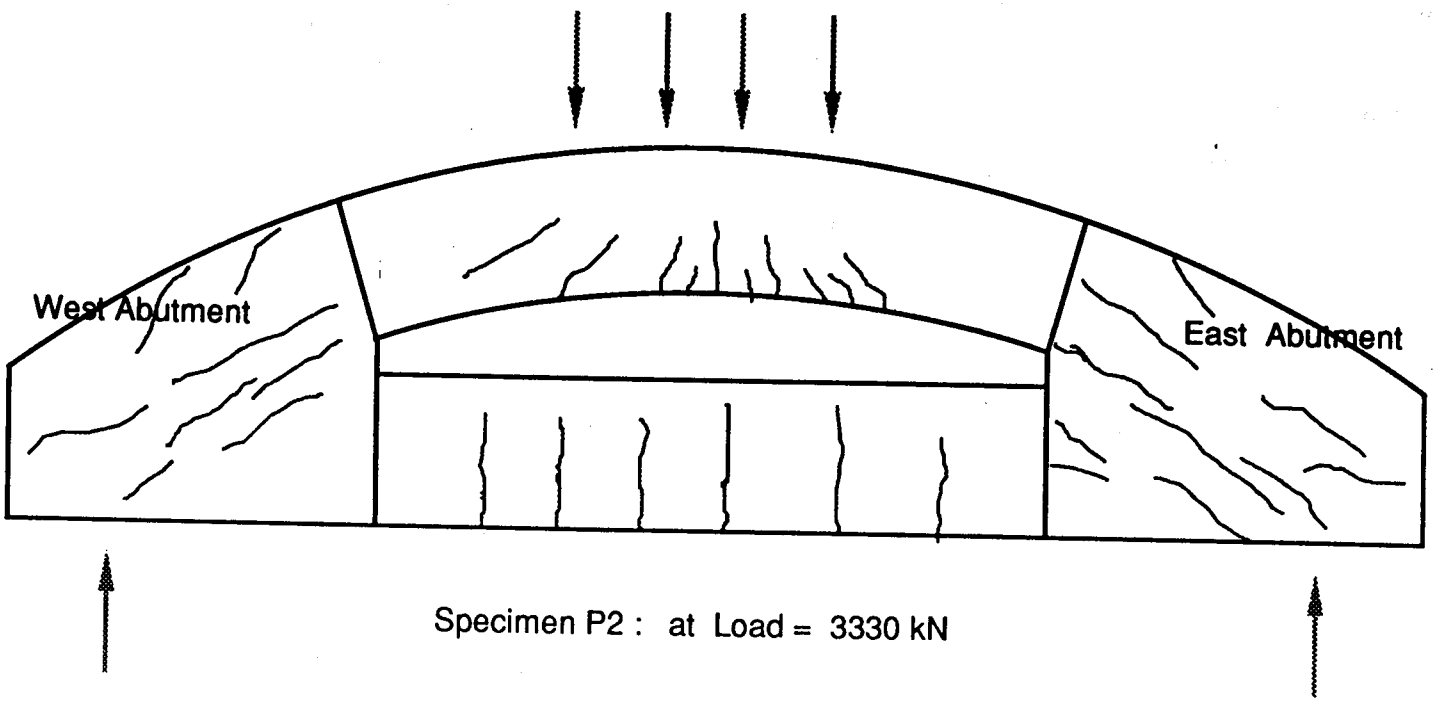

Figure 4.10 Flexural Cracking in Arch Due to Cracking of Prestressed Tie in Specimen P2

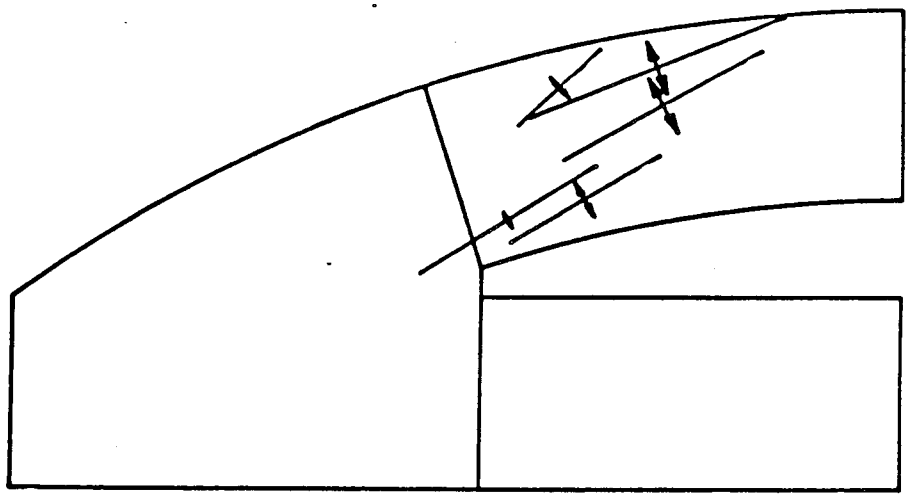

(a) 2 500 kN

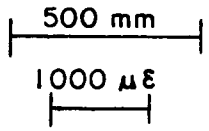

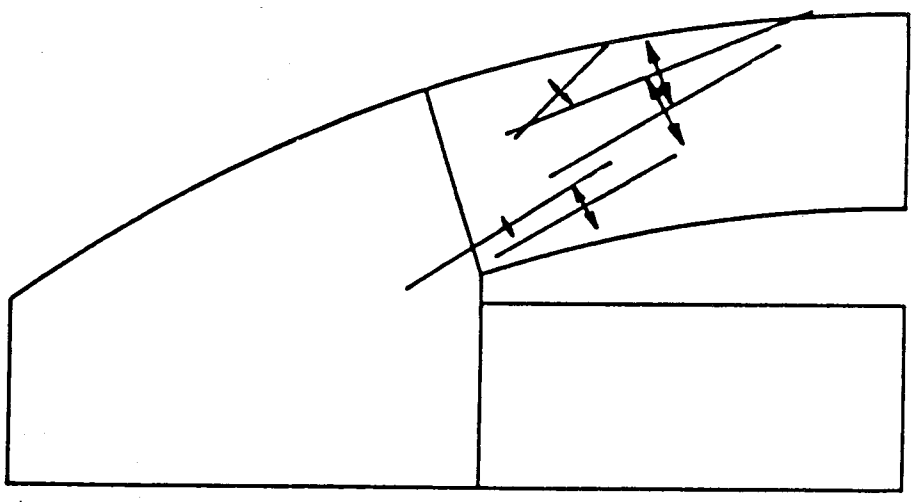

(b) 2 800 kN

Figure 4.11 Principal Strain Plots for Specimen P2

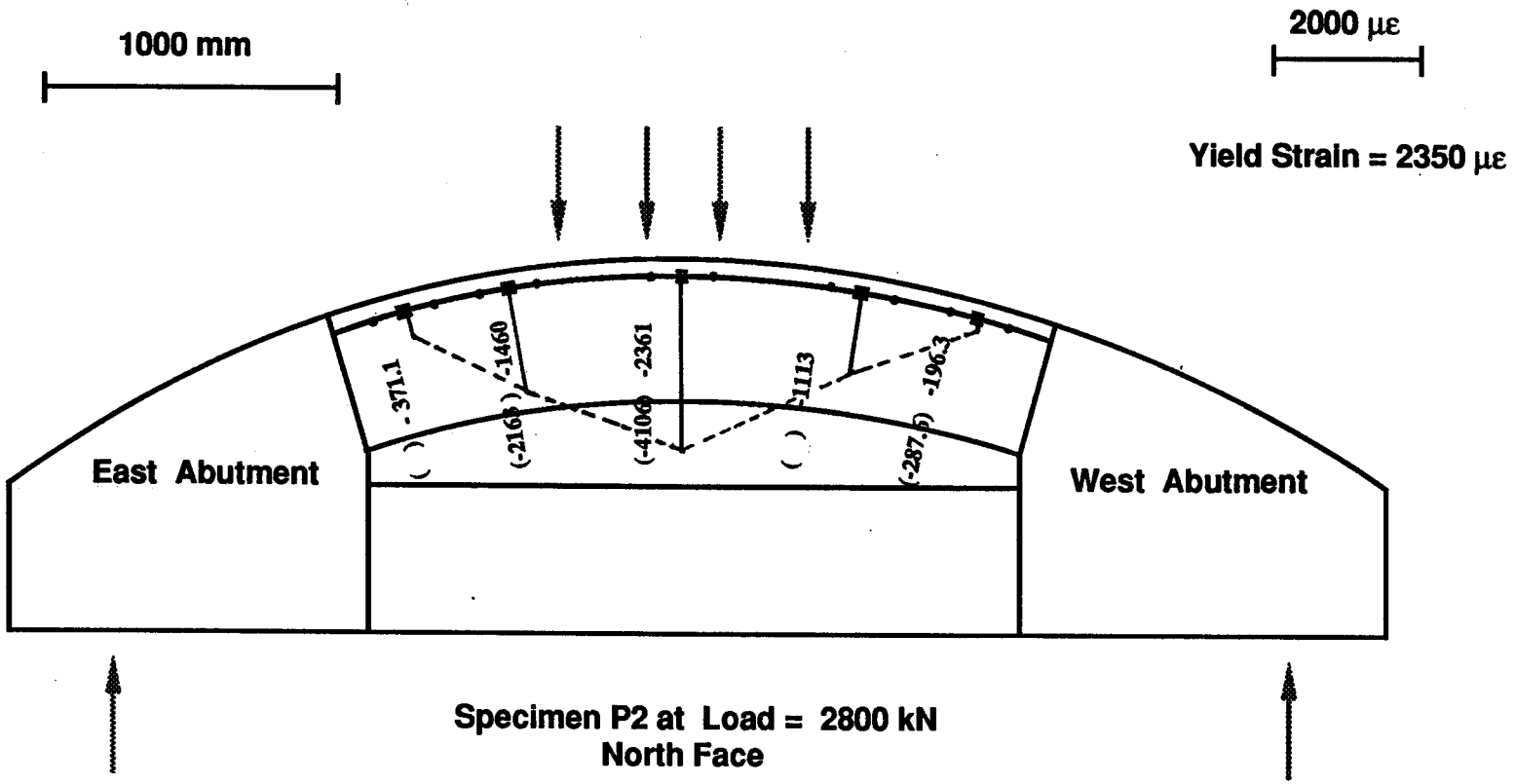

Figure 4.12 Measured Strain Distribution in Top Reinforcing Bars for Specimen P2

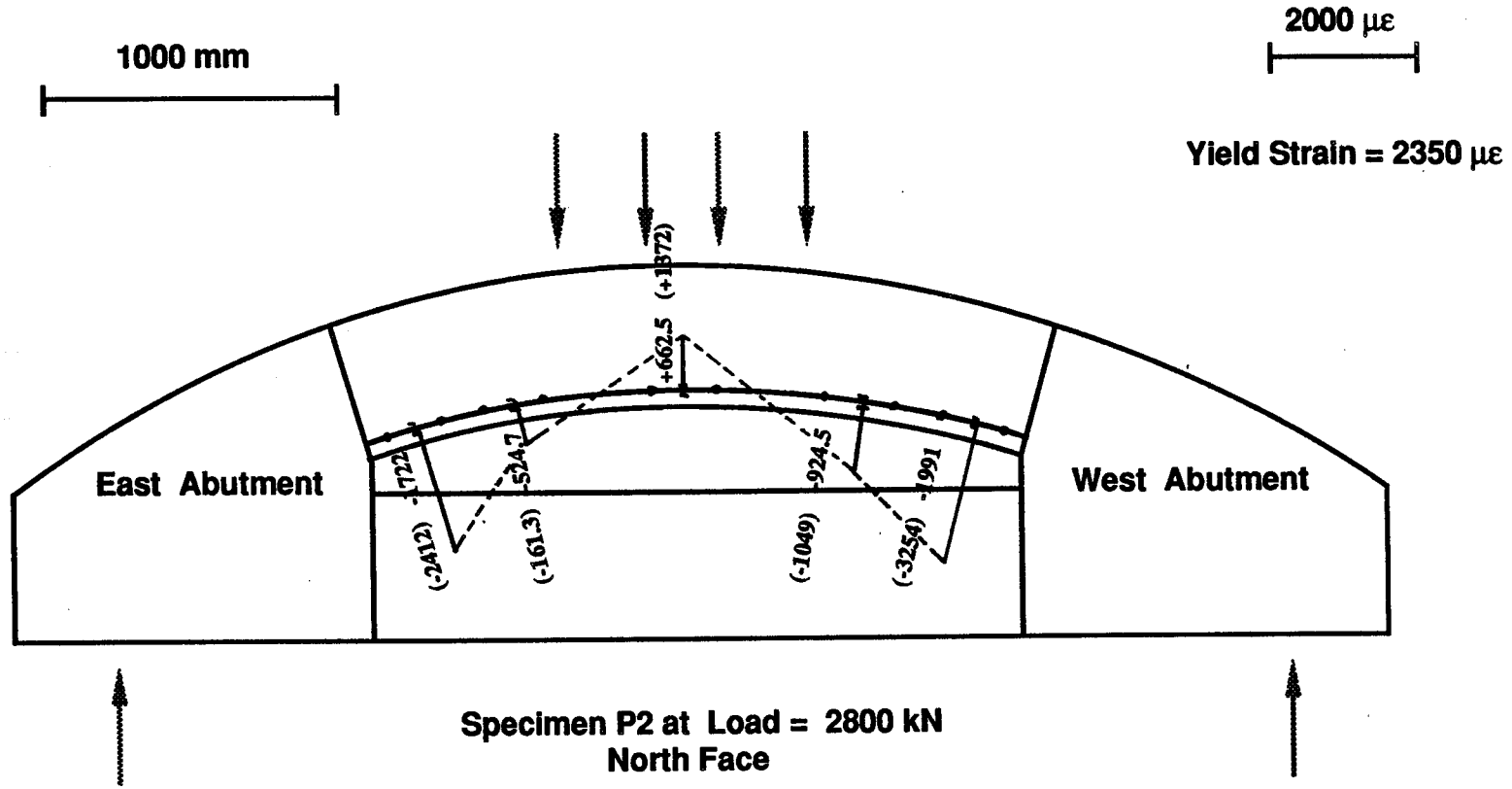

Figure 4.13 Measured Strain Distribution in Bottom Reinforcing Bars for Specimen P2

test; there was only a very small decompression in the tendons within the central region owing to the applied load.

4.3 V-Shaped Arch Specimens: A-Series

4.3.1 Failure Loads, Reactions, End-Forces and Moments

The measured ultimate loads, support reactions, and comments regarding the failure of each of the A-Series specimens are given in Table 4.2. Also shown are the average effective pressures applied to the specimen. For all specimens subjected to load condition I (four point loads) this value is obtained by dividing the applied load by the area 250 mm x 800 mm. For specimens A1 and A2 subjected also to load condition II (MTS platten only), the area is 250 mm x 400 mm. It is to be noted that these load intensities are well in excess of ice pressures. However, they may be within the range of other possible forms of impact on offshore structures such as ship impact (Brown and Perry, 1979, Brakel and Oostlander, 1979).

Referring to Table 4.2, it is seen that the failure load and mode of failure for all the specimens of this type was approximately the same. Also, as will be shown in Sect. 4.3.2, each specimen had approximately the same type of load-deflection response. For this reason, the test results for specimen A1 will be discussed in detail in Sect. 4.3.3 and the results of the remaining specimens will be presented in Sect. 4.3.4.

Table 4.2 Failure Loads and Description of Failure for A-Series V-Shaped Arch Specimens

Specimen	Failure Load (kN)	Effective Pressure (MPa)	Comments and Description of Failure
A1-I	6072 max.	30.4	Load Condition I. First crushing at 5700 kN at top of west strut (Fig. 4.17).
-II	6294	62.9	Load condition II. First crushing under applied load at 5500 kN. More crushing in west strut at 5700 kN. Explosive failure at 6294 kN (Fig 4.20).
A2-I	6003 max.	30.1	Load Condition I. First crushing at 5600 kN in west strut .
-II	6070	60.7	Load condition II. First crushing under MTS head at 5500 kN. Crushing under applied load continues until failure (Fig. 4.23 (a)).
A3	6202	31.1	First crushing at 5800 kN, halfway down on top surface of east strut. Failure of east strut at 6202 kN. (Fig. 4.23(b)).
A4	6385	31.9	First crushing in east strut at 5600 kN, vertical cracking under middle two load points. Explosive failure of east strut at 6385 kN (Fig. 4.24(a)).
A5	6057	30.3	First crushing at west strut at 5600 kN, east strut at 5700 kN. Explosive failure of west strut at 6057 kN. Bars buckled between ties.

In order to develop a strut-and-tie model to describe the load-carrying mechanism for this specimen subjected to a given loading, it is necessary to determine the forces and moments acting at the ends of the specimen at that particular applied load. These were determined from the measured loads, reactions, and strains in the steel beam.

The free-body diagram of a typical A-series specimen is shown in Fig. 4.14(a). The calculated shear forces acting at the west and east ends of the specimen are denoted V_{oW} and V_{oE}, respectively. Similarly the axial forces are denoted P_{oW} and P_{oE} and the moments are denoted M_{oW} and M_{oE}. In Fig. 4.14(b) are shown the free-body diagrams of the abutments, together with part of the steel beam. Shown on the steel beam are the forces and moments which can be determined from the electrical resistance strain gauge measurements and the known material and section properties of the steel beam. A total of 24 strain gauges were mounted on the steel beam on each side of center as shown in Fig. 4.15. The moment and axial force were determined at these two locations. Because the magnitudes of these forces and moments are quite sensitive to each strain gauge reading and because the distribution of strain across the cross-section is really three-dimensional, a least-squares regression analysis was performed to determine the best-fit plane describing the strain distribution. A computer program was written to do this and to determine the regression coefficient. If for a given load step, the regression coefficient was less than

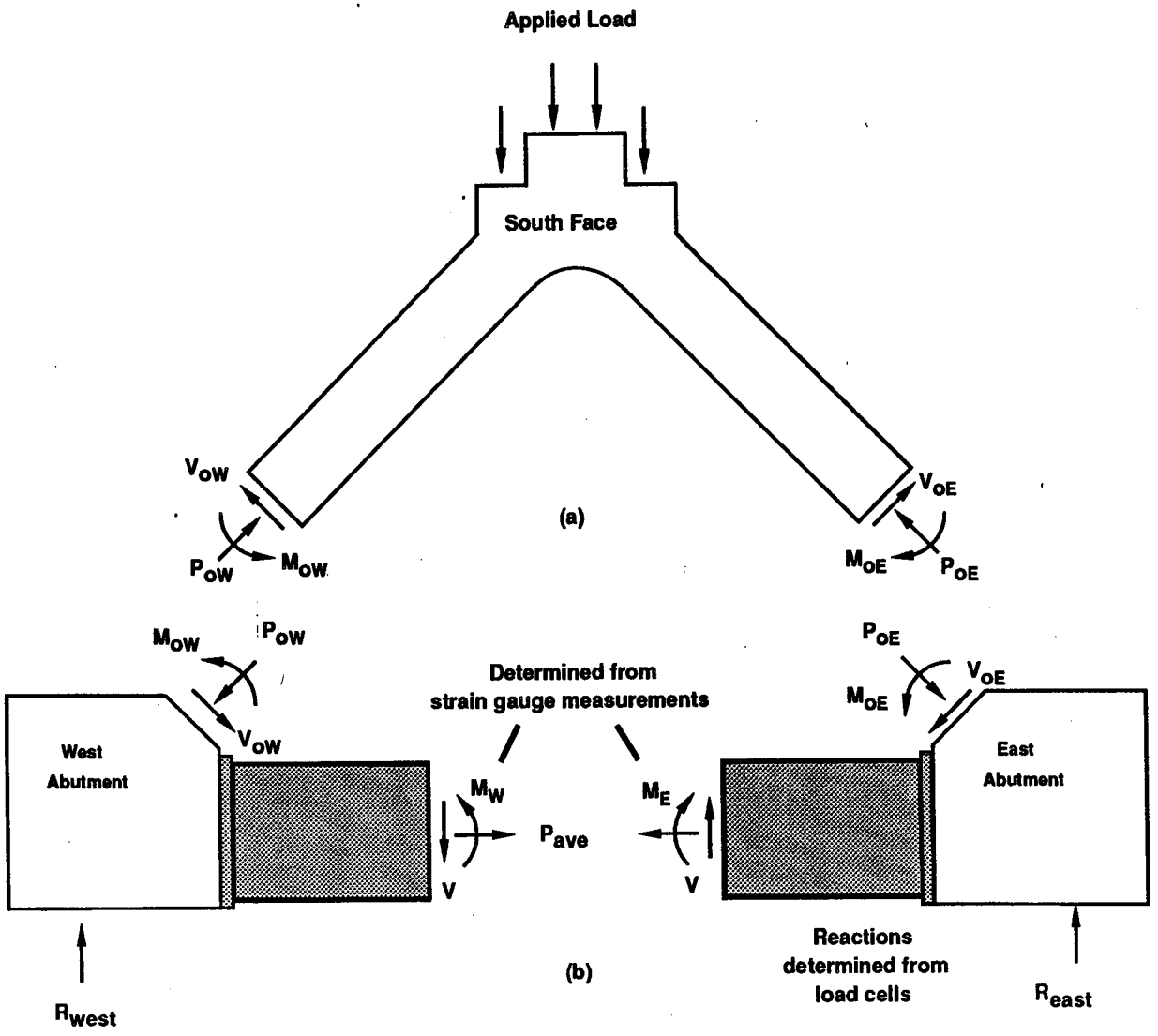

Figure 4.14 Free-Body Diagrams for Typical A-Series Specimens

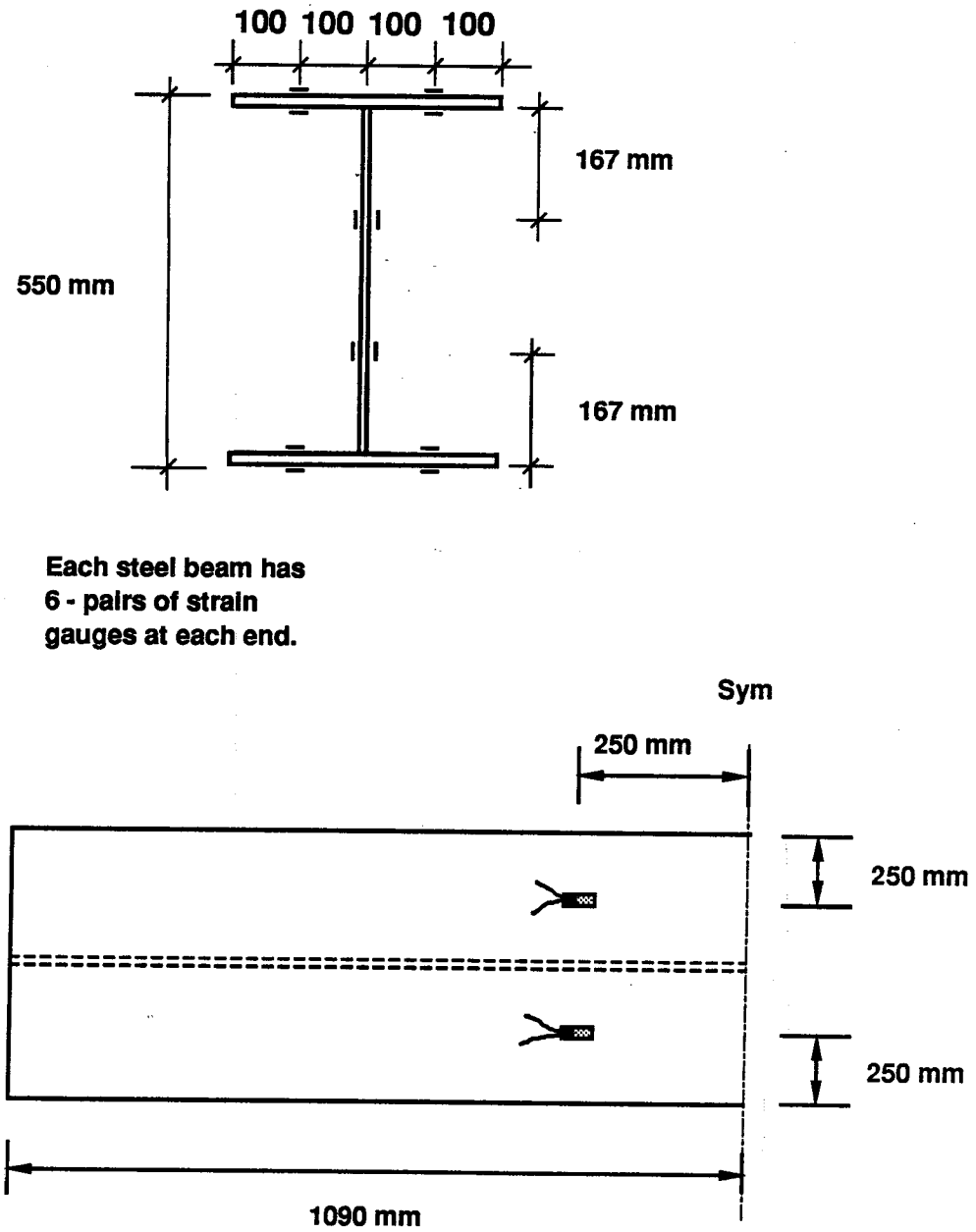

Figure 4.15 Arrangement of Strain Gauges on Steel Beam

0.99, the program would sample each reading to see if dropping any one channel would improve the regression. When it was necessary to drop one gauge, the regression coefficient was typically better than approximately 0.95 and usually the same gauge was found to be suspect for all readings in the test. After determining these forces and moments, the shear force acting in the steel beam could then be determined from the moments since the distance between the two points is known to be 500 mm. The axial force is taken to be the average of the forces determined at the two locations.

Since the reaction is known for each free-body diagram in Fig. 4.14(b), there are only three unknowns which can then be solved from the equations of static equilibrium. A listing of the computer program used to perform the above calculations is included in Appendix A.

Having determined the axial forces and moments acting at the ends of the specimen, a check on the overall equilibrium is performed. Vertical and horizontal equilibrium of the specimen is ensured since the average steel beam axial force was used and since the reactions sum to equal the applied load. Any unbalance in moment is distributed to the ends of the arch in proportion to the error.

The measured loads, reactions, and calculated end forces and moments for Specimen A1 are presented in Sect. 4.3.3. The results for the remaining specimens are discussed

in Sect. 4.3.4.

4.3.2 Load Deflection Response

The measured load-deflection curves for each of the A-Series specimens are shown in Fig. 4.16. The load values are those measured using the MTS pressure transducer. The deflection plotted is the deflection of the second load point although all four load points displaced approximately the same amount. The portion of the displacement due to support settlement has been subtracted from these values. For specimens A1 and A2, which were subjected to a second load condition, both load deflection curves are shown.

4.3.3 Test Results for Specimen A1

The ultimate load and failure mode for this specimen has been presented in Table 4.2. The load-deflection response was presented in Fig. 4.16. The method for determining the end forces and moments from the steel beam strains was discussed in Sect. 4.3.1. The results of this analysis for Specimen A1 for load cases I and II are shown in Tables 4.3 and 4.4 respectively. In the interest of brevity, the results for every second load step are given in the table. The definitions of each of the terms may be seen in Fig. 4.14. Results for the important load steps referred to in various parts of this thesis are shown in bold type.

Under load condition I, Specimen A1 was undamaged until an applied load of 5700 kN was reached. This corresponds to

Table 4.3 Measured Loads Reactions and Calculated End-Forces for Specimen A1 (Load Condition I)

SPECIMEN A1 (Load Condition I)				ANALYSIS FOR ARCH ENDS						
					WEST				EAST	
Load (kN)	Rwest (kN)	Reast (kN)		Po (kN)	Mo (kNm)	Vo (kN)		Po (kN)	Mo (kNm)	Vo (kN)
194.78	96.98	97.8		130.05	-9.96	2.45		135.28	-2.39	7.68
392.35	195.08	197.26		263.76	-18.17	3.45		273.98	-4.34	13.67
596.56	296.57	299.99		399.29	-27.71	5.61		416.22	-4.5	22.54
783.95	389.61	394.34		524.42	-33.12	8.24		546.1	-3.93	29.92
997.6	495.93	501.67		665.94	-38.36	14.51		690.9	-5.28	39.47
1179.96	587.18	592.78		786.22	-46.98	13.05		821.31	3.63	48.14
1387.42	690.5	696.92		922.19	-48.7	23.37		957.69	1.24	58.86
1774.86	883.99	890.87		1181.73	-48.86	35.8		1219.21	3.71	73.29
2161.45	1077.07	1084.38		1445.9	-42.98	45.41		1482.97	8.19	82.48
2575.59	1283.68	1291.91		1725.13	-37.23	59.19		1762.03	12.11	96.1
2958.74	1475.21	1483.53		1987.41	-28.45	70.45		2021.7	16.3	104.74
3358.54	1674.67	1683.87		2242.22	-43.11	85.73		2289.12	21.72	132.63
3741.69	1866.57	1875.12		2504.94	-35.66	96.17		2549.61	26.42	140.84
3956.59	1967.78	1988.8		2648.52	-31.62	92.68		2705.06	30.12	149.21
4459.68	2217.59	2242.09		2986.92	-29.03	105.15		3048.32	35.28	166.56
4741.21	2357.08	2384.13		3222.28	26.52	99.79		3252.76	33.86	130.27
4969.43	2470.01	2499.42		3386.02	34.28	96.71		3417.22	38.95	127.91
5047.61	**2506.03**	**2541.58**		**3450.63**	**45.93**	**86.02**		**3483.19**	**42.8**	**118.57**
5287.57	2625.52	2662.05		3611.48	42.84	93.93		3644.95	39.66	127.41
5495.86	2729.22	2766.64		3748.72	37.99	102.12		3784.05	36.49	137.45
5664.17	**2814.53**	**2849.64**		**3888.39**	**53.92**	**87.45**		**3917.73**	**46.02**	**116.79**
5784.14	2874.27	2909.88		3972.93	54.47	88.39		4001.63	44.66	117.09
5987.45	2975.49	3011.96		4112.17	54.58	95.95		4137.82	38.15	121.6
6072.43	**3018.53**	**3053.9**		**4176.32**	**57.91**	**95.28**		**4198.59**	**37.52**	**117.54**

Table 4.4 Measured Loads Reactions and Calculated End-Forces for Specimen A1 (Load Condition II)

SPECIMEN A1 (Load Condition II)				ANALYSIS FOR ARCH ENDS						
					WEST				EAST	
Load (kN)	Rwest (kN)	Reast (kN)		Po (kN)	Mo (kNm)	Vo (kN)		Po (kN)	Mo (kNm)	Vo (kN)
447.93	221.4	226.53		461.56	114.24	-132.31		449.05	84.44	-144.83
961.37	479.51	481.85		811.09	99.17	-124.54		804.33	83.78	-131.3
1478.99	739.37	739.62		1152.44	83.95	-107.21		1153.02	84.51	-106.63
1968.61	985.38	983.23		1478.01	79.23	-87.48		1479.5	85.31	-85.99
2483.97	1243.86	1240.11		1818.5	78.06	-62.95		1819.39	85.77	-62.07
2948.74	1477.14	1471.6		2133	86.9	-40.16		2125.24	82.81	-47.92
3463.49	1735.98	1727.51		2483.42	95.69	-15.83		2464.9	78.08	-34.35
3978.25	1993.76	1984.49		2829.16	98.93	7.53		2805.52	73.89	-16.11
4461.34	2234.37	2226.97		3149.06	94.71	29.18		3125.47	66.7	5.59
4927.79	2466.67	2461.12		3461.38	89.68	45.67		3438.81	60.33	23.09
5424.21	2713.19	2711.03		3792.55	82.05	61.78		3773.72	53.51	42.96
5972.29	2984.7	2987.59		4163.76	76.22	75.58		4147.48	43.69	59.29
6173.86	3080.7	3093.17		4308.63	78.08	63.87		4301.72	45.71	56.95
6060.57	3022.81	3037.76		4240.23	82.68	49.54		4235.94	50.7	45.25
6140.54	3061.2	3079.34		4295.68	81.62	49.25		4292.77	46.72	46.34
6162.19	3070.53	3091.66		4308.45	79.81	49.75		4307.58	43.45	48.88
6245.48	3111.29	3134.19		4360.65	76.21	55.5		4360.73	38.55	55.58
6257.15	3117.1	3140.05		4367.25	74.31	56.59		4367.89	37.53	57.22
6268.81	3122.17	3146.64		4377.19	74.09	52.78		4379.94	38.41	55.53
6293.8	3133.89	3159.91		4396.43	76.79	53.09		4397.3	35.34	53.96
6290.46	3131.5	3158.97		4395.58	76.63	49.84		4398.19	35.76	52.45

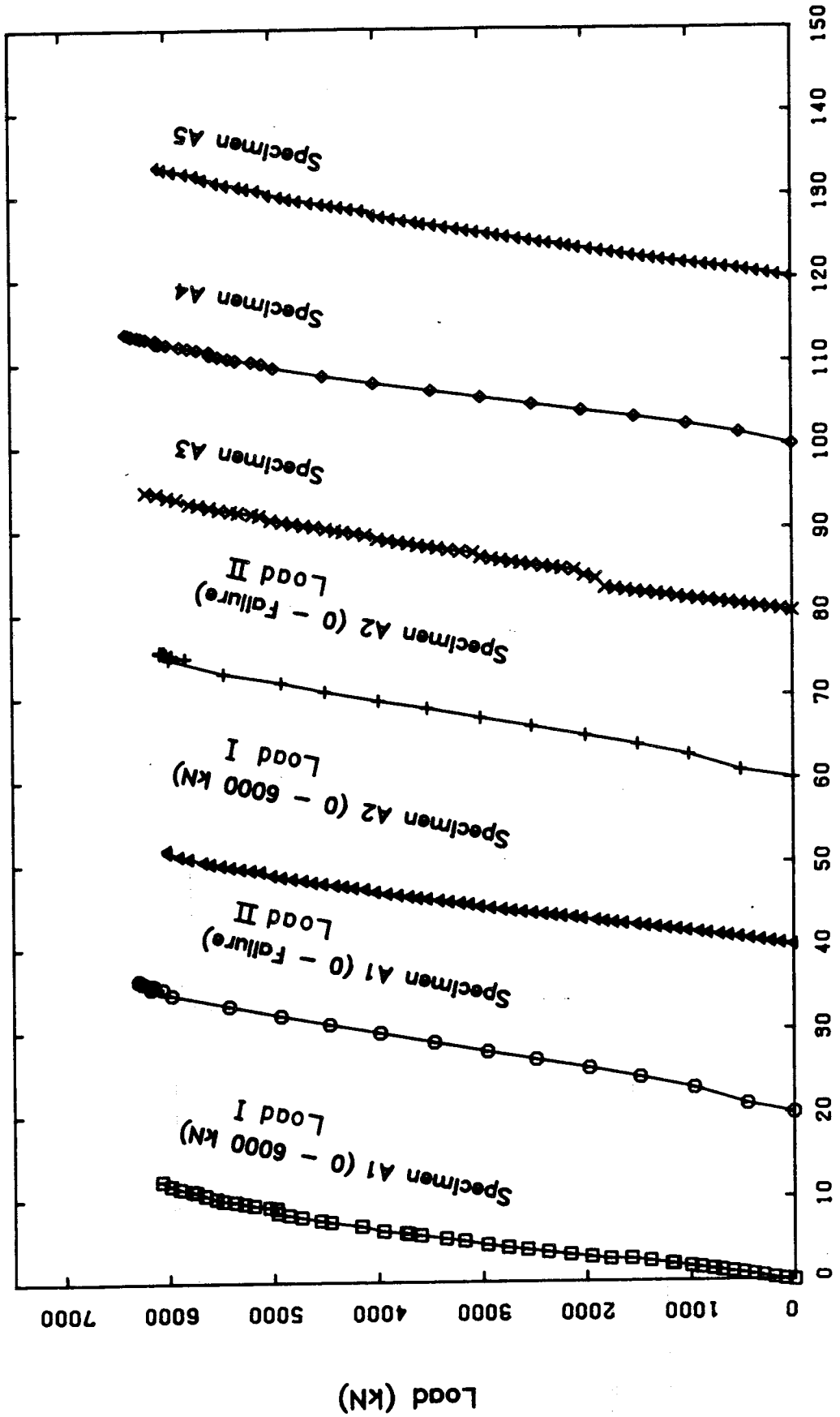

Figure 4.16 Load vs. Midspan Displacement for A-Series Specimens

an average load intensity of 28.5 MPa on the 250 mm x 800 mm area. At this load, crushing was observed at the top of the west strut near the first load point. Cracking and spalling were observed on all three faces of the specimen in this region as shown in Fig. 4.17. These cracks were approximately parallel and were oriented with the principal compressive strain trajectory. This type of distress was typical of all A-Series specimens. As the load was increased, more crushing was observed at this point and further down the strut.

In Fig. 4.18, the measured principal strains are shown plotted on the specimen. These were taken at an applied load of 5000 kN. Using the same criteria as for the circular arch specimens, strain rosettes which gave principal strains with standard deviations in excess of about 10% of the mean principal strain were omitted in this plot. The orientation of the principal strains was consistent throughout the test. The principal compression strains were more or less parallel with the legs of the arch with larger values observed at the lower inside rosette (rosette 2 in Fig. 4.18) and at the upper outside rosette (rosette 7). This suggests the presence of bending in this region. For safety reasons, an abbreviated set of concrete strain readings were taken at an applied load of 5700 kN. These principal strains are shown in Fig. 4.19. The results are seen to be similar in orientation to those taken at the lower load. As will be shown in Chapter 6, the load carrying mechanism for this

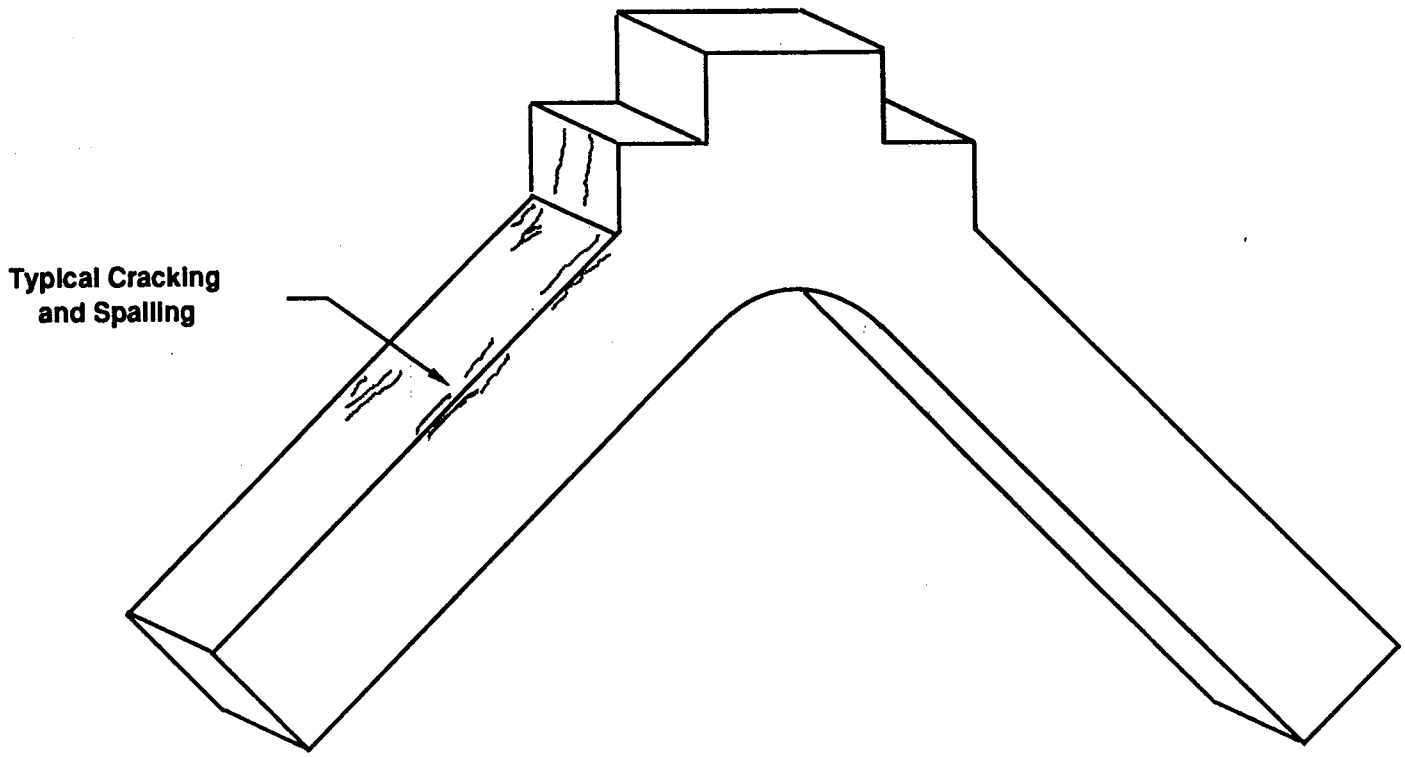

Figure 4.17 Typical Cracking and Spalling for A-Series Specimens

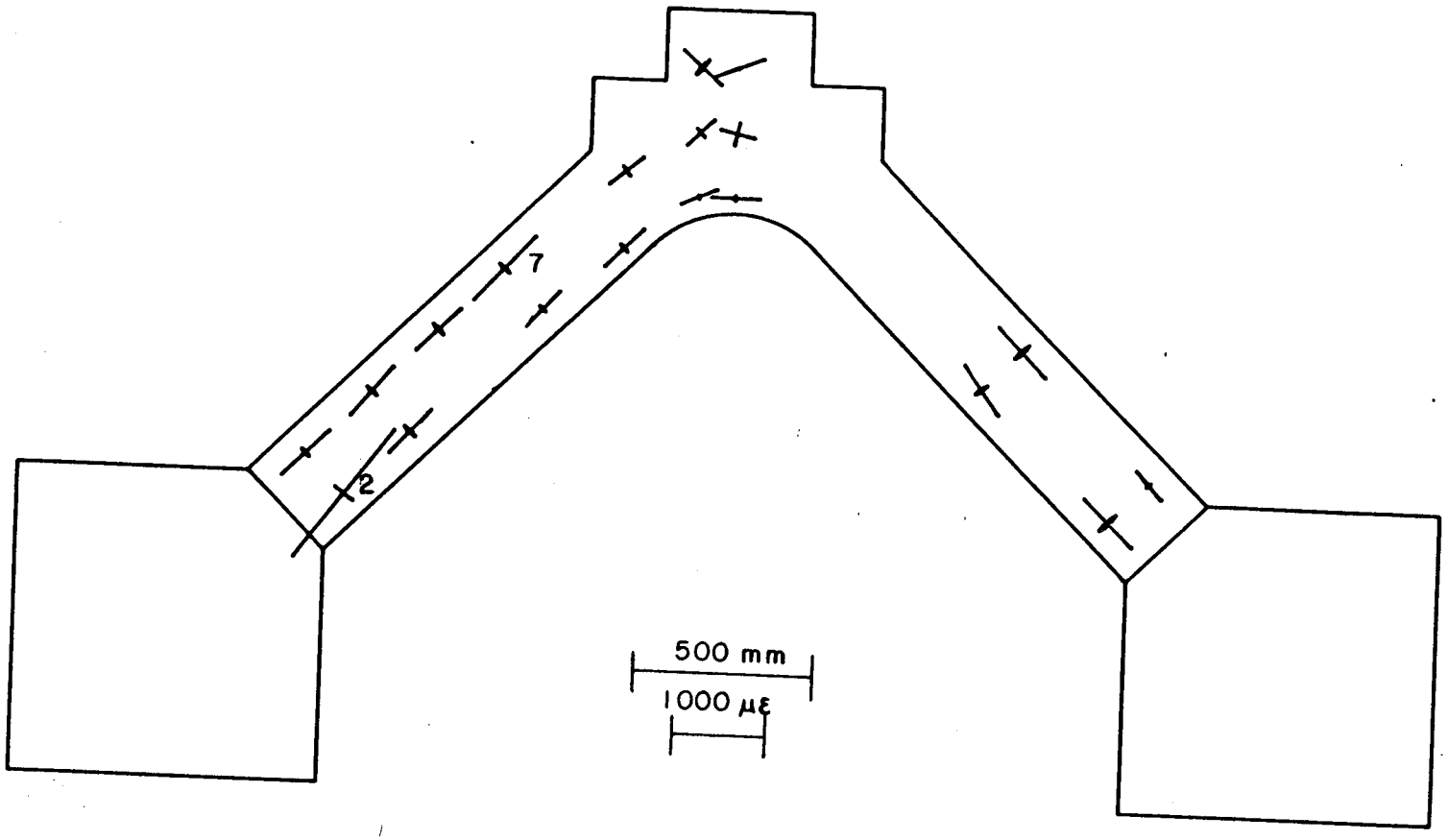

Figure 4.18 Principal Strain Plot for Specimen A1 at 5000 kN (Load Condition I)

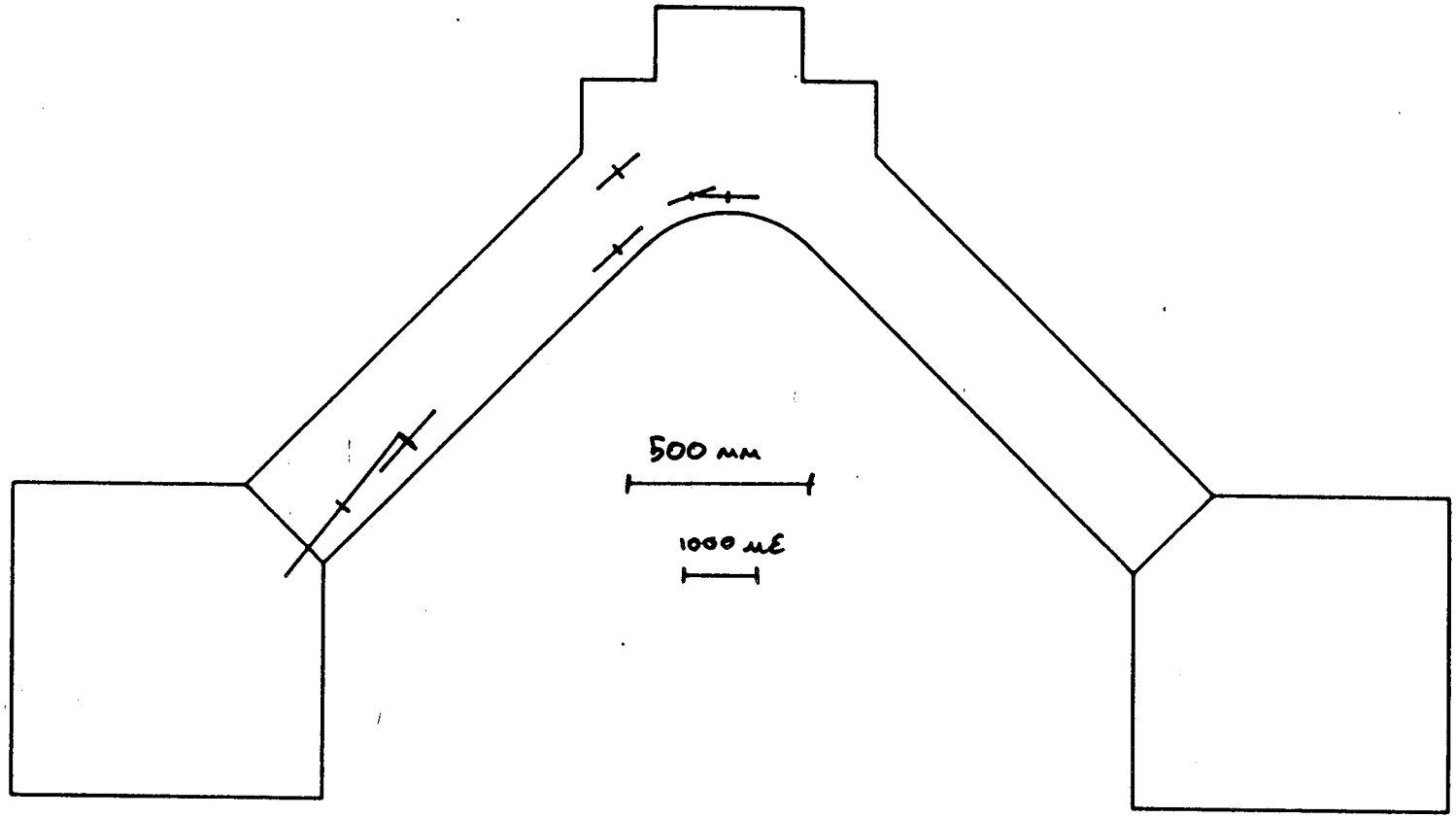

Figure 4.19 Principal Strain Plot for Specimen A1 at 5700 kN (Load Condition II)

structure subjected to this loading involves approximately uniaxial compression in the two struts.

After an applied load of 6000 kN (or 30.0 MPa), the specimen was unloaded, the load application devices were removed, and the specimen was loaded to failure using the platten of the testing machine. Under load condition II, the first signs of crushing were observed under the applied load at 5500 kN. This corresponds to an average intensity of 55.0 MPa on the 250 mm x 400 mm area. Further signs of crushing on the west strut were observed at 5700 kN. Failure was abrupt and explosive and occurred at an applied load of 6294 kN (or 62.9 MPa). The failure occurred at the top of the two struts as shown in Fig. 4.20. After failure, the specimen was loaded again and as the load was applied the top of the specimen pushed through in planes defined by vertical sections on each side of the loaded region. Since the tops of each of the two struts had crushed, little resistance was provided. The load required to do this was approximately 1000 kN.

The measured strains in the longitudinal reinforcement at an applied load of 5664 kN under load condition I are shown plotted at the appropriate locations on the top and bottom reinforcement in Figs. 4.21 and 4.22, respectively. Values are plotted at this load since this is the last load at which manual readings were taken and since a detailed strut-and-tie model is developed for this load. In this figure, all strains are compressive and are shown plotted

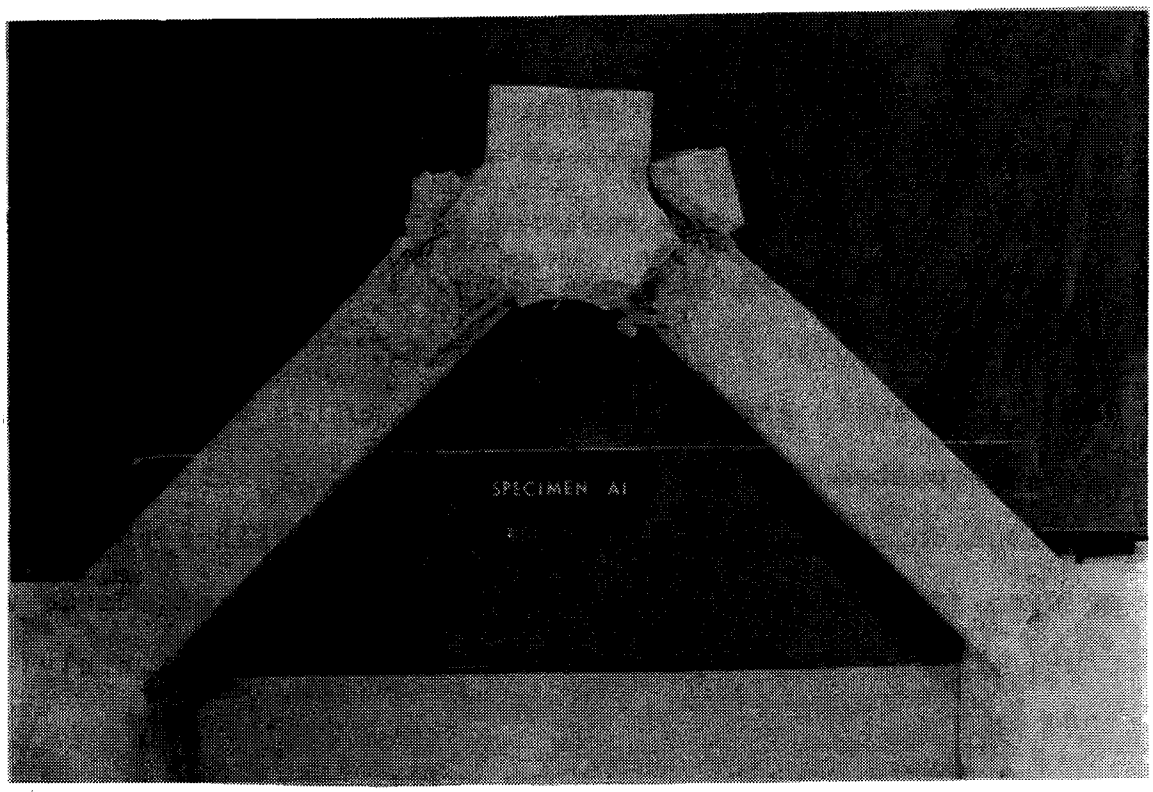

Figure 4.20 Failure Mode for Specimen A1

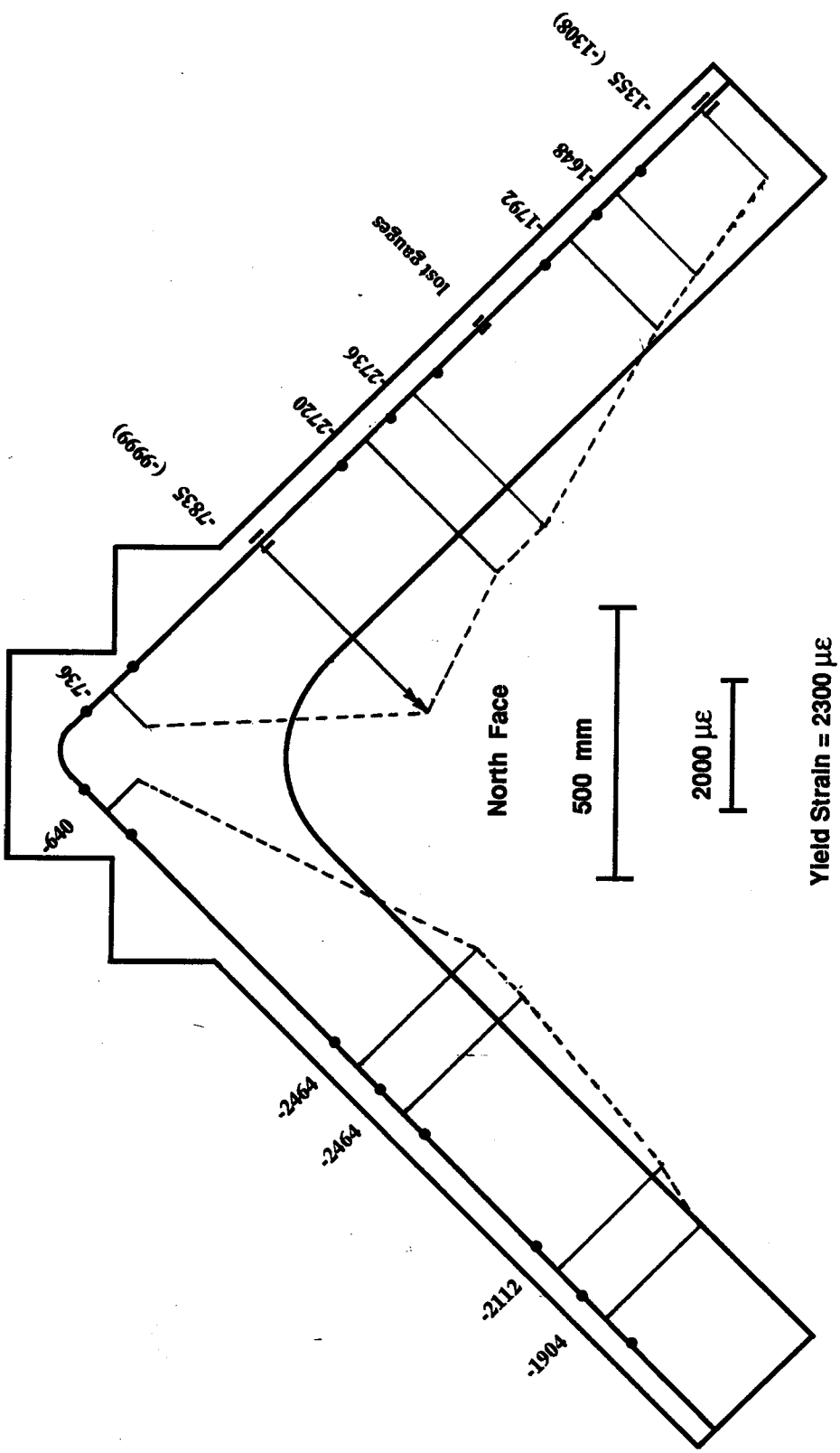

Figure 4.21 Measured Strain Distribution in Top Reinforcing Bars for Specimen A1

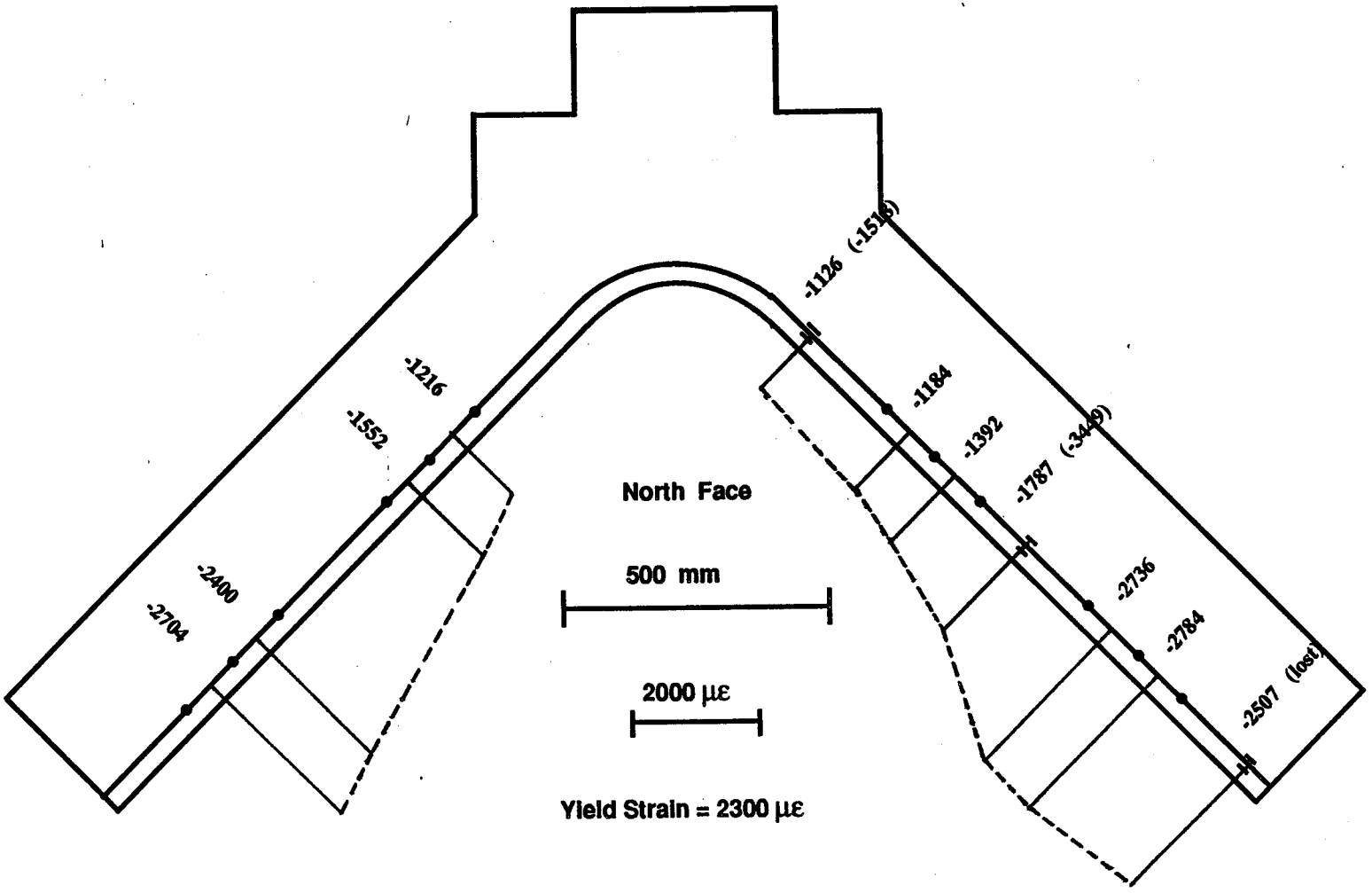

Values in ( ) are taken at ultimate load = 6294 kN

Figure 4.22 Measured Strain Distribution in Bottom Reinforcing Bars for Specimen A1

above the bar. Scales are as indicated on the drawing. At the locations where electrical resistance strain gauges were mounted and readings could be recorded automatically, the strain measurements at the ultimate load (6294 kN) are shown as indicated in brackets ( ).

It is observed that the top 15M bars reached the yield strain in compression at the upper end of the strut. Also, the bottom bars were yielding in compression at the lower end of the strut. The 6 mm stirrups did not reach yield at any location.

4.3.4 Test Results for Specimens A2-A5

The measured ultimate loads, support reactions, and comments regarding the failure of each of these specimens were presented in Table 4.2. The load-deflection response of these specimens was presented in Sect. 4.3.2. Specimen A2 was loaded with load condition I and II. Specimens A3-A5 were loaded to failure using the load application rollers (load condition I). For each specimen, the measured forces and moments in the steel beam and the calculated forces and moments acting at the ends of the specimen were determined as described in Sect. 4.3.1. As stated in Sect. 3.2.2.2 there was a noticable shift in the calculated end forces and moments for the specimens which had one set of rollers removed. It was decided that these calculated forces are likely not reliable. In any case the overall behavior of these specimens was such that Specimen A1 can be taken to be

representative of the A-series specimens.

As suggested above, Specimens A1-A5 exhibited similar behavior in terms of failure load, type of failure, and load-deflection response. In addition, the measured concrete strains in all of the A-Series specimens were similar. For this reason it was thought unnecessary to show the principal strain plots. Photographs of the failure modes for these specimens are shown in Figs. 4.23 and 4.24.

The measured strains in the top and bottom bars for Specimens A2 to A5 are shown in Figs. 4.25 to 4.32. The general distribution of the strains is analogous to that of Specimen A1. As in the case of Specimen A1, the 6 mm stirrups did not reach yield at any location.

4.4 V-Shaped Arch Specimens: B-Series

4.4.1 Failure Loads, Reactions, End-Forces, and Moments

The measured ultimate loads and comments regarding the failure modes of Specimens B1 and B2 are given in Table 4.5. These specimens were loaded through the same load application system as the A-Series specimens. The nominal area under the applied load is 250 mm x 800 mm. The average effective pressures given in Table 4.5 are determined by dividing the ultimate load by this area. It is noted that these pressures are within the range of ice pressures anticipated on offshore structures subjected to high magnitude concentrated patch loads.

Table 4.5 Failure Loads and Description of Failure for Specimens B1 and B2

Specimen	Failure Load (kN)	Effective Pressure (MPa)	Comments and Description of Failure
B1	964.4 (max. load)	4.82	First flexural cracks observed at midspan at 150 kN (or 0.75 MPa). First diagonal cracks at 300 kN (or 1.5 MPa). Load carried by "fan action" and by "direct strut action" or "arching action" (see Figs. 4.34 and 4.35). Crushing observed at the inside soffit of the vertical leg at 840 kN (or 4.2 MPa). Carried max. load in ductile failure mode.
B2	774.7	3.87	First flexural cracks observed at midspan at 150 kN (or 0.75 MPa). First diagonal cracks at 300 kN (or 1.5 MPa). Load carried by "fan action" and by "direct strut action" or "arching action" (see Figs. 4.34 and 4.35). Failure of diagonal in west shear span at 762.9 kN. Load reduced, as more load applied stirrups failed. Crushing observed at the inside soffit of the vertical leg after peak load.

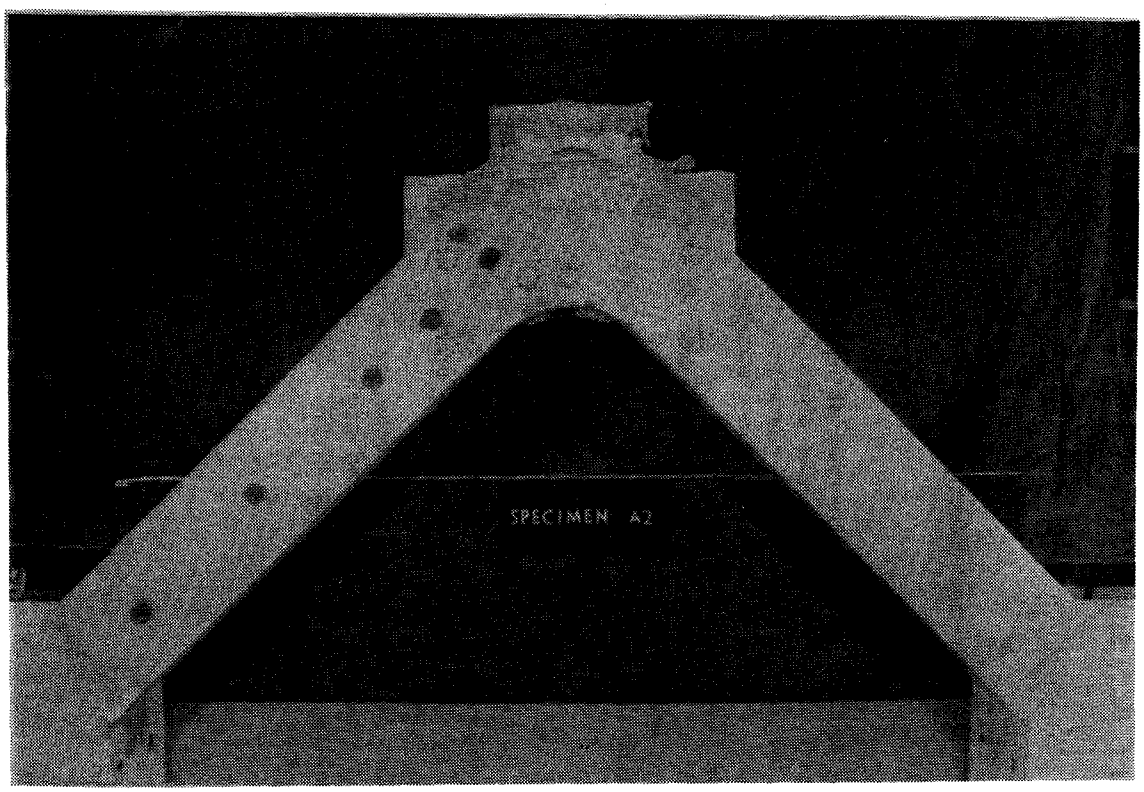

a

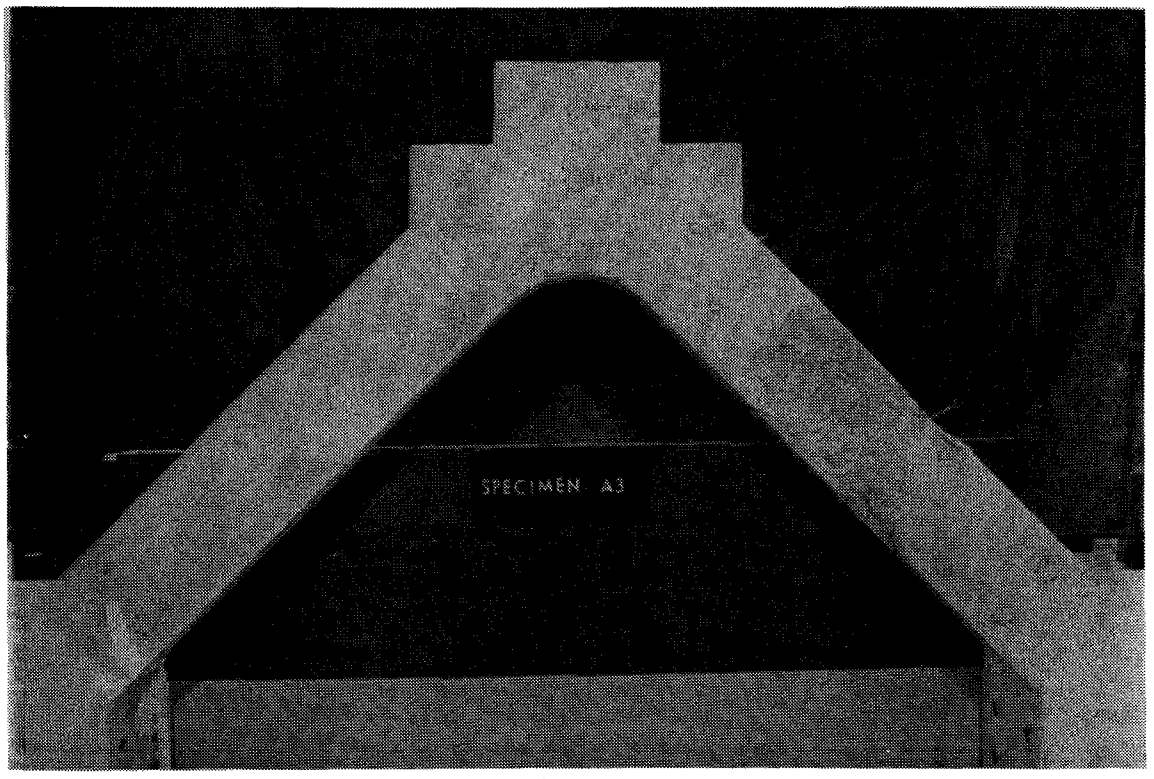

b

Figure 4.23 Failure Modes for Specimens A2 and A3

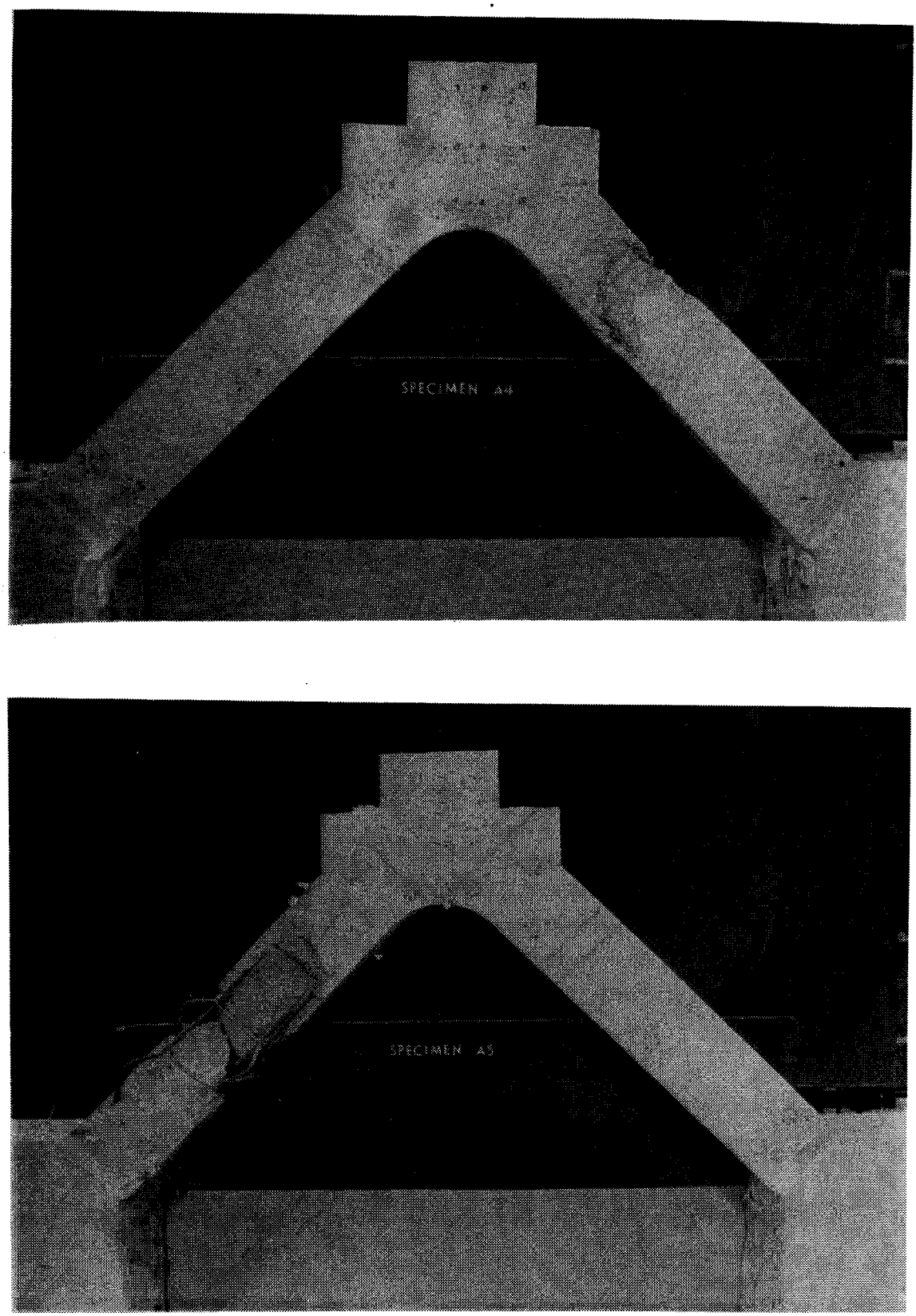

Figure 4.24 Failure Modes for Specimens A4 and A5

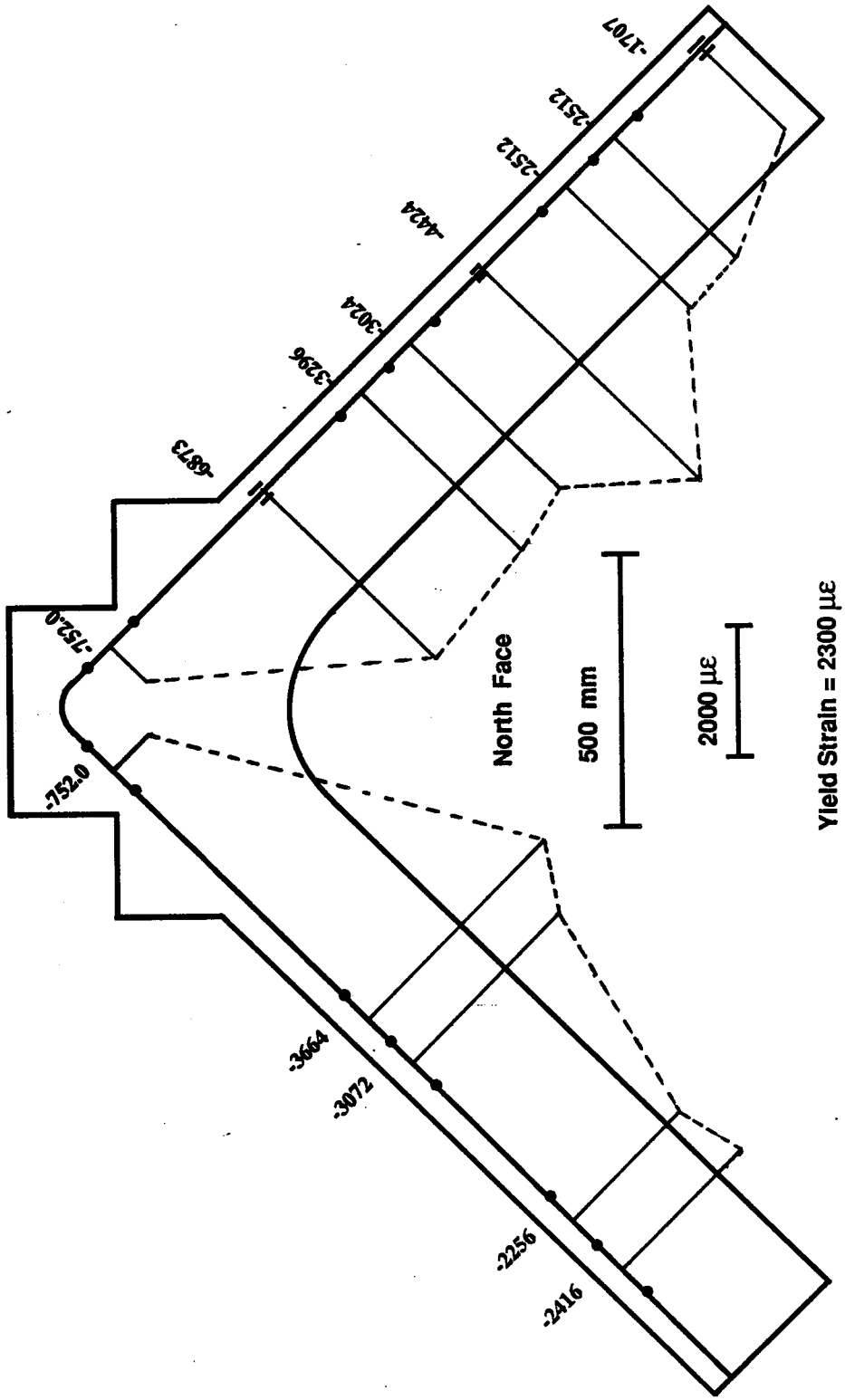

Figure 4.25 Measured Strain Distribution in Top Reinforcing Bars for Specimen A2

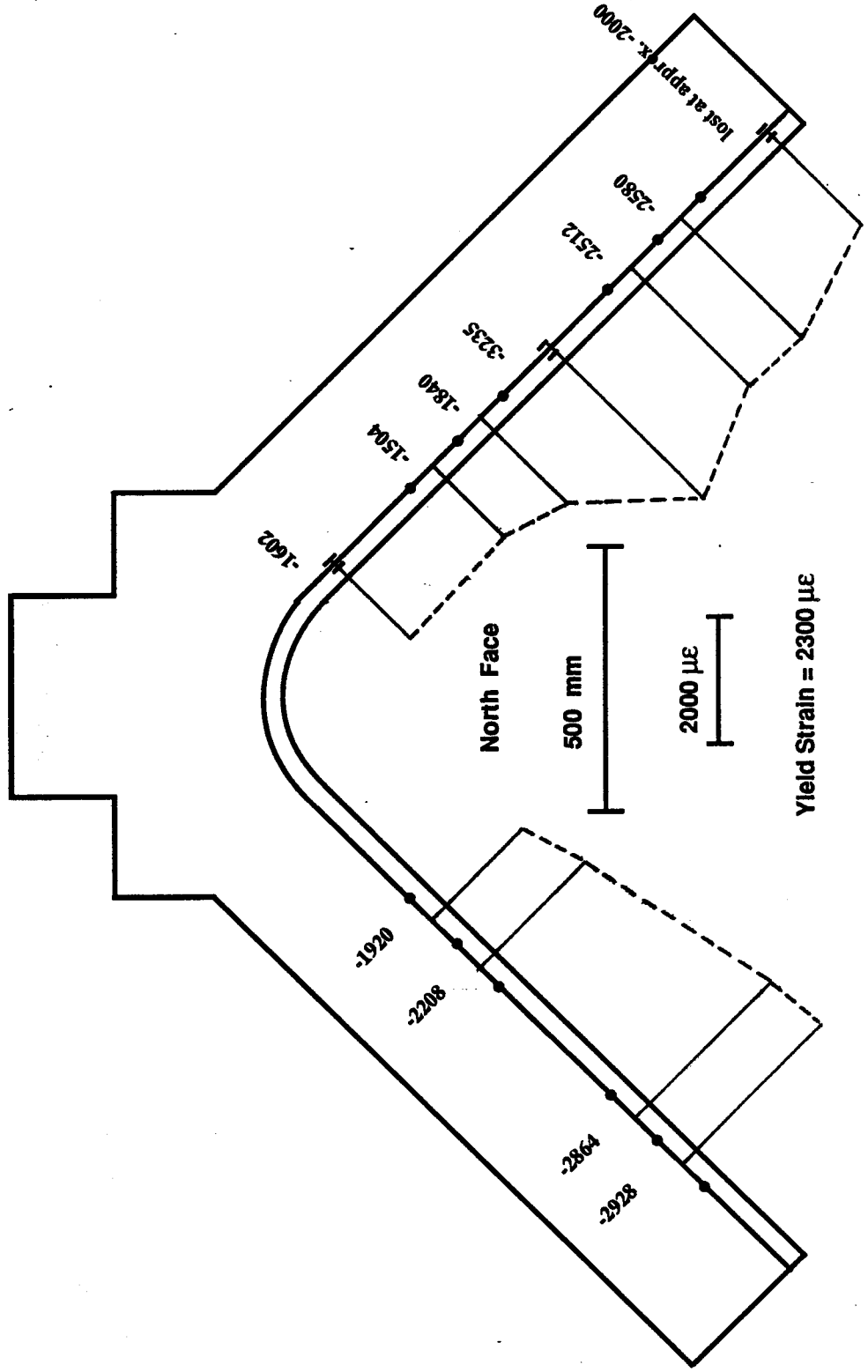

Figure 4.26 Measured Strain Distribution in Bottom Reinforcing Bars for Specimen A2

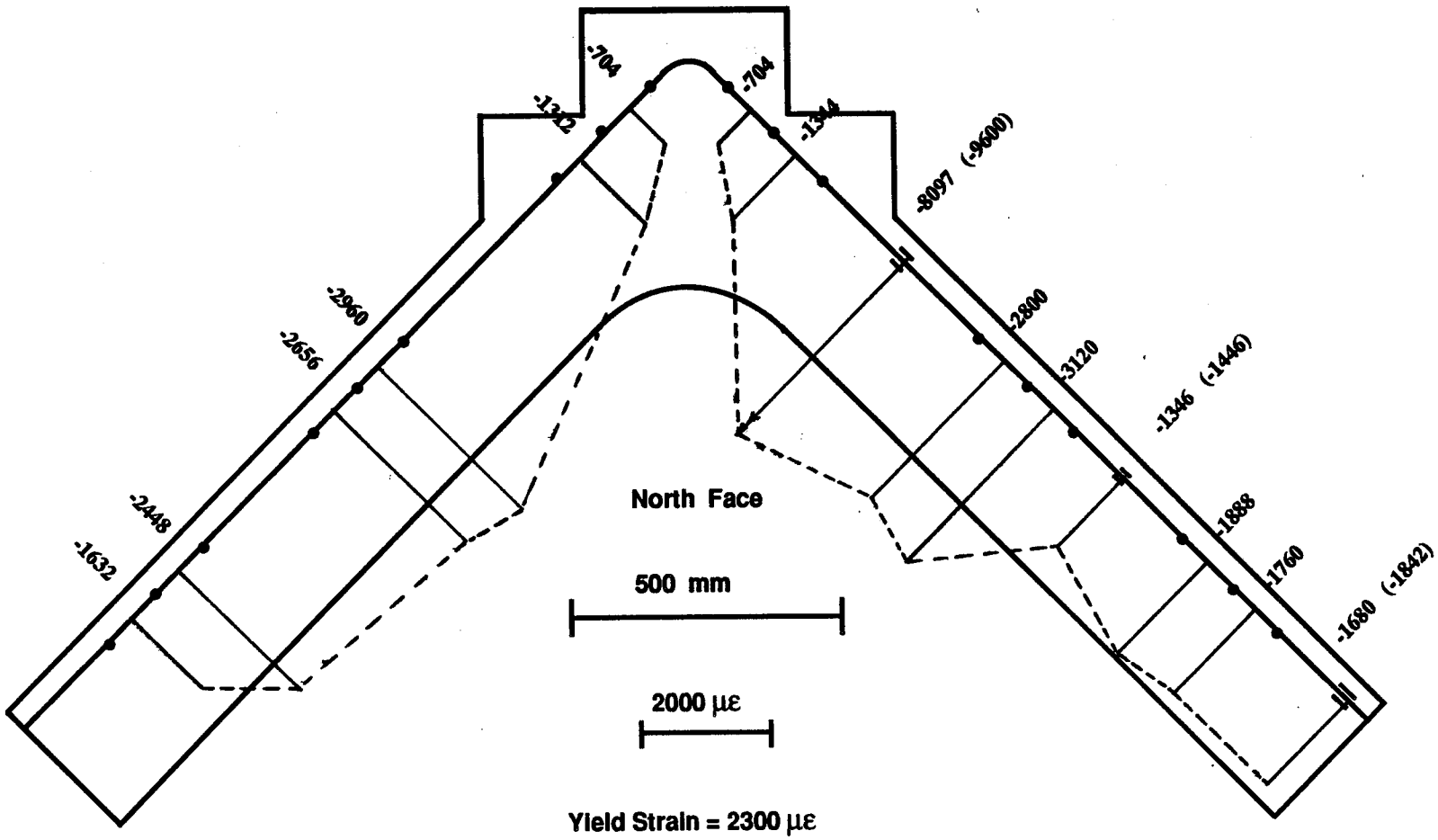

Values in ( ) are taken at ultimate load = 6202 kN

Figure 4.27 Measured Strain Distribution in Top Reinforcing Bars for Specimen A3

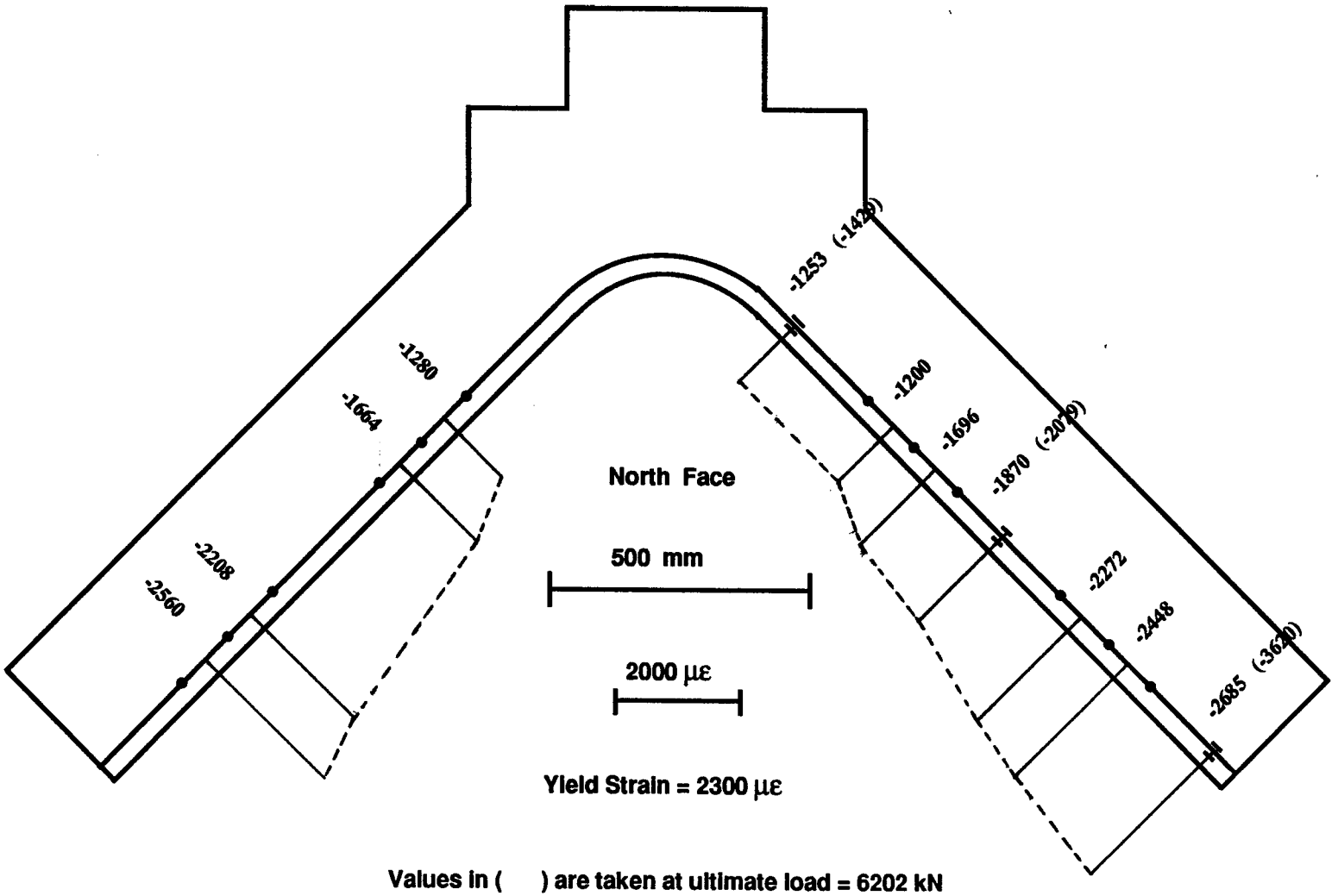

Figure 4.28 Measured Strain Distribution in Bottom Reinforcing Bars for Specimen A3

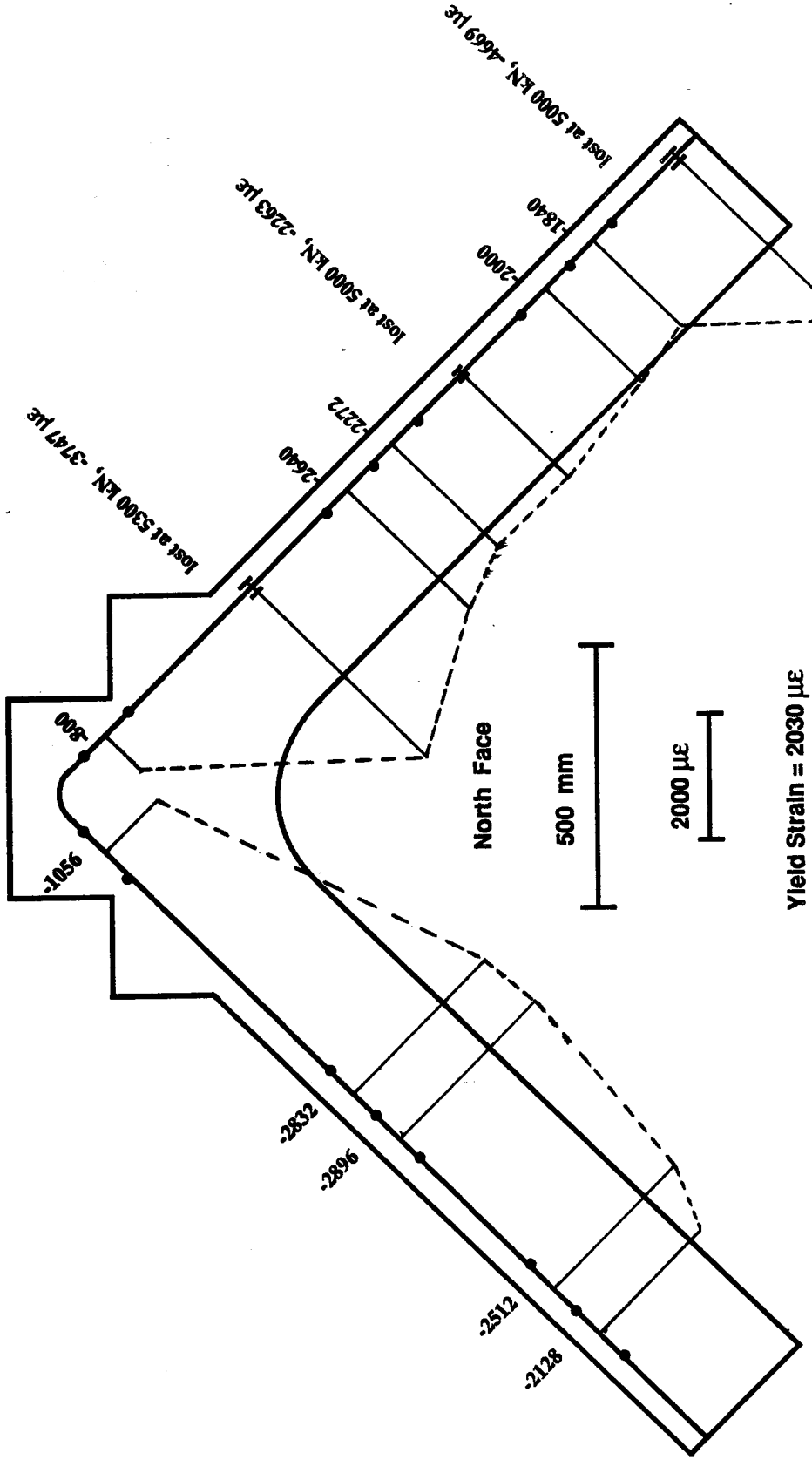

Figure 4.29 Measured Strain Distribution in Top Reinforcing Bars for Specimen A4

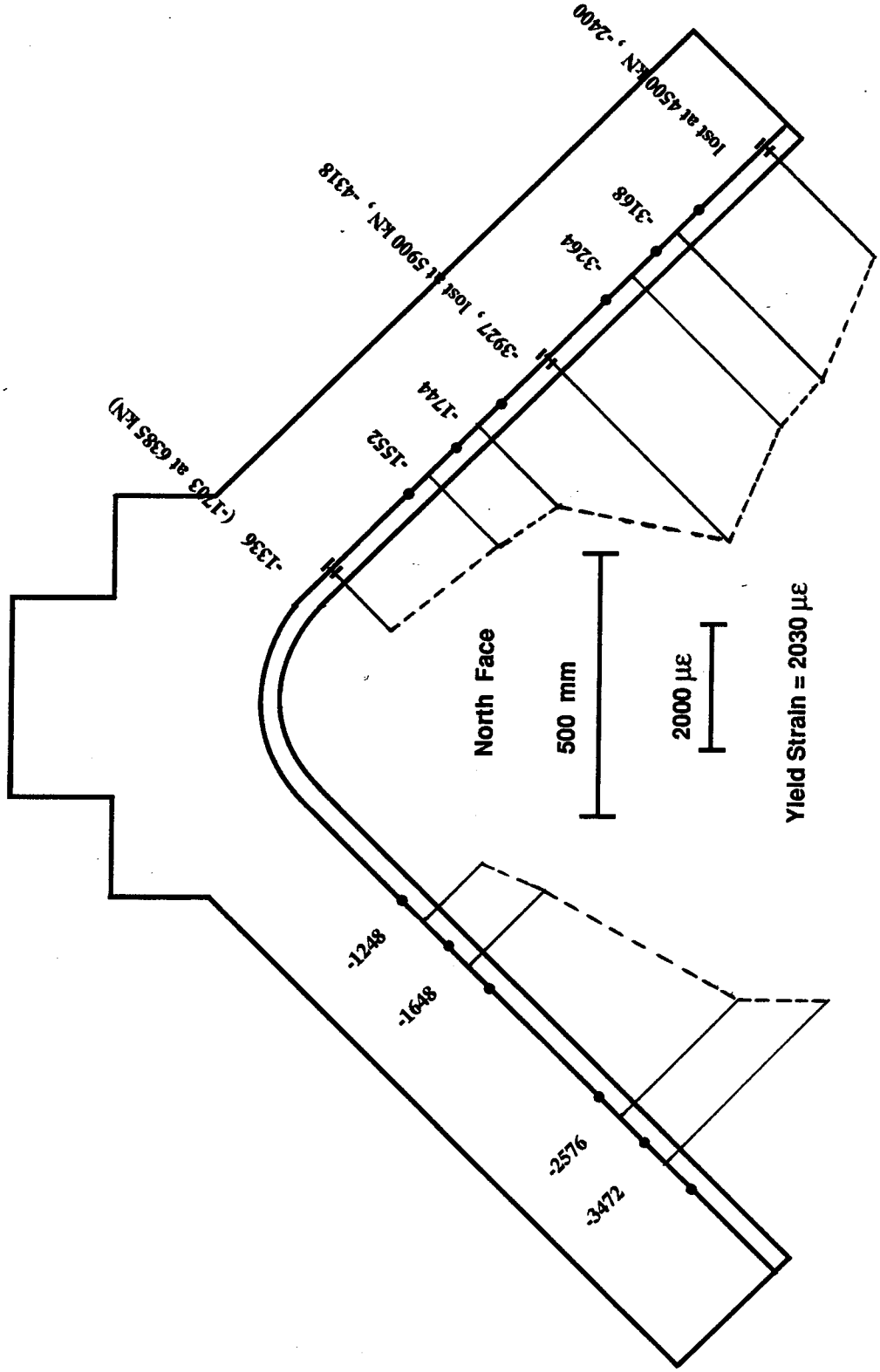

Figure 4.30 Measured Strain Distribution in Bottom Reinforcing Bars for Specimen A4

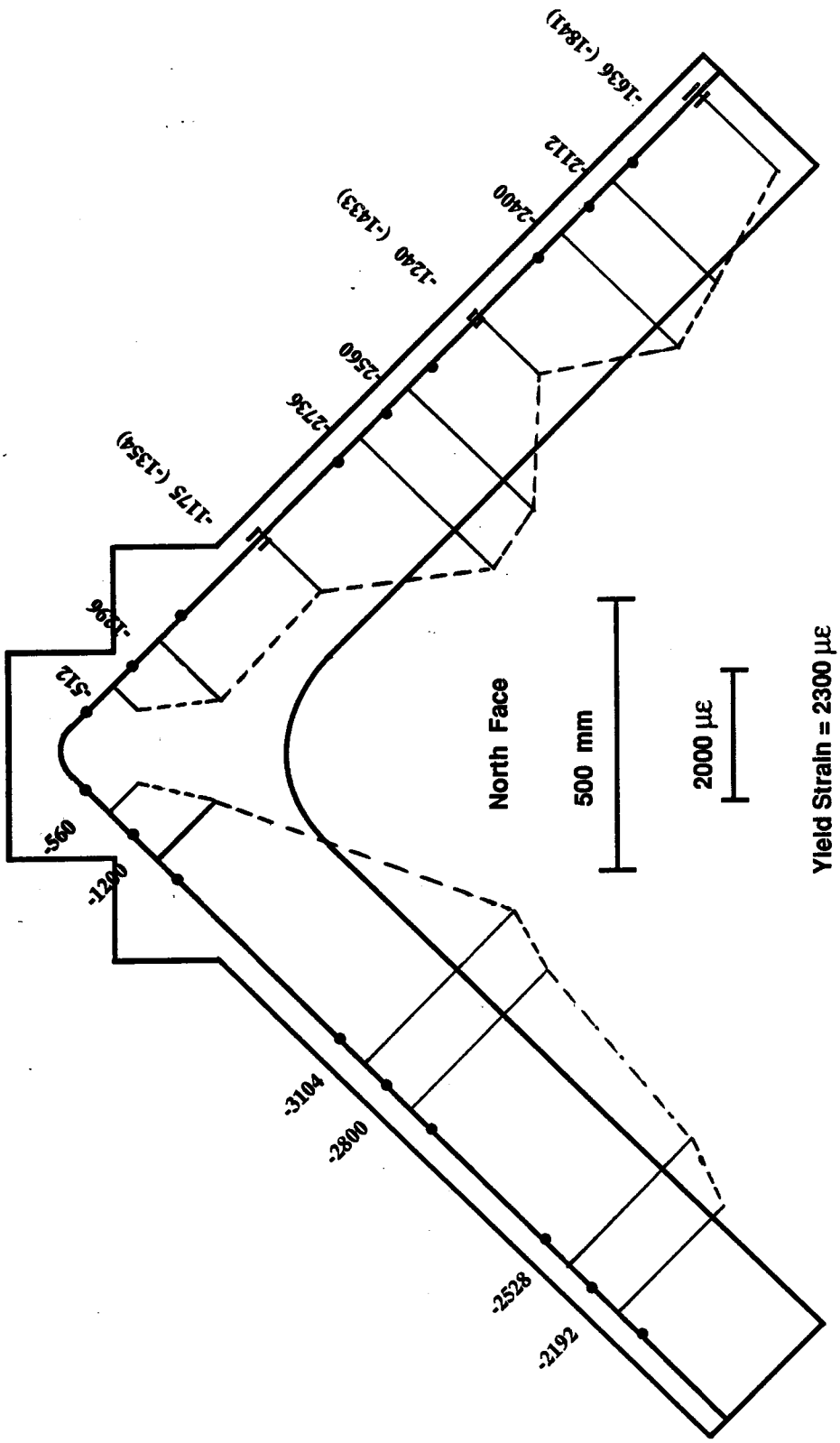

Figure 4.31 Measured Strain Distribution in Top Reinforcing Bars for Specimen A5

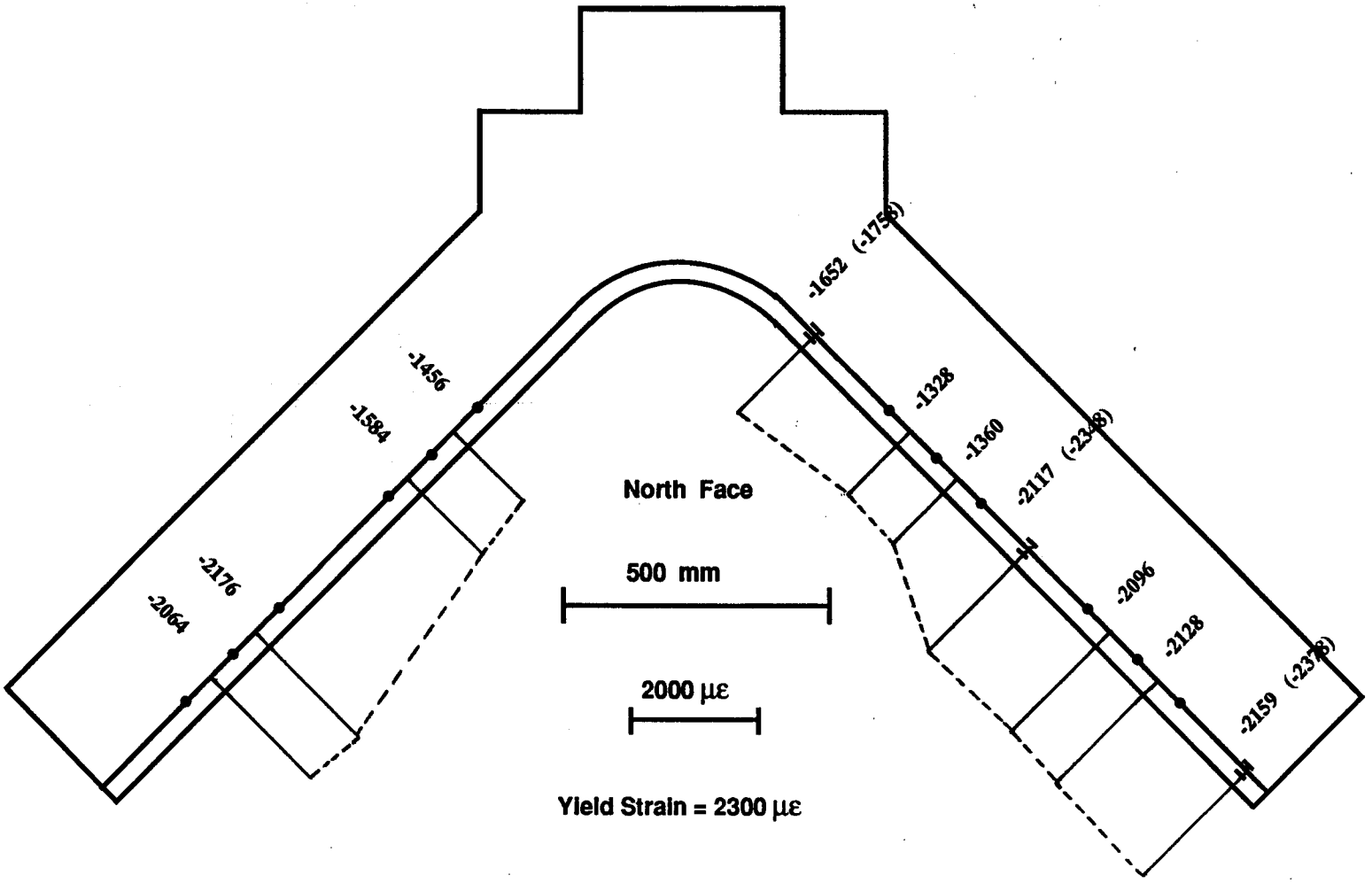

Figure 4.32 Measured Strain Distribution in Bottom Reinforcing Bars for Specimen A5

Both specimens exhibited a ductile failure mode although the increased stirrup spacing in Specimen B2 led to a lower failure load and lesser ductility than in the Specimen B1.

The measured loads, reactions, and calculated end-forces and moments for Specimens B1 and B2 are given in Sect. 4.4.3 and Sect. 4.4.4 respectively. These were determined in the manner described in Sect. 4.3.1 with minor changes in the geometry due to the different test set-up. It should be noted that these end forces will include the reactions to the compressive membrane forces which developed in the B-Series tests.

4.4.2 Load-Deflection Response

The measured load deflection curves for Specimens B1 and B2 are shown in Fig. 4.33. In this thesis all of the load deflection plots are drawn to the same scale to allow direct comparison between specimens (see Fig. 4.16 to compare to the A-Series loading condition). The load values are those measured using the MTS pressure transducer. The deflection plotted is the deflection of the second load point. This is the location of the maximum static moment and typically the largest deflection measured during the test. The portion of the deflection due to support settlement has been subtracted from these values.

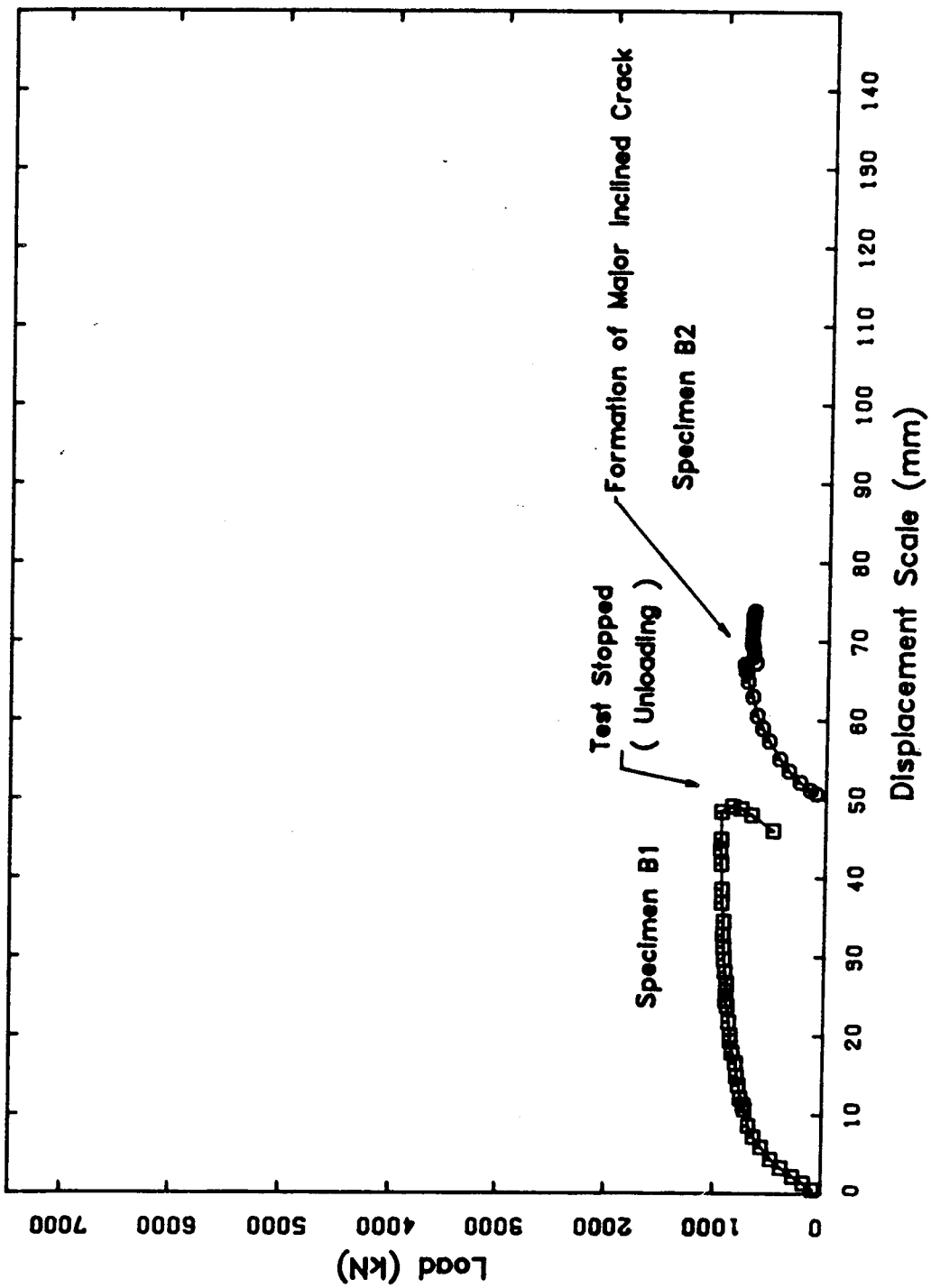

Figure 4.33 Load vs. Midspan Displacement for B-Series Specimens

4.4.3 Test Results for Specimen B1

The ultimate load and failure mode for this specimen has been presented in Table 4.5. The load-deflection response was presented in Fig. 4.33. The measured loads, reactions, and calculated end forces are given in Table 4.6. The same notation and sign conventions are used here as in the A-Series specimens, as shown in Fig. 4.14. The procedure to determine the end forces and moments is as discussed in Sect. 4.3.1. In the B-Series tests, the west end is the raised end which was supported on the steel pedestal (Fig. 3.17). For the summary in Table 4.6, the results selected are for loads beginning with the first load after the cracking load and then in increments of approximately 100 kN until near failure, where smaller increments were chosen. Results which are referred to in various parts of this thesis are shown in bold type.

The load was applied in increments of 50 kN. First cracking was observed in the form of flexural cracks at midspan at an applied load of 150 kN. First diagonal cracks were observed at 300 kN. By 450 kN (or 2.25 MPa) the crack pattern was established as being a combination of fan cracks and inclined cracks. On each side of the loaded region between the first load point and the support, there were upper and lower regions of fan cracking. In between the upper and lower fans, there was generally a region of parallel inclinded cracks running between the support and the load point as shown in Fig. 4.34. This suggests the

Table 4.6 Measured Loads, Reactions and Calculated End-Forces for Specimen B1

SPECIMEN B1 **ANALYSIS FOR ARCH ENDS**

				WEST				EAST		
Load (kN)	Rwest (kN)	Reast (kN)		Po (kN)	Mo (kNm)	Vo (kN)		Po (kN)	Mo (kNm)	Vo (kN)
233.29	74.39	158.90		36.05	22.45	115.52		117.77	-19.44	-36.05
330.70	104.10	226.60		53.51	32.62	162.77		167.93	-29.17	-53.51
425.20	133.20	292.00		71.36	41.02	207.67		217.53	-40.03	-71.36
678.80	211.10	467.70		137.67	80.84	322.93		355.87	-74.29	-137.67
836.80	**257.90**	**578.90**		**184.43**	**96.46**	**394.74**		**442.06**	**-114.09**	**-184.43**
914.30	**278.80**	**635.50**		**209.98**	**107.87**	**432.95**		**481.35**	**-139.38**	**-209.98**
950.20	287.80	662.40		218.15	113.06	451.66		498.54	-146.68	-218.15
964.40	291.10	673.30		222.10	114.35	458.60		505.80	-150.77	-222.10

formation of a direct strut on each side of the applied patch load. The direct struts on each side suggest that arch action was occurring in this region as shown in Fig. 4.35. This is discussed in more detail in the development of the strut-and-tie models in Sect. 6.4 and 6.5.

By 750 kN (or 3.75 MPa) most major cracking had developed as shown in Figs. 4.36(a) and (b). The fan action at the top and bottom of the west shear span, and the direct strut between the load point and the support can be seen in Fig. 4.36(a) identified by the white arrow. In Fig. 4.36(b) is shown the maximum moment region in which a plastic hinge (white arrow) has formed below load point 2. In this high moment, low shear region most cracking is flexural cracking with diagonal cracking confined to the outer regions of midspan. A plastic hinge had also formed at the top of the vertical leg as identified by the white arrow in Fig. 4.37. Fanning and direct strut action in the east shear span are also suggested in this figure. At 840 kN (or 4.2 MPa) some new cracks had formed and crushing was observed at the inside soffit of the pedestal (Fig. 4.34 and Fig. 4.37 (white arrow)).

The specimen carried further load and by 964.4 kN (or 4.82 MPa) the load was increasing only very slightly and the deflection was still increasing as shown in Fig. 4.33. At this point the limit of travel in the load application system was reached and the test was stopped. The unloading branch of the curve shown in Fig. 4.33 is approximately

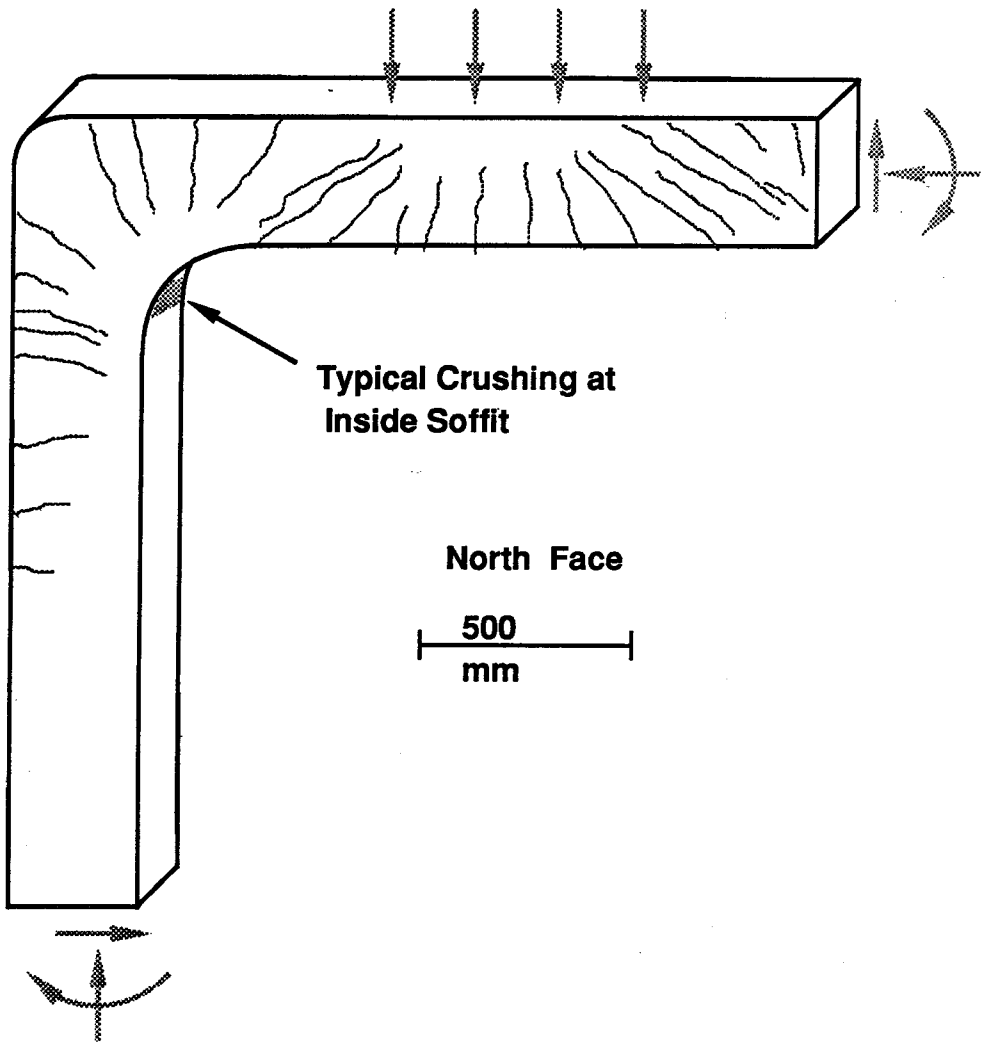

Figure 4.34 Typical Crack Pattern and Damage Zones for B-Series Specimens

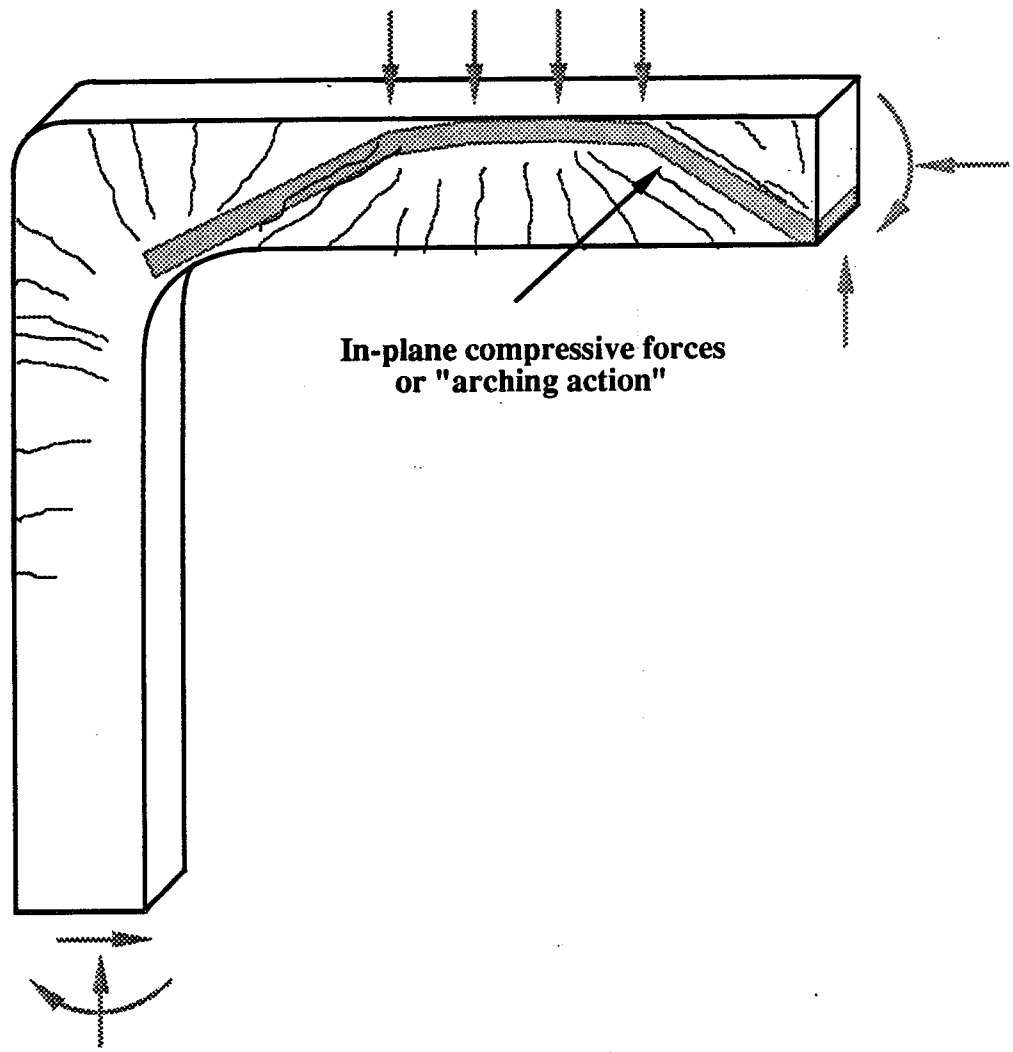

Figure 4.35 Development of Arch Action in B-Series Specimens

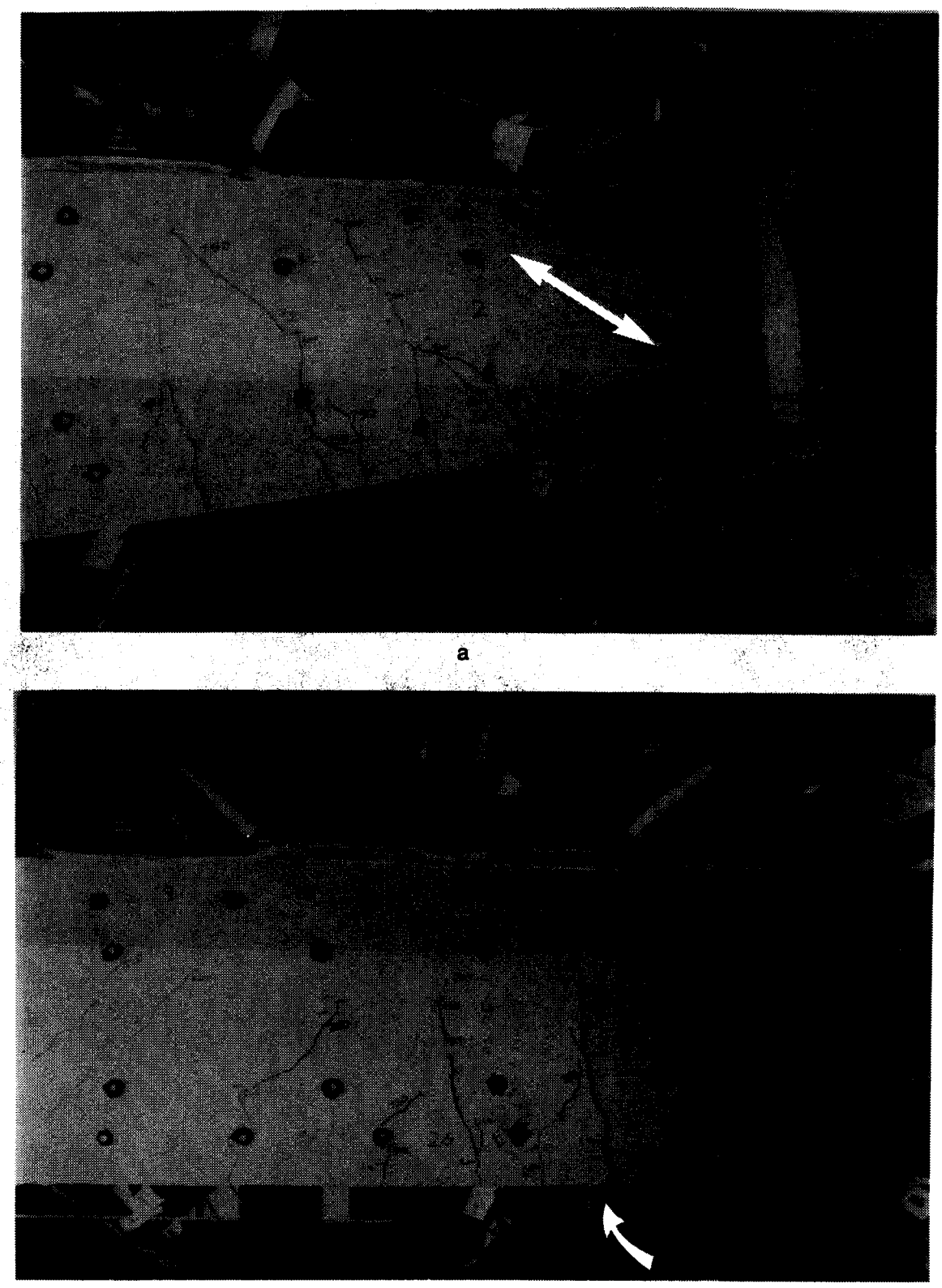

a

b

Figure 4.36 Crack Pattern in West Shear Span and at Midspan for Specimen B1

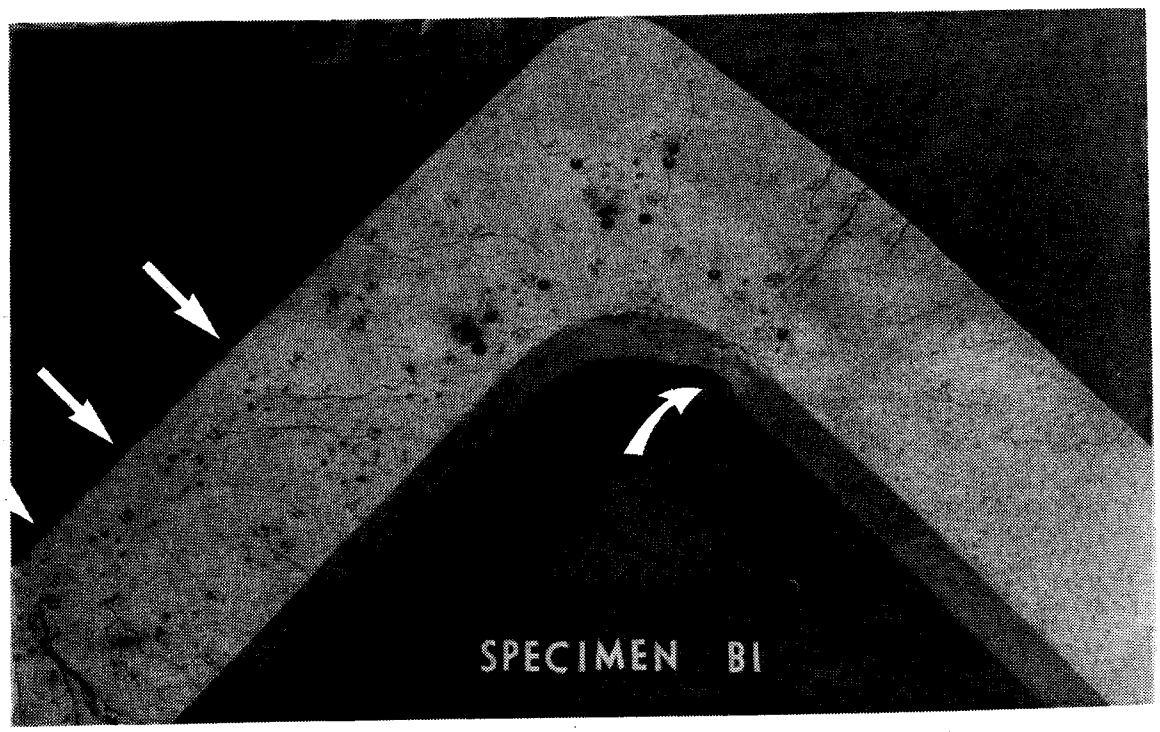

Figure 4.37 Final Crack Pattern in East Shear Span, Corner, and in Pedestal for Specimen B1

parallel to the slope of the loading portion. The overall crack pattern of the specimen is shown in Fig. 4.38.

In Figs. 4.39 and 4.40, the measured principal strains in the concrete at applied loads of approximately 200 kN and 840 kN, respectively, are shown plotted on the specimen. The rosette locations are as shown in Fig. 3.30. The results of the strain rosettes were omitted from this plot on the same basis as in the A-series tests although many tended to be lost due to the large size and number of cracks. The plots are shown on the south face of the specimen which is the side the rosettes were mounted on for Specimens B1 and B2. These plots are particularly useful when compared with the cracking photos, with the assumed strut-and-tie model presented in Sect. 6.5, and with the principal stress plots from the finite element analysis presented in Sect. 7.5.3.

The measured strains in the longitudinal 15M reinforcement at an applied load of 836.8 kN are plotted at the appropriate locations on the top and bottom reinforcement in Figs. 4.41 and 4.42, respectively. This is the last load at which manual readings were taken. In the figure, tensile strains are positive and are plotted on the outside of the bar. Scales are as indicated. At the locations where strain gauges were mounted, the strains at the ultimate load are also plotted and are shown in brackets ( ). The locations and magnitudes of the largest strains are consistent with the crack pattern and the development of the plastic hinges.

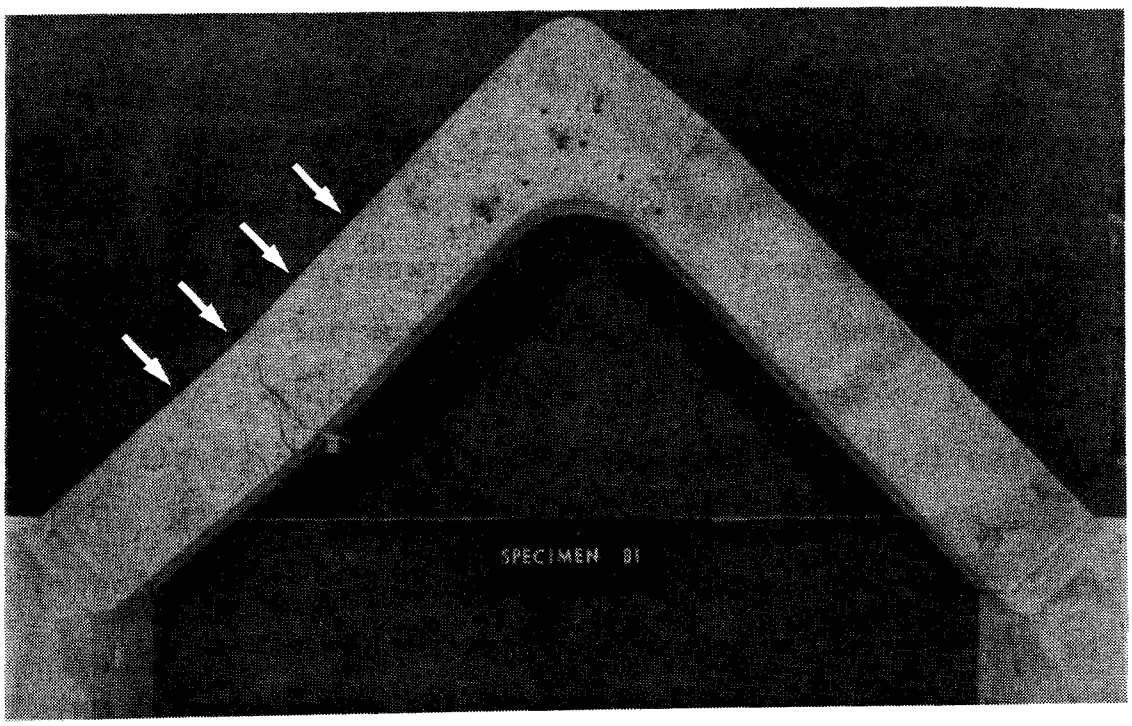

Figure 4.38 Final Overall Crack Pattern for Specimen B1

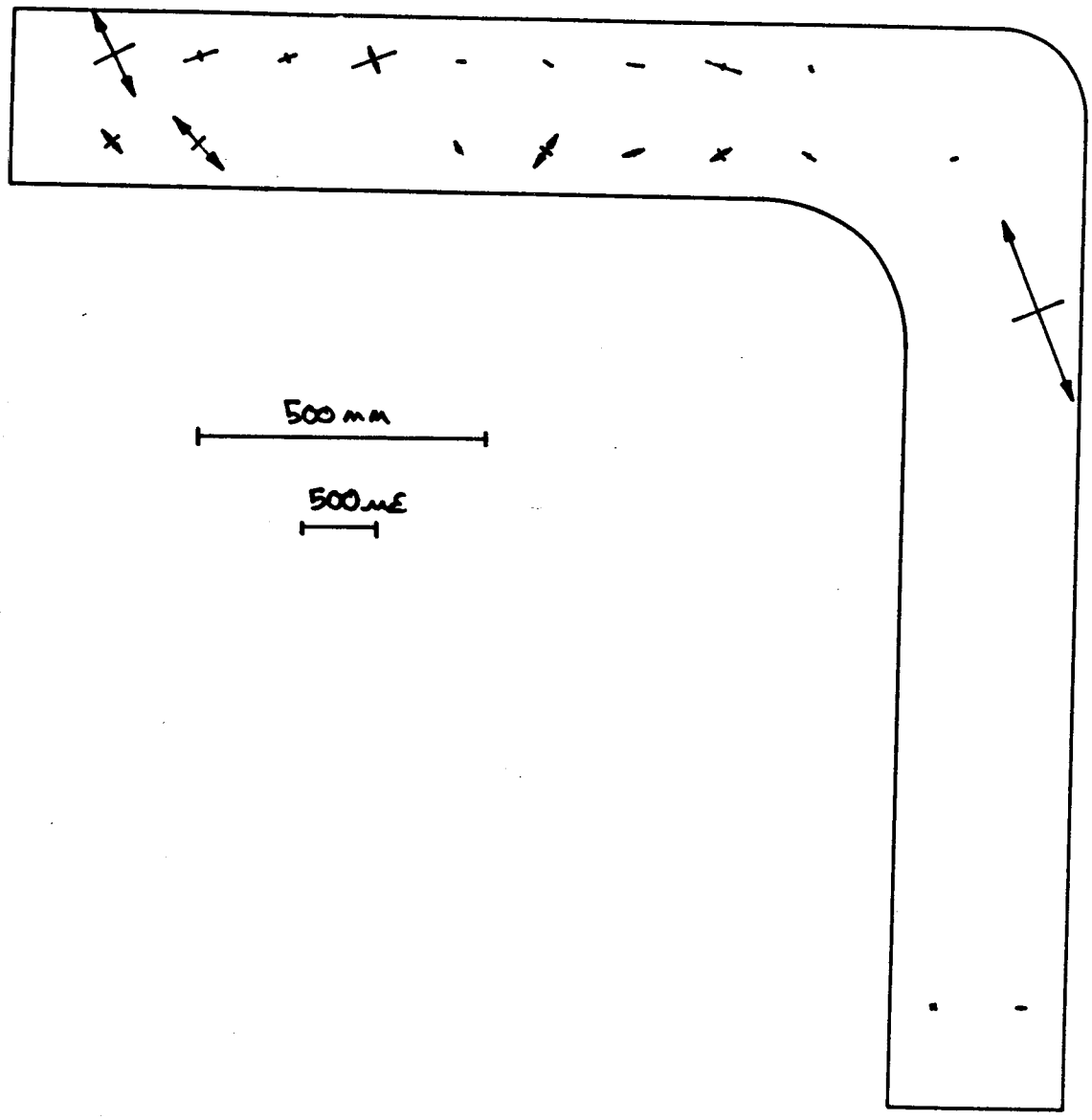

Figure 4.39 Principal Strain Plot for Specimen B1 at 200 kN

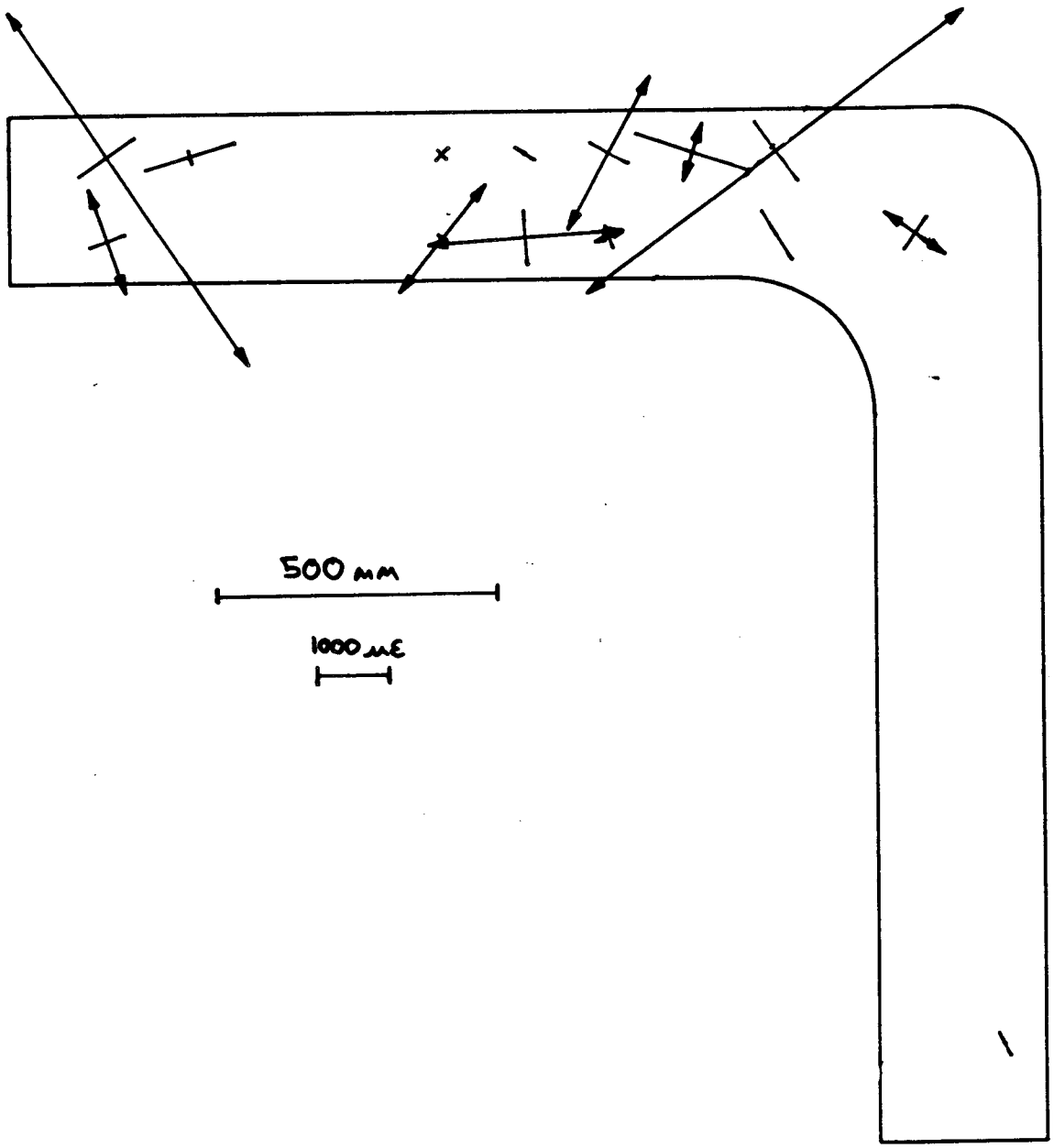

Figure 4.40 Principal Strain Plot for Specimen B1 at 840 kN

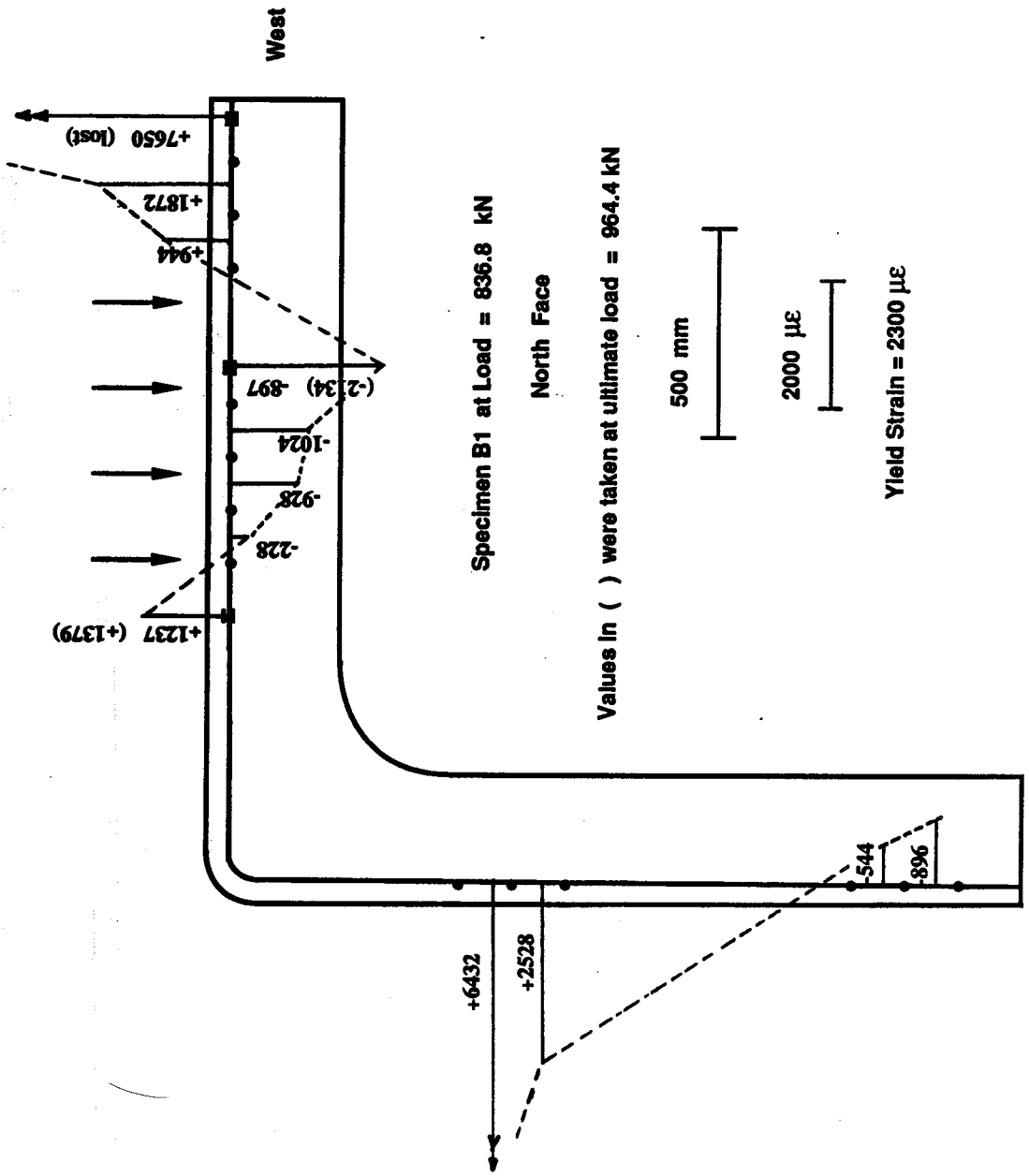

Figure 4.41 Measured Strain Distribution in Top Reinforcing Bars for Specimen B1

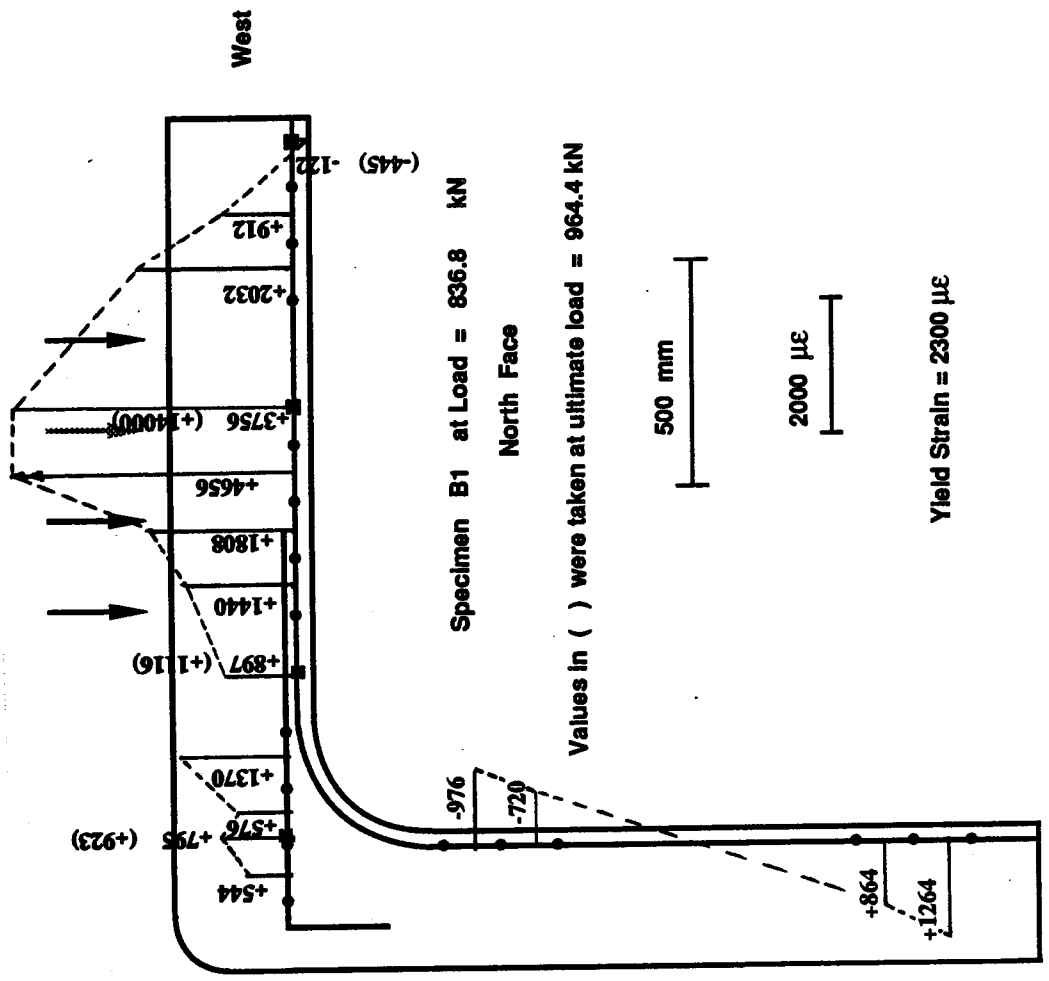

Figure 4.42 Measured Strain Distribution in Bottom Reinforcing Bars for Specimen B1

At the last DEMEC measurements, at an applied load of approximately 840 kN, the 6 mm stirrups had not reached yield. However, the stirrups between the supports and the first load point on each side picked up load dramatically between loads of 750 kN and 840 kN. In some cases the strains in the stirrups at these locations increased 100% in this interval. Based on this and on one set of stirrups in the west shear span on which electrical resistance strain gauges were mounted it is expected that the stirrups in the west shear span were yielding at the ultimate load of 964.4 kN. The same conclusions were made concerning the east shear span. These two regions correspond to regions of maximum shear. In the region between the load points and in the vertical leg where the shear forces are much lower, the measured strains in the stirrups suggest that the stirrups did not reach yield.

4.4.4 Test Results for Specimen B2

The measured ultimate load and the load-deflection response for Specimen B2 were presented in Sections 4.4.1 and 4.4.2, respectively. The specimen was loaded in the same manner as Specimen B1. Cracking occurred at approximately the same locations and at approximately the same load levels. The load-carrying mechanisms are approximately the same and the load-deflection response is similar except that Specimen B2 failed at the lower load. This is principally due to the fact that Specimen B2 had fewer stirrups. Failure

was due to the propagation of a major diagonal crack through the series of fan cracks in the top of the region near the west support. The major crack extended from the bottom of the specimen to the first load point. This occurred at an applied load of 774.7 kN (or 3.87 MPa) which is approximately 80% of the ultimate load of Specimen B1.

The measured loads, reactions, and calculated end-forces and moments are given in Table 4.7. The results presented in Table 4.7 begin with the load after the first cracking load and then in increments of approximately 100 kN until near failure where a smaller increment was chosen. Results which are referred to in various parts of this thesis are shown in bold type.

Figures 4.43-4.45 show the same regions of Specimen B2 that were discussed for Specimen B1 in Sect. 4.4.3. The photos were taken at approximately the same load as Specimen B1, 750 kN (or 3.75 MPa). In this case however, Specimen B2 had reached its maximum load and the load had dropped off (see Fig. 4.33). The same comments given in Sect. 4.4.3 regarding the formation of cracking, load-carrying mechanisms, and plastic hinges also apply to Specimen B2. An important difference is the size of the large diagonal crack in Specimen B2 (Fig. 4.43(a)) versus the small fan-type cracking at this location at the top of Specimen B1 (Fig. 4.36(a)). It appears that the crack opened due to the yielding of the fewer number of stirrups in the region. Another important difference is the presence of flexural

Table 4.7 Measured Loads, Reactions, and Calculated End-Forces for Specimen B2

SPECIMEN B2 **ANALYSIS FOR ARCH ENDS**

				WEST				EAST		
Load (kN)	Rwest (kN)	Reast (kN)		Po (kN)	Mo (kNm)	Vo (kN)		Po (kN)	Mo (kNm)	Vo (kN)
245.79	77.09	168.70		49.25	30.92	114.35		131.44	-19.85	-49.25
348.40	106.60	241.80		75.90	36.90	153.79		194.61	-31.30	-75.90
439.50	135.60	303.90		94.89	43.82	195.15		244.35	-42.70	-94.89
539.50	165.80	373.70		115.08	39.64	229.94		309.56	-47.87	-115.08
650.60	198.80	451.80		141.48	43.26	273.82		376.78	-60.94	-141.48
697.00	212.50	484.50		157.00	52.46	296.29		400.71	-73.41	-157.00
762.90	**231.10**	**531.80**		**173.36**	**62.54**	**330.32**		**432.58**	**-88.05**	**-173.36**
774.70	**234.20**	**540.50**		**178.21**	**63.61**	**334.97**		**439.73**	**-92.20**	**-178.21**
707.00	211.20	495.80		176.55	38.03	283.40		423.60	-89.91	-176.55

cracks at the bottom of Specimen B2 near the support in Fig. 4.43(a). These cracks are absent in Specimen B1 (Fig. 4.36(a)). This is discussed further after the presentation of the reinforcing strains.

The measured principal concrete strains at applied loads of 200 kN and 700 kN are shown plotted on the specimen in Figs. 4.46 and 4.47 respectively. The lower load step corresponds to first cracking. The higher load is the last load at which manual readings were taken. The plots are shown on the south face of the specimen. These principal strain plots are useful when compared with the cracking photos, with the assumed strutand-tie model presented in Sect. 6.5, and with the principal stress plots from the finite element analysis presented in Sect. 7.5.3.

The measured strains in the longitudinal reinforcement at an applied load of 698.1 kN are plotted at the appropriate locations on the top and bottom reinforcement in Figs. 4.48 and 4.49, respectively. This load is the last load at which manual readings were taken. In the figure, tensile strains are positive and are plotted above or to the left of the bar. Scales are as indicated in the figure. At the electrical resistance strain gauge locations, strains at the ultimate load are also plotted and are shown in brackets ( ). It is interesting to note that the bottom bars in the west shear span experienced small tensile strains at ultimate while in Specimen B1 at the same spot the bars were in compression. Although this appears to be a contradiction

a

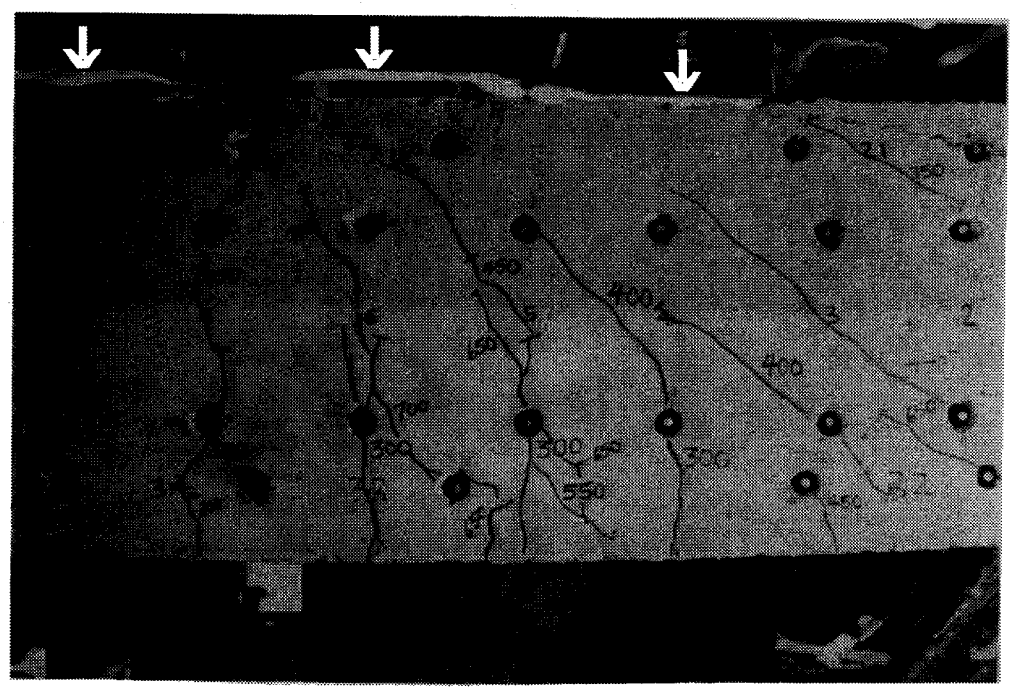

b

Figure 4.43 Crack Pattern in West Shear Span and at Midspan for Specimen B2

Figure 4.44 Final Crack Pattern in East Shear Span, Corner, and in Pedestal for Specimen B2

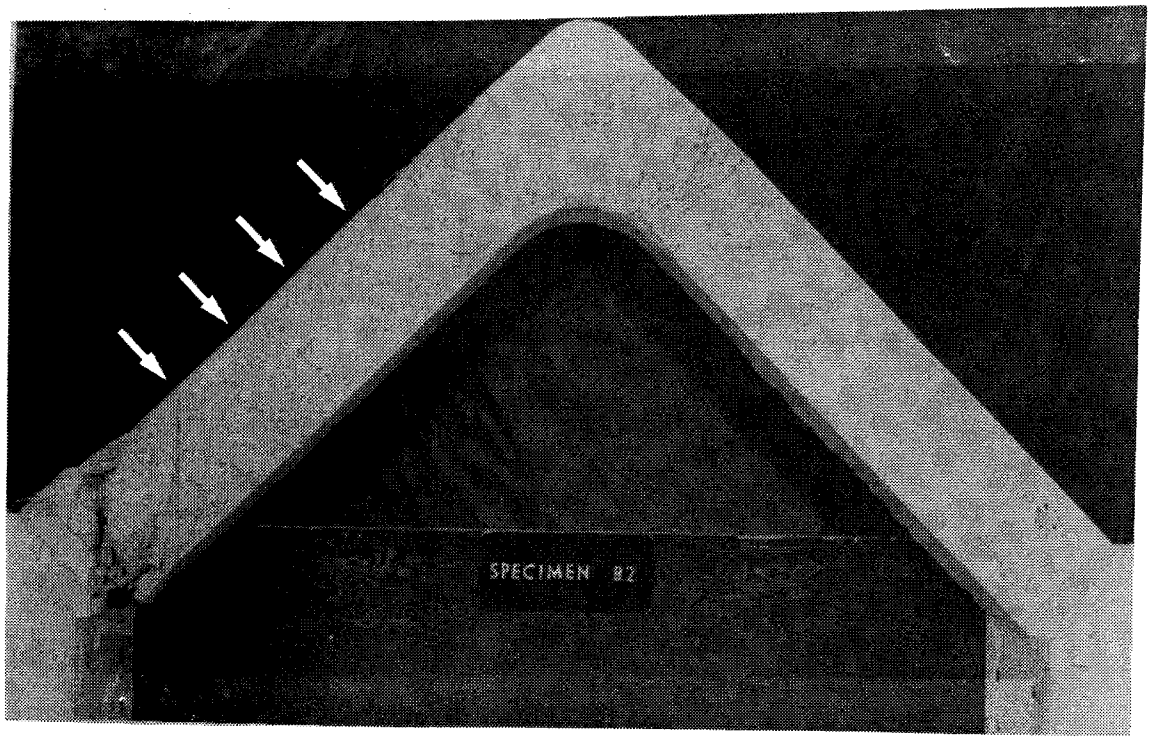

Figure 4.45 Final Overall Crack Pattern for Specimen B2

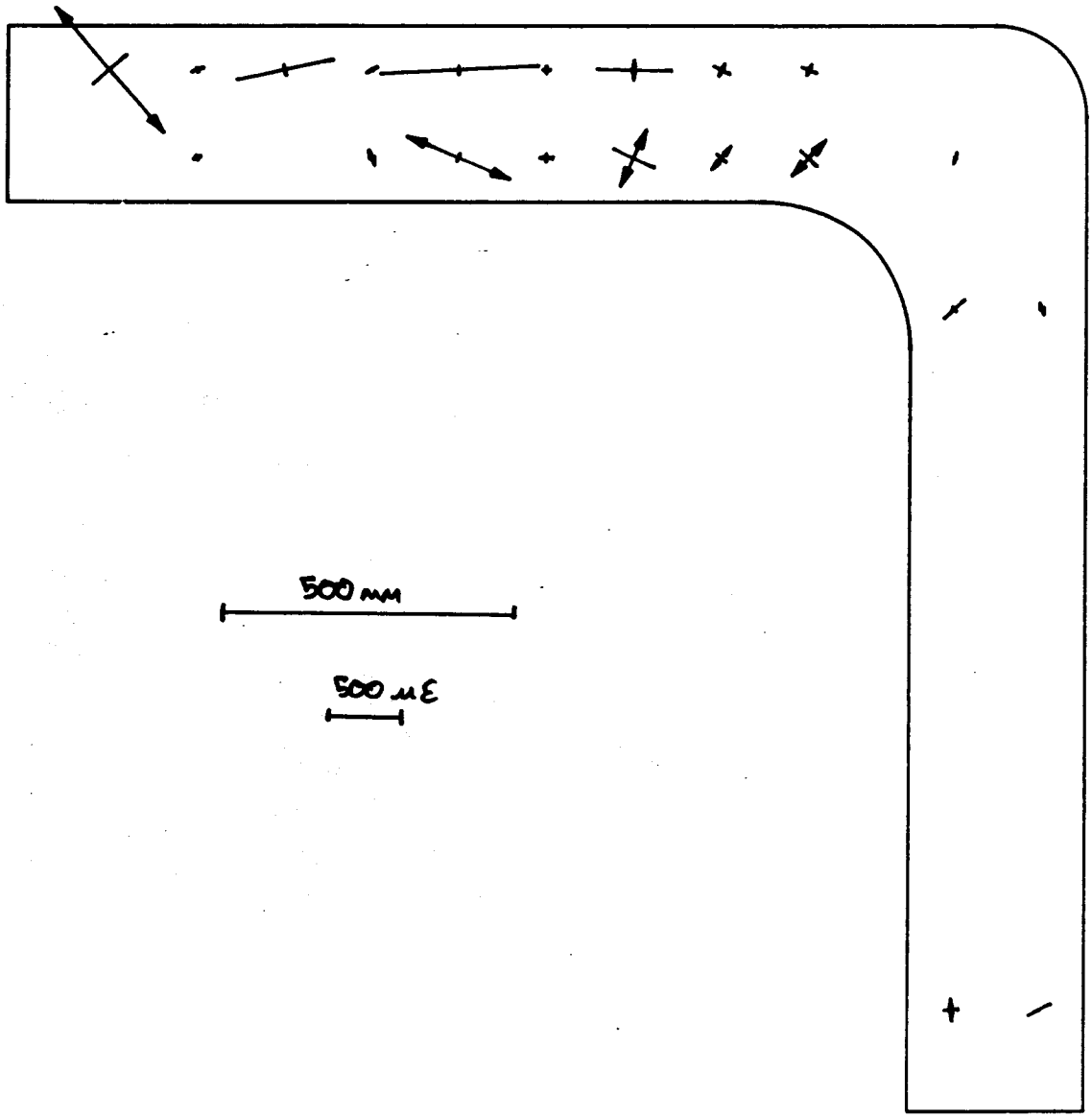

Figure 4.46 Principal Strain Plot for Specimen B2 at 200 kN

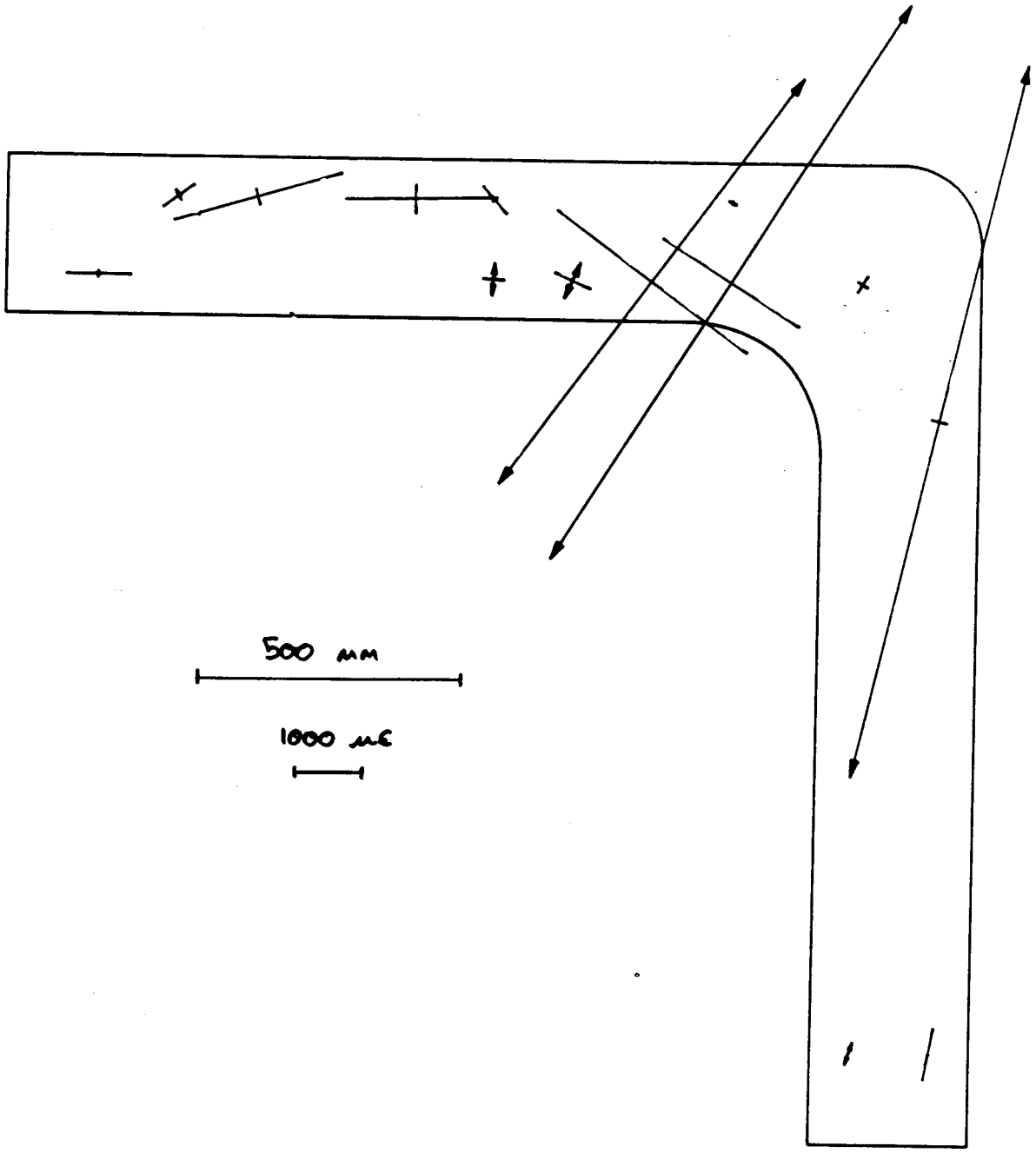

Figure 4.47 Principal Strain Plot for Specimen B2 at 700 kN

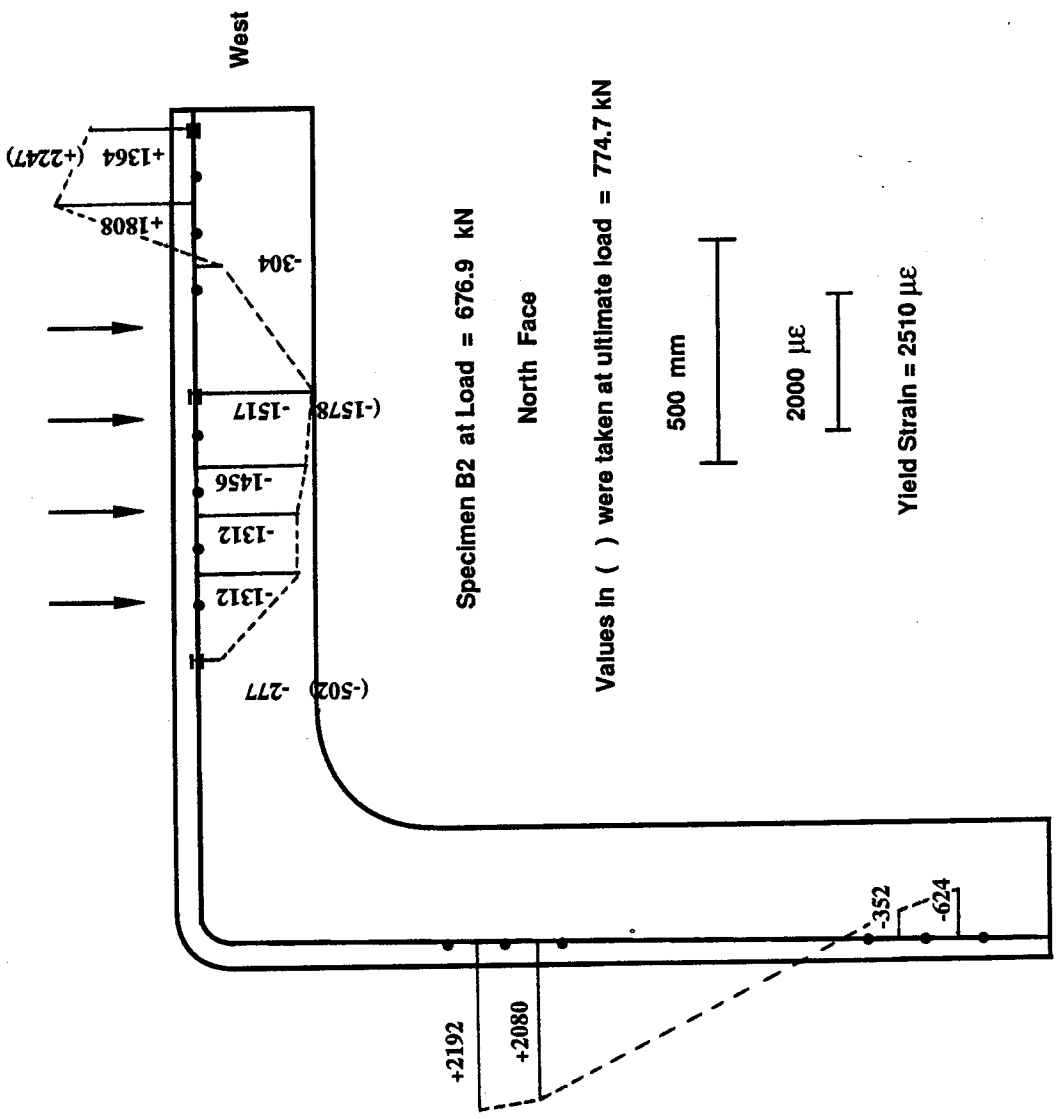

Figure 4.48 Measured Strain Distribution in Top Reinforcing Bars for Specimen B2

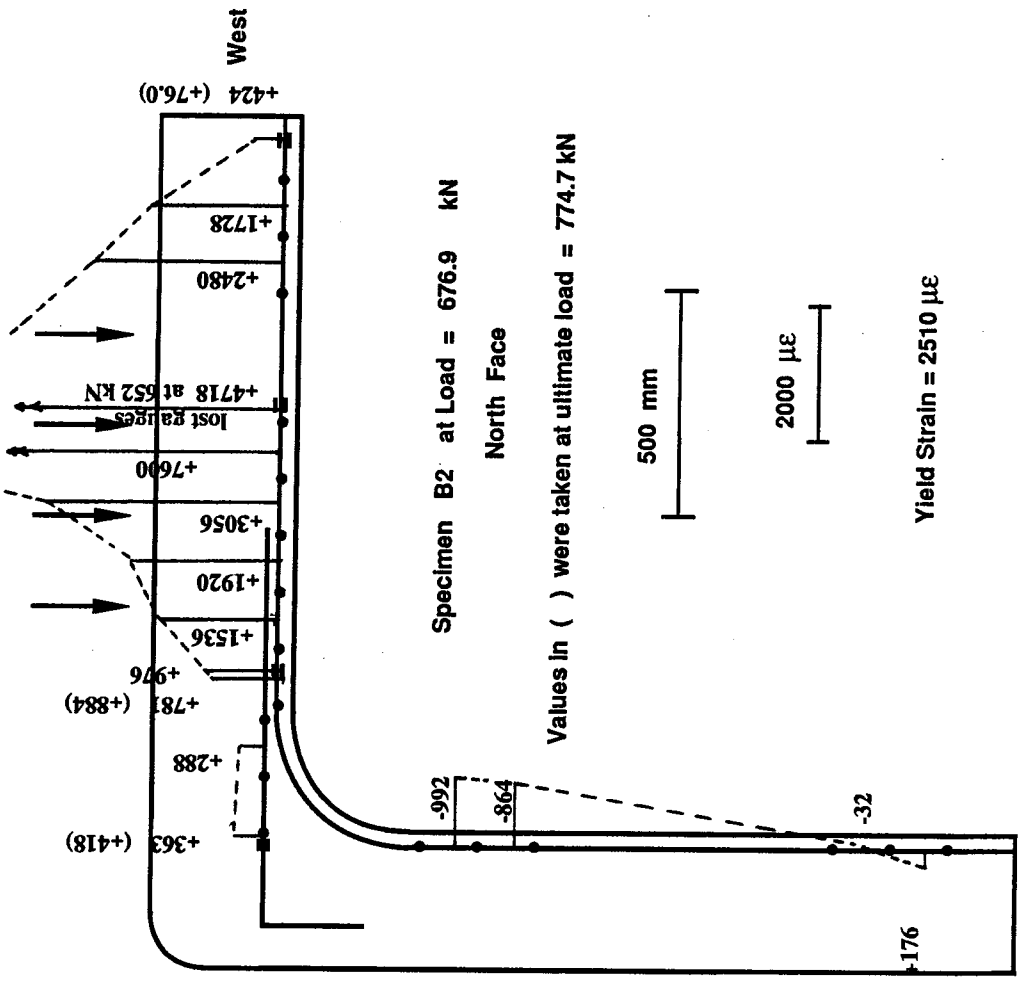

Figure 4.49 Measured Strain Distribution in Bottom Reinforcing Bars for Specimen B2

since it might be expected that compressive strains would be more likely in this region of negative moment it can be explained by the strut-and-tie models discussed in Chapter 6. This is a good illustration of how the presence of shear reinforcement influences the way in which the structures carries the load.

As will be shown in the development of the strut-and-tie models in Sects. 6.4 and 6.5, each stirrup in a fan region, such as in the lower part of the west shear span, must carry the vertical component of a diagonal compression strut. The horizontal component of the force in this strut is what changes the force in the longitudinal reinforcement. In the case of Specimen B1, which had the greater number of stirrups in this shear span, there are sufficient stirrups to permit the reduction of the tension force in the bottom reinforcement to the extent that it actually became compressive. In Specimen B2, however, insufficient stirrups were available to reduce the tensile force to zero and the measured strains indicated a small tensile force remaining in these bars at the support.

At the last DEMEC measurements, at an applied load of approximately 700 kN, the first two sets of 6 mm stirrups in from the west support were already yielding. In the east shear span, one set of stirrups had reached yield and the others were starting to carry load. The stirrups in between the load points and the stirrups in the vertical leg were not yielding.

5. STRUT-AND-TIE MODELLING

5.1 General

The basic elements of the strut-and-tie model are presented in this section in order that the concepts may be applied in Chapter 6.

The strut-and-tie model (STM) is in general terms an extension of the truss analogy proposed by Ritter (1899) and Morsch (1909) which forms the basis of the shear provisions in various reinforced concrete design codes (CAN3 A23.3-M84, ACI 318-83). Improvements over the past twenty-five years (Drucker, 1961; Leonhardt, 1965; Rusch, 1964; Kupfer, 1964; Nielsen et al., 1978; Mueller, 1978; Marti, 1980; Thurlimann, 1983) have led to the adoption of the method into European (CEB-FIP Model Code, 1978) and North American (CAN3 A23.3-M84) codes. The above researchers have demonstrated that the technique is applicable to beams, deep beams, and corbels, and that the strut-and-tie model constitutes a lower bound solution in the plasticity sense. In this thesis, the term strut-and-tie model is used as the generic term while the term truss model is reserved for beams.

As part of a discussion report for the proposed revisions to the CEB-FIP Model Code, Schlaich et al. (1987) have proposed that strut-and-tie models be used for design of all types and all regions of reinforced and prestressed concrete structures. This represents a significant change in

philosophy for reinforced concrete design. Instead of using conventional design procedures for the majority of the structure with additional guidance from procedures based on test results, rules of thumb, or past experience, they propose a consistent design procedure for all regions. The strut-and-tie models presented in Chapter 6 have been developed with this in mind.

5.2 Strut-and-Tie Models

5.2.1 Basic Concepts

Reinforced concrete structures carry ultimate loads by developing a system of compressive stress fields interacting with tension ties in such a way that equilibrium between applied loads and reactions is achieved.

In a STM, the compressive stress distribution is idealized as a statically equivalent compressive stress field having a maximum stress equal to the effective concrete strength, f_{ce} where $f_{ce} = \nu f'_c$. The main factors influencing the selection of the effective concrete strength, f_{ce}, are the multiaxial internal state of stress, the presence of cracking and the presence of reinforcement. Generally, the effectiveness factor ν is less than or equal to 1.0 although in certain cases the additional strength due to biaxial or triaxial states of compression may be recognized, provided the internal forces creating the stress state are caused by external loads which act simultaneously.

The effectiveness factor has generated much discussion in the literature (Nielsen et al., 1978; Thurlimann, 1978; CEB-FIP Model Code, 1978; Bach et al., 1980; Ramirez, 1984). Based on tests of deep beams, Rogowsky and MacGregor (1983) suggest that the accuracy of the truss model is more sensitive to the selection of the truss model itself than to the selection of ν. It must be remembered that the compressive cylinder strength is itself a rather vague representation of in-situ strength and is at best only a bench mark strength measurement for real structures. In this study the selection of ν will be discussed when required.

In certain cases the presence of compression reinforcement may be recognized. Compressive stress fields are discussed in more detail in Sect. 5.2.4.

The tensile stresses are resisted by prestressing or reinforcing bars or concrete tensile stress fields. A tie may model a single reinforcing bar or a group of reinforcing bars as long as it is placed at the centroid of the reinforcement. In the case of a tensile stress field, the tie is placed at the centroid of the stress field. Tension ties are discussed in more detail in Sect. 5.2.3.

Struts and ties are joined together at curved or polygonal regions called nodal zones. Nodal zones are discussed in more detail in Sect. 5.2.5.

The resulting STM model is, to varying degrees depending on the structure and the loading, an idealized model of the load carrying mechanisms present in the

structure at ultimate. As suggested by Marti (1985), "in reality, the concrete tensile strength and bond stresses are mobilized under increasing load to achieve as stiff a response as possible. Cracking indicates the successive development of new static systems and the bond may gradually deteriorate. Eventually the load may be carried by strut-and-tie action".

5.2.2 B and D Regions

Reinforced concrete structures may be divided into separate design regions based on elastic strain distribution and load paths (Schlaich and Weischede, 1982). The regions of a structure in which the strain distributions are linear (plane sections remain plane) are referred to as B regions where B stands for beam or Bernoulli.[1] For uncracked B regions, stresses may be calculated from the bending and torsional moments, shears, and axial forces using section properties. For cracked B regions, design methods based on the truss model may be used.

D regions are regions having geometrical or statical discontinuities. In these regions, the strain distribution is nonlinear. Examples of D regions are regions near supports, openings, changes in geometry, or concentrated loads (Fig. 5.1). Based on St. Venant's principle, Schlaich and Weischede (1982) suggest that a D region may be assumed to extend approximately one depth, h, away from geometrical

---

[1] The contribution of M. Navier notwithstanding

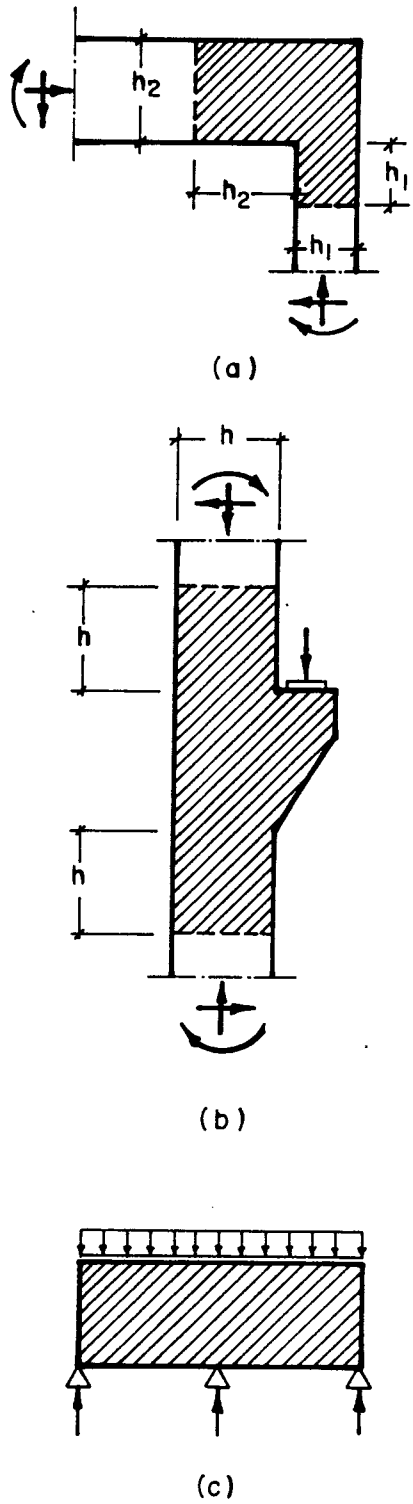

Figure 5.1 Typical D Regions

or statical discontinuities. Uncracked D regions may be analyzed using linear elastic finite element analysis. After cracking, D region behaviour is such that the traditional design procedures are typically empirically derived based on test results (corbels, deep beams). These requirements usually give guidance only concerning the provision of reinforcement and no attempt is made to quantify stresses in the concrete. As a result, the load carrying mechanism is obscurred to the designer. A more consistent design of reinforced concrete structures is possible if strut-and-tie models are used to design these and all regions of the entire structure.

5.2.3 Tension Ties

In a STM a tie force represents the total tension force assumed to be acting at a given location.

Typically reinforcement is provided to resist the tensile stresses and this reinforcement is positioned such that its centroid is collinear with the assumed tension tie (Fig. 5.2). Generally the reinforcement is assumed to be capable of providing a force equal to $A_s f_y$. In addition to providing the required amount of reinforcement at the proper location, it is also necessary to ensure that assumed forces can be developed in the reinforcement where required. For example, the tension tie in Fig. 5.2(a) provides a reaction to one face of the nodal zone and the reinforcement must have sufficient anchorage behind the nodal zone to develop

this force as shown in Fig. 5.2(b).

If the tension tie represents the total force carried by an uncracked tension stress field then the tie is located at the centroid of the stress field. Research is needed in this area concerning what value the 'effective tensile strength' of the concrete should be. Schlaich et al. (1987) suggests that until further research is available, the tensile strength of the concrete should only be used to maintain equilibrium where no progressive failure is expected. They go on to suggest simple recommendations concerning stress redistribution and the size of the cracked failure zone relative to the area of the surrounding concrete. Work concerning the application of fracture mechanics to concrete may be useful to solve this problem (for example Bazant, 1980, 1983; Willam, 1984). The tensile strength of the concrete is not explicitly used in the development of STM in this study although it is always implicitly used as discussed in Sect. 5.2.6. The use of a tensile stress field is illustrated in Chapter 6.

5.2.4 Compressive Stress Fields

In a strut-and-tie model, compressive stress fields are used to model the way in which the compressive stresses are carried by the concrete. The three basic compressive stress fields are the strut or parallel stress field (Fig. 5.3a), the bottle stress field (Fig. 5.4a) and the fan (Figs. 5.5-5.8).

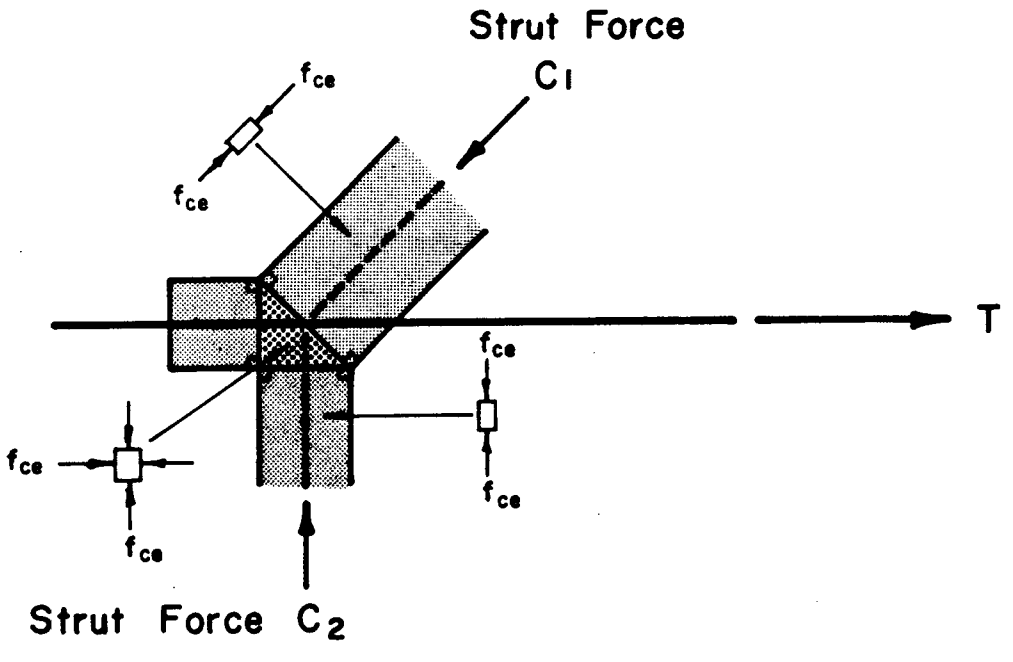

(a)

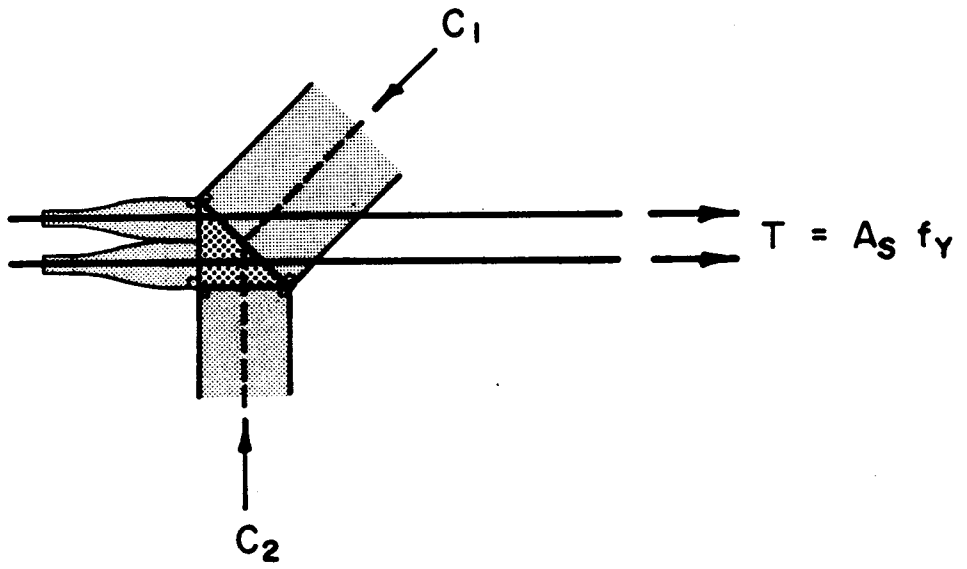

(b)

Figure 5.2 Tension Tie and Reinforcement

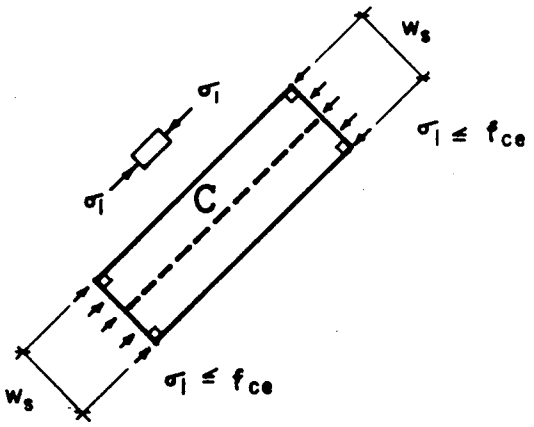

(a)

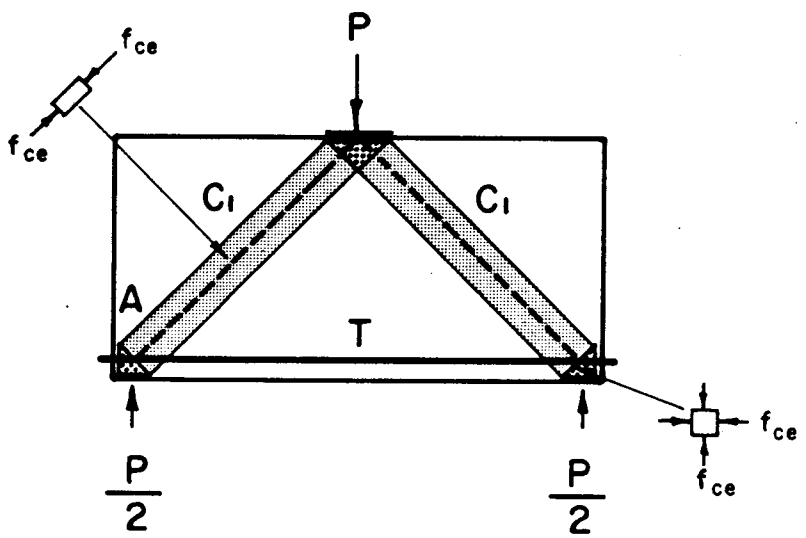

(b)

Figure 5.3 Strut or Parallel Stress Field and Application

5.2.4.1 Struts

The strut (Fig. 5.3a) represents a region of concrete of width w_s and thickness t assumed to be stressed uniaxially to a stress equal to the effective concrete strength, f_{ce}. The maximum compressive principal stress, σ_1 is assumed to be equal to f_{ce} and the minimum compressive principal stress σ_2 is assumed to be zero. If the strut is stressed to f_{ce} and C/t is the compressive force per unit thickness then the width of the strut is $w_s = C/tf_{ce}$. This stress field is largely hypothetical since in the actual structure, the stresses will generally spread out creating transverse tensile stresses. It is, however, simple to apply as shown in Fig. 5.3(b).

This figure shows a possible STM of a deep beam subjected to a concentrated load. The model is a simple truss with the struts carrying the compressive force C_1 and the tie providing the tension T. The 'shear' P/2 is carried by the vertical component of the compression strut. The stress in the struts is assumed to be f_{ce}. Each strut must have a vertical component equal to P/2 and horizontal component T. The reaction P/2, strut force C, and tie force T must be concurrent at the node A.

For equilibrium the nodal zone at A must have principal stresses $\sigma_1 = \sigma_2 = f_{ce}$. Nodal zones are sometimes referred to as 'hydrostatic' nodal zones although this would imply that $\sigma_1 = \sigma_2 = \sigma_3 = f_{ce}$ and in most problems plane stress conditions are assumed ($\sigma_3 = 0$). Nodal zones are discussed

in Sect. 5.2.5.

It is possible that a strut could contain compression reinforcement. This situation is not discussed in the literature and since it will be used in Chapter 6 it will be discussed briefly here. If the strut in Fig. 5.3a contains compressive reinforcement it is expected that the steel could carry a portion of the load. This situation is similar to a reinforced concrete column subjected to uniaxial compression. The potential problem of the reinforcement buckling is covered in the reinforced concrete column literature (for eg. Bresler and Gilbert, 1961; Pfister, 1964). In practice this is accounted for by limiting the tie spacing. If the bars in the strut are prevented from buckling by ties or in any other way it is reasonable to allow them to carry the full design strength $A_s f_y$ provided that adequate provisions exist to develop the bars. The concrete in the strut may be assumed to be stressed to f'_c. The area of concrete which is displaced by the bars should be accounted for. The STM of a column region subjected to eccentric load is discussed in Chapter 6.

5.2.4.2 Bottle-Shaped Stress Fields

The bottle-shaped stress field in Figure 5.4a attempts to account for the transverse tensile stress which develops when a load spreads outward from a width w_1 to a width w_2. The stress field has thickness t and length P. The load is assumed to be applied uniformly over the area w_1 x t. The length ℓ measures the length over which the compressive

stress trajectories spread out and then become parallel again. The length ℓ is generally related to w_2. This type of behaviour can be modelled with the simple STM shown superimposed on the stress field.

Schlaich et al. (1987) give values for the load which can be safely carried by this stress field for uncracked plain concrete and for reinforced concrete. For plain concrete, the values are based on an elastic analysis considering limits on cracking ($\sigma_t < f_{ce}/15$) and on crushing (biaxial tension-compression failure criterion). For reinforced concrete regions the limiting values are based on yielding of the transverse reinforcement in the tie T, and on crushing in the neck region (biaxial compression-compression failure criterion). This analysis was accomplished using the strut-and-tie model shown in Fig. 5.4a. For this reason the STM representation is generally as useful as the stress field.

Figure 5.4b shows an application of this STM representing the spread of prestressing force P, when applied to a reinforced concrete end block and the resulting transverse tensile stresses. Typically reinforcement is necessary to take the 'bursting' stresses in this region.

5.2.4.3 Centered Fans

A centered fan stress field is shown in Figure 5.5a. The surfaces AB and DE have constant radii of curvature r_o and r, respectively. The principal stress along AB is σ_o, directed radially outwards. Equilibrium of a wedge-shaped

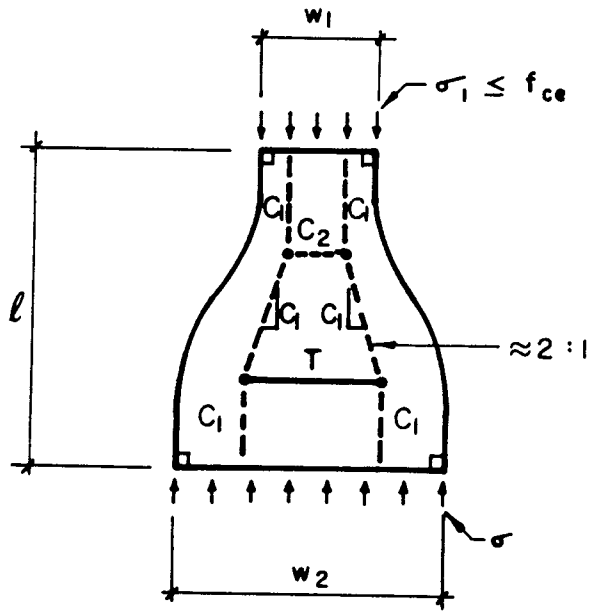

(a)

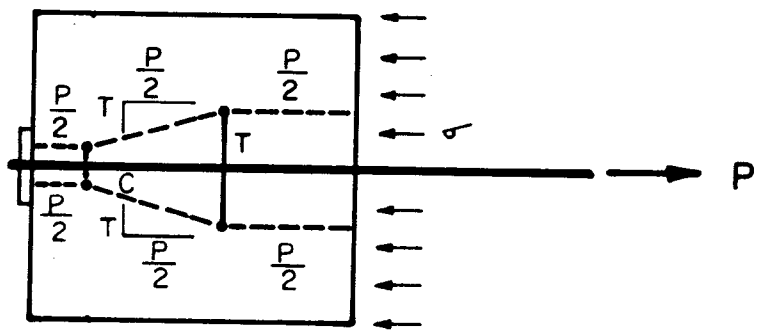

(b)

Figure 5.4 Bottle-Shaped Stress Field and Application

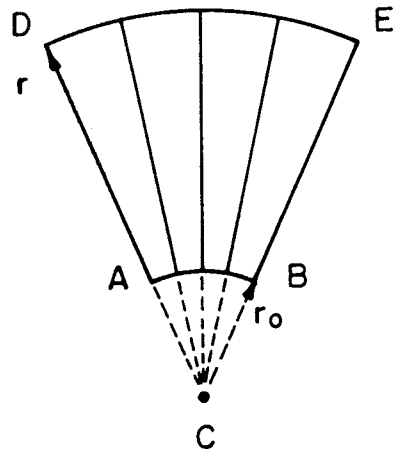

(a)

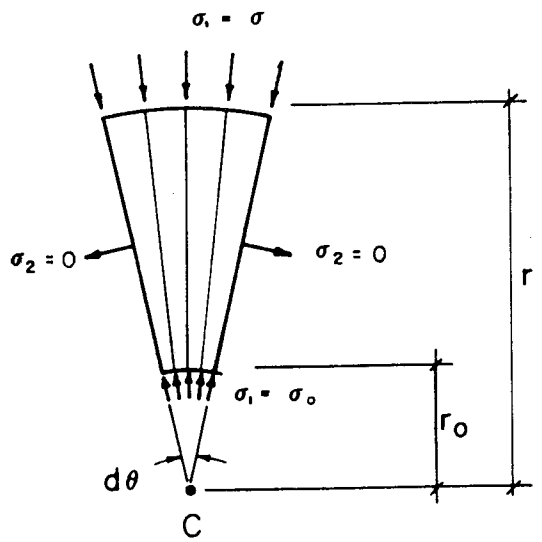

(b)

Figure 5.5 Centered Fan

segment $d\theta$ along any of the radial fan lines requires that the principal stress along DE be given by:

$$\sigma = \frac{r_o}{r}\sigma_o \qquad [5.1]$$

The principal stress perpendicular to a radial fan line is set equal to zero. This stress field was developed to describe the transverse tensile stresses which develop due to the spreading of forces (Thurlimann et al., 1983; Thurlimann, 1984).

A model which illustrates a centered fan is shown in Fig. 5.6. The force R_o is such that the stress in the strut below AB is f_{ce} and the nodal zone AB is stressed biaxially to f_{ce}. The stress along DE is given by Eqn. 5.1 as

$$\sigma = \frac{r_o}{r} f_{ce} \qquad [5.2]$$

The nodal zone DE is stressed biaxially to σ. The force T represents the transverse tension required as the force R_o spreads from width w_1 to width w_2.

The magnitude of force T may be determined from geometry and equilibrium. If the spreading angle is θ_o then

$$r_o = \frac{w_1}{2 \sin \theta_o} \qquad [5.3]$$

and the height h_o of the node AB is given by

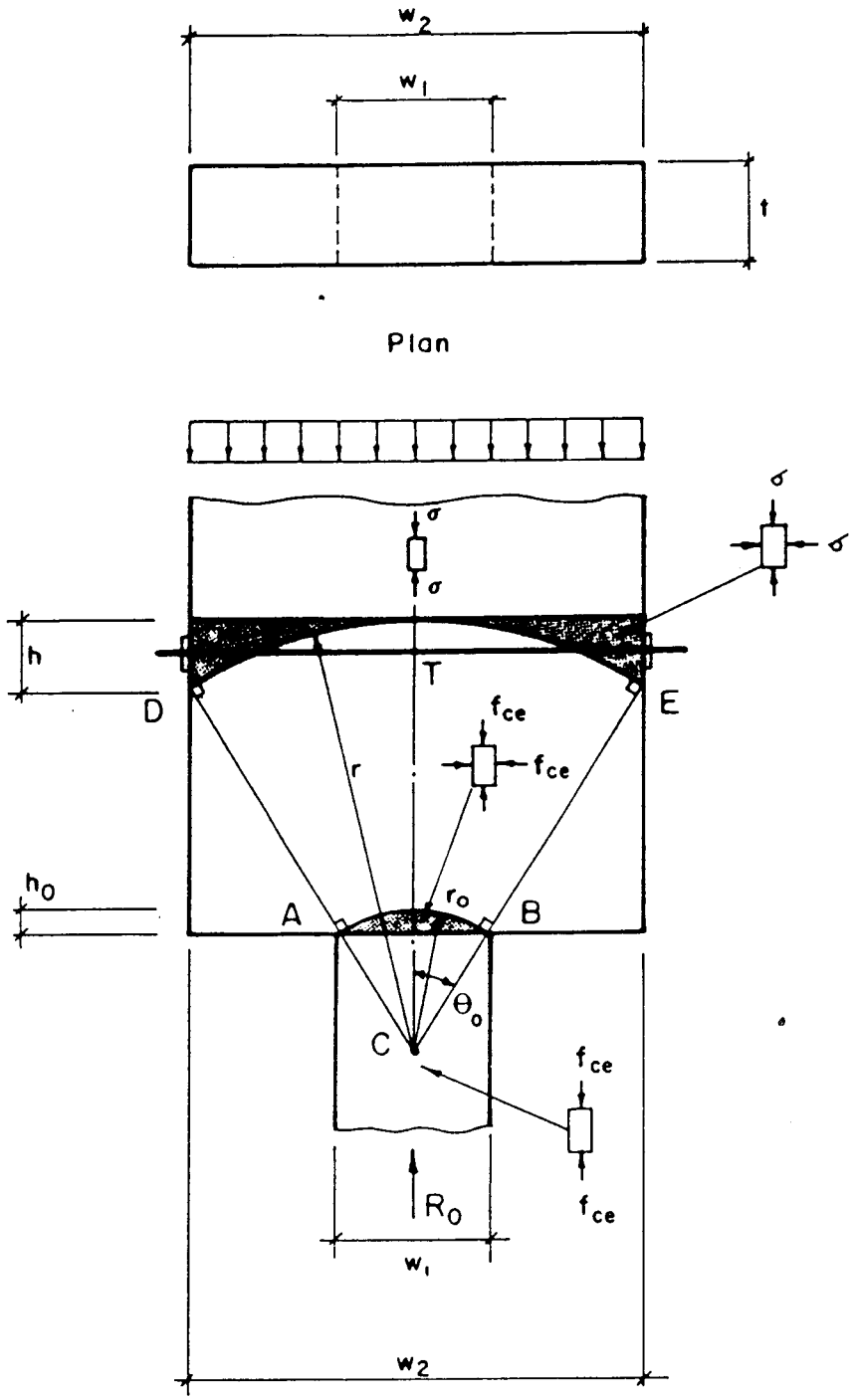

Figure 5.6 Application of Centered Fan Stress Field to Spreading of a Force

$$h_o = r_o(1-\cos\theta_o) = \frac{w_1}{2\sin\theta_o}(1-\cos\theta_o) \qquad [5.4]$$

From horizontal equilibrium along a vertical section through the centerline,

$$T = h\ t\ \sigma = h_o\ t\ f_{ce} \qquad [5.5]$$

If h_o is substituted from Eqn. 5.4, then

$$T = \frac{w_1 t f_{ce}}{2}\ \frac{(1-\cos\theta_o)}{\sin\theta_o} \qquad [5.6]$$

and finally

$$T = \frac{R_o}{2}\tan\frac{\theta_o}{2} \qquad [5.7]$$

The same result may be obtained using the STM shown in Fig. 5.7. The result suggests that reinforcement capable of resisting T given by Eqn. 5.7 should be provided for spreading force situations such as this.

Thurlimann et al. (1983) recommend that for most applications the spreading angle θ_o may be taken to be 45° . Thus $\theta_o/2$ = 22.5° and T = 0.21 R_o. If the STM shown with the bottle-shaped stress field in Fig. 5.4 is used a similar result is obtained, T = 0.25R_o.

Thurlimann et al. (1983) recommend further that the required reinforcement be distributed 1/3A_s in the first half of the spreading zone and 2/3A_s in the top half. For

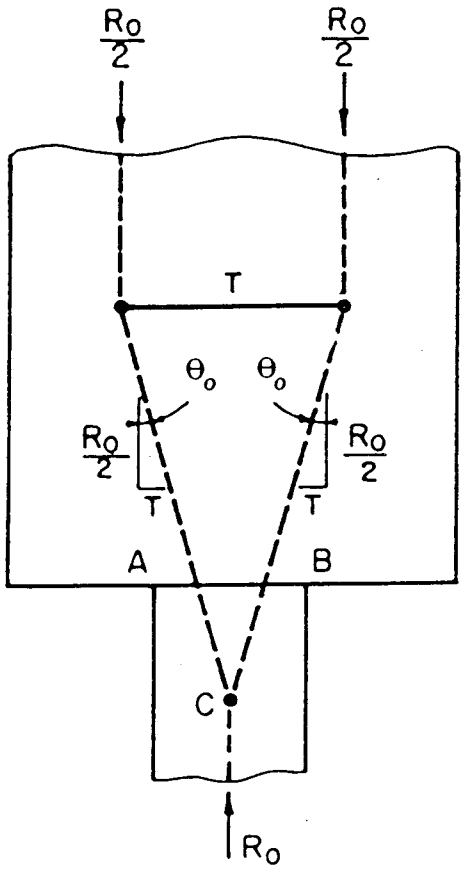

Figure 5.7 STM for Centered Fan Stress Field

bottle-shaped stress fields it is recommended that the reinforcement be distributed over the lower 0.8 ℓ in Fig. 5.4a.

5.2.4.4 Decentered Fans

If the radius of curvature of the nodal surface varies, the fan is called a decentered fan (Thurlimann et al., 1983). In Fig. 5.8(a) line AO represents the locus of the radii to points along the nodal surface AB and along the top surface DE. It can be shown that if the principal stresses, σ_1 and σ_2 along DE are constant then the radii must vary in such a way that DE and AB are parabolas (Mueller, 1978; Marti, 1980). If the principal stresses in the nodal zone are equal ($\sigma_1 = \sigma_2$) then the fan lines will be perpendicular to the surface AB. As in the case of the centered fan, σ_1 will vary along each fan line with radial position in the manner given by Eqn. 5.2 and the value of σ_2 is zero perpendicular to each fan line. Because the line DE is not perpendicular to the fan lines there must be both a normal stress and a shear stress on the top surface of the fan.

This stress field can be used to model a uniformly loaded deep beam as shown in Fig. 5.8(b). The beam has width b and uniform load p. If the nodal zone ABC has $\sigma_1 = \sigma_2 = -f_{ce}$, then the principal stresses in the nodal zone DEG are $\sigma_1 = -f_{ce}$ and $\sigma_2 = -p/b$. For horizontal equilibrium the height of the nodal zone AC must be equal to the height of the nodal zone EF.

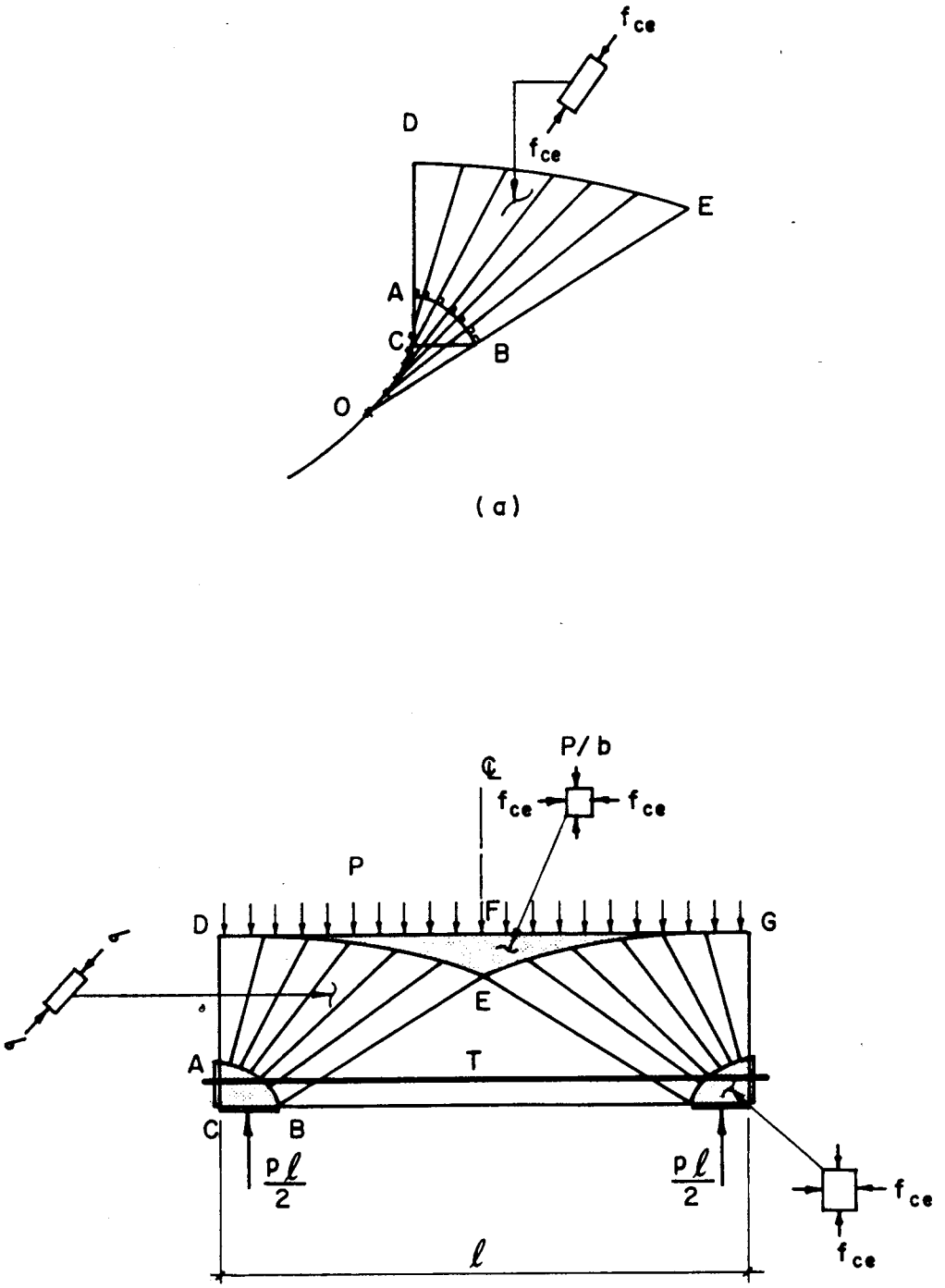

Figure 5.8 Parabolic Decentered Fan and Application

A uniformly loaded corbel is shown in Fig. 5.9a. In this case the top surface of the fan stress field is horizontal with constant vertical stress and varying tangential stress and the nodal surface will be hyperbolic. This stress field will be discussed in more detail since it is used in subsequent sections of this thesis.

The equation of the nodal surface through OAB is represented by the hyperbolic equation (Marti, 1980) :

$$(\eta + 1 - \omega_o)^2 - \zeta^2(\frac{f_{ce}}{p} - 1) = (1-\omega_o)^2 \qquad [5.8]$$

in which the ζ and η axes through O are non-dimensional and the height h is taken to be 1.0 (Fig. 5.9(b)). If the corbel is assumed to have unit thickness, then T, H, and V are forces per unit width and p is the uniformly distributed load applied to the corbel.

The nodal zone ABC has $\sigma_1 = \sigma_2 = -f_{ce}$. The principal compressive stress varies along each radial line from a maximum f_{ce} along AB to a lesser value at the surface DE. Along the fan line, σ_2 is assumed to be equal to zero so that each line may model the location of a crack. This implies that the tensile strength of the concrete is ignored.

The magnitude of σ_1 at any point may be determined by considering the equilibrium of a typical fan line passing through that point. Figure 5.10(a) shows the hyperbolic surface AB and the variation of fan centers O_A to O_B . The

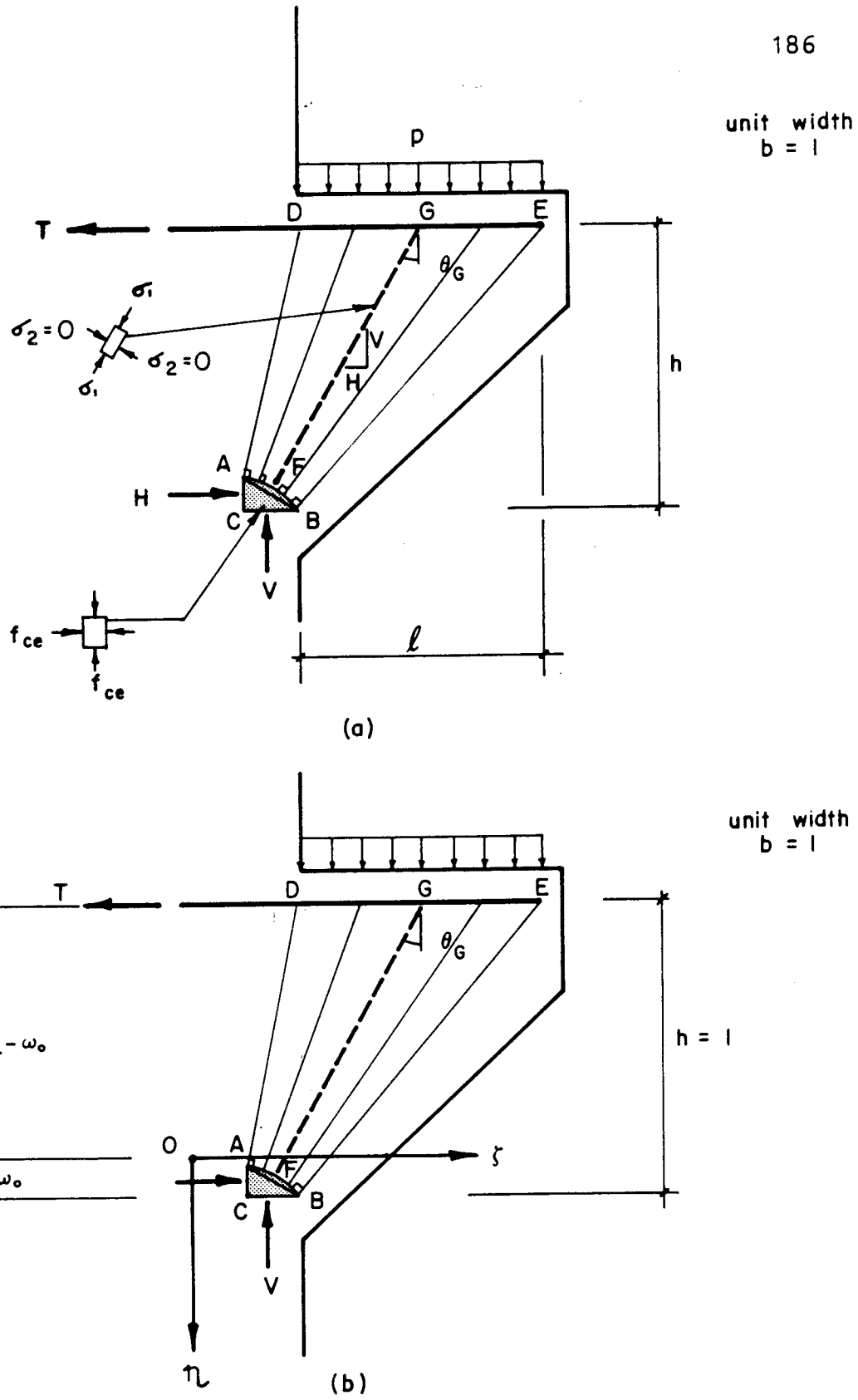

Figure 5.9 Hyperbolic Decentered Fan and Application

center of the typical fan line FG is at point O_F and the radius from O_F to F is r_F. The curve O_A - O_B represents the locus of all fan radii. The free body diagram of the small sector of fan FG is shown in Fig. 5.10(b). Using the same procedure as for the centered fan in Fig. 5.5, equilibrium in the radial direction of the small sector of fan FG gives:

$$\sigma_{1G} = \frac{r_F}{r_G} f_{ce} \qquad [5.9]$$

Similarly, the variation of the principal stress σ_1 along FG can be determined and is shown in Fig. 5.11(a).

The magnitude of the principal stress at G, σ_{1G}, can be related to the normal load p, and the angle θ_G using Mohr's Circle as shown in Fig. 5.11(b). The stresses on the horizontal plane at point G are the normal stress p and the shear stress τ_G. For a given value of p and θ, τ and σ_1 can be determined from Eqns. 5.10 and 5.11

$$\tau = p \tan \theta \qquad [5.10]$$

$$\sigma_1 = \frac{2p}{1 + \cos 2\theta} \qquad [5.11]$$

The procedure used when applying this stress field depends on the problem and which geometric parameters and forces are known at the start. In all problems force and moment equilibrium must be satisfied. To illustrate the solution using non-dimensional coordinates, a fan stress

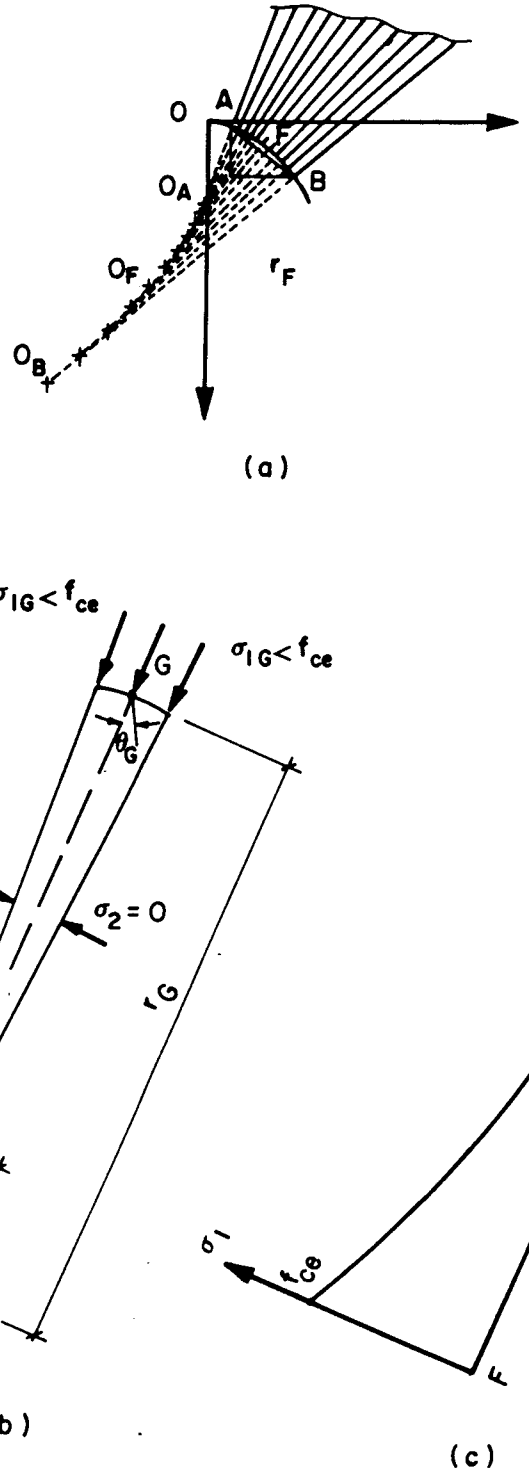

Figure 5.10 Hyperbolic Nodal Surface, Free-Body Diagram of Fan-Sector, and Variation in Principal Stress Along Fan

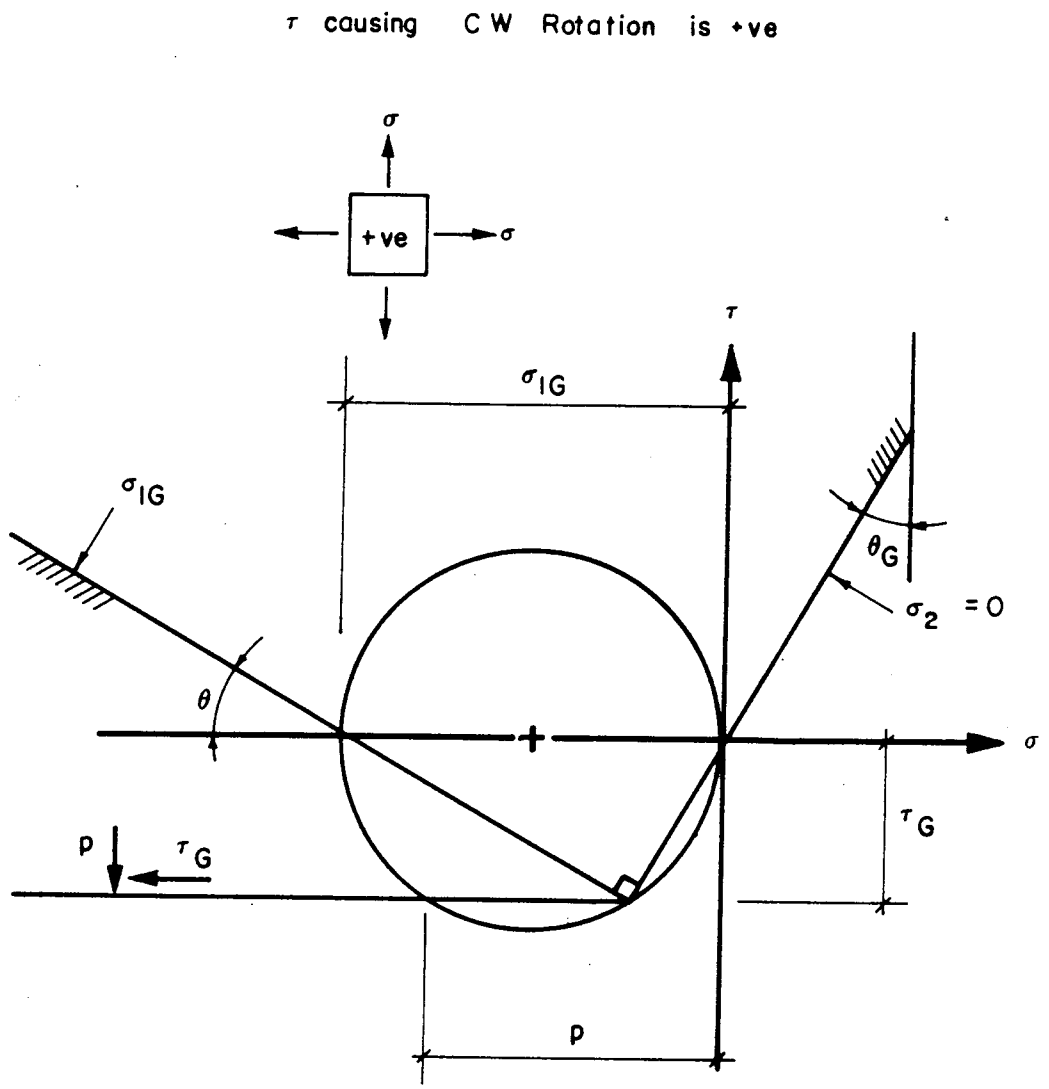

Figure 5.11 Mohr's Circle for Stress Transformation

field applied to a uniformly loaded steel-concrete composite beam will be discussed (O'Flynn, 1987). The test specimen simulates a portion of an ice-resisting wall for an offshore structure (Fig. 5.12).

In this case, the reinforcement is external to the beam. The tensile strength of the concrete is ignored and the tie force is provided by the steel plates. Shear transfer is assumed to be provided by friction and mechanical shear connectors. The applied load is assumed to be carried to the supports by three zones which are composed of hyperbolic fan stress fields (Fig. 5.12a).

Zone 1 is responsible for carrying the load on the cantilever to the support. The necessary fan is assumed to have a top surface length ℓ equal to the length of the cantilever and a height h equal to the depth of the concrete core (Fig. 5.13). With the additional assumption that point B of the nodal surface coincides with the outer edge of the support, the complete fan geometry is known for the assumed value of f_{ce}.

The horizontal distance x_{BC} is known from vertical equilibrium of the whole stress field.

$$x_{BC} f_{ce} = p\ell \qquad [5.12]$$

By summing moments about any point, the vertical distance y_{AC} can be determined. Thus, the horizontal force must be

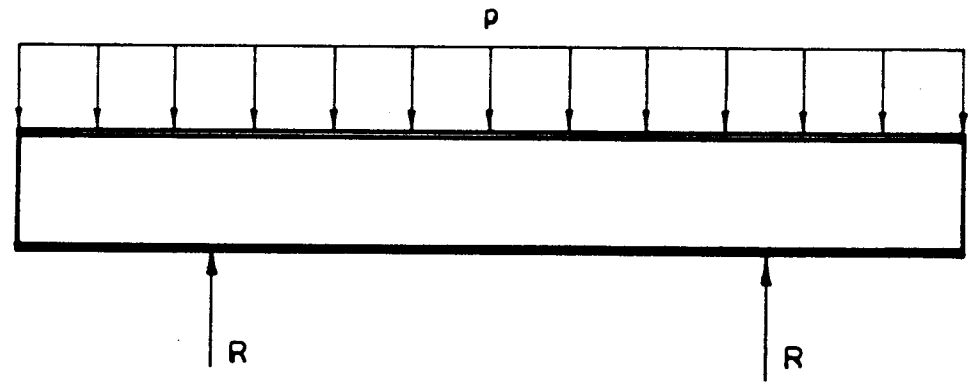

(a)

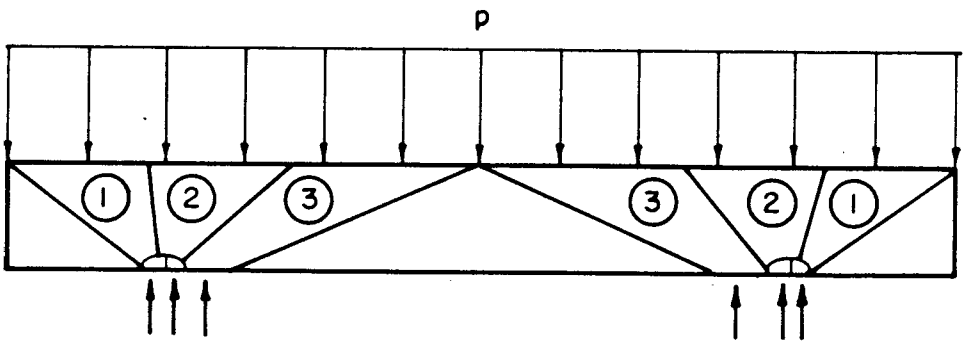

(b)

Figure 5.12 Fan Stress Fields Applied to Composite Beam

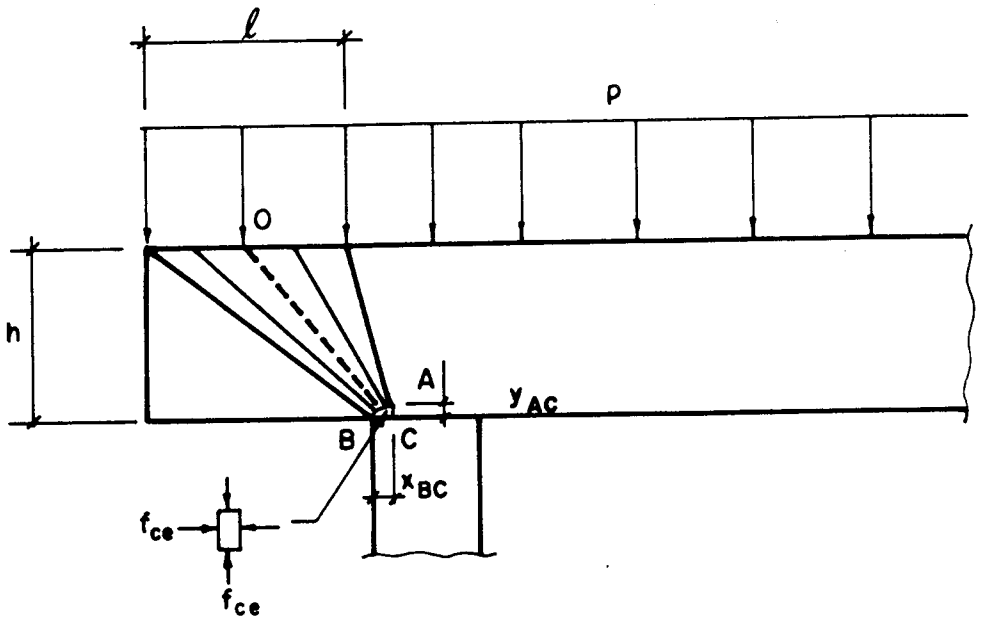

(a)

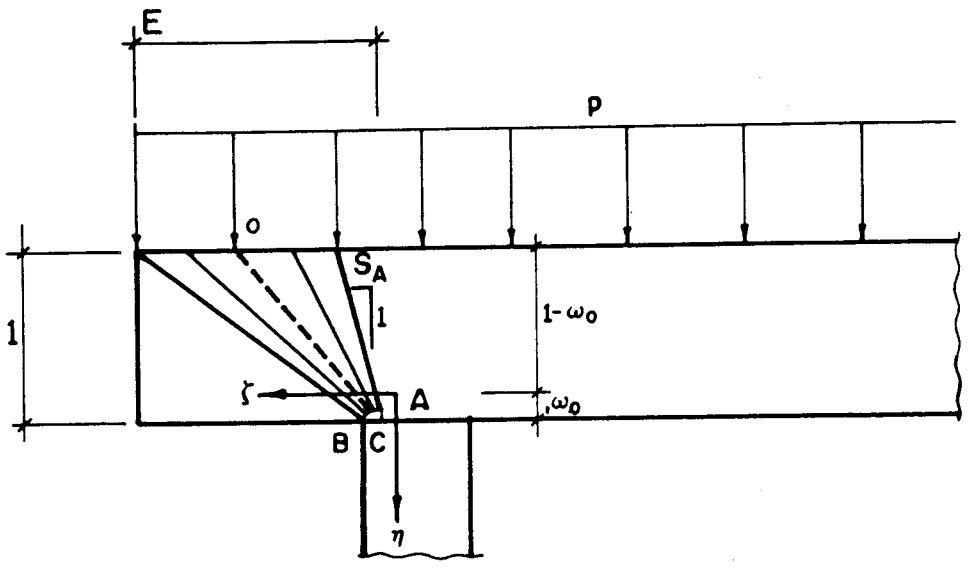

(b)

Figure 5.13 Details of Zone 1 and Normalized Fan Stress Field

$$H = y_{AC} f_{ce} \qquad [5.13]$$

which must also be equal to the tie force representing the tension T in the top steel plate assuming the required shear stresses may be transferred adequately to the steel plate.

If the distribution of the shear stresses is of interest then the equation of the nodal surface must be determined (Eqn. 5.8). The normalized fan stress field may be used to do this (O'Flynn, 1987). First, Eqn. 5.8 is differentiated to determine the slope of the fan line through point A, $1/s_A$.

$$s_A = \frac{\zeta_A((f_{ce}/p) - 1)}{(1 - (y_{AC}/h))} \qquad [5.14]$$

s_A is known for this case so that Eqn. 5.14 may be rearranged to give ζ_A.

$$\zeta_A = \frac{s_A(1 - (y_{AC}/h))}{((f_{ce}/p) - 1)} \qquad [5.15]$$

The coordinates of point A are (ζ_A, η_A) where η_A is obtained by substituting y_A into Eqn. 5.8. If Eqn. 5.15 is substituted into Eqn. 5.8, an equation for ω_o is obtained.

$$\omega_o = 1 - (1 - \frac{y_{AC}}{h})(1 - \frac{s_A^2}{((f_{ce}/p) - 1)})^{1/2} \qquad [5.16]$$

The coordinates of point B are (ζ_B, ω_o). Substituting these into Eqn. 5.8 gives Eqn. 5.17

$$\zeta_B = \left[\frac{\omega_o(2 - \omega_o)}{((f_{ce}/p) - 1)}\right]^{1/2} \qquad [5.17]$$

Since ω_o is known from Eqn. 5.16, ζ_B may be determined. As a check on horizontal and vertical equilibrium the following equations must be satisfied.

$$V = [\zeta_B - \zeta_A]\ h\ f_{ce} \qquad [5.18]$$

$$H = [\omega_o - \eta_A]\ h\ f_{ce} \qquad [5.19]$$

Moment equilibrium may also be verified by taking moments about any point.

If E is the non-dimensional coordinate measured along the top surface from the η axis, then

$$\frac{\tau}{p} = \tan\theta = \frac{E - \zeta}{1 - \omega_o + \eta} \qquad [5.20]$$

Vertical equilibrium of the whole stress field dictates that for any coordinate E,

$$\zeta = \frac{p}{f_{ce}} E \qquad [5.21]$$

From Eqn. 5.8, 5.20 and 5.21, it can be shown that the ratio τ/p may be expressed as

$$\frac{\tau}{p} = \left[\frac{(1 - \omega_o)^2}{E^2(1 - (p/f_{ce}))^2} + \frac{(p/f_{ce})}{(1 - (p/f_{ce}))}\right]^{-1/2} \qquad [5.22]$$

Eqn. 5.22 may be used to determine the shear stress distribution which must be transferred to the steel plate. A typical distribution of normal and shear stresses is shown in Fig. 5.14.

The analysis of the beam continues with the development of Zone 2 and Zone 3. Some iterations are required before the analysis is complete (O'Flynn, 1987).

The use of the hyperbolic fan stress field is discussed further in Sect. 5.2.6.4 and applied in Chapter 6.

5.2.5 Nodal Regions

The regions where compressive struts and tension ties meet are called nodal zones. The nodal zone is an idealized representation of the way in which the compressive stress fields and tension ties intersect.

Nodal zones may be classified according to the type and number of forces which intersect there. When three forces meet, equilibrium requires that the forces be concurrent. When three compressive forces meet, the nodal zone is called a CCC nodal zone (Fig. 5.15(a)). Typically the magnitude of the stress in each of the struts is taken to be equal to f_{ce}. This means that the line of action of each force will be perpendicular to one side of the nodal zone and that the widths of the sides are in the same proportion as the magnitudes of the forces. The state of stress of the nodal zone will be $\sigma_1 = \sigma_2 = - f_{ce}$. The force triangle will be similar to the triangle ABC of the nodal zone. The nodal

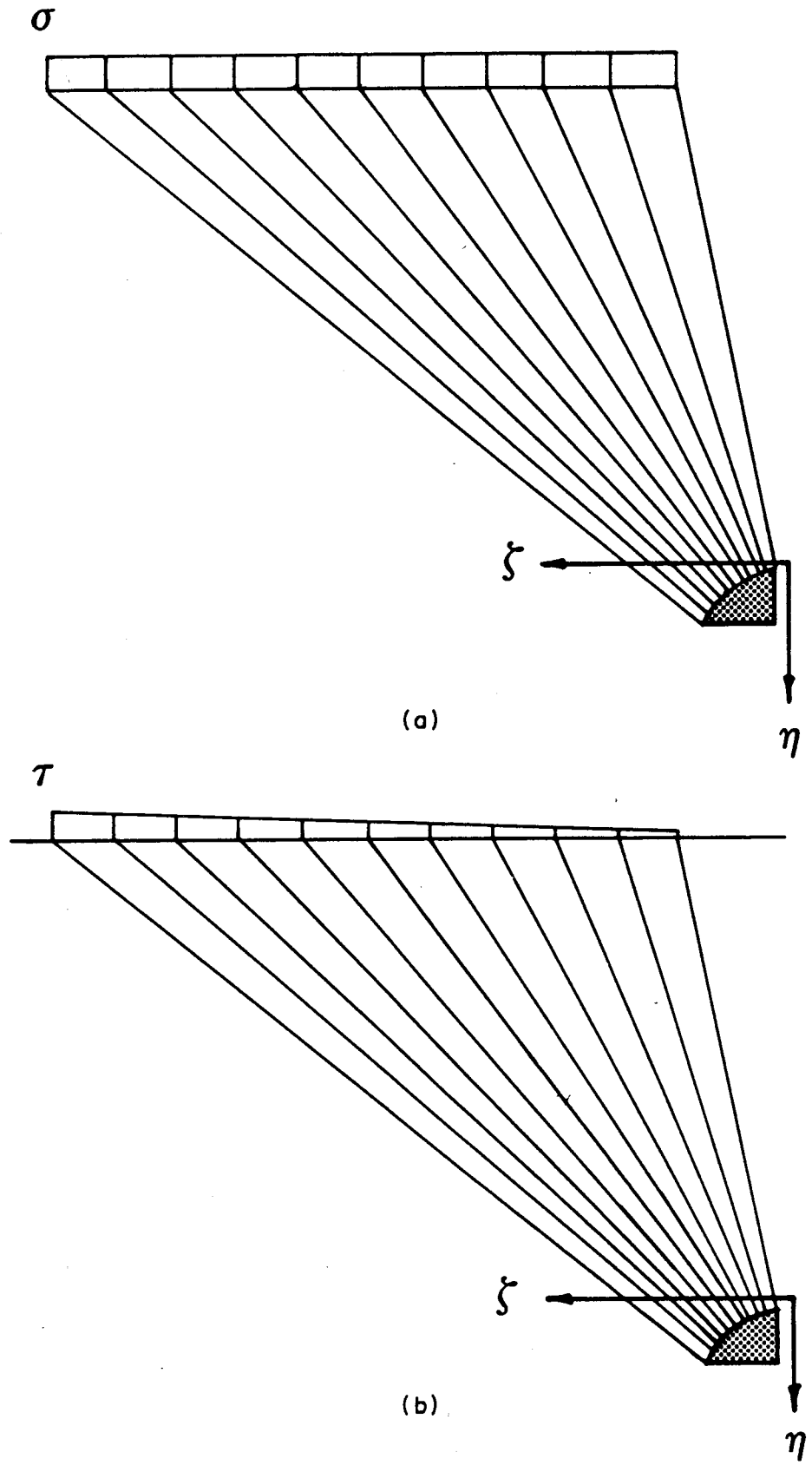

Figure 5.14 Normal and Shear Stress Distribution for Zone 1

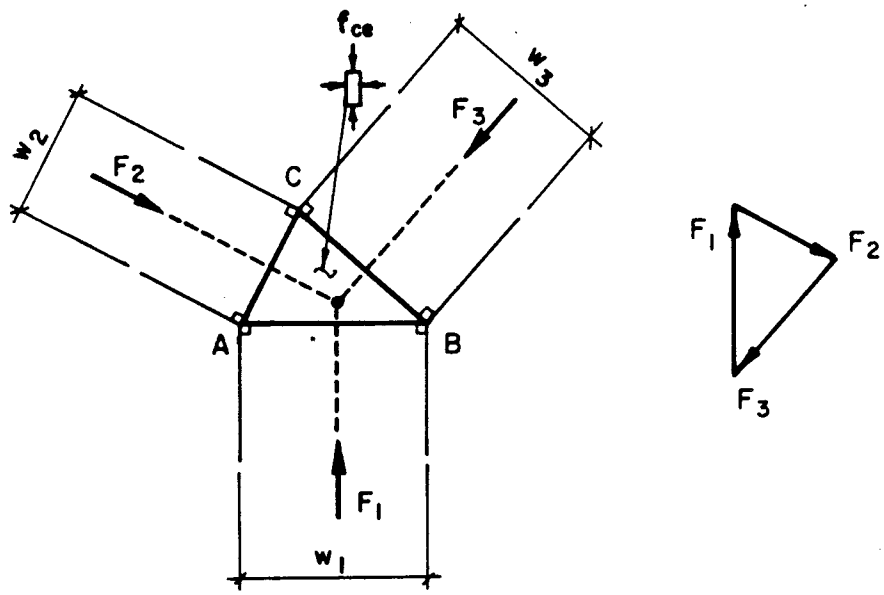

(a)

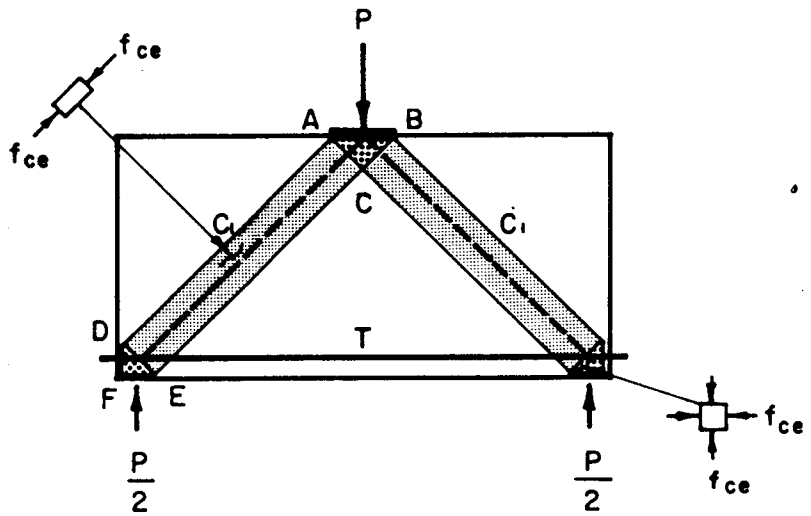

(b)

Figure 5.15 Triangular CCC Nodal Zone with Equal Stresses

zone, ABC of Fig. 5.15(b) is an example of a triangular CCC nodal zone with equal stresses. The load P is applied through a bearing plate of width greater than or equal to the width AB such that the stress along AB is $-f_{ce}$. Similarly, the widths of the struts are such that the principal stresses along AC and BC are also $-f_{ce}$.

A CCC nodal zone with curved surfaces is shown in Fig. 5.16(a). An application of this nodal zone is found in the uniformly loaded deep beam in Fig. 5.16(b). In this nodal zone the principal stresses are $\sigma_1 = -q/b$ and $\sigma_2 = -f_{ce}$ where q is the applied load and b is the width of the beam. The surfaces AC and BC are the top surfaces of parabolic decentered fans as discussed in Sect. 5.2.4.4. Principal stresses along AC and BC vary according to the geometry of the fan. It is seen that the fan lines are not perpendicular to the nodal surface. By considering horizontal equilibrium it can be shown that the width of the nodal zone at C must be equal to the height of the nodal zone at DF.

In a CCT nodal zone, two compressive forces meet a tension tie. A CCT nodal zone may be triangular (Fig. 5.17(a)) or it may have curved surfaces (Fig. 5.17(b)). If the stresses in the struts are equal to f_{ce}, then the nodal zone has $\sigma_1 = \sigma_2 = -f_{ce}$. The line of action of each force and each fan line is perpendicular to the surface of the nodal zone.

CCT zones are often idealized as having an anchor plate which allows the tie to develop outside the nodal zone so

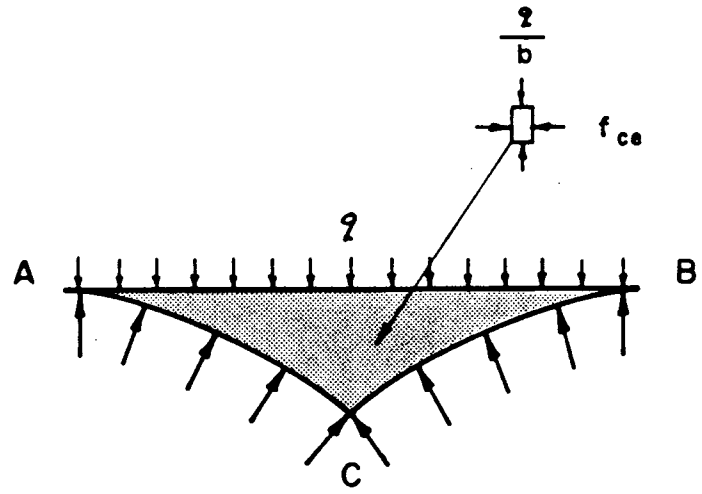

(a)

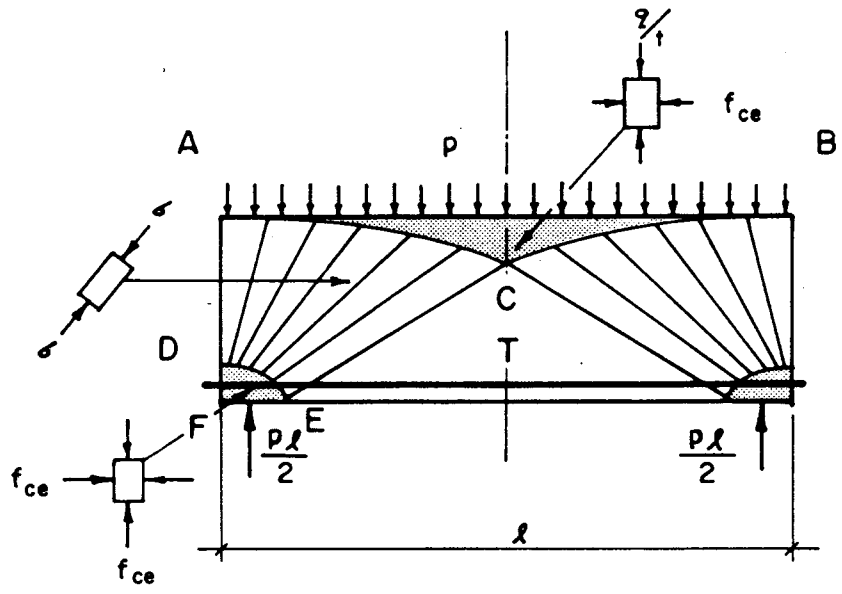

(b)

Figure 5.16 Curved CCC Nodal Zone and Application

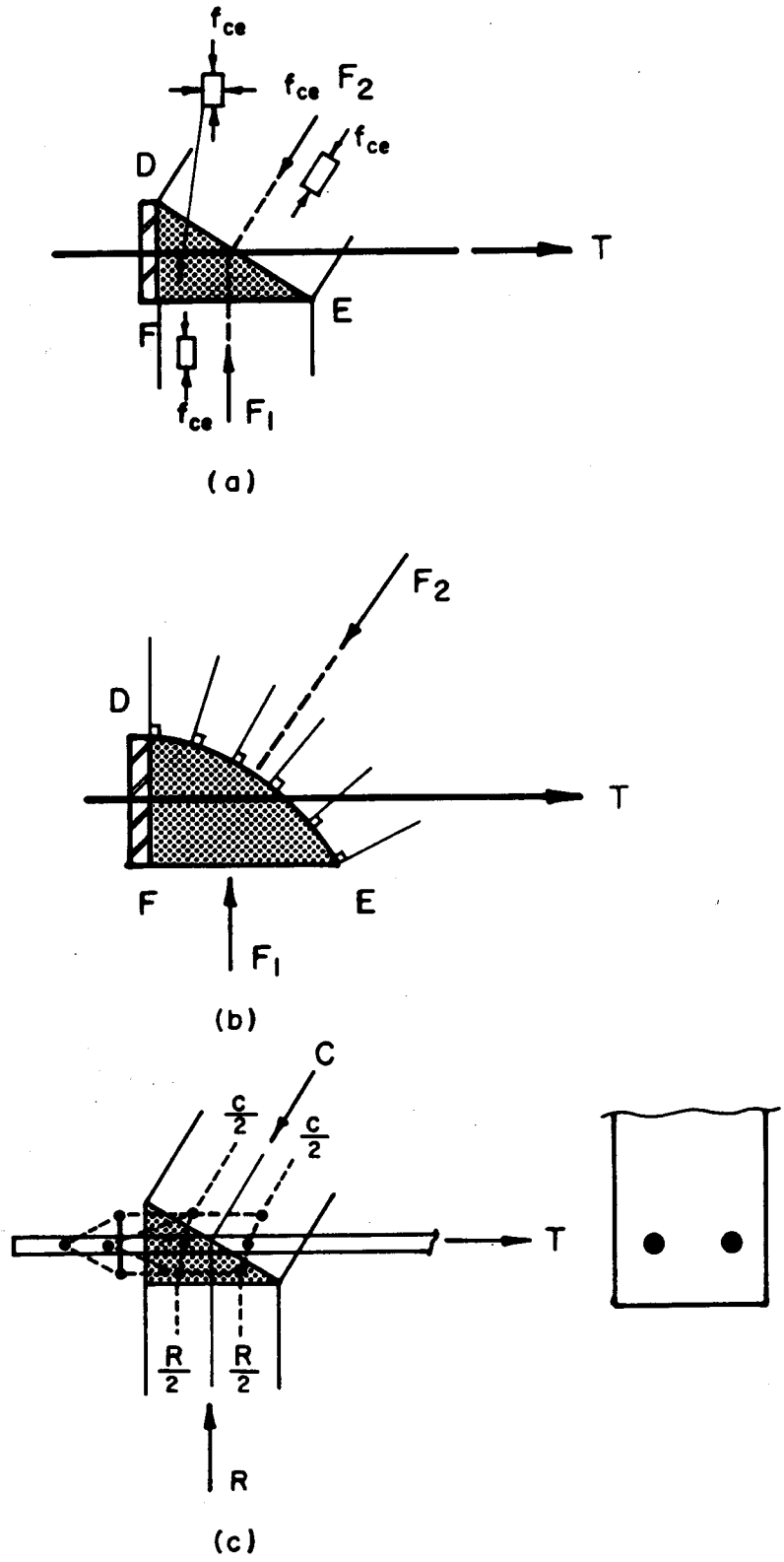

Figure 5.17 CCT Nodal Zone

that the nodal zone behaves like a CCC nodal zone through which a tension tie passes. It is because of this strain discontinuity that the recommended effective concrete strength for CCT nodes is often reduced (Schlaich et al. 1987; CAN3 A23.3-M84). The nodal zone DEF in Fig. 5.15(b) and in Fig. 5.16(b) is a typical example of a CCT node.

Typically, anchor plates are not used, and the reinforcement represented by the tension tie must develop by bond and/or hook anchorages. The force in a reinforcing bar is transferred to surrounding concrete by compressive stresses. It is because these stresses change direction that transverse tensile stresses ("splitting stresses") develop. In regions where these transverse stresses are limited or prevented, straight bar anchorage or bond is enchanced. In a CCT region at a support, for example, the reactive force and the strut act to prevent the formation of the transverse tensile stresses thereby improving the bond. However, outside the region of the joint, sufficient anchorage must be provided for the force remaining in the bar. Before a CCT node can be completed, the anchorage of the tension tie must be ensured.

A strut-and-tie model can be used to describe the bond mechanism for reinforcing bars with and without the confining pressure from the reaction (Fig. 5.17(c)). The struts and ties are seen to correspond to the stress distribution assumed in Fig. 5.17(a). Although models for bond such as these may be found in the literature (Schlaich

and Weischede, 1982; Schlaich and Schafer, 1984), there is little guidance as to how these are developed or how these might be used in practice. At the present time, it is recommended that applicable design codes be used to determine the required development lengths (Schlaich et al., 1987). It is clear that careful and systematic research is needed on the topic of bond, force transfer mechanisms and the STM. Force transfer mechanisms are discussed in more detail in Sect. 5.2.6.

Other three-force nodal zones are the CTT and TTT nodal zones. A typical CTT nodal zone occurs where stirrups, longitudinal reinforcement, and a compressive stress field meet, as in the case of beams with shear reinforcement. This case is discussed in Sect. 5.2.6.2. Because it will be required in Chapter 6, a special CTT node from a typical frame closing joint will be discussed in Sect. 5.2.6.4. TTT nodal zones exist only rarely and will not be discussed here. These and other three-force nodal zones are discussed conceptually by Schlaich and Schafer (1984), Marti (1985) and Schlaich et al. (1987).

When more than three forces act at a nodal zone, the forces will not all be concurrent. Such is the case in the nodal zone where four compressive forces meet shown in Fig. 5.18(a) . The forces F_1, F_2, F_3 and F_4 are in equilibrium. The struts each have $\sigma_1 = - f_{ce}$ and $\sigma_2 = 0$ and the nodal zone has $\sigma_1 = \sigma_2 = -f_{ce}$. As a result, the width of the sides vary in the same proportion as the forces and the struts are

perpendicular to the sides.

It is seen that the forces are non-concurrent. However, F_5, the resultant of F_3 and F_4, is concurrent with F_1 and F_2 at point 0. The forces F_3 and F_4 must intersect at point 0' which is along the line of action of F_5. If any three of the four forces are known then the other force is easily determined.

Node ABCD is taken from the strut-and-tie model for Specimen B1 (Node EE, Fig. 6.49). F_1, the applied load, and F_2, the compressive force at the point of maximum moment, are both known. F_3, the force carried by fan action, and F_4, the compressive force in the top chord are not known. Their magnitudes and directions were evaluated after assuming the percentage of the total shear to be carried by strut and by fan action. As shown in Fig. 5.18(b), fan action requires that the nodal surface have a curved (hyperbolic) surface. However, the fan must be statically equivalent to F_3, having horizontal and vertical components H and V, respectively.

In this section, various nodal configurations were discussed. In particular, whenever a tension tie provides a force to a nodal zone the force in the reinforcing must be transferred via compressive stresses to the concrete. In most cases simple development length considerations will suffice. In other cases the force transfer mechanisms need to be investigated. Some of these situations are discussed in the next section.

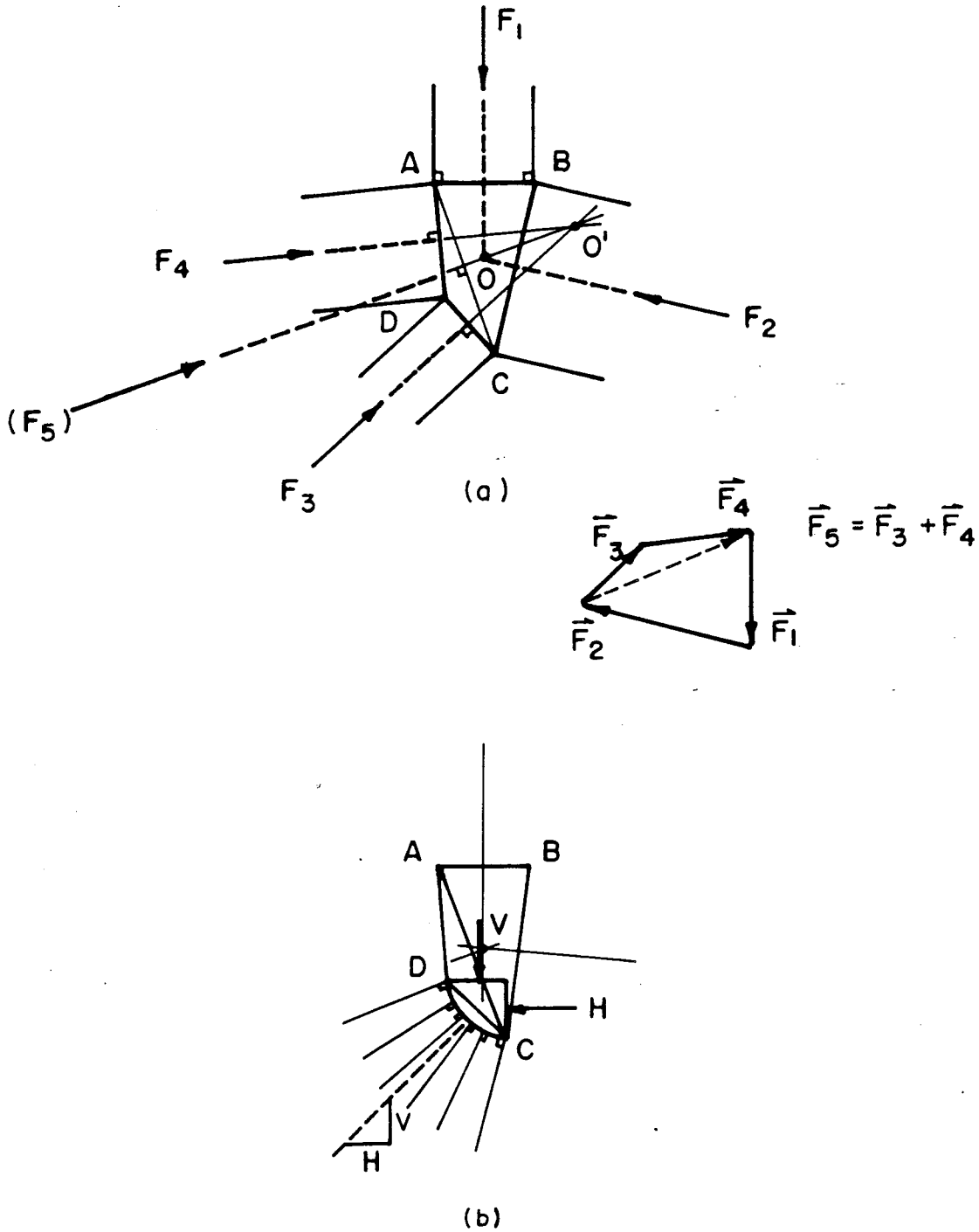

Figure 5.18 Nodal Zone with Four Forces (from Specimen B1)

5.2.6 Force Transfer Mechanisms and the Strut-and-Tie Model

5.2.6.1 Anchorage of Straight Bars

In a pull-out test, a reinforcing bar is embedded in a block of concrete or a concrete cylinder and a hydraulic jack is used to pull the bar out of the specimen (Fig. 5.19(a)). If the embedment length ℓ is sufficiently long, the stress in the bar will reach yield, $f_s = f_y$, before the bar pulls out.

The stresses in the bar are gradually transferred to the concrete over the length l (Fig. 5.19(b)). The mechanisms responsible for this stress transfer are referred to as 'bond' and the stresses at the idealized concrete-reinforcing bar interface are referred to as 'bond-stresses' (Fig. 5.19(c)). If f_s is equal to f_y, then the average bond stress, μ_{AVE}, acting on the surface of the bar is given by Eqn. 5.23.

$$\mu_{AVE} = \frac{A_b f_y}{\pi d_b l} = \frac{\pi^2 d_b^2 f_y}{\pi d_b l} = \frac{d_b f_y}{4l} \qquad [5.23]$$

In recent bond literature (ACI Committee 408, 1966; Rehm, 1968; Tempfers, 1973; Orangum et al., 1977) it is generally accepted that for deformed bars which are loaded near the maximum bond strength, the primary force transfer mechanism is through the bearing of inclined compressive struts on the bar deformations (Fig. 5.20(a)). If adequate concrete exists around the bar the compressive stresses radiate uniformly from the bar requiring circumferential

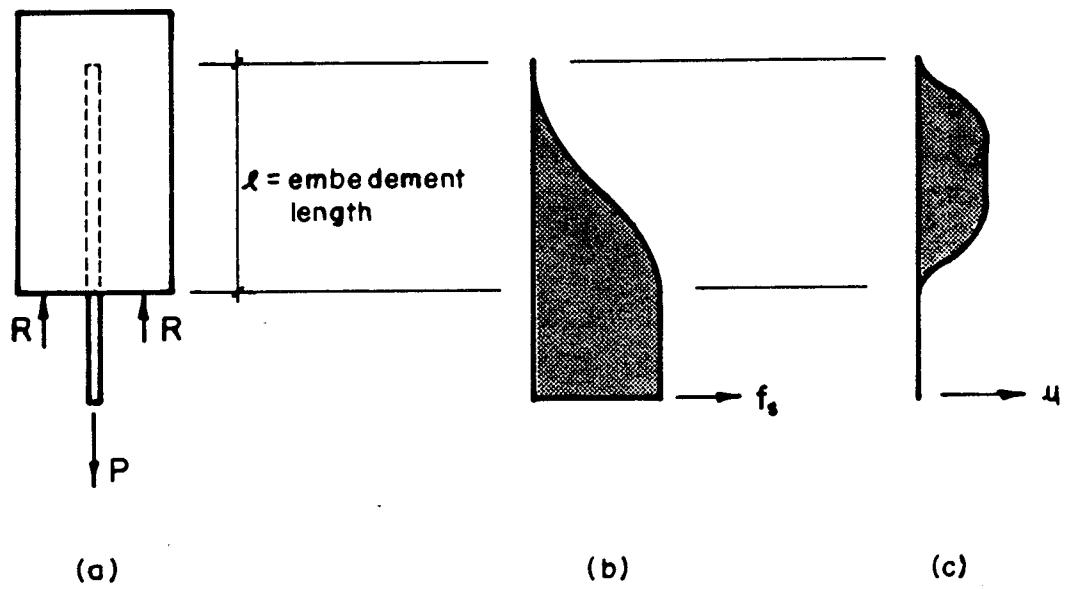

Figure 5.19 Stress Distributions in a Pull-Out Test

tensile stresses in the concrete for equilibrium (Fig. 5.20(b),(c)). The circumferential stresses are analagous to hoop stresses. The longitudinal components of the compressive stresses are what are responsible for 'bond'.

Typically failure will involve splitting of the concrete due to the circumferential stresses (Fig. 5.20(d)). The principal factors affecting the load at which a splitting failure occurs are the tensile strength of the concrete, the change in bar stress over a given length (i.e. the length over which the bond is required to develop), and the minimum distance to the surface of the concrete or to the next bar (Orangun et al., 1977).

Because bond stresses vary along the length of the bar and because of the variety of situations in real structures, the CSA Code uses the concept of development length. The development length, l_d, is the minimum length of embedment over which the stress in the bar can increase from zero to the yield stress f_y. The development length is evaluated as the product of the basic development length, l_{db}, and modification factors which are intended to account for the influence of casting position on the concrete surrounding the bar, bars with yield strength in excess of f_y, lightweight concrete, and conditions which affect the formation of the circumferential tensile stresses.

The pull-out test is not representative of the situation in a beam. This is because beams exhibit flexural cracking which greatly affects the distribution of the bond

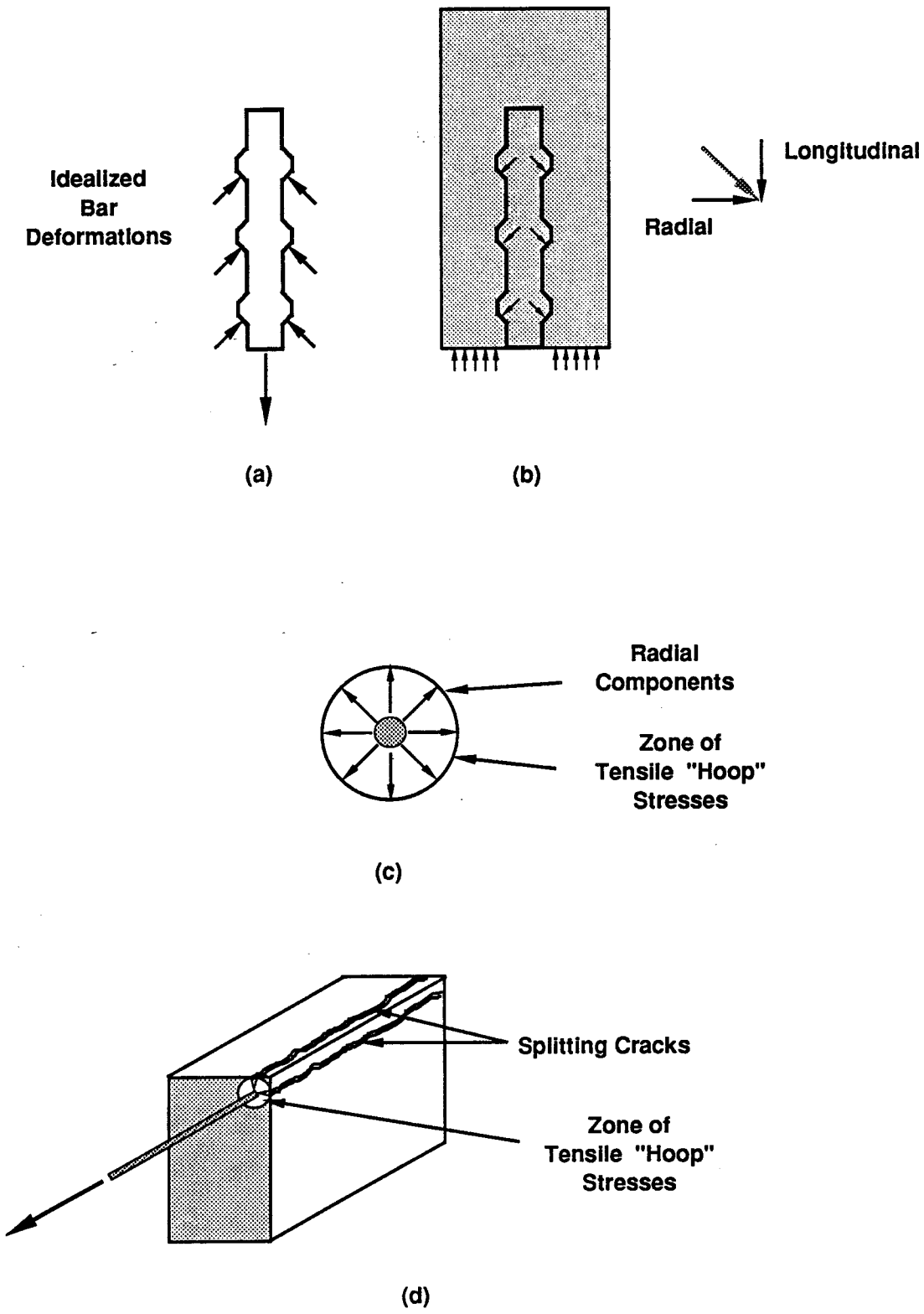

Figure 5.20 Bearing Stresses and Components in Pull-Out Test

stresses. Consequently, small beam tests have been used to evaluate recommendations for the development length l_{db}.

If the development lengths required by the CSA Code are substituted into Eqn. 5.23, the average 'design' bond stress assumed in the code may be determined. Assuming f_y = 400 MPa and assuming all modification factors are 1.0 the curves in Fig. 5.21 may be drawn. It is seen from the figure that for smaller bars and higher concrete strengths the term l_{db} not less than $0.058d_bf_y$ in Clause 12.2.2 of the Code governs the development length and the limiting bond stress for f_y = 400 MPa is 4.3 MPa. For comparison the ultimate bond stress from the CEB-FIP Model Code is shown in the same figure. At 50 MPa, the maximum bond stress is 4.5 MPa.

It should be noted that the Code equations for development length include a factor (x 1.25) to allow for the possibility of overstrength reinforcement, i.e. when we specify f_y = 400 MPa we actually provide for f_s = 500 MPa. The design bond strengths in Fig. 5.21 should be increased by 25% to get the "ultimate" bond strengths. If this is done, then the limiting value for smaller bars and higher concrete becomes 5.4 MPa instead of 4.3 MPa.

The CSA Code has modification factors for development length which attempt to account for a variety of conditions. There are two effects which are not accounted for, however, and these will be discussed next.

Beam reinforcement is typically surrounded by stirrups and such stirrups will cross the potential splitting planes

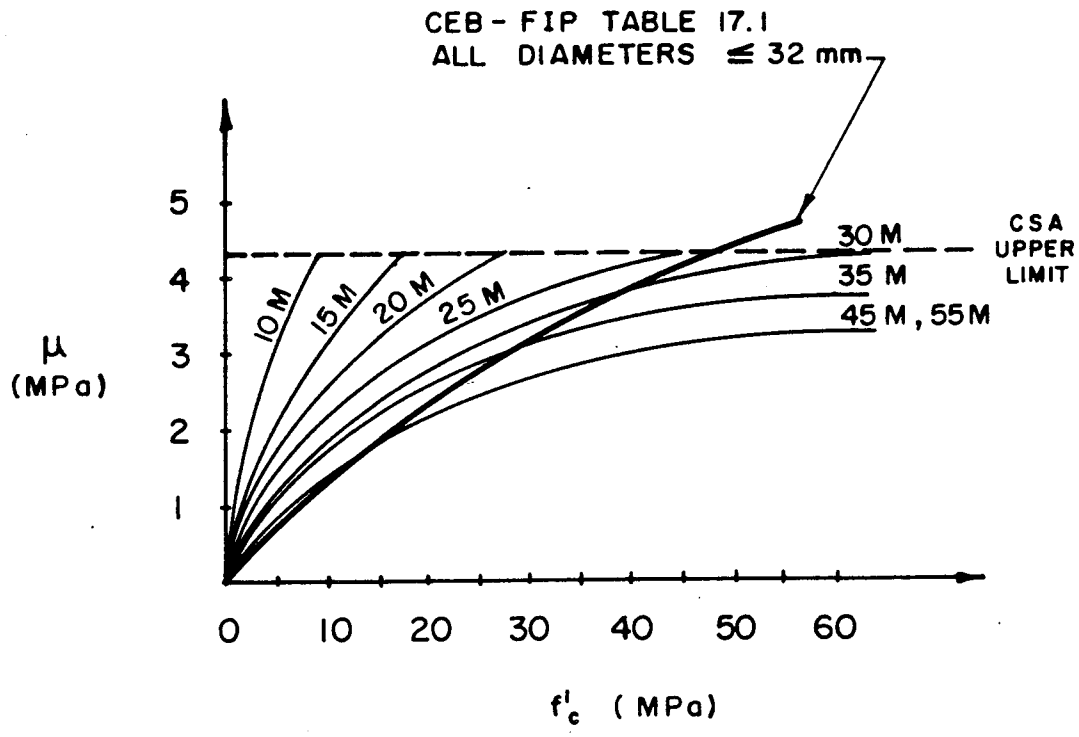

(a)

Figure 5.21 Design Bond Strengths for Deformed Bars Based on CSA Code (f_y=400 MPa) and CEB-FIP Model Code

discussed above. The splitting failure is thus delayed and the bond strength improved. This is not accounted for in the CSA Code and many of the beam tests used to determine the Code expressions did not include this parameter.

A second effect is the beneficial effect of transverse compression when applied over all or part of the development length. Although specific research in this area is quite limited, tests (Untrauer and Henry, 1965; Robins and Standish, 1982) indicate significant increases in bond strength when lateral pressure is applied to pull-out specimens and to beam test specimens. This situation is not addressed by the CSA Code. As discussed in Sect. 5.2.5, this situation occurs at the supports of deep beams where the reinforcement must develop full or nearly full capacity over a short distance.

It is difficult to provide development length or bond strength requirements that are applicable for all situations. The modification factors discussed above attempt to account for some of the variation. Even so, the variety of ways that forces are transferred into reinforcement make the problem a difficult one. For example, based on the forgoing discussion, the forces must be transferred differently in a pull-out test than in a beam with stirrups, or deep beam, or slab, or corbel, or beam-column connection etc.. In all of these cases however, the same basic mechanisms of force transfer must be operating. In attempting to treat all of the practical possibilities with

one requirement, the code values for bond strength are necessarily conservative. It is known from tests, that significantly higher bond strengths may be achieved over short anchorage lengths (Berggren, 1965).

It is useful to consider the strut-and-tie model proposed by Schlaich and Schafer (1984). This models the anchorage of a straight bar in a pull-out test with adequate concrete cover surrounding the bar. Friction is assumed to be prevented where the reaction is applied to the test specimen. The STM is based on stress trajectories (Fig. 5.22(a)). The compressive stresses are modelled by compressive struts, while the tensile stresses are modelled as ties (Fig. 5.22(b)). The struts are responsible for transferring the bond stresses to the deformations of the bar. This is assumed to occur by bearing as discussed above. The tensile strength of the concrete is responsible for the tie forces. Since the tensile stresses actually project radially from the bar, the model represents one plane of the actual specimen. Although details of the model are not discussed, it does provide a useful conceptual model. From the model, it is apparent how the factors discussed above influence the bond strength.

5.2.6.2 Beams with Stirrups

A beam containing stirrups must be able to transfer diagonal compressive stresses in the web to the longitudinal reinforcement and to the stirrups.

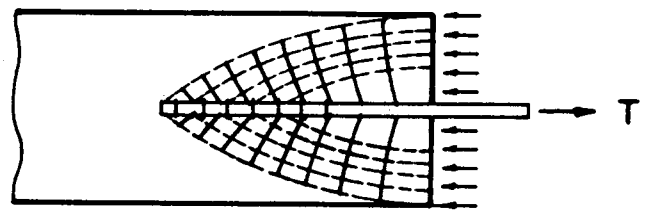

(a)

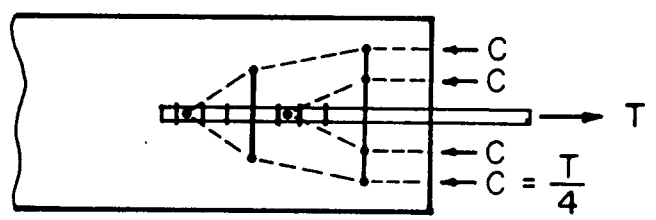

(b)

Figure 5.22 STM for Anchorage of Straight Bars

The 45° truss model was proposed by Ritter (1899) and Morsch (1902) to model the shear behavior of reinforced-concrete beams. In this model, the tensile strength of the concrete is neglected and the diagonal compressive stresses are assumed to act at 45° to the beam axis. The diagonal compressive stresses, f_{CD}, are assumed to act uniformly over the depth of the beam as shown in Fig. 5.23(a). For uniformly spaced stirrups, equilibrium of one stirrup (Fig. 5.23(b)) requires that the horizontal component of the diagonal compressive stresses in the concrete be balanced by the tensile force in the longitudinal reinforcement and the vertical component of the concrete stresses be resisted by the force in the stirrup $A_v f_y$. The tensile force in the longitudinal reinforcement due to shear is called N_v and for the 45° truss, N_v is equal to V. The force N_v is recognized but not specifically accounted for in the ACI Code and the CSA Simplified approach. Instead, bars are required to be extended a specified distance past where they are no longer needed for flexure.

In this approach and in the variable angle truss model and the Detailed Approach of the CSA Code, it is not clear how the forces discussed above are transferred to the reinforcement. Based on the previous discussion we may speculate that the transfer takes place through bearing and bond stresses. In a high shear/low moment region where there are, for instance, only two longitudinal bars it is clear that the total vertical stresses in the concrete must bear

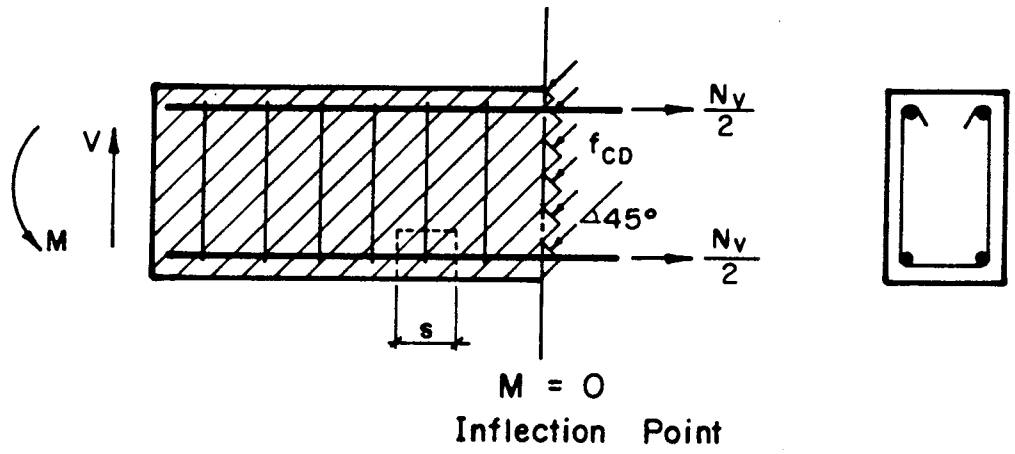

(a)

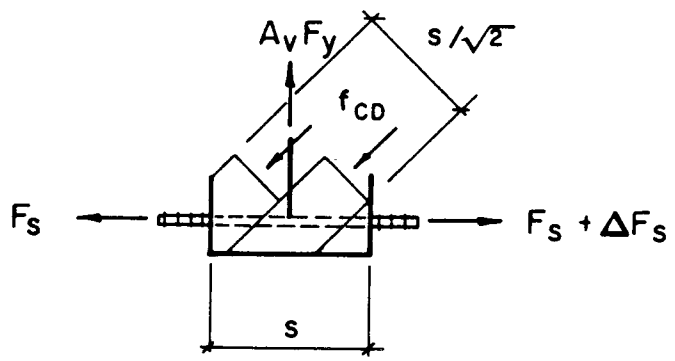

(b)

Figure 5.23 45° Diagonal Compressive Stresses and Equilibrium of One Stirrup

on the longitudinal bars in order to activate the stirrups. Furthermore, over the same distance, the total horizontal stresses must be transferred to the longitudinal reinforcement by bond. Suitable questions regarding this might be:

1. For the absolute maximum shear force, what bond and bearing stresses are implicit in the Code approach?
2. To what extent is the stirrup effective in the confinement and improvement of the bond strength?
3. Spalling is recognized in the Detailed Approach of the CSA Code. How are the forces transmitted differently if spalling has occurred on the sides of the beam? On the sides and the top surface?

It appears that further research is necessary to answer these questions.

An adaptation of a strut-and-tie model proposed by Schlaich and Schafer (1984) is shown in Fig. 5.24. The STM in Fig. 5.24(a) shows how the compressive diagonal stresses must converge in elevation to a CTT nodal zone ABC. The bottle-shaped stress field shown best describes this. The nodal zone is anchored vertically by the stirrup force $A_v f_y$ and horizontally by the bond force represented by ΔT. As shown in Fig. 5.24(b) the stress field must also converge in the cross section to the nodal zone. This very effectively illustrates the three-dimensional nature of the problem. The 'three-dimensional bottle-shaped stress field' is seen to be in equilibrium with the stirrup force $A_v f_y/2$ and the lateral

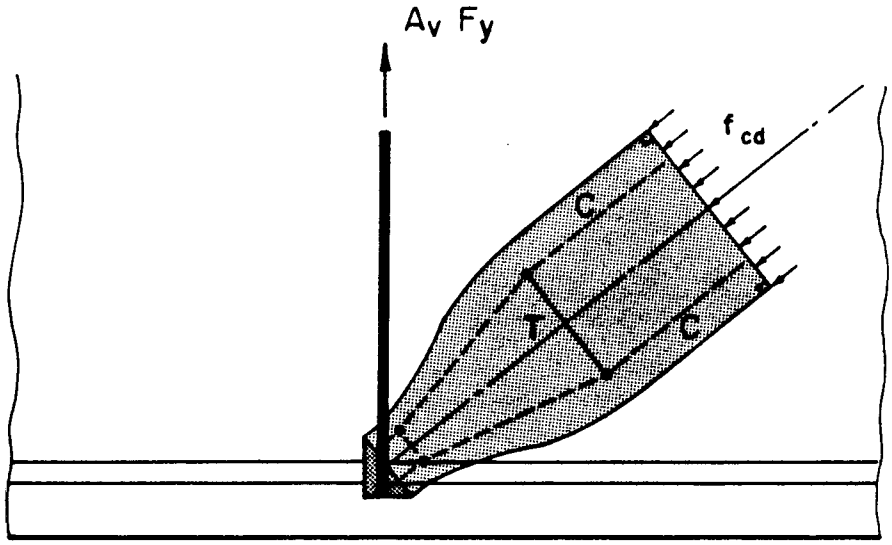

(a)

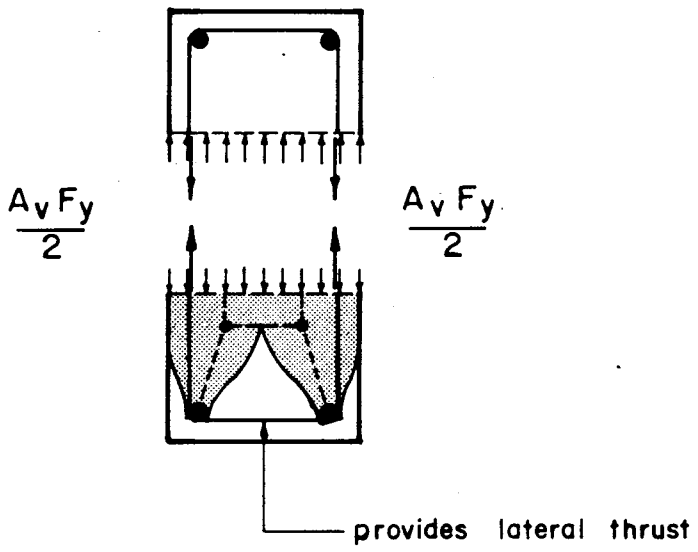

(b)

Figure 5.24 STM of Nodal Zone at a Stirrup

thrust provided by the closed stirrup.

5.2.6.3 Steel-Concrete Composite Beam

The situation is somewhat different in the steel-concrete composite beam shown in Fig. 5.12. As discussed in Sect. 5.2.4.4, the load is assumed to be carried to the supports via fan shaped stress fields. With this assumption it is assumed that the vertical load, V, is distributed uniformly as a normal stress, p, and the horizontal load, H, is distributed as the tangential or shear stress, τ, which varies along the steel plate. In the reinforced concrete beams discussed above the width of the compressive diagonals was much greater than the width of bearing on the reinforcement. Furthermore, depending on the bar layout, assumptions are necessary regarding how the tangential stresses are transferred. In the case of the composite beam, the external reinforcement (i.e. the steel plate) has the same width as the fan. Consequently, the normal and tangential stresses evaluated from the fan are the same as the stresses which must be transferred to the plate.

$$\sigma_N = p \qquad [5.24]$$

$$\sigma_T = \tau \qquad [5.25]$$

The magnitude of p is known, and the distribution of τ may be determined from Eqn. 5.22. The distribution of these stresses has been determined for the fan from Zone 1 and is

shown in Fig. 5.25. As suggested in Sect. 5.2.4 these stresses are assumed to be transferred by bearing (Fig. 5.25(a)) and by friction and mechanical shear connectors (Fig. 5.25(b)). If the coefficient of friction between the concrete and the steel plate is taken to be 0.6 as specified in the shear friction section of the CSA Code, then mechanical shear connectors are required where τ/p exceeds 0.6 (Fig. 5.25(c)).

5.2.6.4 Joints Subjected to Closing Moments

As a final illustration, the force transfer mechanisms associated with a knee-joint subjected to closing moments will now be discussed. A strut-and-tie model which includes a fan stress field is proposed for this type of joint.

A knee-joint subjected to closing moments is shown in Fig. 5.26(a). Tests indicate that cracking will generally occur as shown (Kemp and Mukherjee, 1968; Nilsson, 1973). The forces acting on the joint may be idealized as shown in Fig. 5.26(b). The outer reinforcing bars will generally yield and for equilibrium of the joint, the bars must transfer a force equal to $\sqrt{2}A_s f_y$ This is assumed to occur in the region of the bend. However even for recommended reinforcement ratios (Kemp and Mukherjee, 1968) the bearing stresses on the bars are high enough to suggest that the bearing must occur over a distance larger than this. Furthermore, the diagonal compressive stresses do not intersect the reinforcement orthogonally at all locations and the stresses must be transferred by normal stresses and

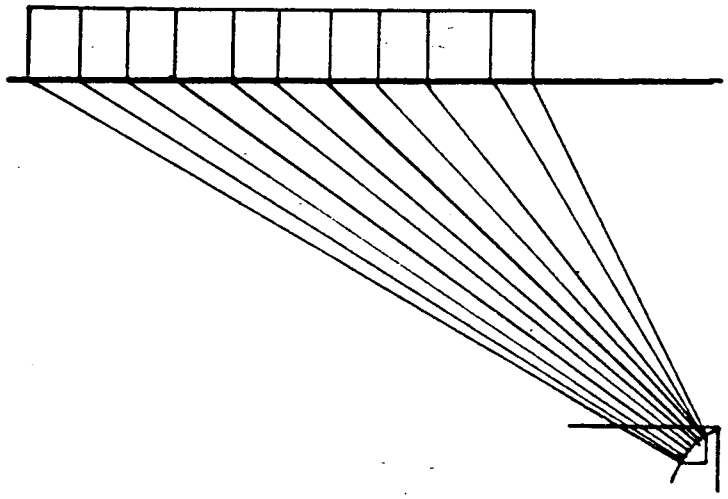

(a)

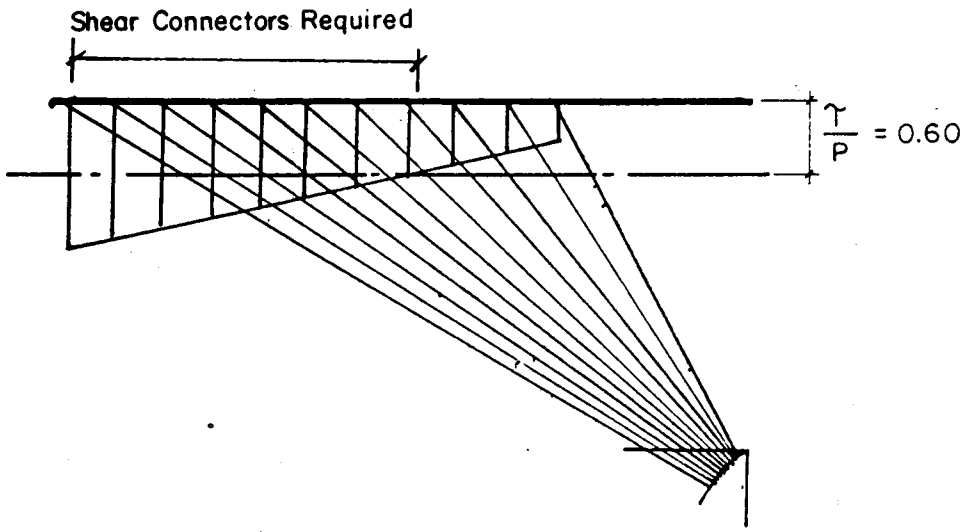

(b)

Figure 5.25 Normal and Shear Stress Distribution for Zone 1

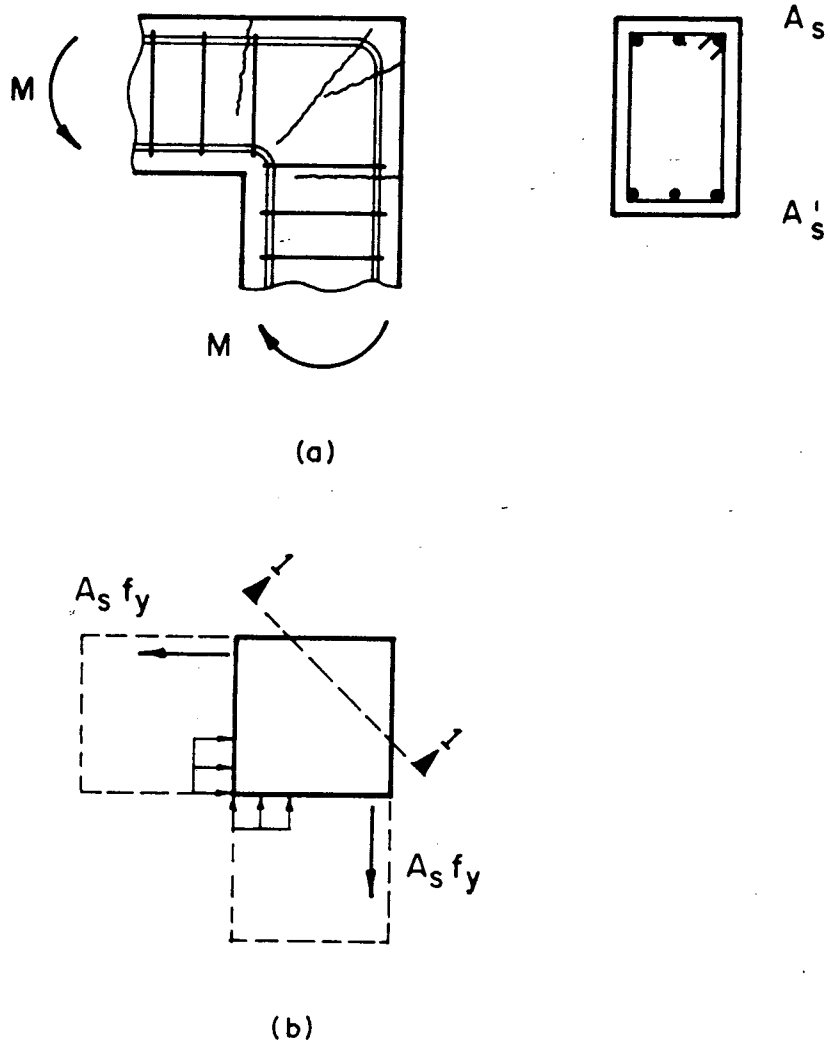

Figure 5.26 Knee-Joint Subjected to Closing Moments

tangential or bond stresses.

It is suggested that the diagonal stresses actually fan out to the outer reinforcement through a series of struts as in Fig. 5.27(a). This is appealing since it uses more of the concrete along a section through the joint (Sect. 1-1 Fig. 5.26(b)), and it activates the bond strength along the bar suggesting that the forces are transferred rather more gradually to the reinforcement. The fan stress field in Fig. 5.27(b) can be used to model this behavior. Actually, two fans are proposed, one on each side of the diagonal A-IP. For equal moments and no shear and axial forces, the left-hand fan is the mirror image of the right-hand fan. Otherwise the two fans will differ. In deriving the left-hand fan, it is assumed that the horizontal surface at mid height of the bars to the left of the bend is uniformly loaded. For the right-hand fan, it is assumed that the surface through the vertical bars has the uniform load. It should be noted that the lines representing the two surfaces intersect at the point denoted I.P..

The normal stress p and the tangential stress τ are determined from the fan stress field assuming a unit width of beam. These are equilibrated by the reinforcement and the area over which these stresses act must be determined. Considering the bearing stresses resulting from the normal stress p, it is assumed that the bearing width is the sum of the widths of the reinforcing bars. Assuming we have n bars of equal diameter, d_b, then the normal (bearing) stress is

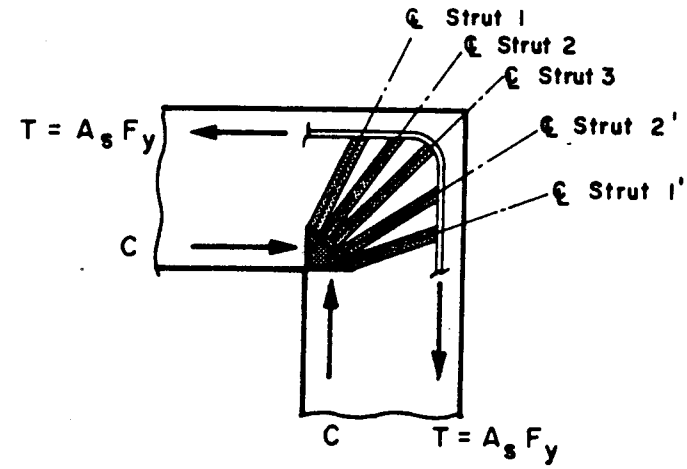

(a)

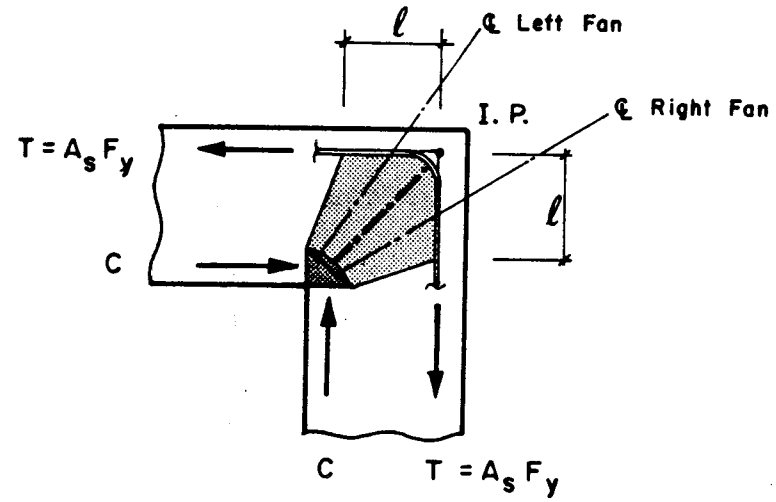

(b)

Figure 5.27 Fan Stress Field for Closing Joint

given by Eqn. 5.26.

$$\sigma_N = p \frac{b}{nd_b} \qquad [5.26]$$

If the tangential (bond) stress is distributed evenly over the surface area of the bar then σ_T (i.e. μ) is given by Eqn. 5.27.

$$\mu = \sigma_T = \tau \frac{b}{n\pi d_b} \qquad [5.27]$$

Assuming that there are three bars as shown in Fig. 5.26, the stress distribution in the plane of any one fan line will be similar to that shown in Fig. 5.28(a) and the three-dimensional nature of the problem is as shown in Fig. 5.28(b). In this case, each of the bottle-shaped stress fields is assumed to carry one-third of the total load. The properties of the bottle-shaped stress field were discussed in Sect. 5.2.4. The stress field requires a tensile stress distribution shown by the ties T. These tensile stresses are resisted by the tensile strength of the concrete. This is the cause of the potential 'splitting crack' which has been observed in tests (Nilsson, 1973). It is possible to use the STM shown to check that the tensile strength of the concrete has not been exceeded in the closing joint.

The distribution of the normal and bond stresses from this will be similar to those shown in Fig. 5.29. The magnitude of these stresses will depend on the values of A_s,

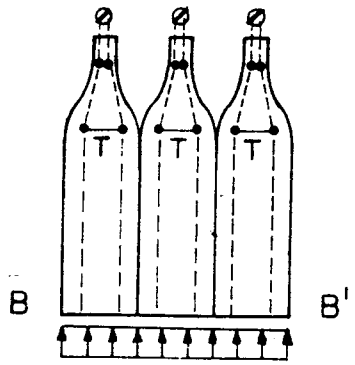

(a)

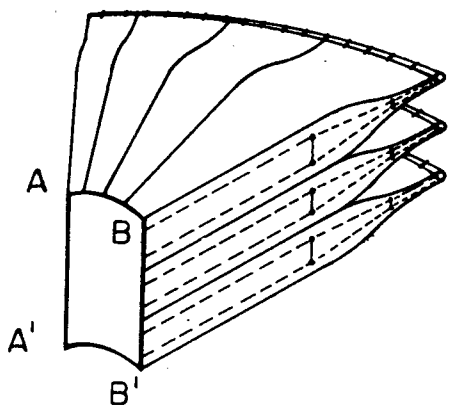

(b)

Figure 5.28 Three-Level Bottle Stress Field for Bearing on Three Bars

b, d, the number and size of bars, and the length, ℓ, over which the fan spreads. The procedure for determining these stresses is discussed next.

Determining the Normal and Bond Stress Distributions

The procedure for determining the assumed bond stress distribution for a corbel-type fan stress field was outlined in Sect. 5.2.4. A microcomputer program, 'FANS', was developed to assist in performing these calculations and, in particular, to assist in determining the assumed normal and bond stress distributions for the case when all or part of the stress field is developed over a circular rebar surface. This occurs for instance in the closing-joint model proposed above. First the procedure by which these stresses may be determined will be discussed. Then the program 'FANS' will be discussed briefly. The potential use of the microcomputer to assist in strut-and-tie modelling is discussed in Sect. 5.4.

Referring to the fan stress field in Fig. 5.27(b), it is seen that the left-hand fan develops partly along the horizontal surface, and partly along the circular surface. For a chosen length, ℓ, the fan stress field can be developed as described above extending from the intersection point (I.P.) as shown in Fig. 5.30(a). In this case each fan carries half of the horizontal and vertical loads and, knowing the geometry, the fan stress field in can be

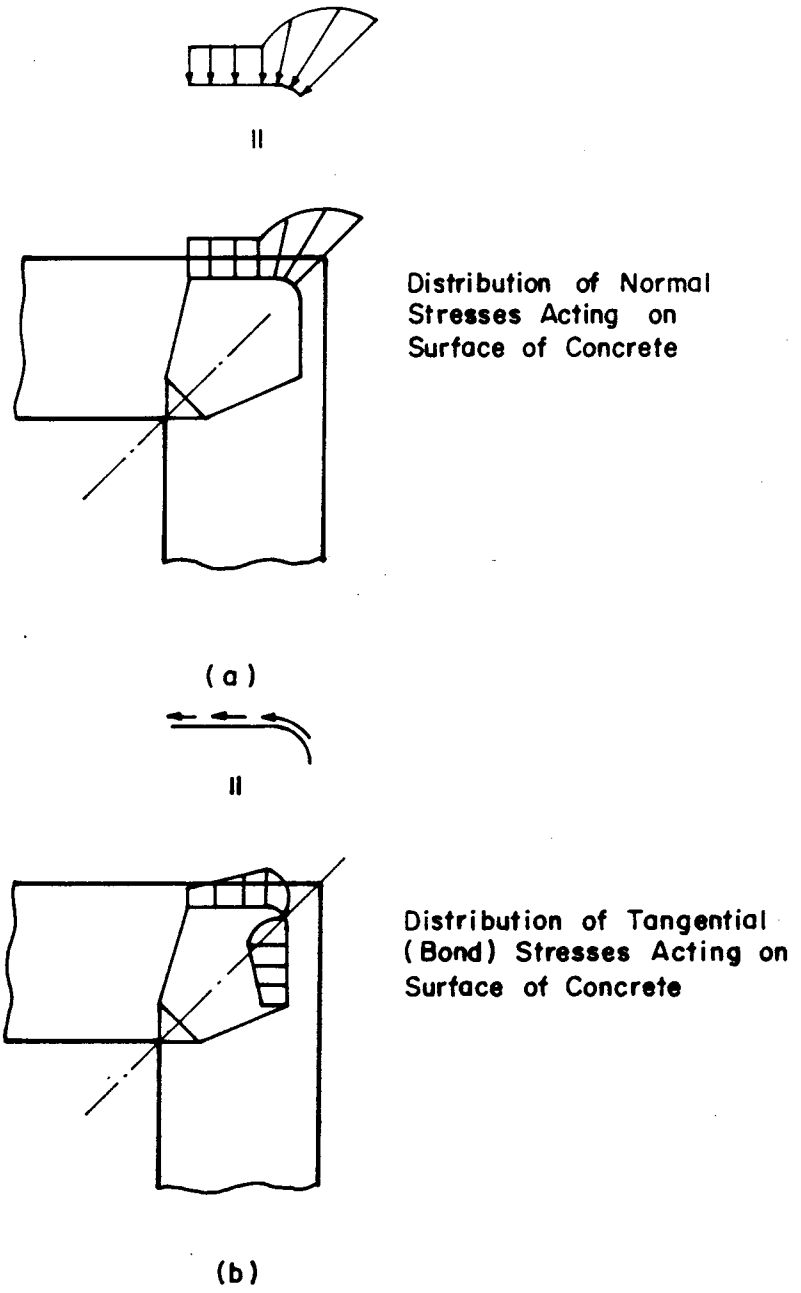

Figure 5.29 Normal and Bond Stress Distributions for Closing Joint

developed.

In Fig. 5.30(a), ξ and η are the coordinates (normalized by dividing by h), E is the normalized coordinate along the top surface, and X_1/h and R/h are normalized dimensions necessary to define the circular surface. The top surface, corresponding to the centerline of the reinforcement, is the surface which is assumed to have the uniform stress p. Thus along the surface between E_A and E_B, the normal stress, σ_N, is given by Eqn. 5.26, and the bond stress, μ, is given by Eqn. 5.27.

Along the circular surface at the bend, the principal compressive stress required for equilibrium will be greater than the value which would exist along the hypothetical horizontal surface between E_1 and E_B. As discussed earlier, the principal compressive stress is a function of position along the fan line. A portion of a typical fan line is shown in Fig. 5.30(b) including part of the stress field which makes contact with the circular reinforcement. For the fan line shown, with center at O, r is the non-dimensional radius to the nodal surface, r_u is the non-dimensional radius to the horizontal upper surface, and r_L is the non-dimensional radius to the surface at the center of the bar. Equilibrium along any fan line dictates that

$$r = \frac{\sigma_{1U}(r_U - r)}{f_{ce} - \sigma_{1U}} \qquad [5.28]$$

where σ_{1u} and f_{ce} are known and $(r_u - r)$ may be calculated

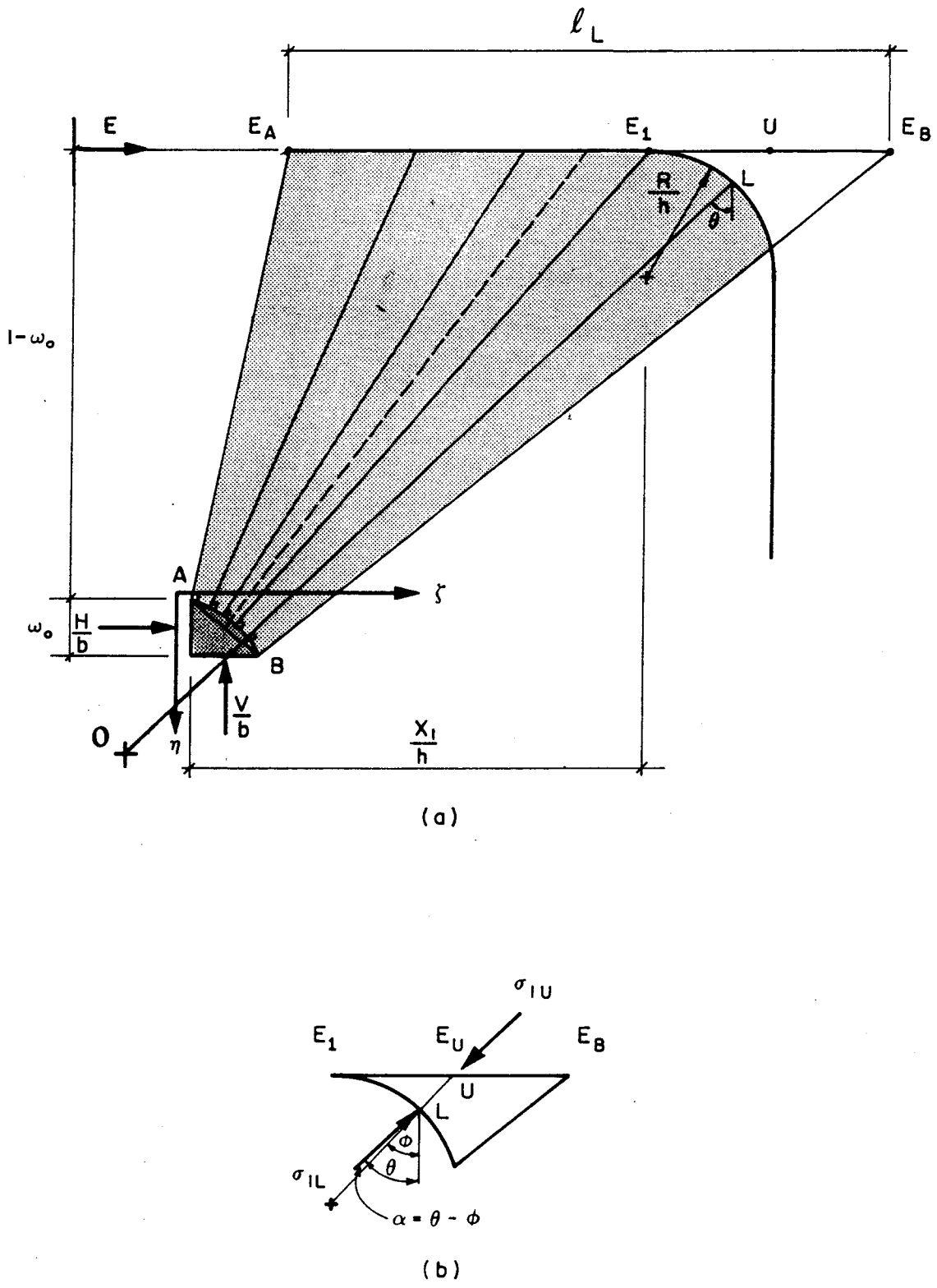

Figure 5.30 Details of Normalized Fan Stress Field for Left Hand Fan

from the geometry. The value of r_L needs to be calculated by determining the coordinates of the intersection point between the circular arc of non-dimensional radius R/h and the fan line through point U having slope θ. This simply involves the solution of a quadratic equation and the selection of the correct intersection point of the two that are numerically possible.

Having determined r_L and r, the value of the principal compressive stress at the lower surface, σ_{1L}, can be determined using Eqn. 5.9 as follows

$$\sigma_{1L} = \frac{r}{r_L} f_{ce} \qquad [5.29]$$

The principal stress acting on the lower surface, σ_{1L}, will have components p' and τ' which are normal and tangent to the surface respectively. These are determined analytically or by using Mohr's Circle as in Fig. 5.31. In Fig. 5.31, θ is the angle of the fan line from vertical, ϕ is the radial position angle to point L (Fig. 5.30), and α is the angle between the θ-plane and the ϕ-plane.

Since p' and τ' are the stresses acting over the full width of the beam, the stresses on the reinforcement σ_N and μ, will be proportionally larger according to Eqns. 5.26 and 5.27. Having determined these stresses for one location, the procedure may be repeated for others if necessary.

Usually the procedure is repeated since the location of the maximum values are not always obvious. This makes the

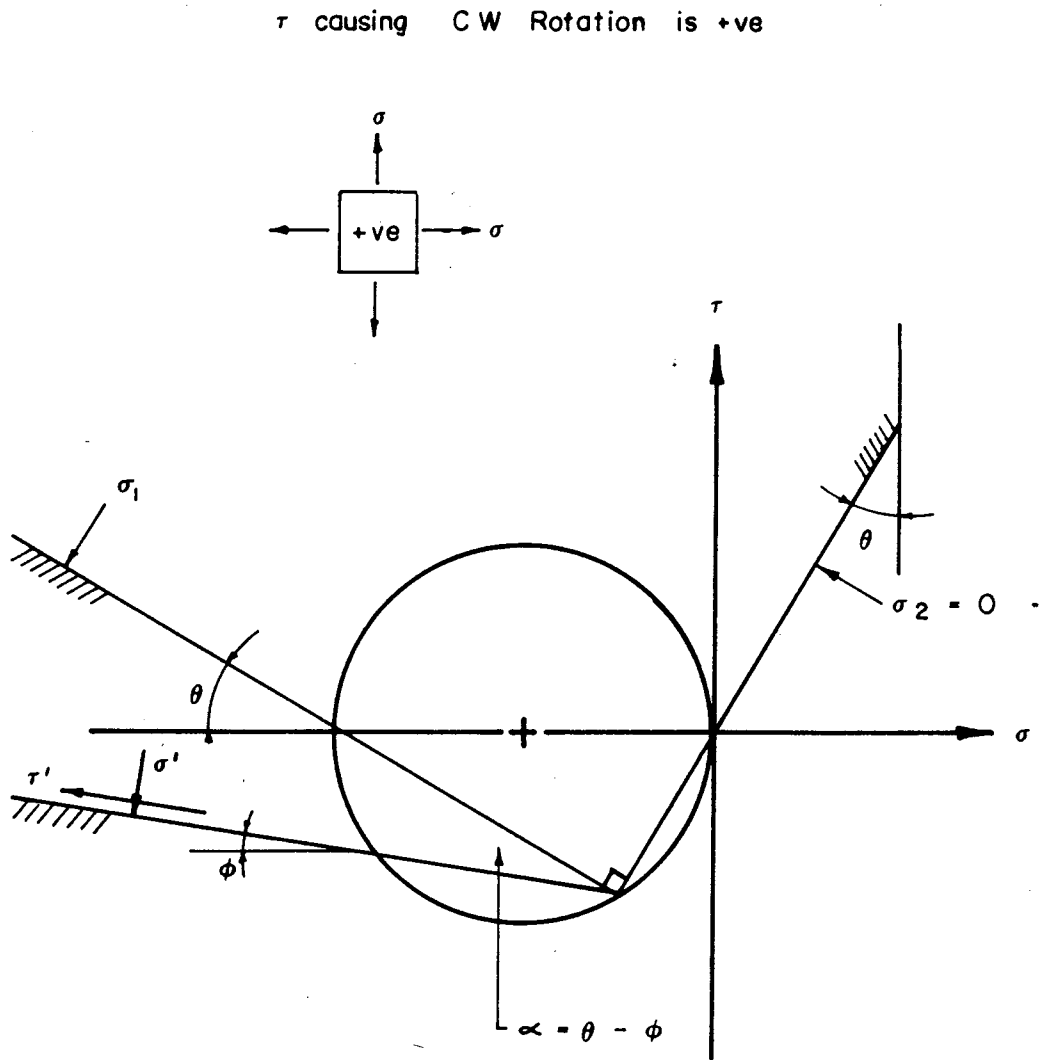

Figure 5.31 Mohr's Circle for Stress Transformation to Circular Surface

use of the microcomputer advantageous. 'FANS' is a microcomputer program written in Microsoft FORTRAN77 which performs calculations for hyperbolic decentered fan stress fields. The program has approximately 1500 lines and the .EXE file requires about 180000 bytes. The program uses commercially available, FORTRAN callable, graphics subroutines. Plots may be directed to the screen or to a file for plotting on an HP7475 plotter.

Given the values of H/b, V/b, h, f_{ce}, and perhaps X_1/h and R/h if required, the program will first ask whether the fan might develop over a horizontal surface, or horizontal and circular surfaces, or a vertical surface, or vertical and circular surfaces. It will then prompt for ℓ, the length of the fan. The input data is then written to the result file.

The program then determines the boundaries of the stress field and defines the equation of the nodal surface. Then, for each type of surface included in the fan, it will determine the normal and tangential stresses at small intervals along the fan. The stresses are then integrated over the surface and a check on equilibrium is made. The results are then written to the result file.

If desired, various plots are available and these may be displayed on the screen or sent to a plot file. The program can plot the stress field including the nodal surface and the ζ and η axes, and the location of the reinforcing. It can also plot the normal and tangential

stress distribution along the surface. To make the results more general, the stresses plotted are the stresses acting over the width b. These are adjusted manually by the user according to the size and number of reinforcing bars. Also, the nodal zone of the decentered fan is plotted to a larger scale.

After the plots are displayed, the program prompts for a new fan length, ℓ, or the program can be terminated. More details of the program and a listing are given in Appendix B. The program is illustrated in the application of the model to the closing-joint of Specimen B1 which is discussed next.

Closing Joint from Specimen B1

The closing joint model discussed above will now be applied to the closing-joint detail of Specimen B1 shown in (Fig. 5.32(a)).

The forces and end moments for this region are determined from statics using the measured reactions (Sect. 4.4). These values correspond to an applied load of 914.3 kN or 92% of the ultimate load. The development of the entire strut-and-tie models for Specimens B1 and B2 are presented in Chapter 6.

A strut-and-tie model for this closing joint is shown in Fig. 5.32(b). The model is seen to be more complicated than the simple closing-joint model in Fig. 5.27 owing to the presence of shear forces and axial forces. As a result,

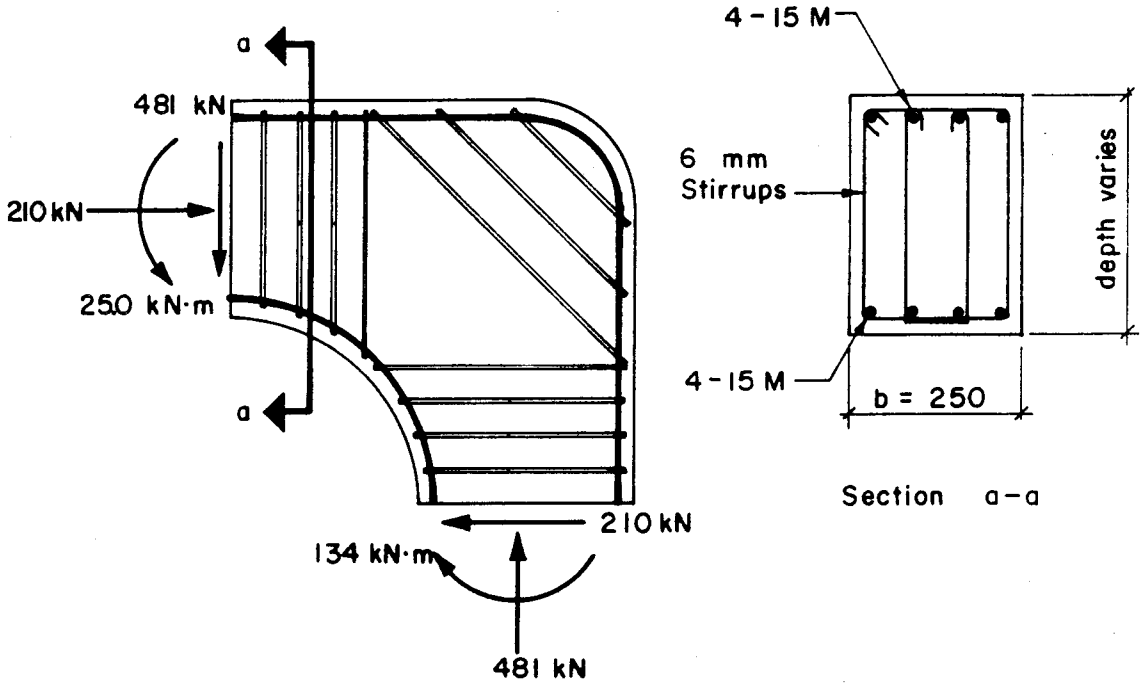

(a)

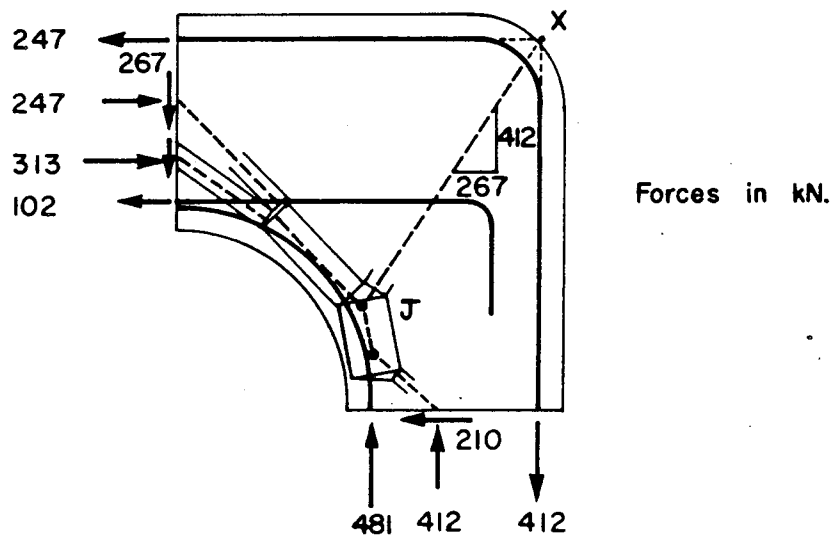

(b)

Figure 5.32 Closing Joint from Specimen B1 and STM

the strut JX is not symmetrical with respect to the reinforcement. However, for equilibrium, the strut must pass through the intersection point of the tie forces, point X (Fig. 5.33(a)).

The nodal zone ABC has horizontal and vertical forces acting on it which equilibrate the tie forces T_L and T_R. The positions of A, B, and X and the slope of the strut are known from the STM. It is possible to chose two struts which are statically equivalent to the original strut (Fig. 5.33(b)). The left and right struts have horizontal and vertical components such that equilibrium of nodal zone ABC is maintained. These struts correspond to left and right fan stress fields as shown in Fig. 5.34(a) and (b).

The boundaries of the two fans were chosen roughly based on the observed crack pattern shown in Fig. 4.37. After establishing these boundaries, values of β_R and β_L were then estimated to be $\beta_R = 41°$ and $\beta_L = 69°$. This defines point D and the values of ℓ_L and ℓ_R are then easily determined from the geometry. Having completely defined the two fans, the assumed distribution of the normal and bond stresses acting on the surface of the concrete can be determined. This may be done following the procedure discussed above.

The stress fields shown in Fig. 5.34 and the stress distributions shown in Fig. 5.35 and 5.36 were determined and plotted using program 'FANS'. The distribution of the normal stresses (σ_N) acting on the surface of the concrete

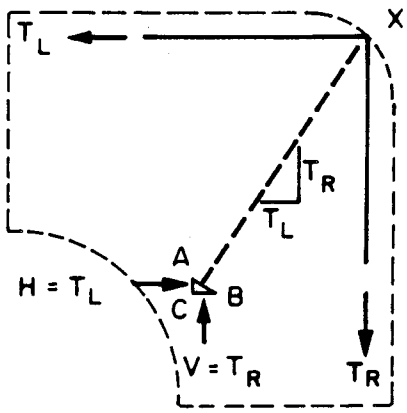

(a)

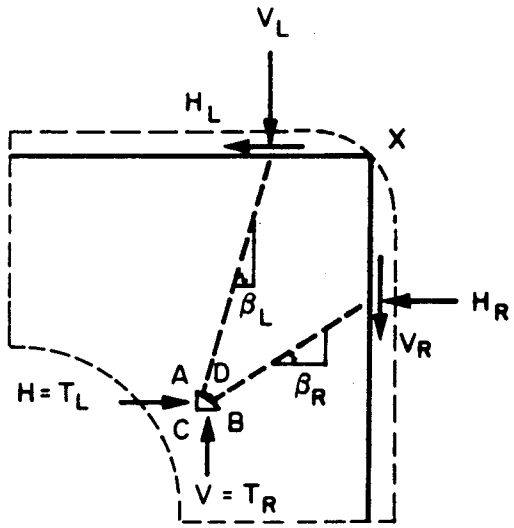

(b)

Figure 5.33 Proposed Left and Right Struts in Closing Joint

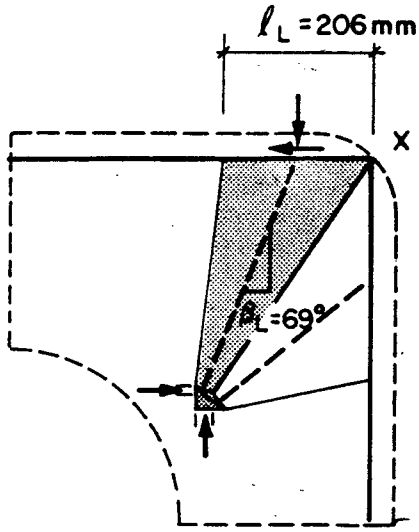

(a)

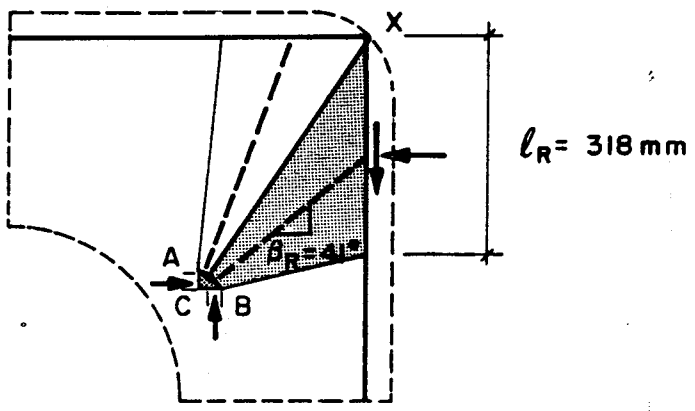

(b)

Figure 5.34 Left and Right Fan Stress Fields for Specimen B1

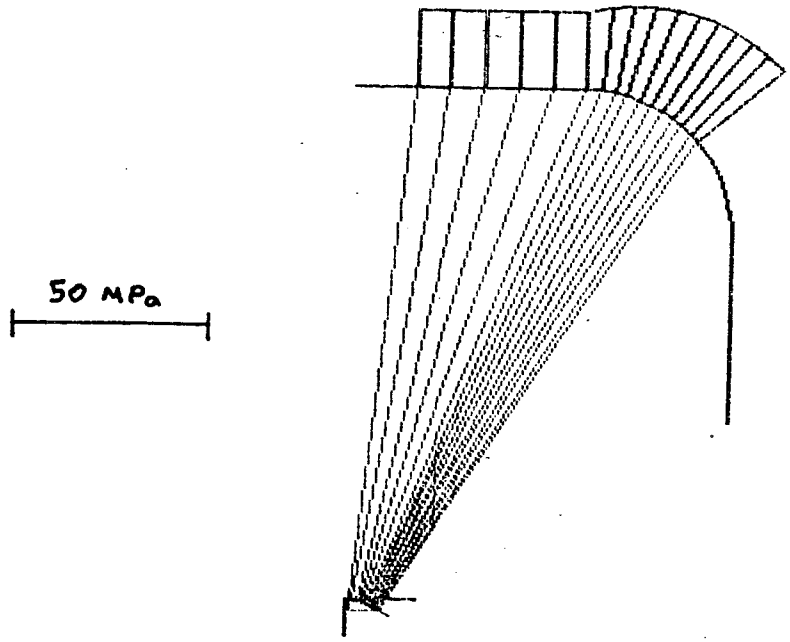

Normal Stresses

(a)

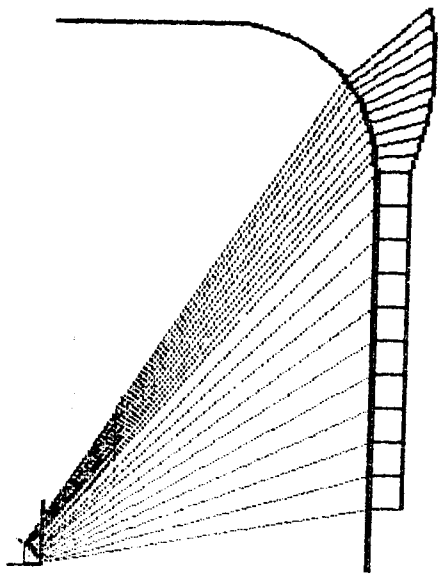

Normal Stresses

(b)

Figure 5.35 Calculated Normal Stress Distribution for Left and Right Fans

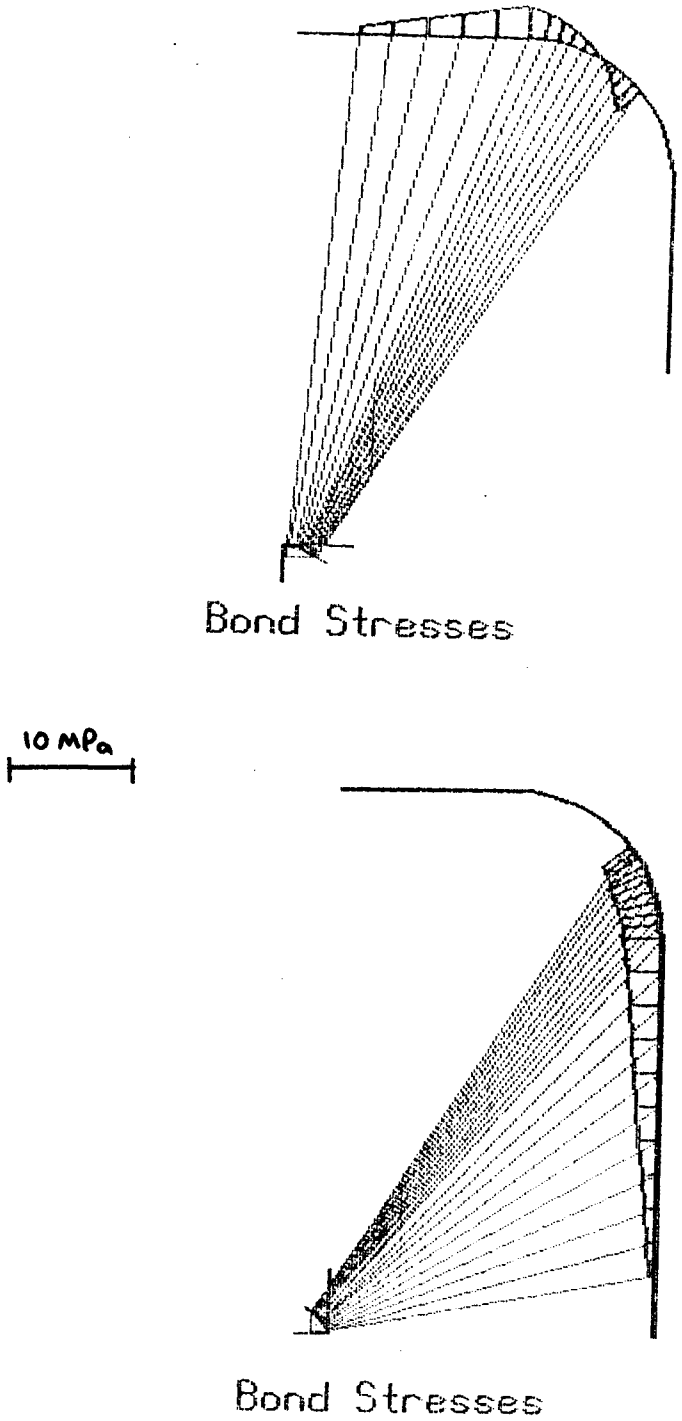

Figure 5.36 Calculated Bond Stress Distribution for Left and Right Fans

is shown in Fig. 5.35. The values are plotted on the surface of the concrete, normal to the surface. The magnitude of these stresses was determined assuming a width of bearing equal to the width of 4-15M bars (nd_b = 64 mm in Eqn. 5.35). The normal stresses are plotted to the scale shown in the plot.

The values of the normal stresses for the left fan are shown in Fig. 5.35(a). The stresses are plotted using the convention shown in Fig. 5.29. For the left stress field, the maximum value of σ_N is approximately 26 MPa and this occurs in the bend of the reinforcement. The average value of σ_N over the total length is approximately 20 MPa. The normal stresses for the right fan are shown in Fig. 5.35(b). The maximum value of σ_N is approximately 28 MPa while the average value is approximately 14 MPa. The maximum value occurs within the bend of the reinforcement as shown. As expected, these bearing stresses are quite large, but they are much less than f_{ce} taken to be 53.6 MPa or the limit on bearing stresses given in the CSA Code $\phi_c 0.85 f'_c$ = 50.6 MPa using ϕ_c = 1.0.

The distribution of the tangential or bond stresses μ acting on the surface of the concrete is shown in Fig. 5.36. The bond stresses are plotted using the convention shown in Fig. 5.29. In Eqn. 5.27 it was assumed that the bond area is equal to the surface area of 4-15M bars ($n\pi d_b$ = 201 mm² per mm .

In the left stress field, the maximum value of μ is approximately 2.4 MPa and this occurs at the beginning and mid-point of the bend (Fig. 5.36(a)). The mean value of μ over the left fan is 1.3 MPa. The maximum value of μ corresponding to the right stress field is 3.2 MPa which occurs within the bend of the reinforcement. The mean value of μ over the right fan is 2.4 MPa. These can be compared to the limiting values for bond strength used for development length in the CSA Code (μ = 4.3 MPa) or the maximum value given in the CEB-FIP Model Code (μ = 4.5 MPa) .

The assumed stress fields are statically admissible and in no location are the resulting stresses excessive. It is suggested that the stress fields adequately model the transfer of forces from the concrete to the reinforcement.

5.3 General Modelling Procedures

If the structure consists of a single D region, the strut and tie forces are determined directly from the applied loads and statically determinate reactions. This applies to deep beams and corbels.

In order to develop the strut-and-tie model for structures which are statically indeterminate or are composed of D and B regions, the reactions must be determined by structural analysis. Generally a linear elastic analysis is suitable although in extreme cases where the structure is heavily cracked and forming plastic hinges a nonlinear analysis would be more acceptable. Suggestions

regarding the structural analysis for the ultimate and serviceability limit states are given by Schlaich et al. (1987).

An elastic analysis has the advantage of being simple and readily available and it is suitable for checking serviceability. Generally speaking the elastic analysis could be any of the standard techniques although the stress distribution obtained from a linear elastic finite-element analysis is very useful when developing the strut-and-tie model.

In developing the strut-and-tie model it is helpful to realize that most B regions can be designed using the truss model (CEB-FIP Model Code) or truss model based on the compression field theory (CAN3 A23.3-M84). The results of this provide the internal forces at the junctions with any adjacent D regions. Once the forces at the boundary of a Dregion are known it is possible to develop the load path within the region. The majority of D regions contain a very clear load path and involve more or less standard models.

Structures are generally insensitive to small deviations in the position of the reinforcement and to some extent will carry the load in a manner consistent with how they are reinforced. It has been suggested that the strut-and-tie model with the least volume and shortest length of ties is best (Schlaich and Weischeide, 1982; Schlaich et al., 1987). This assumes that the loads try to follow a load path which minimizes forces and deformations

and since the ties are much more deformable than the concrete struts which have much larger volume and lower strains, the model with the least and shortest ties more closely models the actual behaviour. Research is recommended in this area.

It has been suggested that the struts and ties should be oriented following the elastic stress trajectories (Schlaich and Schafer, 1984). This should limit the amount of redistribution required after cracking. Schlaich and Schafer state that this approach will provide a conservative ultimate strength design and they recognize the potential benefit in being able to use the same elastic analysis for serviceability design. If the elastic stress distribution is not known, then the strut-and-tie model can be based on an estimate of the load path.

In all cases it is important to consider the ductility of the model. It is necessary to ensure that the rotation capacity of the structure is not exceeded at any location before the assumed state of stress exists in the remainder of the structure. In highly stressed regions this should be fulfilled if the struts and ties were oriented with the elastic stress trajectories and the internal forces were determined from an elastic analysis since these forces are maximum prior to redistribution. In regions that are normally or lightly stressed the struts and ties may deviate considerably from the elastic stress distribution allowing the reinforcement to be arranged according to practical

considerations. Such is the case in a typical B region where stirrups are provided orthogonally to the principal reinforcement rather than along the principal tensile stress trajectories.

In very special cases it may be necessary to use a nonlinear finite element analysis. This can be difficult for design since the reinforcement and perhaps even the geometry are not known at the start. For these special cases the recommended technique is to first use an elastic finite element analysis to develop a strut and tie model to provide a check of the geometry and proportion the reinforcement for ultimate strength. Then if desired, a nonlinear finite element analysis can be used to check the completed design. It is recommended in all cases that a strut and tie model be used to verify the results of a nonlinear finite element analysis. The greater the degree of sophistication of the structure (and of the computer program) the greater the need for a simple design check.

5.4 Computer Aided Strut-and-Tie Modelling

Developing a strut-and-tie model requires simple calculations based only on equilibrium and geometry. For B regions in beams and for the most common D regions "standard" models may be used. However for other situations trial and error procedures are often required and the calculations and drawings may become laborious.

The numerical power and graphical capabilities of a microcomputer offer attractive possibilities in this area. The degree of sophistication of a computer aided design (CAD) package for strut-and-tie modelling could vary from a simple drafting tool to an interactive problem-oriented language environment perhaps including some sort of expert system interface. It is possible that this could be combined with a finite element analysis program which could determine and display the elastic stress trajectories upon which the strut-and-tie model could be superimposed. If the principle of minimum strain-energy criteria (Sect. 5.2.3) is shown to be suitable for evaluating the optimal strut-andtie model, the necessary calculations for model optimization could easily be done in the same computer program.

A small step in this direction is the computer program 'FANS'. Given strength and geometric properties this interactive program will determine the equation of the nodal surface, evaluate the normal and tangential stress distribution for fan stress fields, and show the results on the screen. A printout of the calculations may be obtained and drawings may be produced on various output devices. Fan stress fields which develop on horizontal linear surfaces, vertical linear surfaces, and circular surfaces are considered.

The program was developed to study the details of the closing joint model discussed in Section 5.2.6.4 in which the assumed normal and tangential stress distributions

around the joint are of interest. It is also useful for determining the assumed tensile stress distribution in the steel plates and the requirements for shear connectors for the steel-concrete composite beam in Fig. 5.12.

The program was developed in MS-FORTRAN for use on any MS-DOS based microcomputer. The program listing is given in Appendix B.

6. STRUT-AND-TIE MODELS AND COMPARISONS WITH TEST RESULTS

6.1 General

In this Chapter strut-and-tie models are presented which explain the load carrying mechanisms for each of the test specimens. The shear forces, axial forces, and moments at the ends of each specimen were developed from the measured loads, reactions and steel beam strains as described in Chapter 4. Then for a given load and end reactions, statically admissible stress fields were developed which utilize the reinforcement present in the specimen. The selection of the appropriate stress field was guided by the measured reinforcing strains and crack patterns.

The strut-and-tie model (hereinafter referred to as STM) developed for a test specimen subjected to a given loading and measured reactions constitutes an analytical tool as opposed to a design tool. The model is more difficult to develop since fewer assumptions are made. However the analytical STM can present a very good description of how the load is carried in all regions of the specimen. As a result, the STM may be used with more confidence in the design of that type of structure. In the following, the analytical models are discussed and compared to the measured behavior of the test specimens.

6.1.1 Effective Concrete Strengths

For each of the strut-and-tie models presented in this Chapter, it is necessary to assume an effectiveness factor, ν. The effectiveness factor was discussed briefly in Sect. 5.2.1.

It is possible to use different effectiveness factors for nodal zones experiencing different states of stress, as suggested in Clause 11.4.7.5 of CAN3 A23.3 M84. For uniform diagonal compression fields, the compressive strength of the concrete can be expressed as a function of the transverse principal tensile strain (Clause 11.4 CAN3 A23.3 M84). These methods are most suitable for simple problems.

In this study, a constant effectiveness factor is assumed for each STM. This is consistent with work by others (Thurlimann, 1984; Marti, 1985a and 1985b; Rogowski and MacGregor, 1986; O'Flynn, 1987).

The following considerations affected the choice of the effectiveness factors used in this study.

1. The material properties were measured for each specimen.
2. Since test results were available there was very little uncertainty in the load carrying mechanism(s).
3. As stated in Sect. 5.2.1, Rogowski and MacGregor (1983) suggest that the accuracy of the truss model is more sensitive to the selection of the truss model than to the selection of ν. This is confirmed by Marti, 1985a.
4. In specimens exhibiting primarily compressive behavior and/or specimens which contain reinforcement of

sufficient quantity to increase the confinement of the concrete, a high value of ν seems reasonable.

Based on the foregoing, the value of ν was taken to be a constant value of ν=0.90 throughout this study. Suggestions for design are discussed in Chapter 8.

6.2 Circular Arch Specimens

6.2.1 Introduction

In the following, the development of the STM for the first preliminary test specimen P1 will be discussed. The model proposed is a simple 'funicular' STM. Specimen P2 contained post-tensioned stirrups and as discussed in Chapter 4 the full capacity of the specimen could not reached. Furthermore development of a model to include the post-tensioned stirrups would require more accurate knowledge of the forces and moments acting at the ends of the arch. As a result, the development of a model for Specimen P2 will not be discussed in this thesis.

6.2.2 Simple Funicular Model

The geometry and load arrangement for Specimen P1 is shown in Fig. 6.1. The prestressed tension tie afforded adequate support to the arch so that a lower bound estimate of the strength of the specimen can be obtained using the simple STM shown in Fig. 6.2.

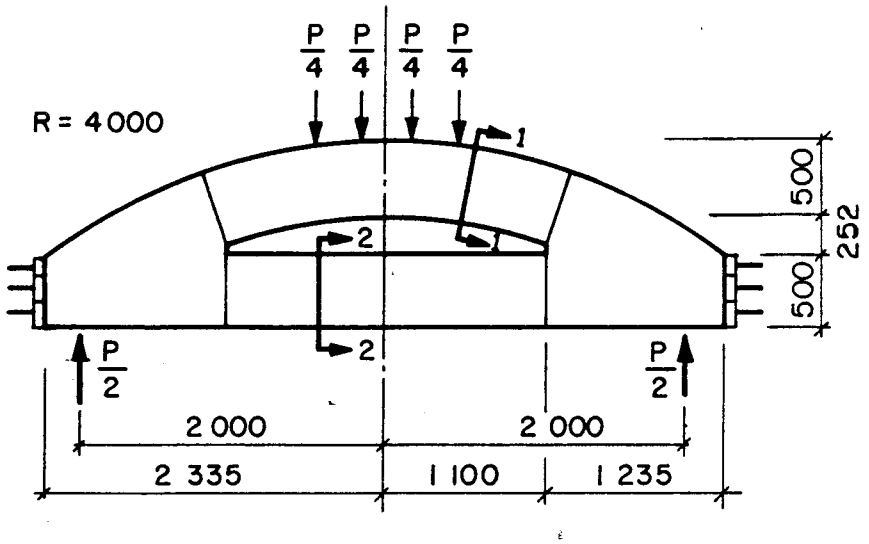

(a)

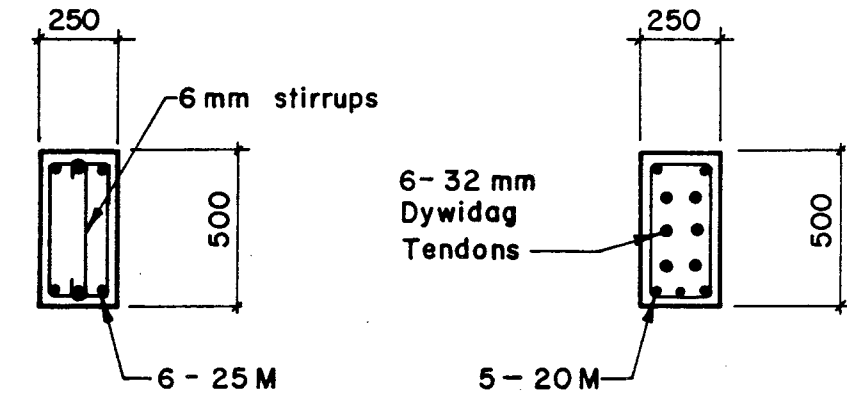

(b)

Figure 6.1 Geometry and Load Arrangement for Specimen P1

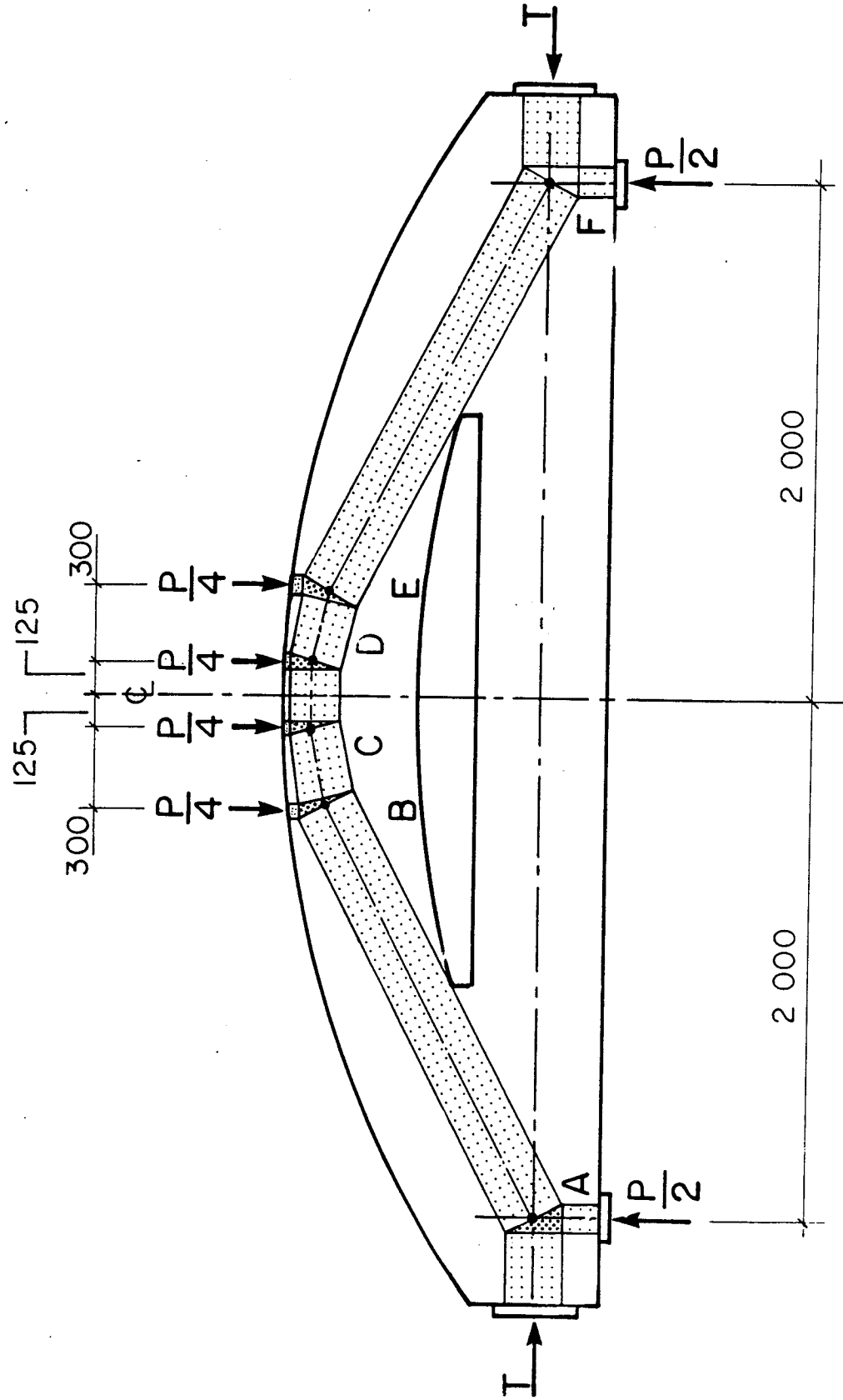

Figure 6.2 Simple STM for Circular Arch Specimens

The shape of the STM must be affine to the shape of the bending moment diagram which would result from the same load applied to a simple beam of equal span. The load path to the supports is the funicular shape for this load. Since this funicular shape fits entirely within the boundary of the specimen, the entire load can be carried by the compression struts. This means that the capacity of the stirrups is not accounted for in this STM. Also, the strength of the longitudinal reinforcement is not included. In the model, P is the total applied load, P/2 is the magnitude of the reactions, and T is the tie force provided by the prestressed tension member.

The value of the applied load P depends on the choice of f_{ce}. Using ν = 0.9 and the mean cylinder strength f'_c = 35.0 MPa, then the maximum load P is determined from this STM to be P = 2030 kN. Since the maximum load carried by this specimen was 2900 kN, the test/predicted ratio for this model is 1.43. These correspond to effective ice pressures of 8.12 and 11.6 MPa, respectively, acting over the loaded area as discussed in Chapter 4. The longitudinal reinforcement in the arch section was not included in this STM. If this were done, the test/predicted ratio would be less than 1.43. The eccentricity of the assumed thrust line between points A and B in Fig. 6.2 is such that tension would be expected at the outer fiber of the specimen. Cracks were not observed in this location in the test.

Similar models can be developed for other load conditions. In all cases the simple model provides a fast method to gain a lower bound estimate of the strength of the specimen. This can be useful for preliminary design or for checking results from more sophisticated analyses. It can also be used to study details in the prototype structure such as the required wall thickness, the spacing of the bulkheads, and the magnitude of the thrust necessary to support the arch. Finally it should be noted that the circular arch is more efficient for distributed loadings than for this loading.

6.3 V-Shaped Arch Specimen A1

6.3.1 Introduction

In the following, the development of four different strut-and-tie models will be developed for Specimen A1. The first two models are simple 'funicular' models for two different load conditions. The third model was developed from the end forces and moments determined from the measured loads, reactions and steel beam strains. The fourth STM is a more detailed model which illustrates how the compression reinforcement can be included in the model. The assumptions particular to each STM will be reviewed in each case.

6.3.2 Simple Funicular Models

The geometry and load arrangements for Specimen A1 are shown in Figs. 6.3 and 6.4. The first load condition (Fig. 6.3) represents load case I in the test in which the specimen was subjected to load applied through the load distribution beam, knife-edges, and four rollers. The second load condition (Fig. 6.4) represents load case II in the test in which the specimen was loaded by the platten of the testing machine directly. In both cases the specimen was supported on knife edges and rollers.

As discussed in Chapter 4, the behavior of the A-series specimens was governed primarily by the behavior of the straight portion of the specimen in uniaxial compression. This suggests that the stiffness of the steel beam used to provide restraint to the specimen was such that the simple STM is adequate to model this behavior. The advantages of this type of STM were discussed in Sect. 6.2.2.

The STM developed for Specimen A1 subjected to load condition I assuming rigid supports is shown in Fig. 6.5. To develop this model the effectiveness factor was taken to be $\nu = 0.9$. Using $\nu = 0.9$ and the mean concrete cylinder strength $f'_c = 62$ MPa, the effective concrete strength f_{ce} is taken to be 56 MPa. The presence of compression reinforcement and the tensile strength of the concrete were ignored. Based on this model, the predicted capacity of the specimen is P = 5504 kN. The specimen carried 6100 kN without failure. The average load intensities corresponding

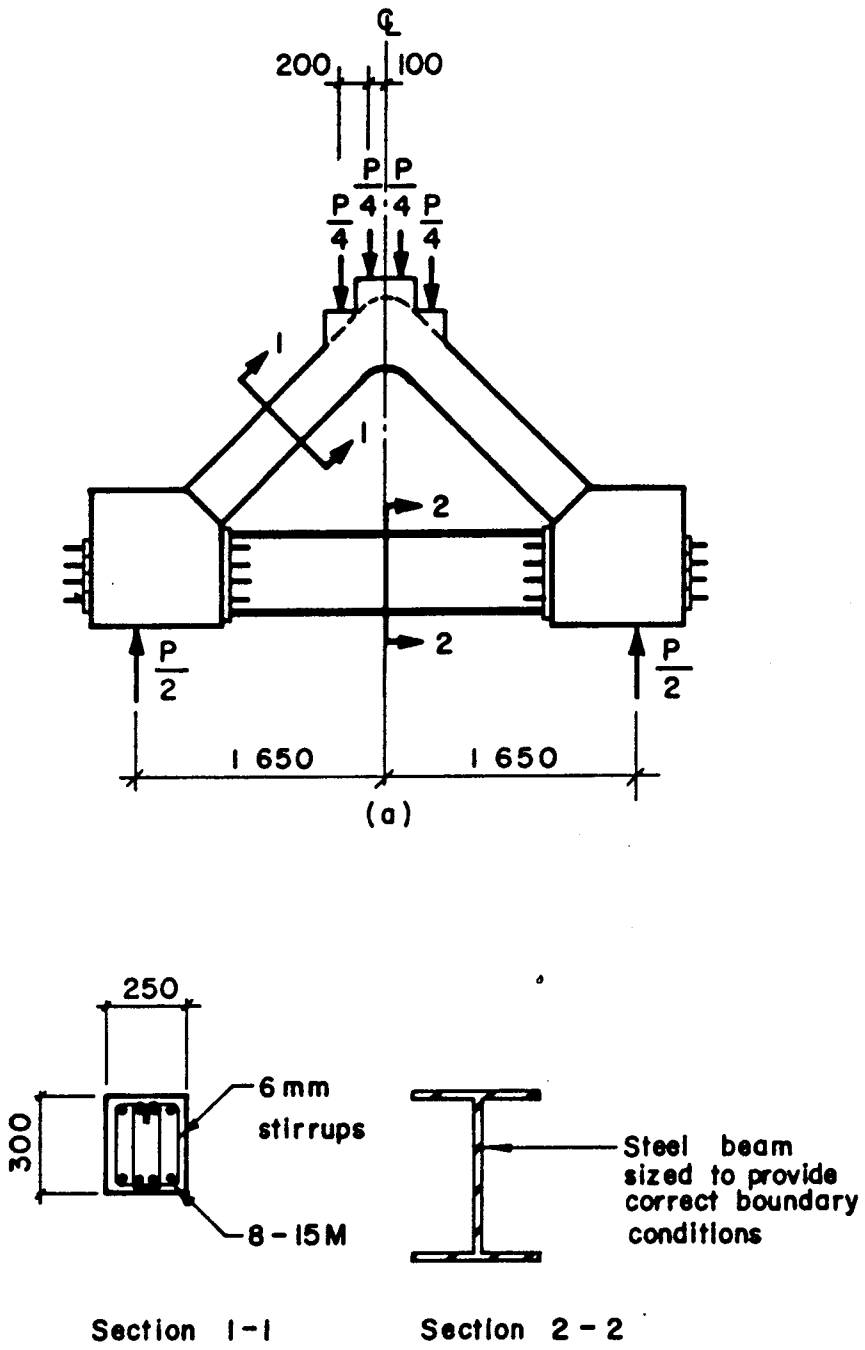

Figure 6.3 Geometry and Load Arrangement for Specimen A1 - Load Condition I (0 - 6000 kN)

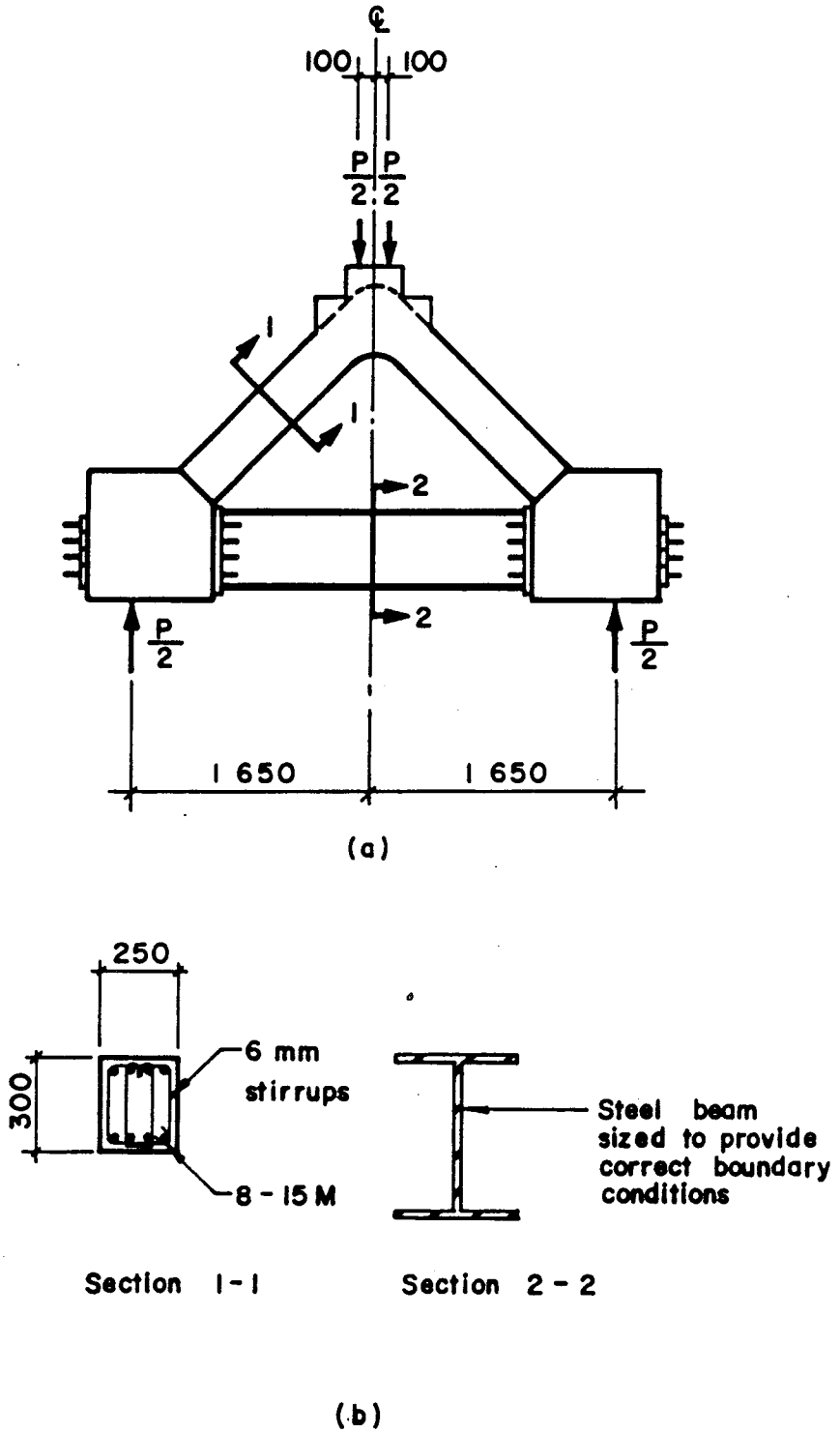

Figure 6.4 Geometry and Load Arrangement for Specimen A1 - Load Condition II

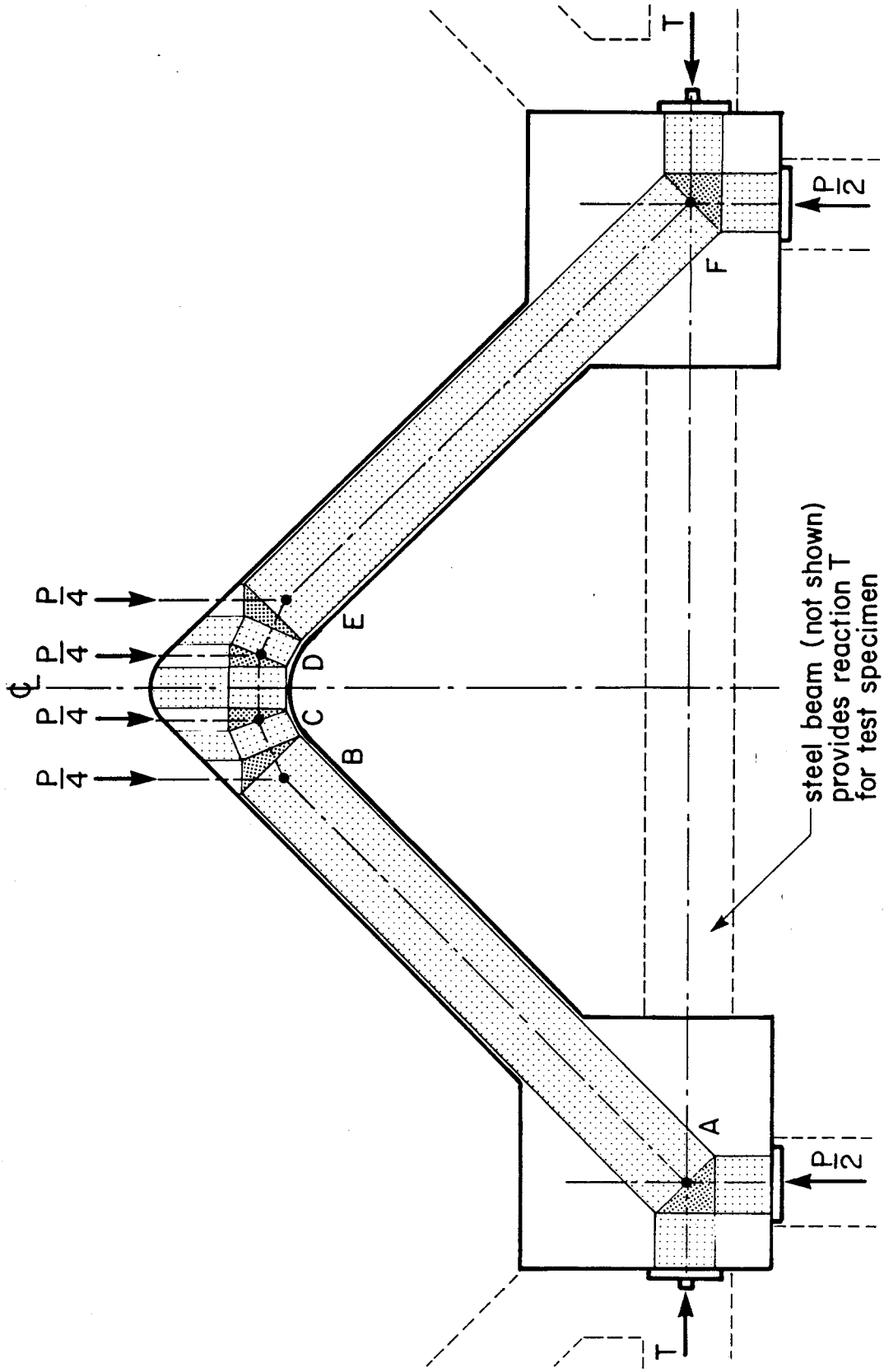

Figure 6.5 Simple STM for Specimen A1 - Load Conditon I

to these loads are 27.5 MPa and 30.5 MPa respectively.

The shape of the STM (ABCDEF) must be affine to the shape of the bending moment diagram which would result from the same load applied to a simple beam of equal span. Because this "funicular load path" fits within the boundary of the specimen, the load can be assumed to be carried entirely by the compression struts. This means there is no "shear" and the stirrups in the specimen function only as column ties (i.e. providing confinement and preventing buckling of the compression reinforcement). It should be noted that the full width of the specimen cannot be used in strut AB because of the required slope of strut BC. That is, if strut AB becomes wider, then strut BC must pass outside the boundary of the specimen. This can be an important consideration for determining the optimum radius of the inside soffit.

This is an extremely efficient structure for this type of loading. However for a different loading or for the same loading but different structure, this may not be the case. This type of STM can be useful for determining the optimum shape of the structure. In general, this structure will be less efficient if the load is applied over a wider area. However, as discussed in Chapter 2 for the design of structures subjected to ice loads, the fact that the ice pressure decreases as the loaded area increases will compensate somewhat for this.

The STM developed for this specimen subjected to load condition II is shown in Fig. 6.6. The model is analgous to the previous model. The shape of the STM is affine to the bending moment diagram and the load is carried by the compressive struts. In this case the load is applied over a smaller area. However, the full STM can be developed and the load intensity is simply $f_{ce} = \nu f'_c = 56$ MPa. This applied over the full width of nodes B and C gives P = 5600 kN. The specimen failed at the load 6294 kN or 63 MPa load intensity.

For both load conditions, the simple STM gives a reasonable lower bound estimate of the strength of the structure.

6.3.3 Simple STM Based on Measured Forces and Moments

In the previous strut-and-tie model it was assumed that the load was carried entirely by the compression struts. The presence of the compression reinforcement and the tensile strength of the concrete were ignored. The effective concrete strength f_{ce} was assumed to be 56 MPa as in the previous case.

The forces and moments acting at the ends of the specimen were determined from the measured loads, reactions, and the steel beam strains. An applied load of 5048 kN was chosen to illustrate the development of this STM. This load level represents 83% of the maximum load for this load condition. This load was selected as it was determined that

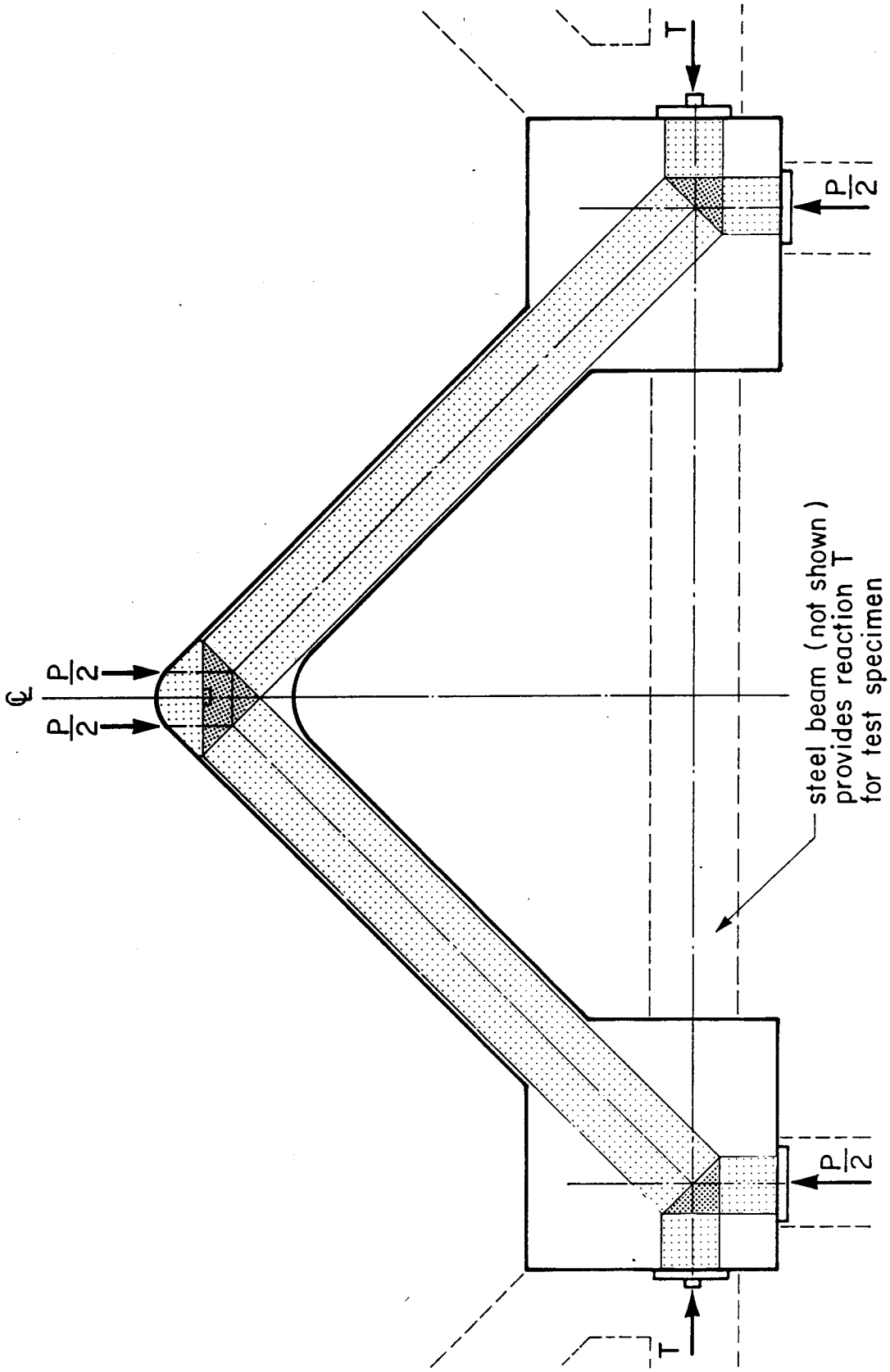

Figure 6.6 Simple STM for Specimen A1 - Load Conditon II

the resulting struts reached the geometrical limit of the specimen. The forces and moments acting at the ends of the specimen for this load are shown in Fig. 6.7. For simplicity the values used are the average of the values measured at the two ends.

The central region of the specimen, where the load is applied and where the section changes shape, is clearly a D-region (Fig. 6.8). The two straight portions are matching B-regions. The forces and moments acting at the ends of the B and D regions are shown in Fig. 6.9(a) and (b) respectively. The principal difference between the previous STM and the one developed here is the presence of end moments and shears. As suggested earlier, this is due to the finite stiffness of the steel beam providing lateral and bending support. As the arch spreads out, moments and therefore shears are introduced and the STM is no longer funicular. The shear in the specimen must be resisted by an appropriate change in slope of the struts.

At this load level (5048 kN), the specimen showed no signs of crushing or cracking. The measured stirrup strains were small. The principal strain plot in Fig. 6.10 was developed from the measured concrete strains. This plot is repeated here from Fig. 4.18. As seen in the plot, large compressive strains were measured at this load and the larger strains are such that the presence of the bending moments may be detected at each end of Region I (double curvature).

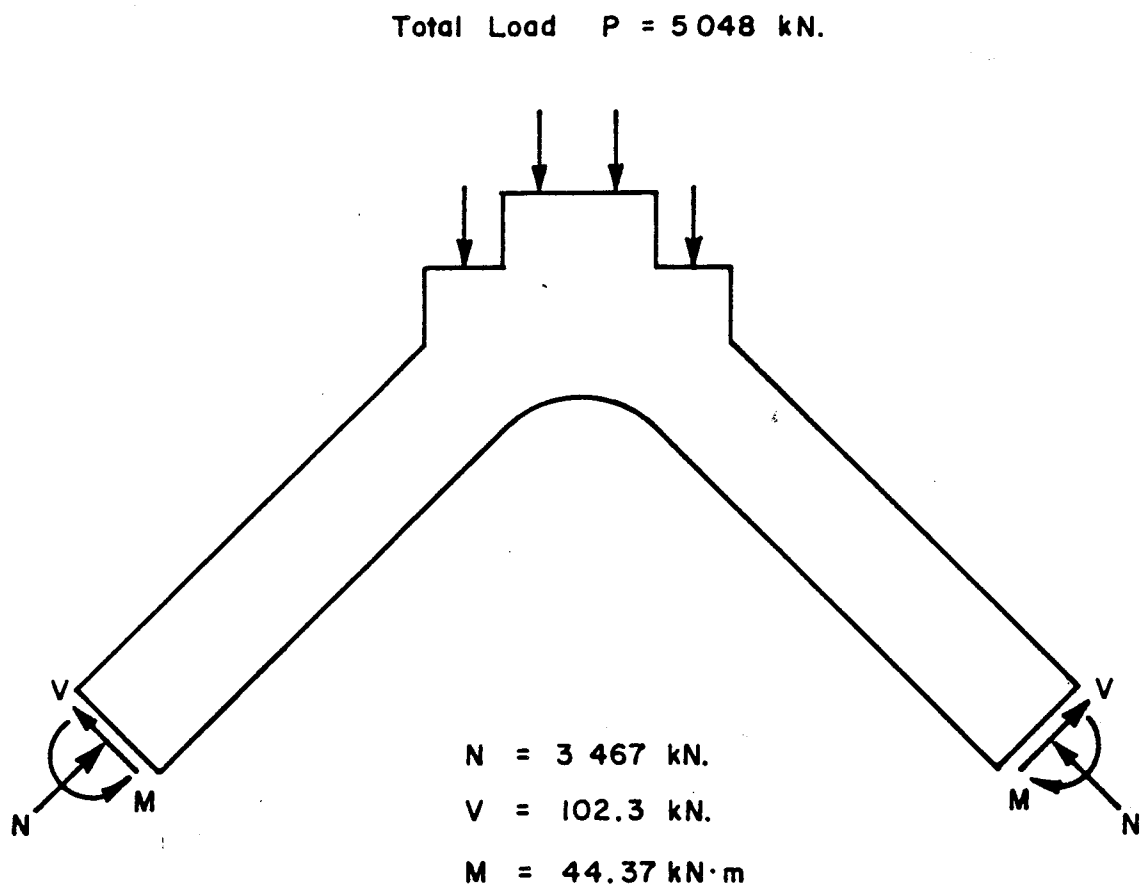

Figure 6.7 Forces and Moments at Ends of Specimen A1 at Load = 5048 kN

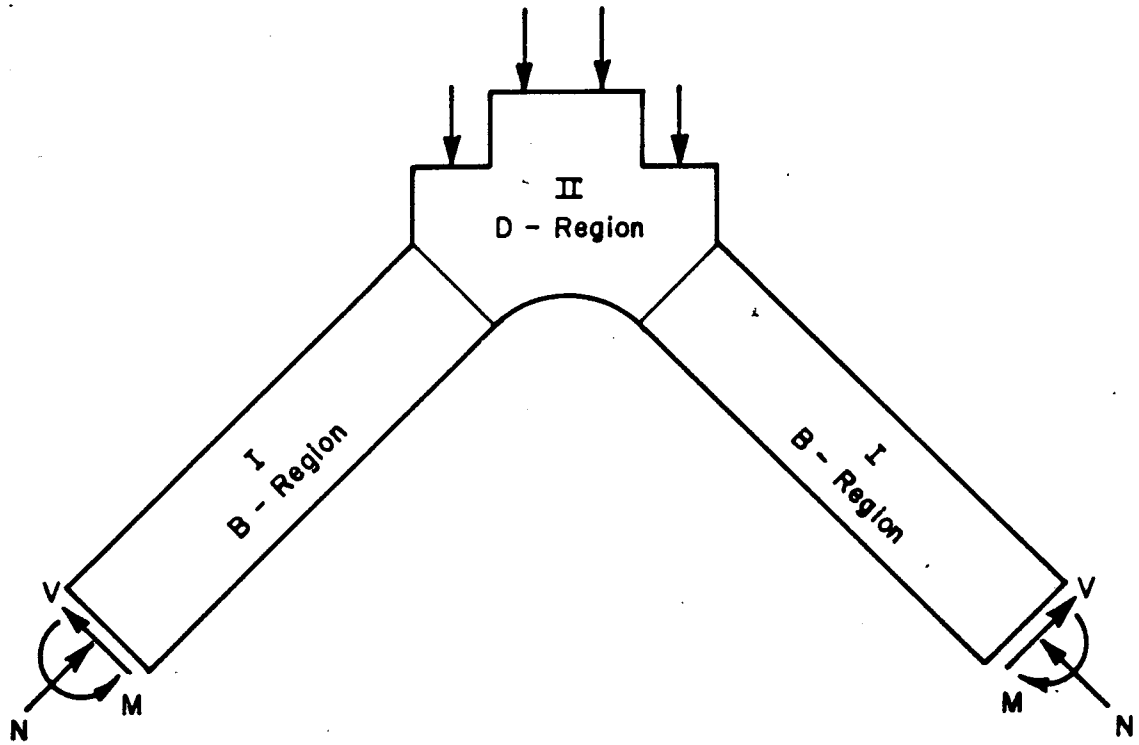

Figure 6.8 'D' and 'B' Regions in Specimen A1

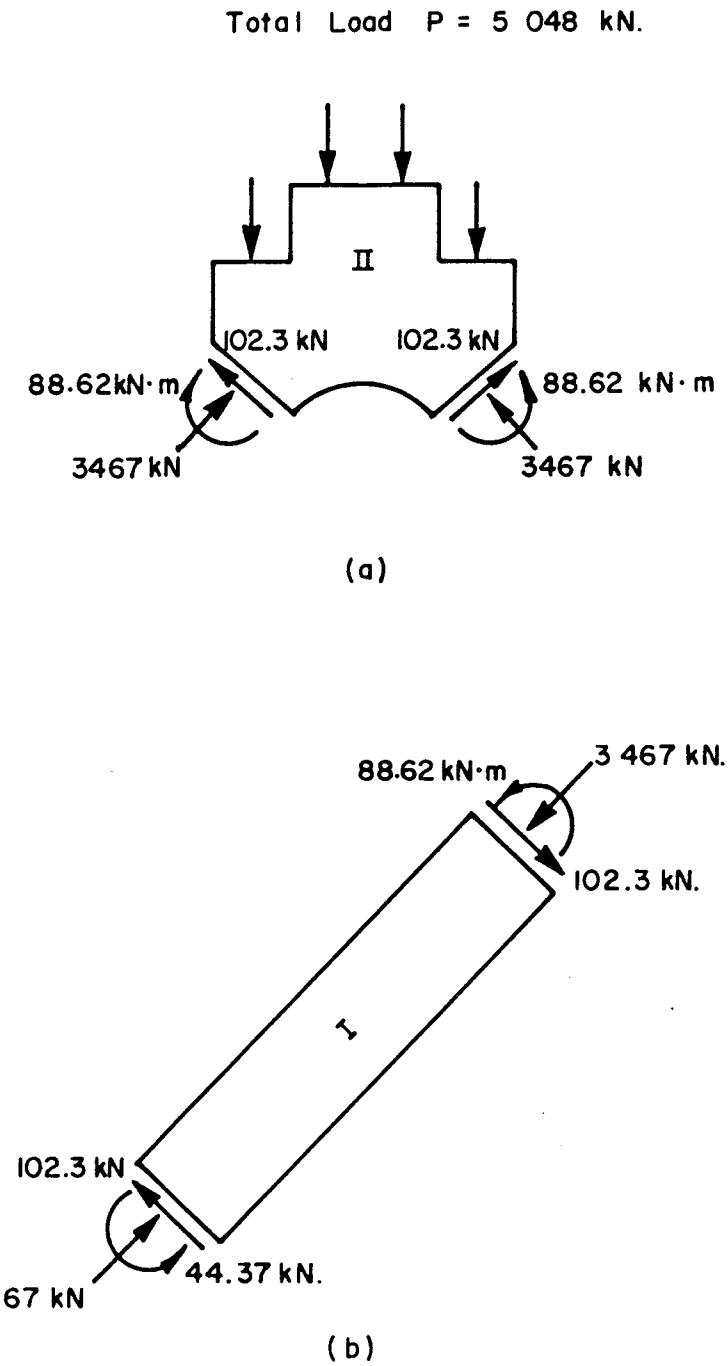

Figure 6.9 Forces and Moments at Ends of D and B Regions at Load = 5048 kN

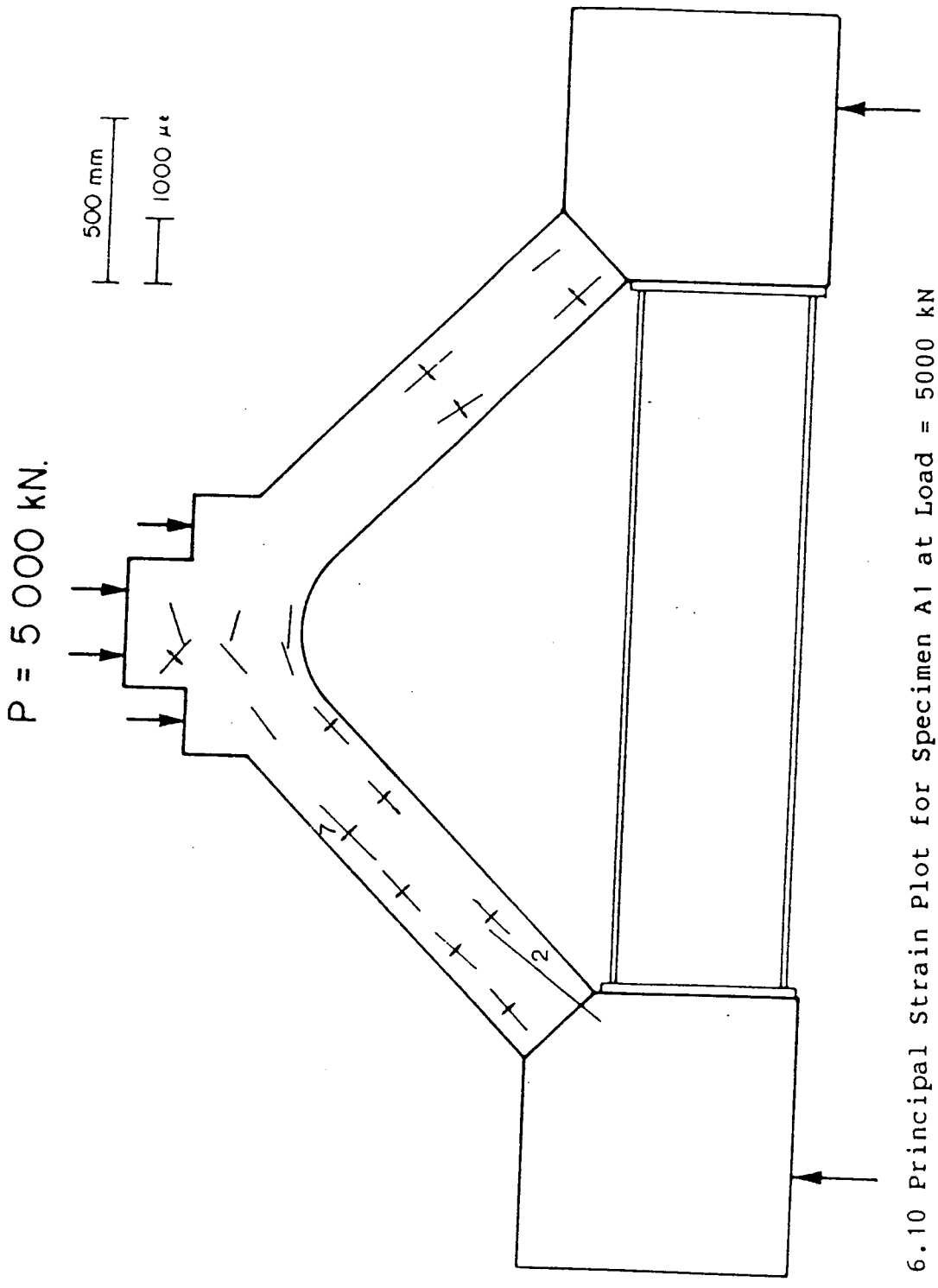

Figure 6.10 Principal Strain Plot for Specimen A1 at Load = 5000 kN

The STM developed for this specimen based on the end forces and moments in Fig. 6.9 is shown in Fig. 6.11. Using f_{ce} = 56 MPa the width of strut AB was determined. The end moment at A is such that the eccentricity of the 3467 kN force must be 12.8 mm. Since the position of the lower edge of the strut is within the specimen this is satisfactory and the procedure is repeated at the top end of Region I. The eccentricity of the axial force at the top must be e = 25.6 mm. The line between these two points represents the line of action of the resultant force acting on Region I. This is strut AB which has horizontal and vertical components as shown. The top edge of the strut AB is seen to be close to the limit of the specimen. Since the location and size of the load at B' is known, point B is located at the intersection of struts AB and B'B. Strut BC is known since it must have the same horizontal component as strut AB and a vertical component equal to P/4. The location of point C is the intersection of strut BC and the strut C'C. Alternatively the elevation of points C and D can be determined by summing moments about the bottom of Region I since the force in strut CD must be equal to the horizontal component of strut AB. The nodal zones can then be sketched simply by "thickening-up" the strut lines. Note that the STM is symmetrical with respect to the centerline of the specimen.

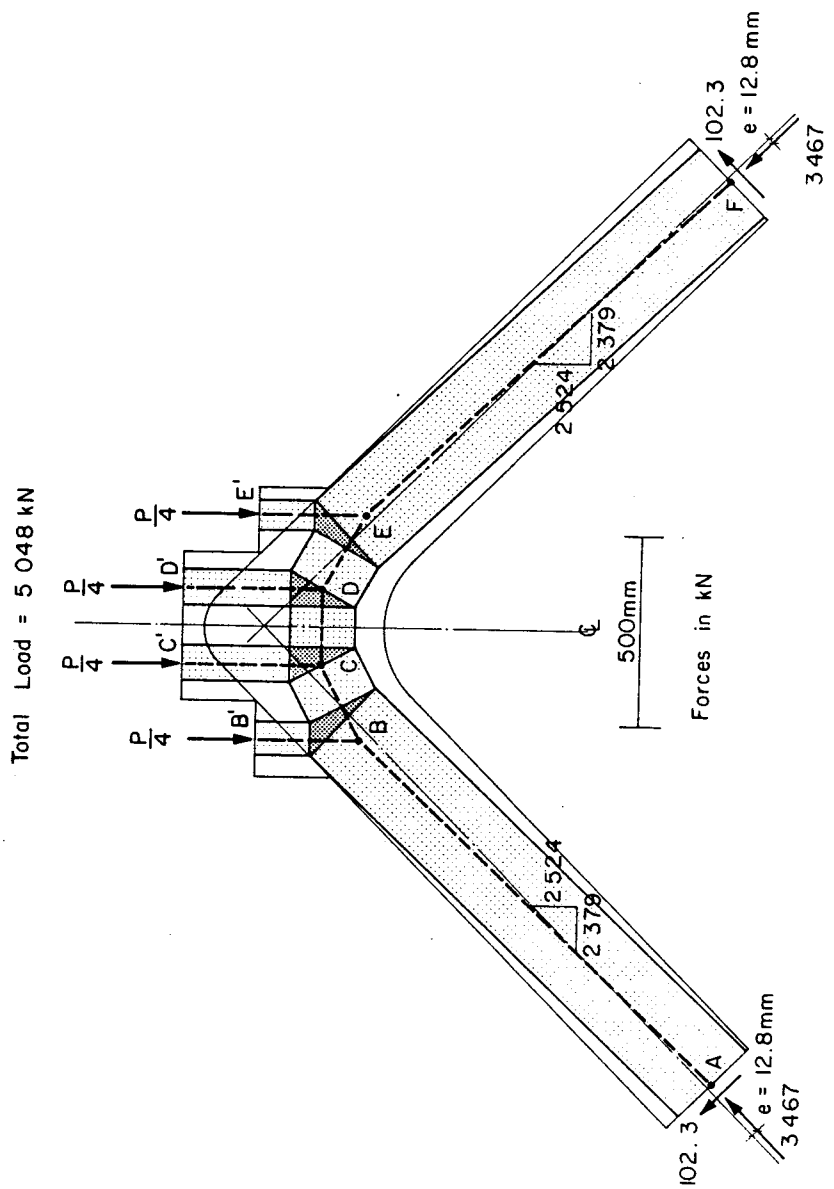

Figure 6.11 STM Based on Measured End Forces and Moments at Load = 5048 kN

6.3.4 STM Based on Measured Forces and Moments and Using Compression Reinforcement

The STM developed from the measured end forces and moment including the compression reinforcement is necessarily more complex than the other models presented in Sect. 6.3 for three main reasons. The additional forces carried by the reinforcement must be carried throughout the STM requiring greater detail. Also the greater axial load and moment are such that a linear stress distribution is not possible and additional assumptions are required. Finally, because the concrete and the reinforcement each take part of the load it becomes necessary to account for the area of concrete displaced by the bars.

In Sect. 5.2.4 it was suggested that for a column subjected to axial load only, the force carried by the column bars could be added to the concrete contribution provided that the bars have adequate development and are prevented from buckling by having adequate tie spacing. In such cases the bar forces will be assumed to be constant. When the axial load is eccentric, that is when moment is present, the force in the bars must change over the length of the region. This can only be achieved by fan action as will be shown in the following development.

The STM will be developed for the forces shown in Fig. 6.12 which were from the measured results from an applied load P = 5664 kN. This corresponds to 93% of the maximum load for this load condition. The forces acting at the ends

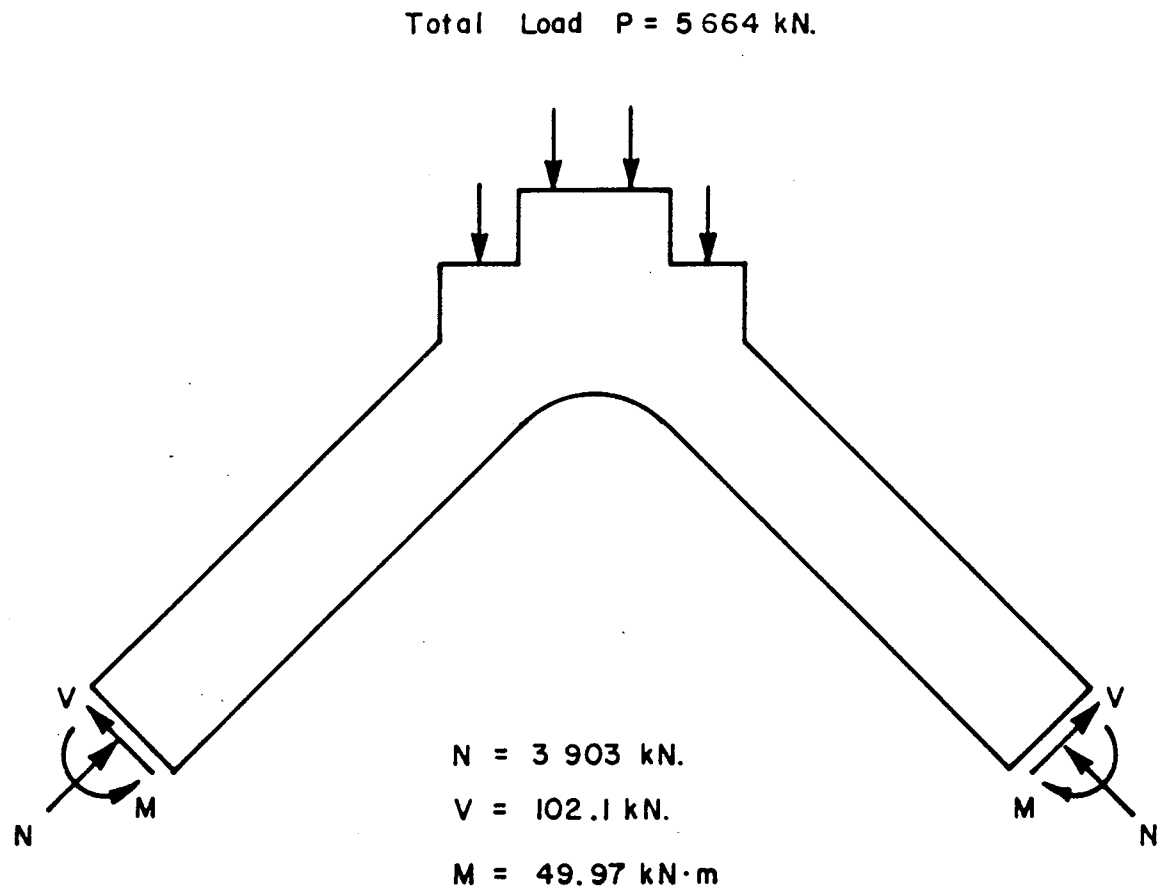

Figure 6.12 Forces and Moments at Ends of Specimen A1 at Load = 5664 kN

of Regions I and II are shown in Fig. 6.13(a) and (b) respectively. At 5700 kN during the test, the first signs of crushing and spalling were observed at the top outside surface. This suggests that the load corresponds very nearly to the capacity of the section.

The loads are too large to consider a linear-elastic transformed section analysis for the B-region in Fig. 6.13(a). However the forces acting in the reinforcement and in the concrete can be determined easily using a strain compatibility analysis and a representative stress-strain curve (Todeschini et al., 1964). This was done using the measured material properties. The resulting forces were then used to develop the STM for this region as well as the STM for the neighbouring D-region.

The assumed distributions of the end forces on the B-region are shown in Fig. 6.14. The corresponding forces acting at the ends of the D-region are also shown in Fig. 6.14. The STM consistent with these forces and utilizing the compression reinforcement is shown in Fig. 6.15. The convention proposed for the compression reinforcement is that it be shown as a dotted line similar to compression struts. In order to include the compression reinforcement it is assumed that the compression reinforcement has adequate development length.

Having selected the end forces, the development of the model is straightforward. The change in compressive force in the reinforcement between A and C, and between H and F can

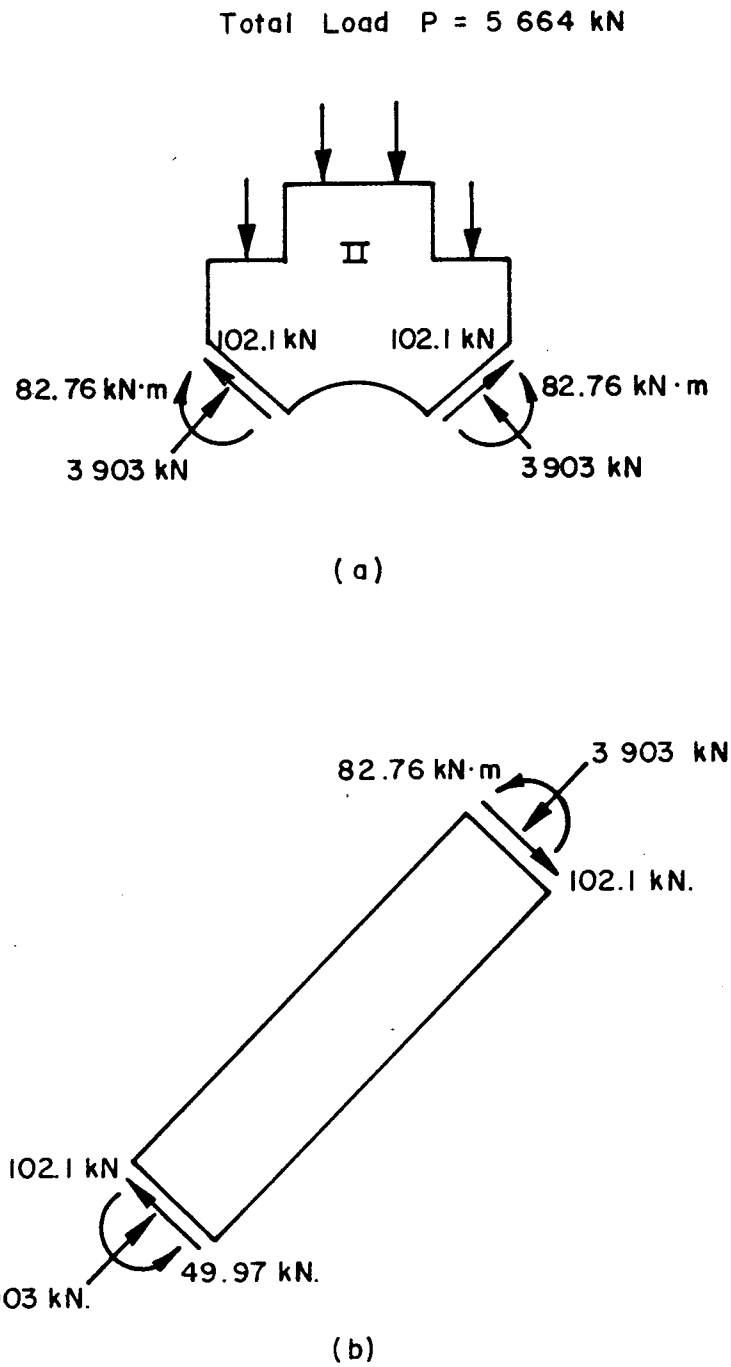

Figure 6.13 Forces and Moments at Ends of Regions I and II at Load = 5664 kN

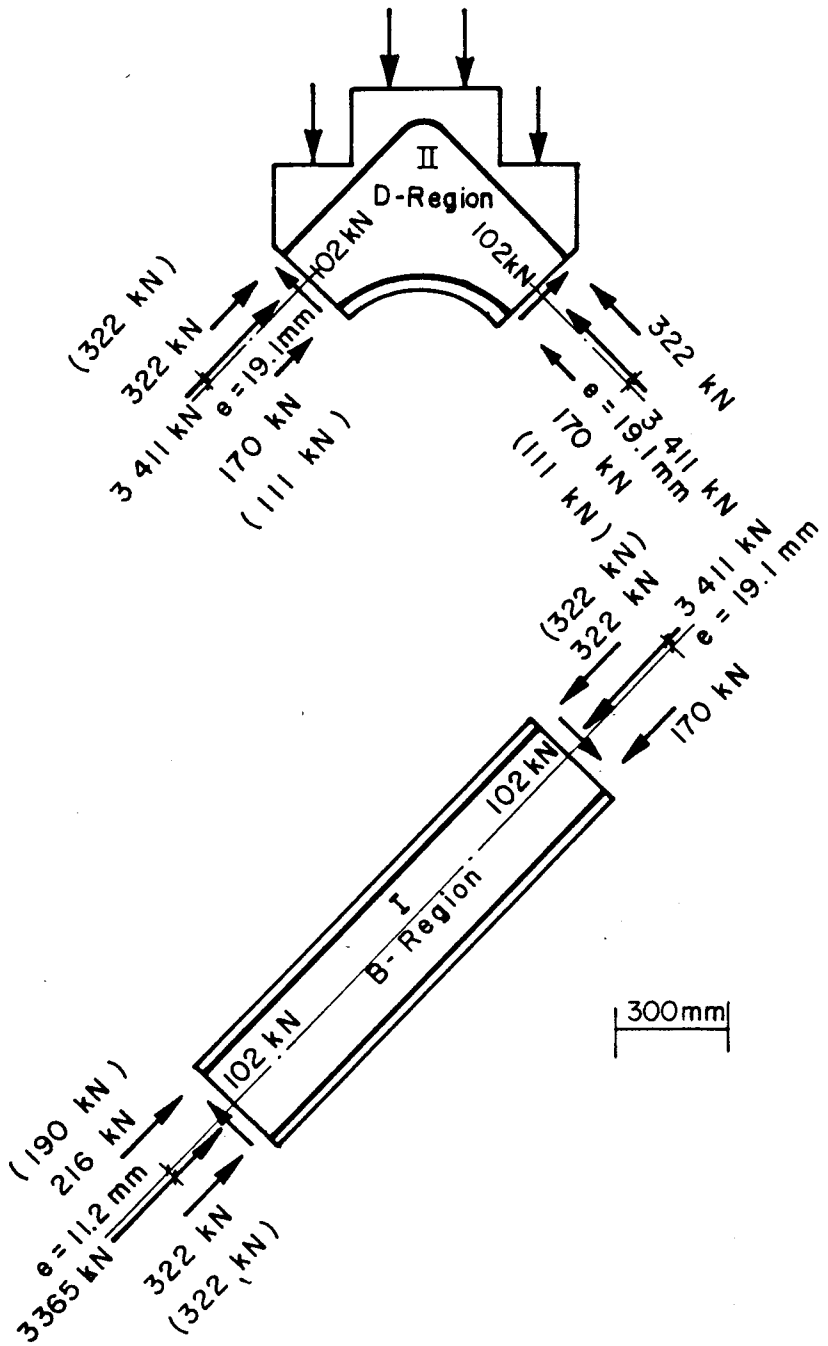

Figure 6.14 End Forces Acting on Regions I and II

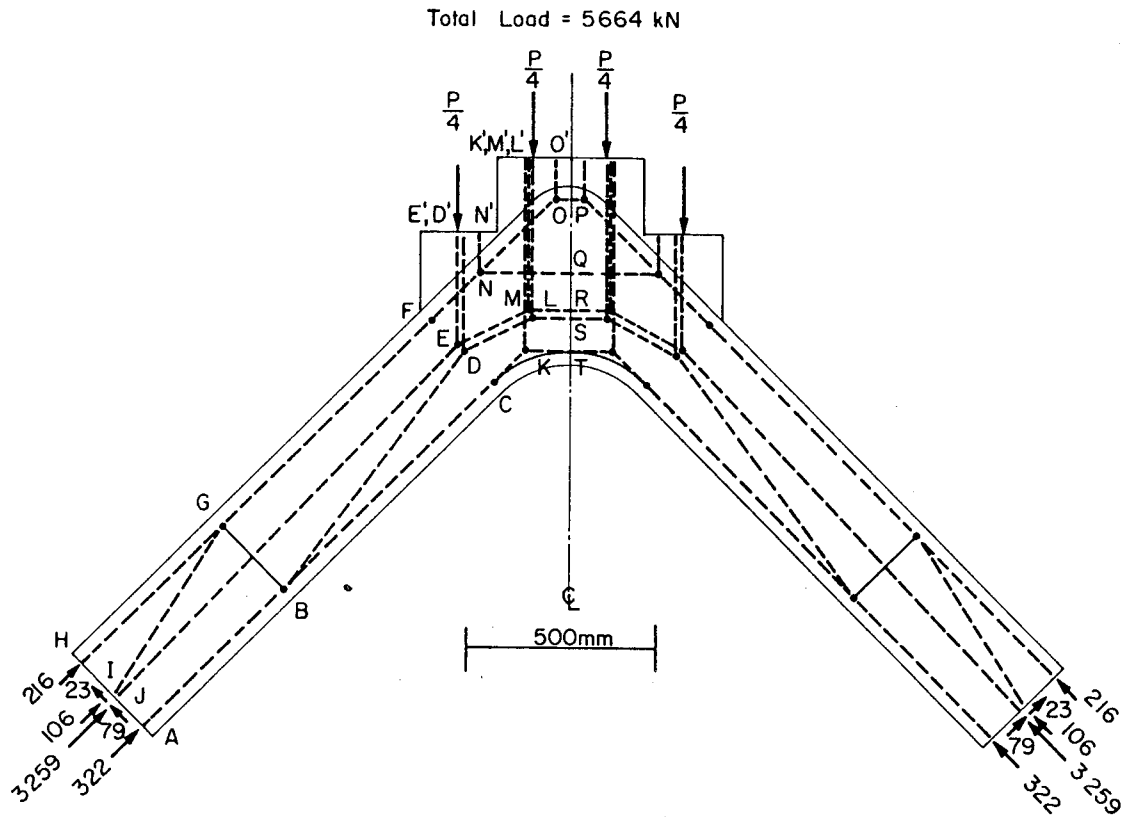

Figure 6.15 STM Based on Measured End-Forces and Including Compression Reinforcement

only be achieved by fans whose centerlines are given by struts DB and IG respectively. The shear on the B-region, 102 kN, is shared by these struts and by the main strut JE. The proportions are fixed since the slope of strut JE is predetermined by the eccentricities of J and E. The shear carried by the fans is taken by the tie GB which represents the action of stirrups or since the concrete is uncracked, a tensile stress field in the concrete. If it is to represent a concrete tensile stress field, then some consideration is warranted regarding the selection of f_{te}, the effective tensile strength of the concrete. The concrete within the stress field will be subjected to biaxial tension-compression and it is recognized that the tensile strength of the concrete is reduced in the presence of compressive stresses (see Fig. 7.2). A simplified qualitative assessment, proposed by Schlaich et al. (1987) is shown in Fig. 6.16. A relationship reduces f_{te} linearly with the compressive stress. That is, as the assumed value of f_{ce} increases, the allowable value of f_{te} decreases from a maximum of f'_t to zero as in Eqn. 6.1. The value of f'_t is taken to be the split cylinder strength.

$$f_{te} = (1 - \nu) f'_t \qquad [6.1]$$

In this case the stress distribution is assumed to correspond to the Todeschini distribution using f'_c = 61.6 MPa and an effectiveness factor is not taken per se.

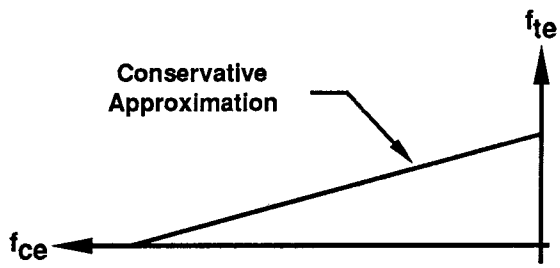

Figure 6.16 Simplified Assessment of Biaxial Tensile-Compressive Strength of Concrete

However, for the purposes of illustration, ν can be taken to be 0.9. Using Eqn. 6.1 gives $f_{te} = 0.1f'_t = 0.37$ MPa for Specimen A1. The required length of the tensile stress field is given by Eqn. 6.2

$$\ell = \frac{V}{bf_{te}} = \frac{23 \times 10^3}{250 \times 0.37} = 249 \text{ mm} \qquad [6.2]$$

The length ℓ will correspond to the length of the fans centered at G and B. Clearly there is more than sufficient capacity to take the 23 kN shear force in the concrete if desired.

Each of the forces acting at the boundary of the D-region must turn to become horizontal at the centerline of the specimen (Fig. 6.15). Each strut will carry part of the load with the two concrete struts carrying the majority, and the compression steel carrying the rest. It was assumed that the bottom compression steel picks up load only from load point 2 (second from the left) via strut K'K. The load transfer mechanism is modelled by struts CK, KT, and KK' but it will actually occur in a combination of bearing, bond, and arch action. However, the essential features are modelled since the steel is in compression at T and at C and the load is applied in between. The location of point K is the intersection of the lines tangent at C and T. Next it was assumed that the top steel develops 50% of its load from load point 1, and 50% from load point 2. The locations of N and O are chosen to position the strut at the innermost edge

of the applied load strut.

The remainder of the shear in each region must be carried by the concrete struts which start at E and D and end at R and S. In all cases the struts must be statically equivalent to the assumed forces in Fig. 6.14. As a final check, the magnitude and location of the forces in struts OP, NQ, MR, LS and KT must be such that the free-body diagram of one-half of the D-region is in equilibrium.

For comparison to the assumed distribution, the forces measured in the reinforcement at the ends of Region I are indicated in Fig. 6.14 by parentheses. The assumed and measured forces are seen to be in good agreement.

6.4 V-Shaped Arch Specimen B2

6.4.1 Introduction

An applied load of 762.9 kN was chosen to illustrate the development of the STM for Specimen B2. This load level represents 98% of the maximum load measured at failure (774.7 kN) and corresponds to an effective ice pressure equal to 3.87 MPa acting over the loaded area. The procedure to develop the STM for other load levels near ultimate is the same. The forces and moments acting at the ends of Specimen B2 at this load level were given in Table 4.7 and are shown in Fig. 6.17. These were determined from the measured applied load and reactions and the strains in the steel beam as discussed in Chapter 4. Included in these end

forces are the reactions to the compressive membrane forces which developed in the test.

Once the forces acting at the boundary of the specimen have been determined the next step in the modelling process is to divide the specimen into smaller regions as shown in Fig. 6.18. This is based on the identification of B and D regions as discussed in Chapter 5. There are no clear rules for the development of the boundaries of these regions but some guidance may be obtained from the crack patterns observed in the test (Fig. 6.19) and from the principal stress plots from a finite-element analysis (Fig. 6.20). Figures 6.19 and 6.20 have been repeated here from Figures 4.45 and 7.20, respectively. In addition, several regions are familiar D-regions such as Region III in which it may be assumed that the shear is carried partly by direct strut action and partly by fan action. From statics we may determine the forces and moments acting at the ends of each of these seven regions. Strut-and-tie models were then developed for these regions. The resulting complete model is shown in Fig. 6.21. In Fig. 6.21, struts and fan centerlines are indicated by dashed lines and the tension ties are indicated by solid lines. Nodes and other important points in the model are indicated by letters. Important nodal zones are drawn in detail and the struts associated with the "arching" or compressive membrane action are shown in full thickness. The scale on the drawing represents 1.0 m. The development of the STM for each of the seven regions will be

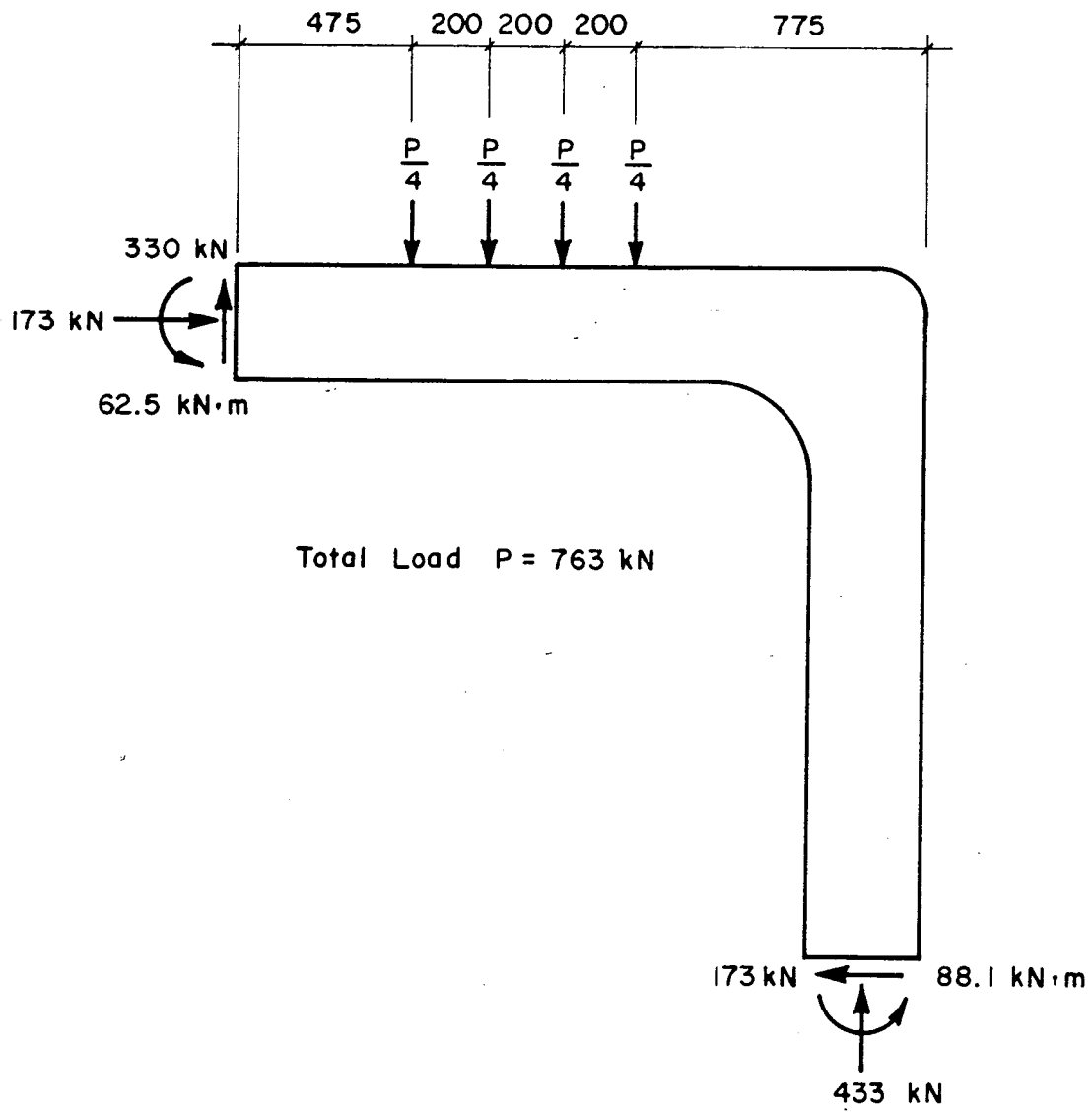

Figure 6.17 End-Forces and Moments for Specimen B2 at Load = 763 kN

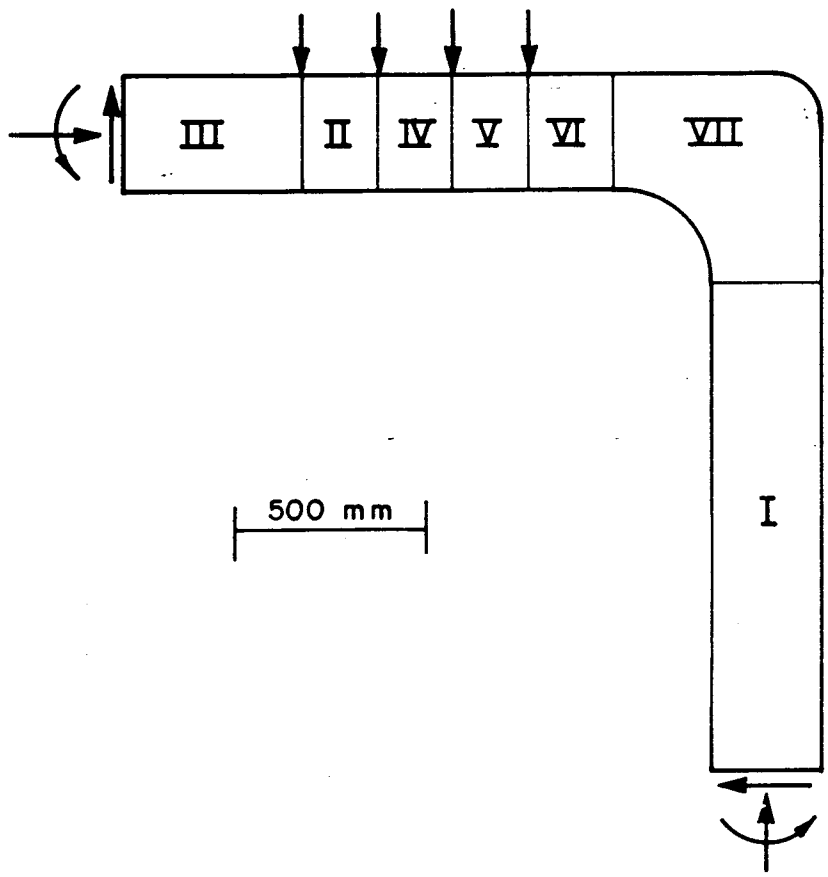

Figure 6.18 Design Regions for Specimens B1 and B2

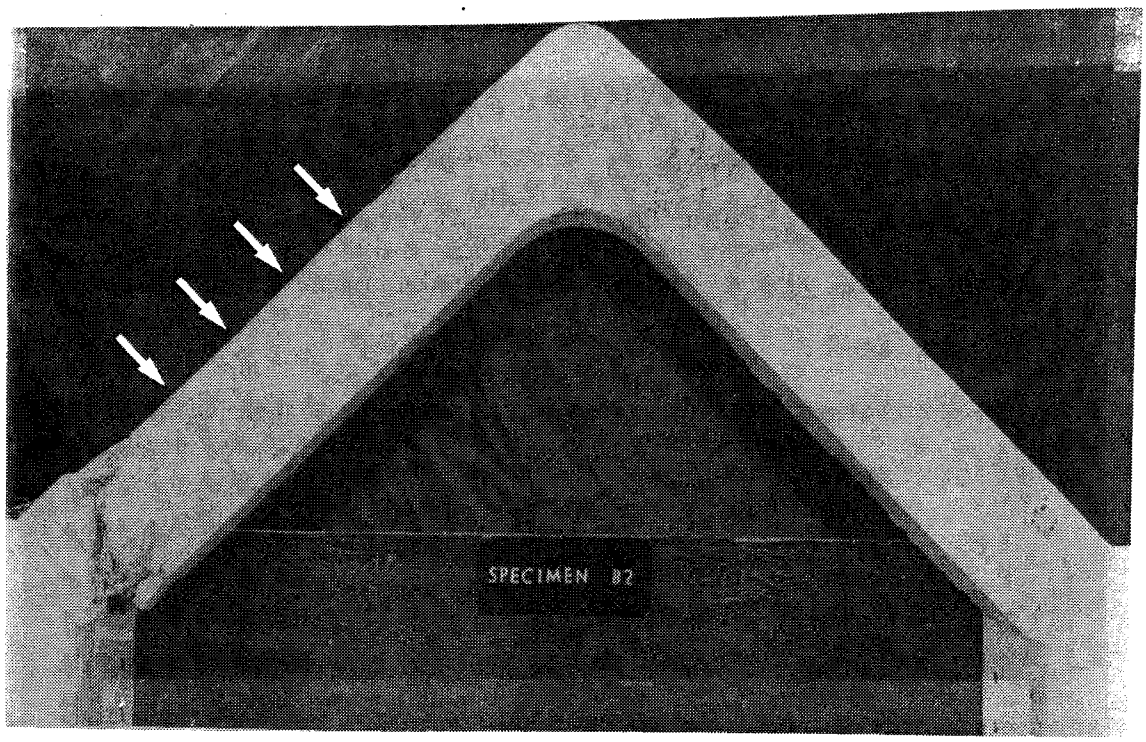

Figure 6.19 Final Overall Crack Pattern for Specimen B2

discussed separately after reviewing the assumptions common to the complete STM.

The following assumptions were used to develop the STM for Specimen B2.

5. $f_{ce} = \nu f'_c = 48.0$ MPa
   using $\nu = 0.9$ and mean concrete cylinder strength $f'_c = 53.3$ MPa
6. $f_y = 430$ MPa, $f_u = 645$ MPa, $A_s f_y = 343$ kN for No. 15M longitudinal steel, $E_s = 178360$ MPa
7. $f_y = 476$ MPa, $f_u = 681$ MPa, $A_v f_y = 60.8$ kN for each set of 6 mm stirrups, $E_s = 185300$ MPa
8. The maximum stress in the reinforcement was allowed to exceed the yield stress in locations where this occurred in the test.
9. The presence of compression steel was not specifically recognized.

6.4.2 Region I

Region I is assumed to begin at the base of the specimen and extend to where the curved section begins. The forces acting at the ends of Region I and the reinforcement present in this region are shown in Fig. 6.22. The DEMEC gauge locations used to measure reinforcement strains are indicated by dots at the proper location.

The measured strains in the reinforcement are summarized in Fig. 6.23. These strains are from DEMEC readings taken at the last load at which DEMEC readings were

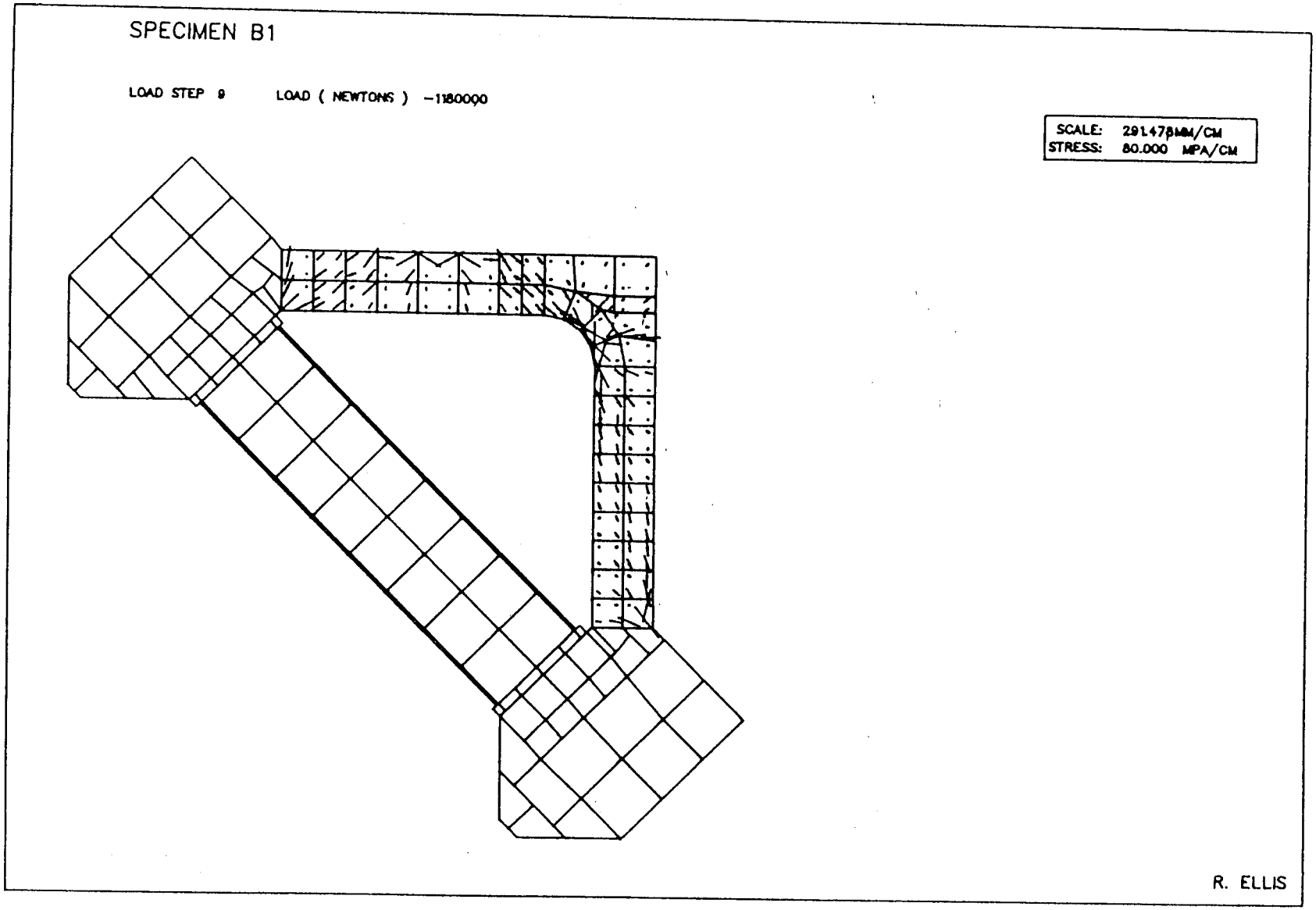

Figure 6.20 Principal Stress Plot From Finite Element Analysis

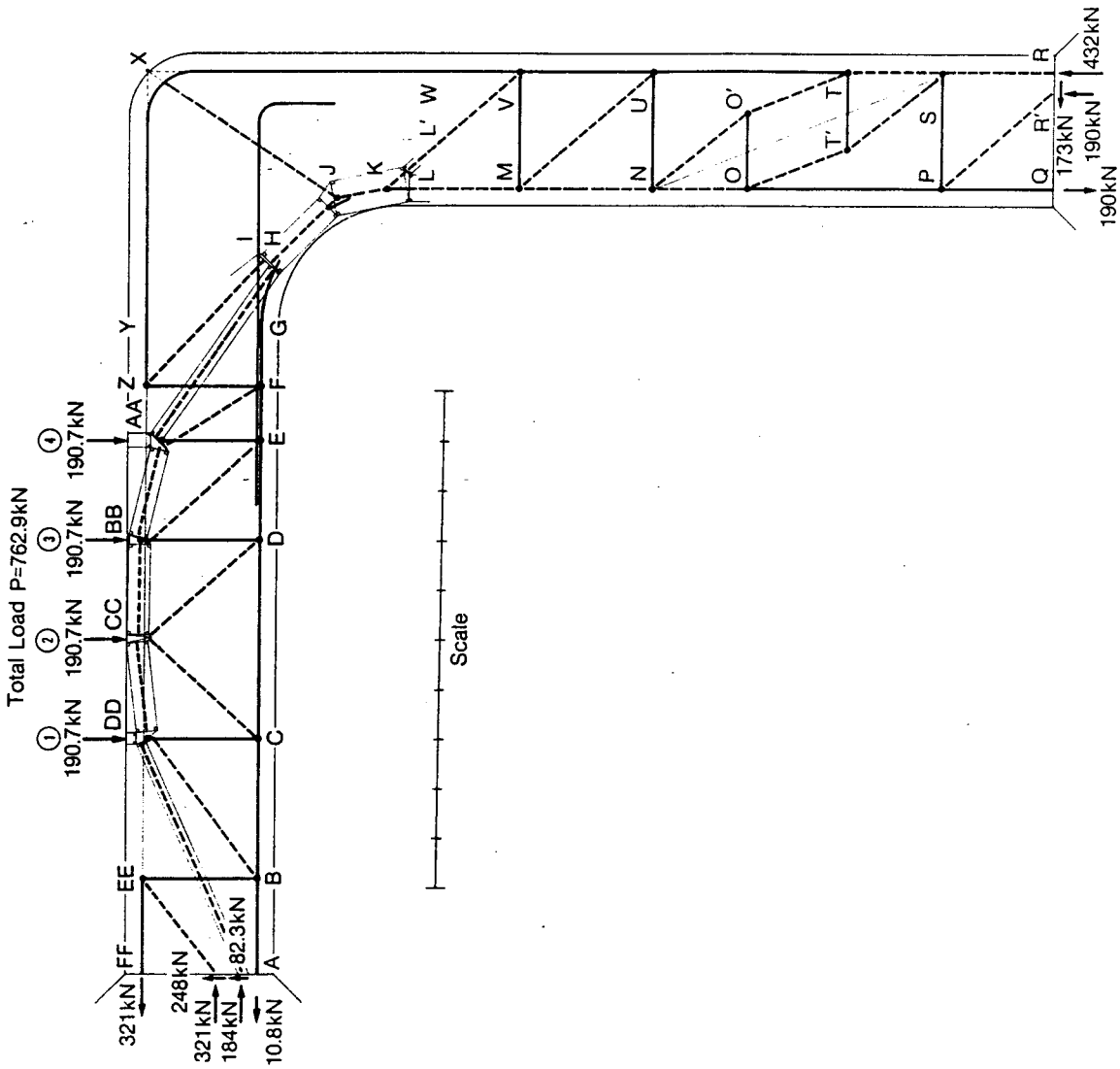

Figure 6.21 STM for Specimen B2 Based on Measured End-Forces at Load = 763 kN

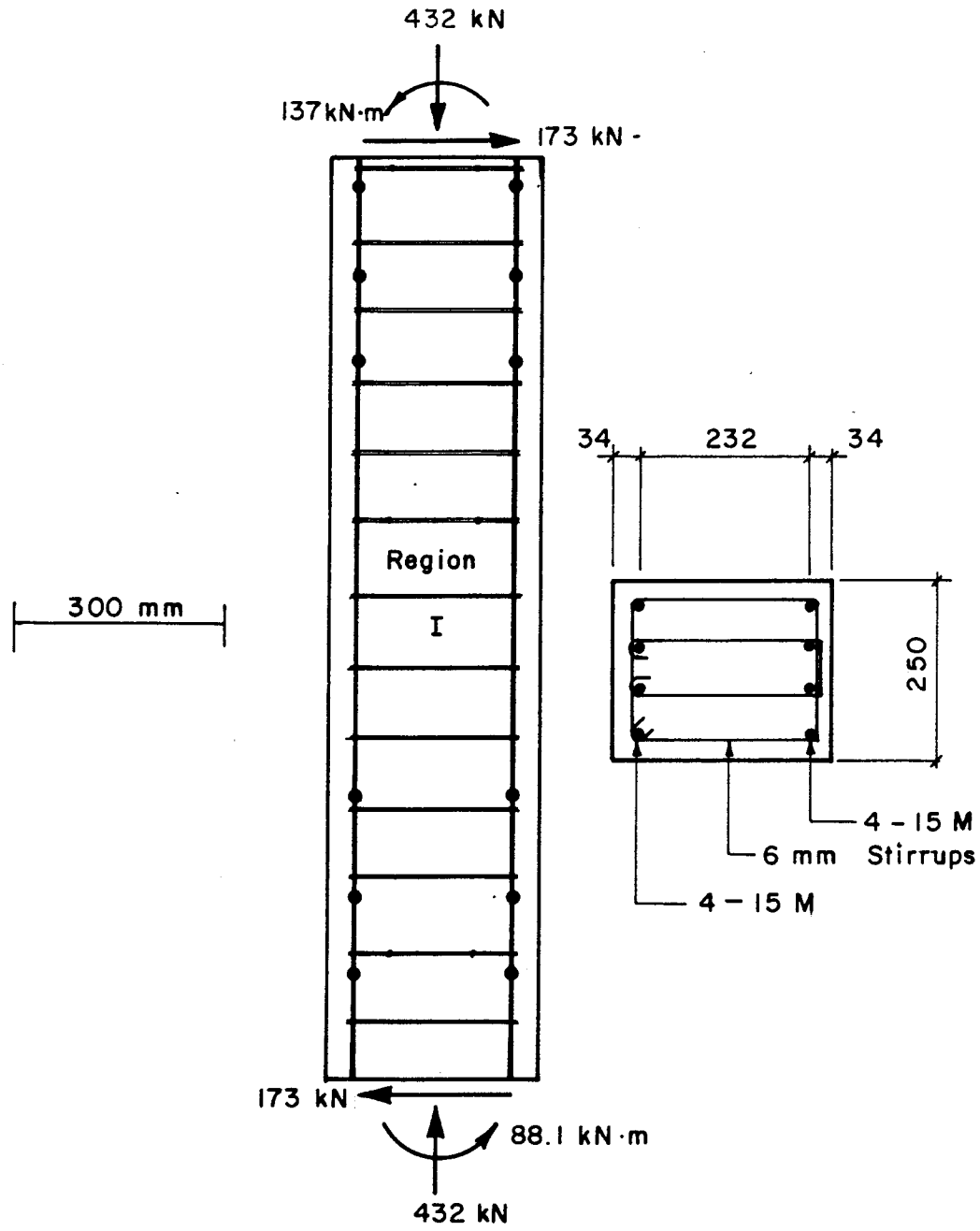

Figure 6.22 End Forces and Reinforcement Layout for Region I of Specimen B2 at Load = 763 kN

taken, 675 kN. This load represents 88.5% of the load considered in developing the STM. It is observed that at this load the stirrups are well below the yield strain. The strains in the longitudinal reinforcement are also well below the yield strain at all locations except in the tension reinforcement at the top. These observations are consistent with the observed crack pattern shown in Fig. 6.19.

The STM developed for this region is shown in Fig. 6.24. To develop this model it was first observed that the shear V = 173 kN is relatively low, and the axial load and moments are such that the resultant will fall within the kern limits of the section between points T and O. Between points N and S the resultant falls within the tension and compression chords. A line from S to N represents the locus of the resultant force.

The shear and axial load are constant in Region I and the strut SN must have x-component equal to 173 kN and y-component equal to 432 kN. The y-component must be carried by struts RS and MN and the widths of these struts can be checked assuming they are stressed to f_{ce}. The x-component (173 kN) of strut NS must be carried by the ties PS and NU. This requires only 3 sets of stirrups each.

Strut PR' will have an x-component equal to 173 kN. The y-component of PR' is equal to the tension in the tie PQ. The magnitude of this tension is not known but it can be estimated from the strain measurements near point P taken at

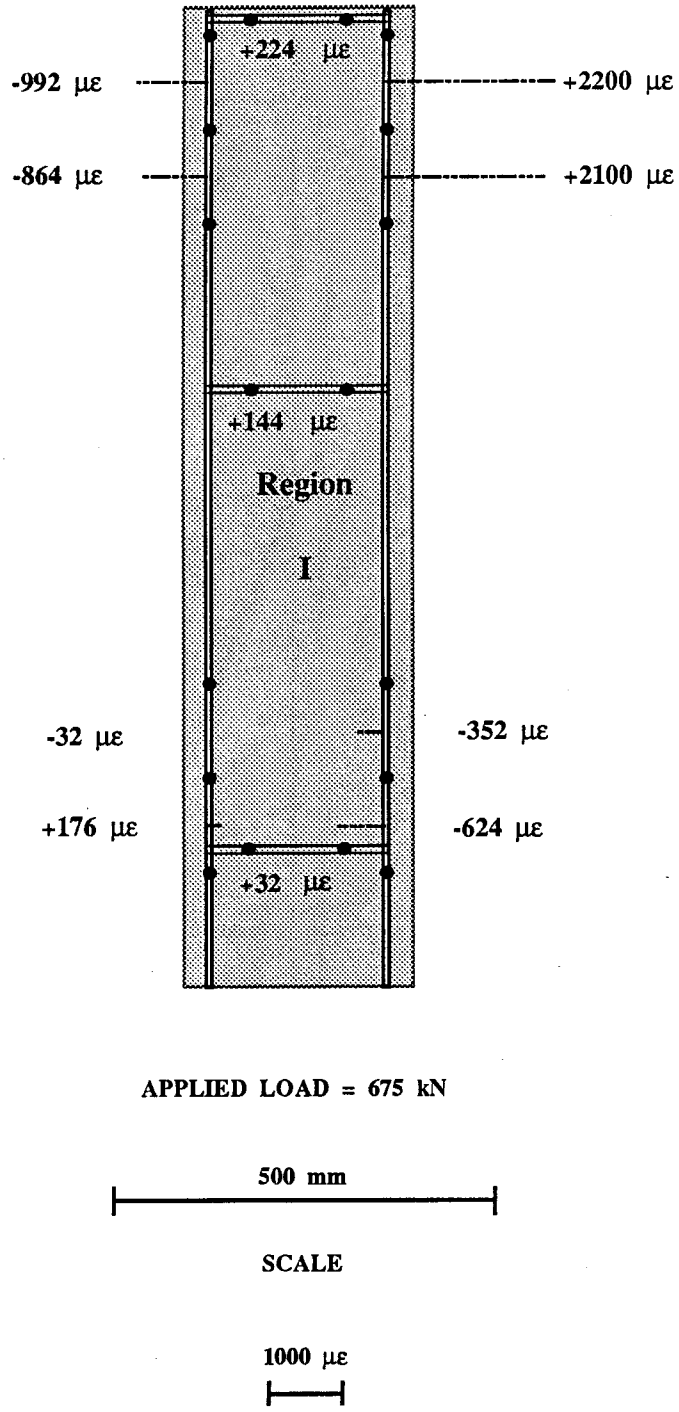

Figure 6.23 Measured Strains in Reinforcement in Region I at Load = 675 kN

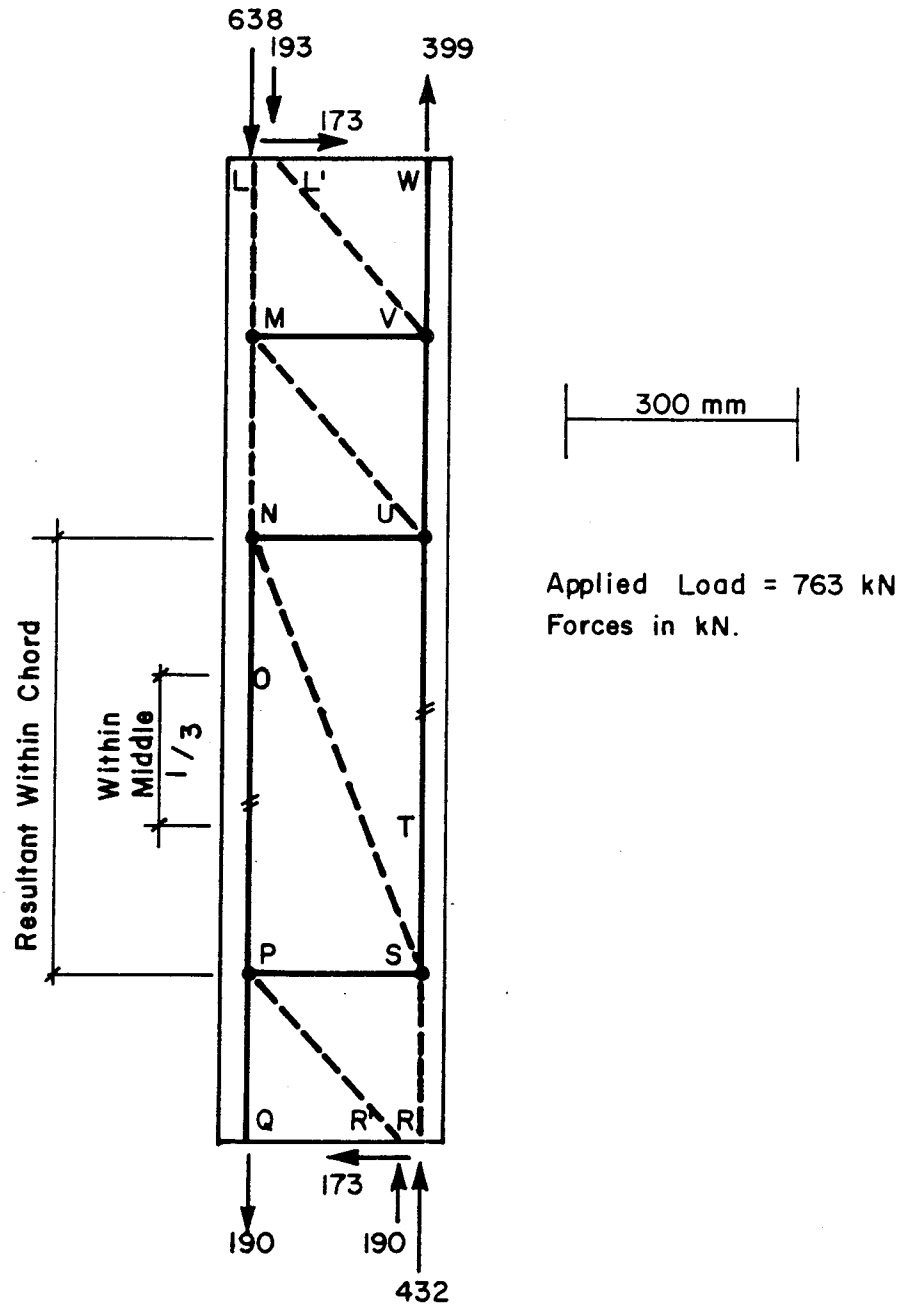

Figure 6.24 STM for Region I for Forces in Fig. 6.22.

the lower load 675 kN. The value shown in Fig. 6.24 was sufficiently accurate based on an estimate of the slope of strut PR'. It is noted that the strut PR' is actually the centerline of a fan stress field and the tension at Q will actually decrease gradually from Q to a point beyond P.

The shear V = 173 kN is carried in the top part of the region by the tie MV and the x-components of struts MU and VL'. If the location of the tie MV is assumed to be 275 mm from point U, then the y-component of strut MU must be 205 kN. This is added to the force in strut NM to produce the force in strut LM, 638 kN, and the width of this strut is checked. The force in the tie UV must also be equal to the y-component in strut MU. The total force in the tie VW is obtained by assuming the slope of the strut VL'. The final slope of the strut VL' is such that the y-component is 193 kN which when added to the tie force UV produces the total tie force 399 kN. Referring to the strains measured in the reinforcement corresponding to tie VW (at 675 kN), it is expected that at this load (763 kN), the maximum tension would be above the yield strength $A_s F_y$ = 343 kN. The location of L' is confirmed by summing moments at this section. Finally, it is also necessary to ensure that strut VL' and strut ML meet in such a way that the resultant strut is within the boundaries of the specimen (see Fig. 6.21).

A more detailed STM for the region between N and S is shown in Fig. 6.25. In this model it is recognized that the compressive forces will tend to spread out in going from S

to N. The resulting tensile stresses require the tension ties TT' and OO'. The ties are assumed to be located at the points where the resultant passes through the kern of the section. The force in each tie will be equal to the shear force 173 kN which could easily be supplied by the uniformly spaced stirrups in this region.

In order to compare assumed and measured forces acting on the reinforcement it is necessary to extrapolate from the measured strains shown in Fig. 6.23 because the DEMEC points were not be at the ends of the region for practical reasons, and because for safety reasons the last readings were taken at an applied load of 675 kN rather than at the load 763 kN considered in the STM. In Fig. 6.20, the forces estimated from linearly extrapolated strains are shown in brackets ( ) for comparison to the forces assumed in the STM.

6.4.3 Region II

Region II is assumed to be the region between load point 1 and load point 2, the point of maximum moment. The forces acting at the ends of the region are shown in Fig. 6.26(a) and the reinforcement present in this region is shown in Fig. 6.26(b).

The measured strains in the reinforcement at an applied load of 675 kN are summarized in Fig. 6.27. Shown in Fig. 6.27(a) are the strains in the top steel for the main part of the specimen comprised of regions II-VI. Region II is shown shaded. The strains in the bottom steel and in the

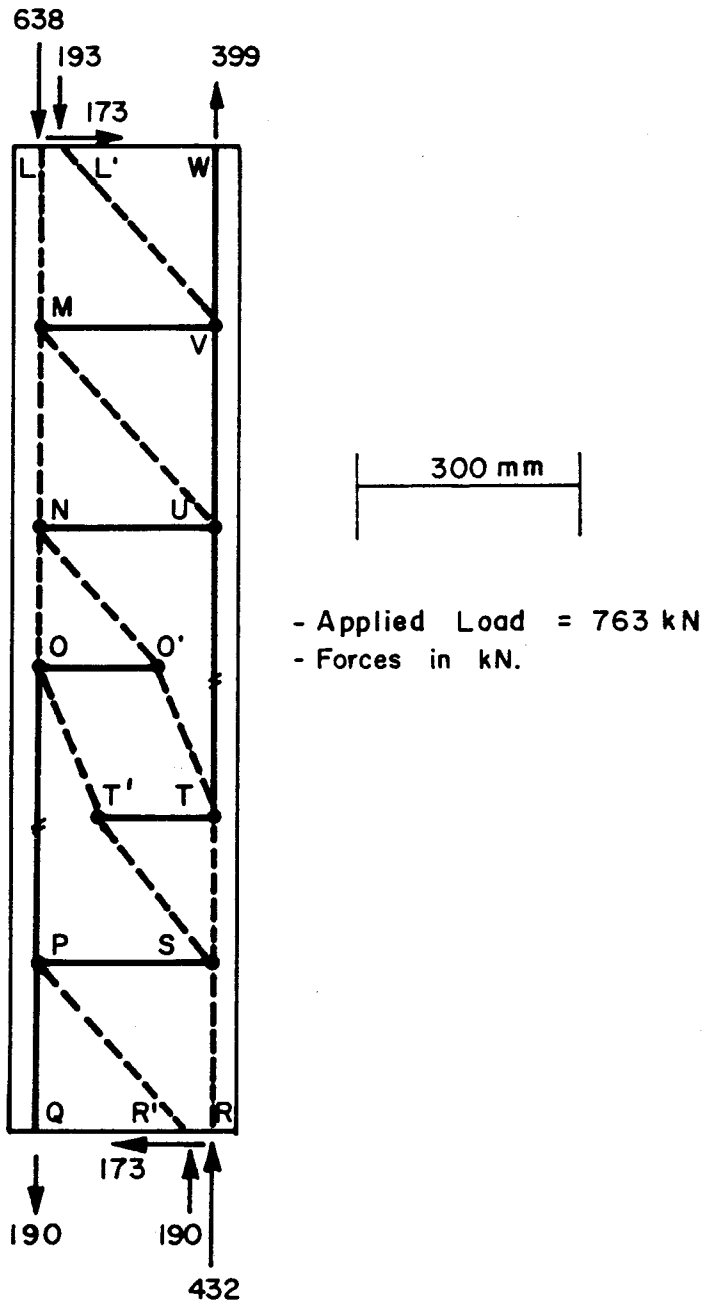

Figure 6.25 More Detailed STM for Region I

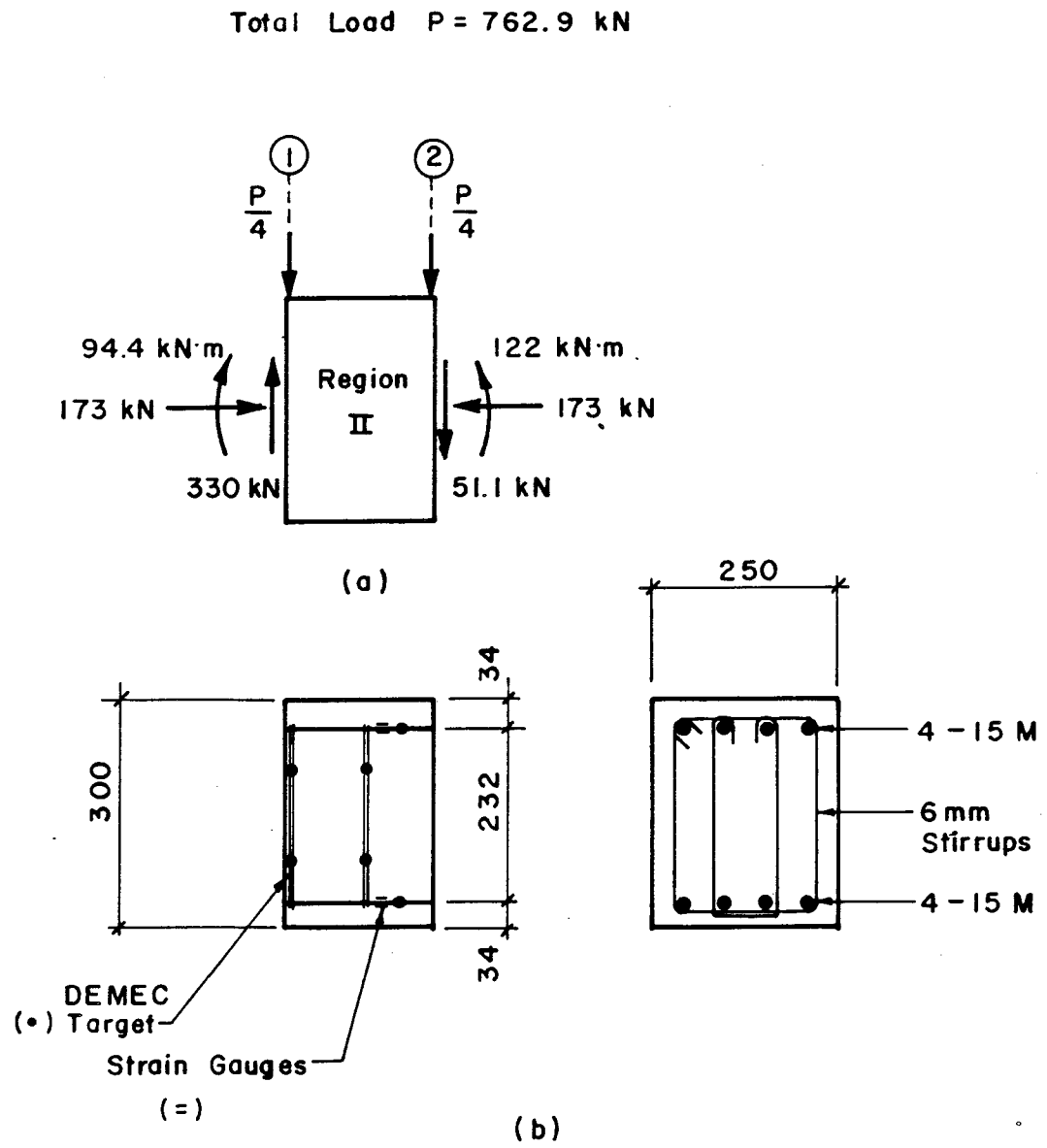

Figure 6.26 End Forces and Reinforcement Layout for Region II at Load = 763 kN

stirrups are shown in Fig. 6.27(b) and (c) respectively. It is observed that at this load the maximum strains in the bottom reinforcement are significantly above the yield strain. The strains in the top reinforcement are below the yield strain at the support where they are tensile, and at midspan where they are compressive. Also shown in Fig. 6.27(a) and (b) are the strain readings from the electrical resistance strain gauges that were still functioning at an applied load of 773 kN.

The STM developed for Region II is shown in Fig. 6.28. Based on the axial load and moment under load point 2 and using f_{ce} = 48.0 MPa, the required depth of the nodal zone at CC can be determined. This requires a force T = T_{max} = 415 kN. Then, based on the strain measurements at point C the force in the bottom reinforcement there was assumed to be equal to $T_C = A_s F_y$ = 343 kN. If the tie location is assumed to be at point C, directly below load point 1, the horizontal component of the strut CC-C is equal to the difference between T_{max} and T_C. The horizontal component of strut CC-DD is known since the sum of this and T_C must equal the axial force on the section, 173 kN. The internal lever arm z to point DD is then known. The vertical components of struts CC-C and CC-DD are determined by trial and error. This is most easily done by varying the slope of one of the struts until the combination of the two struts matches the nodal zone at CC. The final solution to this requires the vertical component of the strut CC-C to be 79.2 kN and that

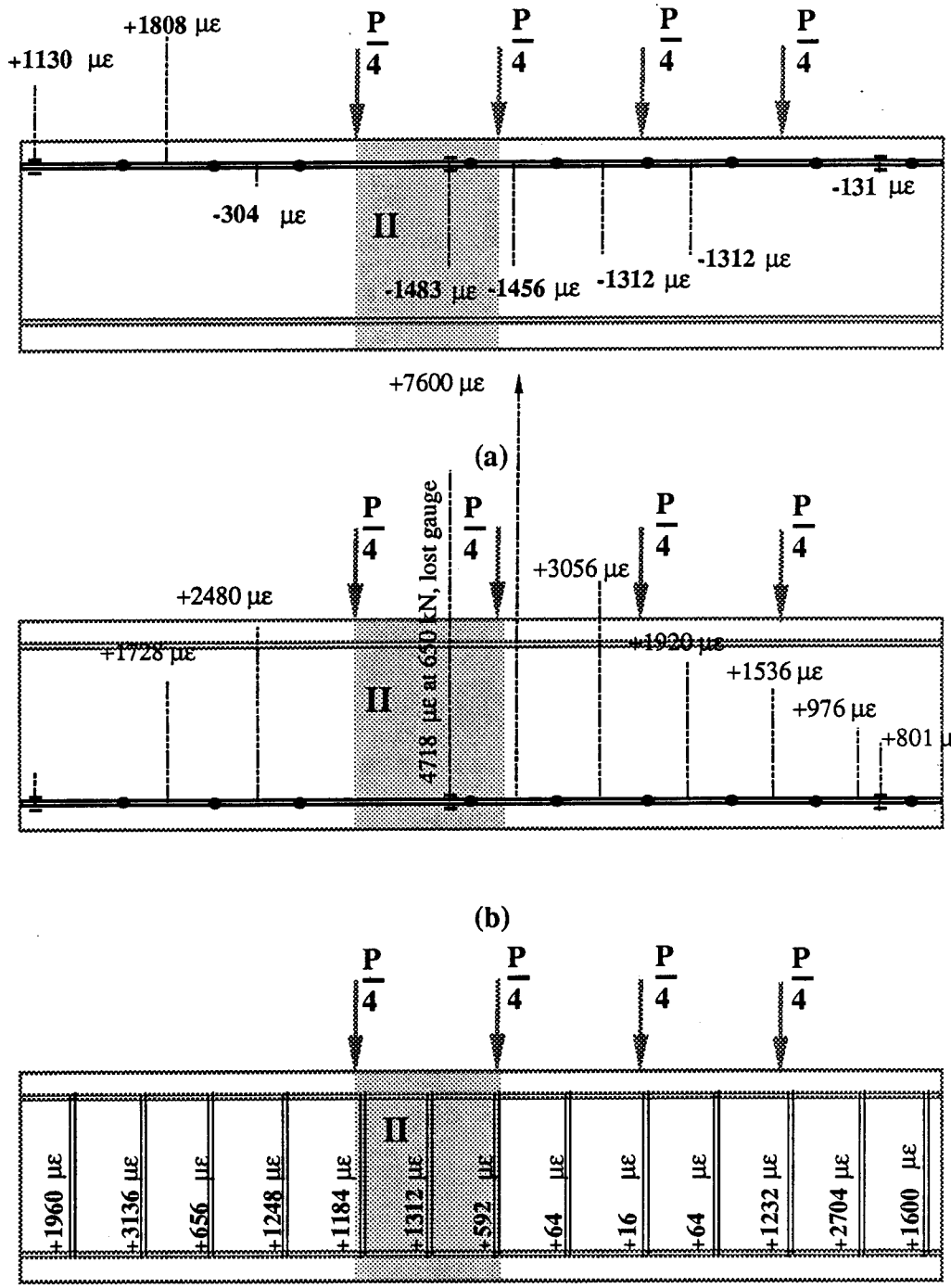

Figure 6.27 Measured Strains in Reinforcement in Region II at Load = 675 kN

of the strut CC-DD to be 60.4 kN. This defines all struts and ties within Region II.

It is then only necessary to ensure that the widths of the struts do not exceed the geometric limits of the section. This is assured if the nodal zones are sketched as shown. Also it was determined that sufficient stirrups exist to provide the force 79.2 kN tie C-DD. This relatively small force is easily taken by the stirrups.

The measured and assumed forces in the reinforcement are compared in the STM of Fig. 6.28. Where they are known, the measured forces are shown surrounded by parentheses. The DEMEC gauge under load point 2 gave a strain of +7600 $\mu\epsilon$ at 675 kN. The electrical resistance strain gauges located on the bottom reinforcement at the point of maximum moment were lost at a strain near +5000 $\mu\epsilon$ corresponding to the applied load 650 kN. Strains of this magnitude correspond to the yield plateau of the stress-strain curve for this reinforcement (Fig. 3.23). At a lower load of 600 kN these strains were +2900 $\mu\epsilon$ which is also on the yield plateau. The change in these values suggests that although we cannot extrapolate to the higher load 763 kN, we can expect the strains to be along or above the yield plateau. The assumed force (415 kN) corresponds to approximately +20 000 $\mu\epsilon$ on the stress-strain curve which is in the strain hardening portion. This is thought to be reasonable.

The force in the reinforcement at C was assumed to be equal to the yield strength because the measured strains

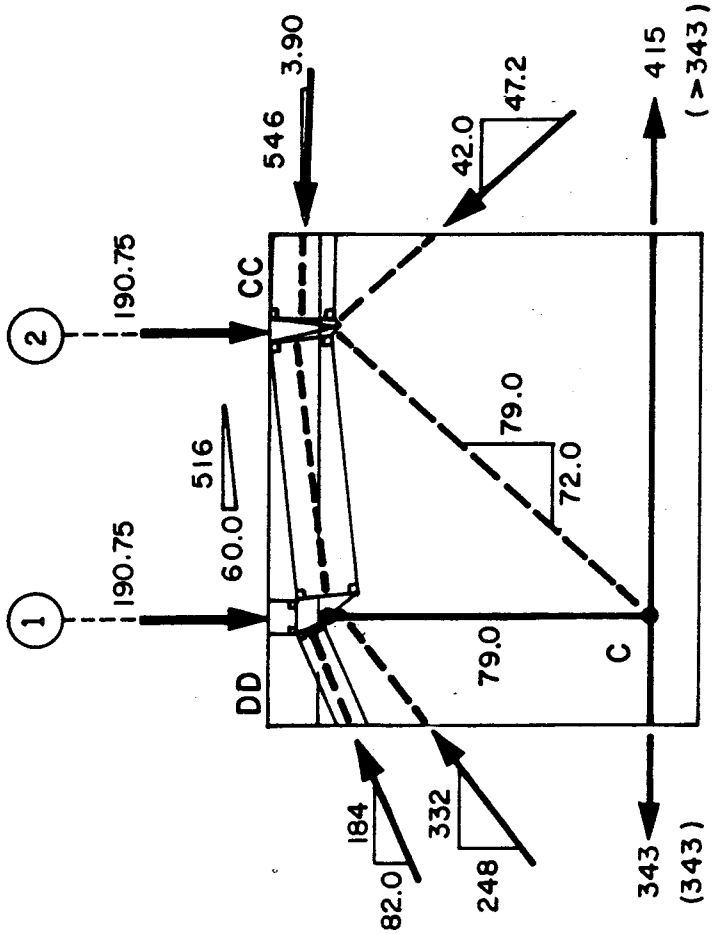

Figure 6.28 STM and Internal Forces for Region II at Load = 763 kN

suggested that at the applied load 763 kN the bars would still be within the yield plateau. The measured and assumed forces are the same at this location.

6.4.4 Region III

Region III is the region between the support and load point 1. The forces acting at the ends of this region are shown in Fig. 6.29(a) and the reinforcement present in this region is shown in Fig. 6.29(b).

The measured strains in the reinforcement at an applied load of 675 kN are summarized in Fig. 6.30. At the support, the electrical resistance strain gauges were functioning properly at an applied load of 770 kN. The forces in the top and bottom steel, at FF and A respectively, were determined based on these measurements. The force in the bottom steel at point C was determined in Region II to be 343 kN. From the measured stirrup strains it is observed that at 675 kN, the stirrups nearest the support are already yielding while the stirrups further away had not yet reached yield.

For a region such as this with a relatively low shear-span to depth ratio and subjected to the forces shown in Fig. 6.29(a), it is reasonable to assume that part of the shear is carried by stirrup action and the remainder by direct strut action. A review of the crack pattern observed in this region (Fig. 6.31) suggests that this is a good assumption. Figure 6.31 is repeated here from Fig. 4.43. The relative magnitudes of the strut action and fan action

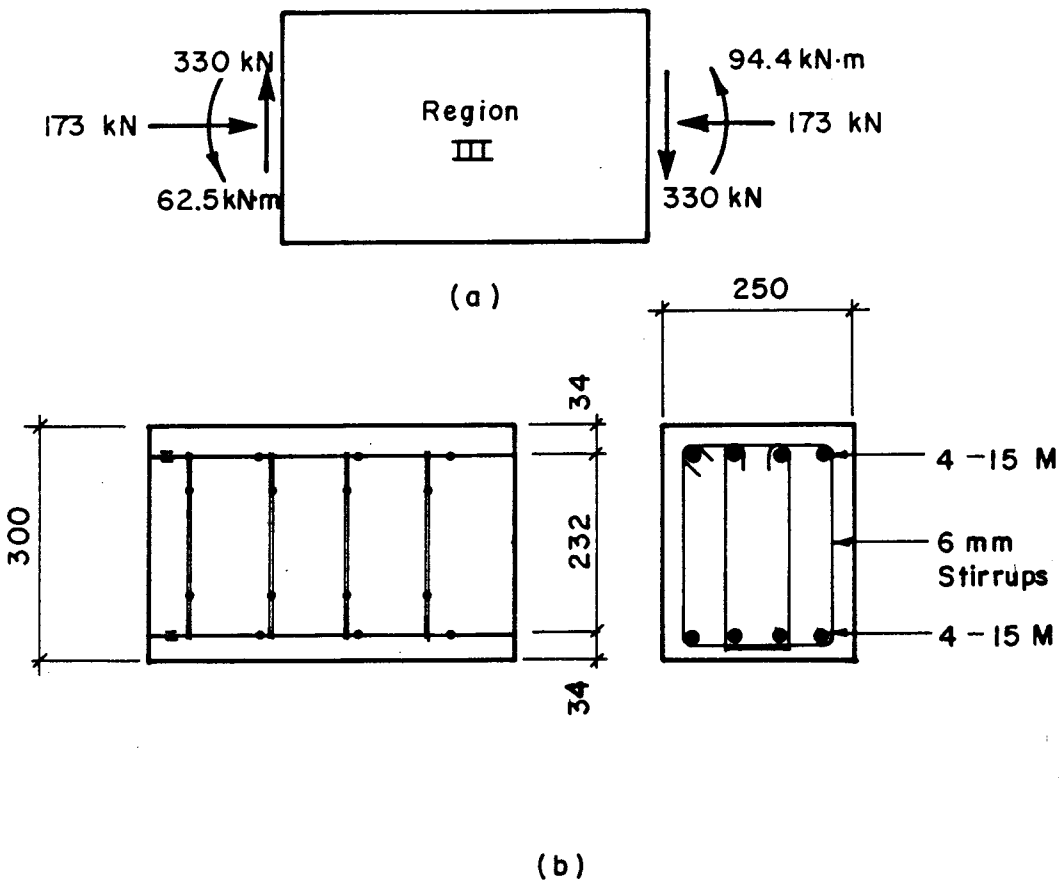

Figure 6.29 End Forces and Reinforcement Layout for Region III at Load = 763 kN

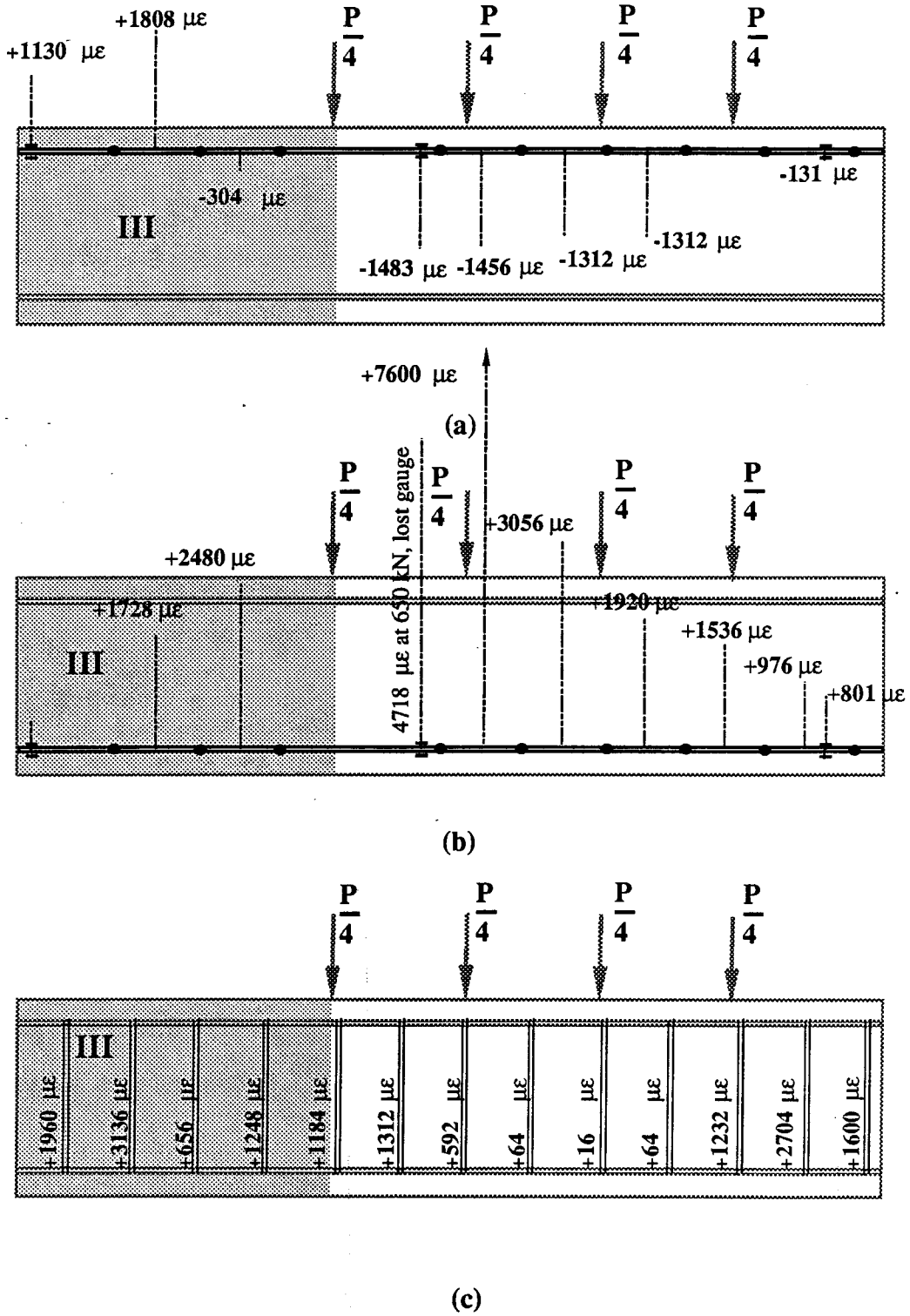

Figure 6.30 Measured Strains in Reinforcement in Region III at Load = 675 kN

should depend on the amount of shear reinforcement.

The STM developed for Region III is shown in Fig. 6.32. The horizontal component of the (fan) strut through B is known since it is responsible force for decreasing the force in tie AC from 343 kN to 10.8 kN. The horizontal component in the strut DD-A' is then known from node DD. The section can only be in equilibrium if the horizontal component of the (fan) strut A"-EE is equal to the force in the tie FF-EE (= 320.6 kN).

Various positions of A' and A" are possible which are statically admissible relative to the end moment at that section. The position of A' and A" also depends on the amount of the shear assumed to be carried by strut DD-A' and tie B-EE. The position of A', A", and the tie B-EE are interrelated and the final solution is obtained by trial and error. In this case, the slope of the strut DD-A' was chosen and location of the tie B-EF was determined by evaluating the (fan) strut DD-B. It is then only necessary to check the width of the struts and the availability of reinforcement.

In Fig. 6.32 the measured forces in the reinforcement are indicated by parentheses. In this case the assumed and measured forces are the same.

6.4.5 Region IV

Region IV is assumed to correspond to the region betwen the load points 2 and 3. The forces acting at the ends of this region are shown in Fig. 6.33(a) and the reinforcement

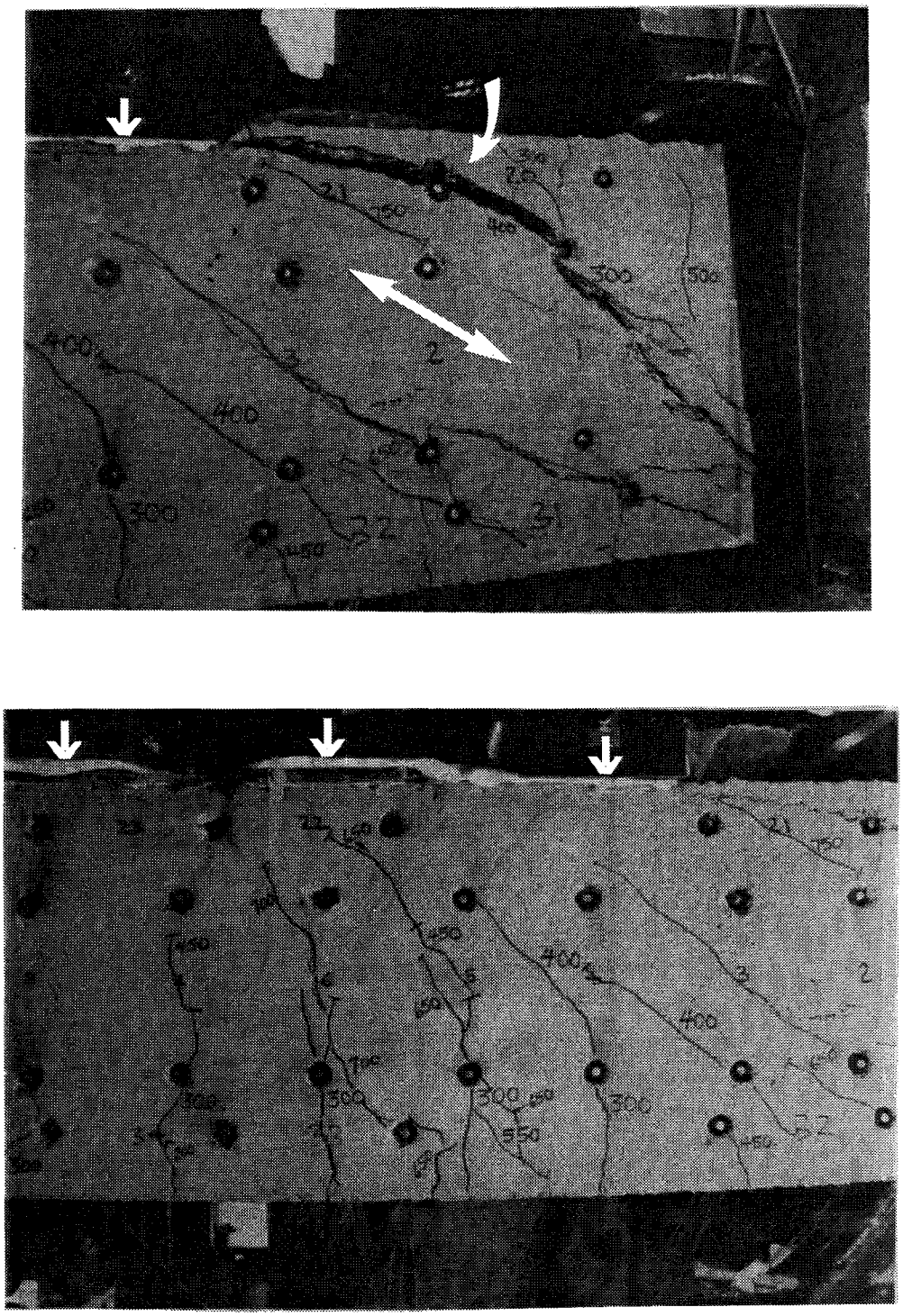

Figure 6.31 Crack Pattern in West Shear Span and at Midspan for Specimen B2

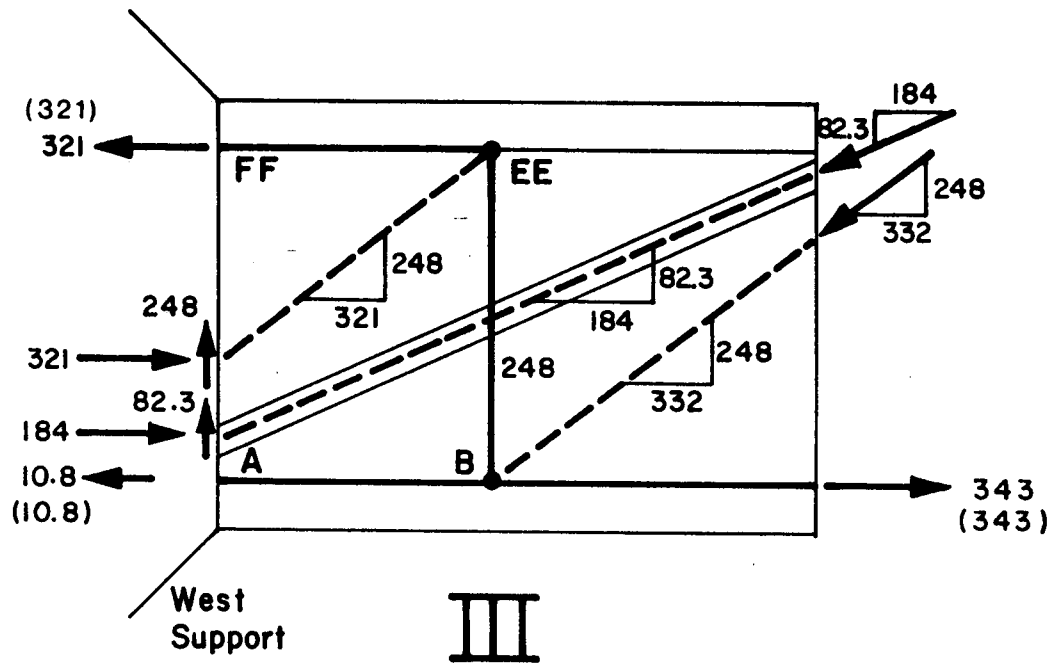

Figure 6.32 STM and Internal Forces for Region III at Load = 763 kN

present in this region is shown in Fig. 6.33(b).

The measured strains in the reinforcement at an applied load of 675 kN are summarized in Fig. 6.34. The force in the tie at the point of maximum moment was determined to be 415 kN in Region II. The strain measurements in Fig. 6.34(b) suggest that the force in the tie to the right of D should be above the yield strength at the applied load 763 kN. Since the magnitude is not known a magnitude was chosen which is intermediate between the yield strength, 343 kN, and the value 415 kN. It was also assumed that the tie location coincides with load point 3. A value of T_D = 373 kN was chosen. This requires the internal lever arm to be slightly less than that at node CC. The resulting STM for this region is shown in Fig. 6.35. Since this is a region of high moment and low shear, it is reasonable that the strut CC-BB should have a very flat slope. Because of this, almost all of the shear in this region is carried by the stirrups.

The widths of all struts are then checked and it must be determined whether sufficient reinforcement is available to provide the assumed tie forces. In this case, the small shear force 51.1 kN requires less than one set of stirrups. Since the force in the reinforcement at D is not known accurately the measured and assumed forces cannot be compared.

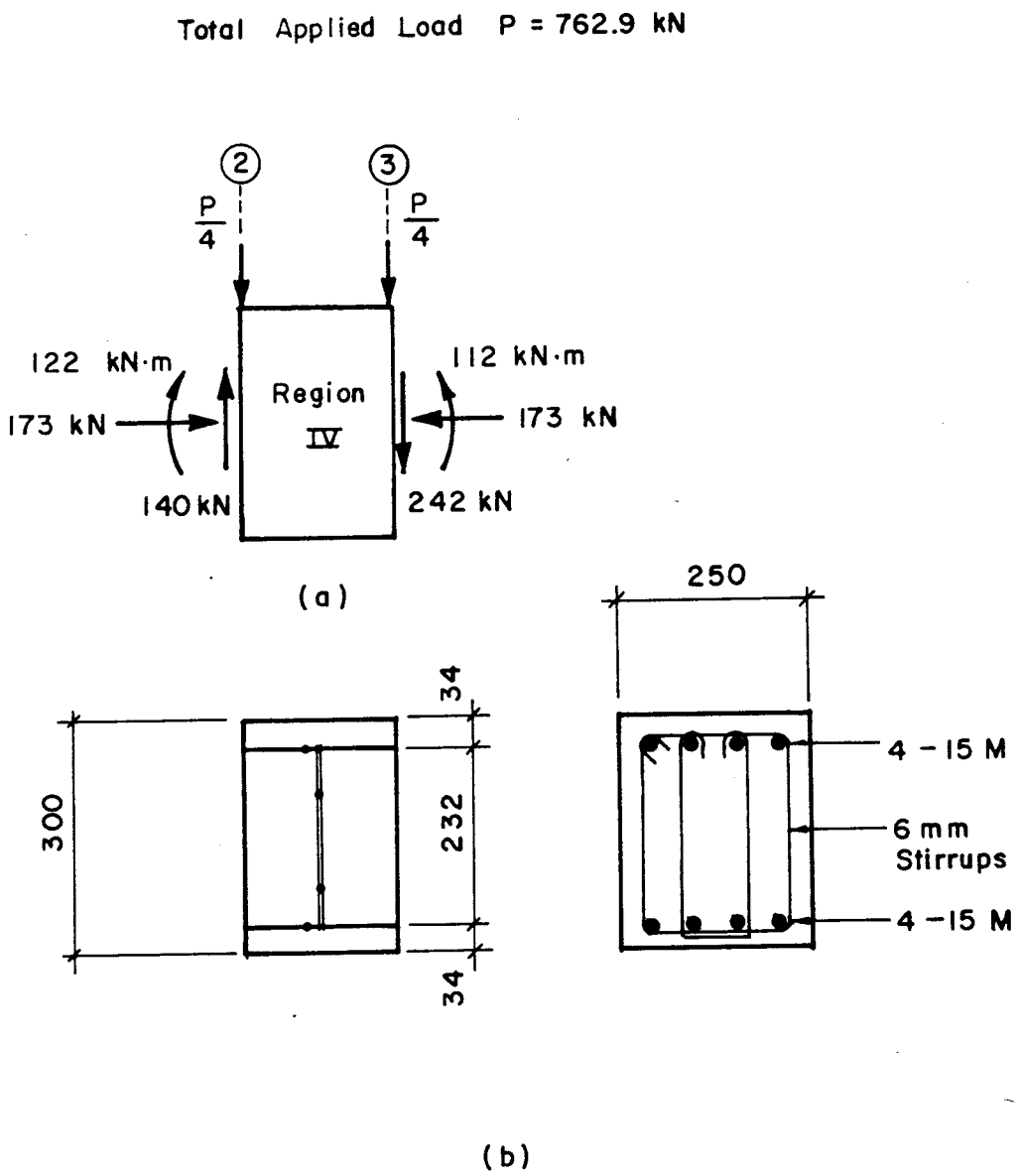

Figure 6.33 End Forces and Reinforcement Layout for Region IV at Load = 763 kN

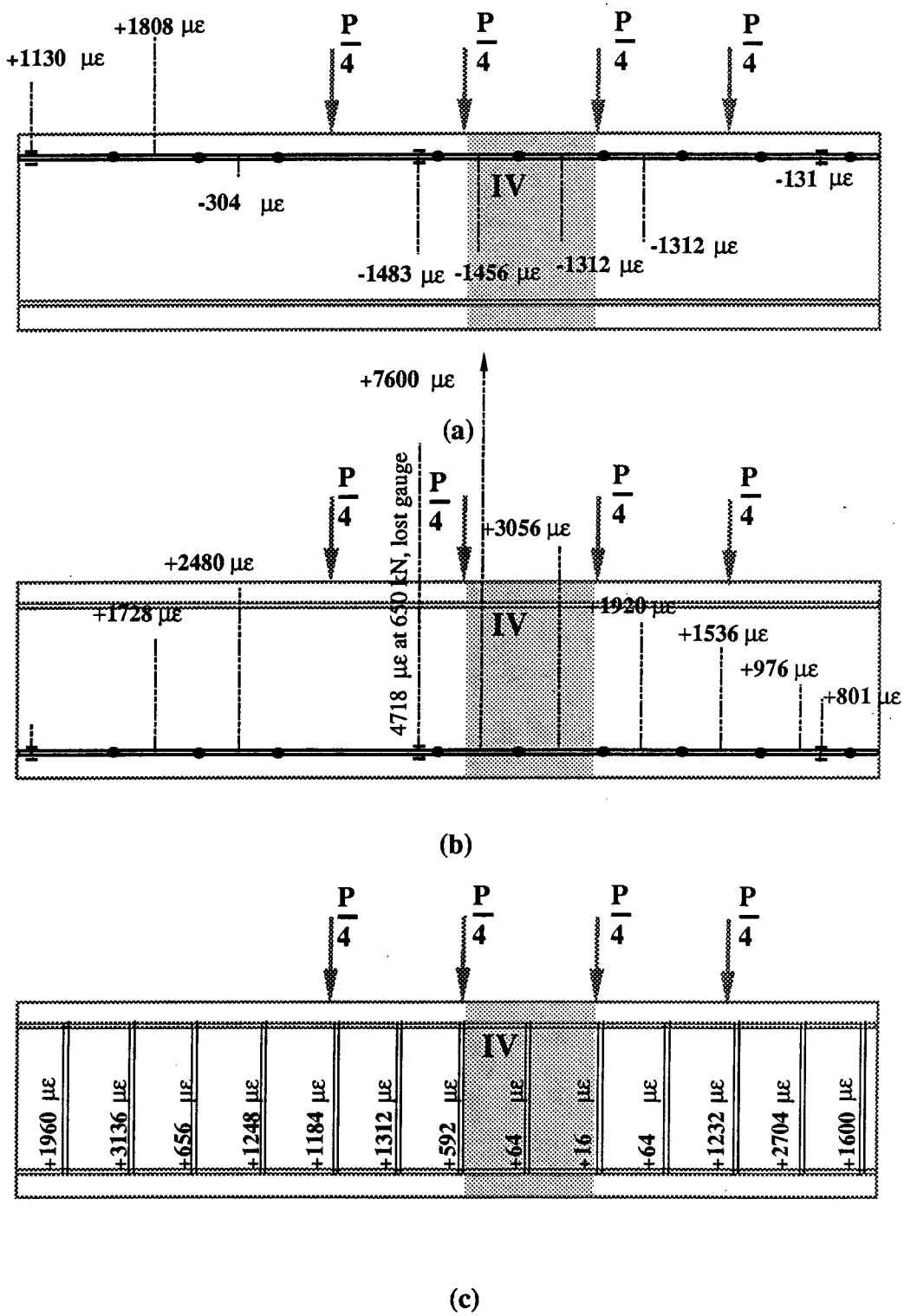

Figure 6.34 Measured Strains in Reinforcement in Region IV at Load = 675 kN

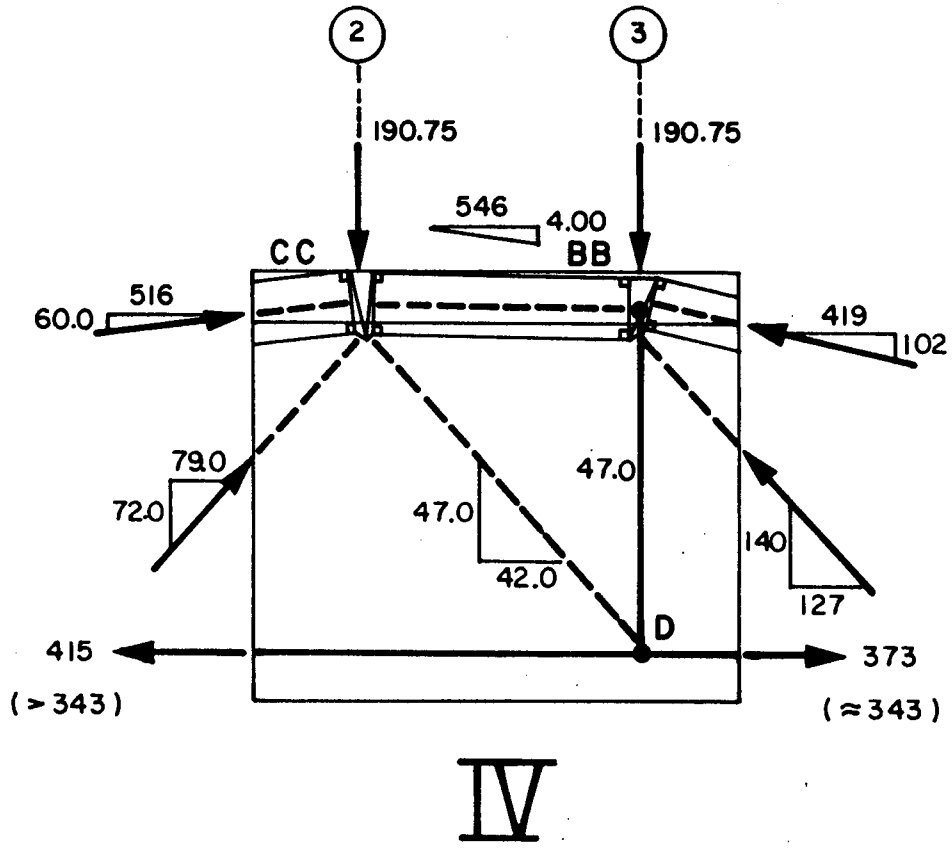

Figure 6.35 STM and Internal Forces for Region IV at Load = 763 kN

6.4.6 Region V

Region V is assumed to be the region between load points 3 and 4. The forces acting at the ends of this region at an applied load of 763 kN are shown in Fig. 6.36(a) and the reinforcement in this region is shown in Fig. 6.36(b). Additional bottom reinforcement in the form of hooked bars are present in this region as shown in Fig. 3.19. It is assumed that these bars do not have sufficient development to contribute to Region V.

The measured strains at the load 675 kN are shown in Fig. 6.37. The STM developed for this region for the applied load 763 kN is shown in Fig. 6.38. The procedure to develop this model from the measured strains is similar to that described above for the other regions. The force in the tie at point E was determined to be 246 kN by extrapolating from the strains measured at the load 675 kN. This defines the magnitude of the internal lever arm, z, to point AA. The tie force at D is known from the calculations for Region IV to be 373 kN. The shear in this region is taken by the vertical components of the (fan) strut BB-E and the strut BB-AA. The horizontal components of these struts are known since that of strut BB-E is equal to the difference between the tie forces at D and E, and the horizontal component of AA-BB must be such that their sum equals the horizontal component of strut CC-BB. With the assumption that the tie AA-E is positioned at the location of load point 4, the STM can be completed. The measured and assumed forces are shown

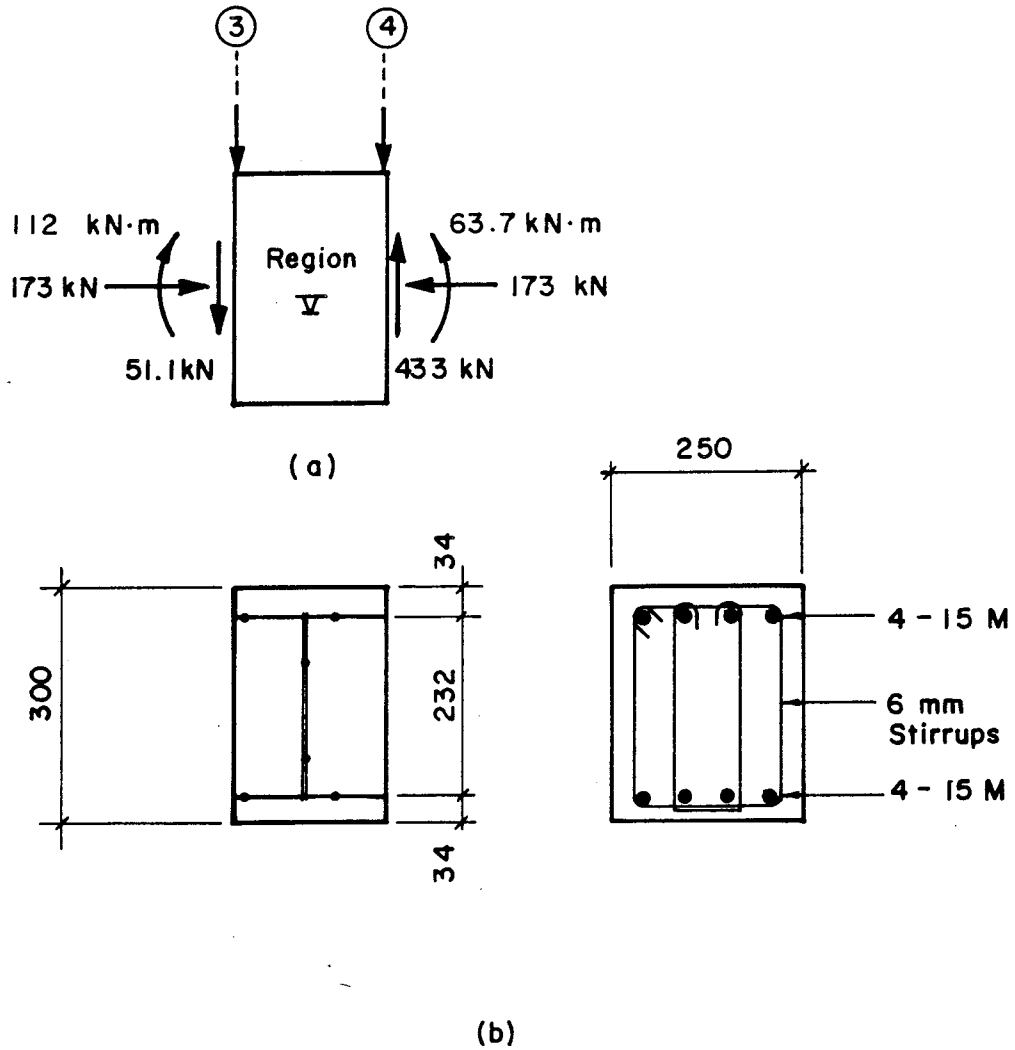

Figure 6.36 End Forces and Reinforcement Layout for Region V at Load = 763 kN

together in Fig. 6.38.

6.4.7 Region VI

Region VI is assumed to be the region between load point 4 and the point where the curved section begins. The forces acting at the ends of this region at an applied load of 763 kN are shown in Fig. 6.39(a) and the reinforcement in this region is shown in Fig. 6.39(b).

The measured strains at the load 675 kN are shown in Fig. 6.40. The crack pattern observed in the test is shown in Fig. 6.41 (Fig. 4.44 is repeated here). As in the case of Region III the shear in this region is assumed to be carried partly by the stirrups and partly by direct strut action. A review of the crack pattern in Fig. 6.41 supports this assumption. The STM proposed for this region is shown in Fig. 6.42. The tie force at point E was determined to be 246 kN in Region V. Based on the available strain measurements, it was assumed that the top bars at point Y were below yield. It was also assumed that the hooked bars which are lapped with the bottom bars in this region carry the full force remaining in the bottom steel at point G. This force is then anchored in Region VII.

Based on the strain measurements in the stirrups, it was assumed that approximately four sets of stirrups may have reached yield within this region at the load 763 kN. The location of the tie FZ which corresponds to the centroid of the stirrup forces, and the slope of the strut AA-F (i.e.

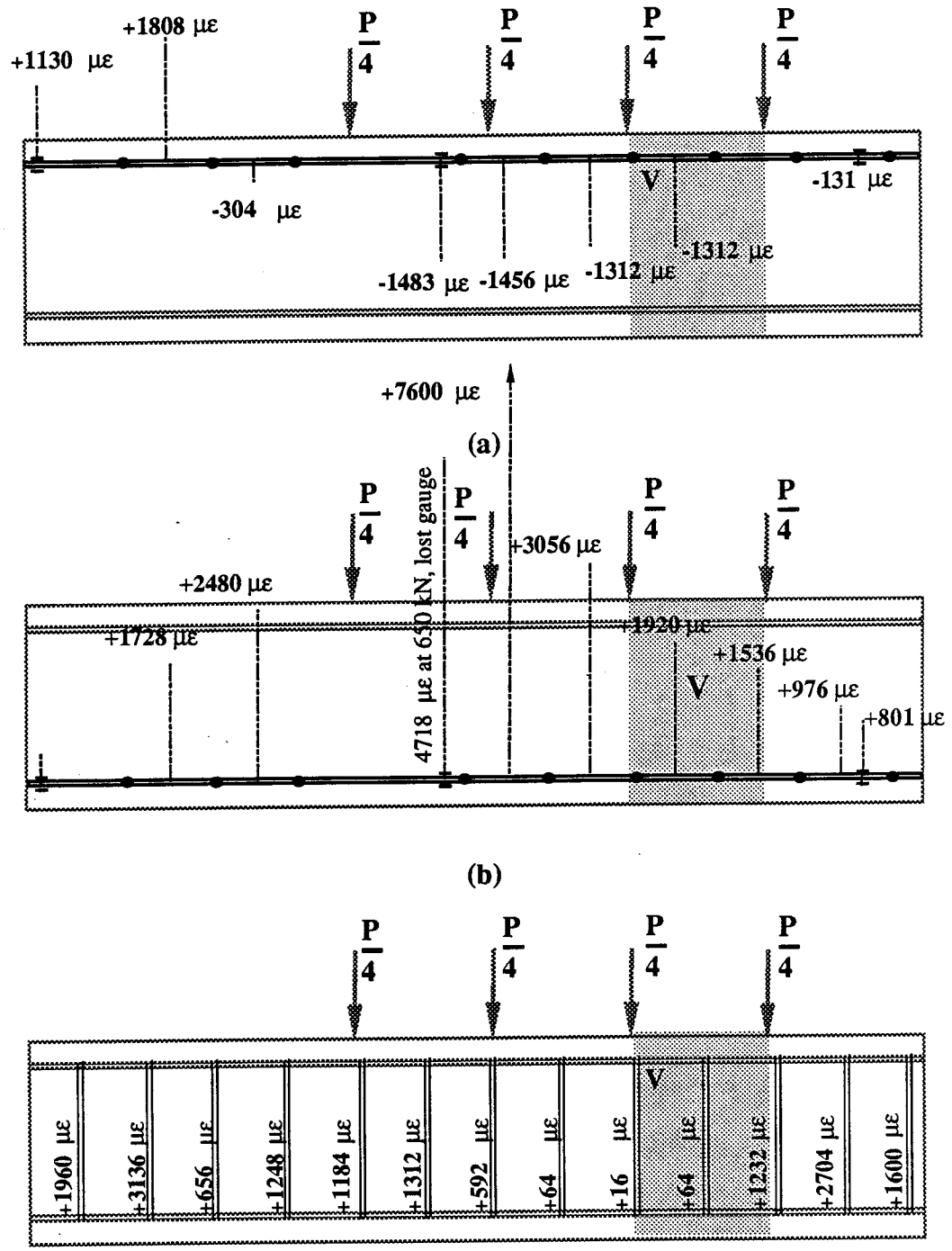

Figure 6.37 Measured Strains in Reinforcement in Region V at Load = 675 kN

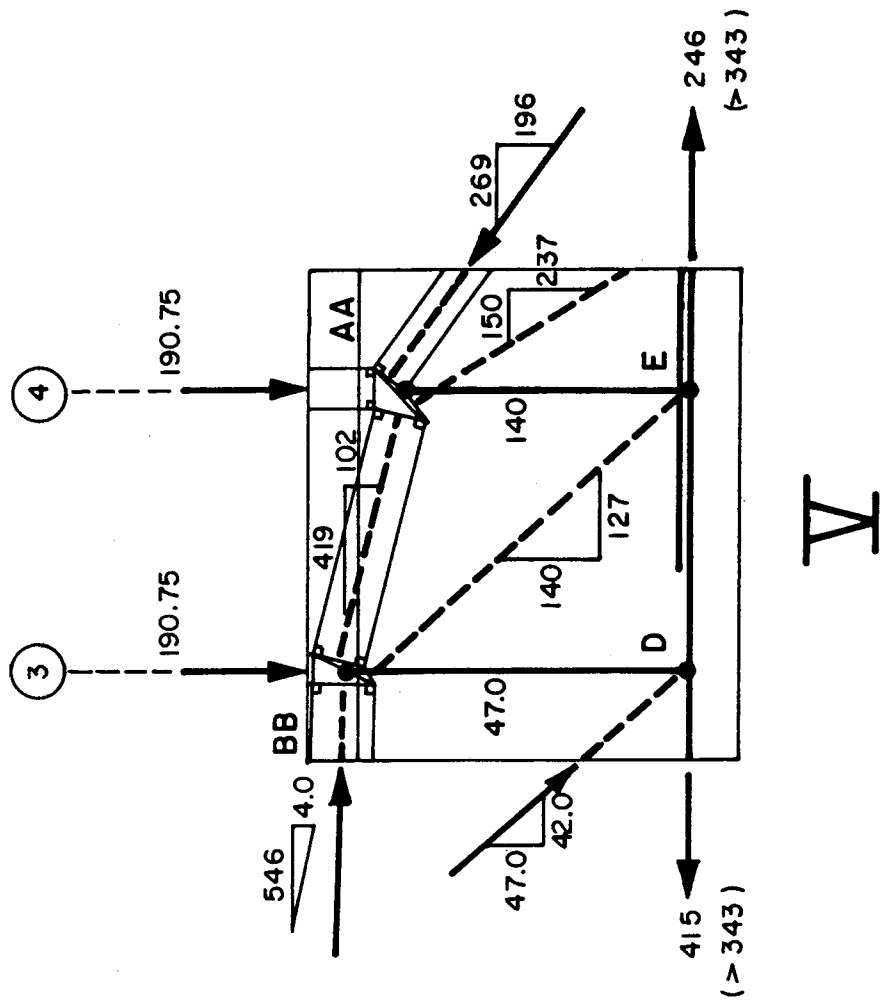

Figure 6.38 STM and Internal Forces for Region V at Load = 763 kN

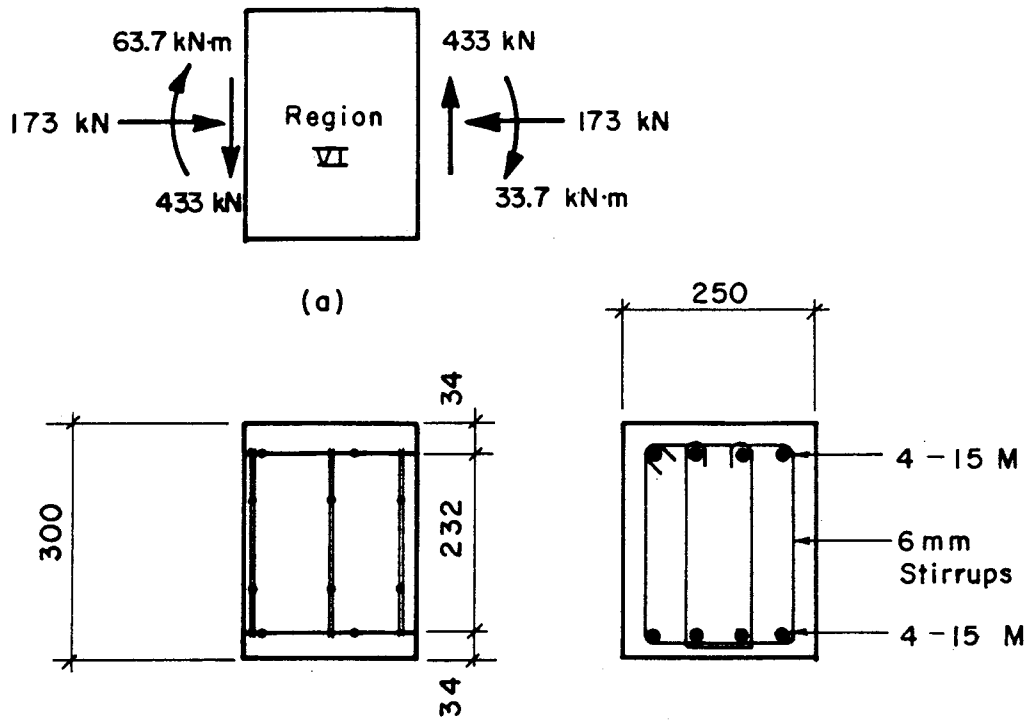

Figure 6.39 End Forces and Reinforcement Layout for Region VI at Load = 763 kN

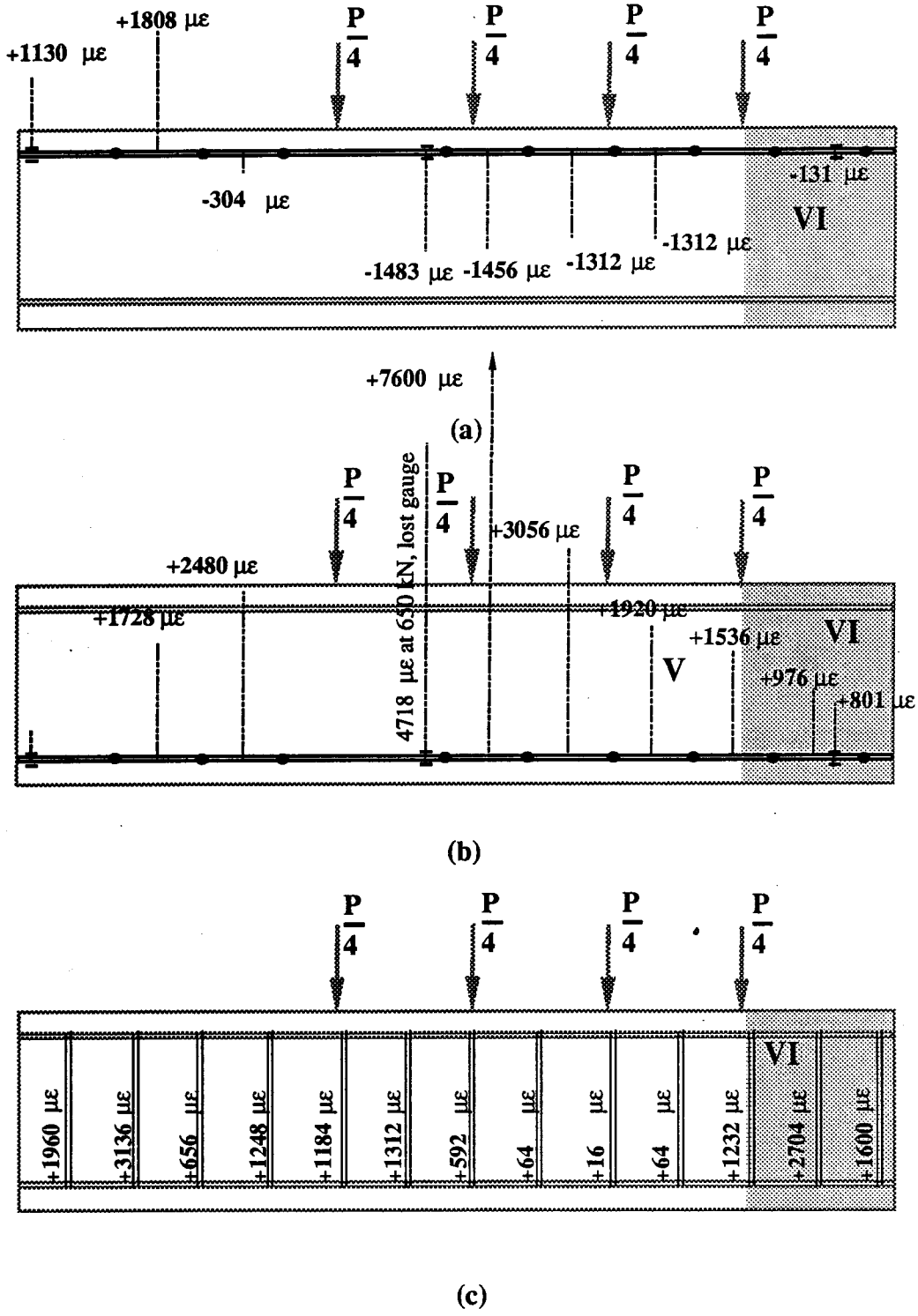

Figure 6.40 Measured Strains in Reinforcement in Region VI at Load = 675 kN

Figure 6.41 Final Crack Pattern in East Shear Span, Corner, and Pedestal for Specimen B2

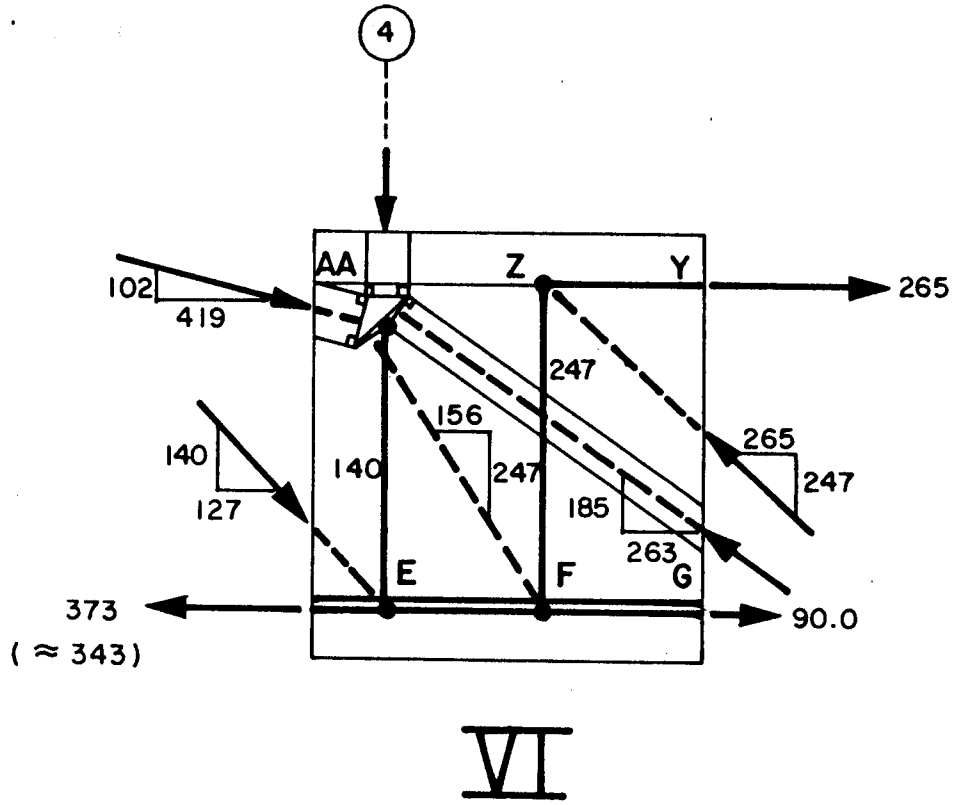

Figure 6.42 STM and Internal Forces for Region VI at Load = 763 kN

fan resultant) were varied until the force carried by the stirrups and the tie force at G seemed reasonable based on the strain measurements.

The results shown are obtained if the distance between E and F is 110 mm and the slope of AA-F is 57.8°. This requires the tie force at G to be 89.7 kN and the horizontal and vertical components of the strut AA-G' to be as shown. The tie force at Y was determined to be 265 kN by varying the slope of strut ZG". As shown in Fig. 6.42, the measured and assumed tie forces are the same at point E. At points Y and G the measured forces are not shown since they were not measured.

6.4.8 Region VII

Region VII provides a transition between Region I and Region VI. The forces acting at the ends of this region at an applied load of 763 kN are shown in Fig. 6.43(a). The principal reinforcement is shown in Fig. 6.43(b). Reinforcement not used explicitly in the development of the STM is not shown (see Fig. 3.20). This D-region is essentially a knee-joint subjected to closing moments, axial loads and shears. The behavior of this type of joint has been discussed in Section 5.2.6.4.

The STM developed for this region subjected to these forces is shown in Fig. 6.44. The tie force at W and the force in strut KJ are known from the calculations associated with Region I. The tie force at Y, the strut ZH, and the

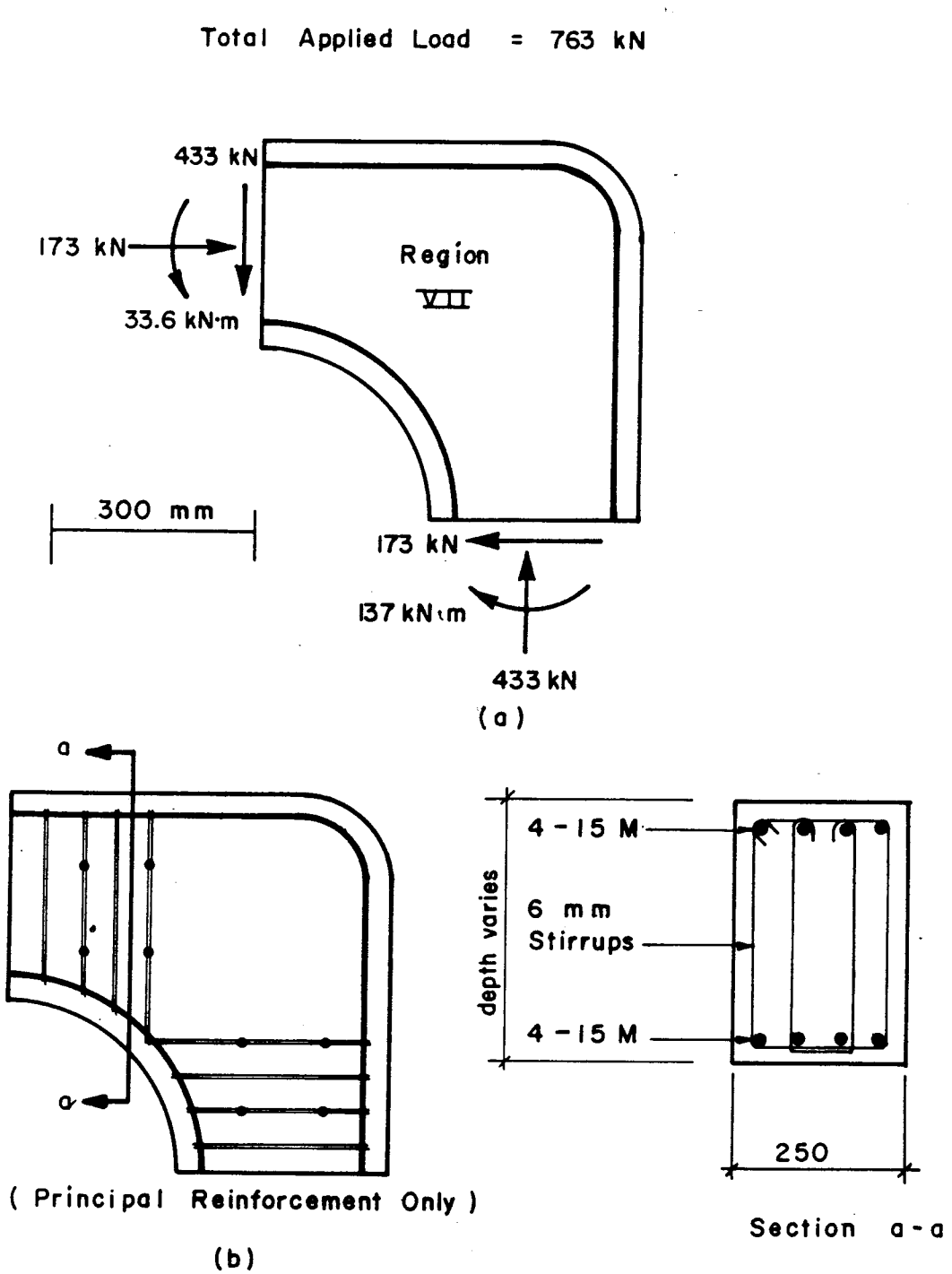

Figure 6.43 End Forces and Reinforcement Layout for Region VII at Load = 763 kN

strut AA-H were determined in the calculations for Region VI. The width of the combined strut HJ must not exceed the limits of the geometry. It should be noted that the strut HJ passes very near the inside soffit. In the test, spalling was observed in this location (Fig. 6.41).

The nodal zone at H is a multi-force nodal zone where three struts and one tie meet. The tie force at I is the force provided by the hooked bars at point G, 89.7 kN. This determines the width of the nodal zone at I. Since the position of node H is affected by the assumed slope and width of the struts in Region VI, several iterations were necessary before the final configuration was achieved.

The CCC (three compression force) nodal zone at J will be such that the strut JX must pass through point X, the intersection point of ties YX and WX. The slope of strut JX will then be given by the magnitude of the tie forces at Y and W. As discussed in Section 5.2.6.4, the force in strut JX will be transferred to the reinforcement by fan action. The details of the two fans developed for this region are shown in Fig. 6.45. As discussed in Sect. 5.2.6.4, the slopes of the two fans are chosen based on what seems to fit the geometry. The assumed values of θ_L and θ_R are 69.0° and 41.4° respectively. This results in left and right fan-lengths of 218 mm and 322 mm respectively.

The compressive stresses, σ_N, acting on the concrete where it bears on the reinforcement are plotted for the left and right fans in Fig. 6.46. The magnitude of these stresses

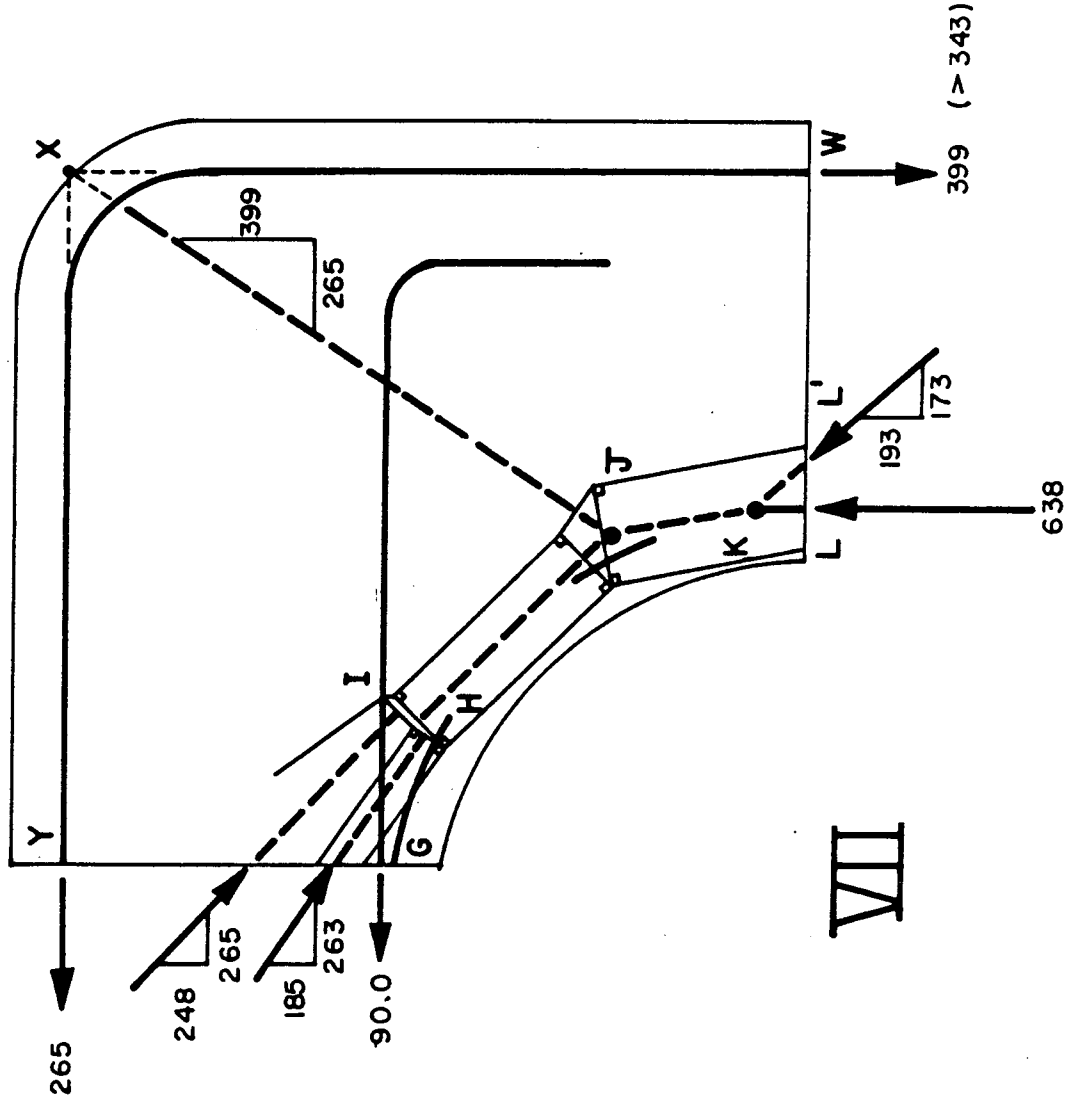

Figure 6.44 STM and Internal Forces for Region VII at Load = 763 kN

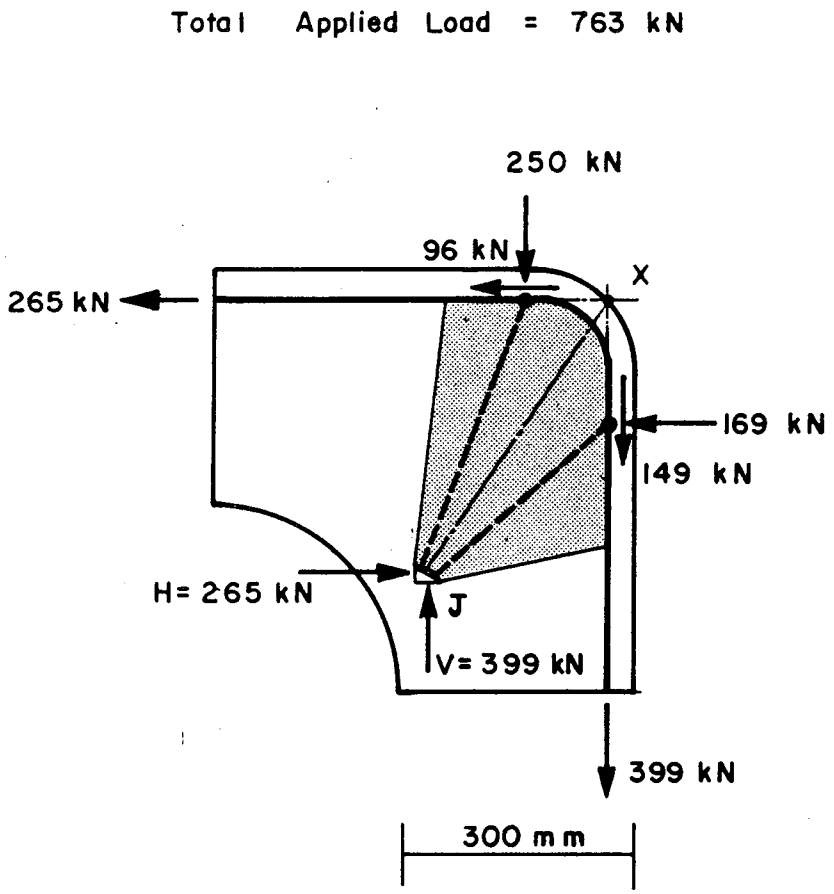

Figure 6.45 Details of Left and Right Fans for Region VII

was determined assuming a width of bearing equal to the width of 4-15M bars, nd_b = 64 mm in Eqn. 5.26. The scale of the stress plot is as indicated in the drawing. The assumed fans are such that the maximum compressive normal stress in the two fans is 27 MPa and the average value is 17 MPa. Although these values are quite large, they are less than f_{ce} = 48 MPa.

The tangential or bond stress distribution for the left and right fans is shown in Fig. 6.47. The magnitude of the stresses is plotted normal to the line representing the surface of the concrete. Values above the line tend to cause CCW rotation of the stress field with respect to the ζ - η origin. Values below the line cause CW rotation of the stress field. The bond area was assumed to be equal to the surface area of 4-15M bars and $n\pi d_b$ = 201 mm² per mm in Eqn. 5.27. The maximum bond stress in this stress field is 3.2 MPa occurring in the right fan. The overall average bond stress in the two fans is 1.9 MPa. These values are less than the limiting bond strength values implied in the CSA or CEB-FIP Codes (see Fig. 5.21). Having completed the two fan stress fields which are statically equivalent to strut JX, the development of the STM for Specimen B2 is completed.

6.4.9 Summary

The STM in Fig. 6.21 was developed for a load level corresponding to 98% of the ultimate load. The model was developed from the calculated end forces and moments

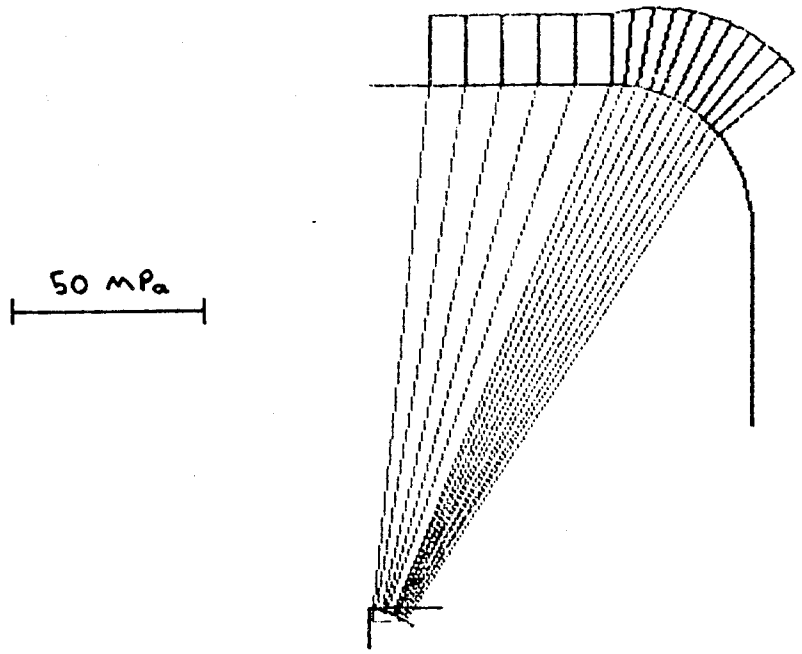

Normal Stresses
(a)

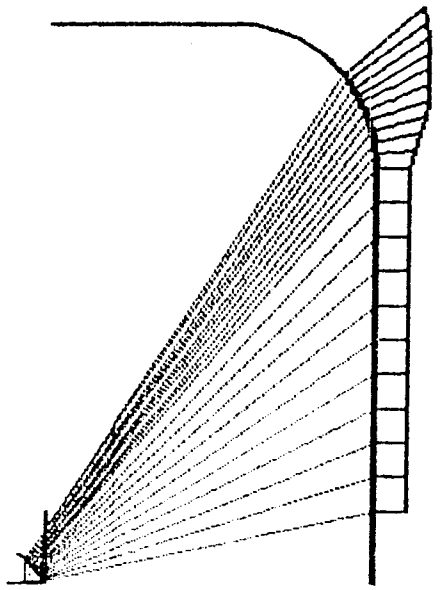

Normal Stresses
(b)

Figure 6.46 Normal Stress Distribution for Left and Right Fans at Load = 763 kN

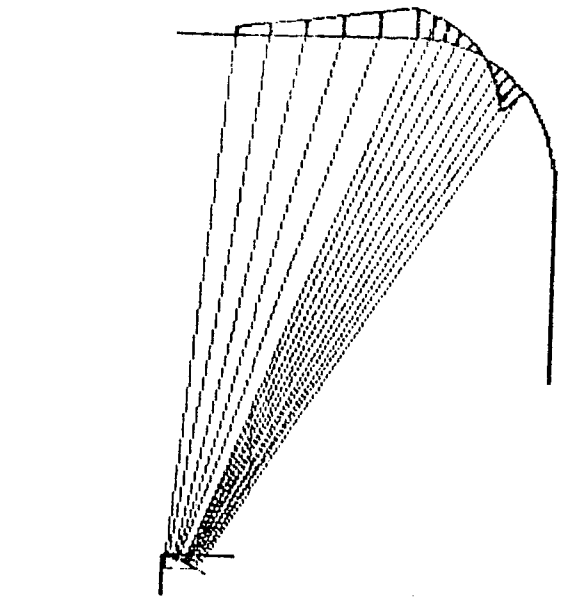

Bond Stresses

(a)

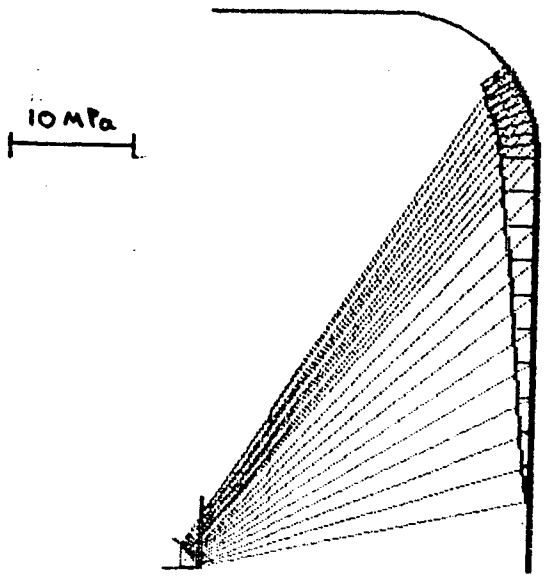

Bond Stresses

(b)

Figure 6.47 Bond Stress Distribution for Left and Right Fans at Load = 763 kN

(including the compressive membrane force). Where ever possible, the forces in the ties were determined from the measured reinforcing strains and therefore there is good agreement with the test results. The model is consistent with the load carrying mechanisms observed in the test. Since the required widths of the struts did not exceed the limits of the specimen at any location, it is concluded that the model gives a safe and realistic estimate of the ultimate strength of the specimen. This was done assuming an effectiveness factor of ν=0.90. Recommendations for design are given in Chapter 8.

6.5 V-Shaped Arch Specimen B1

6.5.1 Summary of the Development of the STM for Specimen B1

The load chosen to illustrate the STM for Specimen B1 was 914.3 kN. This load level represents 95% of the maximum load and corresponds to an effective ice pressure of 4.6 MPa acting on the loaded area. The forces and moments acting at the ends of Specimen B1, as calculated from the measured reactions and steel beam strains, were presented in Table 4.6. The values at 914.3 kN are shown in **bold** in the table. These forces and moments are summarized in Fig. 6.48. As in the case for Specimen B2, the reactions include the compressive membrane forces which developed in the test.

Since the geometry and loading are the same as in Specimen B2, the Specimen B1 is divided into the same B and

D regions (Fig. 6.18). Using the end forces and moments in Fig. 6.48, and the measured reinforcing strains, strut-and-tie models were developed for each of these regions. The complete STM for Specimen B1 is shown in Fig. 6.49.

The following assumptions were used to develop the STM for Specimen B1.

1. $f_{ce} = \nu f'_c$ = 53.6 MPa using ν = 0.9 and mean concrete cylinder strength f'_c = 59.5 MPa
2. f_y = 400 MPa, f_u = 645 MPa, $A_s f_y$ = 320 kN for No. 15M longitudinal steel, E_s = 188800
3. f_y = 476 MPa, f_u = 681 MPa, $A_v f_y$ = 60.8 kN for each set of 6 mm stirrups, E_s = 185300 MPa
4. The maximum stress in the reinforcement was allowed to exceed the yield stress in locations where this occurred in the test.
5. The presence of compression steel was not specifically recognized.

6.5.2 Summary

The STM in Fig. 6.49 was developed for a load level corresponding to 95% of the ultimate load. The model was developed from the calculated end forces and moments (including the compressive membrane force). Where ever possible, the forces in the ties were determined from the measured reinforcing strains and therefore there is good agreement with the test results. The model is consistent

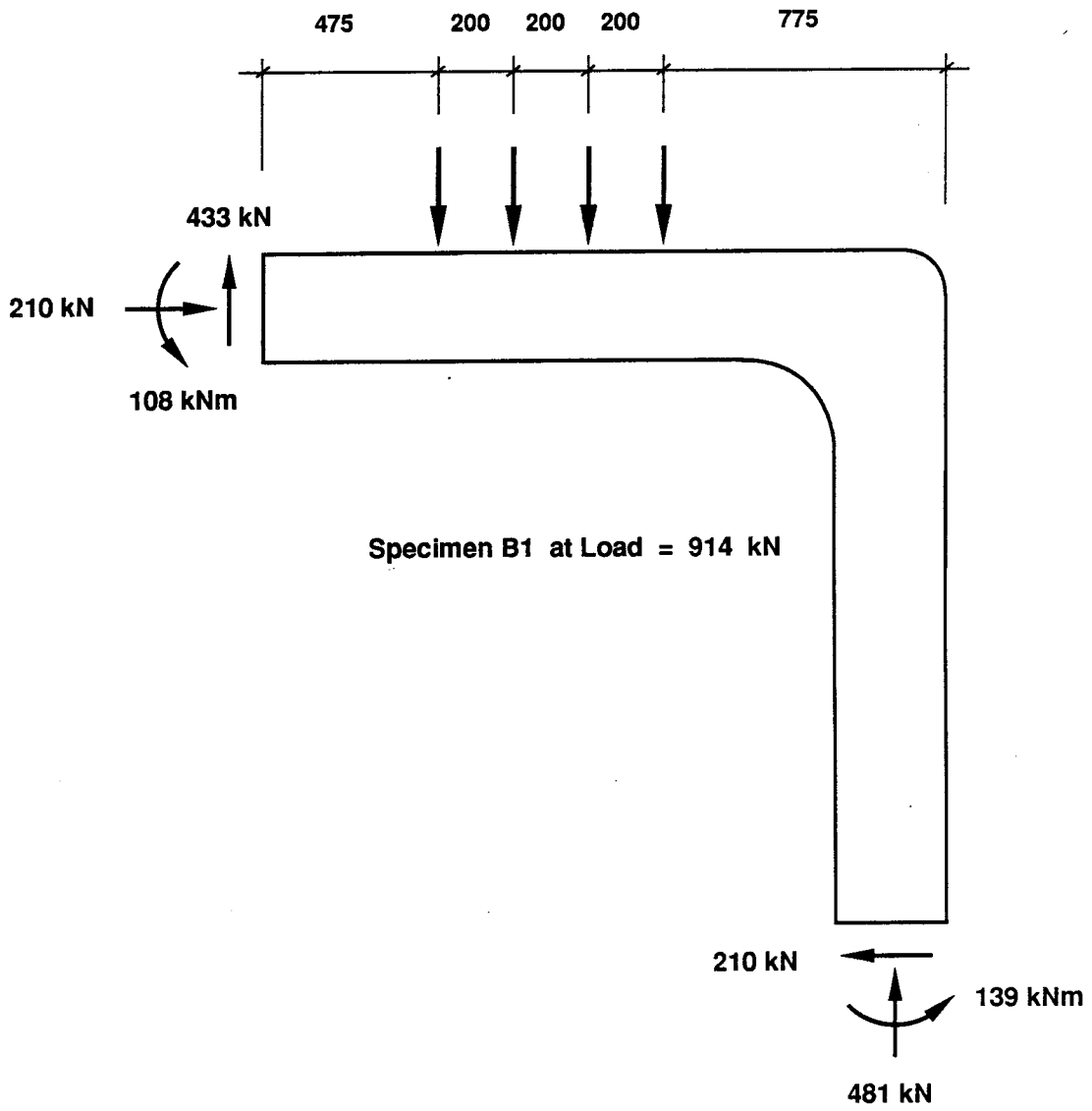

Figure 6.48 End-Forces and Moments for Specimen B1 at Load = 914 kN

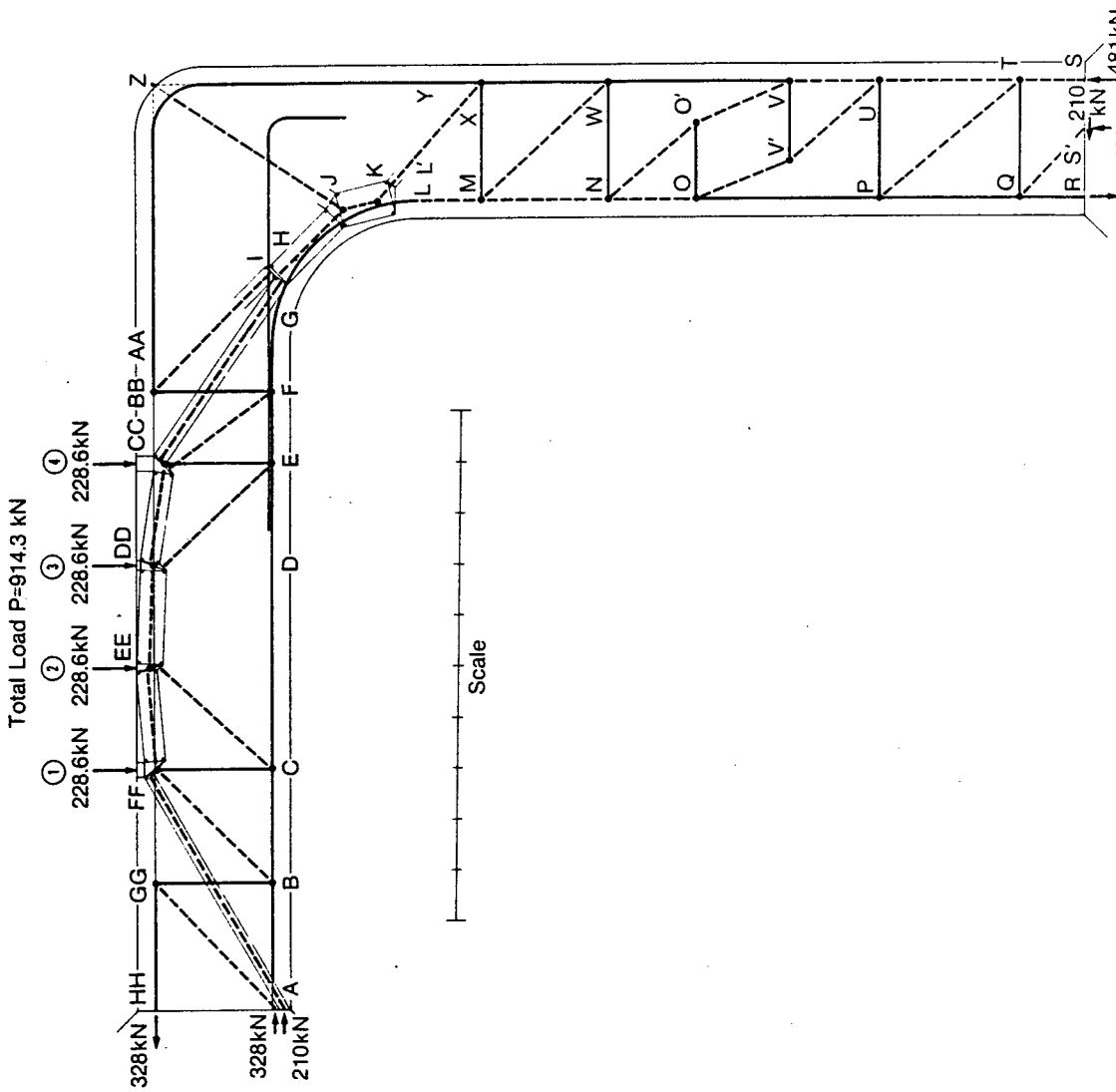

Figure 6.49 STM for Specimen B1 Based on Measured End-Forces at Load = 914 kN

with the load carrying mechanisms observed in the test. Since the required widths of the struts did not exceed the limits of the specimen at any location, it is concluded that the model gives a safe and realistic estimate of the ultimate strength of the specimen. This was done assuming an effectiveness factor of ν=0.90. Recommendations for design are given in Chapter 8.

7. FINITE ELEMENT ANALYSIS AND COMPARISONS WITH TEST RESULTS

7.1 Introduction

As suggested in Chapter 2, it is possible to use non-linear finite element analyses to study the behavior of reinforced-concrete (R/C) ice-resisting walls. This method has been employed successfully in the preliminary analysis of offshore structures subjected to ice loads (Gerwick et al., 1981; Iding, Bresler, and Gerwick, 1985; Vos and den Hertog, 1987).

The detailed requirements of such an analysis and the limited availability of suitable computer programs restrict the use of this type of analysis to specialists. However, because of the importance of the method and because of certain advantages that it offers, the application of non-linear finite element analyses to R/C ice-resisting walls will be discussed in this Chapter.

The objectives of such an analysis are 1) to study the response of the overall structure in terms of the flow of forces through the ice-resisting wall, to the supporting walls, and in to the base of the structure. 2) to predict the local behavior of the ice-resisting wall subjected to intense ice loading.

Of particular interest is the latter analysis, which provides information regarding the stresses in the concrete and reinforcements, failure mode, and energy absorption properties of the ice-resisting wall.

7.2 Finite-Element Analysis of R/C Ice-Resisting Walls

7.2.1 Global Analysis

Typically a 'global' three-dimensional elastic analysis is performed on the structure to assess the overall behavior of the structure and to provide information necessary for a more detailed local analysis.

In the global analysis, plate and beam elements might be used to model all or a portion of the overall structure. The reinforced concrete is modelled as an elastic isotropic material.

The ice loading should be modelled realistically. This means that several analyses will actually be required to model correctly the spreading of the ice load. As the loaded area increases the ice intensity tends to decrease as discussed in Sect. 2.1.

7.2.2 Local Analysis

To predict the local behavior of the ice wall a more detailed model is constructed representing a small portion of the structure. This would include part of the supporting walls but would concentrate primarily on the ice-resisting wall itself. The spacing of the bulkheads or supporting walls in a R/C offshore structure are generally far enough apart that the wall will have significant one-way action (Boyd and Bruce, 1984). Thus a suitable model might include a two-dimensional, plane-strain representation of a unit

height of the wall. To adequately model the boundary conditions for this model, information from the three-dimensional analysis is used to provide guidance in selecting elastic spring stiffnesses to represent the forces and moments acting at the boundaries of the two-dimensional model. These will include axial springs and rotational springs (Iding et al., 1985; Vos and de Hertog, 1987).

A suitable finite element model consists of two-dimensional plane strain solid elements representing the concrete, and one-dimensional elements representing the reinforcement. To adequately predict the behavior of the ice-resisting wall, appropriate constitutive models must be implemented in the analysis. The material model for the concrete must consider cracking, compression and tension softening, the variation of the shear modulus with crack strain, and the effects of confinement. The material model for the reinforcing must consider yielding and strain hardening. Aspects of material behavior are discussed in more detail in the next section. A computer program FEPARCS (Elwi and Murray, 1980; Balakrishnan and Murray, 1986) is discussed briefly and applied in the next section.

7.3 Applications and Comparisons with Test Results

7.3.1 Objectives

The objectives of this study were to evaluate the use of nonlinear finite element analysis as a design/analysis

tool for use on R/C ice-resisting walls and to compare with the experimental results presented in this thesis. In particular, the location and extent of cracking and damaged zones, the cracking load, the ultimate load and mode of failure, and the reinforcing strains were of interest. This analysis has been performed with a view towards simplicity and practical application as opposed to material model refinement.

7.3.2 Description of FEPARCS

7.3.2.1 General

A computer program FEPARCS (Elwi and Murray, 1980; Balakrishnan and Murray, 1987) was developed for the non-linear finite element analysis of plane and axisymmetric reinforced and/or prestressed concrete structures. The version of the program used throughout this study included the following enhancements:

1. variable node, isoparametric Lagrangian and Serendipity elements up to bi-cubic order.
2. an embedded reinforcement formulation which optionally includes bond-slip.
3. the use of a fixed crack or strain rotating crack procedure in the non-linear solution.
4. a simple constitutive model for concrete but which includes all of the considerations discussed in Sect. 7.2.2.

It has been demonstrated (Balakrishnan and Murray, 1987) that this program provides reliable predictions of the structural behavior of reinforced concrete beams exhibiting failure by:

1. steel yielding (flexural failure mode)
2. beams without web reinforcement failing by diagonal tension
3. beams with web reinforcement failing by shear-compression
4. deep beams failing in compression (failure of compression strut)
5. deep beams failing by concrete crushing at the supports.

7.3.2.2 Material Models for Concrete and Reinforcing Steel

Because of the above successes, the constitutive model for concrete which was used in this study is that developed by Balakrishnan and Murray, 1987. This relatively simple model accounts for all of the factors discussed in Sect. 7.2.2, namely

1. Cracking
2. Tension softening and tension stiffening
3. Strain hardening at high compressive stress
4. Strain softening
5. Reduction of shear modulus with crack strain.

The assumed uniaxial stress strain curve for concrete is shown in Fig. 7.1(a). In this figure, f_{cu} is the compressive strength of concrete, f_{tu} is the tensile

strength of concrete, ϵ_{cr} is the cracking strain, ϵ_{ut} is the tensile strain at which the tensile stress has reduced to zero, and ϵ_{yield} is the yield strain of the reinforcement. At any given time, the concrete is assumed to be strained monotonically and to be in one of five damage regions "-2" to "+2" as defined in Fig. 7.1(b). The shear modulus, G, is assumed to vary according to Fig. 7.1(c).

Under biaxial stress conditions, the concrete is considered to be orthotropic after cracking and the orthotropic axes are oriented with the direction of cracking. The peak values of the stress-strain curve in Fig. 7.1(a), f_{cu} and f_{tu}, are then assumed to vary with the failure envelope in Fig. 7.2. The biaxial failure envelope proposed by Balakrishnan and Murray (1987) is that developed by Kupfer et al. (1969, 1973) and Kupfer and Gerstle (1973) with a small modification in the tension-compression region.

In Fig. 7.2, f'_c is the uniaxial compressive strength and f'_t is the uniaxial tensile strength. In this thesis concrete cylinder strengths were available for f'_c, and f'_t is taken to be equal to 60% of the modulus of rupture beam tests. These are consistent with the recommendation of Balakrishnan and Murray (1987). The initial elastic modulus of the concrete ($E_c^{(0)}$) in Fig. 7.1(a)) is taken from the measured stress-strain curve from the concrete cylinder tests. It is also recommended that the compressive strain hardening modulus ($E_c^{(-1)}$) in Fig. 7.1(a)) be taken as $0.05E_c^{(0)}$ for concrete confined by stirrups, and that the

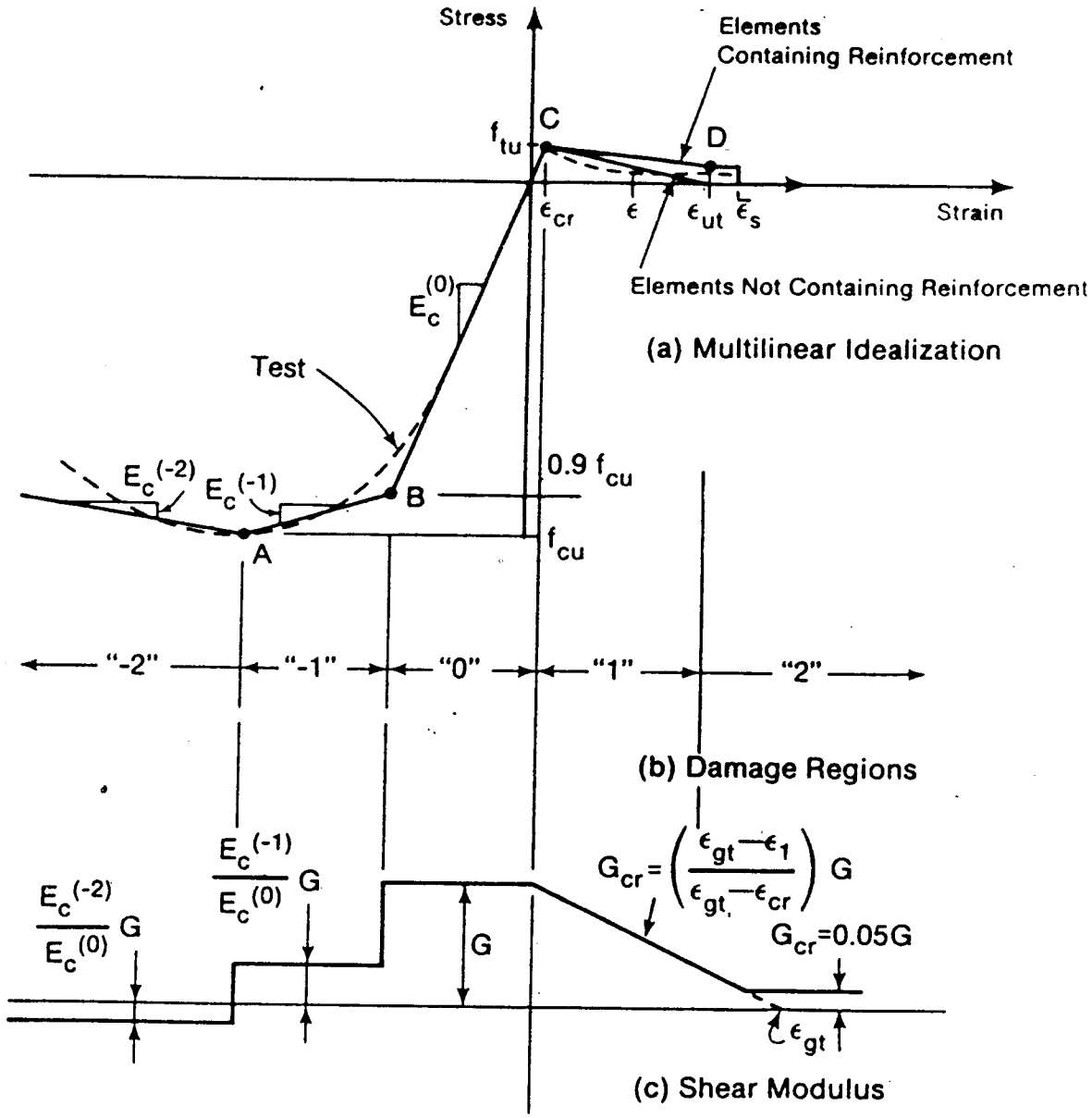

Figure 7.1 Assumed Strain Dependence of Concrete Properties

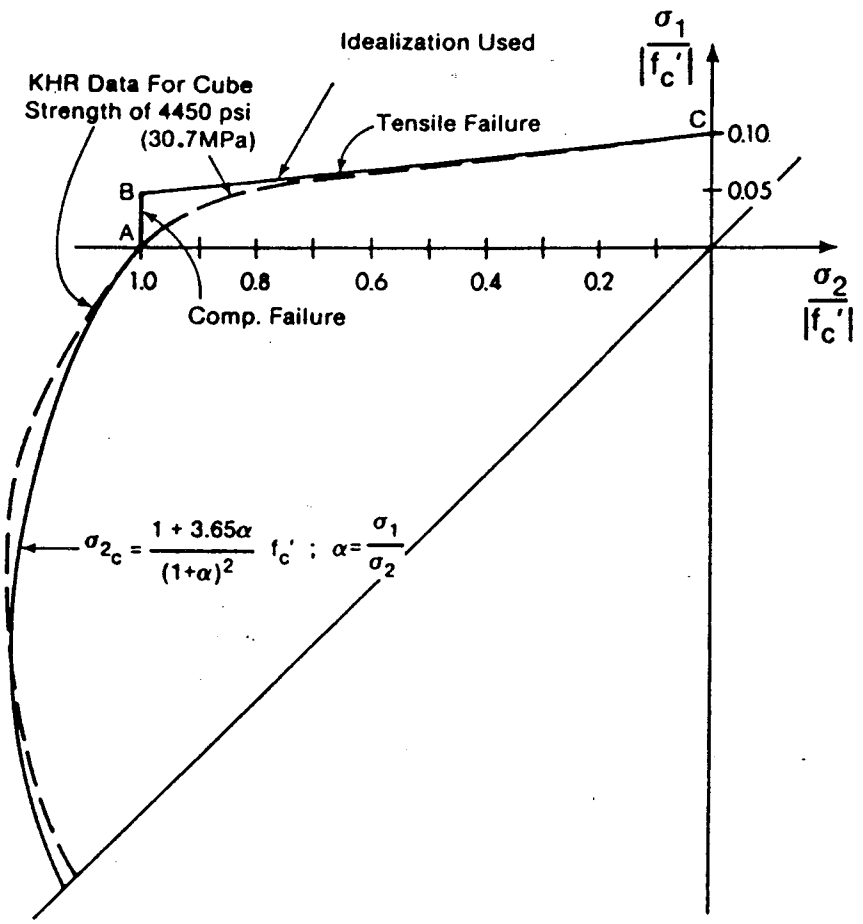

Figure 7.2 Peak Strength Envelope for Biaxial Stress Conditions

strain softening modulus ($E_c^{(-2)}$) in Fig. 7.1(a)) be taken as $-0.05\ E_c^{(0)}$.

In Fig. 7.1(c) is shown the assumed variation of the shear modulus. Within Regions (-1) and (-2) the value of G is determined from the values of $E_c^{(-2)}$, $E_c^{(-1)}$, and $E_c^{(0)}$. In the tension region after cracking, Region 1, the shear modulus is reduced according to the expression shown in the figure, to a minimum shear retention factor of 5% of the uncracked modulus. In the applications given in Sect. 7.3.3 - 7.3.4, it was desired to use one relationship for all of the analyses in order to keep the problem simple. The basic relationships are taken to be those recommended above. For each problem, the input material parameters will be presented in tabular form.

In the applications which follow, the reinforcing steel stress-strain curve is modelled using a bi-linear representation derived from tension coupon tests. The behavior in compression is assumed to be the same as the behavior in tension. The properties of the bi-linear representation are given for each problem.

7.3.2.3 Numerical Solution Procedure

The numerical solution procedure was the same for all specimens analyzed. A standard Newton-Ralphson iterative procedure with the stiffness matrix of the structure updated at every iterate was used.

Generally, the specified tolerances on the convergence of the incremental norms of the displacement and unbalanced

force vectors were 0.1% and 1.0%, respectively. The failure load is assumed to have been reached when the displacement and force vector norms fail to converge within the specified number of iterations or if the structure stiffness matrix contains a zero or negative term on the diagonal.

7.3.3 Circular Arch Specimen P1

Details of the geometry, reinforcing and material properties of Specimen P1 have been presented in Chapter 3. The test results were presented in Sect. 4.2.

The finite element mesh layout, made up of bi-linear elements, is shown in Fig. 7.3. One half of the specimen is modelled since the structure, loading, and reinforcement were symmetrical about the centerline. Reinforcing elements representing the 25M longitudinal bars were modelled at the correct location in the specimen. The stirrups were lumped at the gauss points for each element following the recommendations of Balakrishnan and Murray (1987). The material properties from Chapter 3 and the input parameters for the analysis are summarized in Table 7.1. In this analysis, a fixed crack approach was used. The effects of bond-slip were not accounted for.

In the test, the specimen was loaded to failure in 100 kN increments and near ultimate, 50 kN increments. First cracking was observed at an applied load of 2100 kN in the form of diagonal cracks between the abutment and the first load point (Fig. 4.2). The principal load carrying mechanism

Table 7.1 Material Properties and Input Parameters for Specimen P1

Concrete	
E_c	23000 (MPa)
G	9600.0 (MPa)
ν (Poisson's Ratio)	0.2
f'_c	35.0 (MPa)
f'_t (60% of f_r)	2.90 (MPa)
ε_{ut}	0.0012 mm/mm
Reinforcing Steel	
E_s	204000 (MPa)
f_y	480 (MPa)
E_{sh} (Strain Hardening)	4100 (MPa)
A_s (Top and Bottom)	1500 (mm^2)

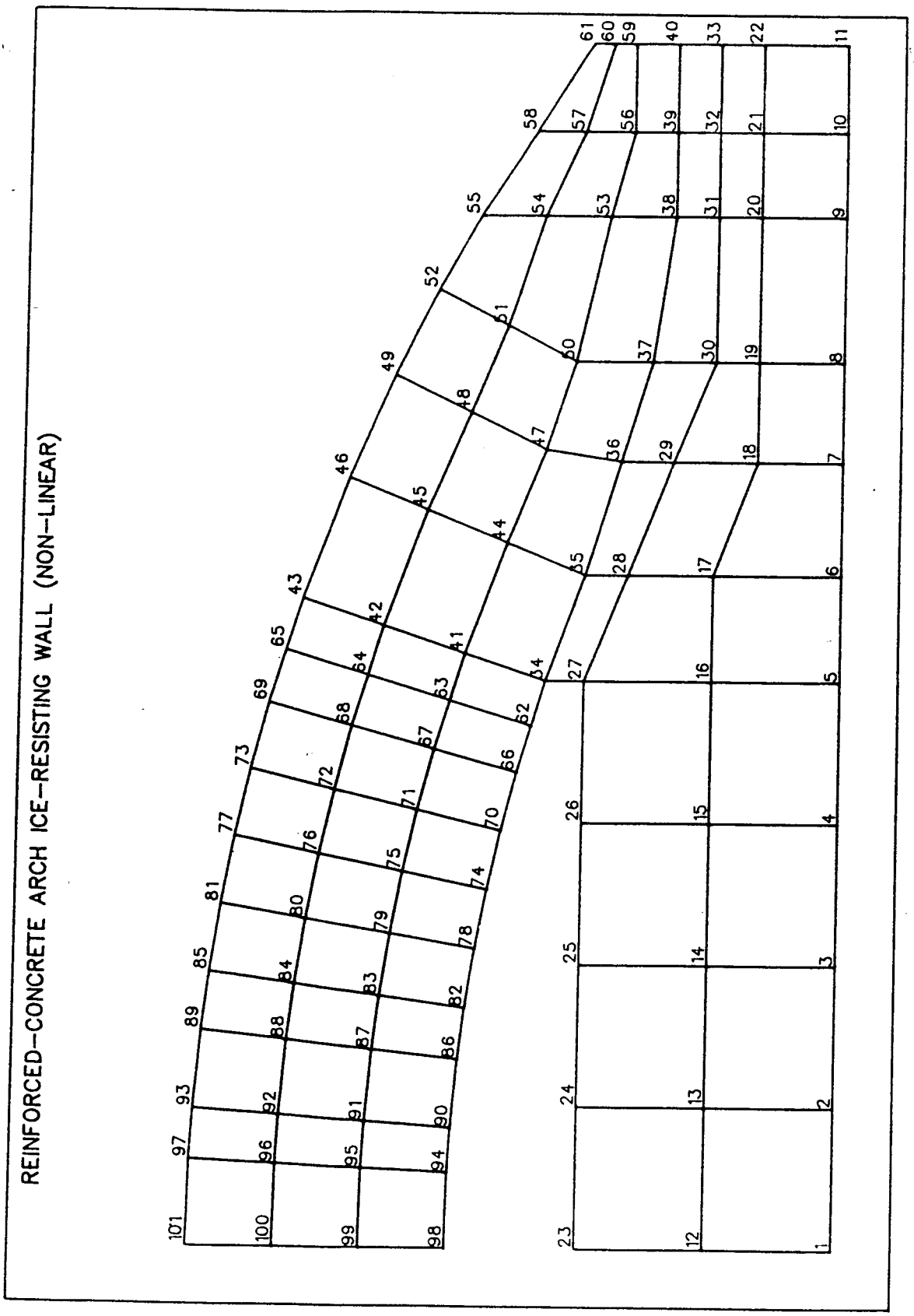

Figure 7.3 Finite Element Mesh Layout for Specimen P1

was in the form of a direct strut between the abutments and the outer load points. Failure occurred in the west strut at an applied load of 2900 kN (Fig. 4.3).

In the finite element analysis, the first two load steps were 800.0 kN each. Following this the load steps were 200.0 kN each until 2600 kN when a negative term on the main diagonal was obtained. From this point, a load step of 80.0 kN was used. At 2760 kN, the failure load was reached as solution could not be obtained past this point. This compares favorably with the test result, 2900 kN. The test-to-predicted ratio is 1.05. Referring to Fig. 7.4, the experimental and analytical load vs. midspan deflection curves are seen to be in close agreement.

In the analysis the first diagonal cracks formed between the first load point and the abutment at an applied load of 2000 kN which compares to 2100 kN in the test (Test/Predicted = 1.05). These cracks are shown in Fig. 7.5 which shows all of the damaged zones in the specimen. In these plots, a single line at the Gauss point indicates that the cracking strain has been exceeded at that location and the damage region is either Region +1 or Region +2. If the location is in the compression hardening zone (Region -1) or the compression softening zone (Region -2), this is indicated by lines with arrowheads at both ends. A cross with arrowheads on both lines indicates that at that Gauss point, the concrete has reached compression hardening (-1) or compression softening (-2) and was cracked at a previous

load step. In this case at the load 2100 kN (Fig. 7.5), all of the crack locations are in the +1 stage.

At a slightly higher load, 2200 kN, some of the elements in the region of the diagonal strut are in the compression strain hardening region and were previously cracked (Fig. 7.6). This trend continued until the failure load, 2760 kN, was reached. At this failure load, the cracking and damage plot contains many double arrowhead crosses in between the abutment and the first load point (Fig. 7.7). Several of these had reached the crushing limit (-2) in addition to being cracked. This corresponds to a test/predicted ratio = 1.05. The failure of the concrete in the compression strut is in agreement with the observed failure mode. The compression 'strut' can be identified in the principal stress plot shown in Fig. 7.8. The results of this analysis are similar to the analysis of the Rogowski and MacGregor (1983) deep beam as performed by Balakrishnan and Murray (1987).

The distribution of the steel strains in the top and bottom bars at the load 2600 kN predicted by this analysis are shown in FIgs. 7.9 and 7.10, respectively. In these figures the measured distribution of the strains at an applied load of 2500 kN are repeated from Figs. 4.6 and 4.7 for comparison. The magnitude and overall distribution of the predicted strains is similar to measured strains. It should be mentioned that at large strains, a large difference in strain corresponds to a small difference in

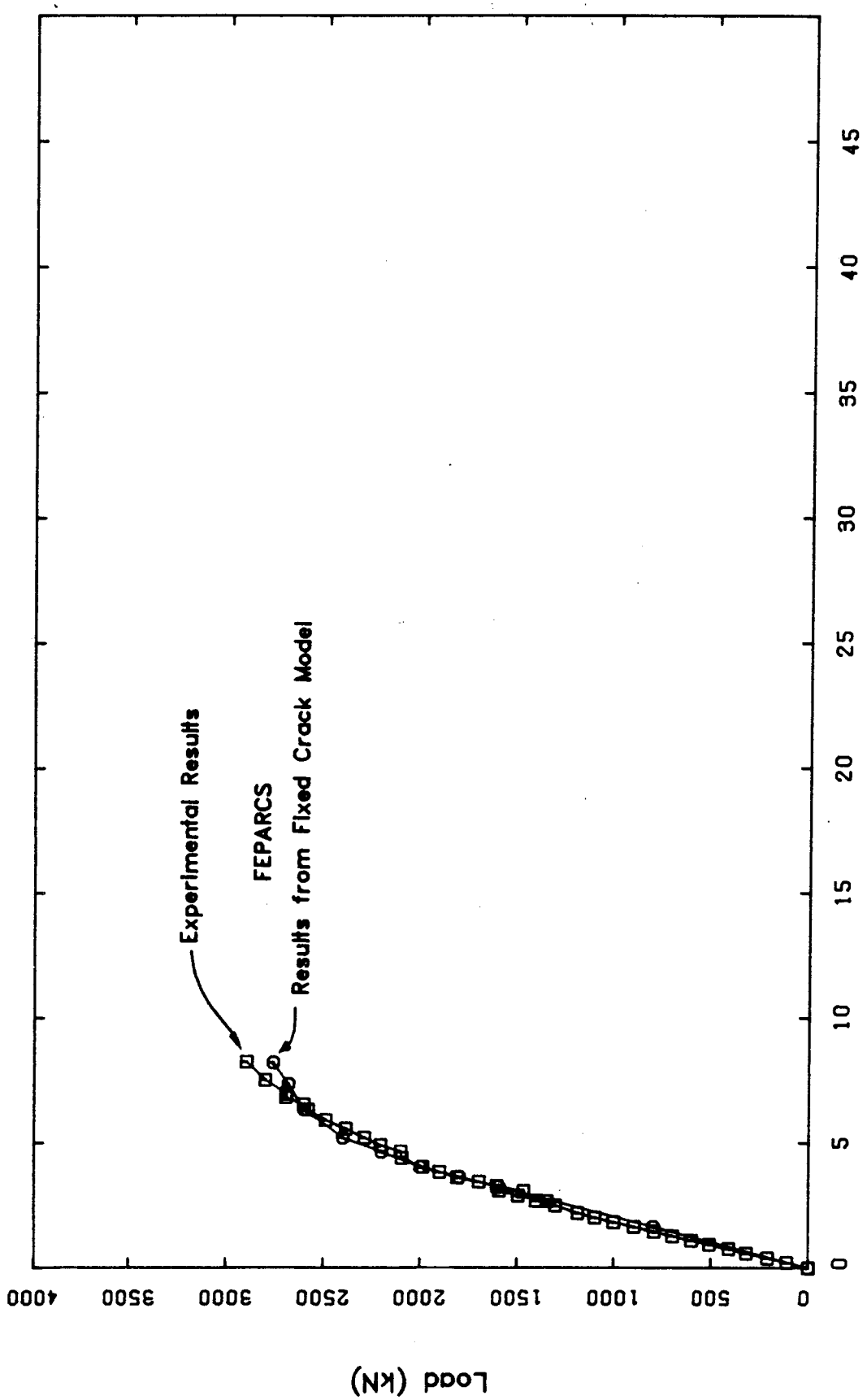

Figure 7.4 Experimental and Analytical Load vs. Midspan Displacement Curves for Specimen P1

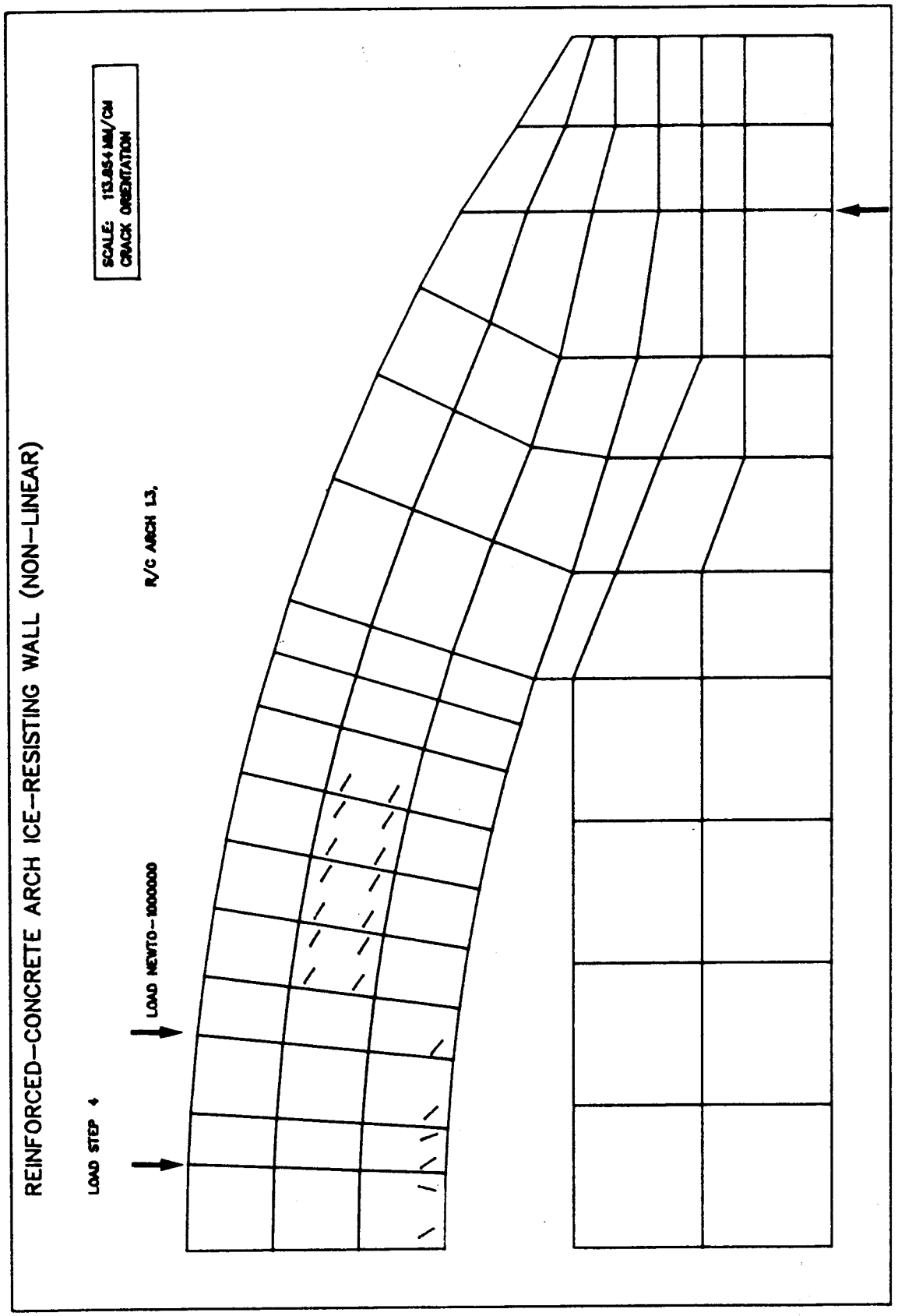

Figure 7.5 First Cracking in the Analysis of Specimen P1 (2000 kN)

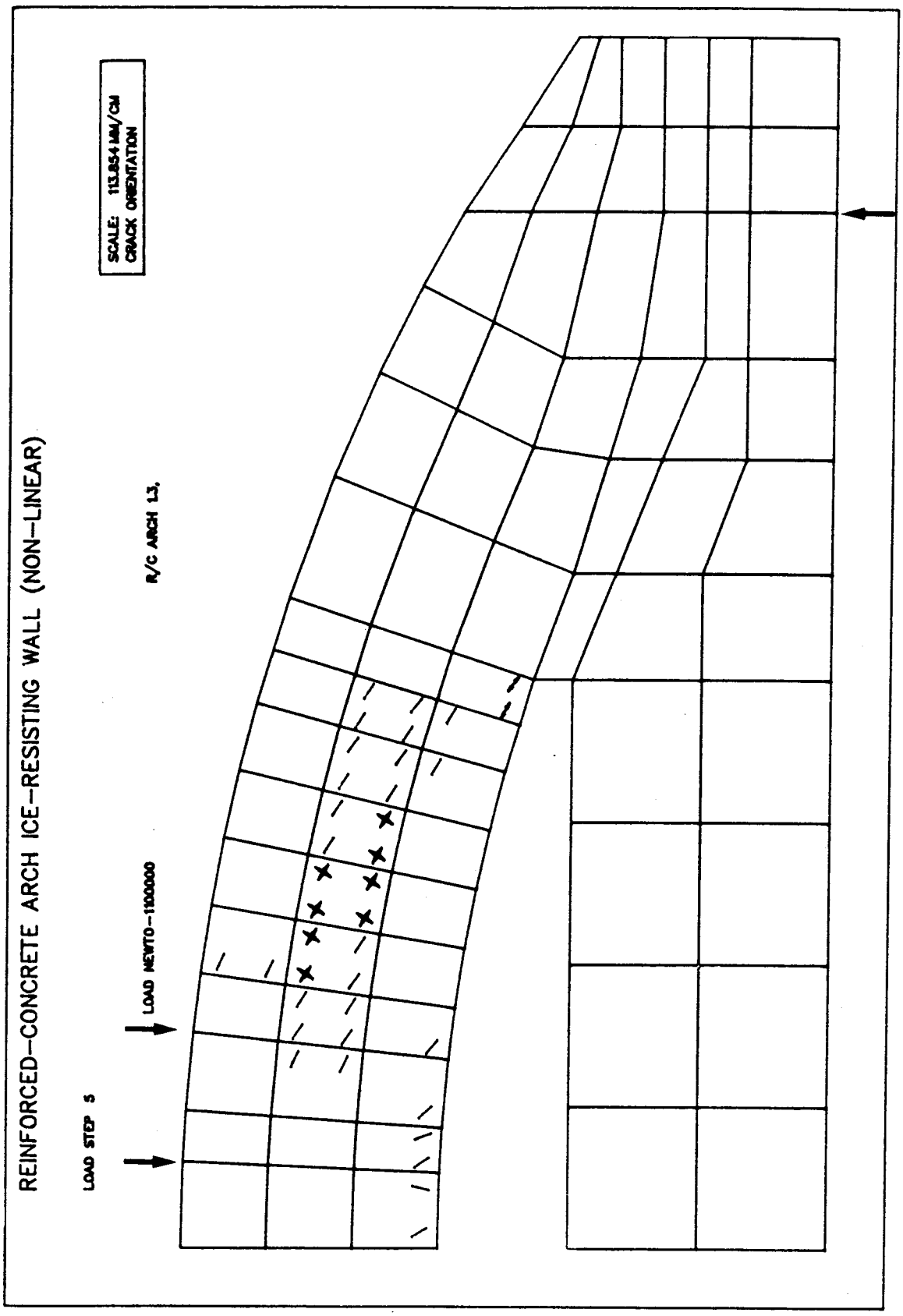

Figure 7.6 First Compression Strain Hardening in the Analysis of Specimen P1 (2200 kN)

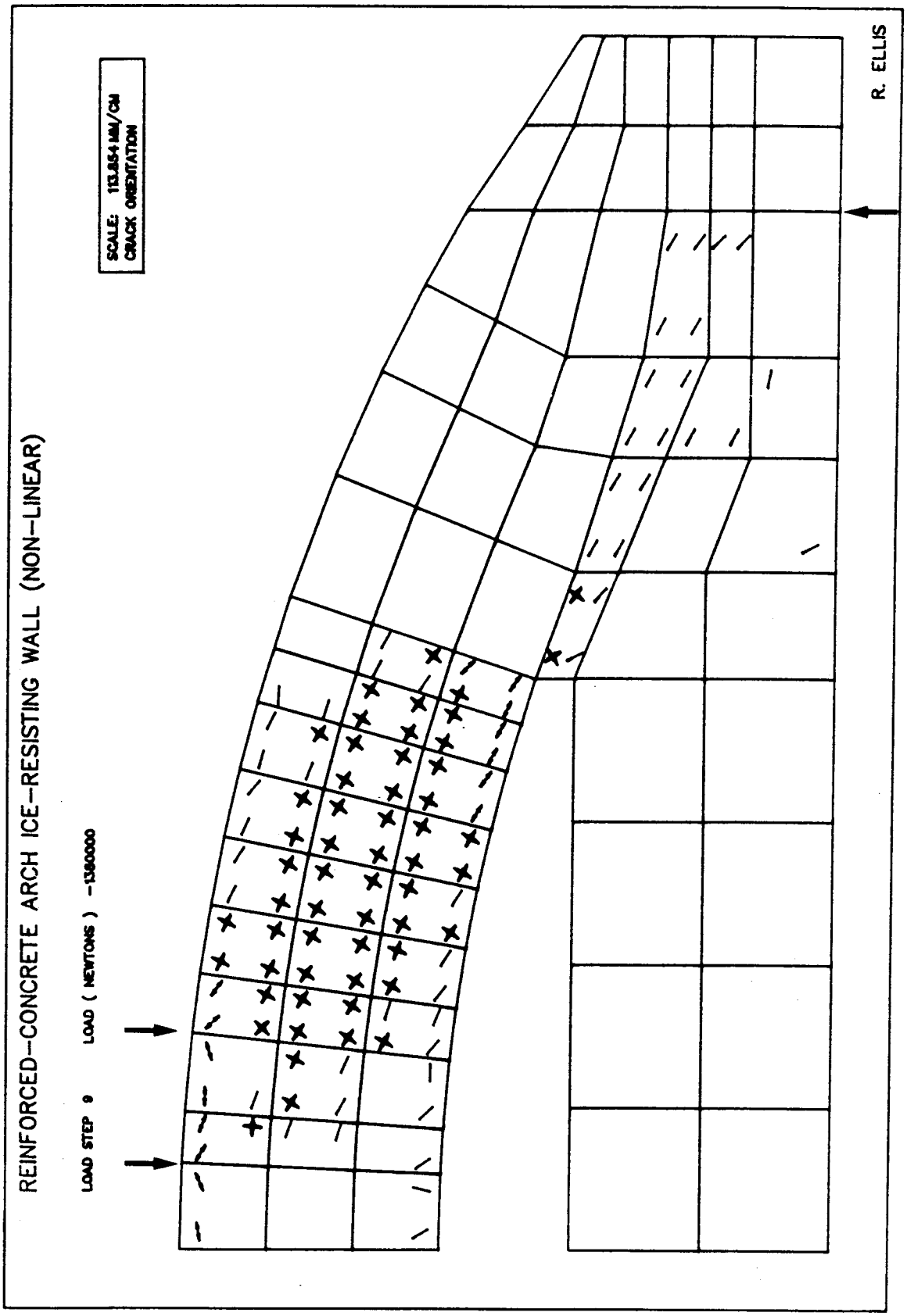

Figure 7.7 Damaged Zones at the Failure Load for Specimen P1 (2760 kN)

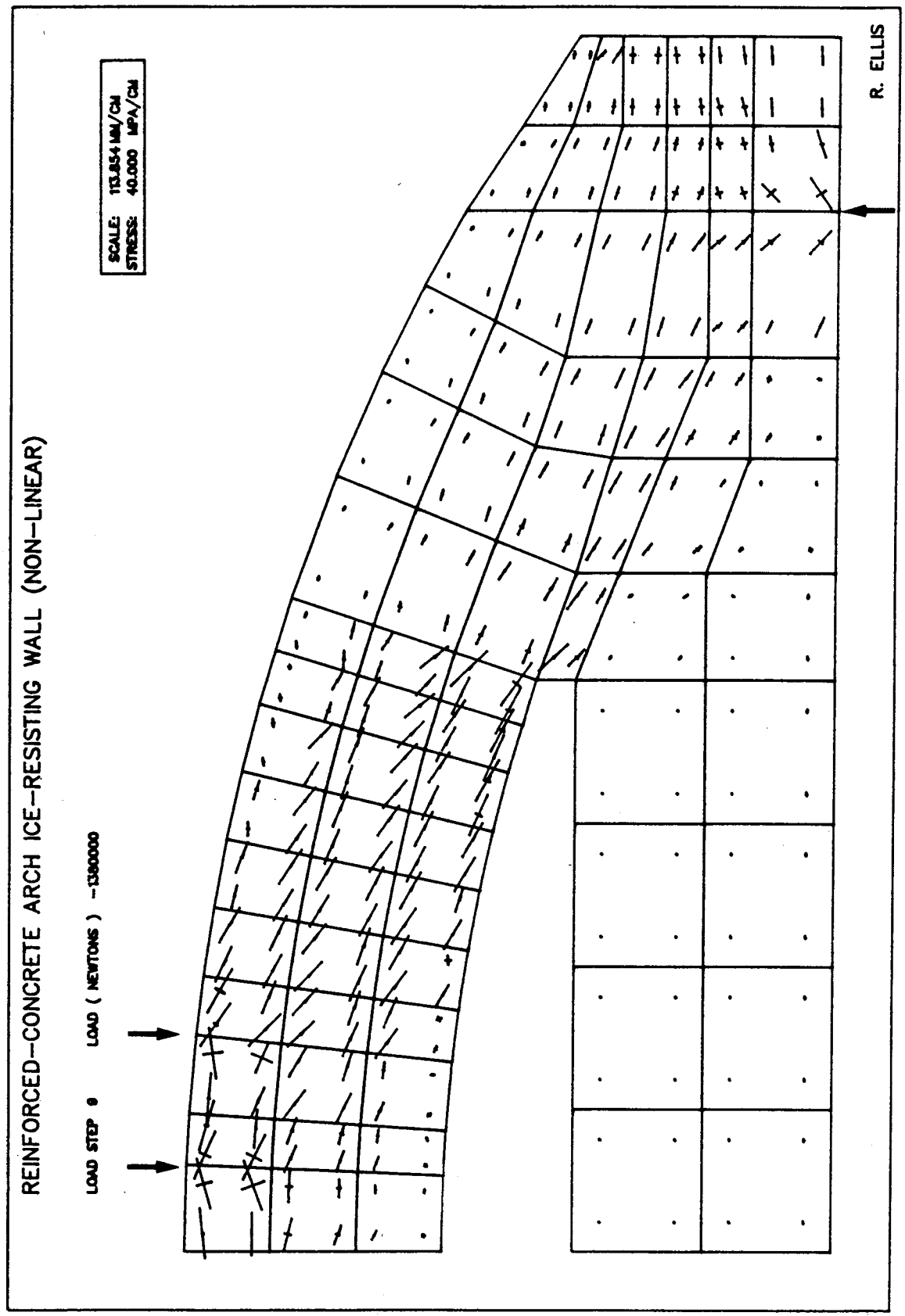

Figure 7.8 Principal Stress Plot at the Failure Load for Specimen P1 (2760 kN)

stress.

It is concluded that the bi-linear elements using a fixed-crack approach give a reasonable prediction of the load-deflection response, cracking/crushing pattern, failure load and mode of failure, and the distribution of stresses in the concrete and strains in the reinforcement.

7.3.4 V-Shaped Arch Specimen A1

Details of Specimen A1 have been presented in Chapter 3. The test results were presented in Sect. 4.3.

The finite element mesh layout is shown in Fig. 7.11. One-half of the structure is modelled since the structure, loading, and reinforcement are symmetric. Bi-linear elements were used throughout except where geometry made it advantageous to use variable node cubic elements. Three material types were used for the solid elements. In the specimen area the actual properties of the concrete (Chapter 3) and the actual thickness of the specimen were used. In the abutments, elements having a thickness equal to the actual thickness were used. A material having the same elastic properties as the first material was used since this region was heavily confined and prestressed. The steel beam was modelled using the actual thickness of the endplates, flanges, and web and the measured elastic properties of the steel were used. Reinforcing elements were used to represent the 15 M longitudinal bars and the 6 mm stirrups. The longitudinal bars were modelled at the correct location

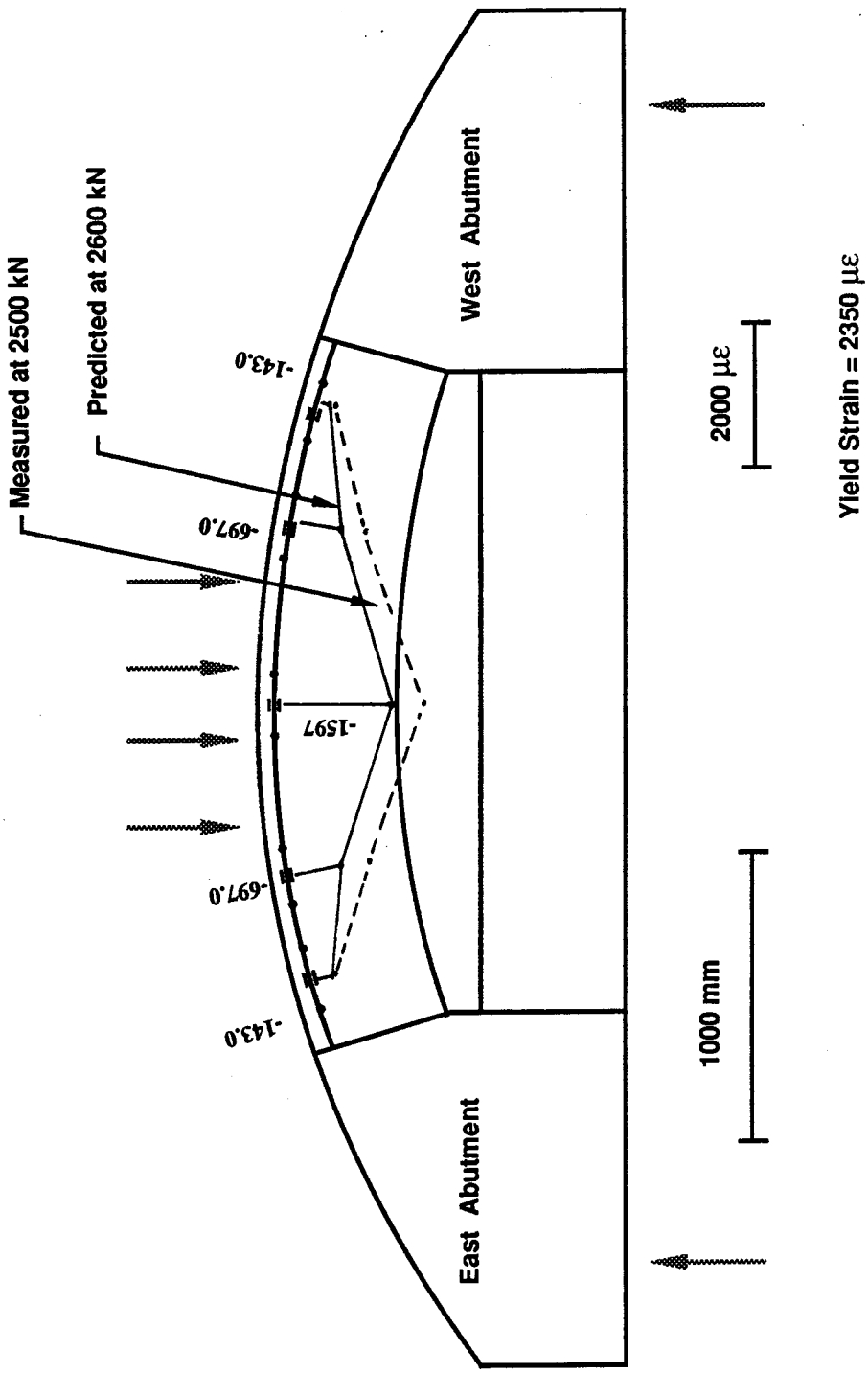

Figure 7.9 Predicted and Measured Strains in Top Reinforcement for Specimen P1

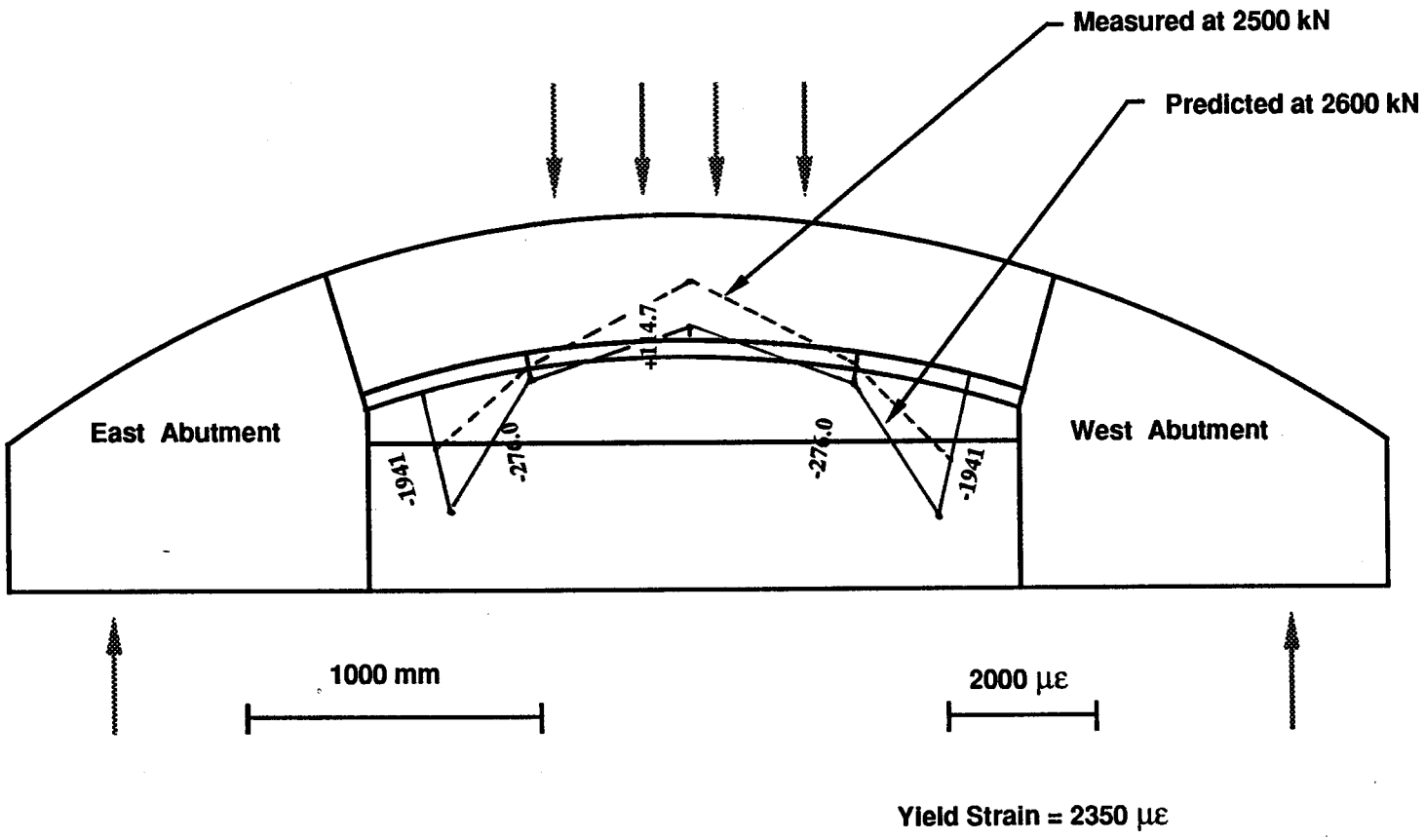

Figure 7.10 Predicted and Measured Strains in Bottom Reinforcement for Specimen P1

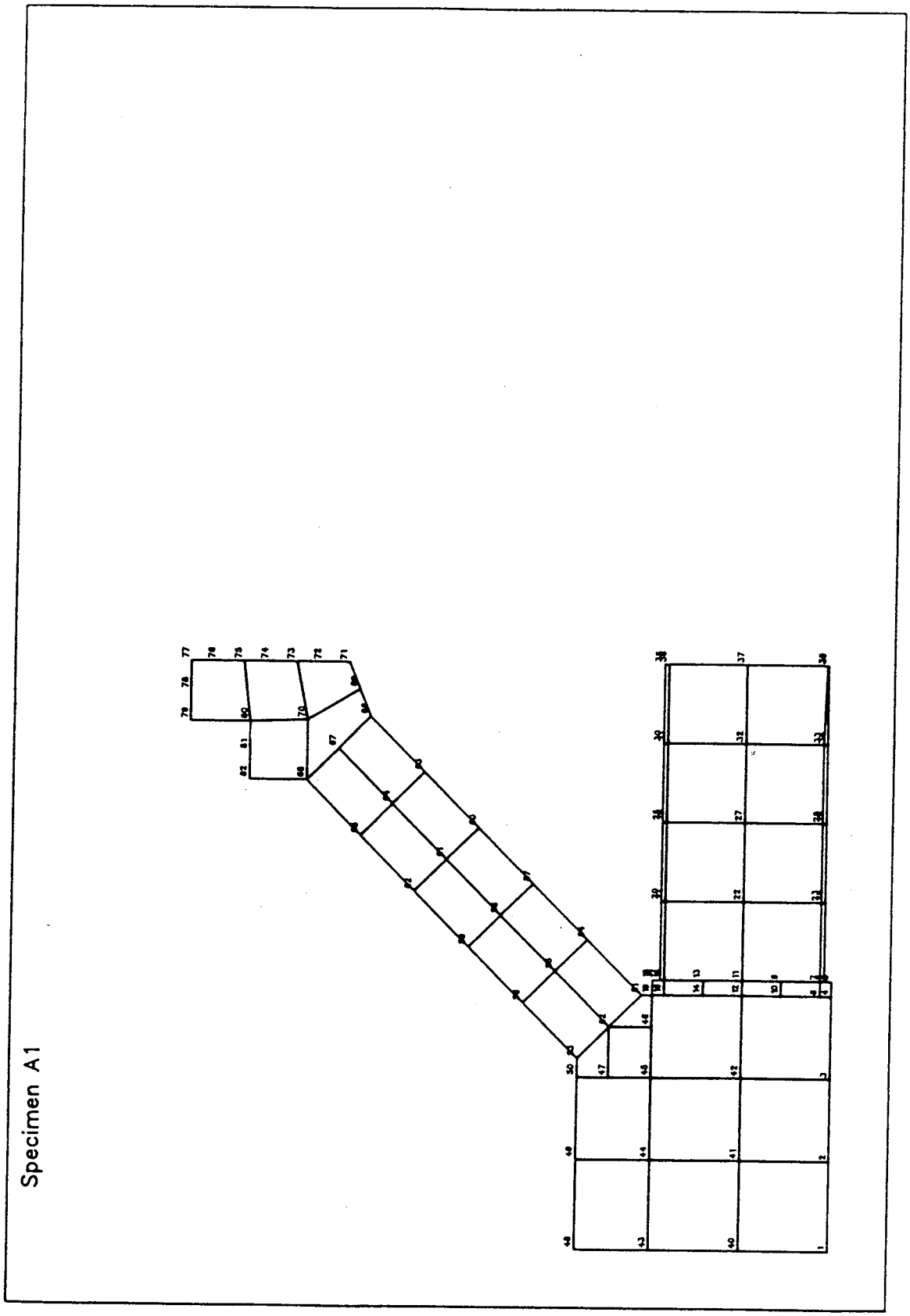

Figure 7.11 Finite Element Mesh Layout for Specimen A1

whereas the 6 mm stirrups were lumped at the gauss points for each element. The input parameters used in the analysis are summarized in Table 7.2. In the analyses of the V-shaped arch specimens a strain rotating crack approach was used. The effects of bond-slip were not accounted for.

In the test of Specimen A1 under load condition I, load increments of 100 kN were used from zero to the maximum load 6072 kN. The first observable signs of distress, in the form of crushing, were observed at 5700 kN at the top of the west strut (Figs. 4.17 and 4.20). As suggested by the measured principal strains (Figs. 4.18 and 4.19) and as discussed in Chapter 6, the load carrying mechanism is the direct strut action in the straight portions of the arch. At the maximum load, 6072 kN, the extent of the crushing and spalling had spread lower down the strut. The specimen was unloaded, the rollers were removed, and the specimen was loaded to failure without the rollers (load condition II).

In the finite element analysis, the specimen was loaded with load condition I since the majority of specimens were failed with this load condition and more measurements were taken during this loading sequence. Five 1000 kN load steps were used up to 5000 kN applied load. Then a 500 kN load step was applied. After 5500 kN, the solution failed to converge and a 250 kN loadstep was used. After 5750 kN, 100 kN load steps were used until 6050 kN. Beyond this load, convergence could not be obtained. The experimental and analytical load-deflection curves are shown in Fig. 7.12.

Table 7.2 Material Properties and Input Parameters for Specimen A1

Concrete	
E_c	27498 (MPa)
G	11500 (MPa)
ν (Poisson's Ratio)	0.2
f'_c	61.8 (MPa)
f'_t (60% of f_r)	3.03 (MPa)
ε_{ut}	0.0022 mm/mm
Reinforcing Steel	
E_s	190000 (MPa)
f_y	400 (MPa)
E_{sh} (Strain Hardening)	2150 (MPa)
A_s (Top and Bottom)	800 (mm^2)

The analytical response is seen to be stiffer than the test.

In the analysis, the first signs of cracking were vertical 'splitting' cracks, one in each of the load pedestals, at a load of 3000 kN. At 4000 kN there was no new cracks. At 5000 kN a 'splitting' crack appeared near the top of the straight portion of the arch, towards the outer face. As the load was increased, no further damaged zones were predicted until the load 5750 kN. As shown in Fig. 7.13, the two uppermost elements in the straight portion (i.e. 'strut') of the arch have reached the strain hardening zone in compression (Damage Region -1) in addition to the original 'splitting' cracks. The situation is the same in the first load pedestal. This corresponds to first crushing in the test at 5700 kN (Test/Predicted Ratio=0.99).

At the failure load in the analysis, 6050 kN, the top element in the strut has reached the peak strength (Region -2) in addition to the 'splitting' crack that appeared at 5000 kN (Fig. 7.14). Of the eight Gauss points in these top two elements, six of these had reached damage zone (-1) or (-2). The failure of the concrete in compression at this location is consistent with the crushing and spalling observed in the test. As shown in Fig. 4.20, this is the location in which failure of Specimen A1 occurred. The failure occurred at 6294 kN corresponding to a test/predicted ratio of 1.04. In Fig. 7.15, the principal stress plot at the failure load, 6050 kN, is shown. The overall distribution of stresses is consistent with the

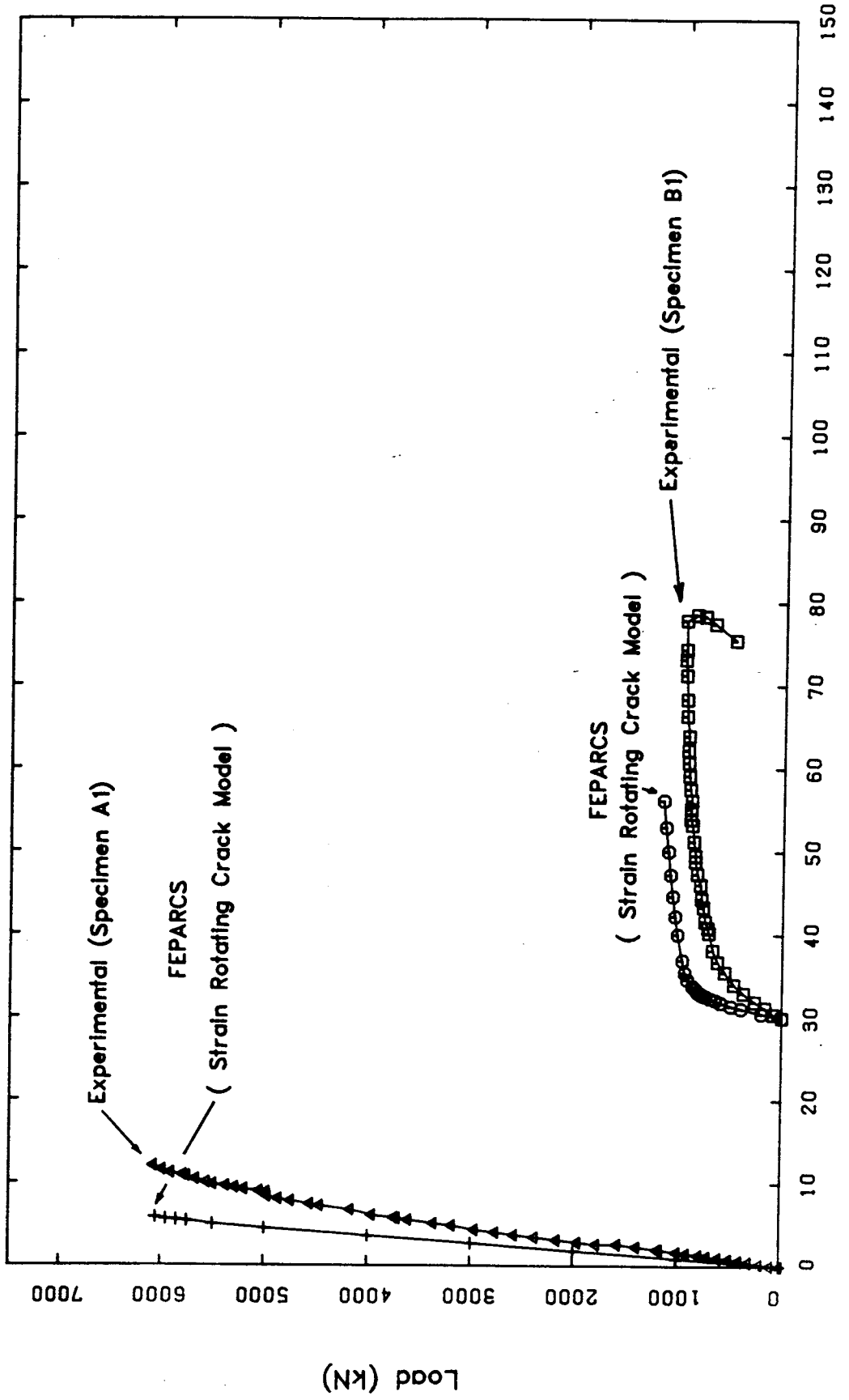

Figure 7.12 Experimental and Analytical Load vs. Midspan Displacement Curves for V-Shaped Arch Specimens

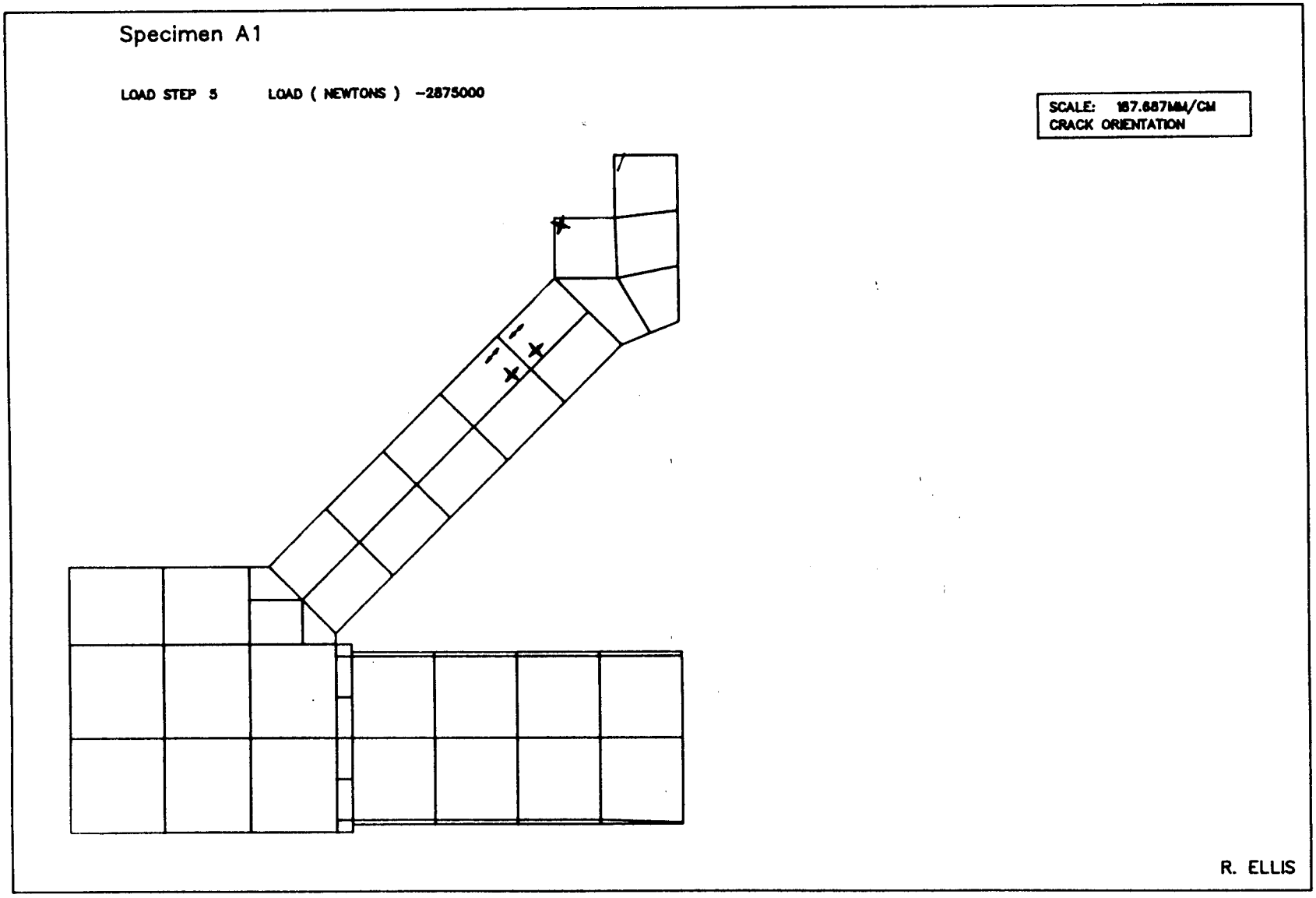

Figure 7.13 First Crushing in the Analysis of Specimen A1 (5750 kN)

observed behavior (Fig. 4.18) and the strut-and-tie models presented in Chapter 6.

The predicted distribution of strains in the top and bottom reinforcement are shown in Figs. 7.16 and 7.17, respectively. This is done at the load 5750 kN in order to compare to the measured distribution repeated from Figs. 4.21 and 4.22. The measured and predicted distributions are seen to be similar. It should be mentioned that at large strains, a large difference in strain corresponds to a small difference in stress.

7.3.5 V-Shaped Arch Specimen B1

Details of Specimen B1 have been presented in Chapter 3. The test results for this specimen were presented in Sect. 4.4.

The finite element mesh layout is shown in Fig. 7.18. Bilinear elements were used except where geometry made it advantageous to use variable-node cubic elements. In the specimen area, the measured properties of the concrete were used and the actual thickness of the specimen was specified. The abutments were modelled using the measured elastic properties of the concrete and the actual thickness. The steel beam was modelled using the measured elastic properties of the steel and the actual thickness of the end-plates, flanges, and web. Reinforcing elements were used to represent the 15M longitudinal bars and the 6 mm stirrups in each of the elements in the specimen region. The 15M bars

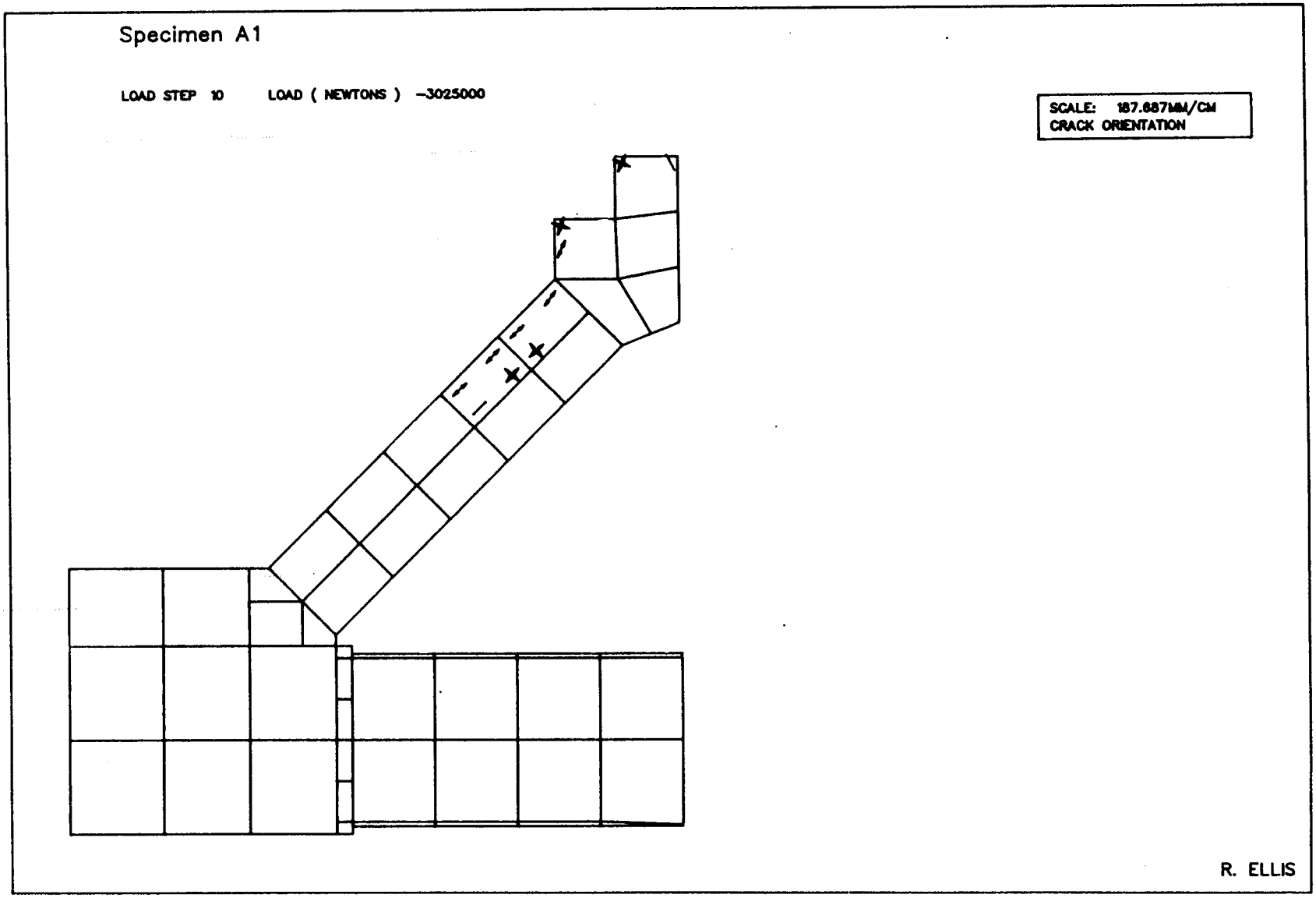

Figure 7.14 Damaged Zones at the Failure Load for Specimen A1 (6050 kN)

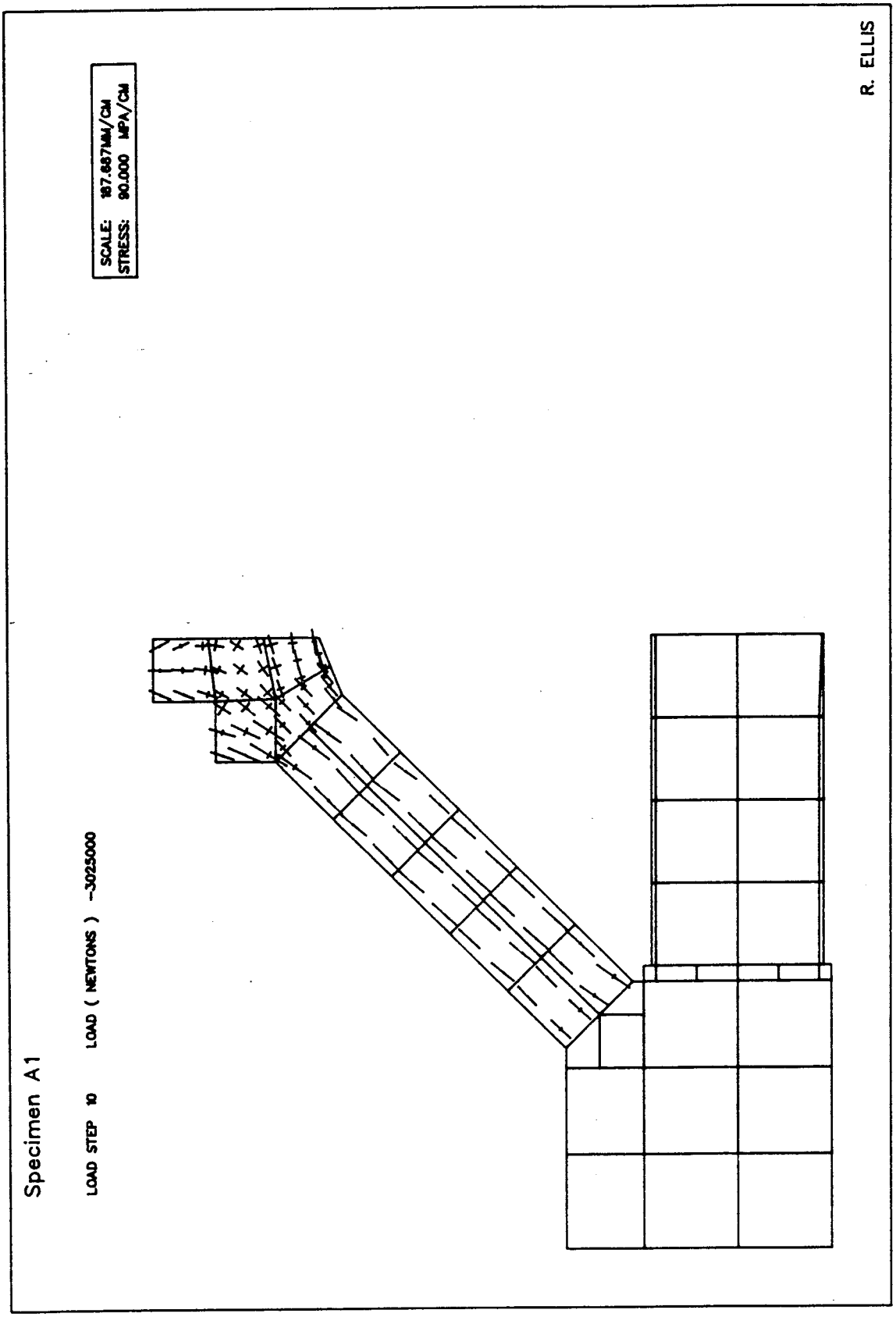

Figure 7.15 Principal Stress Plot at the Failure Load for Specimen A1 (6050 kN)

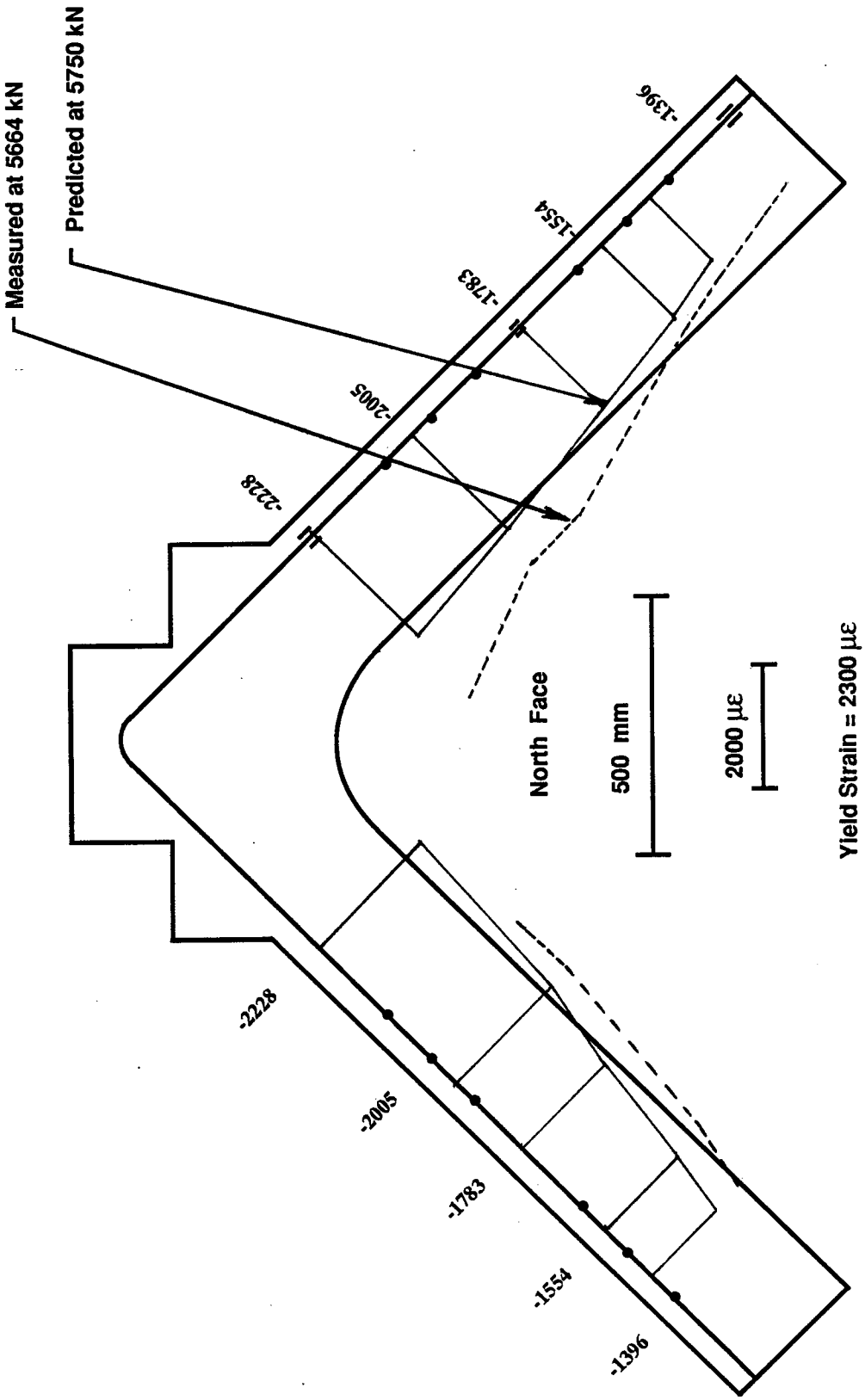

Figure 7.16 Predicted and Measured Strains in Top Reinforcement for Specimen A1

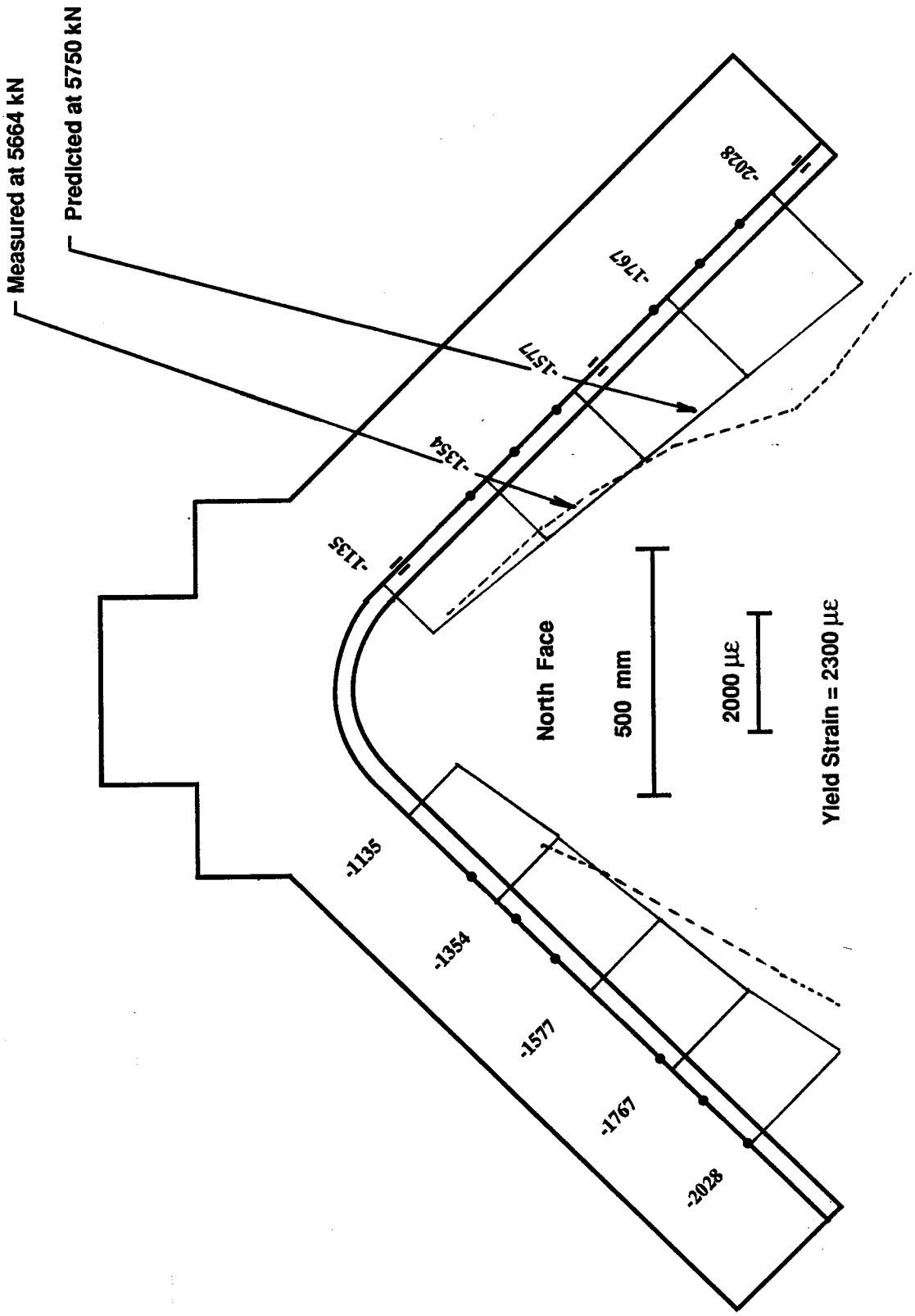

Figure 7.17 Predicted and Measured Strains in Bottom Reinforcement for Specimen A1

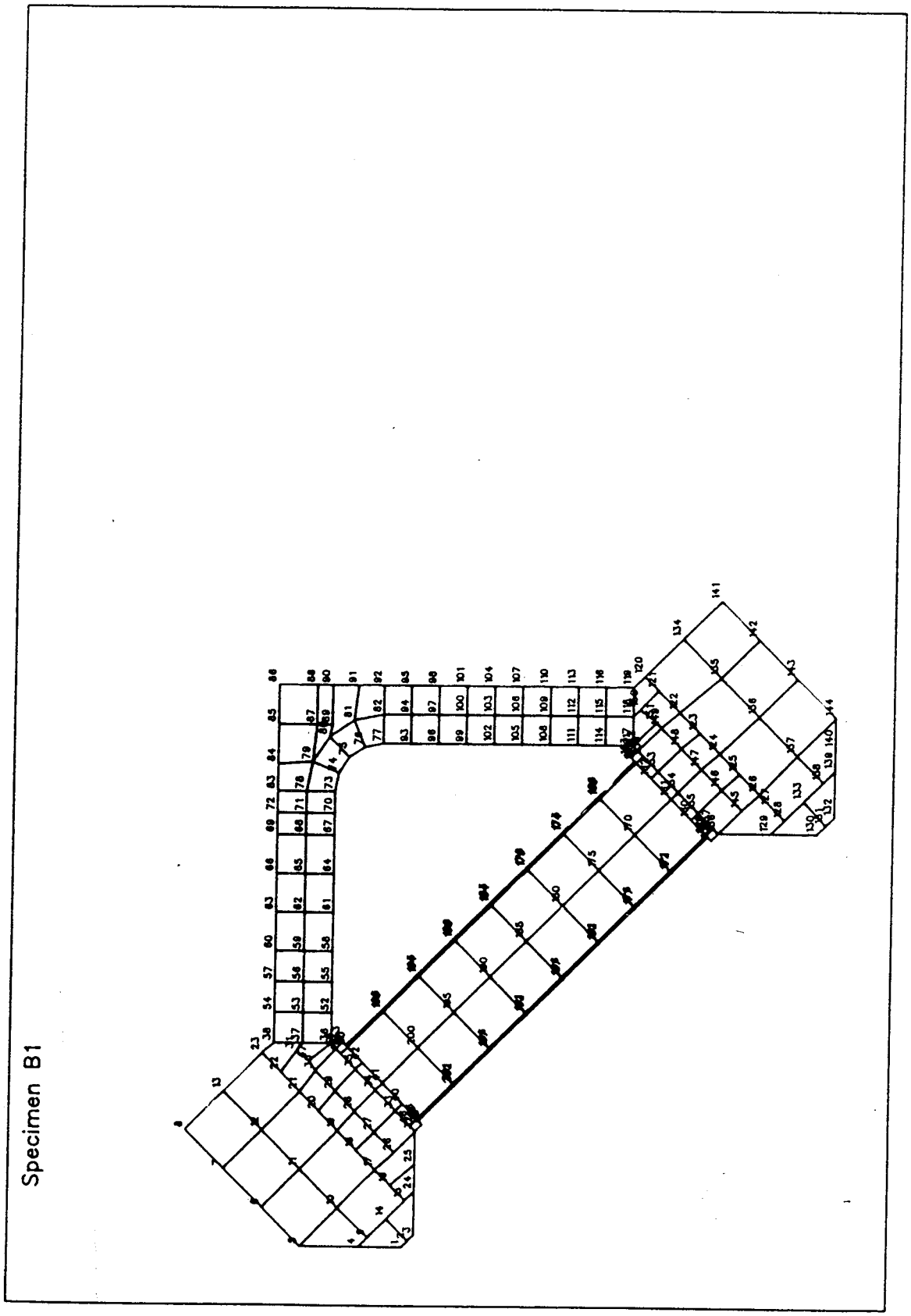

Figure 7.18 Finite Element Mesh Layout for Specimen B1

were modelled at the correct location whereas the 6 mm stirrups were lumped at the gauss points. The input parameters used in the analysis of Specimen B1 are summarized in Table 7.3. As in the case of Specimen A1, a strain rotating crack model was used and the effects of bond-slip were not accounted for.

In the test of Specimen B1, load increments of approximately 50 kN were used from zero to 750 kN. At this load, cracking and deformations were such that smaller load increments of approximately 10 kN were used until the maximum load of 964.4 kN was reached and the specimen was unloaded. This load was thought to be representative of the ultimate load of the structure since plastic hinges and very large flexural cracks had formed.

In the finite element analysis, the size of the load increment was 100 kN up to 600 kN when the increment was reduced to 50 kN. After 750 kN, this was reduced to 25 kN which was satisfactory until 1150 kN. From this point on 10 kN load increments were applied until a load of 1180 kN was reached, beyond which solution could not be obtained. This compares to the maximum load in the test, 964.4 kN. The test-to-predicted ratio is 0.82 (i.e. predicted load is 18% too large). Referring to the experimental and analytical load vs. midspan deflection curves shown in Fig. 7.4, the finite element analysis is seen to be stiffer than the measured response, and the predicted load is about 18% larger than the maximum measured load.

Table 7.3 Material Properties and Input Parameters for Specimen B1

Concrete	
E_c	31500 (MPa)
G	13125 (MPa)
ν (Poisson's Ratio)	0.2
f'_c	59.5 (MPa)
f'_t (60% of f_r)	3.83 (MPa)
ε_{ut}	0.00244 mm/mm
Reinforcing Steel	
E_s	190000 (MPa)
f_y	400 (MPa)
E_{sh} (Strain Hardening)	2150 (MPa)
A_s (Top and Bottom)	800 (mm^2)

In the analysis, the first cracks were flexural cracks (Region +1) which appeared at midspan at an applied load of 200 kN. This compares to first the flexural cracking at 150 kN in the test (Test/Predicted=0.75). As the load was increased, the locations which developed cracking increased in number and were distributed in the same way as in the test (Figs. 4.34 and 4.38). The extent and orientation of the cracking predicted by the analysis at the load 850 kN are shown in Fig. 7.19. The load 850 kN is of interest since this is approximately the load at which the plots in Figs. 4.40-4.42 were made. At this load, the majority of cracks represent damage regions +1. However the flexural cracks at the top near the abutment, and at the bottom at midspan, and at the top outside of the vertical leg correspoond to damage zones of +2 (large, wide cracks). These correspond to the formation of plastic hinges observed in the test. At one location, namely at the bottom soffit near the abutment, the principal compressive stress is within the compression hardening zone (Region -1).

The principal stress plot for this specimen at the load 850 kN is shown in Fig. 7.20. Referring to this, to the crack pattern in Fig. 7.19, to the observed crack pattern (Figs. 4.34 and 4.38), and to the strut-and-tie model shown in Fig. 6.49, the trend towards the load carrying mechanisms described in Sects. 6.4 and 6.5 is evident. The displacements of the structure are illustrated in Fig. 7.21 in which the deformed mesh (solid lines) is shown

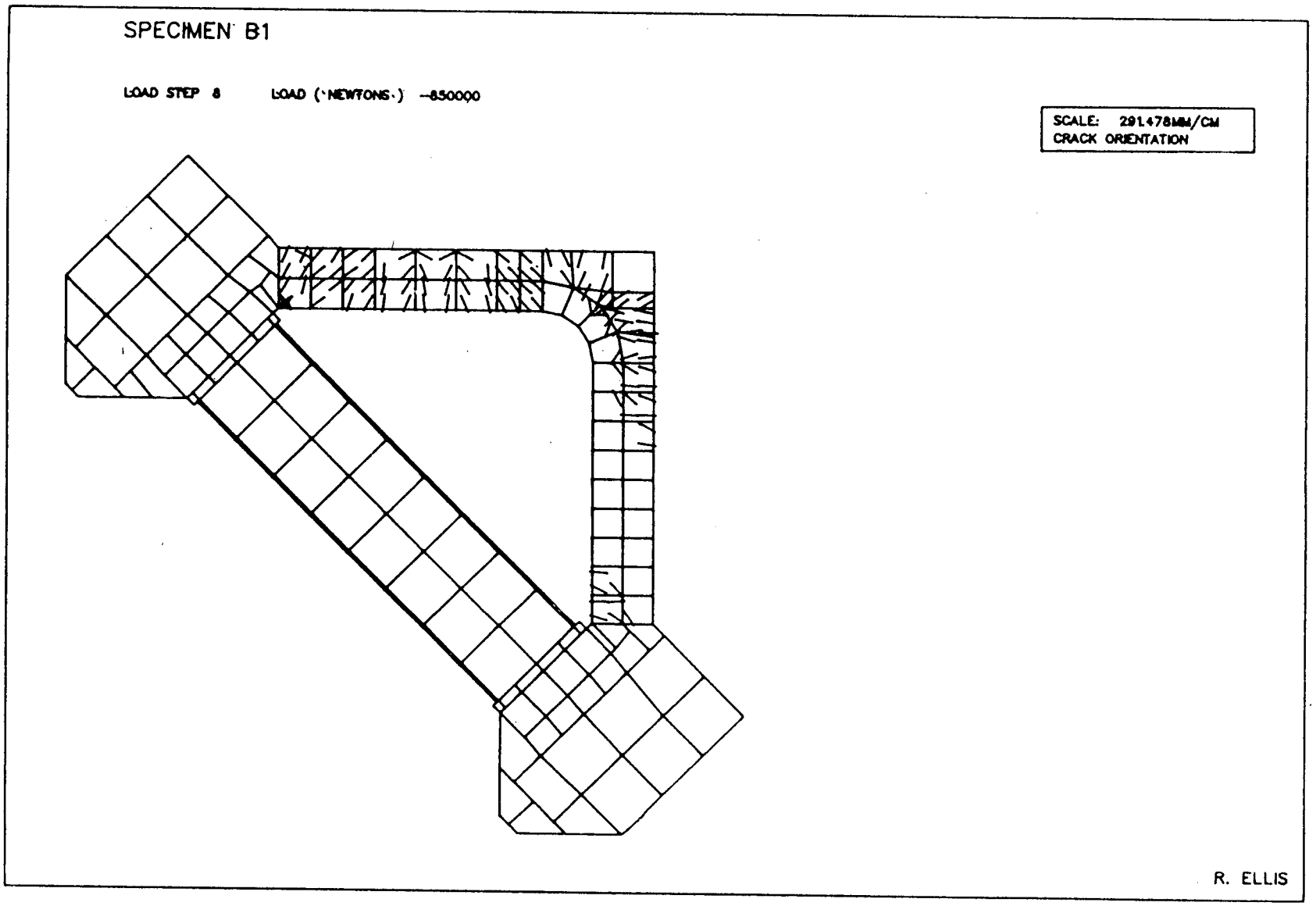

Figure 7.19 Predicted Cracking in Specimen B1 at 850 kN

superimposed on the undeformed mesh (dotted lines). In this plot the displacements are magnified by a factor of 5.0. The displacements are quite small at this load.

The crack pattern at the failure load, 1180 kN is shown in Fig. 7.22. At this load, the overall crack pattern is very similar to that at 850 kN. However at the failure load, about 50% of the cracks are large, wide cracks (Region +2). Furthermore crushing is observed (Region -2) at the inside soffit in the corner. The peak compressive strength was also exceeded at the base of the vertical leg, under the applied load points, and at the bottom soffit near the support. The principal stress plot at this load, shown in Fig. 7.23, is consistent with the load carrying mechanisms discussed in Sect. 6.4 and 6.5. For comparison to Fig. 7.21, the predicted displacements of the structure at failure are shown in Fig. 7.24.

The predicted distribution of strains in the top and bottom reinforcement are shown in Figs. 7.25 and 7.26, respectively. This is done at the load 850 kN which is closest to the load at which the measured strain plots are shown (Fig. 4.41 and 4.42). The measured and predicted distributions are seen to differ in several locations. This is probably due to use of simple bilinear elements, which cannot undergo large bending deformations, and to the use of a rather coarse mesh through the thickness of the specimen. Both of these things were chosen because simplicity was one of the constraints of the analysis. It should be emphasized

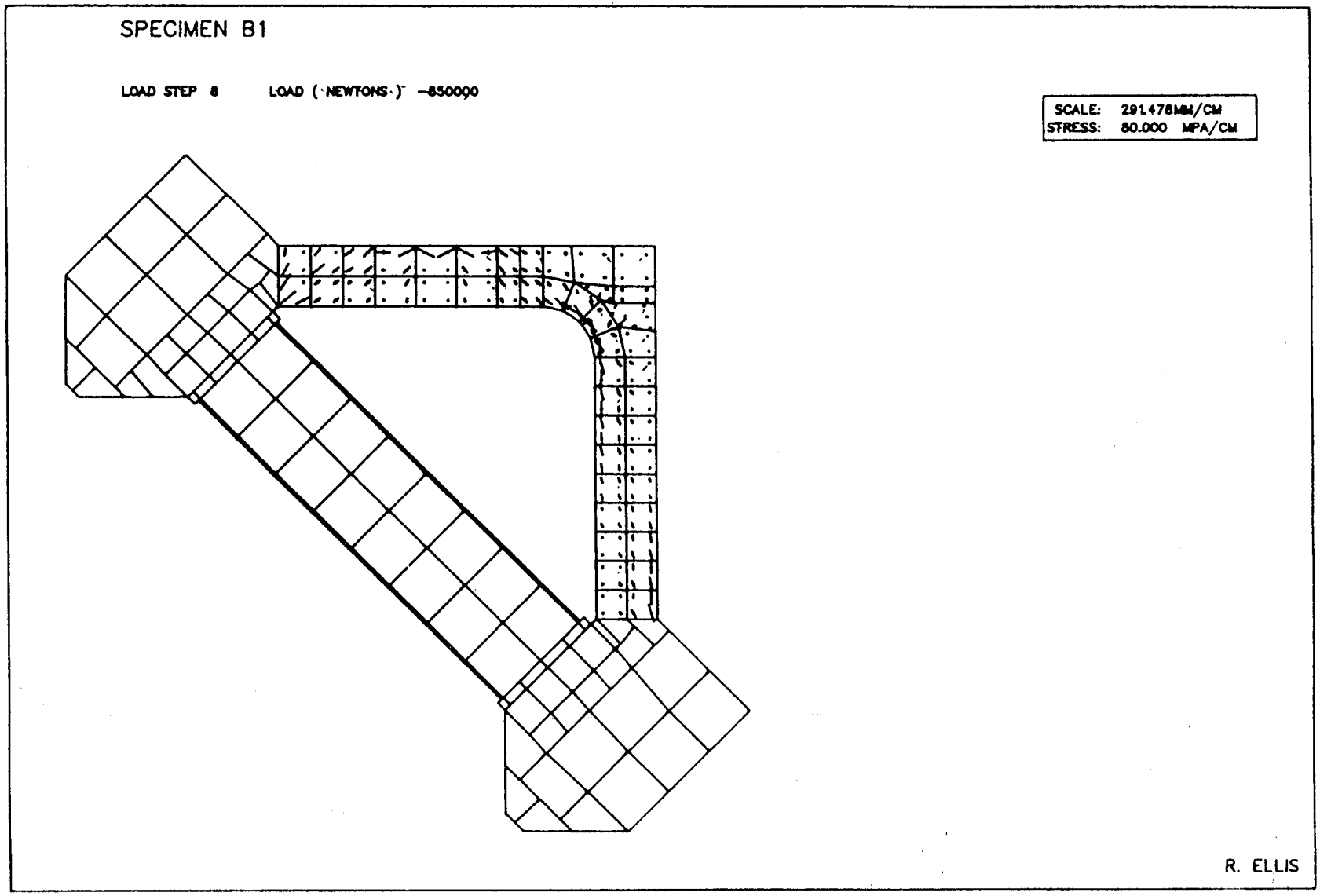

Figure 7.20 Principal Stress Plot for Specimen B1 at 850 kN

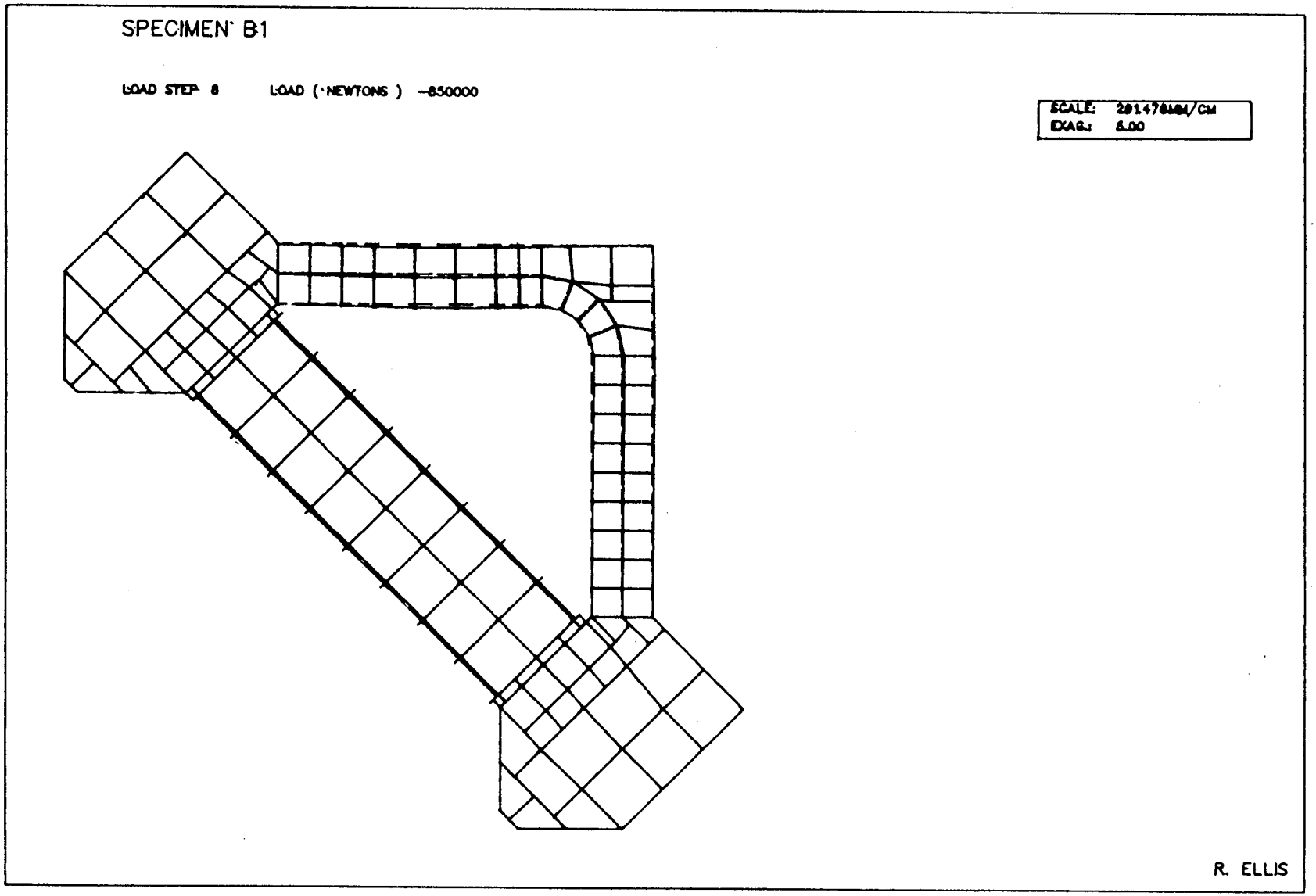

Figure 7.21 Deformed Mesh for Specimen B1 at 850 kN

that large differences in strain will correspond to small differences in stress at higher strain levels.

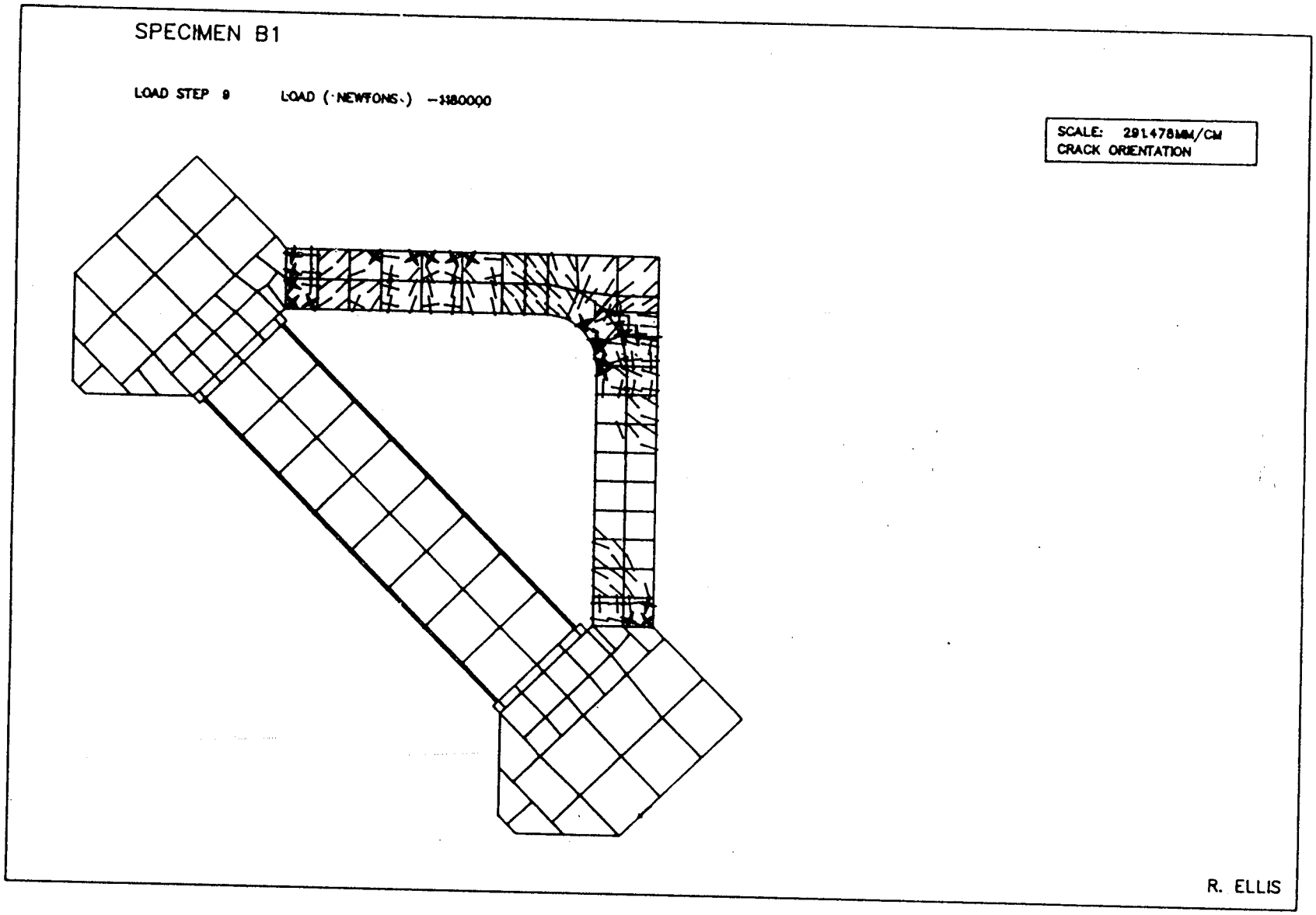

Figure 7.22 Predicted Cracking and Damaged Zones in Specimen B1 at Failure

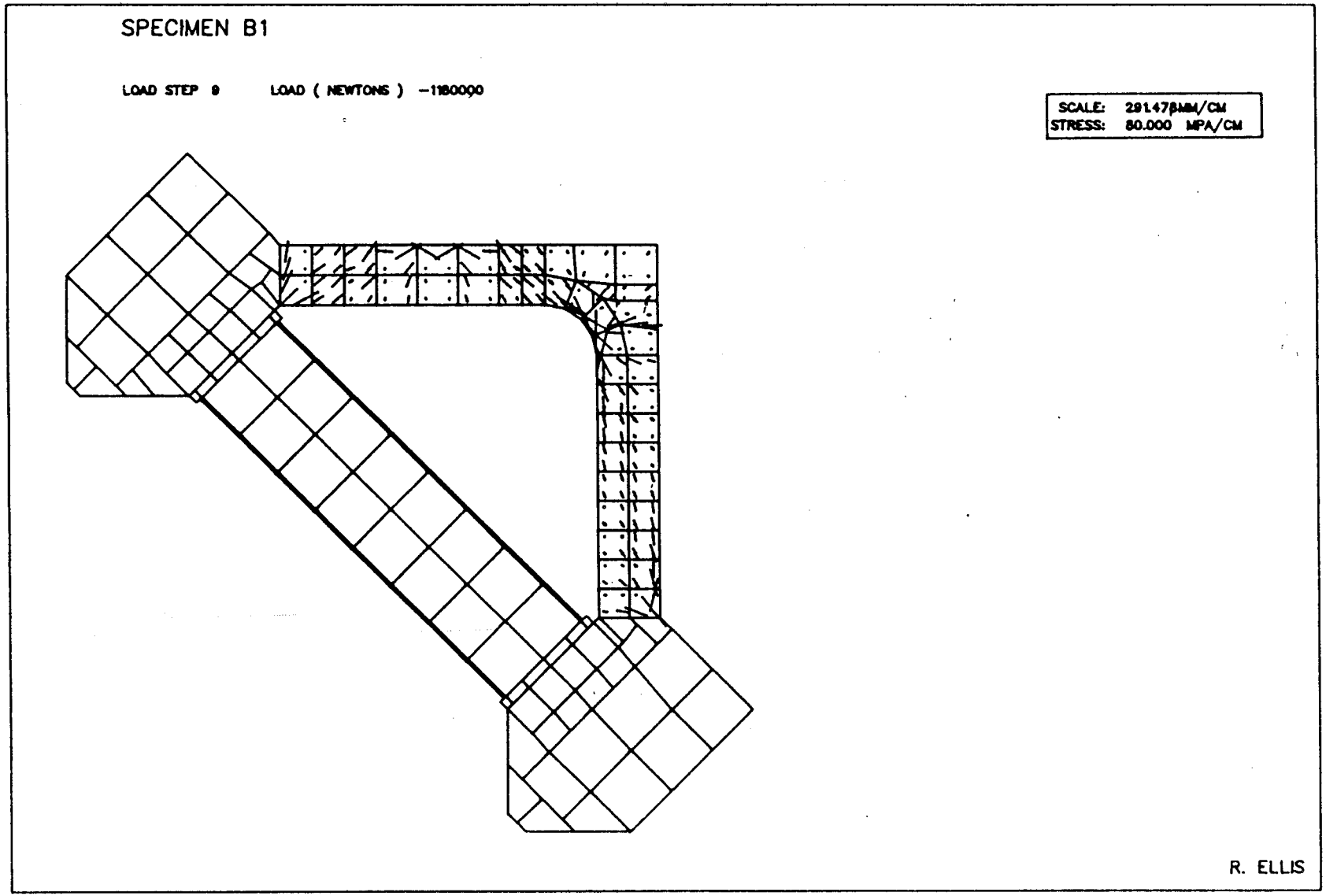

Figure 7.23 Principal Stress Plot for Specimen B1 at Failure

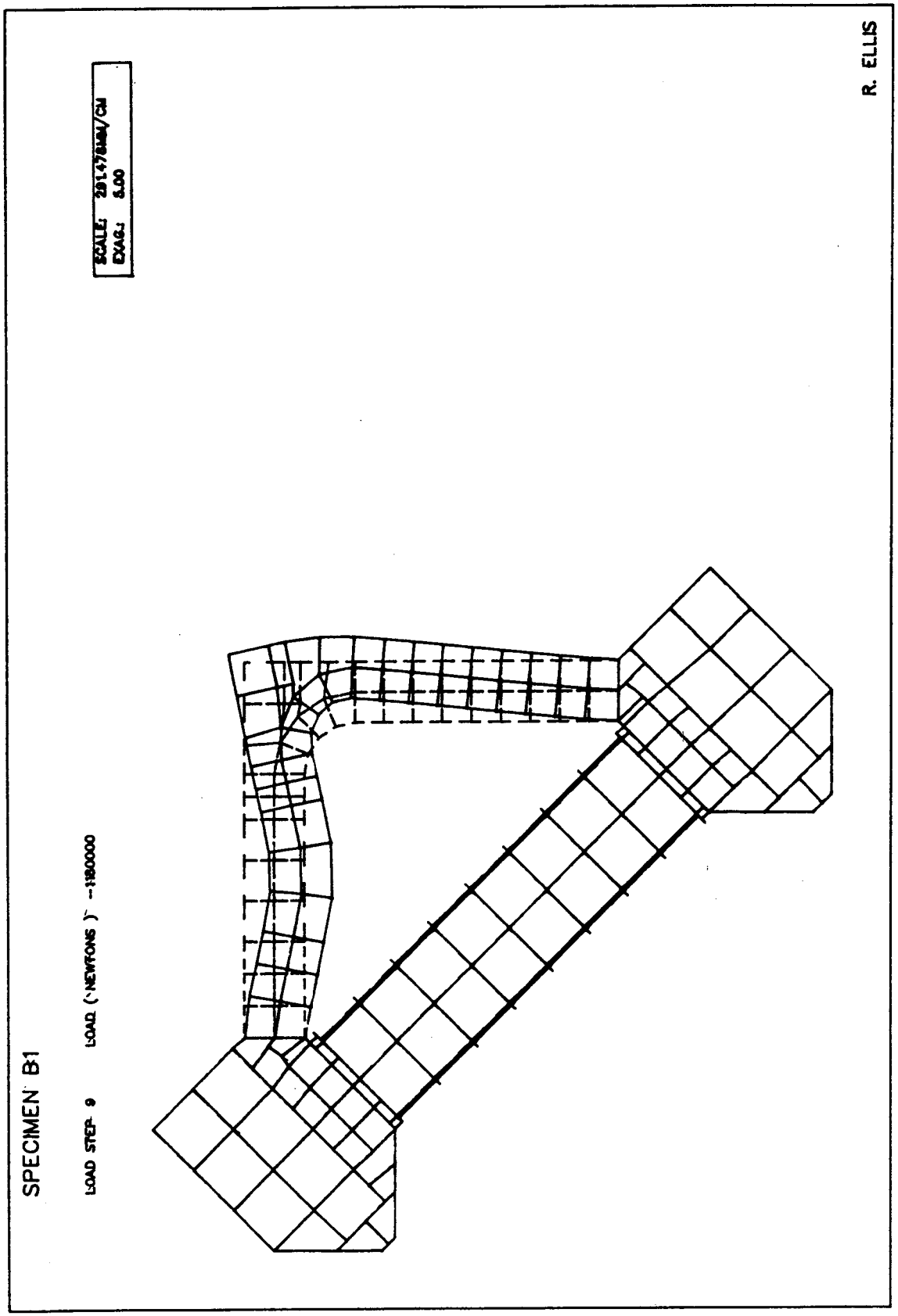

Figure 7.24 Deformed Mesh for Specimen B1 at Failure

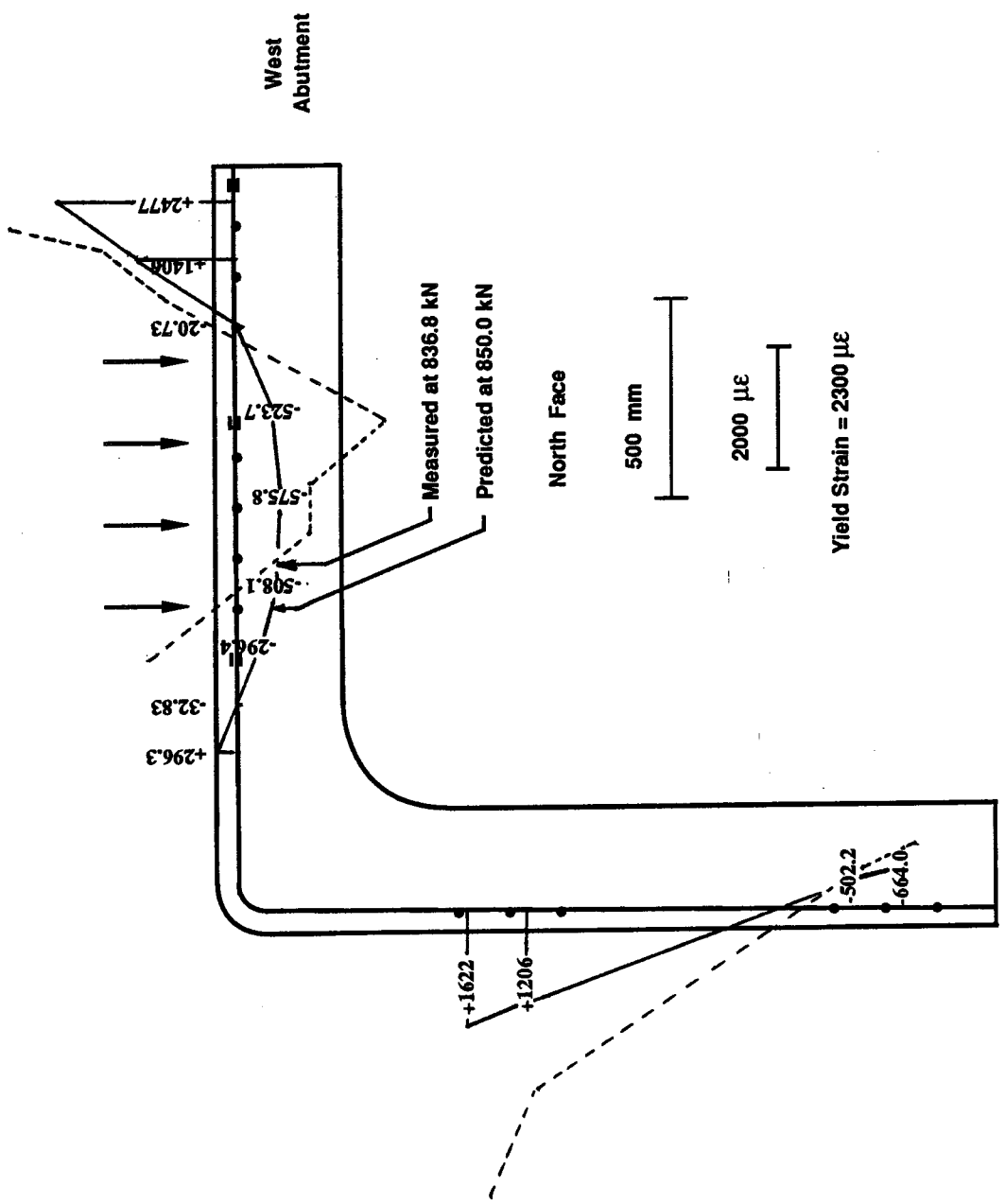

Figure 7.25 Predicted and Measured Strains in Top Reinforcement

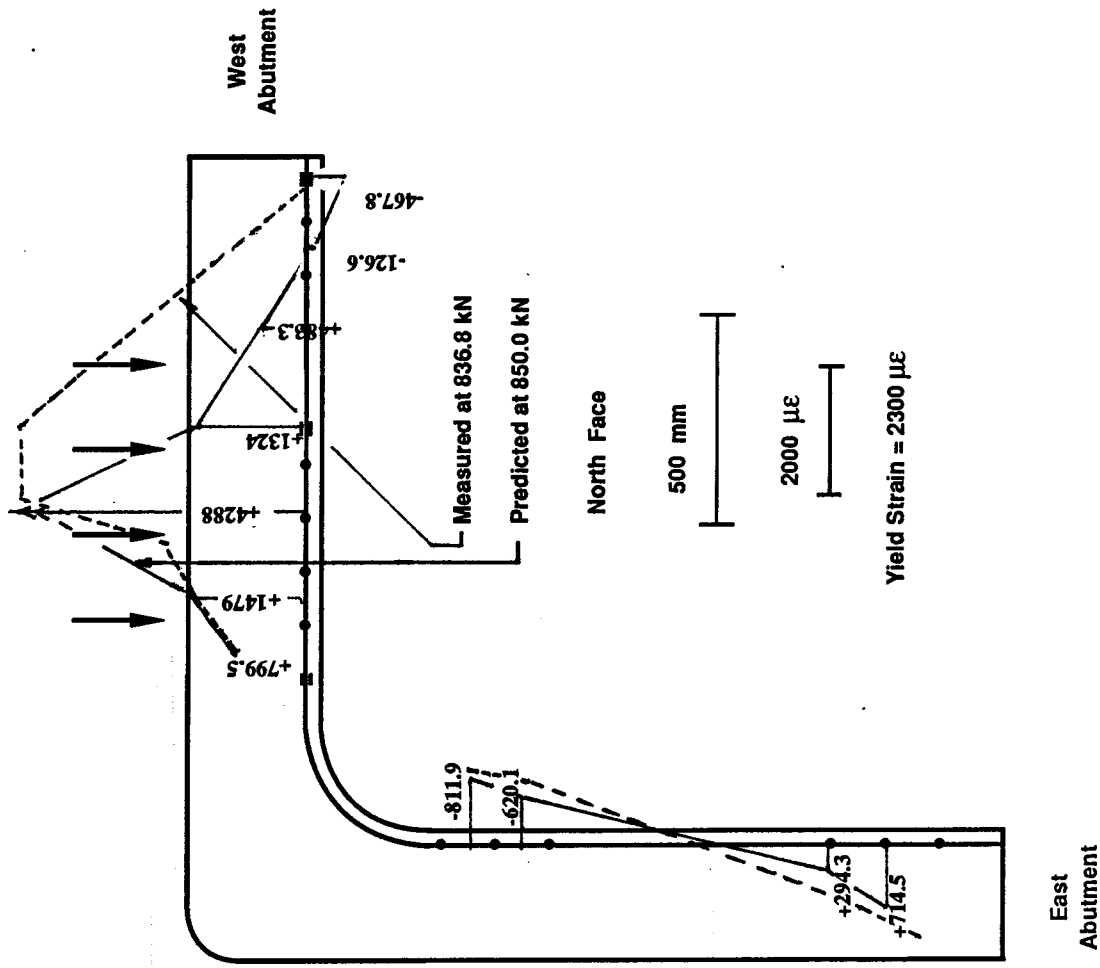

Figure 7.26 Predicted and Measured Strains in Bottom Reinforcement for Specimen B1

8. SUMMARY, CONCLUSIONS AND RECOMMENDATIONS

8.1 Summary and Conclusions

8.1.1 General

Tests were conducted to investigate the behavior of typical reinforced concrete ice-resisting walls for offshore structures. Two approximately 1/4 scale circular arch specimens and seven approximately 1/4 scale V-shaped arch specimens were tested. Both types of specimen were subjected to high-magnitude centrally-placed patch loads. In the B-Series V-shaped arch specimens, the patch load was placed at the midspan of one side of the arch.

The effects of the following on the behavior of these types of structures were of interest:

1. Shape of the arch (Circular or V-shaped)
2. Direction of loading (Symmetric loading at midspan or load applied to one side of the arch)
3. Reinforcing ratio of longitudinal reinforcement
4. Reinforcing ratio of shear reinforcement
5. Stiffness of lateral and bending support provided the arch.

The experimental research program was described in Chapter 3 and the test results were presented in Chapter 4.

Chapter 5 was devoted to the topic of strut-and-tie modelling. Since the transfer of forces between the reinforcement and the concrete has not been given adequate

treatment in the literature, and because it is critically important in all R/C design methods, the use of strut-and-tie models as a research tool to study this problem is also discussed. Corner joints under the action of closing moments were studied to illustrate the application of this concept. A microcomputer program, FANS, was developed to assist in the problem and to illustrate the potential use of the microcomputer and microcomputer graphics to assist in the design of reinforced concrete structures.

Strut-and-tie models were developed for each specimen to examine the applicability of this approach to the design of these types of structures. Simple strut-and-tie models, detailed models including compression reinforcement and recognizing the material nonlinearity, and detailed models based on the measured end forces and moments and measured reinforcing strains were developed. The latter models include the compressive membrane forces which developed in the test.

The applicability of nonlinear finite element analysis to these types of structures was examined. In particular the potential use in predicting the extent of cracking, for the servicability limit state, and the failure load and mode of failure were of interest.

8.1.2 Circular Arch Specimens

Circular arch shaped ice-resisting walls have the advantage that the shape encourages favourable structural behavior. Specimen P1, although it was effectively unreinforced in shear, carried approximately 8.4 MPa over the middle 1/4 span before cracking. At failure, the effective ice pressure was 11.6 MPa. Failure was abrupt and resulted from the developement of a major diagonal crack between the first load point and the support. It is expected that this would become a more ductile failure mode if shear reinforcement were present. Specimen P2 contained post-tensioned stirrups which increased the strength of the specimen significantly over that of Specimen P1. Specimen P2 carried over 12.0 MPa without cracking in the arch. As discussed in Sect. 4.2.4, this test had to be stopped after cracking the prestressed tie beam. It is concluded that the circular arch specimens are capable of carrying loads in excess of typical ice pressures (see Fig. 1.2).

The simple strut-and-tie model presented in Sect. 6.2 was developed using ν=0.90 and ignoring the contribution of the reinforcement. The assumed load carrying mechanism is consistent with the measured cracks and principal strains in the concrete. It can be concluded that this type of model, using ν=0.90 gives an adequate lower bound estimate of the ultimate strength of Specimen P1 (test/predicted =1.43). If contribution of the shear reinforcement and the longitudinal reinforcement were included in the analysis it is expected

that this would give a test/predicted ratio closer to 1.0.

The finite element analysis for Specimen P1 presented in Sect. 7.3.3, gave a reliable prediction of the load-deflection response, the location and extent of cracking (Test/Predicted=1.05), and the failure load (Test/Predicted=1.05) and mode of failure. This was achieved using 4-node linear elements to represent the concrete, a fixed-crack formulation, and a concrete model which includes the following:

1. Cracking
2. Tension softening
3. Strain hardening at high compressive stress
4. Strain softening
5. Reduction of shear modulus with crack strain.

It is concluded that this type of analysis satisfies the objectives of Sect. 7.3.1.

8.1.3 V-Shaped Arch Specimens Loaded by Symmetrical Patch Load at Midspan (A-Series)

As discussed in Sect. 6.3, the symmetric patch load placed at midspan is the load condition which V-shaped arches are most suited for. It can be concluded that specimens having this geometry can carry loads applied in this manner, well in excess of those that would result from typical ice pressures. The effect of the test variables was relatively minor and Specimen A1 can be taken to be representative of the other A-Series tests. Specimen A1

carried 5700 kN (or 25 MPa) before first crushing was observed under load condition I. As suggested by the measured principal strains in the concrete (Fig 4.18) the principal load-carrying mechanism is direct strut action. Failure under load condition II at 6294 kN occurred by crushing at the top of the west strut.

The strut-and-tie models were presented in Sect. 6.3.2. Using these models, good estimates of the ultimate strength of the specimen were obtained using ν=0.90 (5600 kN as compared to 6294 kN in the test for a test/predicted ratio of 1.12 for the model in Fig. 6.6). The assumed load carrying mechanism is consistent with the measured cracks and the principal strains in the concrete.

Based on the finite element analysis for Specimen A1 presented in Sect. 7.3.4, it is concluded that a reliable prediction of the ultimate load and failure mode can be obtained using 4-node linear elements to represent the concrete, a strain rotating-crack formulation, and a concrete material model which includes the same effects listed in Sect. 8.2.1. In the analysis, first crushing occurred in the straight portion of the arch at a load of 5750 kN and in the test, the first visible sign of distress was at 5700 kN. However, the predicted load-deflection response was much stiffer than the measured response. This is not viewed as a serious criticism of the analysis since the analysis satisfies the principal objectives given in Sect. 7.3.1.

8.1.4 V-Shaped Arch Specimens Loaded by Patch Load to One Side (B-Series)

This proved to be the critical load condition for the V-shaped arches in terms of cracking, failure load, and the requirements for the detailing of the reinforcment. It can be concluded that this type of load condition should be considered in the design of these structures. Specimen B1 carried a maximum applied load of 964.4 kN (or 4.82 MPa). The failure mode was ductile with large flexural and diagonal cracks, and yielding of the reinforcement. Specimen B2 contained fewer stirrups and failed at a load of 774.7 kN (or 3.86 MPa). Failure was abrupt as a major crack formed along the diagonal cracks that had formed between the abutment and the first load point. Failure was accompanied by yielding of the reinforcement. It is concluded that these specimens are capable of carrying loads in the range of typical ice pressures (see Fig. 2.1).

The detailed strut-and-tie models developed from the measured end forces and moments and reinforcing strains were presented in Sects. 6.4 and 6.5. The model for Specimen B1 was developed for the load 914.3 kN (or 4.57 MPa) which represents 95% of the failure load, 964.4 kN (or 4.82 MPa). The model for Specimen B2 was developed for the load 763 kN (or 3.80 MPa) which represents 98% of the failure load, 774.7 kN (or 3.87 MPa). As suggested in Sect. 6.4 these loads were chosen for the development of the model but the approach would be identical for a different applied load. It

is concluded that these strut-and-tie models are suitable for design since they gave good representation of the load carrying mechanisms acting at ultimate in the tests and gave good estimates of the ultimate strengths of the specimens. In addition, a constant value of ν=0.90 was shown to give good results compared with the test results.

Based on the finite element analysis for Specimen B1 presented in Sect. 7.3.5, it is concluded that a reliable prediction of the cracking load and crack pattern, failure load and mode of failure can be obtained using 4-node linear elements to represent the concrete, a strain rotating-crack formulation, and a concrete material model which includes the same effects listed in Sect. 8.2.1. The predicted failure load was 18% greater than the measured load which is considered satisfactory in this case. The predicted strains and measured strains differed at several locations. The overall load-deflection response was in agreement with the measured but the predicted response was stiffer than the measured response. These shortcomings are probably the penalty for using the simple 4-node linear element which does not have the ability to undergo large bending deformations, and to some extent the use of a rather coarse mesh.

8.2 Recommendations

8.2.1 Analysis and Design of Reinforced Concrete Ice-Resisting Walls

In general it is recommended that for a specified ice pressure vs. area curve as in Fig. 2.1, the analysis and design of the ice-resisting wall should include the following.

8.2.1.1 Global Analysis

For each of the load conditions, perform a global analysis of the structure to determine the appropriate boundary conditions for a local analysis. This could be achieved by a linear elastic finite element analysis.

8.2.1.2 Develop Strut-and-Tie Models

Using the forces and moments determined from the above analyses, develop strut-and-tie models to proportion the reinforcment for the ultimate strength design, to study the detailing requirements for the different load conditions, and to refine the geometry if necessary (i.e. shape, thickness, bulkhead spacing etc.). It should be noted that certain reinforcement may not necessary for one loading, but may be required for others.

The development of the STM will be much simpler than the detailed analytical models presented in Chapter 6 since the reinforcement is proportioned assuming it is stressed at most to f_s. Fewer assumptions are necessary in design, and

as long as the resulting model satisfies the limits on material stresses and is statically admissible, it will provide a safe lower bound solution.

In all of the strut-and-tie models, a value of ν=0.90 was found to give a good prediction of the ultimate strength. To satisfy CAN3 A23.3 M84, the design of the ice-resisting wall would need to use appropriate load factors, the material factors given in the code (ϕ_c=0.6, and ϕ_s=0.85) and the values of ν implied in Clause 11.4.7.5.. The draft CAN3 S474 standard for offshore structures uses ϕ_c=0.67.

Careful attention should be paid to reinforcing details to ensure that adequate load transfer is provided both for the load path through the structure and in the development of the reinforcing. Particular attention is required in the detailing of joints. These must have adequate ductility to develop the full capacity of the surrounding regions.

8.2.1.3 Final Design Check and Servicability Check

The servicability check on cracking may require a nonlinear finite element analysis. This must be a detailed analysis and it should include the requirements outlined in Sect. 7.3.2.2. It appears that it is more important to use a realistic concrete material model than to use overly sophisticiated elements.

The analysis can be based on the boundary conditions determined in the global analysis. The same analysis can be extended to the ultimate limit state to

provide additional information and to compare with the strut-and-tie models.

8.3 Future Research

There is a need for more research into several areas pertaining to offshore structures in ice environments for eg. the refinement of ice loading and ice-structure interaction, the design of efficient and economical ice-resisting walls.

Pertaining more to the goals of this thesis, there are a number of areas that warrant further investigation.

1. These tests were conducted on 'beam'(i.e.plane stress) specimens. Experimental and analytical work is necessary to study the three-dimensional behavior of these ice-resisting walls subjected to intense patch loads and to develop the necessary three-dimensional strut-and-tie models.
2. These tests considered two possible patch loadings. There is a need for tests on other more uniformly distributed loadings.
3. The prototype structure will have significant amounts of prestressing, vertically and horizontally. Slab specimens could be tested which incorporate this reinforcment as well as the actual three-dimensional nature of the problem. As in the tests reported in this study, the provision of the appropriate boundary constraints is a major consideration.

4. The reinforcing ratios were taken to be estimates of what is likely to be required in a prototype structure. The reinforcing details were also estimated based on the requirements of this test. An investigation into the reinforcing requirements of a prototype structure and the necessary details would be useful.
5. These tests were conducted using medium and high strength concrete. It is probable that very high strength concrete, and semi-light weight concrete would be used in prototype structures. There is a need for research into the effectiveness factors and/or the strength reduction factors appropriate for these types of concrete.
6. Since the proposed strut-and-tie models are applicable to reinforcement which is internal (reinforcing bars) or external (steel plates), it is possible that arch shaped ice-resisting walls could use external reinforcement on one or both sides of the wall. Tests on the type and amount of shear connection, and shear reinforcement necessary would be useful.
7. The proposed method to investigate the servicability limit state is to use finite element analysis. However, the designer is lacking servicability requirements for concrete offshore structures. Research is needed in order that the cracking limits can be specified.

REFERENCES

Abrams, D.A., 1913. Tests of Bond Between Concrete and Steel, University of Illinois, Engineering Bulletin No. 71.

ACI Committee 318, Building Code Requirements for Reinforced Concrete, (ACI 318-77), American Concrete Institute, Detroit, Michigan, 1977.

ACI Committee 318, Building Code Requirements for Reinforced Concrete, (ACI 318-83), American Concrete Institute, Detroit, Michigan, 1983.

ACI Committee 357, Guide for the Design and Construction of Fixed Offshore Concrete Structures, (ACI 357R-78), American Concrete Institute, Detroit, Michigan, 1978.

American Petroleum Institute. 1982. Planning, Designing, and Constructing Fixed Offshore Structures in Ice Environments, API Bulletin 2N, Dallas, TX.

ACI Committee 408. 1966. Bond Stress - The State of the Art. ACI Journal Proceedings. Vol. 63, No. 11. November, pp. 1161-1190. Discussion pp. 1569-1570.

Allyn, N.F., 1986. Global and Local Ice Loads Including Dynamic Effects, Ice/Structure Interaction, PERD Task

6.2 Program Evaluation Workshops, Canada Oil and Gas Lands Administration, May-June, pp. I-1 - I-36.

American Petroleum Institute, 1982. Planning, Designing and Constructing Fixed Offshore Structures in Ice Environments. API Bulletin 2N. Washington, D.C.

Bach, F., Nielson, M.P., and Braestrup, M.W., 1980. Shear Tests on Reinforced Concrete T-Beams. Series V, U, X, B, S, Copenhagen, Technical University of Denmark, Structural Research Laboratory Report No. R-120.

Balakrishnan, S., and Murray, D.W., 1986. Finite Element Prediction of Reinforced Concrete Behaviour. Structural Engineering Report No. 138, Department of Civil Engineering, University of Alberta, Edmonton, Alberta, July. 487 p.

Balakrishnan, S., and Murray, D.W., 1987. Prediction of Response of Concrete Beams and Panels by Nonlinear Finite Element Analysis, Proceedings IABSE Colloquium, Delft. pp. 393-404.

Bazant, Z.P., and Cedolin, L. 1980. Fracture Mechanics of Reinforced Concrete, ASCE Journal of the Engineering Mechanics Division, Vol. 106 (EM6), pp. 1287-1306.

Bazant, Z.P., and Oh, B.H. 1983. Crack Band Theory for Fracture of Concrete, Materials and Structures, RILEM, Paris. Vol. 16, pp. 155-177.

Bercha, F.G., Brown, T.G., and Cheung, M.S., 1985. Local Pressure in Ice/Structure Interactions, Proceedings of the Conference Arctic ;85, San Francisco, California, March, pp. 1243-1251.

Bhula, D.N., Birdy, J.N. and Bruen, F.J., 1984. Design of Concrete Gravity Structures to Withstand Concentrated Ridge and Flow Impact Loads. Proceedings of the Offshore Technology Conference, Houston, Texas, Vol. 3, pp. 515-522.

Birdy, J.N., Bhula, D.N., Smith, J.R. and Wicks, S.J., 1985. Punching Resistance of Slabs and Shells used for Arctic Concrete Platforms. Proceedings of the Offshore Technology Conference, Houston, Texas. Vol. 1, pp. 135-149.

Boyd, A.C., and Bruce, J.C., 1984. The Promise and Practice of Concrete Construction in Ice Infested Waters. Proceedings of the FIP/CPCI Symposia, Calgary, Canada. Vol. 2, pp. 31-40.

Brackel, J., and Oostlander, L.J., 1979. Concentrated

Loading on a Thick Walled Concrete Cylinder. Proceedings, 2nd International Conference on Behavior of Off-Shore Structures, London, England, pp. 299-308.

Bresler, B., and Gilbert, P.H., 1961. Tie Requirements for Reinforced Concrete Columns. ACI Journal, Vol. 58, No. 5. Nov. pp. 555-569.

Brondiem-Nielsen, T. 1975. Optimum Design of Reinforced Concrete Shells and Slabs. Structural Research Laboratory, Technical University of Denmark, Copenhagen, Denmark. pp. 189-200.

Brown, I.C., and Perry, S.H., 1979. Transverse Impact on Beams and Slabs. Proceedings, 2nd International Conference on Behavior of Off-Shore Structures, London, England, pp. 357-368.

Brown, T.G., Kocaman, A., Punj, V., and Bercha, F.G., 1986. Iceberg-Structure Interaction: Global and Local Loads, Proceedings of the Fifth International Symposium on Offshore Mechanics and Arctic Experiences, Tokyo, Japan, April.

Bruen, F.J., Byrd, R.C., Vivatrat, V. and Watt, B.J., 1982. Selection of Local Ice Pressures for Arctic Systems. Proceedings of the Offshore Technology Conference,

Houston, Texas, Vol. 3, pp. 417-435.

CAN3 A23.2-M77, 1977. Methods of Test for Concrete. National Standard of Canada, Canadian Standards Association, Rexdale, Ontario.

CAN3 A23.3-M84, 1984. Design of Concrete Structures for Buildings. National Standard of Canada, Canadian Standards Association, Rexdale, Ontario.

CAN3 G40.21-M81. 1981. Structural Quality Steels. 1981. National Standard of Canada, Canadian Standards Association, Rexdale, Ontario.

CEB-FIP, 1978. Model Code for Concrete Structures. CEB-FIP International Recommendations, Third Edition, Comite Euro-International du Beton, Paris. 384 pp.

Chen, W.F., 1982. Plasticity in Reinforced Concrete. McGraw-Hill Book Company, New York.

Clark, L.A., 1978. The Provision of Tension and Compression Reinforcement to Resist In-Plane Forces. Magazine of Conrete Research, Cement and Concrete Association, London, Vol. 28, No. 94, March, pp. 155-162.

Collins, M.P., Mitchell, D., 1986. A Rational Approach to

Shear Design - The 1984 Canadian Code Provisions. Proceedings, Journal of the ACI, 83(6), pp. 925-933.

Croasdale, K.R., 1984(a). Sea Ice Mechanics; A General Overview. Marine Technology Society Journal. Vol. 18, No. 1, pp. 8-16.

Croasdale, K.R., 1984(b). Ice Interaction with Structures: Recent Developments and Future Trends, Artic Technology Conference, Calgary, Alberta. September.

Deleuil, G., and Zaleski-Zamenhof, C.G., 1984. A Methodology of Evaluation of Iceberg Loads on Fixed Offshore Structures. Proceedings of the FIP/PCI Symposia, Calgary, Canada, Vol.2, August, pp. 54-58.

Det Norske Veritas. 1977 (1981). Rules for the Design, Construction, and Inspection of Offshore Structures. Oslo, Norway.

Drucker, D.C., 1961. On Structural Concrete and the Theorms of Limit Analysis. IABSE Proceedings. Vol. 21. pp. 49-59.

Ellis, R.M., 1985. Structural Design of Roller and Knife-Edge Supports. Manual of Lab Practice, I.F. Morrison Structures Laboratory, University of Alberta,

Edmonton, Canada.

Ellis, R.M., and Nelson, S.W., 1988. The Practical Importance of Computer Graphics for Efficient Engineering in the Design Office Environment. Proceedgings of the Third International Conference on Computing in Civil Engineering, Vancouver, B.C., August, pp. 157-166.

Elwi, A.A., and Murray, D.W., 1980. Nonlinear Analysis of Axisymmetric Reinforced Concrete Structures. Structural Engineering Report No. 87., Dept. of Civil Engineering, University of Alberta, Edmonton, Canada.

Federation Internation de la Precontraint, 1977. Recommendations for the Design and Construction of Concrete Sea Structures, 3rd Ed., FIP Commission on Concrete Sea Structure. FIP Administrative Offices, Slough, England.

Gerwick, B.C., Litton, R.W., and Reimer, R.B., 1981. Resistance of Concrete Walls to High Concentrated Ice Loads. Proceedings of the Offshore Technology Conference, Houston, Texas, Vol. 3, pp. 425-436.

Iding, R.H., Bresler, B., and Gerwick, B.C., 1985. Failure Modes in Concrete Structures due to Ice Loads.

Proceedings of the ASCE Conference Arctic '85, San Francisco, Ca., March, pp. 643-652.

Kemp, E.L., and Mukherjee, P.R., 1968. Inelastic Behaviour of Concrete Knee Joints. The Consulting Engineer, October, pp. 44-48.

Kupfer, H., 1964. Erweitesung des Morsch'schen Fachweskanalogie mit Hilfe des Prinzips vom Minimum des Formandesungsarbiet (Generalization of Morschs's Truss Analogy using the Principle of Minimum Strain Energy), Bulletin d'Information No.40. Comite Euro-International du Beton, Paris, January, pp.44-57.

Kupfer, H., and Gerstle, K., 1973. Behaviour of Concrete Under Biaxial Stresses, ASCE Journal of the Engineering Mechanics Division, Vol. 99, EM4, pp. 853-866.

Kupfer, H., Hilsdorf, H.K., and Rusch, H., 1969. Behaviour of Concrete Under Biaxial Stresses, ACI Journal, Vol. 66, No. 8, pp. 656-666.

Leonhardt, F., 1965. Reducing the Shear Reinforcement in Reinforced Concrete Beams and Slabs. Magazine of Conrete Research, Vol. 17, No. 53, December, 187 p.

MacGregor, J.G., Baskin, K.L., and Ellis, R.M., 1984. A

Review of Design Guidelines for Concrete Fixed Offshore Structures - A Canadian Perspective. CFER, Centre for Frontier Engineering Research Report 84-02, Edmonton, Alberta.

Marti, P., 1980. Zur Plastichen Berechnung von Stahlbeton, Dissertation No. 6602, ETH Zurich.

Marti, P., 1985.(a) Basic Tools for Reinforced Concrete Beam Design. ACI Journal, January/February, pp. 46-56.

Marti, P., 1985.(b) Plasticity in Reinforced Concrete, University of Toronto, CIV 1163 S Lecture notes.

Marti, P., 1987. Application of Plastic Analysis to Shear Design of Reinforced Concrete Members, University of Toronto, February (unpublished).

Matshishi, M., Nishimaki, K., Takeshita, H., and Iwata, S., 1977. On the Strength of New Composite SteelConcrete Material for Offshore Structure, Proceedings of OTC, Paper No. 2804, Houston, Texas, pp. 589-594.

Mellor, M., 1983. Mechanical Behaviour of Sea Ice. U.S. Army Cold Regions Research and Engineering Laboratory Monograph 83-1, Hanover, New Hampshire, June, 105 p.

Morsch, E., 1909. Concrete-Steel Construction. English Translation by E.P. Goodrich, McGraw-Hill Book Company, New York, 368 pp. (Translation from third edition of Der Eisenbetonbau, first edition, 1902).

Muller, P., 1978. Plastische Berechnung von Stahlbentonscheiben und-balken (Plastic Analysis of Reinforced Concrete Walls and Beams). Report No.83, Institute of Structural Engineering, ETH Zurich, 160 p.

Naaman, A.E., 1982. Optimum Design of Prestressed Concrete Tension Members. ASCE Journal of the Structural Division, Vol. 108, ST8, Aug., pp. 1722-1737.

Napoleao , J., and Kennedy, S., 1987. Unpublished Test Results from Detailed Tests on Concrete Cylinders. I.F. Morrison Structures Lab., University of Alberta.

Neilson, M.P., Braestrup, M.W., Jensen, B.C., and Finn Bach, 1978. Concrete Plasticity, Beam Shear-Shear in Joints-Punching Shear. Special Publication of the Danish Society for Structural Science and Engineering, Technical University of Denmark, Lyngby/Copenhagen, 1978.

Neilson, M.P., 1984. Limit Analysis and Concrete Plasticity, Prentice-Hall, New Jersey.

Nilson, I.H.E., 1973. Reinforced Concrete Corners and Joints Subjected to Bending Moment, Design of Corners and Joints in Frame Structures. Document D7:1973, National Swedish Building Research, Stockholm, Sweden.

O'Flynn, B., 1987. Composite Ice-Resisting Walls. Ph.D. Thesis, Department of Civil Engineering, University of Alberta, Edmonton, Alberta, 254 p.

Orangun, C.O., Jirsa, O., and Breen, J.E., 1977. A Reevaluation of Test Data on Development Length and Splices. ACI Journal, Proceedings, Vol. 74, No. 3, March, pp. 114-122, Discussion, pp. 470-475.

Pfister, J.F., 1964. Influence of Ties on the Behavior of Reinforced Concrete Columns. ACI Journal, Proceedings, Vol. 61, No. 5, March, pp. 521-537.

Ramirez, J., 1984. A Truss Analysis of the Shear and Torsional Strength of Beams. Ph.D. Thesis, University of Texas at Austin, 1984.

Ritter, W., 1899. Die Bauweise Hennebique, Schweizerische Bauzeitung, Zurich, February.

Robins, P.J., and Standish, I.G., 1982. Effect of Lateral Pressure on Bond of Reinforcing Bars in Concrete.

Proceedings of the International Conference on Bond in Concrete, Paisley, Scotland, June, pp. 262-272.

Rogowsky, D.M., MacGregor, J.G., 1983. Shear Strength of Deep Reinforced Concrete Continuous Beams, Structural Engineering Report No. 110, University of Alberta, Edmonton, Alberta, November.

Rogowsky, D.M., MacGregor, J.G., and Ong, S.Y., 1983. Tests of Reinforced Concrete Deep Beams. Structural Engineering Report No.109, Department of Civil Engineering, University of Alberta, Edmonton, Alberta.

Rogowsky, D.M. and MacGregor, J.G., 1986. The Design of Reinforced Concrete Deep Beams, Concrete International: Design and Construction, Vol. 8, No. 8, August, pp. 49-58.

Rusch, H., 1964. Uber die Grenzen der Anwendbarkeit der Fachwerkanalogie bei der Berechnung der Schubfesigkeit von Stahlbetonbalken (On the limitations of applicability of the truss analogy for the shear design of reinforced concrete beams). Festschrift F. Campus "Amici et Alumni", Universite de Liege.

Schlaich, J., Weischede, D., 1982. Ein praktisches Verfahren zum methodischen Bemsessen und Konstruieren im

Stahlbetonbau. (A practial method for the design and detailing of structural concrete). Bulletin d'Information No. 150. Comite Euro-International du Beton, Paris, March.

Schlaich, J., Schafer, K., and Jennewein, M., 1987. Towards a Consistent Design of Reinforeced and Prestressed Concrete, PCI Journal, May-June.

Slowski, S., and Vivatrat, V., 1983. Selection of Design Ice Pressures and Applications to Impact Load Prediction. Proceedings, POAC, Helsinki, Finland. Vol. 2, pp. 909-919.

Tepfers, R., 1973. A Theory of Bond Applied to Overlapped Tensile Reinforcement Splices for Deformed Bars. Division of Concrete Structures, Chalmers University of Technology, Goteborg, Sweden, Publication 73:2, 328 p.

Thurlimann, B., Marti, P., Pralong, J., Ritz, P. and Zimmerli, B., 1983. Anwendung der Plastizitaestheories auf Stahlbeton (Application of the Theory of Plasticity to Reinforced Concrete), Institute for Structural Engineering, ERH, Zurich, 252 pp.

Thurlimann, B., 1984. Plasticity Applied to Reinforced Concrete. Lecture Notes, Civ E 672, University of

Alberta. Oct. 1984.

Untrauer, R.E., and Henry, R.L., 1965. Influence of Normal Pressure on Bond Strength. ACI Journal, Vol. 62, pp. 577-585.

Vecchio, F.J., Collins, M.P., 1982. Response of Reinforced Concrete to In-Plane Shear and Normal Stresses, Publication No. 82-03, Department of Civil Engineering, University of Toronto, March.

Vivatrat, V. and Slowski, S., 1983. A Probabilistic Basis for Selecting Design Ice Pressures and Ice Loads for Arctic Offshore Structures. Proceedings of the Offshore Technology Conference, Houston, TX.. pp. 121-131.

Vos, C.J., and den Hertog, D., 1987. Ultimate Capacity of an Iceberg Loaded Gravity Base Structure. Proceedings IABSE Colloquium, Delft. pp. 425-435.

Watt, B.J., Ice Load Considerations for Concrete Structures, Proceedings of the FIP/CPCI Symposia, Calgary, Canada, Vol. 2, August, pp. 43-53.

Wheen, R.J., 1979. Prestressed Concrete Members in Direct Tension. ASCE Journal of the Structural Division. Vol. 105, No. ST7, July, pp. 1471-1487.

Willam, K.J., 1984. Experimental and Computational Aspects of Concrete Fracture. Proceedings of the International Conference on Computer-Aided Analysis and Design of Concrete Structures. Dejanic et al, Eds., Split, Yugoslavia. Part I, pp. 33-69.

Yee, A.A., Masuda, F.R., Kim, C.N., Doi, D.A. and Daly, L.A., 1984. Concrete Module for the Global Marine Concrete Island Drilling System. Proceedings of the FIP/CPCI Symposia, Calgary, Canada, Vol. 2, August, pp. 2330.

Zia, P., Preston, H.K., Scott, N.L., and Workman, E.B., 1979. Estimating Prestress Losses (ACI-ASCE Committee in Prestressed Concrete Recommended Procedure). Concrete International, Vol. 1, No. 6, June. pp. 32-38.

APPENDIX A LISTING OF COMPUTER PROGRAM FOR THE STATISTICAL ANALYSIS OF THE STEEL BEAM STRAINS

```
C     |---------------------------------------|
C     |             REED M. ELLIS             |
C     |       DEPT OF CIVIL ENGINEERING       |
C     |          REED'S STEEL BEAM            |
C     |         ----------------------        |
C     |             ASSISTED BY               |
C     |         PALANIMUTHU SUNDARARAJ        |
C     |---------------------------------------|
C
C
C
C                 12                1
C                  .....................
C                 |.....................|
C                           |   |
C                  11       |   |      2
C                     10 |  |   |  | 3
C                           |   |
C                           | ..|.........)......... Y
C                           | | |          MY
C                        9  | | |  | 4
C                           | | |
C                        8  | | |     5
C                  .........|.|.|.........
C                  |........|.|.|........|
C                           |
C                        7  |     6
C                           |  MZ
C                           |
C                           Z
C
C
C ************************************************************
C
C     GAUGES 13-24 : SIMILAR ARRANGEMENT
C
C ************************************************************
C             3 = STRAIN GAUGE LOCATIONS
C     FILES : 4 = PRE-GLIP FILE ( I.D.'S GAUGES 1-24 )
C             5 = .DO DATA
C             6 = INTERMEDIATE RESULTS
C             7 = END MOMENT CALCS
C             9 = OUTPUT
C
C ************************************************************
C
C
      DIMENSION NCON(24),DATA(150,110),DAT(150,110),TEMP(110)
      DIMENSION  Z1(12),  Y1(12), LOADN(25), S1(150,6), S2(150,6)
      DIMENSION  Z2(12),  Y2(12), ISTUFF(5), DISP(150,6),
     & DISPL(6),      PT1T(150),PT1B(150), PT2T(150), PT2B(150)
```

```
      REAL INER, INER2, LOAD
      REAL MY1,MY2,MZ1,MZ2
      CHARACTER TITLE*25
C
      CALL TIME(6,0,ISTUFF)
C
C     READ IN CROSS-LINKAGE DATA GIVING POSITIONS OF GAUGES
C     1-24 AND LOAD MAGNITUDES IN .DO FILE
C     ------------------------------------------------- C
C
      READ(4,101) TITLE
  101 FORMAT(A)
      PRINT*, TITLE
      READ(4,*,END=999)(NCON(I),I=1,24), NCONL, LCRW,LCRE,NOM1,NOM2,
     & NOM3,NOM4
C
C      NOM1 AND NOM2 ARE USED TO MANUALLY SELECT WHICH ONE OR
C      AT MOST TWO CHANNELS ARE TO BE OMITTED. THE DEFAULT IS
C      WHEN NOM1 IS  SPECIFIED AS -VE. THEN, THE PROGRAM
C      DECIDES WHICH CHANNEL TO OMIT BASED ON THE COEFF OF DETER.
C      NOM3 AND NOM4 ARE FOR END 2 (13-24).
C
 999  PRINT*,'NCON',NCON(1),NCON(24),'NCONL',NCONL,LCRW,LCRE,
     & NOM1,NOM2,NOM3,NOM4
C
C
      NUM1 = 0
      NUM2 = 0
C
C     READ IN LOAD ZERO VALUES
C     ----------------------- C
      READ(5,*)NOM,NGAUGE,NLOAD,ND1,ND2,ND3,NT,NT,NT
   1  FORMAT(13X,I3,5X,I3,6(6X,I2))
C
C     READ IN FAKE .DO FILE ( IF SPECIFIED BY ND1=-1 )
C     ------------------------------------------------ C
      PRINT*, 'NGAUGE',NGAUGE,'NLOAD',NLOAD
C
        IF(NOM.EQ.-1.OR.NOM.EQ.-9) THEN
        READ(5,*)(LOADN(K),K=1,NLOAD)
        DO 11 I=1,NLOAD
           READ(5,*)(DAT(I,J),J=1,NGAUGE)
           DO 12 J=1,24
              DAT(I,J)=DAT(I,J)*1E-6
 12        CONTINUE
 11     CONTINUE
C
C            READ DISPLACEMENTS FOR B TYPE
C
      DO 121 J=1,6
 121   READ(5,*) (DISP(I,J), I=1,NLOAD)
C
C
C           READ ECCENTRICITIES
      READ(4,*) E1,E2
```

```
C
         GO TO 888
      ENDIF
C
C
      READ(5,2)(TEMP(I),I=1,NGAUGE)
   2  FORMAT(21(2X,5(E13.6,2X)/))
C
C     READ IN ALL READINGS AT ALL LOAD STEPS FROM .DO FORMAT
C     ------------------------------------------------------ C
      DO 10 I=1,NLOAD
         READ(5,*)DUMMY
         READ(5,2)(DAT(I,J),J=1,NGAUGE)
  10  CONTINUE
C
C     PUT STRAIN GAUGES 1-24 IN DATA ( AS PER PRE-GLIP FILE # 4 )
C         AND CONVERT MICROSTRAIN READINGS INTO STRESS(MPa)
C     ------------------------------------------------------------ C
 888  DO 20 I=1,NLOAD
         DO 30 J=1,24
            DATA(I,J)=DAT(I,NCON(J))*200000
   30    CONTINUE
   20 CONTINUE
C
C
C     READ IN X-SECT. AREA, Iy (INER), Iz (INER2)
C     ------------------------------------------- C
      READ(3,*) AREA, INER, INER2
C
C
C
         PRINT*, 'AREA',AREA,INER,INER2
C
C
C
C
C
C     Z-COORD OF STRAIN GAUGES
C     ------------------------ C
      READ(3,*)(Z1(II), II=1,12)
      READ(3,*)(Z2(II), II=1,12)
C
C
C     Y-COORD OF STRAIN GAUGES
C     ------------------------ C
      READ(3,*)(Y1(II), II=1,12)
      READ(3,*)(Y2(II), II=1,12)
C
C
C     PRINT HEADINGS
C     ------------- C
C
      WRITE(9,89) TITLE, (ISTUFF(I),I=3,5), (ISTUFF(I),I=1,2)
   89 FORMAT('1',10X,A25,2X,
     +'ANALYSIS OF STEEL BEAM STRAINS   DATE: ',3A4,
```

```
     + 4X,'TIME: ',2A4,///)
C
          IF(NOM1.LT.0) THEN
          WRITE(9,87)
  87  FORMAT(40X,'CHANNELS AUTOMATICALLY DELETED'//)
          ELSE
          WRITE(9,88) NOM1,NOM2,NOM3,NOM4
  88  FORMAT(40X,'CHANNELS MANUALLY DELETED : ',2I2,' AND ',2I2//)
          ENDIF
C
      WRITE(9,90)
 90   FORMAT(35X,'END 1',41X,'END2'/)
      WRITE(9,91)
 91   FORMAT(4X,'#',3X,'LOAD(KN)',5X,'P(KN)',5X,'MY(KNm)',
     +3X,'MZ(KNm)',2X,'OMIT',3X,'R',
     +11X,'P(KN)',5X,'MY(KNm)',3X,'MZ(KNm)',
     +2X,'OMIT',3X,'R')
      WRITE(9,92)
 92   FORMAT(3X,'--',3X,'--------',5X,'------',4X,'-----',
     +'--',3X,'-------',2X,'----',2X,'-----',
     +8X,'-----',5X,'-------',3X,'-------',
     +2X,'----',2X,'-----'/)
C
C
C
      WRITE(7,789) TITLE,(ISTUFF(I),I=3,5), (ISTUFF(I),I=1,2)
 789  FORMAT('1',10X,A25,2X,'ANALYSIS FOR ARCH ENDS   DATE: ',3A4,
     + 4X,'TIME: ',2A4,//)
      WRITE(7,7895) E1,E2
7895  FORMAT('USING ',2F5.3)
      WRITE(7,790)
790   FORMAT(45X,'WEST',31X,'EAST',25X,'CLOSURE'/)
      WRITE(7,791)
791   FORMAT(4X,'#',3X,'Load(KN)',4X,'Rwest',3X,' Reast ',
     +2X,'Po (KN)',1X,'Mo (KNm)',3X,'Vo (KN)',
     +10X,'Po (KN)',2X,'Mo (KNm)',2X,'Vo (KN)',
     +3X,'Vert %',1X,'Horiz %',3X,'Mom %')
      WRITE(7,792)
792   FORMAT(3X,'--',3X,'--------',3X,'------',3X,'------',
     +3X,'-------',2X,'--------',3X,'------',
     +10X,'------',3X,'-------',3X,'-------',3X,'-----',2X,
     +'------',4X,'------'/)
C
C
      DO 1000 K=1,NLOAD
C
C
      N12 = 12
        PRINT*, ' '
        PRINT*, 'ECHO CHECK FOR LOAD = ', DAT(K,NCONL)
         DO 1001 MM=1,N12
 1001       PRINT*, MM, DATA(K,MM),Z1(MM),Y1(MM)
         DO 1002 MM=1,N12
 1002       PRINT*, DATA(K,MM+12),Z2(MM),Y2(MM)
        PRINT*, ' '
```

```
C
      LOAD = ABS( DAT(K,NCONL) )
C
C     MAIN AXIS BENDING ( MY ) AND AXIAL FORCE ( P ) CALC
C       AND MZ,   BY REGRESSION PLANE.
C     ------------------------------------------------- C
C     REGRESSION AND CALC
C     ------------------ C
      DO 905 II=1,12
  905   TEMP(II)=DATA(K,II)
C
      CALL COEFF(12,Y1,Z1,TEMP,A,B,C,RY1,NOM1,NOM2)
C
C
      IF (NOM1.LT.0) THEN
C
      IF(ABS(RY1).LT.0.99) CALL DROP(12,Y1,Z1,TEMP,A,B,C,RY1,NUM1)
      ENDIF
C
      C1 = C
      B1 = B
C
C
C     AREA = BEAM X-SECTIONAL AREA  ************************
C     INER = MOMENT OF INERTIA OF BEAM  ********************
C     INER2 = WEAK AXIS " " "           ********************
C
      P1 =  C * AREA      *1E-3
      MZ1 = A * INER2     *1E-6
      MY1 = B * INER      *1E-6
C
       PRINT*,'END1 A  ',A,' B  ',B, 'C  ',C, 'RY1= ',RY1
         PRINT*, LOAD,P1,MY1,MZ1
C
C              AND NOW FOR END 2 , GAUGES 13 - 24
C
      DO 906 II=13,24
  906   TEMP(II-12)=DATA(K,II)
C
      CALL COEFF(12,Y2,Z2,TEMP,A,B,C,RY2,NOM3,NOM4)
C
      IF (NOM1.LT.0) THEN
C
      IF(ABS(RY2).LT.0.99) CALL DROP(12,Y2,Z2,TEMP,A,B,C,RY2,NUM2)
      ENDIF
C
      C2 = C
      B2 = B
C
      P2 =  C*AREA     *1E-3
      MZ2 = A*INER2    *1E-6
      MY2 = B*INER     *1E-6
C
C
      RWEST = ABS( DAT(K,LCRW) )
```

```
      REAST = ABS( DAT(K,LCRE) )
      SUM = RWEST + REAST
C
C
        PRINT*,'END2 A= ',A,'B= ',B,'C= ',C, 'RY2= ',RY2
        PRINT*, LOAD,P2,MY2,MZ2
C
C      GENERATE PAIRS FOR PLOTTING
       N1 = NLOAD + 1
      IF(K.EQ.1) WRITE(8,870) N1
  870 FORMAT(/1X,'LOAD VS REACTIONS',
     & /,' 0.0 100.0 1200.0 8.0',
     & /,' 0.0 100.0 1200.0 5.0',
     & /I4,' 0 0 0 0 .075',
     & / ' 0.0,    0.0')
       WRITE(8,880) LOAD, SUM
  880 FORMAT(F10.2,', 'F10.2)
C
      PT1T(K) = -275.*B1 + C1
      PT1B(K) =  275.*B1 + C1
      PT2T(K) = -275.*B2 + C2
      PT2B(K) =  275.*B2 + C2
C
C
C       CALL TO END-MOMENT CALCS
C       use ave. P
C
      PO = (P1+P2)/2.
C
      P1 = PO
      P2 = PO
C
C     ALSO LET THE LOAD = SUM OF REACTIONS
C           REVISE THE LOAD TO SUM TO THE REACTIONS
C           IF NOT ALREADY DONE SO IN THE .DO FILE
C
      LOAD = SUM
C
      IT = 1
        IF(NOM.EQ.-1.OR.NOM.EQ.-9) THEN
C
       DO 111 JJ=1,6
  111  DISPL(JJ) = DISP(K,JJ)
C
      IT = 2
C     USE FIRST ONE FOR B2.1 WHICH WAS REVERSED
       IF(NOM.EQ.-9) THEN
       CALL ENDMOM(IT,LOADN(K),LOAD,RWEST,REAST,
     & P2,MY2,P1,MY1,E1,E2,DISPL)
       ELSE
       CALL ENDMOM(IT,LOADN(K),LOAD,RWEST,REAST,
     & P1,MY1,P2,MY2,E1,E2,DISPL)
       ENDIF
       ELSE
       CALL ENDMOM(IT,K,LOAD,RWEST,REAST,P1,MY1,P2,MY2,E1,E2,DISPL)
```

```
      ENDIF
C
C      WRITE RESULTS TO FILE 9
C
      IF (NOM1.LT.0) THEN
C
        IF(NOM.EQ.-1.OR.NOM.EQ.-9) THEN
      WRITE(9,100)LOADN(K),LOAD,P1,MY1,MZ1,NUM1,RY1,P2,
     + MY2,MZ2,NUM2,RY2
      ELSE
C
      WRITE(9,100)K,LOAD,P1,MY1,MZ1,NUM1,RY1,P2,MY2,MZ2,NUM2,
     + RY2
  100 FORMAT(2X,I3,2X,F8.2,2X,2(3(1X,F9.3),2X,I3,4X,F5.3,4X))
C
      ENDIF
C
      ELSE
C
        IF(NOM.EQ.-1.OR.NOM.EQ.-9) THEN
      WRITE(9,102)LOADN(K),LOAD,P1,MY1,MZ1,NOM1,NOM2,RY1,P2,
     + MY2,MZ2,NOM3,NOM4,RY2
      ELSE
C
      WRITE(9,102)K,LOAD,P1,MY1,MZ1,NOM1,NOM2,RY1,P2,MY2,MZ2,
     + NOM3,NOM4,RY2
  102 FORMAT(2X,I3,2X,F8.2,2X,2(3(1X,F9.3),1X,2I2,4X,F5.3,4X))
C
C
      ENDIF
C
      ENDIF
C
 1000 CONTINUE
C
      WRITE(8,887)
       DO 2000 K=1,NLOAD
C
C      GENERATE MORE PAIRS FOR PLOTTING
C
      LOAD = ABS( DAT(K,NCONL) )
      LEND = 1
      WRITE(8,875) LOAD, LEND
  875 FORMAT(1X,'STRESS PROFILES FOR LOAD = ',F8.2,' END ',I3,
     & /,'-50.0  10.0 50.0 5.0',
     & /,' 275.0 25.0 -275. 8.0',
     & /,'  12 1 0 0 0 .075')
      DO 2500 L=1,12
       WRITE(8,885) DATA(K,L), Z1(L)
  885 FORMAT(F9.3,', 'F7.1)
 2500 CONTINUE
      WRITE(8,886)
  886 FORMAT(1X,' 2 0 0 0 0 .075 ')
       WRITE(8,885) PT1T(K), Z1(1)
       WRITE(8,885) PT1B(K), Z1(6)
```

```
C     WRITE(8,887)
  887 FORMAT(' ')
C
C
      LEND = 2
      WRITE(8,876)
  876 FORMAT(1X,'  12 1 0 0 0 .075')
      DO 3000 L=1,12
       WRITE(8,885) DATA(K,L+12), Z2(L)
 3000 CONTINUE
      WRITE(8,886)
       WRITE(8,885)  PT2T(K), Z2(1)
       WRITE(8,885)  PT2B(K), Z2(6)
      WRITE(8,887)
 2000 CONTINUE
C
C
      STOP
      END
C
C     STATISTICS SUMMATIONS
C     -------------------- C
C
      SUBROUTINE  COEFF(N,X,Y,Z,A,B,C,R,NOMA,NOMB)
C
C
      DIMENSION X(12), Y(12), Z(12)
C
      A=0.
      B=0.
      C=0.
      SX=0.
      SY=0.
      SZ=0.
      SXS=0.
      SYS=0.
      SZS=0.
      SXY=0.
      SXZ=0.
      SYZ=0.
      ICOUNT = 0
C
      IF(NOMA.GT.0) THEN
      DO 12 KK=1,12
      IF(KK.EQ.NOMA) GOTO 12
      IF(KK.EQ.NOMB) GOTO 12
         SX=SX+X(KK)
         SY=SY+Y(KK)
         SZ=SZ+Z(KK)
         SXS=SXS+X(KK)**2
         SYS=SYS+Y(KK)**2
         SZS=SZS+Z(KK)**2
         SXY=SXY+Y(KK)*X(KK)
         SXZ=SXZ+X(KK)*Z(KK)
         SYZ=SYZ+Y(KK)*Z(KK)
```

```
          ICOUNT = ICOUNT + 1
       12 CONTINUE
          NP = ICOUNT
          GOTO 13
          ELSE
          NP = N
          DO 1 J=1,N
             SX=SX+X(J)
             SY=SY+Y(J)
             SZ=SZ+Z(J)
             SXS=SXS+X(J)**2
             SYS=SYS+Y(J)**2
             SZS=SZS+Z(J)**2
             SXY=SXY+Y(J)*X(J)
             SXZ=SXZ+X(J)*Z(J)
             SYZ=SYZ+Y(J)*Z(J)
C
C            PRINT*, J, '  X= ',X(J),' Y= ',Y(J),' Z= ',Z(J)
C
C
       1     CONTINUE
          ENDIF
C
C         LINEAR REGRESSION :   Z =  AX + BY + C
C       IN THIS CASE WE ARE ACTUALLY SOLVING STRESS = AY +BZ +C
C
       13  D = 0.0
          D1 = 0.0
          D2 = 0.0
          D3 = 0.0
C
          D = SXS*(NP*SYS - SY**2) - NP*SXY**2 + 2*SX*SY*SXY - SYS*SX**2
C
C         A= Y-SLOPE ;   B=Z-SLOPE ; C = INT ;   R=CORR. COEFF. ;
C
          D1 = NP*SXZ*SYS - SXZ*SY**2- NP*SXY*SYZ + SXY*SY*SZ + SX*SYZ*SY
         &      - SX*SYS*SZ
          D2 = SXS*(NP*SYZ - SY*SZ) - SXZ*(NP*SXY - SX*SY)
         &      + SX*(SXY*SZ - SYZ*SX)
          D3 = SXS*(SYS*SZ - SYZ*SY) - SXY*(SXY*SZ - SYZ*SX)
         &      + SXZ*(SXY*SY - SX*SYS)
          A = D1/D
          B = D2/D
          C = D3/D
          R = ( NP * SYZ - SY*SZ )/ SQRT( (NP*SYS-SY**2)*(NP*SZS -SZ**2) )
C
           PRINT*, 'NP  SX SY SZ SXS SYS SZS SXY SXZ SYZ D D1 D2 D3 R'
           PRINT*, NP,SX,SY,SZ,SXS,SYS,SZS,SXY,SXZ,SYZ,D,D1,D2,D3,R
C
C
C                 R IS THE COEFF. OF DETERMINATION BETWEEN THE
C                 STRAIN AND THE Z POSN ON THE BEAM = A MEASURE
C                 OF THE ACCURACY OF MY.
C
C
```

```
C
      SIGAVE = SZ/NP
      PRINT*, '**** AVE STRESS = ',SIGAVE
      PRINT*, '**** BASED ON ',NP,' VALUES'
      RETURN
      END
C
C
C
C     DROP :   A SUBROUTINE TO CHECK IF DROPPING ANY 1 OF
C              THE 12 STRAIN POINTS IMPROVES CORR.COEFF.(R)
C     ------------------------------------------------- C
C        INITIALLY, R is less than 0.99
C
      SUBROUTINE DROP( N,X,Y,Z,A,B,C,R, NUM)
C
C   X IS THE Y POSN, Y IS THE Z POSN, Z IS THE STRESS.
C
      DIMENSION X(12), Y(12), Z(12)
      NOMA = 0
      NOMB = 0
      NUM=0
      DO 1 I=1,N
         TEMPX=X(I)
         TEMPY=Y(I)
         TEMPZ=Z(I)
         X(I)=X(N)
         Y(I)=Y(N)
         Z(I)=Z(N)
         X(N)=TEMPX
         Y(N)=TEMPY
         Z(N)=TEMPZ
C
       CALL COEFF(11,X,Y,Z,AN,BN,CN,RYN,NOMA,NOMB)
C
C     IF(I.EQ.4) THEN
C         PRINT*,'** I=4 **  ',AN,BN,CN,RYN
C         PRINT*,' X Y Z OMIT',N,X(N), Y(N), Z(N)
C         PRINT*,' X Y Z  N  ',I,X(I), Y(I), Z(I)
C     ENDIF
         IF(ABS(RYN).GT.ABS(R)) THEN
            NUM=I
            A=AN
            B=BN
            C=CN
            R=RYN
         ENDIF
         TEMPX=X(I)
         TEMPY=Y(I)
         TEMPZ=Z(I)
         X(I)=X(N)
         Y(I)=Y(N)
         Z(I)=Z(N)
         X(N)=TEMPX
         Y(N)=TEMPY
```

```
        Z(N)=TEMPZ
C
C
C
C
 1    CONTINUE
      RETURN
      END
C
      SUBROUTINE ENDMOM(ITYPE,K,LOAD,RWEST,REAST,
     & P1,MY1,P2,MY2,E1,E2,DISPL)
      REAL MOM, MOW, MOE, LOAD, MY1, MY2
      DIMENSION DISPL(6)
C
C   CALCULATES THE END MOMENTS, SHEARS, AXIAL FORCES
C   AT THE ENDS OF THE SPECIMENS FROM THE STEEL
C   BEAM END FORCES. EVALUATES CLOSURE
C   BY CHECKING EQUILIBRIUM. ASSUMES END1
C   OF THE STEEL BEAM IS AT THE EAST END.
C
C   WEST END
C
      IF(ITYPE.EQ.2) THEN
C
C      B-SERIES
C
      V1= (MY1-MY2)/0.5
      V2 = V1
      MOW =  -RWEST*E1 -V2*0.956 + MY2 + P2*0.444
      POW = (P2-V2)/1.41421
      VOW = RWEST - (P2+V2)/1.41421
C
C    EAST END
C
C
      MOE =  REAST*E2 + V1*0.956 + MY1 + P1*0.444
      POE =  REAST + (V1+P1)/1.41421
      VOE =  (V1-P1)/1.41421
C
C      CHECK CLOSURE BY EQUILIBRIUM ON SPECIMEN PART ONLY
C
C     CALL DEFL(DISPL,LOAD,V,STATIC)
C
      STATIC =  LOAD/4.*(0.475 + 0.675 + 0.875 + 1.075)
      VERT = (VOW + POE -LOAD)*100./LOAD
      HORIZ = (POW + VOE)*100./LOAD
      DIFF = STATIC - POE*1.7 + MOE - MOW - VOE*1.7
      CORR = DIFF
      EPER = MOE/(MOE - MOW)
      WPER = MOW/(MOE - MOW)
C
C
C   PROPORTION ERROR IN MOMENT TO EACH END
C
C
```

```
      MOE = MOE - ABS(EPER)*CORR
      MOW = MOW + ABS(WPER)*CORR
      DIFF = STATIC - POE*1.7 + MOE - MOW - VOE*1.7
      MOM = DIFF * 100./STATIC
C
      ELSE
C
C     TYPE 1 SPECIMENS
C
      E1 = 0.444
      E2 = E1
      V1= (MY1-MY2)/0.5
      V2 = V1
      MOW =  -RWEST*E1 -V2*0.956 + MY2 + P2*0.444
      POW = (RWEST+P2-V2)/1.41421
      VOW = (RWEST-P2-V2)/1.41421
C
C     EAST END
C
C
      MOE =  -REAST*E2 + V1*0.956 + MY1 + P1*0.444
      POE =  (REAST+V1+P1)/1.41421
      VOE =  (REAST+V1-P1)/1.41421
C
C      CHECK CLOSURE BY EQUILIBRIUM
C
      VERT = ( (VOW+POW+VOE+POE)/1.41421-LOAD )*100./LOAD
      HORIZ = (POW-VOW+VOE-POE)*100./(1.41421*LOAD)
      MOM = (LOAD*1.206 - POE*1.7 -VOE*1.7
     & + MOE - MOW)*100./(LOAD*1.206)
C
C
      ENDIF
C
C     PRINT*, '**********',LOAD,RWEST,REAST
      WRITE(7,100)K,LOAD,RWEST,REAST,POW,MOW,VOW,
     + POE,MOE,VOE,VERT,HORIZ,MOM
 100  FORMAT(2X,I3,2X,6(1X,F8.2),9X,6(1X,F8.2))
C
      RETURN
      END
C
C
C
      SUBROUTINE DEFL(DISPL,LOAD,V,STATIC)
C
      DIMENSION D(5), H1(50),V1(50), THETA(5), DISPL(6)
      REAL LOAD
      DATA D / 325., 3*200., 325./
C
C      SUBROUTINE TO PERFORM EQUILIBRIUM CHECK ON
C               DISPLACED GEOMETRY
C
C
      H = 0.
```

```
      V = 0.
      STATIC = 0.
      DO 10 I=1,5
      THETA(I) = ATAN( ( DISPL(I) - DISPL(I+1) )/D(I) )
10    PRINT*, DISPL(I), DISPL(I+1), THETA(I)
      DO 20 I=1,4
      V1(I) = LOAD/4. * COS( ( THETA(I) + THETA(I+1) )/2. )
      H1(I) = LOAD/4. * SIN( ( THETA(I) + THETA(I+1) )/2. )
      PRINT*, V1(I), H1(I)
      H = H + H1(I)
20    V = V + V1(I)
      STATIC =  V1(1)*0.475 +V1(2)*.675+V1(3)*.875+V1(4)*1.075
     & + H*1.94
      PRINT*, ' '
      PRINT*, 'LOAD ',LOAD,' V ',V,' H ',H
      PRINT*, ' '
      RETURN
      END
```

APPENDIX B COMPUTER PROGRAM "FANS" FOR ANALYSIS OF FAN STRESS FIELDS

```
C   PROGRAM FANS
C_____________________________
C
C                    F  A  N  S
C                   ___________
C
C        to evaluate the stress components
C        on curved and linear surfaces due to
C        hyperbolic fan stress fields.
C        For any surface or group of surfaces.
C        It assumes that the horizontal surface
C         has the uniform pressure
C
C
C
C
C
C
C             BY R. M. ELLIS
C             DEPT. OF CIVIL ENGINEERING
C             UNIVERSITY OF ALBERTA
C             1987/1988
C             VERSION 1.1 SPRING 1988
C
C          CHANNEL  5= -- INPUT FILE
C          CHANNEL  6= -- OUTPUT FILE
C
C          PLOTTING TO FILE, SEE PLOT88 MANUAL
C
      COMMON/FP/EU(35),ZETA(35),ETA(35),TANB(35),BETA(35),DBETA(35),
     +          THETA(35),DTHETA(35),RHOU(35),HRHOU(35),SIG1U(35),
     +          RX(35),HRX(35),EL(35),GAMA(35),DGAMA(35),
     +          RHOL(35),HRHOL(35),SIG1L(35),PP(35),TP(35),
     +          DELRHO(35),TAOU(35), HSUM(35), VSUM(35), HTERM1(35),
     +          HTERM2(35),HTERM3(35), VTERM1(35),VTERM2(35),VTERM3(35),
     +          DELG(35),RADF(35),TANF(35),ALPHA(35),DALPHA(35),
     +          P,FC,FCOP1,RW0,H,EUA,EUB,W0,ZETAA,ZETAB,ETAA,
     +          ICOL,NTYPE,BOND(35),NORM(35),W(35),ITITLE,
     +          X0(35),Y0(35),XPTN(35),XPTB(35),YPTN(35),YPTB(35),SCALE
C
C
      DIMENSION  EFAN(35),ZFAN(35),YFAN(35),BARX(21),BARY(21)
      REAL NFAN(35)
C
      REAL L,LO2,NL(35),NLMAX,N(35),NORM
C
      CHARACTER*1 IANS,IY
      CHARACTER*30 ITITLE
C
      REV = 1.2
C           REVISED CONVENTION FOR PLOTTING STRESSES
```

```
C
C
      CALL GETDAT(IYR,IMON,IDAY)
      CALL GETTIM(IHR,IMIN,ISEC,IDUM)
C
      PI = 3.141592654
C
      OPEN(5, FILE= ' ')
      OPEN(6, FILE= ' ')
C
      WRITE(*,2500) IHR,IMIN,ISEC,IYR,IMON,IDAY,REV
      WRITE(6,2500) IHR,IMIN,ISEC,IYR,IMON,IDAY,REV
 2500 FORMAT(/27X,'   F  A  N  S ',
     * //19X,'ANALYSIS OF FAN STRESS FIELDS',
     * //,10X, 'TIME OF RUN  : ',I2.2,':',I2.2,
     *':',I2.2,5X,'DATE : ',
     *I4,' ',I2.2,' ',I2.2, //25X,'VERSION  :',F4.1//)
C
      WRITE(6,*) ' '
C
       READ(5,'(A30)' ) ITITLE
       READ(5,*) HOB,VOB,FC,H
       READ(5,*) PSCALE
       READ(5,*) FACTN,SCALEN
       READ(5,*) FACTB,SCALEB
C
C   READ  RADIUS AND DISTANCE TO START OF CIRCULAR ARC '
C
       READ(5,*)  R,X1
C
       READ(5,*)  IOPORT,MODEL
C
   5  WRITE(*,*)  'CHOOSE TYPE OF SURFACE : '
      WRITE(*,*)  '       1 = HORIZONTAL SURFACE ONLY '
      WRITE(*,*)  '       2 = COMBINED SURFACES '
      WRITE(*,*)  '    -ve = STOP '
C
       READ(*,*)  NTYPE
C
      IF(NTYPE.LT.0) GO TO 999
C
      WRITE(*,*)  'ENTER LENGTH OF FAN   L/2 '
      WRITE(*,*)  '    - VE = STOP '
       READ(*,*)  LO2
C
      IF(LO2.LT.0.1) GO TO 999
C
C    INITIALIZE PLOTTING DEVICE
C
C     IOPORT = 97
C     MODEL =  97
C
C
      L = 2. * LO2
C
```

```
      FX = 0.0
      FY = 0.0
C
      P = VOB/L
      FCOP1 = FC/P -1.
      H1 = HOB/FC
      H1OH = HOB/FC/H
      RH1OH = 1. - H1OH
      S = ( (H-H1/2.)*HOB/VOB  + VOB/2./FC - LO2 )/ ( H - H1 )
      DBETAA = ATAN2(1.,S) * 180./PI
      ZETAA = S*RH1OH/FCOP1
      W0 = 1. - RH1OH*SQRT( 1. - S**2/(FCOP1)  )
      RW0 = 1. - W0
      VAR = W0 * (2.- W0)/FCOP1
      ZETAB = SQRT( VAR )
C
       CALL HYPER(FCOP1,RW0,ZETAA,ETAA)
C
       CALL HYPER(FCOP1,RW0,ZETAB,ETAB)
C
      HOR = ( ZETAB - ZETAA )
      VDIFF = HOR - VOB/FC/H
      VDIFF = VDIFF * 100.
C
C     EVALUATE TOP SURFACE PARAMETERS AND E INCREMENT
C
      EUB = ZETAB * FC / P
      EUA = ZETAA * FC / P
      TANBB = ( RW0 + ETAB )/( EUB - ZETAB )
      BETAB = ATAN(TANBB)
      DBETAB = BETAB * 180./PI
C
      WRITE(6,*) ' '
      WRITE(6,'(A30)' )  ITITLE
      WRITE(6,*) ' '
      WRITE(6,'(2(A9,F8.3))') ' H/b =   ',HOB,'  V/b =  ',VOB
      WRITE(6,'(A9,F8.3)')  ' Fc  =   ',FC, ' h   =   ',H
      WRITE(6,'(A15,F8.3)') 'FAN HALF-LENGTH = ',LO2
      WRITE(6,'(A15,F8.3)') ' FAN LENGTH  = ',L
      WRITE(6,'(A14,F8.3)') ' Radius   R  = ',R
      WRITE(6,'(A14,F8.3)') ' Distance X1 = ',X1
      WRITE(6,'(A21,F8.3)') ' UNIFORM STRESS P  = ', P
C
      WRITE(6,*) ' '
      WRITE(6,'(A16,F8.3)')  ' PLOT SCALE   = ', PSCALE
      WRITE(6,'(A18,2F8.3)') ' FACTN , SCALEN = ', FACTN,SCALEN
      WRITE(6,'(A18,2F8.3)') ' FACTB , SCALEB = ', FACTB,SCALEB
      WRITE(6,'(A18,2I4)') ' IOPORT, MODEL  = ', IOPORT,MODEL
C
      WRITE(6,*) ' '
      WRITE(6,'(A21,F8.3)') ' UNIFORM STRESS P  = ', P
      WRITE(6,'(A14,F10.7)') ' FC/P - 1    = ',FCOP1
      WRITE(6,'(A14,F10.7)') ' 1 - H1/H    = ',RH1OH
      WRITE(6,'(A14,F10.7)') ' Slope S     = ',S
      WRITE(6,'(A14,F10.7)') ' Angle BETAA = ',DBETAA
```

```
      WRITE(6,'(A14,F10.7)') ' Angle BETAB = ',DBETAB
      WRITE(6,'(A14,F10.7)') ' ZETA A      = ',ZETAA
      WRITE(6,'(A14,F10.7)') ' ETA A       = ',ETAA
      WRITE(6,'(A14,F10.7)') ' ZETA B      = ',ZETAB
      WRITE(6,'(A14,F10.7)') ' ETA B       = ',ETAB
      WRITE(6,'(A14,F10.7)') ' W0          = ',W0
      WRITE(6,'(A14,F10.7)') ' EUA         = ',EUA
      WRITE(6,'(A14,F10.7)') ' EUB         = ',EUB
      WRITE(6,'(A14,F10.7)') ' HORIZ DIFF % = ',HDIFF
      WRITE(6,'(A14,F10.7)') ' VERT  DIFF % = ',VDIFF
C
C
      IJ = 0
C
      CALL IPLOT(H,PSCALE,SCALE,IOPORT,MODEL)
C
       SFACTN = SCALE / ( SCALEN * 25.4 )
       SFACTB = SCALE / ( SCALEB * 25.4 )
C
C
      IF(NTYPE.EQ.1) THEN
      ICASE = 1
      NINC = 10
      EINC1 = (EUB-EUA)/NINC
      GO TO 10
      ELSEIF(NTYPE.NE.2) THEN
      WRITE(6,*)'**** ERROR **** INCORRECT TYPE OF SURFACE  =  ', NTYPE
      WRITE(6,*) ' '
      ENDIF
C
      EC1 = X1/H + ZETAA
C
      RS = R/H
      X2 = X1 + R
      EC2 = EC1 + RS
C
      IF(EUA.LT.EC1) THEN
C
C   CASE I ; COMBINED, BUT BEGINS ON HORIZONTAL SURFACE
C
      NINC = 10
C     NINC = 5
      EINC1 = ( EC1 - EUA )/NINC
C
      ELSE
C
C   CASE II ; BEGINS ON CIRCULAR SURFACE
C
      GOTO 20
      ENDIF
C
C
C ***************************************************************************
C     HORIZONTAL SURFACE
C ***************************************************************************
```

```
C
  10  CONTINUE
C
C             INITIALIZE  IN CASE PLOTS ARE REQUESTED
C
      CALL IPLOT(H,PSCALE,SCALE,IOPORT,MODEL)
C
C
      ISKIP = 1
      IF(NTYPE.NE.1) ISKIP = 2
C
      ICOL = 14
      ICOUNT = NINC + 1
C
      DO 50 I=1,ICOUNT
C
      EU(I) = EUA + EINC1 * (I-1)
C
      ZETA(I) = EU(I) * P / FC
      CALL HYPER(FCOP1,RW0,ZETA(I),ETA(I))
      TANB(I) = ( RW0 + ETA(I) )/( EU(I) - ZETA(I) )
      BETA(I) = ATAN(TANB(I))
      DBETA(I) = ATAN(TANB(I)) * 180./PI
      THETA(I) = PI/2. - BETA(I)
      DTHETA(I) = 90. - DBETA(I)
      RHOU(I) = SQRT( (EU(I) - ZETA(I))**2 + ( RW0 + ETA(I) )**2 )
      HRHOU(I) = RHOU(I) * H
C
C     EVALUATE PRINCIPAL STRESS SIG1U
C
       SIG1U(I) = 2. * P  / ( 1. + COS(2. * THETA(I)) )
C
C     EVALUATE THE SHEAR STRESS THAT GOES WITH P
C
       TAOU(I) = P * TAN( THETA(I) )
C
C
      RX(I) = SIG1U(I) * RHOU(I) / ( FC - SIG1U(I) )
      HRX(I) = RX(I) * H
C
C       BACK SUBSTITUTE TO FIND NL(I)
C
      NL(I) = 0.0
      DELRHO(I) = 0.0
      RHOL(I) = RHOU(I) - DELRHO(I)
      HRHOL(I) = RHOL(I) * H
C
C
      SIG1L(I) = FC*RX(I) / (RX(I) + RHOL(I))
C
      ALPHA(I) = THETA(I)
      DALPHA(I) = ALPHA(I)*180./PI
      SIGN = - 1.0
C
      PP(I) =  SIG1L(I)*COS(ALPHA(I))**2
```

```
      TP(I) =  SIGN * SIG1L(I)*COS(ALPHA(I))*SIN(ALPHA(I))
C
      N(I) = 1.0
C
  50  CONTINUE
C
      DO 75 I=1,ICOUNT
      FACTOR = EINC1 * H
      IF(I.EQ.1) THEN
      FACTOR = EINC1 * H /2.
      ELSEIF(I.EQ.ICOUNT) THEN
      FACTOR = EINC1 * H / 2.
      ENDIF
C
C
      FX = FX - TP(I) * FACTOR
      FY = FY + PP(I) * FACTOR
C
C
  75  CONTINUE
C
       DO 80 I = 1,ICOUNT,ISKIP
       IJ = IJ + 1
       EFAN(IJ) = EU(I)
       NFAN(IJ) = N(I)
       ZFAN(IJ) = ZETA(I)
       YFAN(IJ) = W0 - ETA(I)
       W(IJ) = PI/2.
       NORM(IJ) = PP(I)
       BOND(IJ) = -TP(I)
       X0(IJ) = EU(I)
       Y0(IJ) = 1.0
C
       XPTN(IJ) = X0(IJ)
       XPTB(IJ) = X0(IJ)
C      YPTN(IJ) = Y0(IJ) - NORM(IJ) * SFACTN
       YPTN(IJ) = Y0(IJ) + NORM(IJ) * SFACTN
  80   YPTB(IJ) = Y0(IJ) + BOND(IJ) * SFACTB
       NUMFAN = IJ
C
C
      WRITE(*,*)  'SURFACE  1 = HORIZONTAL SURFACE'
      WRITE(6,*) ' '
      WRITE(6,'(A19,I6)') ' # OF INCREMENTS = ',NINC
      WRITE(6,'(A14,F10.7)') ' EINC1       = ',EINC1
      WRITE(6,*) ' '
C
      WRITE(6,*) '  I      EU(I)      ZETA(I)     ETA(I)  ',
     + ' DBETA(I)    DTHETA(I)'
      WRITE(6,*) ' '
      WRITE(6,200) (I, EU(I), ZETA(I), ETA(I), DBETA(I),
     +    DTHETA(I), I = 1,ICOUNT)
C 200 FORMAT(1X,I2,5F12.8)
C
      WRITE(6,*) '  I     SIG1U(I)      TAOU(I)     HRHOU(I)',
```

```
     + '    HRX(I)          EL(I)         NL(I)'
      WRITE(6,*) ' '
      WRITE(6,210) (I, SIG1U(I), TAOU(I), HRHOU(I),HRX(I),
     +      EL(I), NL(I), I = 1,ICOUNT)
C 210 FORMAT(1X,I2,4F13.8,2F12.8)
C
      WRITE(6,*) '  I     HRHOL(I)      SIG1L(I)     ',
     +  '     DALPHA(I)       PP(I)         TP(I)'
      WRITE(6,*) ' '
      WRITE(6,211)  (I, HRHOL(I), SIG1L(I), DALPHA(I),
     +   PP(I), TP(I), I = 1,ICOUNT)
  211 FORMAT(1X,I2,3F13.8,2F12.8)
C
C
      IF(NTYPE.EQ.1) THEN
      WRITE(6,*) '  IJ      X0(IJ)      Y0(IJ)      XPTN(IJ)',
     +           '  YPTN(IJ)    XPTB(IJ)    YPTB(IJ)  '
      WRITE(6,*) ' '
      WRITE(6,216)  (I, X0(I), Y0(I), XPTN(I),YPTN(I),
     +    XPTB(I),YPTB(I), I=1,IJ)
C 216 FORMAT(1X,I2,6F12.6)
      WRITE(6,*) ' '
      ENDIF
C
C
      WRITE(6,*) ' TOTAL HORIZONTAL FORCE =  ', FX
      WRITE(6,*) ' '
      WRITE(6,*) 'TOTAL VERTICAL FORCE =  ',  FY
      WRITE(6,*) ' '
C
      IF( NTYPE.EQ.1 )  GO TO 2000
C
  20  CONTINUE
C
C    ASSUME IT STARTS AT PT. EC1
C
      ESTART = EC1
C
C    NOW DETERMINE THE
C    CONTRIBUTION FROM THE CIRCULAR ARC
C
C    FIRST FIND NLMAX
C
C
      NLMAX = ( EUB - EC2 )*TANBB
C
      IF(NLMAX.GT.RS) THEN
C
C    I.P.  ON VERTICAL SURFACE
C
      ICASE = 3
C
C  FIND I. PT. WITH CIRCULAR ARC PT. EC2
C
      EAVE = ( EC2 + EUB ) / 2.
```

```
C
      ZETA(1) = EAVE * P / FC
      CALL HYPER(FCOP1,RW0,ZETA(1),ETA(1))
      TANB(1) = ( RW0 + ETA(1) )/( EAVE - ZETA(1) )
      NL(1) = ( EAVE - EC2 ) * TANB(1)
C
      E = EC2
      DELTAE = ( EUB - EC2 ) / 100.
      IF(NL(1).LT.RS) THEN
         E = EAVE
         DELTAE = ( EUB - EAVE ) / 100.
      ENDIF
C
      DO 25 I=1,101
      E = E + DELTAE
      ZETA(1) = E * P / FC
      CALL HYPER(FCOP1,RW0,ZETA(1),ETA(1))
      TANB(1) = ( RW0 + ETA(1) )/( E - ZETA(1) )
      NL(1) = ( E - EC2 ) * TANB(1)
      ELAST = E - DELTAE
C
      IF(NL(1).GT.RS) GO TO 26
   25 CONTINUE
   26 ENEW = E
      DELTAE = ( ENEW - ELAST ) / 100.
      E = ELAST
      DO 27 I=1,101
      E = E + DELTAE
      ZETA(1) = E * P / FC
      CALL HYPER(FCOP1,RW0,ZETA(1),ETA(1))
      TANB(1) = ( RW0 + ETA(1) )/( E - ZETA(1) )
      NL(1) = ( E - EC2 ) * TANB(1)
C
      IF(NL(1).GE.RS) GO TO 28
   27 CONTINUE
   28 CONTINUE
C
      NINC = 10
      EINC2 = ( E - EC1 )/NINC
      NINC3 = 10
      EINC3 = ( EUB - E )/NINC3
      DELN3 = ( NLMAX - NL(1) ) / NINC3
C
      ELSE
C
C   THE I.P. IS ON THE CIRCULAR SURFACE
C
      ICASE = 2
      NINC = 10
      ESTART = EC1
      IF(EUA.GT.EC1) ESTART = EUA
      EINC2 = ( EUB - ESTART )/NINC
      EINC3 = -1
C
      ENDIF
```

```
C
C
C ***********************************************************************
C       THE SURFACE IS A CIRCULAR ARC WITH RADIUS = R
C ***********************************************************************
C
C     DETERMINE FOR EACH EU(I) THE INTERSECTION COORDINATES WITH THE SURFACE
C
C
      ICOL = 14
      CFX = 0.0
      CFY = 0.0
      ICOUNT = NINC + 1
      DO 100 I=1,ICOUNT
      EU(I) = ESTART + EINC2 * (I-1)
C
      ZETA(I) = EU(I) * P / FC
      CALL HYPER(FCOP1,RW0,ZETA(I),ETA(I))
      TANB(I) = ( RW0 + ETA(I) )/( EU(I) - ZETA(I) )
      BETA(I) = ATAN(TANB(I))
      DBETA(I) = ATAN(TANB(I)) * 180./PI
      THETA(I) = PI/2. - BETA(I)
      DTHETA(I) = 90. - DBETA(I)
      RHOU(I) = SQRT( (EU(I) - ZETA(I))**2 + ( RW0 + ETA(I) )**2 )
      HRHOU(I) = RHOU(I) * H
C
C    EVALUATE PRINCIPAL STRESS SIG1U
C
       SIG1U(I) = 2. * P  / ( 1. + COS(2. * THETA(I)) )
C
C    EVALUATE THE SHEAR STRESS THAT GOES WITH P
C
       TAOU(I) = P * TAN( THETA(I) )
C
C
      RX(I) = SIG1U(I) * RHOU(I) / ( FC - SIG1U(I) )
      HRX(I) = RX(I) * H
C
C
      A = 1 + TANB(I)**2
      B = -2.* ( EC1 + EU(I)*TANB(I)**2 - RS*TANB(I) )
      C = EC1**2 + (EU(I) * TANB(I))**2 - 2.*RS*TANB(I)*EU(I)
C
      E1 = -B + SQRT( B**2 -4.*A*C)
      E1 = E1 / 2./A
C        OR
      E2 = -B - SQRT( B**2 -4.*A*C)
      E2 = E2 / 2./A
C
      IF ( E1.LE.EU(I).AND.E1.GE.EC1 ) THEN
C
        EL(I) = E1
C
      ELSEIF ( E2.LE.EU(I).AND.E2.GE.EC1 ) THEN
C
```

```
        EL(I) = E2
C
      ELSE
C
C   ERROR OR EU = EC1, ie WHEN I = 1 EU = EL = EC1
C
      IF(I.EQ.1) THEN
      EL(1) = EC1
C
      ELSE
       WRITE(6,*) ' INTERSECTION pt. NOT WITHIN PRESCRIBED LIMITS'
      ENDIF
C
      ENDIF
C
C       BACK SUBSTITUTE TO FIND NL(I)
C
      NL(I) = ( EU(I) - EL(I) ) * TANB(I)
      N(I) = 1.0 - NL(I)
      DELRHO(I) = SQRT( NL(I)**2 + (EU(I) - EL(I))**2 )
      RHOL(I) = RHOU(I) - DELRHO(I)
      HRHOL(I) = RHOL(I) * H
C
C
      SIG1L(I) = FC*RX(I) / (RX(I) + RHOL(I))
C
      IF(EL(I).EQ.EC1) THEN
      GAMA(I) = PI/2.
      ELSE
      RATIO = (RS - NL(I)) / (EL(I) - EC1)
      GAMA(I) = ATAN(RATIO)
      ENDIF
      DGAMA(I) = GAMA(I)*180./PI
C
      IF(GAMA(I).GT.THETA(I)) THEN
      ALPHA(I) = GAMA(I) + THETA(I) - PI/2.
      SIGN = - 1.0
      ELSEIF(GAMA(I).EQ.THETA(I)) THEN
      ALPHA(I) = 0.0
      SIGN = + 1.0
      ELSEIF(GAMA(I).LT.THETA(I)) THEN
      ALPHA(I) = PI/2. - GAMA(I) - THETA(I)
      SIGN = + 1.0
      ELSE
       WRITE(6,*) ' ERROR ---- GAMA OUTSIDE LIMITS'
       STOP
      ENDIF
C
      PP(I) =  SIG1L(I)*COS(ALPHA(I))**2
      TP(I) =  SIGN * SIG1L(I)*COS(ALPHA(I))*SIN(ALPHA(I))
C
  100 CONTINUE
C
C    EVALUATE DELTA GAMA FOR EACH STRIP
C
```

```
C
      DO 150 I=1,ICOUNT
      IF(I.NE.ICOUNT) THEN
      DELG(I) = ABS( GAMA(I) - GAMA(I+1) )
      ELSE
      DELG(I) = 0.0
      ENDIF
      IF(I.EQ.1) THEN
      FACTOR =  RS * DELG(1)/2. * H
      ELSEIF(I.EQ.ICOUNT) THEN
      FACTOR =  RS * DELG(I-1)/2. * H
      ELSE
      FACTOR =  RS * (DELG(I-1)+DELG(I))/2. * H
      ENDIF
C
      RADF(I) =  PP(I) * FACTOR
      TANF(I) =  TP(I) * FACTOR
C
C
      CFX = CFX + RADF(I)*COS(GAMA(I)) - TANF(I)*SIN(GAMA(I))
      CFY = CFY + RADF(I)*SIN(GAMA(I)) + TANF(I)*COS(GAMA(I))
C
C
C
  150 CONTINUE
C
       IF(ICASE.NE.2) IJ = IJ - 1
C
       DO 180 I=1,ICOUNT
       G = GAMA(I)
       IJ = IJ + 1
       EFAN(IJ) = EL(I)
       NFAN(IJ) = N(I)
       ZFAN(IJ) = ZETA(I)
       YFAN(IJ) = W0 - ETA(I)
       W(IJ) = G
       NORM(IJ) = PP(I)
       BOND(IJ) = -TP(I)
       X0(IJ) = EL(I)
       Y0(IJ) = N(I)
C
C      XPTN(IJ) = X0(IJ) - NORM(IJ) * COS(G) * SFACTN
C      YPTN(IJ) = Y0(IJ) - NORM(IJ) * SIN(G) * SFACTN
       XPTN(IJ) = X0(IJ) + NORM(IJ) * COS(G) * SFACTN
       YPTN(IJ) = Y0(IJ) + NORM(IJ) * SIN(G) * SFACTN
       XPTB(IJ) = X0(IJ) + BOND(IJ) * COS(G) * SFACTB
 180   YPTB(IJ) = Y0(IJ) + BOND(IJ) * SIN(G) * SFACTB
       NUMFAN = IJ
C
      FX = FX + CFX
      FY = FY + CFY
C
C
C     SET REBAR COORDINATES
C     for circular surface
```

```
C     we assume a full 90 degree
C     hook although not all of it
C     need be used by the stress field
C
C
      NSEGS = 20
      DELTA = PI/2./NSEGS
      NSEGS1 = NSEGS + 1
C
      ANGLE = PI/2.
      DO 110 I = 1,NSEGS1
      BARX(I) = EC1 + RS * COS(ANGLE)
      BARY(I) = 1.0 - (RS * ( 1. - SIN(ANGLE) ) )
  110 ANGLE = ANGLE - DELTA
C
C
      WRITE(*,*)  'SURFACE  2 = CIRCULAR SURFACE'
      WRITE(6,*) ' '
C
      WRITE(6,'(A19,I6)') ' # OF INCREMENTS = ',NINC
      WRITE(6,'(A14,F10.7)') ' EINC2       = ',EINC2
      WRITE(6,'(A27,F10.3)') ' RADIUS CIRCULAR SURFACE = ',R
      WRITE(6,*) ' '
      WRITE(6,*) '  I      EU(I)      ZETA(I)     ETA(I)  ',
     + ' DBETA(I)    DTHETA(I)'
      WRITE(6,*) ' '
      WRITE(6,200) (I, EU(I), ZETA(I), ETA(I), DBETA(I),
     +    DTHETA(I), I = 1,ICOUNT)
  200 FORMAT(1X,I2,5F12.8)
C
      WRITE(6,*) '  I     SIG1U(I)      TAOU(I)     HRHOU(I)',
     + '    HRX(I)         EL(I)        NL(I)'
      WRITE(6,*) ' '
      WRITE(6,210) (I, SIG1U(I), TAOU(I), HRHOU(I),HRX(I),
     +      EL(I), NL(I), I = 1,ICOUNT)
  210 FORMAT(1X,I2,4F13.8,2F12.8)
C
      WRITE(6,*) '  I    HRHOL(I)     SIG1L(I)     DGAMA(I)',
     +  '     DALPHA(I)      PP(I)        TP(I)'
      WRITE(6,*) ' '
      WRITE(6,210)  (I, HRHOL(I), SIG1L(I), DGAMA(I), DALPHA(I),
     +   PP(I), TP(I), I = 1,ICOUNT)
C
      WRITE(6,*) '  I    DELG(I)     RADF(I)     TANF(I)'
      WRITE(6,*) ' '
      WRITE(6,215)  (I, DELG(I), RADF(I), TANF(I), I=1,ICOUNT)
  215 FORMAT(1X,I2,3F12.6)
C
C
      WRITE(6,*) ' HORIZONTAL FORCE FROM CIRCULAR SURFACE =  ', CFX
      WRITE(6,*) ' '
      WRITE(6,*) ' VERTICAL FORCE FROM CIRCULAR SURFACE =  ', CFY
      WRITE(6,*) ' '
C
C
```

```
      WRITE(6,*) ' TOTAL HORIZONTAL FORCE =  ', FX
      WRITE(6,*) ' '
      WRITE(6,*) ' TOTAL VERTICAL FORCE =  ',  FY
      WRITE(6,*) ' '
C
C
      ISKIP = 1
C     CALL FNPLOT(EFAN,NFAN,ZFAN,YFAN,NUMFAN)
C
      IF(EINC3.LT.0) GOTO 2000
C
C ***********************************************************************
C       THE SURFACE IS A VERTICAL SURFACE AT LOCATION EC2
C ***********************************************************************
C
C   .  DETERMINE FOR EACH EU(I) THE INTERSECTION COORDINATES WITH THE SURFACE
C
  30  ICOUNT = NINC3 + 1
      ICOL = 14
      DO 125 I=1,ICOUNT
      EU(I) = E + EINC3 * (I-1)
C
      ZETA(I) = EU(I) * P / FC
      CALL HYPER(FCOP1,RW0,ZETA(I),ETA(I))
      TANB(I) = ( RW0 + ETA(I) )/( EU(I) - ZETA(I) )
      BETA(I) = ATAN(TANB(I))
      DBETA(I) = ATAN(TANB(I)) * 180./PI
      THETA(I) = PI/2. - BETA(I)
      DTHETA(I) = 90. - DBETA(I)
      RHOU(I) = SQRT( (EU(I) - ZETA(I))**2 + ( RW0 + ETA(I) )**2 )
      HRHOU(I) = RHOU(I) * H
C
C     EVALUATE PRINCIPAL STRESS SIG1U
C
       SIG1U(I) = 2. * P  / ( 1. + COS(2. * THETA(I)) )
C
C     EVALUATE THE SHEAR STRESS THAT GOES WITH P
C
       TAOU(I) = P * TAN( THETA(I) )
C
C
      RX(I) = SIG1U(I) * RHOU(I) / ( FC - SIG1U(I) )
      HRX(I) = RX(I) * H
C
C    EVALUATE THE POINT OF INTERSECTION WITH THE VERTICAL SURFACE
C
      EL(I) = EC2
C
C       BACK SUBSTITUTE TO FIND NL(I)
C
      NL(I) = ( EU(I) - EL(I) ) * TANB(I)
      N(I) = 1.0 - NL(I)
      DELRHO(I) = SQRT( NL(I)**2 + (EU(I) - EL(I))**2 )
      RHOL(I) = RHOU(I) - DELRHO(I)
      HRHOL(I) = RHOL(I) * H
```

```
C
C
      SIG1L(I) = FC*RX(I) / (RX(I) + RHOL(I))
C
C
      ALPHA(I) = PI/2. - THETA(I)
      DALPHA(I) = ALPHA(I)*180./PI
      SIGN = + 1.0
C
      PP(I) =  SIG1L(I)*COS(ALPHA(I))**2
      TP(I) =  SIGN * SIG1L(I)*COS(ALPHA(I))*SIN(ALPHA(I))
C
 125  CONTINUE
C
      VFX = 0.
      VFY = 0.
      DO 175 I=1,ICOUNT
      FACTOR = DELN3 * H
      IF(I.EQ.1) THEN
      FACTOR = DELN3 * H /2.
      ELSEIF(I.EQ.ICOUNT) THEN
      FACTOR = DELN3 * H / 2.
      ENDIF
C
      VFX = VFX + PP(I) * FACTOR
      VFY = VFY + TP(I) * FACTOR
C
 175  CONTINUE
C
       IJ = IJ - 1
       DO 280 I = 1,ICOUNT,2
       IJ =  IJ + 1
       EFAN(IJ) = EL(I)
       NFAN(IJ) = N(I)
       ZFAN(IJ) = ZETA(I)
       YFAN(IJ) = W0 - ETA(I)
       W(IJ) = 0.0
       NORM(IJ) = PP(I)
       BOND(IJ) = -TP(I)
       X0(IJ) = EC2
       Y0(IJ) = N(I)
C
C      XPTN(IJ) = X0(IJ) - NORM(IJ) *  SFACTN
       XPTN(IJ) = X0(IJ) + NORM(IJ) *  SFACTN
       YPTN(IJ) = Y0(IJ)
       XPTB(IJ) = X0(IJ) + BOND(IJ) *  SFACTB
 280   YPTB(IJ) = Y0(IJ)
       NUMFAN = IJ
C
C
      FX = FX + VFX
      FY = FY + VFY
C
      WRITE(*,*)  'SURFACE  3 = VERTICAL SURFACE'
      WRITE(6,*) ' '
```

```
C
C
      WRITE(6,'(A19,I6)') ' # OF INCREMENTS = ',NINC3
      WRITE(6,'(A14,F10.7)') ' EINC3       = ',EINC3
      WRITE(6,'(A14,F10.7)') ' DELN3       = ',DELN3
C
      WRITE(6,*) '  I      EU(I)      ZETA(I)     ETA(I)  ',
     + ' DBETA(I)    DTHETA(I)'
      WRITE(6,*) ' '
      WRITE(6,200) (I, EU(I), ZETA(I), ETA(I), DBETA(I),
     +    DTHETA(I), I = 1,ICOUNT)
C 200 FORMAT(1X,I2,5F12.8)
C
      WRITE(6,*) '  I     SIG1U(I)      TAOU(I)     HRHOU(I)',
     + '    HRX(I)         EL(I)        NL(I)'
      WRITE(6,*) ' '
      WRITE(6,210) (I, SIG1U(I), TAOU(I), HRHOU(I),HRX(I),
     +      EL(I), NL(I), I = 1,ICOUNT)
C 210 FORMAT(1X,I2,4F13.8,2F12.8)
C
      WRITE(6,*) '  I    HRHOL(I)     SIG1L(I)    ',
     +  '     DALPHA(I)      PP(I)        TP(I)'
      WRITE(6,*) ' '
      WRITE(6,211)  (I, HRHOL(I), SIG1L(I), DALPHA(I),
     +   PP(I), TP(I), I = 1,ICOUNT)
C
C     WRITE(6,*) '  I    DELG(I)     RADF(I)     TANF(I)'
C     WRITE(6,*) ' '
C     WRITE(6,215)  (I, DELG(I), RADF(I), TANF(I), I=1,ICOUNT)
C 215 FORMAT(1X,I2,3F12.6)
C
      WRITE(6,*) '  IJ     X0(IJ)     Y0(IJ)     XPTN(IJ)',
     +           '  YPTN(IJ)    XPTB(IJ)    YPTB(IJ)  '
      WRITE(6,*) ' '
      WRITE(6,216)  (I, X0(I), Y0(I), XPTN(I),YPTN(I),
     +    XPTB(I),YPTB(I), I=1,IJ)
  216 FORMAT(1X,I2,6F12.6)
      WRITE(6,*) ' '
C
      WRITE(6,*) ' HORIZONTAL FORCE FROM VERTICAL SURFACE =  ', VFX
      WRITE(6,*) ' '
      WRITE(6,*) ' VERTICAL FORCE FROM VERTICAL SURFACE =  ', VFY
      WRITE(6,*) ' '
C
      WRITE(6,*) ' TOTAL HORIZONTAL FORCE =  ', FX
      WRITE(6,*) ' '
      WRITE(6,*) ' TOTAL VERTICAL FORCE =  ',  FY
      WRITE(6,*) ' '
C
C
 2000 CONTINUE
C
C     PLOTS PREVIOUSLY INITIALIZED
C
      WRITE(6,*) ' '
```

```
      IY = 'Y'
      WRITE(*,*)  '   '
     WRITE(*,*)  'PLOT STRESS FIELD ? '
     WRITE(*,*)  '  ENTER Y OR N '
      READ(*,'(A1)')  IANS
C
      IF(IANS.EQ.IY) THEN
C
C             PLOT FANS
C
      CALL FNPLOT(EFAN,NFAN,ZFAN,YFAN,NUMFAN)
C
C             PLOT THE REINFORCING STEEL
C
      CALL RPLOT(NTYPE,BARX,BARY,SCALE,NSEGS)
C
C             PLOT THE FAN BOUNDARIES
C
      CALL FPLOT(FCOP1,ZETAA,ETAA,ZETAB,W0,SCALE)
C
      CALL PLOT(0.,0.,999)
      ENDIF
C
      WRITE(*,*)  '   '
     WRITE(*,*)  'PLOT NORMAL STRESSES ? '
     WRITE(*,*)  '  ENTER Y OR N '
      READ(*,'(A1)')  IANS
C
     IF(IANS.EQ.IY) THEN
C
C             PLOT NORMAL STRESSES
C
      SCALE=1.0
      CALL IPLOT(H,PSCALE,SCALE,IOPORT,MODEL)
      CALL FNPLOT(EFAN,NFAN,ZFAN,YFAN,NUMFAN)
      CALL RPLOT(NTYPE,BARX,BARY,SCALE,NSEGS)
      CALL FPLOT(FCOP1,ZETAA,ETAA,ZETAB,W0,SCALE)
      CALL NORMPL(IJ)
      CALL PLOT(0.,0.,999)
      ENDIF
C
      WRITE(*,*)  '   '
     WRITE(*,*)  'PLOT BOND STRESSES ? '
     WRITE(*,*)  '  ENTER Y OR N '
      READ(*,'(A1)')  IANS
C
      IF(IANS.EQ.IY) THEN
C
C             PLOT BOND STRESSES
C
      SCALE=1.0
      CALL IPLOT(H,PSCALE,SCALE,IOPORT,MODEL)
      CALL FNPLOT(EFAN,NFAN,ZFAN,YFAN,NUMFAN)
      CALL RPLOT(NTYPE,BARX,BARY,SCALE,NSEGS)
      CALL FPLOT(FCOP1,ZETAA,ETAA,ZETAB,W0,SCALE)
```

```
      CALL BONDPL(IJ)
      CALL PLOT(0.,0.,999)
      ENDIF
C
       WRITE(*,*)  '    '
      WRITE(*,*)  'PLOT ZOOM OF NODAL ZONE ? '
      WRITE(*,*)  '  ENTER Y OR N '
       READ(*,'(A1)')  IANS
C
      IF(IANS.EQ.IY) THEN
      SCALE=1.0
      CALL IPLOT(H,PSCALE,SCALE,IOPORT,MODEL)
      CALL NPLOT
      CALL PLOT(0.,0.,999)
      ENDIF
C
      GO TO 5
C
  999 STOP
      END
C **********************************************************************
C
      SUBROUTINE HYPER(FCOP1,RW0,ZETA,ETA)
C
      ETA = SQRT( FCOP1*ZETA**2 + RW0**2 ) - RW0
C
      RETURN
      END
C
C **********************************************************************
C
      SUBROUTINE IPLOT(H,PSCALE,SCALE,IOPORT,MODEL)
C
      DIMENSION XS(4),YS(4)
C
C    SET SCALE
C
C
      SCALE = PSCALE * 25.4/H
C
       CALL PLOTS(0,IOPORT,MODEL)
C
C
C   FILL SCREEN
C
      XS(1) = 0.0
      XS(2) = 0.0
      XS(3) = 9.8
      XS(4) = 9.8
      YS(1) = 0.0
      YS(2) = 7.4
      YS(3) = 7.4
      YS(4) = 0.0
      ICOL = 7
C     CALL NEWPEN(1)
```

```
C      CALL COLOR(ICOL,IERR)
C      IFILL = 1
C      CALL STFILL(IFILL)
C      CALL FILL(XS,YS,4)
C
C    DRAW RECTANGLE   9.9 X 7.5
C
C
       CALL COLOR(3,IERR)
C      CALL NEWPEN(20)
C
       CALL PLOT(0.0,0.0,-3)
C      CALL PLOT(0.0,7.5,2)
C      CALL PLOT(9.9,7.5,2)
C      CALL PLOT(9.75,7.5,3)
C      CALL PLOT(9.75,0.0,2)
C      CALL PLOT(0.0,0.0,2)
C
C     MOVE ORIGIN TO (0.75,0.75)
C
        CALL PLOT(0.75,0.75,-3)
C
       CALL OFFSET(0.,SCALE,0.,SCALE)
C
   99  RETURN
       END
C ***************************************************************************
C
       SUBROUTINE FNPLOT(EFAN,NFAN,ZFAN,YFAN,NUMFAN)
C
       DIMENSION  EFAN(35),ZFAN(35),YFAN(35)
       REAL NFAN(35)
C
C
C
C  NOW PLOT FAN LINES AT EACH INCREMENT
C       .
       ICOL = 14
       CALL COLOR(ICOL,IERR)
       CALL NEWPEN(1)
C
       DO 10 K=1,NUMFAN
        CALL PLOT(ZFAN(K),YFAN(K),13)
  10    CALL PLOT(EFAN(K),NFAN(K),12)
C
C
       RETURN
       END
C ***************************************************************************
C
       SUBROUTINE RPLOT(NTYPE,BARX,BARY,SCALE,NSEGS)
C
       DIMENSION BARX(21),BARY(21)
C
C      PLOT REBAR
```

```
C
      CALL COLOR(4,IERR)
      CALL NEWPEN(2)
C
C   THICK RED PEN
C   AND MOVE TO START OF HORIZONTAL BAR
C
       CALL PLOT(0.0,1.0,13)
      IF(NTYPE.EQ.1) THEN
       X = 8.8 * SCALE
       CALL PLOT(X,1.0,12)
       RETURN
       ELSE
       X = BARX(1)
       CALL PLOT(X,1.0,12)
       ENDIF
C
C
       CALL PLOT(BARX(1),BARY(1),13)
      DO 10 J=2,NSEGS
      XLAST = BARX(J)
      CALL PLOT(BARX(J),BARY(J),12)
  10  CONTINUE
C
      Y = 1.0 * SCALE
      CALL PLOT(XLAST,Y,12)
C
C
      RETURN
      END
C **********************************************************************
C
      SUBROUTINE FPLOT(FCOP1,ZETAA,ETAA,ZETAB,W0,SCALE)
C
      DIMENSION XT(3),YT(3)
C
      RW0 = 1. - W0
C
      CALL COLOR(0,IERR)
      CALL NEWPEN(1)
C
C   PLOT NODAL ZONE
C
      YA = W0 - ETAA
       CALL PLOT(ZETAA,0.0,13)
       CALL PLOT(ZETAA,YA,12)
       CALL PLOT(ZETAB,0.0,12)
       CALL PLOT(ZETAA,0.0,12)
C
C   FILL NODAL ZONE
C
      XT(1) = 1.01 * ZETAA / SCALE
      XT(2) = 1.01 * ZETAA / SCALE
      XT(3) = 0.95 * ZETAB / SCALE
      YT(1) = 0.95 * YA / SCALE
```

```
      YT(2) = YT(1) * 0.02
      YT(3) = YT(1) * 0.02
      CALL COLOR(0,IERR)
      CALL STFILL(3)
      CALL FILL(XT,YT,3)
C
C     CALL COLOR(5,IERR)
      CALL COLOR(0,IERR)
      CALL NEWPEN(2)
C
C  PLOT HYPERBOLIC NODAL SURFACE
C
      ZMAX = ZETAB * 1.2
      XINC = ZMAX / 30.
      X = 0.0
C      CALL COLOR(0,IERR)
C     CALL NEWPEN(2)
C      CALL PLOT(0.,W0,13)
C     XL = ZETAB * 2.
C      CALL PLOT(XL,W0,12)
C      CALL PLOT(0.,W0,13)
C     YL = - .05
C      CALL PLOT(0.,YL,12)
       CALL PLOT(0.,W0,13)
C     CALL COLOR(5,IERR)
      CALL COLOR(0,IERR)
      CALL NEWPEN(2)
        DO 10 I = 1,30
        X = X + XINC
        CALL HYPER(FCOP1,RW0,X,Y)
        Y = W0 - Y
 10     CALL PLOT(X,Y,12)
      CALL COLOR(0,IERR)
      CALL NEWPEN(2)
       CALL PLOT(0.,W0,13)
      XL = ZETAB * 2.
       CALL PLOT(XL,W0,12)
       CALL PLOT(0.,W0,13)
      YL = - .05
       CALL PLOT(0.,YL,12)
C
      RETURN
      END
C ***********************************************************************
C
      SUBROUTINE NPLOT
C
      COMMON/FP/EU(35),ZETA(35),ETA(35),TANB(35),BETA(35),DBETA(35),
     +          THETA(35),DTHETA(35),RHOU(35),HRHOU(35),SIG1U(35),
     +          RX(35),HRX(35),EL(35),GAMA(35),DGAMA(35),
     +          RHOL(35),HRHOL(35),SIG1L(35),PP(35),TP(35),
     +          DELRHO(35),TAOU(35), HSUM(35), VSUM(35), HTERM1(35),
     +          HTERM2(35),HTERM3(35), VTERM1(35),VTERM2(35),VTERM3(35),
     +          DELG(35),RADF(35),TANF(35),ALPHA(35),DALPHA(35),
     +          P,FC,FCOP1,RW0,H,EUA,EUB,W0,ZETAA,ZETAB,ETAA,
```

```
     +          ICOL,NTYPE,BOND(35),NORM(35),W(35),ITITLE,
     +          X0(35),Y0(35),XPTN(35),XPTB(35),YPTN(35),YPTB(35),SCALE
C
      REAL L,LO2,NL(35),NLMAX,N(35),NORM
C
      DIMENSION XT(3),YT(3),XS(4),YS(4)
C
      CHARACTER*1 CARRAY
      CHARACTER*30 ITITLE
C
      RW0 = 1. - W0
      PI = 3.1415927
C
C
C     SET SCALE
C
      XMAX = 2.5 * ZETAB
      YMAX = 1.0
      S1 =  XMAX / 9.0
      S2 =  YMAX / 6.0
      SCALE = S1
      IF(S1.LT.S2) SCALE = S2
C
C     INITIALIZE PLOTTING DEVICE
C
      IOPORT = 97
      MODEL =  97
C
       CALL PLOTS(0,IOPORT,MODEL)
C
C    FILL SCREEN
C
      XS(1) = 0.0
      XS(2) = 0.0
      XS(3) = 9.8
      XS(4) = 9.8
      YS(1) = 0.0
      YS(2) = 7.4
      YS(3) = 7.4
      YS(4) = 0.0
      ICOL = 7
C     CALL NEWPEN(1)
C     CALL COLOR(ICOL,IERR)
C     IFILL = 1
C     CALL STFILL(IFILL)
C     CALL FILL(XS,YS,4)
C
C    DRAW RECTANGLE   9.9 X 7.5
C
C
      CALL COLOR(3,IERR)
      CALL NEWPEN(20)
C
       CALL PLOT(0.0,0.0,-3)
       CALL PLOT(0.0,7.5,2)
```

```
      CALL PLOT(9.9,7.5,2)
      CALL PLOT(9.75,7.5,3)
      CALL PLOT(9.75,0.0,2)
      CALL PLOT(0.0,0.0,2)
C
C     MOVE ORIGIN TO (4.00,4.75)
C
      CALL PLOT(4.00,4.75,-3)
C
      CALL OFFSET(0.,SCALE,0.,SCALE)
C
      CALL COLOR(0,IERR)
      CALL NEWPEN(1)
C
C    PLOT NODAL ZONE
C
      YA =  -ETAA
      YB =  - W0
      CALL PLOT(ZETAA,-W0,13)
      CALL PLOT(ZETAA,YA,12)
      CALL PLOT(ZETAB,-W0,12)
      CALL PLOT(ZETAA,-W0,12)
C
C    FILL NODAL ZONE
C
      XT(1) = 1.05 * ZETAA / SCALE
      XT(2) = 1.05 * ZETAA / SCALE
      XT(3) = 0.95 * ZETAB / SCALE
      YT(1) = - W0 /SCALE
      YT(2) = - ETAA /SCALE
      YT(3) = - W0 /SCALE
      CALL COLOR(0,IERR)
      CALL STFILL(3)
      CALL FILL(XT,YT,3)
C
C    PLOT FAN BOUNDARY
C
      CALL COLOR(3,IERR)
      CALL NEWPEN(2)
C
      CALL PLOT(ZETAA,YA,13)
      X =  ZETAA + ( EUA - ZETAA ) / 5.0
      Y =  YA + ( RW0 +  ETAA ) / 5.0
      CALL PLOT(X,Y,12)
      CALL PLOT(ZETAB,YB,13)
      X =  ZETAB + ( EUB - ZETAB ) / 5.0
      Y =   YB + 1.0 / 5.0
      CALL PLOT(X,Y,12)
C
C  PLOT HYPERBOLIC NODAL SURFACE  AND AXES
C
      CALL COLOR(0,IERR)
      CALL NEWPEN(2)
C
      ZMAX = ZETAB * 1.2
```

```
      XINC = ZMAX / 50.
      X = 0.0
C      CALL PLOT(0.,0.,13)
C     XL = 3.5 * SCALE
C      CALL PLOT(XL,0.,12)
C      CALL PLOT(0.,0.,13)
C     YL = -3.5 * SCALE
C      CALL PLOT(0.,YL,12)
       CALL PLOT(0.,0.,13)
      CALL COLOR(3,IERR)
      CALL NEWPEN(2)
C
        DO 10 I = 1,50
        X = X + XINC
        CALL HYPER(FCOP1,RW0,X,Y)
        Y =  -1.0  * Y
 10     CALL PLOT(X,Y,12)
C
      CALL COLOR(0,IERR)
      CALL NEWPEN(2)
       CALL PLOT(0.,0.,13)
      XL = 3.5 * SCALE
       CALL PLOT(XL,0.,12)
       CALL PLOT(0.,0.,13)
      YL = -3.5 * SCALE
       CALL PLOT(0.,YL,12)
C
      XINC = ( EUB - EUA ) / 10.
C
      CALL COLOR(14,IERR)
      CALL NEWPEN(1)
C
C
C   PLOT FANS AND RADIUS FANS
C
      DO 20 I=1,11
C
       XU = EUA + XINC * (I-1)
C
       X = XU * P / FC
       CALL HYPER(FCOP1,RW0,X,Y)
       TANBX = ( RW0 + Y )/( XU - X )
       BETAX = ATAN(TANBX)
       THETAX = PI/2. - BETAX
       RHOUX = SQRT( ( XU - X )**2 + ( RW0 + Y )**2 )
C
C    EVALUATE PRINCIPAL STRESS SIG1U
C
       SIG1UX = 2. * P  / ( 1. + COS(2. * THETAX) )
C
C
       RXX = SIG1UX * RHOUX / ( FC - SIG1UX )
C
       XR = X - RXX * COS(BETAX)
       YR = RXX * SIN(BETAX) + Y
```

```
      YR = -1.0 * YR
C
C   PLOT EACH FAN
C
      Y =  -1.0  * Y
       CALL PLOT(X,Y,13)
      XU = X + ( XU -  X ) / 5.0
      YU = Y + ( RW0 - Y ) / 5.0
       CALL PLOT(XU,YU,12)
C
C   PLOT EACH RADIUS
C
     CALL COLOR(13,IERR)
     CALL NEWPEN(1)
C
       CALL PLOT(X,Y,13)
      XR = XR / SCALE
      YR = YR / SCALE
       CALL PLOTD(XR,YR,2)
     CALL COLOR(14,IERR)
     CALL NEWPEN(1)
C
      CARRAY = CHAR(3)
      CALL SYMBOL(XR,YR,0.15,CARRAY,90.,-1)
C       CALL PLOT(XR,YR,12)
C
  20  CONTINUE
C
  99  RETURN
      END
C ***************************************************************************
C
      SUBROUTINE NORMPL(IJ)
C
      COMMON/FP/EU(35),ZETA(35),ETA(35),TANB(35),BETA(35),DBETA(35),
     +          THETA(35),DTHETA(35),RHOU(35),HRHOU(35),SIG1U(35),
     +          RX(35),HRX(35),EL(35),GAMA(35),DGAMA(35),
     +          RHOL(35),HRHOL(35),SIG1L(35),PP(35),TP(35),
     +          DELRHO(35),TAOU(35), HSUM(35), VSUM(35), HTERM1(35),
     +          HTERM2(35),HTERM3(35), VTERM1(35),VTERM2(35),VTERM3(35),
     +          DELG(35),RADF(35),TANF(35),ALPHA(35),DALPHA(35),
     +          P,FC,FCOP1,RW0,H,EUA,EUB,W0,ZETAA,ZETAB,ETAA,
     +          ICOL,NTYPE,BOND(35),NORM(35),W(35),ITITLE,
     +          X0(35),Y0(35),XPTN(35),XPTB(35),YPTN(35),YPTB(35),SCALE
C
      REAL L,LO2,NL(35),NLMAX,N(35),NORM
      CHARACTER*30 ITITLE
C
C  SCALE FOR STRESSES RELATIVE TO CURRENT SCALE
C
C     CALL COLOR(0,IERR)
      CALL COLOR(2,IERR)
      CALL NEWPEN(2)
C
       CALL SYMBOL(-.40,-0.40,0.15,'Normal Stresses',0.0,15)
```

```
      CALL SYMBOL(-.40,-.70,0.20,ITITLE,0.0,30)
C
      DO 50 I = 1,IJ
      CALL PLOT(X0(I),Y0(I),13)
      X = XPTN(I)
      Y = YPTN(I)
 50   CALL PLOT(X,Y,12)
C
     CALL NEWPEN(2)
      CALL PLOT(XPTN(1),YPTN(1),13)
C
      DO 100 I = 2,IJ
      X = XPTN(I)
      Y = YPTN(I)
100   CALL PLOT(X,Y,12)
C
C
      RETURN
      END
C ***********************************************************************
C
      SUBROUTINE BONDPL(IJ)
C
      COMMON/FP/EU(35),ZETA(35),ETA(35),TANB(35),BETA(35),DBETA(35),
     +          THETA(35),DTHETA(35),RHOU(35),HRHOU(35),SIG1U(35),
     +          RX(35),HRX(35),EL(35),GAMA(35),DGAMA(35),
     +          RHOL(35),HRHOL(35),SIG1L(35),PP(35),TP(35),
     +          DELRHO(35),TAOU(35), HSUM(35), VSUM(35), HTERM1(35),
     +          HTERM2(35),HTERM3(35), VTERM1(35),VTERM2(35),VTERM3(35),
     +          DELG(35),RADF(35),TANF(35),ALPHA(35),DALPHA(35),
     +          P,FC,FCOP1,RW0,H,EUA,EUB,W0,ZETAA,ZETAB,ETAA,
     +          ICOL,NTYPE,BOND(35),NORM(35),W(35),ITITLE,
     +          X0(35),Y0(35),XPTN(35),XPTB(35),YPTN(35),YPTB(35),SCALE
C
      REAL L,LO2,NL(35),NLMAX,N(35),NORM
      CHARACTER*30 ITITLE
C
C
C     CALL COLOR(0,IERR)
      CALL COLOR(2,IERR)
C     CALL NEWPEN(1)
      CALL NEWPEN(2)
C
      CALL SYMBOL(-.40,-0.40,0.15,'Bond Stresses',0.0,13)
      CALL SYMBOL(-.40,-.70,0.20,ITITLE,0.0,30)
C
C
      DO 50 I = 1,IJ
      CALL PLOT(X0(I),Y0(I),13)
      X = XPTB(I)
      Y = YPTB(I)
 50   CALL PLOT(X,Y,12)
C
     CALL NEWPEN(2)
      CALL PLOT(XPTB(1),YPTB(1),13)
```

```
C
      DO 100 I = 2,IJ
      X = XPTB(I)
      Y = YPTB(I)
 100  CALL PLOT(X,Y,12)
C
C
      RETURN
      END
```